METEORIC PHENOMENA IN THE EARTH'S ATMOSPHERE

INVESTIGATIONS OF METEORS

No. 2

B. L. Kashcheyev, V. N. Lebedinets, M. F. Lagutin

Translation of: "Meteornyye yavleniya v atmosfere Zemli," Issledovaniya meteorov. Izdatel'stvo "Nauka" [Science Publishing House] 260 pp., Moscow 1967.

[RESULTS OF RESEARCH IN INTERNATIONAL GEOPHYSICAL PROJECTS]

Date of Translation: April 1968

Translated by Bellcomm Inc.
under NASA Contract NASw-417.

TABLE OF CONTENTS

TABLE OF CONTENTS (cont'd)

Book by B.L. Kashcheyev, V.N. Lebedinets and M.F. Lagutin

Transliterated title: Meteornyye yavleniya v atmosfere Zemli.

Approved for printing by the Interdepartmental Geophsyical Committee under the Presidium of the USSR Academy of Sciences

Editor: A.D. Podol'skiy. Technical Editor A.P. Yefimova

Sent to typesetting on 4 July 1966. Assigned for printing on 3 January 1967

Format 70X108 1/16 Printed sheet 22.75

Printing run: 1,275 copies. Publishing number 1108/66. Printing order: 1087

"Science" Publishing House, Moscow, K-62, Podsosenskiy pereulok, 21

Second Typography of "Science" Publishing House, Moscow, G-99, Shubinskiy per. 10.

ABSTRACT

From November 1959 through December 1960 at the Kharkov Polytechnical Institute series of radar measurements of radiants and velocities of individual meteors were carried out. The pulse-diffraction method was used to measure velocities; the method of triangular reception of radio-waves reflected from forming meteor trail was used for measuring radiant position. The orbits of 12500 meteor bodies were obtained. Measurements of meteor rates, meteor trail drifts, initial radius of ionized meteor trails were also carried out according to the program of the IGY—IGC.

In Chapter I the physical theory of radiometeors is discussed. The ionization curves for meteors being borne by meteor bodies of various masses are obtained. In Chapter II the selectivity of observations in relation to declination of radiants and meteor velocities is discussed. Formulas for receiving density of meteor stream from measured meteor rates are obtained. In Chapter III the equipment and technique for measuring velocities and radiants of meteors are described. Errors of measurements are analysed. As the result of the statistical analysis of the orbit catalogue 195 meteor streams and associations are found. The obtained distribution of orbits of meteor bodies is compared with the results of photographic observations.

METEORIC PHENOMENA IN THE EARTH'S ATMOSPHERE

PREFACE

A thorough study of the upper layers of the atmosphere and also of the interplanetary and near-Earth cosmic space led to the development of new trends in research, developing at the confluence of several sciences. One of them is the study of meteors and the related phenomena in the Earth's atmosphere by the radar method. The radar observations permit one to obtain information concerning the meteor bodies, concerning their movement in interplanetary space, and concerning the ionization produced by them in the atmosphere. In distinction from the optical observations (visual and photographic), the radio observations can be conducted at any time of day and under any weather conditions, which is particularly valuable during a study of the diurnal and seasonal variations of the population of meteors, and also in a study of the diurnal meteor streams and of the streams acting during very brief time intervals. The radar observations of meteors permit us to study the diurnal and seasonal variations of the atmospheric density in the meteor zone. The measurements of the drifts of the ionized meteor trails proved to be an irreplaceable means for a detailed study of the circulation of the atmosphere. By the program of the International Quiet Sun Year (IQSY), the conduct of such measurements was provided for in many countries.

In spite of a number of advantages, the radar method can not completely replace the other methods of studying meteors. A thorough study of the meteoric material in the solar system and the phenomena, related with meteors, in the Earth's atmosphere, requires the use of various methods, of which the most valuable are the radar and photographic observations of meteors, and also of the direct measurements on artificial Earth satellites and space rockets.

The studies of the meteor phenomena by the radar method conducted in the Kharkov Polytechnical Institute (KPI) from 1957 - 1963 include practically all of the basic trends. The extensive statistical material accumulated during these years permit us to derive a number of conclusions concerning the structure of the aggregation of the meteor bodies in the environs of the Earth orbit, concerning the physical processes in the ionized meteor trails, and concerning their effect upon the noticeability of meteors during the radio observations. We studied the regular and irregular movements of the atmosphere in the meteor zone. We compiled the largest catalog in the world, containing 12,500 individual orbits of meteor bodies.

The present report summarizes the studies of the meteors and the related phenomena based on various radar measurements of meteors more brilliant that approximately $+7^{m}$, conducted in the KPI. In writing the monograph, the authors utilized the material published previously both by themselves and by other

co-workers at the Institute. Chapters 1 and 2 were written by V. N. Lebedinets, chapter 3 by B. L. Kashcheyev, chapter 4, jointly by B. L. Kashcheyev, V. N. Lebedinets and M. F. Lagutin.

The authors express appreciation to the group at the Department of the Fundamentals of Engineering at the KPI for their aid in preparing the manuscript and the catalog of orbits for printing. The authors consider it necessary to remark that the successful development of the studies on the meteors was largely promoted by the member of the Interdepartmental Geophysical Committee under the Presidium of the USSR Academy of Sciences, Professor V. V. Fedynskiy, for which the authors express deep gratitude to him.

CHAPTER 1

PHYSICAL THEORY OF METEORS

In the radar observations on the waves $\lambda \gtrsim 8$ m, basically there are registered the meteors weaker than +5 stellar magnitude, forming the ionized trails with a linear electron density $\alpha < 10^{12}$ electrons/cm. In the present report, the physical theory of meteors is regarded with reference to the radar method of investigations, therefore the basic attention is diverted to the evaporation of small meteor bodies and to the processes of the formation and destruction of the ionized meteor trails. The physical theory of optical meteors will interest us only in those cases when the results of the optical observations are necessary for verifying the basic initial precepts of the physical theory of radio meteors. For the sake of brevity, we will call the radio meteors simply meteors, being registered by the radio engineering means.

The fundamentals of the modern physical theory of meteors was laid in the reports of Gaede [1], Opik [2, 3], Spiral' [4], Fisher [5], and others. Subsequently, the physical theory of meteors was developed in the writings of a large number of Soviet and foreign astronomers and physicists.

SIMPLEST PHYSICAL THEORY OF METEORS

In its movement in the atmosphere, a meteor body experiences collisions with the air molecules, as a result of which a braking occurs, heeding an evaporation of the body. The problem of the motion in the atmosphere can be reversed considering the meteor body stationary, while the air molecules are considered to be moving towards it with the velocity v of the body. During the time dt, the meteor body encounters the mass of air

$$dM_a = S\rho v dt, \tag{1.1}$$

where S equals the area of the frontal section of a meteor body, ρ equals density of the atmosphere. This air mass has the kinetic energy relative to the motion dE_a and the quantity of motion dp_a

$$dE_a = dM_a \frac{v^2}{2} = \frac{1}{2} S\rho v^3 dt, \tag{1.2}$$

$$dp_a = dM_a v = S\rho v^2 dt. \tag{1.3}$$

From the law of the conservation of a quantity of motion, we find the braking of a meteor body:

$$M\frac{dv}{dt} = -\Gamma S\rho v^2, \tag{1.4}$$

where M equals mass of meteor body, Γ equals resistance factor (portion of the quantity of motion of the impinging molecules of air, being transmitted to the body).

The area of the frontal section of a meteor body is expressed by its mass and density δ:

$$S = AM^{2/3}\delta^{-2/3}, \tag{1.5}$$

where A equals the coefficient of the form. For a spherical body

$$A = \left(\frac{9\pi}{16}\right)^{1/3} = 1.21. \tag{1.6}$$

From (1.4) and (1.5), the equation for the braking of a meteor body will be written as follows:

$$\frac{dv}{dt} = -\Gamma A M^{-1/3}\delta^{-2/3}\rho v^2, \tag{1.7}$$

in the derivation of the braking equation, we did not take into account the Earth's attraction, since during the movement of a meteor body in the atmosphere at the cosmic velocity, it is much less than the force of the air resistance.

Assuming that the energy transmitted to a meteor body by the air molecules is expended in its evaporation, from (1.2) and (1.5), we derive the equation of the evaporation of a meteor body

$$\frac{dM}{dt} = -\frac{\Lambda}{2Q} S\rho v^3 = -\frac{\Lambda A}{2Q} M^{2/3}\delta^{-2/3}\rho v^3, \tag{1.8}$$

where Λ equals the heat transfer factor (portion of kinetic energy of the impinging air molecules, transmitted to the meteor body), Q equals the force of evaporation of one gram of meteor substance.

The atoms and molecules evaporating from the surface of a meteor body have the initial velocity of motion relative to the ambient atmosphere, close to the velocity of the meteor body. In case of their collisions with the molecules of the atmosphere, there occur the processes of resilient scattering, dissociation, excitation and ionization.

The light force of the meteor I is usually expressed by the kinetic energy of the evaporating meteor substance. Then the equation of the luminescence of the meteor can be written as follows:

$$I = -\frac{\tau}{8\pi}\left(\frac{dM}{dt}\right)v^2 = \frac{\Lambda A\tau}{16\pi Q} M^{2/3}\delta^{-2/3}\rho v^5, \tag{1.9}$$

where τ equals the luminosity factor.

The ionizing capability of meteor atoms is typified by the ionization factor β (β equals the average number of the free electrons, being generated by one evaporated meteor atom). The linear electron density of the trail formed by a meteor is found from the ionization formula

$$\alpha = -\frac{\beta}{\mu m_H v}\left(\frac{dM}{dt}\right) = \frac{\Lambda A\beta}{2Q\mu m_H} M^{2/3}\delta^{-2/3}\rho v^2, \tag{1.10}$$

where μ equals the average atomic weight of the meteor substance, m_H equals the mass of a hydrogen atom.

Let us estimate the value of the braking of a meteor body in the process of its evaporation. Dividing (1.8) into (1.7), we obtain

$$dM = \sigma v dv, \tag{1.11}$$

where

$$\sigma = \frac{\Lambda}{2\Gamma Q}. \tag{1.12}$$

If the values Λ, Γ and Q during the process of evaporation remain constant, integrating (1.11), we obtain

$$M = M_0 e^{-\frac{\sigma}{2}(v_0^2 - v^2)}, \tag{1.13}$$

where M_0 and v_0 equal the mass and velocity, respectively, of a meteor body before the inception of its evaporation.

The value σ can be estimated, assuming Λ equals $\Gamma = 1$. According to Opik [6], the force of evaporation Q is practically identical for the stone and iron meteor bodies and comprises on an average $Q = 8 \cdot 10^{10}$ ergs/g. At these values of Λ, Γ and Q, we obtain $\sigma = 6 \cdot 10^{-12}$ sec^2/cm^2. From (1.13), it is easy to observe that the decrease in the velocity of a meteor body during the evaporation process is slight. Plus, at an average velocity of meteors $v_0 = 40$ km/sec, the reduction in the mass of a meteor body as a result of evaporation by 10 times, is accompanied by a decrease in the initial velocity by only 1 km/sec in all.

The value for σ can be determined more precisely based on the results of the basic photographic observations of the meteors equipped with a shutter, if we conduct the measurements of the velocity, braking and light force of the meteors. According to (1.11)

$$\sigma = \frac{\frac{1}{M}\frac{dM}{dt}}{v\frac{dv}{dt}}, \tag{1.14}$$

from the luminosity equation (1.9), we find

$$\frac{dM}{dt} = -\frac{8\pi I}{\tau v^2}. \tag{1.15}$$

Integrating (1.15) and disregarding the residual mass of the meteor body at the moment of the meteor's disappearance, let us find the mass of the meteor body at the moment t:

$$M = 8\pi \int_t^{t_2} \frac{I}{\tau v^2} dt, \tag{1.16}$$

where t_2 equals the moment of disappearance of the meteor. From (1.14) - (1.16), we obtain

$$\sigma = -\frac{I}{\tau v^3 \frac{dv}{dt} \int_t^{t_2} \frac{I}{\tau v^2} dt}. \tag{1.17}$$

As we have seen, a decrease in the velocity of a meteor body in the process of evaporation is slight, therefore v^2, and also the luminosity factor depending on the velocity can be removed from under the integral sign. Then Eq. (1.17) is simplified:

$$\sigma = -\frac{I}{v\frac{dv}{dt}\int_t^{t_2} I dt}. \tag{1.18}$$

The most complete data concerning the determination of the value and its dependence on velocity according to (1.18) was published by Jacchia [7] in 1958:

v_o, km/sec..	15	20	30	40	50	60	70
log σ	-10.98	-11.08	-11.19	-11.24	-11.31	-11.34	-11.37

The values for σ decrease slightly with an increase in velocity. At an average velocity of meteors $v_o = 40$ km/sec, $\sigma = 5{,}8 \cdot 10^{-12}$ sec^2/cm^2, which is close to the value previously derived.

The estimate given for the value of the braking of meteor bodies indicates that in the integration of the evaporation equation, in a first approximation, the velocity of a meteor body can be considered constant.

Within fairly narrow intervals of heights, the Earth's atmosphere can be considered isothermal and the average molecular weight of air μ_a can be considered constant. Then a variation in the atmospheric density with height h occurs according to the law

$$\rho = \rho_0 e^{-\frac{h-h_0}{H}}, \tag{1.19}$$

where ρ_o equals the density of the atmosphere at the height h_o. The adduced height of a homogeneous atmosphere h depends on the temperature T and upon the average molecular weight of the air:

$$H = \frac{kT}{\mu_a m_H g}, \tag{1.20}$$

where k equals the Boltzmann constant, g equals the acceleration of gravitational force, m_H equals the mass of a hydrogen atom.

If z equals the zenith distance of a meteor's radiant, it is evident that dh equals -v cos zdt,

$$d\rho = \frac{\rho v \cos z dt}{H}. \tag{1.21}$$

From (1.8) and (1.21), we derive

$$\frac{dM}{d\rho} = -\frac{\Lambda A H M^{2/3} v^2}{2Q\delta^{2/3}\cos z}. \tag{1.22}$$

Integrating (1.22), at constant v, we derive

$$M_0^{1/3} - M^{1/3} = \frac{\Lambda A H v_0^2 \rho}{6Q\delta^{2/3}\cos z}. \tag{1.23}$$

Equating to zero the derivative of (1.8), we find the density of the atmosphere ρ_m at the height of the maximum evaporation of a meteor body, h_m:

$$\rho_m = \frac{3QM_m^{1/3}\delta^{2/3}\cos z}{\Lambda A H v_0^2}, \tag{1.24}$$

where M_m equals mass of meteor body at the point of maximal evaporation. From (1.23) and (1.24), we find M_m:

$$M_m = \frac{8}{27} M_0. \tag{1.25}$$

Substituting M_m into (1.24), we derive

$$\rho_m = \frac{2QM_0^{1/3}\delta^{2/3}\cos z}{\Lambda AHv_0^2}; \tag{1.26}$$

From (1.23) and (1.26), we obtain

$$M^{1/3} = M_0^{1/3}\left(1 - \frac{1}{3}\frac{\rho}{\rho_m}\right). \tag{1.27}$$

Substituting (1.27) into the equations of luminosity and ionization, we find the luminous intensity of a meteor and the linear electron density of a meteor trail:

$$I = \frac{\tau M_0 v_0^3 \cos z}{8\pi H}\frac{\rho}{\rho_m}\left(1 - \frac{1}{3}\frac{\rho}{\rho_m}\right)^2, \tag{1.28}$$

$$\alpha = \frac{\beta M_0 \cos z}{\mu m_H H}\frac{\rho}{\rho_m}\left(1 - \frac{1}{3}\frac{\rho}{\rho_m}\right)^2, \tag{1.29}$$

the luminous intensity and the linear electron density of the trail in the point of maximal evaporation

$$I_m = \frac{1}{18\pi}\frac{\tau M_0 v_0^3 \cos z}{H}, \tag{1.30}$$

$$\alpha_m = \frac{4}{9}\frac{\beta M_0 \cos z}{\mu m_H H}. \tag{1.31}$$

From (1.28) - (1.30), we find the distribution of the luminous intensity of a meteor and the linear electron density along the trail:

$$\frac{\alpha}{\alpha_m} = \frac{I}{I_m} = \frac{9}{4}\frac{\rho}{\rho_m}\left(1 - \frac{1}{3}\frac{\rho}{\rho_m}\right)^2. \tag{1.32}$$

From (1.13) and (1.25), we find the reduction in the velocity of a meteor to the point of maximal evaporation:

$$\Delta v_m = v_0 - v_m \approx \frac{1.22}{\sigma v_0}, \tag{1.33}$$

where v_m equals the velocity of a meteor in the point of maximum evaporation. We have listed below the numerical values of Δv_m. The values for σ at various velocities of meteors were taken from the data listed on page

v_0, km/sec..	15	20	30	40	50	60	70
Δv_m, km/sec.	0.78	0.72	0.63	0.52	0.49	0.45	0.41

COMPARISON OF THE SIMPLEST PHYSICAL THEORY OF METEORS WITH OBSERVATIONS

Height of Maximum Evaporation

If we overlook the decrease in the velocity of a meteor body in the process of its evaporation, the point of maximum evaporation should coincide with the point of maximum luminous intensity of the meteor and with the point of maximum linear electron density of the ionized trail of the meteor. Since the density of the atmosphere at various heights at the present time is known with a sufficient degree of accuracy according to the data collected by rocket measurements [8], the height h_m of maximal evaporation of a meteor body can be determined with the aid of Equation (1.26).

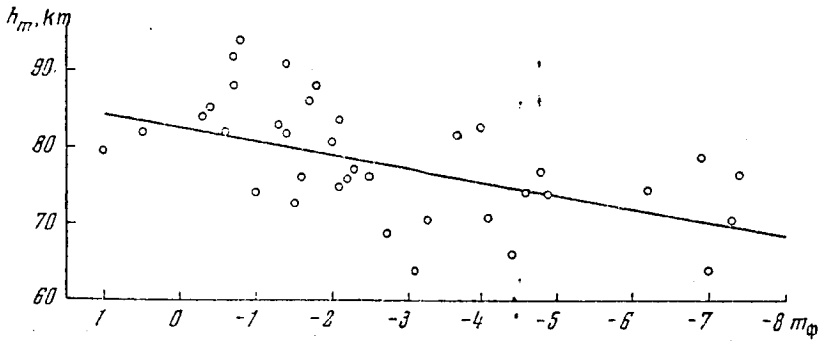

Fig. 1.1. Dependence of the Height of Maximal Luminous Intensity h_m Upon Photographic Absolute Stellar Magnitude for Meteors with Velocities of 25 - 35 km/sec.

In the calculation of ρ_m, we adopted the following values of the parameters entering Eq. (1.26): $\Lambda = 1$, $Q = 8 \cdot 10^{10}$ ergs/g, $H = 6.5$ km, the average value $\cos z = 2/3$. For a spherical body, the coefficient of form $A = 1.21$. From the experiments with iron and aluminum bodies of varying fragmenting form [9], we found the average value $A = 1.7$. Taking into account the gradual smoothing of the form of a meteor body during the evaporation process, we adopt the mean value $A = 1.5$. The luminosity factors at the various velocities of meteors, determining the scale of masses of meteor bodies were computed by Öpik [10].

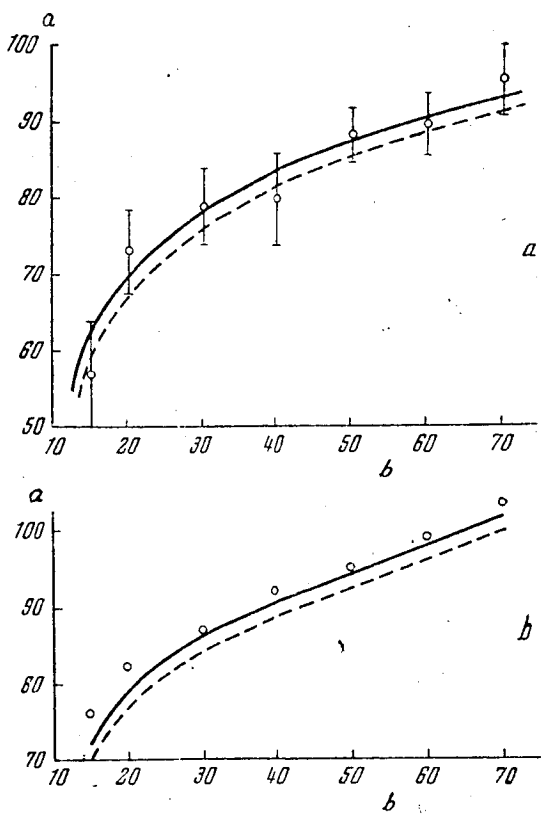

Fig. 1.2. Dependence of Height h_m of Maximal Luminous Intensity Upon Velocity v_o for the Meteors a--2^m; b-0^m. The solid line shows the theoretical dependence of h_m upon v_o at $\delta = 2$ g/cm^3, and the broken line at $\delta = 3.4$ g/cm^3. Key to figure: a) h_m, km; b) v_o, km/sec.

Until now, there have been published the heights of maximal evaporation of around a thousand meteor bodies, found according to the basal photographic observations of meteors. For a comparison with the theory, we utilized the data obtained for about 500 meteors, presented in [11, 12].

Whipple [12] presents the h_m-values for 144 meteors brighter than approximately 0^m, having been observed with the standard photographic cameras. These meteors were divided by us into seven groups based on velocity. In each group, the values of h_m for the individual meteors were reduced to the average values of the velocity and of the zenith distance of the radiant. Then, for each group, based on the method of least squares, we found the dependence h_m upon the stellar magnitude of meteors, m. In Figure 1.1, we have shown such a dependence for the meteors with velocities 25 - 35 km/sec, and also the values for m and h_m for individual meteors in the given group. From the figure it is obvious that at a variation in the maximal luminous intensity of the meteors by one stellar magnitude, h_m on an average changes much less than by 2 km, which agrees well with (1.26).

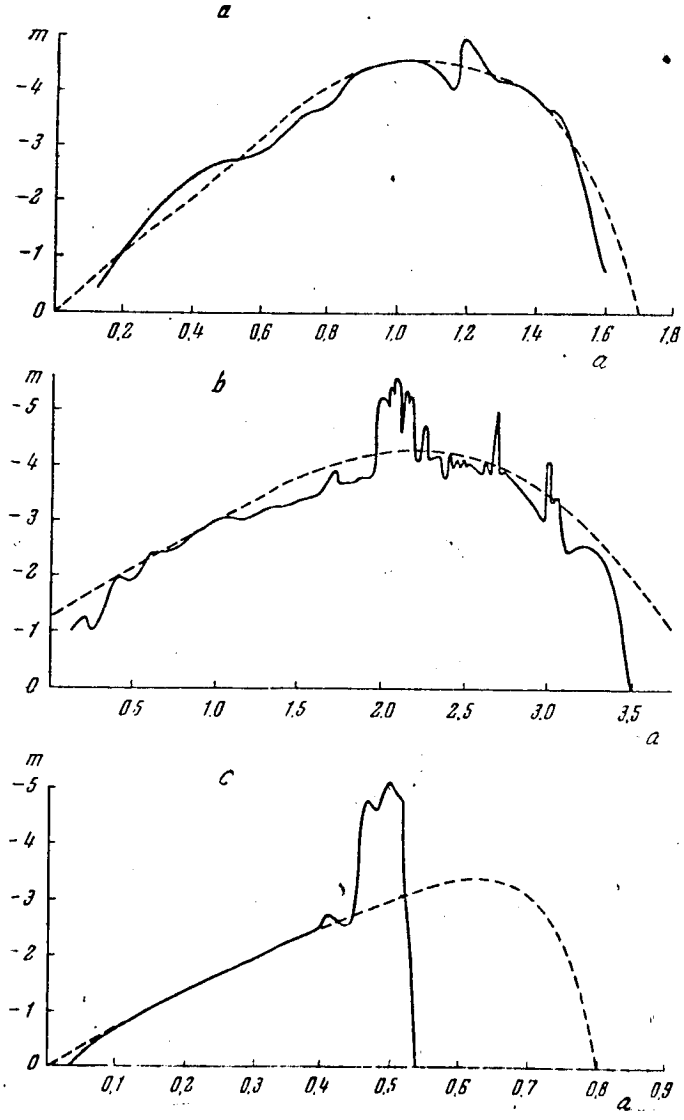

Fig. 1.3. Curves of the Luminous Intensity of Three Photographic Meteors [13] with the Velocities: a- 36 km/sec; b- 26 km/sec; and c- 69 km/sec.
[caption continued, next page]

The broken line indicates the theoretical curves of luminous intensity based on (1.34). Key to figure: a) t, sec.

In Figure 1.2a, a for all the groups of the velocities of meteors, we have shown the average values of h_m for the meteors - 2^m, and also the average deviations of the individual h_m-values from the mean. In the figure, we also show the theoretical dependence of h_m upon v_o at two values of density of meteor bodies: $\delta = 2$ g/cm^3 and $\delta = 3.4$ g/cm^3. The average measured values of h_m agree well with the theoretical ones at $\delta = 2$ g/cm^3, although at $\delta = 3.4$ g/cm^3, not for one of the groups of velocities do the divergences exceed the average spread of values for h_m for the individual meteors. The spread of the individual h_m-values can be explained by the diversity of the form, density and chemical composition of the meteoric bodies, by the dependence of the luminosity factor upon the chemical composition of the meteor body, and by the fluctuations in the density of the atmosphere.

Similar calculations were made by us for 360 meteors brighter than about $+3^m$ of absolute photographic stellar magnitude (m_ϕ), having been observed with the "Super-Schmidt" cameras [11]. In Fig. 1.2, b, we have shown the average measured values of h_m for the meteors with $m_\phi = 0$ at various velocities. We have also shown the theoretical dependence of h_m upon v_o at $\delta = 2$ g/cm^3 and $\delta = 3.4$ g/cm^3. The theoretical heights of the maximal evaporation prove to be systematically less than those observed: at 1 - 2km at $\delta = 2$ g/cm^3 and at 3 - 4 km at $\delta = 3.4$ g/cm^3. The discrepancies increase for the slowest meteors.

Curves of Luminous Intensity

According to (1.32), the form of the luminous intensity curve of a meteor does not depend on the mass of a meteor body, its density and velocity. For a comparison with the observations, in (1.32), it is convenient to transfer from the luminous intensity to the stellar magnitude. Since the values m and I are linked by the relationship m = const-2.5 log I, from (1.32), we derive

$$\Delta m = m - m_m = -0.875 - 1.08\left\{\frac{h_m - h}{H} + 2\ln\left[1 - \frac{1}{3}e^{\frac{h_m - h}{H}}\right]\right\}, \qquad (1.34)$$

where m_m equals the stellar magnitude of a meteor in the maximum of brilliance.

In Fig. 1.3, we have shown the typical luminous intensity curves, obtained from the observations with standard cameras, of three bright meteors [13] with velocities of 36, 25 and 69 km/sec. The first two meteors have standard curves of luminous intensity, while the third is an anomalous meteor with a flare. From the figure, it is evident that the standard curves of the luminous intensity of the bright meteors, obtained from the observations with the standard cameras agree satisfactorily with the theoretical curve (1.34), if we overlook the slight fluctuations in the luminosity of the meteor. At the very end of the trail, the decrease in the brightness of the meteor almost always occurs more quickly than according to (1.34). Sometimes this rapid drop in the brightness is preceded by a small flare. In the scintillating meteors, the curve of the luminous intensity is close to the theoretical one up to the moment of the flare, then for some reason, the evaporation rate of the meteor body increases abruptly.

The observations with the Super-Schmidt cameras revealed significant deviations of the measured curves of the luminous intensity of the faint photographic meteors ($m_\phi = 0^m - +3^m$) from the theoretical [11]. For the curves of the luminous intensity of the faint photographic meteors, the following characteristics are typical.

1) Near the point of the appearance, the luminous intensity of a meteor increases much more quickly than according to (1.34), after which there follows a more gradual increase in the luminous intensity up to the maximum.

2) Below the point of maximum evaporation, the deviations of the observed curves of the luminous intensity from the theoretical are less significant. Usually, the luminous intensity of a meteor decreases more quickly than according to (1.34).

3) The visible parts of the curves of the luminous intensity of meteors are shorter than according to (1.34).

These features of the curves of the luminous intensity of meteors, observed with the Super-Schmidt cameras usually are explained by the fragmenting of the meteor bodies generating them [11, 14, 15]. For a quantitative description of the process of fractionation, certain authors introduced various parameters of fragmentation. B. Yu. Levin [16] introduced the fragmentation parameter F, typifying the relative truncation of the observed part of the curve of luminous intensity of a meteor in comparison with the theoretical one. If we know the excess Δ_{m_0} of the visible stellar magnitude of the meteor in the point of the maximum luminous intensity over the threshold of the sensitivity of the photoplate, based on (1.34) we can find the theoretical difference in the heights of the points of the appearance and disappearance of the meteor $(h_1 - h_2)_{теор}$. Knowing the length of the trail of a meteor on the photoplate and the zenith distance of the meteor's radiant, we find the observed difference of the heights of the points of the appearance and disappearance $(h_1 - h_2)_{набл}$. Then

$$F = \frac{(h_1 - h_2)_{набл}}{(h_1 - h_2)_{теор}}. \qquad (1.35)$$

Hawkins and Southworth [11] present the values of h_1, h_2 and Δm for 360 meteors, photographed with the Super-Schmidt cameras. Using these data, B. Yu. Levin [16] computed the distribution based on the parameter F of the meteor bodies with varying masses. In Fig. 1.4, we have shown the distribution for 2 intervals of masses: $M_0 < 0.003$ g and $0.03 < M_0 < 0.1$ g. From the Figure it is obvious that in the faintest of the photographic meteors, one most often finds $0.5 < F < 0.6$. In the bright meteors, the F-values prove to be less. In this manner, if the parameter F characterizes the fragmentation of the meteor bodies, in the bright meteors, it should be expressed more intensively than in the faint ones. In the following sections, we will return to an explanation of this feature of the variation of the parameter F in the meteors of varying stellar magnitudes.

From a comparison of the simplest physical theory of meteors with the observations, we can make the following conclusions.

1) Eq. (1.26) describes well the average values of the height of the maximal luminous intensity of meteors brighter than about 0^m and its dependence upon the velocity and the stellar magnitude of meteors. For the meteors 0^m - + 3^m, the measured values of h_m are systematically higher by 1 - 3 km than the theoretical ones, furnished by Eq. (1.26).

2) The visible part of the curves of the luminous intensity of meteors brighter than about 0^m during the observations with the standard cameras agrees

satisfactorily with the theoretical part, provided by Eq. (1.32). However, during the observations with the Super-Schmidt cameras, it has been found that Eq. (1.32) yields a greater extent of the trail above h_m as compared with that observed.

3) In the case of the meteors fainter than about 0^m, which are photographed only with the Super-Schmidt cameras, the trails prove to be considerably shorter than according to (1.32). Near the points of the appearance of a meteor, the luminous intensity increases much more rapidly than according to (1.32). Below h_m, the deviations of the measured curves of luminosity from (1.32) are less significant and, as Levin [16] has shown, can usually be explained by the variation in the form of a meteor body during the evaporation process.

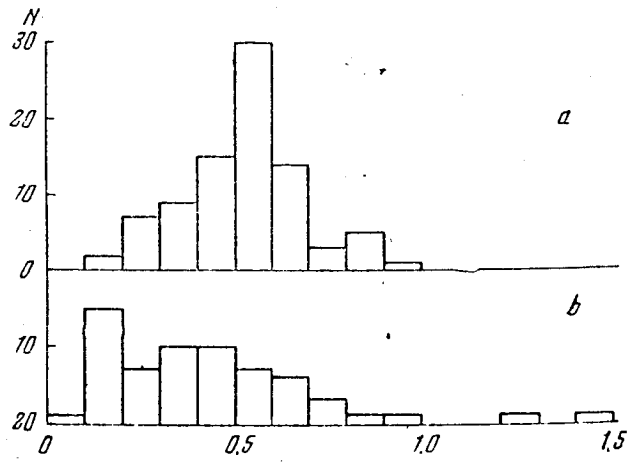

Fig. 1.4. Distribution According to Parameter of Fragmentation of Meteors, Generated by Meteor Bodies with the Masses: a- $M_o < 0.003$ g; b- $0.03 < M_o < 0.1$ g.

The divergences of certain conclusions of the simplest physical theory of meteors with the results of observations indicate that we need a more detailed examination of the process of the interaction of a meteor body with the atmosphere.

DEPENDENCE OF THE RATE OF EVAPORATION OF METEOR BODIES UPON TEMPERATURE

In the derivation of the basic formulas of the simplest physical theory of meteors, it is postulated that in any point of the trajectory of a meteor body, the intensity of its evaporation is determined only by the rate of the receipt of energy, transmitted to the meteor body by the molecules of the atmosphere, and the dependence of the evaporation intensity on the temperature of the body's surface was not considered.

In evaporation in a vacuum, when the molecule's mean free path is longer than the dimensions of the body, the particles, having evaporated from the surface of the body, practically never return; therefore, the evaporation rate should be the same as under the conditions of equilibrium with saturated steam (vapor). In equilibrium with saturated steam, in 1 sec per 1 cm^2 of the body's surface, $1/4\ an v_T$ of molecules are condensed. Here a equals the condensation factor (share of the molecules, arriving from the steam onto the surface of the body,

which (molecules) are condensed on it); n equals the vapor density; v_T equals the thermal velocity of the molecules. The same number of molecules should be evaporated. In this manner, if we know the pressure of the saturated steam and the condensation factor, we can easily find the evaporation rate. Proceeding from these concepts, Langmuir [17] derived the following formula for the rate of evaporation in vacuo:

$$\Delta M = 5.85 \cdot 10^{-5} a p_\mu \sqrt{\frac{\mu}{T}}\ g/cm^2\ sec, \qquad (1.36)$$

where p_μ equals pressure of saturated vapor of the given substance of temperature T, expressed in microns of merc. col., μ equals the molecular weight of the vapor. According to Langmuir, for most of the metals the condensation factor a = 1. For the other substances, the a-value can be less than 1 (up to 0.1 - 0.01).

The tables of the p_μ -values for the metals and a number of inorganic compounds were compiled by Deshman [18], Kubaschewski and Evans [19], Stull [20] et al. The dependence p_μ upon temperature is usually expressed in the form:

$$\log p_\mu = C_1 - \frac{C_2}{T}, \qquad (1.37)$$

where C_1, C_2 equals the constants for the given substance, which can differ somewhat for various temperature ranges. From (1.36) and (1.37), we derive the dependence of the evaporation rate on the temperature:

$$\log(\Delta M) = -4.23 + C_1 + \log a + 0.5 \log \mu - \frac{C_2}{T} - 0.5 \log T. \qquad (1.38)$$

For molten iron, C_1 = 12.00 and C_2 = 19,700° K. Assuming a = 1, from (1.38) we obtain the evaporation rate of molten iron

$$\log(\Delta M) = 8.65 - \frac{19\,700}{T} - 0.5 \log T. \qquad (1.39)$$

At the melting temperature $T_{пл}$ = 1800° K, $\Delta M = 3.5 \cdot 10^{-4}$ g/cm^2 · sec, i.e. the evaporation rate is very low. The intensive evaporation of iron begins at the temperature $T_и \approx 2300 - 2400°$ K.

The calculation of the evaporation rate of stony meteoric bodies is much more complex, since we do not even know their exact chemical composition. Öpik [6] has estimated the evaporation rate of stony meteoric bodies, assuming that their chemical composition is the same as that of the stony meteorites. During the heating of the stony meteorites, there occurs a gradual disintegration of the complex chemical compounds forming their composition. Up to the moment of the inception of their intensive evaporation, only the simplest molecules are included in their composition. Öpik presents the following mean molecular composition of the vapors of stony meteor bodies:

Molecules	SiO_2	MgO	CaO	Fe	S	O_2	Al_2O_3	Remainder
% by weight	43.5	25.1	2.5	15.4	3.8	3.8	3.2	2.7

The mean molecular weight of vapors = 50, the mean atomic weight = 23.

For molten quartz (SiO_2), the pressure of saturated vapor:

$$\log p_\mu = 13.83 - 24{,}400/T.$$

The rate of evaporation

$$\log (\Delta M) = 10.49 + \log a - 24{,}400/T.$$

If we assume a = 1, the temperature of inception of intensive evaporation $T_H \approx 2300 - 2400^\circ$ K. At a = 0.1, $T_H \approx 2600 - 2700^\circ$ K.

For the average composition of stony meteor bodies, Öpik [6] lists the melting temperature $T_{пл} = 1800^\circ$ K and the dependence p_μ on temperature:

$$\log p_\mu = 10.48 - 13{,}500/T.$$

The evaporation rate

$$\log (\Delta M) = 7.10 + \log a - 13{,}500/T - 0.5 \log T. \quad (1.40)$$

At a = 1, the temperature of the inception of the intensive evaporation of the stony meteors bodies $T_H \approx 2100 - 2200^\circ$ K. At a = 0.1, $T_H \approx 2500 - 2600^\circ$ K.

INTERACTION OF SMALL METEOR BODIES WITH THE ATMOSPHERE PRIOR TO THE BEGINNING OF INTENSIVE EVAPORATION

A meteor body, entering the atmosphere from interplanetary space, has an initial temperature close to the equilibrium temperature of an absolutely black body at a distance of 1 astronomical unit (a. u.) from the Sun, $T_o = 280^\circ$. If the dimensions of the body are less than the mean free path of the molecules of the atmosphere at the corresponding height, the interaction of the body with the the atmosphere occurs as a result of collisions with individual molecules. For the small meteor bodies of interest to us, this condition is almost always met. Since the velocity of the meteor body is much greater than the heat velocity of the molecules, we can consider that to the body, there is incident a parallel molecular beam of the atmosphere with identical velocities. At velocities of 11 - 72 km/sec, the kinetic energies of molecules of N_2 and O_2 vary in the limits from 20 to 860 ev.

The impacts of fast particles with a solid target have been studied many times experimentally and theoretically in connection with the investigation of the processes occurring in the electric vacuum devices. This kinetic energy lost by the molecules during collision with a solid target is spent in heating the target, in its fragmentation, in radiation, and also in dissociation, the excitation and ionization of the reflected and fragmented molecules and atoms. At forces of tens and hundreds of electron-volts practically all of the energy lost by the particles is converted to thermal energy of the target.

The nature of the interaction of the fast particle with a solid target depends on the particles' energy. If the energy of a particle is much greater than the binding energy of the atoms in a crystal lattice, the corresponding equipotential surfaces of the interaction encompass the individual atoms in the lattice. In this instance, we can consider that the impinging particle experiences collisions with individual atoms of the solid target.

The energy transmitted by the impinging particle to the target atoms depends on the relationship of the particles' masses. In the case of the stony meteor

bodies, when the mass of the air molecules is larger than the average mass of the body's atoms, the impinging particles impart almost entirely to the body their initial kinetic energy, and fly away from it at velocities close to the heat velocity, corresponding to the temperature of the body's surface. In the case of the iron meteor bodies, the mass of air molecules is less than the mass of iron atoms, and after impact, the molecules can jump away, retaining a part of their original velocity. In this case, the adaptation factor $\varkappa$ (ratio of the energy transmitted by the molecules to the body, to their initial kinetic energy) should be less than unity.

Proceeding from a simplified consideration of the interaction of the impinging particles with the surface of a solid, B. Yu. Levin [21] obtained the following formula for the adaptation factor:

$$\varkappa = \frac{(3\mu + \mu_a)\mu_a}{(\mu + \mu_a)^2}. \qquad (1.41)$$

At $\mu = 56$ (iron meteor body) and $\mu_a = 29$, we obtain $\varkappa = 0.79$.

At the present time, the value for the adaptation factor can be estimated more closely, proceeding from the modern concepts concerning the mechanism of the interaction of fast particles with the surface of a solid. At average velocities of the meteors, the effective section of the back scattering for the collisions of molecules of N_2 and O_2 with iron atoms is less by about one order of magnitude than the square of the mean distance between the iron atoms in a crystal lattice ($5 \cdot 10^{-16}$ cm^2), therefore a considerable share of the impinging particles penetrate within the crystal lattice for a depth of several interatomic distances. After scattering into the lattice, on the return path, the particles can experience recurrent collisions with the atoms of the lattice, leading to an increase in the share of the particles' kinetic energy, which is being transmitted to the body. The value for the adaptation factor can be roughly estimated, assuming that the particles, having experienced two or more collisions, have lost practically all of their kinetic energy to the body. Let us examine a case of a meteor body with a plane frontal surface.

On the body's face, there falls a normal stream of particles with the density N_0. At the depth h, the density of the stream of particles, not having experienced collisions with the body's atoms,

$$N = N_0 e^{-nhQ_d},$$

where n equals the density of atoms in the meteor body, Q_d equals the effective diffusion section. In a unit of volume with the base area of 1 cm^2 and with height dh, at the angle θ (in a system of coordinates connected with the body), $dN(\theta, h)$ particles are scattered:

$$dN(\theta, h) = Nnd\sigma(\theta)\,dh = N_0 n e^{-nhQ_d} d\sigma(\theta)\,dh$$

($d\sigma(\theta)$ - the differential section of scattering at angle θ). Among them, the ones which leave the body, not having undergone repeated collisions,

$$dN(\theta, h)\, e^{nQ'_d h \sec\theta} = N_0 n e^{-nh(Q_d - Q'_d \sec\theta)}\, d\sigma(\theta)\,dh, \qquad (1.42)$$

where Q'_d equals the diffusion section after collision.

The share of the initial kinetic energy, being retained by a particle after collision [22, 23],

$$\varepsilon = 1 - \frac{4\mu\mu_a}{(\mu + \mu_a)^2}\sin^2\chi, \qquad (1.43)$$

where χ equals the scattering angle in a system of masses' center. The angles χ and θ are interrelated by the equation:

$$\tan\theta = \frac{\mu \sin\chi}{\mu_a + \mu\cos\chi}.$$

From (1.42) and (1.43), we find the share of the initial kinetic energy, which is removed by the particles, scattered at the angle θ:

$$d\varepsilon(\theta) = n\left[1 - \frac{4\mu\mu_a}{(\mu+\mu_a)^2}\sin^2\chi\right] d\sigma(\theta)\int_0^\infty e^{-nh\,(Q_d - Q_d'\sec\theta)}\,dh =$$

$$= \left[1 - \frac{4\mu\mu_a}{(\mu+\mu_a)^2}\sin^2\chi\right]\frac{d\sigma(\theta)}{Q_d - Q_d'\sec\theta}.$$

Integrating in respect to θ, we find the adaptation factor:

$$\varkappa = 1 - \int_{\pi/2}^{\pi}\left[1 - \frac{4\mu\mu_a}{(\mu+\mu_a)^2}\sin^2\chi\right]\frac{d\sigma(\theta)}{Q_d - Q_d'\sec\theta}. \qquad (1.44)$$

As will be shown below, in the range of the meteor velocities, the dependence of Q_d upon energy can be represented in the form $Q_d \sim \varepsilon^{-1/2}$. Then

$$Q_d' = \frac{Q_d}{\sqrt{1 - \frac{4\mu\mu_a}{(\mu+\mu_a)^2}\sin^2\chi}}. \qquad (1.45)$$

At energies of tens and hundreds of electron-volts, the scattering section is usually assumed to be spherically symmetrical [22]. Then [23]

$$d\sigma(\theta) = \frac{Q_d}{2}\left[2\frac{\mu_a}{\mu}\cos\theta + \frac{1 + \frac{\mu_a^2}{\mu^2}\cos 2\theta}{\sqrt{1 - \frac{\mu_a^2}{\mu^2}\sin^2\theta}}\right]\sin\theta\,d\theta. \qquad (1.46)$$

From (1.44) - (1.46), we obtain

$$\varkappa = 1 - \frac{1}{2}\int_{\pi/2}^{\pi}\left[2\frac{\mu_a}{\mu}\cos\theta + \frac{1 + \frac{\mu_a^2}{\mu^2}\cos 2\theta}{\sqrt{1 - \frac{\mu_a^2}{\mu^2}\sin\theta}}\right]\frac{\left[1 - \frac{4\mu\mu_a}{(\mu+\mu_a)^2}\sin^2\chi\right]\sin\theta\,d\theta}{1 - \left[1 - \frac{4\mu\mu_a}{(\mu+\mu_a)^2}\sin^2\chi\right]^{-1/2}\sec\theta}. \qquad (1.47)$$

At an assigned value for μ_a/μ, the value can be found by numerical integration. From (1.47) we can obtain the approximate expression

$$\varkappa \approx 1 - \frac{1}{6}\left[1 - \frac{\mu_a}{\mu} - \frac{4\mu\mu_a}{(\mu+\mu_a)^2}\left(\frac{2}{3} - \frac{\mu_a}{\mu} + \frac{1}{3}\frac{\mu_a^3}{\mu^3}\right)\right]. \qquad (1.48)$$

At $\mu_a = 29$, for the iron meteor bodies, we obtain $\varkappa \approx 0.93$.

In the derivation of formulas (1.47) and (1.48), we proceeded from a model of the pairing interaction of the impinging particles with the free atoms of the target and we disregarded the bonding of the atoms in the solid. Such an approach is applicable only in the case of high energies of particles. At low energies, it is necessary to take into account the bonding energy, which leads to an increase in the effective mass of the atoms of the solid taking part in the collision [22]. In this case, in (1.47) and (1.48), it is necessary to replace μ by $\mu_э$: [see next page for equation]

$$\mu_э = \frac{\mu\left(1+\frac{E_п}{E_{от}}\right)}{1-\frac{\mu}{\mu_a}\frac{E_п}{E_{от}}}, \quad E_{от} = \frac{\mu}{\mu+\mu_a}E_0, \tag{1.49}$$

where $E_п$ equals depth of potential hole, in which the atom is located in the solid ($E_п$=20 - 30), $E_{от}$ equals the energy of relative motion of the colliding particles, and E_0 equals the energy of an impinging particle.

From (1.49), it is obvious that the energy of the bonding of atoms in a solid can be disregarded at $E_0 \gtrsim 300$ ev ($v \gtrsim 45$ km/sec). In the case of slow meteors, the allowance for the effective mass of the atoms leads to a decrease in the adaptation factor. At $E_0 \lesssim 60$ ev ($v \lesssim 20$ km/sec), for the iron meteor bodies from (1.48) and (1.49), we obtain $\varkappa \approx 0{,}83$).

Prior to the beginning of the intensive evaporation, a reduction in the mass of the meteor body occurs chiefly as a result of the fragmentation process. The fragmentation of meteor bodies was reviewed by B. Yu. Levin [24] and Öpik [6].

The effectiveness of the pulverization process is typified by the number of the target atoms, which are fragmented by one impinging particle. The theory of this process is still inadequately developed at the present time. According to the results of laboratory measurements [25], at energies E of the particles of hundreds of electron-volts, the dependence of γ upon E can be represented by the empirical formula

$$\gamma \sim (E - E_0).$$

For many substances, the value E_0 comprises about 100 ev. However, in a number of experiments, the dependence of γ upon E is derived in the form of a line passing through the origin of the coordinates ($E_0 = 0$). In the case of energies of particles of hundreds of electron-volts, the precise knowledge of the value for E_0 is of little significance. The careful measurements of the rate of pulverization in the range of energies 10 - 100 ev [26] indicates that at $E \lesssim 100$ ev, the rate of pulverization is very low (γ varies from 0 to 0,3). Since we are interested only in the upper estimation of the rate of pulverization, we assume $E_0 = 0$.

Massey and Barhop [25] present a summary of the γ-values at energies of 500 ev for various combinations of impinging particles and materials of the target. The average value $\gamma = 3$ and the spread of individual values for γ ranges from 0,3 to 9,5. Assuming the average value $\gamma = 3$, the dependence of γ upon E will be written in the following form:

$$\gamma = 6 \cdot 10^{-3} E, \tag{1.50}$$

where E is expressed in electron-volts.

For the further calculations, it is convenient to characterize the effectiveness of the atomization process by the pulverization factor Λ_p, which would enter the equation of the reduction of the mass of a meteor body as a result of the pulverization in the same manner as the heat transfer factor enters the evaporation equation (1.8), at the same value Q for the energy of evaporation. Then prior to the start of the intensive evaporation, the variation in the mass of the meteor body will be described by the equation [see next page]

$$\frac{dM}{dt} = -\frac{\Lambda_p A}{2Q} M^{2/3}\delta^{-2/3}\rho v^3. \qquad (1.51)$$

Setting the adaptation factor $\varkappa = 1$, and disregarding the blocking of the meteor body by the atomized and emitted particles, from (1.50) and (1.51), we derive the upper estimation of the pulverization factor $\Lambda_p \approx 0.025$.

HEATING OF METEOR BODIES

B. Yu. Levin [21, 27] considered the heating of a nonrotating cylindrical meteor body with a plane frontal surface. If the height of the cylinder is sufficiently great, the trailing side will remain continually at a temperature close to the initial temperature of the body. In this case, the calculation of the heating of a meteor body reduces to a solution of the one-dimensional problem of the propagation of heat along a rod bounded on one side, and a prescribed density of heat flow through the base of the rod $\varphi(t)$. The temperature is reckoned from the initial value.

If we disregard the braking and also the loss in energy to the atomization and the heat radiation of the meteor body,

$$\varphi(t) = \frac{1}{2}\Lambda v_0^3\rho = \frac{1}{2}\Lambda v_0^3\rho_0 e^{\frac{vt\cos z}{H}}.$$

The univariate equation of heat conduction

$$\frac{\partial T}{\partial t} - b^2\frac{\partial^2 T}{\partial x^2} = 0, \quad b^2 = \frac{\lambda}{c\delta},$$

where λ equals the heat conduction factor, and c equals heat capacity.

The initial and boundary conditions

$$T(x, -\infty) = 0, \qquad -\lambda\left(\frac{\partial T}{\partial x}\right)_{x=0} = \varphi(t).$$

The solution of the heat conduction equation yields the temperature of the frontal surface

$$T(0, t) = \frac{\Lambda b}{2\lambda}\sqrt{\frac{H}{\cos z}}\rho v_0^{3/2}. \qquad (1.52)$$

The solution presented does not take into account that at a certain temperature, there occurs a melting of the surface layer. This assumption is justified by the following concepts. The values λ and b differ but little for the solid and molten meteor substance. The latent heat of molten meteor substance $Q_{пл}$ is less by about an order of magnitude than the total energy $Q_н$, necessary for heating from temperature T_0 to $T_н$ [6]. Since $Q_{пл}$ is about equal to the energy of heating from 0° K to T_0, at temperatures above the melting temperature in (1.52), it is better to read the temperature from 0° K.

B. Yu. Levin presents the results of calculating the heating of a nonrotating cylindrical meteor body with a flat frontal surface, having the finite length h: [see next page]

$$T_h(0, t) = T(0, t)\left[1 + \frac{2}{e^{\frac{2h}{x_0}} - 1}\right],$$

$$T_h(x, t) = T(0, t)\, e^{\frac{x}{x_0}}\left[1 + \frac{e^{\frac{2x}{x_0}} + 1}{e^{\frac{2h}{x_0}} - 1}\right], \qquad (1.53)$$

$$x_0 = b\sqrt{\frac{H}{v_0 \cos z}}.$$

The case of a nonrotating meteor body with a plane frontal surface leads to the most rapid heating of the frontal surface. Another extreme case is a spherical quickly and irregularly rotating body. Here, the average density of the heat flow through the surface of the body is four times less than for a nonrotating body with a plane frontal surface.

The equation of heat conduction in spherical coordinates

$$\frac{\partial T}{\partial t} - b^2\left(\frac{\partial^2 T}{\partial r^2} + \frac{2}{r}\cdot\frac{\partial T}{\partial r}\right) = 0. \qquad (1.54)$$

The initial condition T (r, - ∞) = 0. The boundary conditions

$$\left(\frac{\partial T}{\partial r}\right)_{r=0} = 0, \qquad (1.55)$$

$$\lambda\left(\frac{\partial T}{\partial r}\right)_{r=r_0} = \frac{1}{4}\varphi(t) = \frac{\Lambda}{8} v_0^3 \rho_0 e^{\frac{vt\cos z}{H}}, \qquad (1.55')$$

where r_0 equals the radius of the body.

The solution will be sought in the form

$$T(r, t) = \frac{1}{r} R(r)\, e^{\frac{vt\cos z}{H}}. \qquad (1.56)$$

Substituting (1.56) into (1.54), we derive the equation for R (r):

$$\frac{d^2R}{dr^2} - \frac{1}{x_0^2} R = 0, \quad x_0 = b\sqrt{\frac{H}{v_0 \cos z}}. \qquad (1.57)$$

The general solution of Eq. (1.57):

$$R(r) = C_1 e^{\frac{r}{x_0}} + C_2 e^{-\frac{r}{x_0}}. \qquad (1.58)$$

From the boundary conditions, we find the constants C_1 and C_2:

$$C_1 = -C_2 = \frac{\Lambda v_0^3 \rho_0 r_0}{16\lambda\left(\frac{1}{x_0}\operatorname{ch}\frac{r_0}{x_0} - \frac{1}{r_0}\operatorname{sh}\frac{r_0}{x_0}\right)}.$$

From (1.56) and (1.58), we find the temperature distribution along the radius of the meteor body:

$$T(r, \rho) = \frac{\Lambda v_0^3 \rho}{8\lambda\left(\frac{1}{x_0}\operatorname{ch}\frac{r_0}{x_0} - \frac{1}{r_0}\operatorname{sh}\frac{r_0}{x_0}\right)} \frac{r_0}{x_0}\operatorname{sh}\frac{r}{x_0} \qquad (1.59)$$

and the surface temperature: [see next page]

$$T(r_0, \rho) = \frac{\Lambda r_0 \rho v_0^3}{8\lambda\left(\frac{r_0}{x_0}\operatorname{cth}\frac{r_0}{x_0} - 1\right)}. \qquad (1.60)$$

BEGINNING OF INTENSIVE EVAPORATION OF METEOR BODIES

By beginning of intensive evaporation, we will connote the moment, starting from which the basic part of the energy being transmitted by the molecules of the atmosphere to the meteor body begins to be expended in its evaporation.

Let us consider the beginning of the intensive evaporation of a rotating spherical meteor body. From (1.38) and (1.60), we find the rate of evaporation from a unit of surface of the meteor body as a function of the atmosphere's density:

$$\log(\Delta M) = -4.23 + C_1 + \log a + 0.5\log\mu - 0.5\log T - \frac{8\lambda C_2\left(\frac{r_0}{x_0}\operatorname{cth}\frac{r_0}{x_0} - 1\right)}{\Lambda r_0 \rho v_0^3}. \qquad (1.61)$$

To evaporation, the energy $Q\,\Delta M$ is expended. Equating its energy, being transmitted to the meteor body by the air molecules, $1/2\,\Lambda\, v_0^3 \rho$, we find the density ρ_{H1} of the atmosphere at the height of the beginning of intensive evaporation:

$$\rho_{H1} = \frac{8\lambda C_2\left(\frac{r_0}{x_0}\operatorname{cth}\frac{r_0}{x_0} - 1\right)}{\Lambda r_0 v_0^3\left[-4.23 + C_1 + \log(aQ\mu^{1/2}) + \log\left(\frac{\rho_0}{\lambda}\right) - \log\left(\frac{r_0}{x_0}\operatorname{cth}\frac{r_0}{x_0} - 1\right) - \frac{3}{2}\log T_H\right]}. \qquad (1.62)$$

According to (1.39) and (1.40), the rate of evaporation increases abruptly even at a slight increase in the temperature near the temperature T_H of the beginning of intensive evaporation, therefore the value $\log T_H$ entering (1.62) and can, with a sufficient degree of accuracy, be considered constant.

From (1.38) and (1.53), similarly we find the density of the atmosphere at the height of the beginning of the intensive radiation of a nonrotating cylindrical body with a plane frontal surface:

$$\rho_{H2} = \frac{2\lambda C_2}{\Lambda x_0 v_0^3\left[1 + \frac{2}{e^{\frac{2h_0}{x_0}} - 1}\right]\left[-4.23 + C_1 + \log(aQ\mu^{1/2}) + \log\frac{x_0}{\lambda} + \log\left(1 + \frac{2}{e^{\frac{2h_0}{x_0}} - 1}\right) - \frac{3}{2}\log T_H\right]}. \qquad (1.63)$$

Let us consider two extreme cases: large and small meteor bodies.

Beginning of Intensive Evaporation of Large Meteor Bodies

At $h_0 \gtrsim 2x_0$ in the case of a nonrotating cylindrical body and at $r_0 \gtrsim 4x_0$ in the case of a rotating spherical body, according (1.62) and (1.63), the height of the beginning of the intensive evaporation practically does not depend on the dimensions of the meteoric body. Such meteoric bodies will be called large. From (1.62) and (1.63), at $h_0 > 2x_0$ and $r_0 > 4x_0$, we obtain $\rho_{H1} \approx 4\,\rho_{H2}$. The pertinent heights of the beginning of intensive evaporation h_{H1} and h_{H2} differ

by about 9 km. As the theoretical height h_H of the beginning of intensive evaporation of large meteor bodies, we assume the average of these two values:

$$h_H = \frac{1}{2}(h_{H1} + h_{H2}). \quad \text{Then} \quad \rho_H = \frac{1}{2}\rho_{H_1} = 2\rho_{H2}.$$

From (1.62) and (1.63), we find the density of the atmosphere at the height of the beginning of intensive evaporation of large meteor bodies:

(1.64)

In Table 1.1, we have shown the heights of the beginning of intensive evaporation (in km) at various velocities for the three types of meteoric bodies: iron, solid stone and unconsolidated (friable) stony ones.

Table 1.1

Bodies	v_0, km/sec						
	15	20	30	40	50	60	70
Iron	73	78	84	88	91	94	96
solid stony	87	91	96	100	103	106	109
Unconsolidated stony	92	97	102	106	109	112	115

In Table 1.1, we have assumed the following values for the parameters entering (1.64) (Table 1.2):

Table 1.2

Bodies	λ, ergs/cm sec degr.	b, cm/sec $^{1}/_{2}$	δ, g/cm^3
Iron [6]	$4 \cdot 10^6$	0.20	7.8
Compact stony [24]	$3 \cdot 10^5$	0.1	3.5
Unconsolidated stony [24]	$2 \cdot 10^4$	0.04	1.0

We assume $\Lambda = 1$, $a = 1$ and the average value $\cos z = 2/3$.

In the calculation of the height h_H of the beginning of intensive evaporation, we did not take into account that somewhat higher than h_H, a part of the energy begins to be expended in evaporation, and the heating of the surface of the meteoric body is slowed down. From (1.61), it can easily be seen that at the height $h_H + 1$ km, less than 10% of the energy transmitted to the body by the air molecules is spent in evaporation. Thus, the transition from the conditions of the heating of a meteoric body to the conditions of intensive evaporation occurs in a narrow range of height of not more than 1 - 2 km.

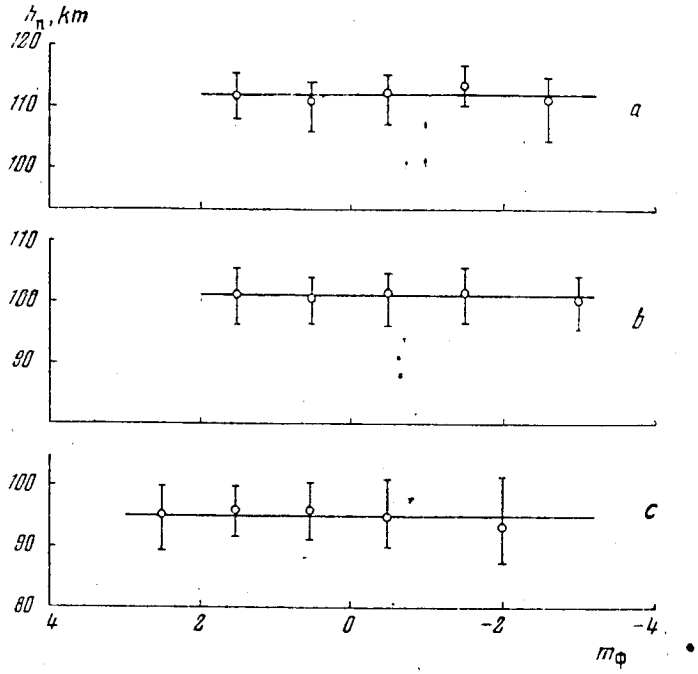

Fig. 1.5. Dependence of the Height of Appearance of Meteors Upon Stellar Magnitude for the Meteors with the Velocities: a- 60 - 72 km/sec; b- 35 - 45 km/sec; and c- 22 - 28 km/sec.

The rate of evaporation of large meteoric bodies around the height $h_н$ increases so rapidly that the heights of the appearance of the bright meteors should be close to $h_н$, if only the sensitivity of the radiation receiver is adequate for detecting a meteor at the height $h_н$. This conclusion can be verified by the results obtained from the photographic observations of the meteors in [12, 28], the authors have presented the heights $h_п$ of appearance of approximately 26, 50 meteors brighter than $+4^m$. All the meteors were divided into several groups according to velocity, and for each group, we obtained the dependence $h_п$ upon absolute stellar magnitude of the meteor in the maximum of brilliance. In Fig. 1.5, we have shown such a dependence for three groups of meteors with velocities 60 - 72, 35 - 45 and 22 - 28 km/sec. We have also indicated the average spread of the individual $h_п$ -values relative to the average. In each group, the individual values of $h_п$ were reduced according to (1.64) to the midpoint of the range of velocities and to the average value cos z = 2/3.

From Fig. 1.5, it is evident that the average heights of the appearance of bright meteors in effect do not depend on their stellar magnitude, which agrees with (1.64). The average spread of the individual values of $h_п$ in Fig. 1.5 comprises around 5 km. This spread can be explained as the diversity of the physical properties and of the physical composition of the individual meteoric bodies, and by the difference in their form and rotation. It is sufficient to remark that the value $h_н$ differs by about 9 km for a nonrotating meteoric body with a plane frontal surface and for a rotating spherical body even in the case of their identical physical properties and chemical composition. Similarly, in the transition from the unconsolidated stony meteoric bodies to the iron ones, the height of the inception of intensive evaporation changes by 18 - 19 kilometers.

In Fig. 1.6, we have shown the theoretical dependence of the height of the beginning of intensive evaporation of large solid stony meteoric bodies upon velocity. The dots indicate the average measured heights of the appearance of bright meteors based on the data in Fig. 1.5. We find a satisfactory agreement of the measured values for $h_п$ with the theoretical values of h_H. If we consider that the meteoric bodies are iron or unconsolidated stony ones, the agreement becomes worse.

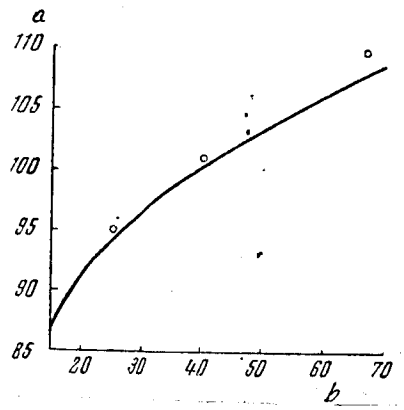

Fig. 1.6. Dependence of Height of Appearance of Bright Meteors Upon Velocity. Key to figure: a) h_H, km; and b) v_o, km/sec.

Beginning of Intensive Evaporation of Small Meteor Bodies

During movement in the atmosphere, the small meteor bodies succeed in becoming heated practically all the way through. According to (1.59), the boundary value of the radius of the meteoric bodies thoroughly heated

$$r_0' \approx 2x_0 = 2b \sqrt{\frac{H}{v_0 \cos z}}. \qquad (1.65)$$

The boundary value of the mass of meteoric bodies

$$M_0' = \frac{32\pi\delta}{3}\left(\frac{b^2 H}{v_0 \cos z}\right)^{3/2}. \qquad (1.66)$$

In Table 1.3, we have shown the values for M'_o (in grams), for the stony and iron meteoric bodies with varying velocities. We have assumed the average value cos z = 2/3.

Table 1.3

Meteoric bodies	v_o, km/sec						
	15	20	30	40	50	60	70
Stony	$3.2\cdot10^{-2}$	$2.1\cdot10^{-2}$	$1.1\cdot10^{-2}$	$7.3\cdot10^{-3}$	$5.2\cdot10^{-3}$	$4.0\cdot10^{-3}$	$3.2\cdot10^{-3}$
Iron (ferrous)	1.14	0.74	0.40	0.26	0.19	0.14	0.11

The intensive evaporation of meteoric bodies with masses $M_o < M'_o$ begins when the entire body is heated to the temperature T_H. The impinging molecules of the atmosphere transmit to the meteoric body the energy

$$\frac{dE}{dt} = \frac{1}{2}\Lambda A M^{2/3}\delta^{-2/3}\rho v^3. \qquad (1.67)$$

Disregarding the braking of a meteor body and the decrease in its mass as a result of atomization, from (1.67) we find the density ρ'_H of the atmosphere at the height h'_H, at which the meteor body completely heated through is heated to the temperature T_H,

$$\rho'_H = \frac{2Q_H M_0^{1/3}\delta^{2/3}\cos z}{\Lambda A H v_0^2}, \qquad (1.68)$$

where Q_H equals the energy required for heating one gram of meteor substance to the temperature T_H.

In the calculation of the heating of meteor bodies, we did not consider the energy losses to the heat radiation of the body. For obtaining the upper estimation of the expenditure of energy to heat radiation, we will consider a meteor body as being an absolutely black body, which is heated uniformly from all sides as a result of rotation. In this case, the energy radiated by a meteor body at the temperature T_H,

$$\frac{dE_H}{dt} = 4\sigma T_H^4 A M^{2/3}\delta^{-2/3}, \qquad (1.69)$$

where σ equals the Stefan-Boltzmann constant. From (1.67) and (1.69), we find the atmospheric density ρ''_H, at which the energy losses to heat radiation of a meteor body at the temperature T_H equal the receipt of energy as a result of collisions with molecules of the atmosphere:

$$\rho''_H = \frac{8\sigma T_H^4}{\Lambda v^3}. \qquad (1.70)$$

In Table 1.4, we have shown the heights h''_H (in km), at which the density of the atmosphere equals ρ''_H, for the stony and for the iron meteoric bodies.

Table 1.4

Meteor bodies	v, km/sec						
	15	20	30	40	50	60	70
Stony	92	96	103	108	113	116	120
Iron	90	94	101	106	111	114	118

From a comparison of the data in Tables 1.1 and 1.4, it is obvious that the difference in heights $h'_H - h_H$ comprises 6 - 12 km for the stony meteor bodies and 19 - 23 km for the iron ones. Since we took the upper estimate of the expenditure of energy to heat radiation, a comparison of the heights h_H and h''_H indicates that in the case of the large meteor bodies, the energy losses to heat radiation can be disregarded.

In the case of small meteor bodies completely heated through, the height h'_H of the inception of the intensive evaporation increases with a decrease in the mass, and, at sufficiently small masses, approaches h''_H. We find the critical value of the mass of meteor bodies M''_0 from the condition $h''_H = h'_H$. From (1.68) and (1.70), we obtain

$$M_0^{''1/3} = \frac{4AH\sigma T_H^4}{Q_H \delta^{2/3} v_0 \cos z}. \qquad (1.71)$$

In the meteor bodies with the masses $M_0 \leqslant M''_0$, the height of the beginning of intensive evaporation is determined from Eq. (1.70).

With allowance for the energy losses to the heat radiation, we have an increase in the reduction of the velocity of the small meteor bodies to the beginning of their intensive evaporation. Disregarding the decrease in the mass of a meteor body as a result of atomization (spraying), from (1.7), we find the velocity of a meteor body with the mass $M_0 \leqslant M''_0$ at the height of the beginning of its intensive evaporation:

$$\ln \frac{v_0}{v''_H} = \frac{\Gamma A H \rho''_H}{M_0^{1/3}\delta^{2/3}\cos z} = \frac{8\sigma T_H^4 \Gamma A H}{\Lambda M_0^{1/3}\delta^{2/3} v''^3_H \cos z}. \qquad (1.72)$$

From (1.72), we find the mass M'''_0 of a meteor body, the velocity of which, up to the beginning of intensive evaporation, decreases by 10%:

$$M_0'''^{1/3} = \frac{10^2 \Gamma A H \sigma T_H^4}{\Lambda \delta^{2/3} v_0^3 \cos z}. \qquad (1.73)$$

In a first approximation, for the meteor bodies with masses $M_0 \geqslant M'''_0$, we can disregard the braking up to the beginning of intensive evaporation. According to (1.70), the height of the beginning of intensive evaporation of small meteor bodies with masses from M'_0 to M'''_0 does not depend on the mass of the meteor body or on its density, or on the zenith distance of the meteor's radiant. In Table 1.5, we have shown the values for M'_0 and M'''_0 (in grams) at different velocities for the stony and iron meteor bodies. We assume $\Lambda = \Gamma = 1$ and the mean value $\cos z = 2/3$.

Table 1.5

Meteor bodies	v, km/sec						
	15	20	30	40	50	60	70
Stony							
M''_0	$4.3 \cdot 10^{-4}$	$1.8 \cdot 10^{-4}$	$5.4 \cdot 10^{-5}$	$2.2 \cdot 10^{-5}$	$1.2 \cdot 10^{-5}$	$6.6 \cdot 10^{-6}$	$4.2 \cdot 10^{-6}$
M'''_0	$4.7 \cdot 10^{-6}$	$3.5 \cdot 10^{-7}$	$0.9 \cdot 10^{-8}$	$6.8 \cdot 10^{-10}$	$0.9 \cdot 10^{-10}$	$1.8 \cdot 10^{-11}$	$4.4 \cdot 10^{-12}$
Iron							
M''_0	$2.7 \cdot 10^{-4}$	$1.1 \cdot 10^{-4}$	$3.4 \cdot 10^{-5}$	$1.4 \cdot 10^{-5}$	$7.6 \cdot 10^{-6}$	$4.2 \cdot 10^{-6}$	$2.6 \cdot 10^{-6}$
M'''_0	$3.0 \cdot 10^{-6}$	$2.2 \cdot 10^{-7}$	$5.7 \cdot 10^{-9}$	$4.3 \cdot 10^{-10}$	$5.7 \cdot 10^{-11}$	$1.1 \cdot 10^{-11}$	$2.8 \cdot 10^{-12}$

From Eqs. (1.70) and (1.72), we can determine more accurately the height of the beginning of intensive evaporation of small meteor bodies with the masses $M_0 < M'''_0$, with allowance for braking. Determining v'''_H, according to the given values v_0 and M_0, from (1.72), and substituting it in (1.70), we find the refined value of the height h'''_H (v'''_H) of the beginning of intensive evaporation. For the meteor bodies with the masses $M_0 = M'''_0$, the difference in heights h'''_H (v_0) - h'''_H (v'''_H) $\approx$ 2 km independently of the initial velocity. With an increase in the mass, the difference in heights decreases. At $M_0 = M'''_0$ for meteors with velocity $v_0 = 40$ km/sec, h'''_H (v_0) - h'''_H (v'''_H) $\approx$ 0.1 km. Thus, for meteor bodies with the masses $M_0 \geqslant M'''_0$, the allowance for the braking has practically no influence on the height of the beginning of intensive evaporation.

The very small meteor bodies expend on heat radiation a considerable part of their kinetic energy, and can be slowed down before they become heated to the temperature of the inception of intensive evaporation. Disregarding the decrease in the mass of the meteor body as a result of atomization, from (1.7), let us find the variation of velocity with height:

$$v = v_0 e^{-\frac{\Gamma A H \rho}{M_0^{1/3}\delta^{2/3}\cos z}}. \tag{1.74}$$

From (1.67) and (1.74), we find the variation, with height, of the energy imparted to the meteor body by the air molecules:

$$\frac{dE}{dt} = \frac{1}{2}\Lambda A M^{2/3}\delta^{-2/3}\rho v_0^3 e^{-\frac{3\Gamma A H \rho}{M_0^{1/3}\delta^{2/3}\cos z}}. \tag{1.75}$$

From (1.69) and (1.75), we find the temperature variation of the meteor body with height:

$$T^4 = \frac{\Lambda \rho v_0^3}{8\sigma} e^{-\frac{3\Gamma A H \rho}{M_0^{1/3}\delta^{2/3}\cos z}}. \tag{1.76}$$

The maximal temperature of a meteor body is reached at the height h'''_m, where the atmospheric density equals:

$$\rho'''_m = \frac{M_0^{1/3}\delta^{2/3}\cos z}{3\Gamma A H}. \tag{1.77}$$

The maximal value of temperature

$$T_m^4 = \frac{\Lambda M_0^{1/3}\delta^{2/3} v_0^3 \cos z}{3\Gamma A H}. \tag{1.78}$$

The critical value of the mass of meteor bodies which are never heated to the temperature $T_н$, is found from the condition $T_m = T_н$.

$$M_0^{IV\,1/3} = \frac{24\Gamma A H e \sigma T_н^4}{\Lambda \delta^{2/3} v_0^3 \cos z}. \tag{1.79}$$

From (1.73) and (1.79), we obtain

$$M'''_0 = 3.6 M_0^{IV}. \tag{1.80}$$

In this manner, the interval of the masses of meteor bodies, for which it is necessary to consider the braking in a calculation of the height of the beginning of intensive evaporation proves to be very narrow. For the critical value of the mass of meteor bodies being heated in the atmosphere to the temperature $T_н$, the atmospheric density at the height of the beginning of their intensive evaporation

$$\rho''_н(M_0^{IV}) = \frac{8 e \sigma T_н^4}{\Lambda v_0^3}. \tag{1.81}$$

Hence, the maximal decrease in a height of the inception of intensive evaporation with allowance for the braking of meteor bodies equals the indicated height of a homogeneous atmosphere.

The meteor bodies with the initial masses $M_0 < M_0^{IV}$ never attained the temperature of the beginning of intensive evaporation. Having lost a part of the mass as a result of atomization, they are slowed down in the upper layers of the atmosphere and settle to the Earth's surface in the form of "micrometeorites". The processes of braking, heating and atomization

of the "micrometeorites" were reviewed in detail by Öpik [29], Whipple [30] and V. G. Fesenkov [31].

ATOMIZATION OF METEOR BODIES

Let us estimate the reduction in the mass of meteor bodies as a result of atomization up to the beginning of their intensive evaporation. Disregarding braking, from (1.51), we find the mass of a meteor body at the height of inception of intensive evaporation

$$M_{\text{н}}^{1/3} = M_0^{1/3} - \frac{\Lambda_p A \dot{H} v_0^2 \rho_{\text{н}}}{6Q\delta^{2/3}\cos z}. \tag{1.82}$$

In the case of large meteor bodies, from (1.74) and (1.82), we derive

$$M_{\text{н}}^{1/3} = M_0^{1/3} - \frac{2\Lambda_p A C_2 \lambda_* H^{1/2}}{3\Lambda b Q \delta^{2/3} v_0^{1/2} \cos^{1/2} z \left(-4.23 + C_1 + \log Q + 0.5 \log \mu + \log \frac{x_0}{\lambda} - \frac{3}{2}\log T_{\text{н}}\right)}. \tag{1.83}$$

The relative decrease in the mass increases with a reduction in M_o. At $\cos z = 2/3$, the reduction in the mass of the large meteor bodies ($M_o > M'_o$) up to the beginning of intensive evaporation comprises less than 1%.

In the case of the meteor bodies, heating completely through, with masses $M''_o < M_o < M'_o$, from (1.68) and (1.82), we derive

$$\left(\frac{M_{\text{н}}}{M_0}\right)^{1/3} = 1 - \frac{\Lambda_p Q_{\text{н}}}{3\Lambda Q} \approx 1 - 2\cdot 10^{-3}. \tag{1.84}$$

The decrease in the mass prior to the beginning of the intensive evaporation comprises around 1%.

In the case of meteor bodies with masses $M'''_o < M_o < M''_o$, from (1.70) and (1.82), we obtain

$$M_{\text{н}}^{1/3} = M_0^{1/3} - \frac{\Lambda_p A H^{4.5} T_{\text{н}}^{1}}{3\Lambda Q \delta^{2/3} v_0 \cos z}. \tag{1.85}$$

The relative decrease in the mass increases with a decrease in the initial mass of a body and with an increase in velocity. At $M_o = M'''_o$ and $v_o = 70$ km/sec, the decrease in the mass amounts to around 50%; at $M_o = M'''_o$ and $v_o = 40$ km/sec, it comprises about 10%. With an increase M_o, the relative decrease in the mass prior to the inception of intensive evaporation decreases quickly.

The cited estimations of the value of atomization indicate that, for meteor bodies with masses $M_o \gg M'''_o$, we can disregard the decrease in the mass prior to the beginning of intensive evaporation.

NUMERICAL VALUES OF COEFFICIENTS Λ AND Γ

If the dimensions of a meteor body are less than the length of the free path of an air molecule at the corresponding height, during the movement of a body in the atmosphere, the formation of a shock wave does not take place. In this case, the heat transfer factor can be represented in the form of the product of the coefficients of adaptation and blocking [24]: [see next page]

$$\Lambda = \varkappa\xi. \tag{1.86}$$

The blocking factor ξ characterizes the decrease in the share of kinetic energy (being transmitted to the meteor body) of the impinging air molecules as a result of their collisions with the atoms and molecules, evaporating from the body's surface, and also with the air molecules escaping after impact with the body.

The blocking (obstructing) of meteor bodies was studied by B. Yu. Levin [24, 32]. However, in the calculation of the blocking factor, he overlooked the dependence of the effective section of diffusion upon the velocity of the colliding particles. The value of the diffusion section was assumed to be the same as under gas-kinetic conditions. In addition, B. Yu. Levin did not take into account that each evaporating or escaping particle in effect can protect the face of a meteor body from the impact of only one air molecule. As a result of this, the estimation of the role of blocking obtained by Levin proves to be exaggerated.

For obtaining the maximal estimation of the effect of blocking of a meteor body by particles, evaporating from its surface, let us consider the case of a body having the form of a circular cylinder with a plane frontal surface. The radius of the cylinder equals r. Let us also assume that the evaporation occurs only in the center of the frontal surface.

The angular distribution of the directions of the heat velocities of the evaporating particles

$$dN(\theta) = \frac{N}{\pi}\cos\theta\, d\omega, \tag{1.87}$$

where θ equals the angle with a normal to the frontal surface, N equals the number of particles evaporating from the frontal surface in one sec, $d\omega$ equals an element of the solid angle. The tangential velocity component of a particle both in a system of coordinates, connected with the meteor body, as well as in a stationary system of coordinates

$$v_{at} = v_a \sin\theta, \tag{1.88}$$

where v_a equals the heat velocity, corresponding to the surface temperature of the body. The normal velocity component of a particle relative to the body

$$v_{an} = v_a \cos\theta,$$

while in a stationary system of coordinates, it is close to the velocity v of the body, since $v \gg v_a$. The full velocity of the particles in a stationary system of coordinates is also close to v.

The evaporating particles experience the first collision with the air molecules on an average through the period Δt after evaporation:

$$\Delta t = \frac{\lambda}{v} = \frac{\mu_a m_H}{Q_d \rho v}, \tag{1.89}$$

where λ equals the mean free path of the evaporating particles in the atmosphere. During the period Δt, the particles separate from the cylinder axis for the distance

$$l_t = v_{at}\Delta t = \frac{\mu_a m_H \sin\theta}{Q_d \rho}\frac{v_a}{v}. \tag{1.90}$$

In the blocking, there participate only those particles which experience the first impact at the distances $l_t \leq r$ from the cylinder axis. From (1.90), let us find the critical value of θ for the particles participating in the blocking:

$$\sin\theta_0 = \frac{Q_d \rho r}{\mu_a m_H} \frac{v}{v_a}. \tag{1.91}$$

Hence, from the total number N of the evaporating particles, in the blocking there participate

$$N_0 = \int_0^{2\pi} \int_0^{\theta_0} dN(\theta) = 2N \int_0^{\theta_0} \sin\theta \cos\theta \, d\theta = N \sin^2\theta_0. \tag{1.92}$$

Each of the N_o particles can shield the frontal surface of the body from the impact of one of the impinging molecules of air.

The number of air molecules impinging on the frontal surface of a meteor body in 1 sec,

$$N_a = \frac{\pi r^2 \rho v}{\mu_a m_H}. \tag{1.93}$$

From (1.91) - (1.93), we find the blocking factor under conditions of weak blocking:

$$1 - \xi = \frac{N_0}{N_a} = \frac{N \mu_a m_H}{\pi r^2 \rho v} \sin^2\theta_0 = \frac{N Q_d^2 \rho v}{\pi \mu_a m_H v_a^2}. \tag{1.94}$$

As will be indicated below, in the range of meteor velocities, the dependence of the effective section of diffusion upon velocity can be represented in the form

$$Q_d = C/v, \tag{1.95}$$

where $C \approx 1.7 \cdot 10^{-9}$ cm^3/sec. From (1.94) and (1.95), we obtain

$$1 - \xi = \frac{C^2 N \rho}{\pi \mu_a m_H v v_a^2}. \tag{1.96}$$

In the derivation of (1.96), we did not consider that certain of the air molecules or evaporating particles, which experience collisions at short distances from the surface of the body, after collision bounce away toward the meteor body and transmit to it their pulse, by the same token decreasing the effect of blocking. As was demonstrated by Levin [24], the consideration of this factor leads to a reduction in the effect of blocking by about 5 times. Then, Eq. (1.94) and (1.96) can be rewritten in the form

$$1 - \xi = \frac{0.2 N Q_d^2 \rho v}{\pi \mu_a m_H v_a^2}, \tag{1.97}$$

$$1 - \xi = \frac{0.2 C^2 N \rho}{\pi \mu_a m_H v v_a^2}. \tag{1.98}$$

During the intensive evaporation when in effect all the energy received by the meteor body is expended to its evaporation,

$$N = \frac{\Lambda \pi r^2 \rho v^3}{2 Q \mu m_H}. \tag{1.99}$$

From (1.98) and (1.99), we get

$$1-\xi=\frac{0.2\Lambda C^2\rho^2 v^2 r^2}{2\mu\mu_a m_{\text{H}}^2 Q v_a^2}. \tag{1.100}$$

We can disregard the blocking, if

$$1-\xi\lesssim 0.1. \tag{1.101}$$

From (1.100) and (1.101), we find the r-values, at which the blocking is slight:

$$r\lesssim\frac{\mu^{1/2}\mu_a^{1/2}m_{\text{H}}Q^{1/2}v_a}{\Lambda^{1/2}C\rho v}. \tag{1.102}$$

Substituting the numerical values of the parameters, for the stony meteor bodies, we get

$$r\lesssim\frac{10^{-3}}{\rho v}. \tag{1.103}$$

Let us compare Eq. (1.103) with the results obtained by Levin [24]. He derived the following condition:

$$r\lesssim\frac{2\cdot 10^8}{\rho v^3}. \tag{1.104}$$

The critical value of r obtained by us for meteor bodies, for which we can overlook the blocking, at v = 40 km/sec proves to be higher than the value found by Levin, by 2 orders of magnitude. The appropriate critical values of the mass of meteor bodies differ by almost 6 orders of magnitude.

Let us estimate the value of blocking at the height of the beginning of intensive evaporation of the large meteor bodies. From (1.63) and (1.100), for the stony meteor bodies, we get

$$1-\xi_{\text{H}}\approx 1.4\cdot 10^{19}\frac{r^2\cos z}{v^3}. \tag{1.105}$$

We can disregard the blocking at

$$r\lesssim 9\cdot 10^{-11}\frac{v^{3/2}}{\cos^{1/2}z}. \tag{1.106}$$

At v = 40 km/sec and cos z = 2/3, we obtain $r\lesssim 0.8$ cm. It can readily be seen that the blocking of the escaping air molecules, and also the atomized meteor atoms and molecules prior to the beginning of the intensive evaporation can be disregarded for the meteor bodies of practically any dimensions.

In the process of evaporation, the blocking increases. We can roughly estimate the blocking at the height of maximal evaporation, taking the density of the atmosphere at height h_m, obtained in the simplest physical theory of meteors. From (1.24) and (1.100), we get

$$1-\xi_m\approx\frac{0.3\,C^2\delta^{2/3}r_0^2\cos^2 z}{\Lambda H^2\mu\mu_a m_{\text{H}}^2 v_a^2 v^2}. \tag{1.107}$$

In the derivation of Eqs. (1.105) - (1.107), we made a number of assumptions, each of which leads to an increase in the blocking effect: 1) we assume

that the evaporation occurs only in the center of the frontal surface; 2) the case of a body with a plane frontal surface leads to the maximal effect of blocking as compared with other forms of meteor bodies; and 3) we overlooked the rotation of the meteor body. Evidently, the blocking can also be disregarded in the case of r-values, slightly higher than the critical values provided by Eqs. (1.105) - (1.107).

In the case of the large meteor bodies with r considerably higher than the critical values yielded by Eqs. (1.105) - (1.107), the blocking can lead to a considerable decrease in the heat conduction factor. In the present report, we will be interested chiefly with the evaporation of small meteor bodies, for which the role of the blocking effect is relatively slight.

In an estimation of the value of the resistance factor, in addition to the impulse transmitted to a meteor body by the air molecules, it is necessary to consider the reactive pulse of the evaporating atoms and molecules [21]. Escaping from the surface of a body with the heat velocity v_a, the evaporating particle imparts to the body the impulse $\mu m_H v_a$. The component of the impulse in a direction opposite to the movement of the body is $\mu m_H v_a \cos\theta$ (where θ equals the angle between the directions of velocities v and v_a). The total pulse transmitted to the meteor body by the evaporating particles per time unit,

$$P = \frac{dM}{dt}\frac{v_a}{4\pi}\int F(\theta, \varphi)\cos\theta d\omega = kv_a\frac{dM}{dt}, \qquad (1.108)$$

where F (θ , φ) equals the angular distribution of the evaporating particles.

Disregarding the reactive pulse of the escaping air molecules, from (1.7), (1.8) and (1.108), we derive the approximate expression for the resistance factor under conditions when the blocking of a meteor body is slight:

$$\Gamma \approx 1 + k\frac{v_a}{2Q}v. \qquad (1.109)$$

For the nonrotating spherical body k = 4/9, for a very quickly rotating body, k ≈ 0. Let us assume the average value k = 2/9. Then, from (1.109), we get

$$\Gamma \approx 1 + 1.3\cdot 10^{-7}v, \qquad (1.110)$$

where v is expressed in cm/sec. The reactive pulse of evaporating particles has the maximal value for nonrotating meteor bodies with a flat frontal surface. In this case, k = 2/3 and

$$\Gamma \approx 1 + 4\cdot 10^{-7}v. \qquad (1.111)$$

Thus, the value of the resistance factor with allowance for the reactive pulse of evaporating particles for various meteors can be changed in the limits from 1 to 4. The mean value of the resistance factor according to (1.110) is a weak function of the meteors' velocity. At constant values for Λ and Q, the value $\sigma = \Lambda/2\Gamma Q$ should decrease slightly with an increase in v. This conclusion agrees with the results of the determinations of the σ-value from the observations presented on page 9.

If we disregard the blocking of a meteor body by the evaporating particles, the numerical values of the factors Λ and Γ will remain practically constant in the evaporation process.

EVAPORATION OF METEOR BODIES

Let us examine the evaporation of meteor bodies of various dimensions, assuming that the numerical values of the factors Λ, Γ and A in the evaporation process will remain constant. In the case of meteor bodies with the masses $M_0 \gg M'_0$, for which the losses of energy to heat radiation are slight, in the integration of the evaporation formula in a first approximation, the braking can be disregarded.

Evaporation of Large Meteor Bodies

Integrating (1.8), in the case of an isothermal atmosphere, we get

$$M^{1/3} = M_0^{1/3} - \frac{\Lambda A H v_0^2}{6Q\delta^{2/3}\cos z}(\rho - \rho_н). \tag{1.112}$$

Equating to 0 the derivative from (1.8), from (1.8) and (1.112), we find the density of the atmosphere at the height of maximal evaporation

$$\rho_m = \frac{3QM_m^{1/3}\delta^{2/3}\cos z}{\Lambda A H v_0^2}.$$

The mass of a meteor body in the point of maximal evaporation

$$M_m^{1/3} = \frac{2}{3} M_0^{1/3} + \frac{\Lambda A H v_0^2 \rho_н}{9Q\delta^{2/3}\cos z}. \tag{1.113}$$

Then

$$\rho_m = \frac{2QM_0^{1/3}\delta^{2/3}\cos z}{\Lambda A H v_0^2} + \frac{1}{3}\rho_н. \tag{1.114}$$

From (1.9), (1.10) and (1.112), let us find the curves of the luminous intensity and ionization below the height of the beginning of intensive evaporation

$$I = \frac{\Lambda A \tau v_0^5}{16\pi Q\delta^{2/3}}\rho\left[M_0^{1/3} - \frac{\Lambda A H v_0^2}{6Q\delta^{2/3}\cos z}(\rho - \rho_н)\right]^2, \tag{1.115}$$

$$\alpha = \frac{\Lambda A \beta v_0^2}{2\mu m_н Q\delta^{2/3}}\rho\left[M_0^{1/3} - \frac{\Lambda A H v_0^2}{6Q\delta^{2/3}\cos z}(\rho - \rho_н)\right]^2. \tag{1.116}$$

At $M_0 > M'_0$, the second term in the right part of Eq. (1.114) comprises less than 10% of the first; hence, dropping it, we introduce an error in the height of maximal evaporation of less than 1 km. The relationship between the first and second terms in the right part of Eq. (1.113) is the same. Dropping the second terms in the right part of Eqs. (1.113) and (1.114), we obtain Eqs. (1.115) and (1.116) of the simplest physical theory of meteors. Then, Eqs. (1.115) and (1.116) can roughly be rewritten in the form

$$I = \frac{\tau M_0 v_0^3 \cos z}{8\pi H}\frac{\rho}{\rho_m}\left[1 - \frac{1}{3}\left(\frac{\rho}{\rho_m} - \frac{\rho_н}{\rho_m}\right)\right]^2, \tag{1.115'}$$

$$\alpha = \frac{\beta M_0 \cos z}{\mu m_н H}\frac{\rho}{\rho_m}\left[1 - \frac{1}{3}\left(\frac{\rho}{\rho_m} - \frac{\rho_н}{\rho_m}\right)\right]^2. \tag{1.116'}$$

Below $h_н$, the curves of the intensity of light (1.115') and of ionization (1.116') are quite close to the curves (1.18) and (1.19), which were derived in the simplest physical theory of meteors. A significant difference from the results of the simplest physical theory of meteors is only

the fact that with allowance for the dependence of the rate of evaporation from the temperature of the surface of a meteor body, the trail in effect breaks off at the height h_H. Above h_H at the range of heights 1 - 2 km, the evaporation rate decreases by about 2 orders of magnitude. The length of the trail proves to be appreciably less than was derived in the simplest physical theory of meteors.

Evaporation of Small Meteor Bodies

The meteor bodies with masses $M_0 < M'_0$ up to the time of the inception of intensive evaporation have already been completely liquefied and heated to a temperature close to T_H. Then the energy required for evaporating one gram of their substance, equals $(Q - Q_H)$. If in the evaporation process, the temperature of the body's surface remains close to T_H, from (1.67), (1.69) and (1.70), we derived the equation of the evaporation, with allowance for the losses in energy to the heat radiation of a meteor body:

$$\frac{dM}{dt} = -\frac{\Lambda A M^{2/3} v^3}{2(Q - Q_H)\delta^{2/3}}(\rho - \rho''_H). \qquad (1.117)$$

Disregarding the braking in the evaporation process, in the case of an isothermal atmosphere, from (1.21) and (1.117), we get

$$M^{1/3} = M_0^{1/3} - \frac{\Lambda A H v_H^2}{6(Q - Q_H)\delta^{2/3}\cos z}\left[\rho - \rho_H - \rho''_H \ln\frac{\rho}{\rho_H}\right], \qquad (1.118)$$

where ρ_H, v_H equals the density of the atmosphere and the velocity of the meteor at the height of the beginning of intensive evaporation.

From (1.10), (1.117) and (1.118), we find the curve of ionization:

$$\alpha = \frac{\Lambda A \beta v_H^2}{2(Q - Q_H)\delta^{2/3}\mu m_H}(\rho - \rho''_H)\left[M_0^{1/3} - \frac{\Lambda A H v^2}{6(Q - Q_H)\delta^{2/3}\cos z}(\rho - \rho_H - \rho''_H \ln\frac{\rho}{\rho_H}\right]^2. \qquad (1.119)$$

Using Eqs. (1.70) and (1.71), let us rewrite Eq. (1.118) in the form

$$\alpha = \frac{64 A^3 H^2 \beta\sigma^3 T_H^{12}}{Q_H^2 (Q - Q_H)\delta^2 v_H^3 \mu m_H \cos^2 z}\left(\frac{\rho}{\rho''_H} - 1\right)\left[\left(\frac{M_0}{M''_0}\right)^{1/3} - \frac{Q_H}{3(Q - Q_H)} \times \right. \qquad (1.120)$$
$$\left. \times \left(\frac{\rho}{\rho''_H} - \frac{\rho_H}{\rho''_H} - \ln\frac{\rho}{\rho_H}\right)\right]^2.$$

Similarly, we derive the curve of the luminous intensity

$$I = \frac{8\tau A^3 H^2 \sigma^3 T_H^{12}}{\pi Q_H^2 (Q - Q_H)\delta^2 \cos^2 z}\left(\frac{\rho}{\rho''_H} - 1\right)\left[\left(\frac{M_0}{M''_0}\right)^{1/3} - \frac{Q_H}{3(Q - Q_H)}\left(\frac{\rho}{\rho''_H} - \frac{\rho}{\rho''_H} - \ln\frac{\rho}{\rho_H}\right)\right]^2. \qquad (1.121)$$

Let us consider two extreme cases.

a) At $M'_0 < M_0 \ll M''_0$: $v_H \approx v_0$, $\rho_H = \rho'_H$ and $\rho'_H \gg \rho''_H$. Assuming in (1.118), $\rho''_H = 0$, we derive

$$M^{1/3} = M_0^{1/3} - \frac{\Lambda A H v_0^2}{6(Q - Q_H)\delta^{2/3}\cos z}(\rho - \rho'_H). \qquad (1.122)$$

The density of the atmosphere and of the masses of a meteor body at the height of maximal evaporation

$$\rho'_m = \frac{3(Q - Q_н) M_m^{1/3} \delta^{2/3} \cos z}{\Lambda A H v_0^2}, \qquad (1.123)$$

$$M_m^{1/3} = \frac{2}{3} M_0^{1/3} \left(1 + \frac{1}{3} \frac{Q_н}{Q - Q_н}\right). \qquad (1.124)$$

From (1.123) and (1.124), we derive

$$\rho'_m = \frac{2\left(Q - \frac{2}{3} Q_н\right) M_0^{1/3} \delta^{2/3} \cos z}{\Lambda A H v_0^2}. \qquad (1.125)$$

From (1.9), (1.10), (1.117) and (1.122), we find the curves of the intensity of light and ionization:

$$I = \frac{\tau M_0 v_0^3 \cos z}{8\pi H} \frac{Q_н}{Q - Q_н} \frac{\rho}{\rho'_н} \left[1 - \frac{1}{3} \frac{Q_н}{Q - Q_н} \left(\frac{\rho}{\rho'_н} - 1\right)\right]^2, \qquad (1.126)$$

$$\alpha = \frac{\beta M_0 \cos z}{\mu m_н H} \frac{Q_н}{Q - Q_н} \frac{\rho}{\rho'_н} \left[1 - \frac{1}{3} \frac{Q_н}{Q - Q_н} \left(\frac{\rho}{\rho'_н} - 1\right)\right]^2. \qquad (1.127)$$

From (1.126) and (1.127), it is evident that the form of the curves of the intensity of light and ionization of meteors, generated by the meteor bodies, the masses of which are enclosed in the limits $M''_0 \ll M_0 < M'_0$, does not depend on M_0, v, δ and z. The ratio of the densities of the atmosphere at the heights of the beginning and end of the trail

$$\frac{\rho'_к}{\rho'_н} = \frac{3Q}{Q_н} - 2. \qquad (1.128)$$

For the stony meteor bodies, $Q/Q_н \approx 4$; hence, the difference in heights of the beginning and end of the trail $h'_н - h'_к = 2.3\ H$. In this manner, the difference in heights of the points of the appearance and disappearance of the meteors, generated by the meteor bodies heating completely through, can not be more than about 15 km.

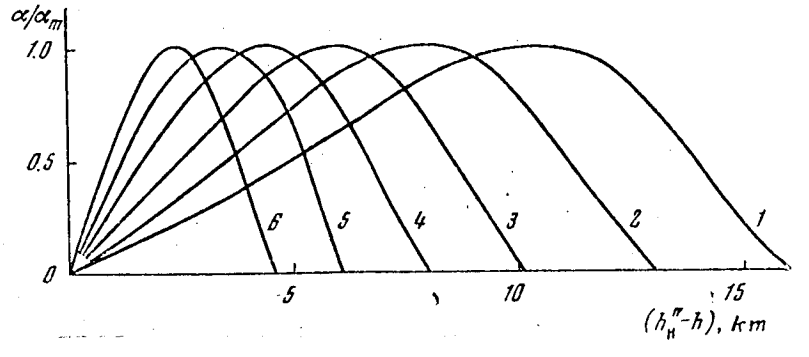

Fig. 1.7. Curves of the Luminous Intensity of Meteors, Generated by Small Meteor Bodies with the Masses:

1 — $M_0 = M_0''$; 2 — $M_0 = 0.16 M_0''$; 3 — $M_0 = 0.025 M_0''$; 4 — $M_0 = 4 \cdot 10^{-3} M_0''$; 5 — $M_0 = 6.2 \cdot 10^{-4} M_0''$; 6 — $M_0 = 10^{-4} M_0''$

b) At $M''_0 < M_0 < M'''_0$: $v_H = v''_H$ and $\rho_H = \rho''_H$. From (1.120) and (1.121), we obtain

$$\alpha = \frac{64A^3H^2\beta\sigma^3T_H^{12}}{Q_H^2(Q-Q_H)\delta^2 v_H''^3 \mu m_H \cos^2 z}\left(\frac{\rho}{\rho''_H}-1\right)\left[\left(\frac{M_0}{M''_0}\right)^{1/3}-\frac{Q_H}{3(Q-Q_H)}\left(\frac{\rho}{\rho''_H}-1-\ln\frac{\rho}{\rho''_H}\right)\right]^2, \quad (1.129)$$

$$I = \frac{8\tau A^3H^2\sigma^3T_H^{12}}{\pi Q_H^2(Q-Q_H)\delta^2\cos^2 z}\left(\frac{\rho}{\rho''_H}-1\right)\left[\left(\frac{M_0}{M''_0}\right)^{1/3}-\frac{Q_H}{3(Q-Q_H)}\left(\frac{\rho}{\rho''_H}-1-\ln\frac{\rho}{\rho''_H}\right)\right]^2. \quad (1.130)$$

The curves of the luminous intensity and ionization at various values of M_0/M''_0 are presented in Fig. 1.7.

In the derivation of Eqs. (1.117) - (1.130), we overlooked the decrease in the velocity of the meteor body during the evaporation process. At M_0, comparable with M'''_0 or less than M'''_0 , it is necessary to take the braking into account. For the obtainment of the upper and lower estimation of the decrease in the velocity in the process of evaporation $\Delta v = v''_H - v$, let us integrate (1.7) at constant M-values:

$$\ln\frac{v''_H}{v} = \frac{A\Gamma H(\rho-\rho''_H)}{M^{1/3}\delta^{2/3}\cos z}. \quad (1.131)$$

We obtained the lower estimation of the decrease in velocity $\Delta v'$ from (1.131), substituting $M = M_0$; we obtained the upper estimation of $\Delta v''$ by substituting M from (1.118). For example, for a meteor body with $M_0 = 10^{-8}$ grams and $v''_H = 40$ km/sec, at the moment when the mass of the body, as a result of evaporation, decreases to the value $M = 0.2 M_0$, we obtain $\Delta v' = 1.2$ and $\Delta v'' = 2.0$ km/sec. The true value for Δv lies between $\Delta v'$ and $\Delta v''$.

The curves of the intensity of light and ionization with allowance for braking should be found from the combined solution of Eqs. (1.7) and (1.117). Under the condition that $\Delta v \ll v''_H$, it is convenient to find a solution by the method of successive approximations. We conducted a numerical integration of Eqs. (1.7) and (1.117) for a series of values for M_0, v''_H and cos z. We found that in the range of values for M_0 from M'''_0 to M''_0, the variation in Δv with height can roughly be represented in the form

$$\Delta v = v''_H k\rho(\rho-\rho''_H), \quad (1.132)$$

where

$$k = \frac{4.5\cdot10^{-5}v''^3_H}{\rho''^3_H}\left(\frac{M'''_0}{M_0}\right)^{\mu},$$

$$\mu = 0.408 + \frac{2.6\cdot10^3}{v_0}. \quad (1.133)$$

From (1.117) and (1.132), we derived the equation of the evaporation of meteor bodies with the masses from M'''_0 to M''_0 with allowance for the braking in the process of evaporation

$$\frac{dM}{dt} = -\frac{\Lambda A M^{2/3}v''^3_H}{2(Q-Q_H)\delta^{2/3}}(\rho-\rho''_H)[1-k\rho(\rho-\rho''_H)]^3. \quad (1.134)$$

From (1.11) and (1.134), we get

$$\frac{dM}{M^{2/3}} = -\frac{\Lambda A H v_{н}''^{2}}{2(Q-Q_{н})\delta^{2/3}\cos z}\left[\frac{\rho-\rho_{н}''}{\rho}-2k(\rho-\rho_{н}'')^{2}+k^{2}\rho(\rho-\rho_{н}'')^{3}\right]d\rho. \qquad (1.135)$$

Disregarding in the right hand part (1.135) the terms of the order $k^2 \rho_{н}''^{4}$, we obtain

$$M^{1/3} = M_{0}^{1/3} - \frac{\Lambda A H v_{н}''^{2}}{6(Q-Q_{н})\delta^{2/3}\cos z}\int_{\rho_{н}}^{\rho}\left[1-\frac{\rho_{н}''}{\rho}-2k(\rho-\rho_{н}'')^{2}\right]d\rho =$$

$$= M_{0}^{1/3} - \frac{\Lambda A H v_{н}''^{2}}{2(Q-Q_{н})\delta^{2/3}\cos z}\left[\rho-\rho_{н}''\left(1+\ln\frac{\rho}{\rho_{н}''}\right)-\frac{2}{3}k(\rho-\rho_{н}'')^{3}\right]. \qquad (1.136)$$

The curve of ionization

$$\alpha = \frac{\Lambda A \beta v_{н}''^{2}}{6(Q-Q_{н})\delta^{2/3}\mu m_{н}}[(\rho-\rho_{н}'')-2k\rho(\rho-\rho_{н}'')^{2}]\times$$

$$\times\left\{M_{0}^{1/3}-\frac{\Lambda A H v_{н}''^{2}}{6(Q-Q_{н})\delta^{2/3}\cos z}\left[\rho-\rho_{н}''\left(1+\ln\frac{\rho}{\rho_{н}''}\right)-\frac{2}{3}k(\rho-\rho_{н}'')^{3}\right]\right\}^{2}. \qquad (1.137)$$

In Fig. 1.8, we have shown the curves of the intensity of light and ionization, found according to (1.137), for the meteor bodies with v_o = 40 km/sec and cos z = 2/3 at various values M_o/M''_o with allowance for braking prior to the beginning and during the process of intensive evaporation. From a comparison of Figs. 1.7 and 1.8, it is obvious that the allowance for the braking has little effect on the form of the curves of the intensity of light and ionization.

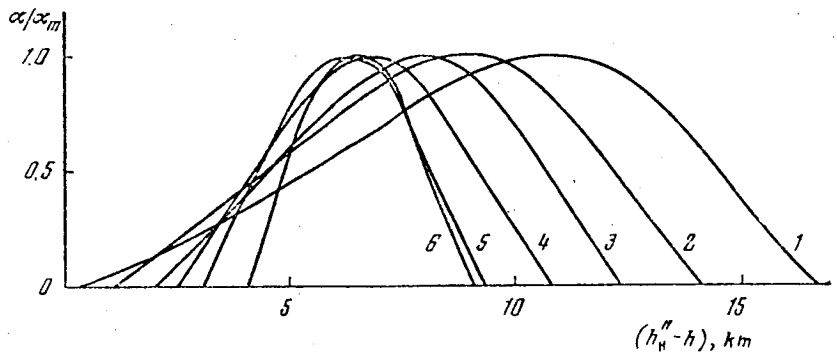

Fig. 1.8. Curves of Luminous Intensity, Computed with Allowance for Braking, for the Meteors Generated by Small Meteor Bodies. The notations are the same as in Fig. 1.7.

In a reduction of the mass of the meteor bodies from M''_o to M'''_o, the difference in the heights of the beginning and end of the trail decreases from about 15 to 5 km. Simultaneously, we have some decrease in the height of the inception of intensive evaporation, so that the height of maximal evaporation increases at this time by not more than 4 km. In this manner, the evaporation of the small meteor bodies with the given initial velocity and masses, varying in a broad range of values from M'''_o to M''_o (at v_o = 40 km/sec, this range includes the variation of M_o by $3 \cdot 10^4$ times), occurs in a narrow range of heights practically with a width of not more than 10 - 12 km. With allowance for the spread of the meteor velocities, this range expands.

If the distribution of the small meteor bodies by velocities has a fairly distinct upper limit, in the atmosphere there should exist a fairly clear upper limit, above which in effect there does not occur the evaporation of meteor bodies (the evaporation of the larger meteor bodies with the masses $M_o > M''_o$ begins below h''_H). If at this time there does not occur a sufficiently effective vertical transport of the evaporated substance during a period in which its basic part succeeds in condensing, in the atmosphere at heights of 90 - 115 km, there should exist an area of increased concentration of atoms of meteoric origin with a fairly distinct upper boundary. The position of this upper boundary is established only by the velocity and chemical composition of the meteor bodies and does not depend on the distribution of the meteor bodies by masses, their density and structure (stability), or upon the zenith distance of the meteors' radiants.

Since the potential of the ionization of a considerable part of the meteor atoms is below the potential of the ionization of the main components of air at this height, the ionizing aadiation passes freely through the higher layers of the atmosphere, and the ions of meteor origin can make a considerable contribution to the formation of the E-layer of the ionosphere. The ionization in the meteor trails introduces a certain contribution to the formation of the night E-layer of the ionosphere. During the meeting of the Earth with the streams of small meteor bodies, there can occur the most considerable increase in the concentration of the ions of meteor origin in certain ranges of heights in the atmosphere, since all the particles in the stream have similar values of velocity, and evaporate in a narrow range of altitudes.

The rocket measurements of the ionic composition of the atmosphere [33] reveal such an area of high concentration of ions of meteoric origin Mg^+, Fe^+, Si^+ and Ca^+ in the narrow range of altitudes 100 - 110 km, with a maximum of around 104 km. With the 15 degree altitude of the Sun above the horizon, the ions of meteoric origin comprise around 40% of all the ions at a height of 105 km. We find a distinct upper boundary of the layer, containing the ions of Mg^+, Fe^+, Si^+ and Ca^+, with a width of the order of 2 km at the height of 108 - 110 km.

DEFORMATION AND FRAGMENTATION OF SMALL METEOR BODIES

Until this time, it was assumed that in the process of evaporation, the form of a meteor body does not change and the basic type of the ablation of meteor bodies is evaporation. Let us consider in more detail the process of the ablation of the small meteor bodies.

Up to the time of the inception of intensive evaporation, the small meteor bodies with the masses $M_o < M'_o$ are already completely liquefied. Under the effect of aerodynamic pressure and forces of surface attraction, the molten meteor body acquires an oblate form.

The deformation of a fused meteor body as a result of aerodynamic pressure on the frontal surface was studied by Öpik [6]. Not indicating the calculation method used by him, he presents only the final results. With the radius [see next page]

$$r \leqslant r_s = \frac{4\sigma}{p_s} \qquad (1.138)$$

(where σ equals the surface attraction factor, $p_s = \Gamma\rho v^2$ equals the aerodynamic pressure) the drop does not experience a noticeable deformation. At $r > r_s$, the drop acquires an oblate form, close to an ellipsoid of revolution. The value of the minor semi-axis of the ellipsoid in this context does not depend on the drop's radius and equals

$$b = \frac{3\sigma}{p_s}. \qquad (1.139)$$

The dependence which Öpik obtained for the extent of the deformation of a drop upon its radius has a discontinuity (the author himself points this out) at $r = r_s$, which is physically inexplicable. Since in Öpik's report, nothing is said concerning the use of the solution method, we are unable to verify its validity.

Let us estimate the value of the deformation, assuming that the drop has the form of an ellipsoid of revolution with the minor axis in the direction of motion. The difference in the pressures, being created by the forces of surface attraction in the planes of the longitudinal and transverse sections of the drop, p_σ is found with the aid of the Laplace formula

$$p_\sigma = \sigma\left(\frac{a}{b^2} + \frac{1}{a}\right) - \frac{2\sigma}{a},$$

where a, b equal the major and minor semi-axis of the ellipsoid (spheroid). Equating p_σ to the aerodynamic pressure at the frontal surface, we get

$$\sigma\left(\frac{a}{b^2} + \frac{1}{a}\right) - \frac{2\sigma}{a} = \Gamma\rho v^2.$$

Expressing b through a and the radius of the undeformed drop r we get

$$\left(\frac{a}{r}\right)^5 - \frac{r}{a} = \frac{\Gamma r v^2 \rho}{\sigma}. \qquad (1.140)$$

According to (1.140), the value of the deformation of a drop at a variation in r changes continuously. Eq. (1.140) can be rewritten in the form

$$\frac{r^3}{b^{5/2}} - b^{1/2} = \frac{\Gamma r^{3/2} v^2 \rho}{\sigma}.$$

In this manner, in distinction from the result obtained by Öpik (1.139), the minor semi-axis of the ellipsoid depends on the radius of the drop.

According to (1.140), a perceptible deformation of drop occurs at

$$\frac{\Gamma r v^2 \rho}{\sigma} \geqslant 1. \qquad (1.141)$$

The critical value of the drop's radius

$$r_3 = \frac{\sigma}{\Gamma v^2 \rho}. \qquad (1.142)$$

From (1.68) and (1.142), we find the critical value of the radius of the meteor bodies, which experience a considerable deformation as early as at the height of the beginning of intensive evaporation

$$r_{\sigma H}^2 = \frac{3\sigma\Lambda H}{8\Gamma\delta Q_H \cos z}. \qquad (1.143)$$

From (1.118) and (1.142), let us find the critical value of the initial radius of the meteor bodies, for which we can disregard the deformation occurring under the effect of aerodynamic pressure in the process of the entire evaporation:

$$r_{\sigma 0}^2 = \frac{3\sigma\Lambda H}{2\Gamma\delta(3Q - 5Q_H)\cos z}. \qquad (1.144)$$

From (1.65) and (1.143), we get

$$\frac{r_0'^2}{r_{\sigma H}^2} = \frac{32\Gamma b^2 \delta Q_H}{3\sigma\Lambda v}. \qquad (1.145)$$

For the molten substance of stony meteorites, at the temperature of the beginning of intensive evaporation averaging $\sigma \approx 360$ dynes/cm [6], for iron $\sigma \approx$ 1200 dynes/cm. From (1.144), we find that in the entire range of the meteor velocities both for the iron and for the stony meteor bodies, $r'_0 > r_{\sigma H}$.

With allowance for deformation, let us consider the evaporation of meteor bodies, the initial radii of which satisfies the condition $r_{\sigma H} < r_0 < r'_0$. Disregarding in the left part of Eq. (1.140) the term r/a (which leads to a certain decrease in the deformation value), we get

$$a = \left(\frac{\Gamma v^2 \rho}{\sigma}\right)^{1/8} r^{1/8}. \qquad (1.146)$$

The equation of the evaporation of a meteor body will have the following form:

$$\frac{dM}{dt} = -\frac{\Lambda}{2(Q - Q_H)} S v^3 \rho = -\frac{\pi\Lambda}{2(Q - Q_H)} v^{19/8} \left(\frac{\Gamma}{\sigma}\right)^{2/8} r^{12/8} \rho^{7/8}. \qquad (1.147)$$

For the isothermal atmosphere (1.147), we can rewrite in the form

$$\frac{dr}{r^{3/8}} = -\frac{\Lambda H v^{14/8}}{8(Q - Q_H)\delta\cos z}\left(\frac{\Gamma}{\sigma}\right)^{2/8} \rho^{2/8} d\rho. \qquad (1.148)$$

Disregarding the braking of a meteor body in the evaporation process, we get

$$r^{3/8} = r_0^{3/8} - \frac{3\Lambda H v_0^{14/8}}{56(Q - Q_H)\delta\cos z}\left(\frac{\Gamma}{\sigma}\right)^{2/8} (\rho^{7/8} - \rho_H'^{7/8}). \qquad (1.149)$$

From (1.9), (1.10), (1.147) and (1.149), we find the curves of the intensity of light and ionization:

$$I = \frac{\tau\Lambda}{16(Q - Q_H)}\left(\frac{\Gamma}{\sigma}\right)^{2/8} v^{19/8}\rho^{7/8}\left[r_0^{3/8} - \frac{3\Lambda H v_0^{14/8}}{56(Q - Q_H)\delta\cos z}\left(\frac{\Gamma}{\sigma}\right)^{2/8}(\rho^{7/8} - \rho_H'^{7/8})\right]^4,$$

$$\alpha = \frac{\pi\Lambda\beta}{2\mu m_H (Q - Q_H)}\left(\frac{\Gamma}{\sigma}\right)^{2/8} v^{14/8}\rho^{7/8}\left[r_0^{3/8} - \frac{3\Lambda H v_0^{14/8}}{56(Q - Q_H)\delta\cos z}\left(\frac{\Gamma}{\sigma}\right)^{2/8}(\rho^{7/8} - \rho_H'^{7/8})\right]^4. \qquad (1.150)$$

At sufficiently intensive deformation, the drop becomes unstable. Öpik [6] evaluated the stability of a molten meteor body, proceeding from the observations of the fragmentation of air bubbles in water, and found the critical value of the radius of a drop, in which the fragmentation begins:

$$r_b = \frac{7{,}5\sigma}{\rho_s}. \qquad (1.151)$$

Such a method of the estimation of the critical radius is quite approximate, since the physical conditions of the fragmentation of air bubbles in water corresponds but little to the conditions of the motion of a liquid drop at a velocity of tens of km/sec in a rarefied gas.

Up to the present time, a number of theoretical studies have been made on the stability of liquid drops in an ultrasonic gas flow, which agree well with the results of the experiments [34 - 38]. The stability of a drop is typified by the Weber number

$$\mathrm{We} = \frac{\Gamma \rho r v^2}{\sigma}. \qquad (1.152)$$

For a nonviscous liquid, the critical value of the Weber number $\mathrm{We}_0 \approx 3.2$. For a viscous liquid, $\mathrm{We}_0 \approx 6.5$. At $\mathrm{We} \approx \mathrm{We}_0$, the drop fragments.

From (1.68) and (1.152), we find the critical value of the radius of meteor bodies, which in a molten state are unstable even at the height of the beginning of intensive evaporation:

$$r_{gH}^2 = \frac{3\sigma \Lambda H \,\mathrm{We}_0}{8\Gamma \delta Q_H \cos z}. \qquad (1.153)$$

From (1.149) and (1.152), we find the critical value of the initial radius of meteor bodies, which preserves the stability in the process of the entire evaporation:

$$r_{g0}^2 = \frac{9}{16} r_{gH}^2 = \frac{27\sigma \Lambda H \,\mathrm{We}_0}{128\Gamma \delta Q_H \cos z}. \qquad (1.154)$$

The initial masses of the meteor bodies with the radii r_{gH} and r_{g0} are signified respectively as M_{gH} and M_{g0}. At $v_0 = 40$ km/sec, for the stony meteor bodies, $M_{g0} \approx 2 \cdot 10^{-3}$ grams and for the iron meteor bodies, $M_{g0} \approx 3 \cdot 10^{-3}$ grams, which corresponds to the meteors of approximately $+5^m$. In this manner, the compact stony and iron meteor bodies generating the meteors weaker than about $+5^m$, should not experience fragmentation.

The meteor bodies with a mass of $M \geqslant M_{g0}$ should experience fragmentation. In this connection, we should differentiate 4 cases.

1) At

$$M_{gH} \leqslant M_0 \leqslant M_0' \qquad (1.155)$$

the meteor body will fragment even at the altitude of the beginning of intensive evaporation. For the stony meteor bodies, condition (1.155) can be fulfilled at $v_0 \lesssim 30$ km/sec, while for the iron ones, it can be fulfilled in the entire range of meteor velocities.

2) At

$$M_{g0} \leqslant M_0 < M_{gH} \text{ и } M_0 \leqslant M_0' \qquad (1.156)$$

the fragmentation occurs after the beginning of intensive evaporation, after the drop's radius has reached the critical value corresponding to the condition $\mathrm{We} = \mathrm{We}_0$. The height h_g, at which fragmentation occurs can be found from the

Eqs. (1.149) and (1.152). Conditions (1.156) both for the stony and for the iron meteor bodies can be fulfilled at any meteor velocities.

3) At

$$M_{g_0} \leqslant M_0 < M_{g_H} \text{ and } M_0 > M'_0 \qquad (1.157)$$

the fragmentation occurs after the body has been melted through, and the radius of the drop has reached the critical value corresponding to the condition We = = We_0.

4) At $M_0 > M_{g_H}$ and $M > M'_0$, the fragmentation occurs after the body has been liquefied completely through.

The fragmentation of a meteor body leads to an increase in the frontal surface and consequently to an increase in the rate of evaporation and braking. It is easy to demonstrate that at $v_0 \geqslant 20$ km/sec in the calculation of the curve of the luminous intensity of a fragmented meteor, we can overlook the braking of the small drops into which the body will fragment.

Since the very small particles can expend to heat radiation a considerable part of their kinetic energy, in an estimation of the value of the droplets' braking, it is necessary to take into account the energy losses to heat radiation.

Dividing the equation of evaporation with allowance for the energy losses to heat radiation (1.117) into the braking equation (1.7), we get

$$\frac{dM}{M} = \zeta v \left(1 - \frac{\rho''_H}{\rho}\right) dv; \quad \zeta = \frac{\Lambda}{2\Gamma(Q - Q_H)}. \qquad (1.158)$$

From (1.68), (1.70) and (1.154), it is easy to show that the density ρ'_H of the atmosphere at the height of the beginning of intensive evaporation of meteor bodies with the radii $r_0 \geqslant r_{g_0}$ always meets the condition $\rho'_H / \rho''_H > 2$. The fragmentation of the molten meteor bodies occurs at a height close to the height of the beginning of intensive evaporation, or below, therefore for obtaining the maximal estimation of the velocity loss by the droplets in the evaporation process, in (1.158), we assume $\rho''_H / \rho =$ = 1/2. Then, integrating (1.158), we get

$$\frac{M_0}{M} = e^{\frac{\zeta}{4}(v_0^2 - v^2)}, \qquad (1.159)$$

where M_0 equals the initial mass of a droplet. From (1.59) we find that at an average velocity of meteors $v_0 = 40$ km/sec, independently of the initial mass of the droplet, to a reduction in its mass by e.g. 5 times, there corresponds a reduction in velocity of less than 2%. Since Eq. (1.159) provides the maximal estimation of the velocity loss, the actual braking will be even less. The allowance for such a trivial decrease in the velocity of the droplets during the evaporation process has practically no effect on the form of the curve of the meteor's luminous intensity.

If we disregard the deceleration (frictional action), the curves of the luminous intensity of meteors, generated by individual droplets can be calculated with the aid of Eq. (1.150). The integral curve of the luminous intensity is obtained as a result of their addition.

As an example, let us consider the evaporation of a compact stony meteor body with $M_o = 0.02$ gram, $v_o = 20$ km/sec and cos $z = 2/3$. The radius of the body satisfies condition (1.155); hence, the fragmentation should occur as early as the height of the beginning of intensive evaporation. It is possible to have different types of fragmentation: the drops can fragment immediately into very fine droplets, each of which will remain stable in the evaporation process, or will experience progressive fragmentation. For example, if a drop is divided into two equal parts, each of them, having travelled about 2 km, will become unstable, and in their turn, will separate into finer parts. This process, in combination with evaporation, will continue until the body has been fragmented into quite fine stable droplets. It is also possible to have a combination of both these types of fragmentation. In Fig. 1.9, the curve 1 of luminous intensity is computed under the assumption that the drop will break into a minimal number of droplets, each of which will remain stable during the evaporation process. For a comparison, we have presented: 2-curve of luminous intensity calculated according to (1.150) without allowance for fragmentation, and 3- the curve of luminous intensity (1.28), provided by the simplest physical theory of meteors. The cross-hatched part of curves 1 and 2 corresponds to the range of heights at which we have the transition from conditions of the heating of a meteor body to intensive evaporation. The value of the luminosity factor is taken from the data of Öpik [10]. In Fig. 1.10, we have presented the analogous curves of the luminous intensity for a meteor generated by an iron meteor body with $M_o = 0.03$ gram, $v_o = 40$ km/sec and cos $z = 2/3$.

The allowance for fragmentation leads to an increase in the maximal brilliance of the meteor, a truncation of the trail, an increase in the deceleration and an increase in the height of maximal evaporation. For instance, the allowance for fragmentation leads to an increase in the maximal luminous intensity of a stony meteor, for which the curve of the luminous intensity is presented in Fig. 1.9, by $0,^m 8$ as compared with the value provided by the simplest physical theory of meteors. The height of the maximal evaporation increases by 3 km. At the threshold of sensitivity of the radiation receiver $m_\phi = +4^m$ introduced by Levin [16], the parameter of fragmentation F, which characterizes the relative truncation of the trail, is obtained as equalling 0.5. Owing to the fragmentation and the subsequent deformation of the droplets, the coefficient of the form of a meteor body reaches the value 3.6, which leads to an increase in the deceleration of the meteor by about 3 times as compared with the case of a nonfragmenting spherical meteor body. For an iron meteor, for which the curve of luminous intensity is shown in Fig. 1.10, the fragmentation parameter $F = 0.3$. We have examined the cases of the fragmentation of a liquefied meteor body into a minimal number of relatively large droplets. In the case of fragmentation into very fine droplets, the fragmentation effects examined above can be manifested much more intensively.

During the movement in the atmosphere of large meteor bodies not heating all the way through, there can occur the blowing away from the body's surface of a film of molten substance by the opposing air flow. This process was studied by Öpik [6]. In the case of stony meteor bodies, the blowing away is made difficult by the high viscosity of the molten meteor substance. In the case of iron meteor bodies not entirely heated through with the initial radii

$$r_0 < \frac{1.6 \cdot 10^7}{v_0}, \text{ cm}$$

where v_o is expressed in cm/sec), according to Opik, the basic mechanism of the reduction of the mass is not evaporation but the blowing away of the molten film. The upper limit of r_o corresponds to the very large meteor bodies, which when moving in the atmosphere form a shock wave.

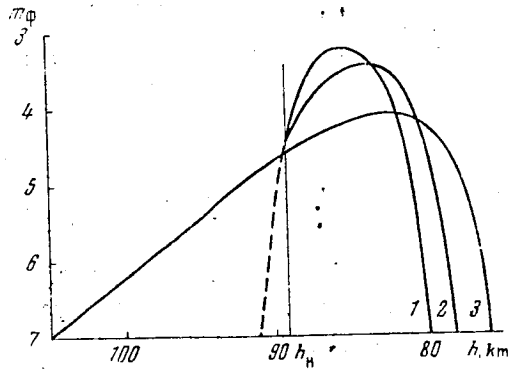

Fig. 1.9. Curves of the Luminous Intensity of a Meteor, Generated by a Compact Stony Meteor Body with M_o = 0.02 g, v_o = 20 km/sec; δ = 3.4 g/cm^3 and cos z = 2/3. 1- with allowance for fragmentation of a molten meteor body; 2- with allowance only for the drop's deformation; 3- the curve provided by the simplest physical theory of meteors.

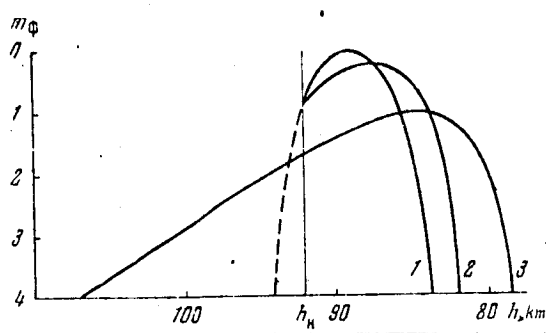

Fig. 1.10. Curves of the Luminous Intensity of a Meteor, Generated by an Iron Meteor Body with M_o = 0.03 g, v_o = 40 km/sec and cos z = = 2/3. The notations are the same as in Fig. 1.9.

In the case of the blowing away of the molten film, the temperature of the body's surface will remain continuously close to $T_{пл}$ and the evaporation from the surface of the body is slight. The original temperature of the droplets forming during the blowing away, is also close to $T_{пл}$. Since the mass of the droplets is much less than the mass of the body (at the separation of large drops from the body, they immediately shatter into smaller parts), prior to the beginning of intensive evaporation, the droplet travels less than one km, and the path being covered by a droplet prior to the completion of of its evaporation is much less than the length of the meteor trail. In connection with this, in the case of the blowing away of the melted film, the rate of evaporation of the meteor substance is close to the rate of the decrease in the mass of the meteor body, and hence is roughly described by the formula

$$\frac{dM}{dt} = -\frac{\Lambda A M^{2/3} \rho v^3}{2 Q_{пл} \delta^{2/3}}, \qquad (1.160)$$

where $Q_{пл}$ equals the energy required to heat and melt 1 g of meteor substance. For iron, $Q_{пл} \approx 1.3 \cdot 10^{10}$ ergs/g.

From (1,9) and (1,160) for the case of an isothermal atmosphere, let us find the atmospheric density at the altitude of the maximal evaporation and the curve of the luminous intensity of the meteor:

$$\rho_m = \frac{2Q_{пл} M_0^{1/3} \delta^{2/3} \cos z}{\Lambda A H v_0^2} + \frac{1}{3} \rho_н, \qquad (1,161)$$

$$I = \frac{\Lambda A \tau v_0^5}{16\pi Q_{пл} \delta^{2/3}} \rho \left[M_0^{1/3} - \frac{\Lambda A H v_0^2}{6 Q_{пл} \delta^{2/3} \cos z} (\rho - \rho_н) \right]^2. \qquad (1,162)$$

The height at which the melting of the surface of an iron meteor begins is 1 - 2 km higher than the height of the beginning of its intensive evaporation, found according to (1,62) or (1,63); hence, the height of the beginning of intensive evaporation of meteor substance is practically the same in the case of both types of ablation of a meteor body (of the evaporation of the body or the blowing away of the melted film). The height of the maximal evaporation proves to be greater by 5 - 10 km than according to (1,114), and somewhat more than for the compact stony body of the same mass. The blowing away of the molten film leads to an appreciable shortening of the meteor trail.

By way of an example, let us consider the curve of the luminous intensity of a meteor being generated by an iron meteor body having the following parameters: $M_o = 1$ g, $v_o = 40$ km/sec, $\cos z = 2/3$ and $A = 1.21$. With the aid of Eqs. (1,62), (1,63) and (1,162), we computed the curves of the luminous intensity for two extreme cases: a spherical rotating meteor body and a non-rotating meteor body with a plane frontal surface. In the first instance, the length of the trail proved to equal 7 - 8 km. The maximal luminous intensity of the meteor is attained immediately after the beginning of the melting of the body. The visual absolute stellar magnitude of the meteor in the maximum of brightness - 3^m, 4 (brighter by 1^m, 6 than according to Eq. (1,30) of the simplest physical theory of meteors). At a threshold of sensitivity of the radiation receiver $+3^m$, we obtain the value of the fragmentation factor $F \approx 0.2$. In the second instance, the length of the trail equals about 12 - 13 km. The maximal luminous intensity of the meteor ($-2,^m 3$) is reached in 5 - 6 km after the beginning of the liquefaction of the body's surface. The value for the fragmentation factor $F \approx 0.4$.

In this manner, we can differentiate three basic types of the ablation of the compact meteor bodies: evaporation, blowing away of the molten film with the subsequent evaporation of the droplets separated from the body; and the fragmentation of the molten meteor body, the extreme case of blowing away, when the mass of the parent body immediately decreases to zero. The role of the various types of ablation is dissimilar for the iron and stony meteor bodies.

Ablation of Iron Meteor Bodies

Evaporation is the basic type of ablation only for the small meteor bodies (heated right through) with the masses $M^{IV}_o < M_o < M_{go}$. In this

connection, in the case of bodies with the masses $M_{\sigma o} < M_o < M_{go}$ in the integration of the equations of the evaporation and deceleration, it is necessary to take into account the deformation of the molten drop, leading to a truncation of the trail, to an increase in the maximal brightness of the meteor and to an increase in the frictional action.

In the range of masses $M_{go} < M_o < M_{g_H}$, there occurs initially the evaporation of the deformed, and then, when the deformation reaches a critical value, the drop fragments. At $v_o = 40$ km/sec, this range of masses corresponds to the meteors of approximately $+5^m$ - $+3^m$.

The meteor bodies with the masses $M_{g_H} < M_o < M'_o$ begin to split up at the heights close to the height of the beginning of intensive evaporation. In the process of evaporation, the progressive splitting of the droplets can take place. In this range of masses of meteor bodies, we can expect the most intensive indications of the effects of fragmentation. In the case of masses close to M'_o, a drop will break into a very large number of fragments, which will lead to an increase in the maximal brightness of the meteor by several stellar magnitudes as compared with the value yielded by the simplest physical theory of meteors, and also to an appreciable increase in the deceleration of the meteor. The height of the maximal luminous intensity of the meteor increases. At $v_o = 40$ km/sec, this range of masses of meteor bodies corresponds to meteors of approximately $+3^m$ - -3^m.

At $M_o > M'_o$, the mass of the meteor body decreases chiefly as a result of the blowing off of the molten film. This leads to a considerable contraction of the meteors' trails, to an increase in the maximal brightness and an increase in the height of the maximal luminous intensity by 5 - 10 km. The deceleration of the meteor does not change at this time (with the exception of a section at the end of the trail, when the body becomes melted right through and fragments). The fragmentation of the body melted right through at the end of the trail leads to the bursting of the meteor.

Ablation of Stony Meteor Bodies

According to the assessment by Öpik [6], in the case of the stony meteor bodies, the blowing away of the molten film does not occur. The more precise calculations by Cook [208] demonstrated that the partial blowing away is also possible in the case of the stony meteor bodies. This question requires further research.

For the small meteor bodies, heating right through, with the masses $M_o^{IV} < M_o < M_{go}$, evaporation comprises the basic type of ablation. In this connection, in the range of masses $M_{\sigma o} < M_o < M_{go}$, it is necessary to take into account the deformation of the molten drop.

The meteor bodies with the masses $M_o > M_{go}$ can experience fragmentation. In this context, the meteor bodies with the masses in the range $M_{g_H} < M_o < M'_o$ become shattered already at the height of the beginning of intensive evaporation (this range of masses differs from zero only at $v_o \lesssim 30$ km/sec, and expands with a decrease in velocity), the others--as early as following the onset of intensive evaporation.

At $M_{go} < M_o \lesssim 10M'_o$, the fragmentation should occur above the point of the maximal evaporation. At $v_o = 40$ km/sec, this range of masses of meteor bodies corresponds to the meteors of approximately $+5^m - 0^m$. Since the fragmentation leads to an abrupt increase in the rate of the evaporation of the meteor substance, the moment of the onset of fragmentation can often coincide with the time of the appearance of the meteor duringthe photographic observations. At $M_o \gg M'_o$, the residue of the meteor body will become melted right through below h_m (all the later, the larger the M_o). The drop forming at this time can experience fragmentation (or even atomization), which leads to the flaring of the meteor; in the case of a very large meteor body, it leads to the frequently occurring final flash of a bright meteor [39].

During the photographic observations of the Draconid meteor stream in 1946 [40], it was revealed that the average height of the appearance of meteors of the stream ($h_n = 97.7$ km) is greater by 7 - 8 km than in the sporadic meteors of the same velocity ($v_o = 23.1$ km/sec). The trails of meteors in the stream prove to be very short. The same anomalously great heights of the appearance, as in the Draconids are found in the individual sporadic meteors of certain other streams [24, 41].

The anomalous heights of the appearance of the Draconids evidently can not be explained within the framework of the concepts concerning the compact stony or iron meteor bodies of the standard chemical composition. Jacchia, Kopal and Millman [40] connect the anomalies of the Draconids with the unusual composition of the meteor bodies of the stream, which is manifested in the ease of their evaporation. In the reports by Levin [24] and Öpik [6], these anomalies are connected with the very unconsolidated structure of the meteor bodies, which leads to their fragmentation. The hypothesis of Jacchia, Kopal and Millman can be somewhat modified if we consider that the meteor bodies in the stream of the Draconids are easily melted and the fusion (melt) has a low viscosity. In this case, the basic mechanism of the ablation will be the blowing away or the spraying of the molten film, which leads to an increase in the height of evaporation and a contraction of the trail. In any of these cases, it is necessary to assume that the meteor bodies in the Draconid stream differ greatly in composition or structure from the basic mass of meteor bodies, generating the sporadic meteors and the meteors of most of the streams.

As was already mentioned above, the photographic observations with the Super-Schmidt cameras revealed a number of features of the meteors $0^m - +4^m$. Jacchia [14] indicates three main features of the faint photographic meteors.

1) A contraction of the trails of meteors as compared with the length of the trail, provided by the simplest physical theory of meteors; a rapid increase in the brightness in the point of appearance, after which there usually follows a more gradual increase of the brightness up to the maximum.

2) An anomalously high deceleration of the meteors in the second half of the visible part of the trail. If we consider that the form of the body is unchanged in the process of evaporation, the density of the atmosphere, found according to the deceleration, that the beginning of the trail proves to be close to the actual one, while at the end of the trail, on an average it proves to be four times higher than the actual.

3) In the photographs taken with a shutter, in the second half of the trail, we often find a blurring of the intervals. The same kind of a blurring sometimes occurs at the end of the trails of the bright meteors. In the case of the meteors 0^m - $+4^m$, it is found more often and in a larger part of the trail.

These features of the faint photographic meteors usually explain the quite unconsolidated structure of the meteor bodies generating them, as a result of which these bodies experience fragmentation [6, 14 - 16, 42].

The noted features of meteors 0^m - $+4^m$ as compared with the findings of the simplest physical theory of meteors and the results of the observations of meteors brighter than 0^m with the standard photographic cameras follow from the above-mentioned more precise theory of the evaporation of the compact stony and iron meteor bodies.

1) With allowance for the dependence of the rate of evaporation upon the temperature of the body's surface, the brightness of a meteor around the height h of the beginning of intensive evaporation at the range of heights 1 - 2 km increases by about 5 stellar magnitudes. Whereupon there usually follows the more gradual increase in the brightness to the maximum. In the case of the iron meteor bodies that are not very large, the brightness maximum can be reached immediately after the onset of the intensive evaporation (e.g., in the above-mentioned example of the ablation of an iron meteor body). Such an abrupt increase in the brightness near the height h should also occur in the bright meteors, however, in effect, it is always the case that the brilliance of a meteor near the height h is below the sensitivity threshold of the standard photographic cameras, therefore prior to the application of the Super-Schmidt cameras, this distinct increase in the brightness of meteors could not be detected from the photographic observations. Even without allowance for the fragmentation and deformation of the molten meteor body, the length of the meteor's trail weaker than approximately $+3^m$ can not be more than 15 km, while in the brighter meteors, the length of the trail increases by about 2 km per stellar magnitude. This factor alone decreases the fragmentation parameter F with the increase in the brightness of the meteors). The allowance for the deformation and fragmentation leads to an even greater contraction of the trails.

2) For the meteors 0^m - $+4^m$, the deformation and fragmentation of the molten meteor bodies begins above the height h_m of the maximal evaporation. The increase of the frontal surface, connected with the progressive fragmentation and deformation of the drops, leads to an increase in the deceleration.

3) The fragmentation of a meteor body above h_m and the differing deceleration of the fragments of varying size will lead to the blurring of the intervals on a considerable part of the photograph of the meteors. In the case of meteors brighter than about 0^m, the fragmentation occurs below h_m and the blurring of the intervals will occur at the very end of the trail.

In this manner, the features of the faint photographic meteors and the occurring fragmentation of the bodies producing them by themselves can not serve as a criterion for a solution of the question concerning the density and

structure of the meteor bodies, hence, both the very unconsolidated as well as the molten dense meteor bodies can become shattered. The selection between these two mechanisms of fragmentation is quite important for a solution of th question concerning the possibility of the fragmentation of small bodies, producing meteors fainter than about $+5^m$, which at the present time can still not be observed photographically.

The compact stony and iron bodies, producing meteors fainter than about $+5^m$ should not experience fragmentation. According to (1.128), the difference in the heights of the beginning and end of the trail of a meteor, being produced by a nonfragmenting body heated right through, should be around 15 km. The fragmentation would have led to a contraction of the trail. According to the results obtained from the radar measurements by Greenhow and Neufeld [43], the average length of trails of meteors $+5^m$ - $+7^m$, obtained from a large number of measurements, equals about 15 km. The average curve of ionization is close to (1.127). The deceleration of the radio meteors also does not indicate the fragmentation of the meteor bodies generating them. In this manner, most of the small meteor bodies producing the meteors fainter than $+5^m$ evidently do not fragment, and to them can be applied the above-mentioned evaporation theory.

We should point out the considerable difference between the meteors in the Draconids stream and the main mass of the faint photographic meteors. The Draconids have anomalously high heights of appearance, which (in combination with the contraction of their trails) also comprises the basic criterion of the very loose structure or the unusual chemical composition of the meteor bodies producing them. The same structure (or composition) can be possessed by the separate sporadic meteor bodies and the meteor bodies of certain streams. From Figs. 1.5 and 1.6, it is evident that the average heights of the appearance of 2500 photographic meteors, both the faint and the bright ones, agree satisfactorily with the theory of evaporation of compact meteor bodies. The same can be stated concerning the heights of the maximal force of the luminosity of meteors brighter than $+4^m$.

The concepts presented permit one to make the following conclusions: the question of the mechanism of the fragmentation of the meteor bodies producing meteors brighter than about $+5^m$, in our opinion at the present time apparently still can not be solved unequivocally and requires further experimental and theoretical study. Since the features which exist in the faint photographic meteors can be explained within the framework of the fragmentation mechanism of the compact meteor bodies that have melted right through, at the present time it does not seem feasible to us to involve, for an explanation of these features, the hypothesis concerning the very unconsolidated structure of most of the small meteor bodies.

COEFFICIENT OF RADIANCE AND SCALE OF MASSES OF OPTICAL METEORS

In the movement of meteor bodies (in the upper atmosphere), the dimensions of which are less than the mean free path of the air molecules at the corresponding height, a shock wave does not form, and the processes of excitation and ionization occur chiefly during the collisions of particles, having evaporated from the body's surface, with the individual air molecules. In the range of meteor velocities, the energy of the electrons is of the

order of the average heat energy of the air molecules, and is much less than the potentials of excitation and ionization of atoms and molecules, therefore the excitation and ionization in the meteor trails can occur only in case of the collisions of the heavy particles.

The substance of the stony meteor bodies evaporates chiefly in the form of molecules (refer to page 16). Since the effective sections of dissociation at the meteor velocities [44] are larger than the sections of diffusion and much larger than the sections of excitation and ionization, most of the evaporated molecules manage to become dissociated before they become excited or ionized. In the spectra of the meteors, the bands of meteor molecules actually do not occur. In connection with this, in a calculation of the factors of radiance and ionization from meteors, we can limit ourselves to a consideration of the collisions of the meteor atoms with the air molecules.

The calculation of the radiance factof during the atomic collisions was conducted in the two reports by Öpik [3, 10]. Öpik determines the radiance factor τ as the portion of the kinetic energy of a meteor body, which converts to the visible radiation in the range of wave lengths 4500 - 5700 A.

In 1933, Opik [3] for the calculation of τ, applied the following semi-empirical theory. Proceeding from the then existing information concerning the effective sections of elastic scattering and ionization during the collisions of various pairs of atoms and ions, Opik demonstrated that the average number of ions forming during one collision can be represented by the empirical formula

$$\beta' = 0.026 \sqrt{\frac{E}{E_i}}, \qquad (1.163)$$

where E_i equals the ionization potential, E equals the energy of relative movement of the colliding particles

$$E = \frac{m_1 m_2 v^2}{2(m_1 + m_2)},$$

m_1, m_2 equal the masses of particles, v equals the relative velocity. Eq. (1.163) is applicable at $\beta' < 1$ and $E > E_i$. For the various pairs of colliding particles, there was found a spread in the experimental values of β' relative to the values provided by Eq. (1.163), by 1.55 times in one direction or another.

Öpik assumed that the probability of the excitation of the colliding particles can also be computed with the aid of Eq. (1.163). There were no experimental data concerning the sections of excitation during the slow collisions of heavy particles, and the validity of this assumption could not be verified. Taking into account the probability of transitions between the various energy levels of the electrons, Öpik found the value τ for the collision of a nitrogen atom with the initial velocity v, which is decelerated in the pairs of atomic iron (T 1.6).

Generalizing the results obtained to the case of the complex composition of meteor bodies and allowing for the possibility of collisions between the evaporated meteor atoms, Öpik found the values of τ for the bright and faint meteors, presented in Table 1.6. For the bright meteors in the range

of velocities of 20 - 60 km/sec, the τ-value can be approximated by the expression

$$\tau = \tau_0 v^p, \tag{1.164}$$

where $p = 1$ and $\tau_0 = 10^{-9}$ sec/cm. At $v < 20$ km/sec, the reduction in τ with a decrease in the velocity occurs more rapidly than according to (1.164).

Proceeding from the spectral sensitivity of the eye and the energy distribution in the spectrum of meteors found by m, Öpik derived the following relationship between the energy I', being radiated in the range of wave lengths 4500 - 5700 Å, and the visual absolute stellar magnitude of a meteor

$$m = 24.6 - 2.5 \quad I'. \tag{1.165}$$

Table 1.6

Coefficient of Radiance $\tau \cdot 10^3$

	v, km/sec						
	10.4	14.8	20.9	29.6	41.8	59.2	83.6
Fe + N	3.6	4.9	6.5	8.5	10.7	12.8	14.5
Bright meteors	0.53	1.14	1.90	2.90	4.10	5.30	6.42
Faint meteors.	0.90	0.95	0.85	0.75	0.65	0.62	0.55

If we know the coefficient of radiance, the mass of the meteor body producing the given meteor can be determined by means of measuring the curve of the luminous intensity and velocity of the meteor. Substituting in the equation of luminescence (1.9) I by $I'/4\pi$ and integrating from the moment of appearance of the meteor t_1 to the moment of disappearance t_2, we get

$$M = 2\int_{t_1}^{t_2} \frac{I'}{\tau v^2}\, dt. \tag{1.166}$$

In (1.166), we do not consider the decrease in the mass of the meteor body prior to the point of appearance of the meteor and the residual mass in the point of its disappearance. The mass of a meteor body can be estimated roughly also based on the luminous intensity of the meteor at the maximum of brightness. From (1.30), we get

$$M_0 = \frac{9\pi H I_m}{2\tau v_0^3 \cos z}. \tag{1.167}$$

This method of determining the masses of the meteor bodies is said to be "photometric", while the masses found with the aid of Eq. (1.166) or (1.167), are said to be "photometric". From (1.164), (1.165) and (1.167), we derive the following scale of the "photometric" masses of bright meteors: a meteor body, flying vertically with the velocity $v_0 = 40$ km/sec, with the mass $M_0 = 0.07$ g, produces a meteor of 0^m of visual absolute stellar magnitude (in the point of maximum light intensity).

In 1955, Öpik [10], re-examined his calculations of the radiance coefficient. He obtained values for τ somewhat lower than he had in 1933, and in effect these were the same for the stony and iron meteor bodies (Table 1.7).

Utilizing more recent determinations of the curve of the spectral sensitivity of the eye, Öpik also obtained a new relationship between I' and the visual stellar magnitude of a meteor

$$m = 24.3 - 2.5 \log I'. \qquad (1.168)$$

Table 1.7

Coefficient of Radiance $\tau \cdot 10^3$

Meteors	v, km/sec						
	10.4	14.8	20.9	29.6	41.8	59.2	83.6
Bright	0.53	1.10	1.46	1.67	2.10	2.60	3.11
Faint	0.71	1.00	0.96	0.64	0.45	0.37	0.30

For the faint meteors, Öpik [45] estimates the dependence of τ upon v by the formula

$$\tau = \frac{2 \cdot 10^3}{v}. \qquad (1.169)$$

In the case of the bright meteors, the dependence of τ on v turns out to be weaker than according to (1.164) ($p \approx 0.5$). At $v = 40$ km/sec, $\tau \approx 2 \cdot 10^{-3}$. From (1.167) and (1.168), we get a new scale of the "photometric" masses of meteors: a meteor body, flying vertically with the velocity $v_0 = 40$ km/sec, with the mass $M_0 = 0.12$ g produces a meteor 0^m of visual absolute stellar magnitude.

In 1957, the first tests were made on the development of artificial meteors [46]. At a height of 80 km, we exploded three cartridges of varying design, which created directed explosions and transmitted a high velocity to the aluminum fragments which formed during the explosion. The artificial meteors were photographed by 5 ground stations with the aid of the Super-Schmidt cameras equipped with a shutter and tracking ballistic cameras with a rotating shutter.

Of the three experiments, only one proved successful. According to the photographs obtained with the Super-Schmidt cameras, we found the curve of the luminous intensity of the meteor and measured the velocity. In the maximum of the brightness, the meteor had the photographic absolute stellar magnitude of -2^m. The initial velocity v_0 of the meteor equals 14.4 km/sec; at the moment of disappearance, it equalled around 12.7 km/sec. The average height of the meteor was 79.2 km. From the laboratory studies it was found that the total mass of the fragments formed during the explosion, $M_0 \approx 0.11$ g. Adopting the relationship between I' and m based on (1.165) and the index of the color of the meteor as -1^m, 8, based on the curve of the luminous intensity of the meteor and the velocity, McCrosky found the value of the factor τ_0 in Eq. (1.164) $\tau_0 = 9 \cdot 10^{-10}$ sec/cm (at $p = 1$).

Adopting a more accurate relationship between I' and m (1.168), we derive that for an aluminum meteor body with the initial velocity $v_0 = 14.4$ km/sec, the radiance factor $\tau = 10^{-3}$. This value practically coincides with

the τ values obtained by Öpik for the average composition of the meteor bodies in 1933 and 1955.

In 1961, the second test was made with an artificial meteor [47]. To a steel fragment with the mass $M_0 = 2.2$ g at a height of 195 km, we imparted the initial velocity $v_0 = 9.8$ km/sec. The chemical composition of the steel was as follows: iron - 68.5%, chromium - 19.2%, nickel - 10.3%, and manganese - 2.0%. The artificial meteor had the zenith distance of the radiant $z = 15^\circ$. The height of the appearance of the meteor $h_n = 69.4$ km, and the height of disappearance $h_k = 62.6$ km. In the maximum of brightness, the meteor had the photographic absolute stellar magnitude - $0,^m 4$. Assuming $p = 1$ McCrosky and Soberman [47] based on a curve of the luminous intensity of an artificial meteor found the value of the coefficient n (1.164) $\tau'_0 = 8 \cdot 10^{-19}$ (in a system in which to the meteor of 0^m photographic magnitude, there corresponds $I' = 1$). This value for τ_0 was adopted by us for pure iron also. Assumming that the luminescence of the iron meteors was caused only by the iron lines, McCrosky and Soberman for the iron meteor bodies, in the composition of which on an average there enters 93% of iron, obtained $\tau'_0 = 7.4 \cdot 10^{-19}$. The lower limit of the value of the radiance factor for the stony meteor bodies can be obtained if we consider only the luminescence of the iron atoms entering their composition. At an average content of the iron in the stony meteorites of 15%, we obtain $\tau'_0 = 1.2 \cdot 10^{-19}$.

The average velocity of an artificial meteor is around 9 km/sec. Assumming the color index at $-1^m, 3$ [7] with the aid of Eqs. (1.164) and (1.168), we can transfer from τ'_0 to τ. For a steel meteor body, we get $\tau = 0.72 \cdot 10^{-3}$. For the iron meteor bodies, $\tau \approx 0.67 \cdot 10^{-3}$ and for the stony ones, $\tau \approx 0.18 \cdot 10^{-3}$. The last value is obviously depressed, since it disregards the radiation of the remaining atoms, other than iron, entering the composition of the stony meteor bodies. Öpik [10], at a velocity of 9 km/sec for the stony and iron meteors, obtained $\tau = 0.26 \cdot 10^{-3}$.

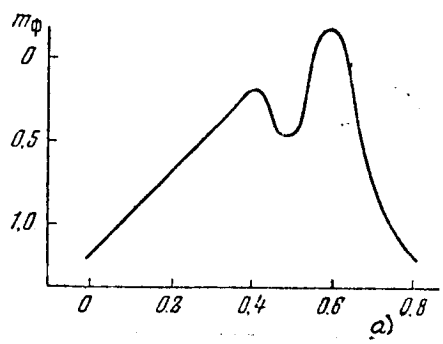

Fig. 1.11. Curve of the Luminous Intensity of an Artificial Meteor [47]. a) t, sec.

The mechanism of the ablation of an artificial meteor body is of interest. A steel fragment has the form of a flat disc with a diameter of 12 mm and a thickness of 2.5 mm. The position of the disc was saabilized by the rotation around the axis, perpendicular to the plane of the disc. McCrosky and Soberman consider that the height h_n of the appearance of an artificial meteor equals 69.4 km is too high for the initial velocity $v_0 = 9.8$ km/sec. From (1.63), for an iron meteor body with a flat frontal surface, having the

initial velocity v_0 = 9.8 km/sec, the zenith distance of the radiant z = 15° and the thickness h_0 = 2.2 mm, we derive the height of the beginning of intensive evaporation, $h_и$ = 70 km, which practically coincides with that obtained from the observations of the height of the meteor's appearance. In Fig. 1.11, we have shown the curve of the luminous intensity of a meteor. As a result of the rapid rotation prior to the moment of the complete melting of the body, from the edges of the disc, there took place a spraying of the molten film. The decrease in the brightness before the attainment of the maximum, having continued for 0.3 sec, is linked by McCrosky and Soberman with the complete melting of the body. The subsequent flare and rapid disappearance of the meteor is evidently connected with the fragmentation of the unstable drop having formed during fusion.

The results obtained from the tests with the artificial meteors indicate that the radiance factors found by Öpik evidently are not far from the true ones, although there is possible a spread in the values for τ, associated with the difference in the chemical composition of the individual meteor bodies.

For the basic photographic observations of meteors with a shutter, the mass of the meteor body can be determined according to the deceleration of the meteor. From the deceleration equation (1.7), we get

$$M^{1/3} = \frac{A\Gamma}{\delta^{2/3}} \frac{\rho v^2}{-\left(\frac{dv}{dt}\right)}. \qquad (1.170)$$

For the transition to the initial mass of a meteor body, it is necessary to consider the reduction in the mass to a given point, which can be done, utilizing Eq. (1.13) or the curve of the luminous intensity of the meteor. The masses of the meteor bodies found with the aid of Eq. (1.170) are said to be the "dynamic" masses.

For a calculation of the "dynamic" masses of meteor bodies, it is necessary to know the value for $\Gamma A/\delta^{2/3}$. Since the "photometric" scale of the masses at the present time has been established with satisfactory accuracy, the problem can be reversed, and, knowing M, from (1.170), we can find the density of the meteor bodies. Substituting in (1.16) I by $I'/4\pi$ and τ by τ'_0 v, we get

$$M = \frac{2}{\tau'_0} \int_{t}^{t_2} \frac{I'}{v^3}\, dt. \qquad (1.171)$$

Excluding from (1.170) and (1.171) M, we obtain

$$K = \frac{\rho v^2}{\left(-\frac{dv}{dt}\right)\left[\int_{t}^{t_2} \frac{I'}{v^3}\, dt\right]^{1/3}}, \qquad (1.172)$$

where

$$K = \frac{1}{\Gamma A}\left(\frac{2\delta^2}{\tau'_0}\right)^{1/3}. \qquad (1.173)$$

All the values standing in the right part of (1.172), can be determined directly from observations. In the integral expression, we replaced τ by τ_0. Since for each meteor, the velocity changes within narrow limits,

such a substitution does not lead to appreciable errors, and we can always revert to τ. Measuring the deceleration and the curves of the luminous intensity of a large number of meteors, Jacchia [48] found the average value for log K = 6,403 (in a photometric system in which I' = 1 for the meteor 0 of visual absolute stellar magnitude). Whipple [42] again processed the data for 88 meteors, using the results obtained from more recent measurements of the density of the atmosphere; he derived the average value log K = 6,321. The average value of the velocity of these 88 meteors v = 29,3 km/sec.

According to Öpik [10], at v = 29,3 km/sec, $\tau = 1{,}65 \cdot 10^{-3}$. Assuming A = 1,5, from (1,182), we get

$$\log \delta = 0.11 + 1{,}5 \log \Gamma. \tag{1,174}$$

With allowance for the reactive impulse of the evaporating molecules, we obtain $\delta = 2{,}2$ g/cm^3, which is close to the average density of the large meteor bodies, estimated by us at the beginning of this chapter in respect to the heights of the maximal luminous intensity of bright meteors.

A discussion of the scale of masses, composed in 1955 by Cook [49] is in order. In the evening from 8 to 9 March 1954, from two points, photographs were made of the luminous trail of a fast meteor (v_o = 70 km/sec), which revealed a systematic movement of the trail downward with a velocity of 30 m/sec. Ascribing this motion to the impulse of the evaporated meteor substance, we were able to estimate the mass of the meteor body and the coefficient of radiance. The value for τ prove to be about 200 times less than the value obtained by Öpik in 1933 [3]. Accordingly, the "photometric" scale of the masses of meteors increased by 200 times. For the matching of the "photometric" and "dynamic" scales of the masses, it was necessary to assume that the meteor bodies have a quite unique unconsolidated structure, and have the average density $\delta = 0{,}05$ g/cm^3.

This scale of masses and the very low density of meteor bodies is utilized in many reports in the interpretation of the results of the observations of meteors. After carrying out the experiments with the artificial meteors [46, 47], a disagreement was found in the new scale of masses with the results of measurements, and in 1963, Whipple [42] concluded that it was necessary to reduce the new scale of masses by about 60 times. Currently, the American researchers have arrived at a scale of masses, differing in all by 2 - 5 times from the "photometric" scale of masses derived by Öpik [42, 47, 50].

COEFFICIENT OF IONIZATION AND THE SCALE OF MASSES OF RADIOMETERS

The kinetic energy of the evaporating meteor atoms decreases during the elastic collisions with the molecules of the atmosphere and is also spent in the ionization and excitation both of the atoms themselves and of the air molecules. The variation in energy E of an atom in a segment of path ds can be written in the form

$$dE = -\left(\frac{1}{2} nEQ_d + n\bar{E}_i Q_i + n\bar{E}_{ex} Q_{ex}\right) ds, \tag{1.175}$$

where n equals density of atmospheric molecules, $\bar{E}_i$, $\bar{E}_{ex}$ equals average values of the potentials of ionization and excitation, Q_i, Q_{ex} equal the

effective sections of ionization and excitation, and Q_d equals the effective diffusion section.

The number of free electrons, generated by an atom in the segment of path ds,

$$dNe = nQ_i ds. \tag{1.176}$$

From (1.175) and (1.176), we get

$$\frac{dN_e}{dE} = -\frac{Q_i}{\frac{1}{2}EQ_d + \overline{E}_i Q_i + \overline{E}_{ex} Q_{ex}}. \tag{1.177}$$

The full number of free electrons, generated by one evaporated meteor atom up to the loss by it of the cosmic velocity,

$$\beta = \int_{E_t}^{E} \frac{Q_i dE}{\frac{1}{2}EQ_d - \overline{E}_i Q_i + \overline{E}_{ex} Q_{ex}}, \tag{1.178}$$

where E_t equals the minimal value of energy at which the ionization can still occur. At the meteor velocities $1/2\ EQ_d$ is much higher than $\overline{E}_i Q_i + \overline{E}_{ex} Q_{ex}$, therefore (1.178) can roughly be rewritten as

$$\beta = 2\int_{E_r}^{E} \frac{Q_i dE}{Q_d E}. \tag{1.179}$$

Thus, for the calculation of the ionization factor, it is necessary to know the effective section of the diffusion and ionization during the collisions of the meteor atoms with the molecules of N_2 and O_2 and their dependence upon velocity.

The first steps in an evaluation of the value of the ionization factor were made as early as 1933 by Öpik [3]. Proceeding from the then available data concerning the sections of elastic scattering and ionization (chiefly during the collisions of atoms of inert gases with their own ions and with the ions of alkali metals), Öpik derived the empirical formula (1.163) for an average number of ions, forming during one collision. In 1955, Öpik [10] continued this work. Taking into account the ionization both in the first and in the subsequent collisions of an atom, he found the number of free electrons γ, forming in a meteor trail, in a calculation for one erg of kinetic energy of the meteor body. In Table 1.8, we have listed the values for γ at different velocities for the stony and iron meteor bodies, and also the β-values corresponding to them.

In the range of velocities of 30 - 70 km/sec, the dependence of β upon v, based on the data in Table 1.8, can be represented as

$$\beta = \beta_0 v^8.$$

For the stony meteor bodies, $\beta_0 = 1.44 \cdot 10^{-21}\ \mathrm{sec^3/cm^3}$.

Table 1, 8

	Meteor bodies	v, km/sec					
		14.8	20.9	29.6	41.8	59.2	83.6
$\gamma \cdot 10^3$	Stony . .	1.0	7.1	18.8	31.6	45.5	59.9
	Iron . .	2 5	13.0	26.6	39.9	52.5	65.9
β	Stony . .	0.0004	0.006	0.031	0.105	0.30	0.80
	Iron . .	0.0025	0.026	0.11	0.32	0.85	2.12

The effective section of diffusion is expressed as follows through the differential section of elastic scattering I (E, θ) [25]:

$$Q_d(E) = 2\pi \int_0^{\pi} (1 - \cos\theta)\, I(E, \theta) \sin\theta d\theta, \qquad (1.180)$$

where θ equals the scattering angle in a system of center of masses.

In the calculation of the effective section of elastic scattering, the classical theory [25] is applicable. The quantum corrections are significant only at small angles of deflection. Since the differential sections of scattering at small angles enter into (1.180) owing to the factor (1 - cos θ) sin θ with very low weights, the quantum and classical formulas for Q_d practically coincide.

The differential section of the scattering is determined by the following classical formula [51]:

$$I(\theta)\, d\omega = \frac{p}{\sin\theta} \frac{dp}{d\theta} d\omega,$$
$$\theta = \pi - 2\int_{r_0}^{\infty} \frac{rd}{r\varphi(r)}, \qquad (1.181)$$

where

$$\varphi(r) = \left[\frac{r^2}{p^2} - 1 - \frac{r^2}{pE} V(r)\right]^{1/2}.$$

Here r equals the internuclear distance, p equals the impact parameter, d ω equals the element of the solid angle, V (r) equals the potential of interaction, and r_o equals the maximal of the roots of equation φ(r) = 0.

If during the collision, there occurs a slight disturbance of the electrostatic potentials and the distribution of the density of the charges in the electron shells of the colliding atoms, the interaction potential can be calculated by a statistical method. From the minimal principle of Lenz and Gensen [52], we obtained the following expression for the interaction potential: [see next page]

$$V(r) = \frac{z_1 z_2 e^2}{r} - e\int\left[\frac{z_1\rho(r_2)}{r_1} + \frac{z_2\rho(r_1)}{r_2}\right]d\tau -$$
$$- \frac{1}{2}\int[V_e(r_1)\rho(r_2) + V_e(r_2)\rho(r_1)]\,d\tau +$$
$$+ \frac{(4\pi)^{1/3}}{5e^{5/3}}\left(\frac{3}{8\pi}\right)\frac{h^2}{m}\int\{[\rho(r_1)+\rho(r_2)]^{5/3} - [\rho(r_1)]^{5/3} - [\rho(r_2)]^{5/3}\}\,d\tau - \quad (1.182)$$
$$- \frac{3}{2}\left(\frac{3}{8\pi}\right)^{1/3}\frac{e^{2/3}}{(4\pi)^{1/3}}\int\{[\rho(r_1)+\rho(r_2)]^{4/3} - [\rho(r_1)]^{4/3} - [\rho(r_2)]^{4/3}\}\,d\tau.$$

Here r_1, r_2 equal the distances to the nuclei of the colliding atoms, $V_e(r_1)$, $V_e(r_2)$ equal the electrostatic potentials, being developed by the unperturbed electron clouds of the atoms $\rho(r_1)$, $\rho(r_2)$ equal the respective densities of the charges of the electron clouds, $d\tau$ equals the element of volume, e, m equals the charge and mass of the electron, and h equals the Planck constant.

Massey and Sida [52] with the aid of Eqs. (1.190) - (1.192) computed the diffusion section for the collisions of the Ca and Ne atoms. In the calculation, it was assumed that the mass of the atom of Ne equals the mass of the atom Ca. The densities of the charges in the electron clouds of the atoms and the electrostatic potentials were obtained from the calculations of the self-coordinated fields by D. R. Hartree and W. Hartree [53] for Ca and by Brown [54] for Ne. We have listed below the values for of Q_d obtained by them for four values of energy. Q_d is expressed in the units πa^2_o, where $a_o = 0.529 \cdot 10^{-8}$ cm equals the radius of the first Bohr orbit.

E, ev	75	150	750	1500
$Q_d/\pi a^2_o$	4.39	3.20	1.34	0.77

The dependence Q_d (E), obtained by them based on the four values of Q_d is approximated by Massey and Sida by the expression

$$Q_d(E) = Q_0(\ln E/C)^2, \quad (1.183)$$

where $Q_o = 0.165\,\pi a^2_o$, C = 12,800 ev. The approximation (1.183) provides an approximately valid value under the gas-kinetic conditions also. For the calculations, it is more convenient to approximate the dependence obtained by Massey and Sida, $Q_d(E)$, by the expression

$$Q_d(E) = C_1/\sqrt{E} + C_2, \quad (1.184)$$

where C_1, C_2 are constants. The approximation of such a type agrees well with the Q_d-value both at the meteor velocities and at the heat velocities. In the case of the meteor velocities $\sqrt{E} \gg C_2$, the dependence $Q_d(E)$ also acquires a quite simple form:

$$Q_d \approx \frac{C_1}{\sqrt{E}} = \frac{C}{v}, \quad (1.185)$$

where $C = 10^{-9}$ cm^3/sec.

An atom of Ca is a typical meteor atom. The calculation for collisions of atoms with the molecules of the atmosphere N_2 and O_2 by this method is impossible, since at the present time, we do not know the self-consistent fields

for the molecules. Therefore, Massey and Sida selected Ne, the ordinal number of which is close to the ordinal numbers of N and O.

Yu. I. Portnygin [55] computed the interaction potential of the typical meteor atoms with the molecules of N_2 and O_2 under the following assumptions: the total electron energy of the system of interacting atoms was determined from a model of the atom according to Thomas-Fermi-Dirac, the molecule was regarded as a rigid system of the dumbbell type (the probability of the oscillatory and rotational excitations is slight), the average potential of interaction of the atom-molecule system was obtained from the orientation-dependent potential of the atom-molecule by a direct averaging based on all possible orientations, wherein it was assumed that the potentials of the systems atom-atom provide the additive contributions to the orientation-dependent potential.

For a calculation of the interaction potential of the system atom-atom, we utilize the expression obtained by Abrahamson [56, 57] from the average value of the minimal and maximal Hamiltonian system,

$$V(r) = \frac{1}{2}\frac{z_1 z_2 e^2}{r}\left[\psi\left(z_1^{1/3} r/a\right) + \psi\left(z_2^{1/3} r/a\right)\right] + \\ + \frac{\pi}{3r}\int\limits_{\text{макс}\,(0,\, r-r_{b1})}^{\text{мин}\,(r_{b2},\, r+r_{b1})} dr_2 \int\limits_{|r-r_2|}^{\text{мин}\,(r_{b1},\, r+r_2)} r_1 r_2 F(r_1, r_2)\, dr_1, \qquad (1.186)$$

where $\psi\left(z^{1/3} r/a\right)$ equals the screening function of Thomas-Fermi-Dirac; $a = 0{,}8853\, a_0$; r_{b1}, r_{b2} equals the boundary radii of the atoms in the Thomas-Fermi-Dirac model;

$$F(r_1, r_2) = \varkappa_k\left\{[\rho(r_1) + \rho(r_2)]^{5/3} - [\rho^{5/3}(r_1) + \rho^{5/3}(r_2)]\right\} - \\ - 2\varkappa_a\left\{[\rho(r_1) + \rho(r_2)]^{4/3} - [\rho^{4/3}(r_1) + \rho^{4/3}(r_2)]\right\};$$

$$\varkappa_k = \frac{3}{10}(3\pi^2)^{2/3} e^2 a_0 \approx 2{,}9 e^2 a_0; \quad \varkappa_a = \frac{4}{3}(3/\pi)^{1/3} e^2 \approx 0.73 e^2.$$

Computing the average values of the Hamiltonian by numerical integration on a computer and substituting the derived values into the orientational-dependent potential of the system atom-molecule, Yu. I. Portnyagin obtained the following expression for the average potential of the atom-molecule system:

$$V(r) = \frac{2\alpha e^{-\beta r}}{d\beta}\left[\operatorname{sh}(d\beta)\left(1 + \frac{1}{\beta r}\right) - \operatorname{ch}(d\beta)\frac{d}{r}\right], \qquad (1.187)$$

where α, β equal constants, d equals half of the interatom distance in a molecule.

The numerical integration of the expressions (1.181) and (1.180) with the potential of interaction (1.187) yields the value of Q_d for the collisions of an atom with a molecule. The values, obtained by Portnyagin of the effective section of diffusion for the collisions of typical meteor atoms (Fe, Ca, O, Mg, Si, etc.) with molecules of the atmosphere N_2 and O_2 in the entire range of meteor velocities are approximated well by the expression

$$Q_d = C/v, \qquad (1.188)$$

where $C = 1{,}7 \cdot 10^{-9}$ cm^3/sec. In this manner, the dependence of Q_d upon velocity proves to be the same as in the report by Massey and Sida. The difference consists only in a certain increase in the numerical value of the coefficient, C. Yu. I. Portnyagin suggests that this divergence is explained by the use, in the report by Massey and Sida, of an expression for the interaction potential (1.182),

which was obtained from the minimal principle and hence provides only the lower estimation of the possible interaction. At the present time, we already have fairly extensive data on the experimental determinations of effective section of the ionization during the collisions of various pairs of atoms, ions and molecules in the range of meteor velocities.

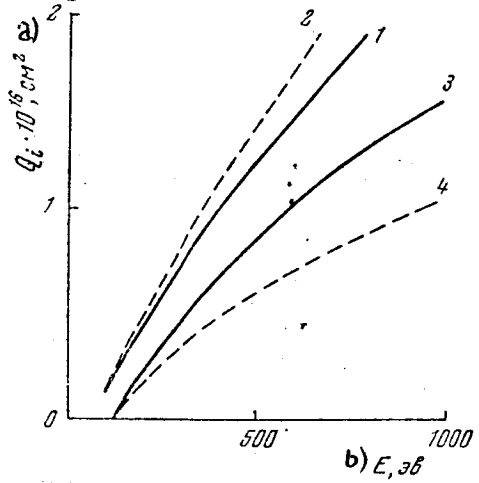

Fig. 1.12. Effective Section of Ionization for Collisions of Atoms and Ions. 1- Ar with Ar; 2- Ar+ with Ar; 3- Ne with Ne; 4- Ne+ with Ne [58]. Key to figure: a) $Q_i \cdot 10^{16}$, cm^2 and b) E, ev

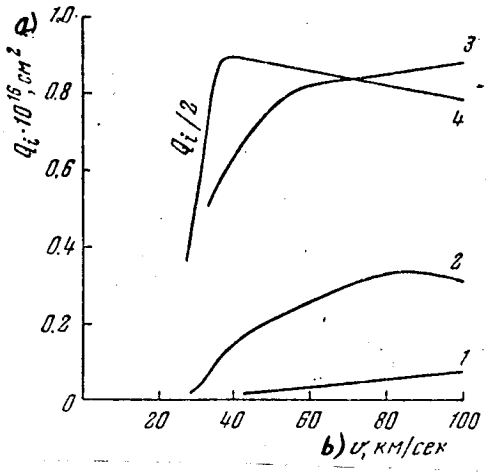

Fig. 1.13. Effective Sections of Ionization for Collisions of Atoms of Alkali Metals with Molecules of the Atmosphere. 1- Na with N_2; 2- K with N_2; 3- Na with O_2; and 4- K with O_2 [63]. Key to figure: a) $Q_i \cdot 10^{16}$, cm^2; and b) v, km/sec.

Massey and Barhop [25] present a summary of the measurements of Q_i, conducted in the 1930s by Rostagni [58], Barry [59], Wolf [60], Frische [61], and others, for the collisions of atoms of inert gases of He, Ne, Ar and Kr with neutral atoms and ions of He, Ne, Ar and Kr, with molecules of H_2, and also with ions of K^+. In Fig. 1.2, we have presented the Q_i-values for the collisions of Ne and Ar with Ne, Ne^+, Ar and Ar^+. In [62], the results are given of the more recent measurements of Q_i for the collisions of K^+ with Ne, Ar, Kr and Xe.

In 1958, Yu. F. Bydin and A. M. Bukhteyev [63] measured the effective sections of ionization for the collisions of atoms of the alkali metals, Na, K, Rb and Cs with molecules of H_2, D_2, N_2 and O_2. In Fig. 1.13, we have presented the values of Q_i for the collisions of atoms of Na and K with the molecules of N_2 and O_2. In 1963, A. M. Bukhteyev and Yu. F. Bydin [64] measured the Q_i-values for the collisions of atoms of Ca with molecules of N_2 and O_2 in the range of velocities 60 - 100 km/sec (Fig. 1.14), and also obtained separate values of Q_i for the collisions of other meteor atoms of Fe, Si and Mg with molecules of N_2 and O_2 at the velocities somewhat higher than the meteor velocities (Table 1.9).

Table 1.9

Atom	v, km/sec	$Q_i \cdot 10^{16}$, cm^2	
		N_2	O_2
Fe	80	0.25	0.8
	100	0.4	1.3
Si	120	0.5	0.7
	143	0.85	1.0
Mg	125	0.2	0.2
	154	0.3	0.3

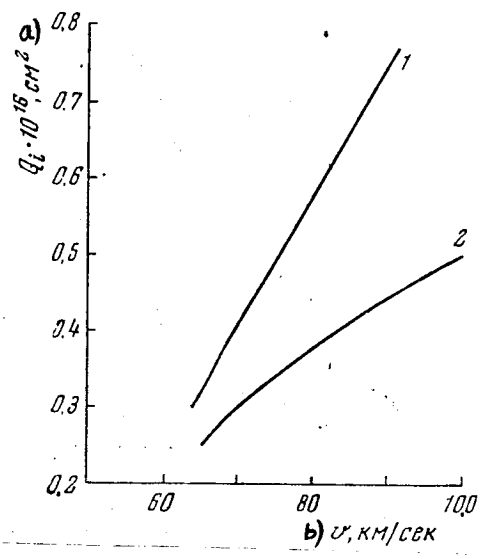

Fig. 1.14. Effective Sections of the Ionization for the Collisions: 1- Ca with O_2; and 2- Ca with N_2 [64]. Key to figure: a) $Q_i \cdot 10^{16}$, cm^2; and b) v, km/sec.

In 1961, Utterbach and Miller [65, 66] measured the sections of ionization for the collisions of the molecules of N_2 and O_2 with N_2 and O_2 in the range of energies ($E - E_i$) from 1 to 1000 ev (Fig. 1.15). The theoretical calculation of the effective section of ionization for the collisions of the pairs of atoms He - He and Ar - Ar at the energies close to the threshold ones, was conducted by Rosen [67, 68]. In Table 1.10, the values obtained for Q_i are compared with the measurement results obtained by Rostagni [58]. We find a satisfactory agreement of the theoretical and measured values of Q_i.

The theoretical calculation of Q_i for the collisions of the Na and O atoms was conducted by Lazarus and Hawkins [69] (Fig. 1.16). From a comparison of Fig. 1.13 and 1.16, it is evident that the dependence of Q_i upon v obtained by Lazarus and Hawkins agrees well with the measurements made by Yu. F. Bydin and A. M. Bukhteyev for the collisions of Na and O_2. In the 30 - 100 km/sec range of velocities, the measured value of Q_i for the collisions of Na and O_2 is about twice as high as the theoretical value for the collisions of Na and O.

From a comparison of the values for Q_i for the collisions of various pairs of atoms, ions and molecules in the range of meteor velocities, we can make the following conclusions.

1) At $v \gtrsim 30$ km/sec, for various pairs of colliding particles, the Q_i-values differ by less than one quarter of magnitude.

2) At energies above the threshold values, we do not find a specific relationship between the Q_i-values and the ionization potential of the colliding particles.

3) We find an increase in Q_i with an increase in the atomic weight of the particles, and also during the collisions of the particles with identical or similar atomic weights.

4) The dependence of Q_i upon v for all pairs of particles has about the same nature: a rapid increase near the threshold and then a more gradual change with an increase in the velocity. For K, Rb, Cs in the range of meteor velocities, the maximum sets in. For the remaining particles, in range of meteor velocities, we find an increase in Q_i with an increase in the velocity. Utilizing the above-listed values for Q_i, let us estimate the value of the ionization factor at various velocities of the meteors.

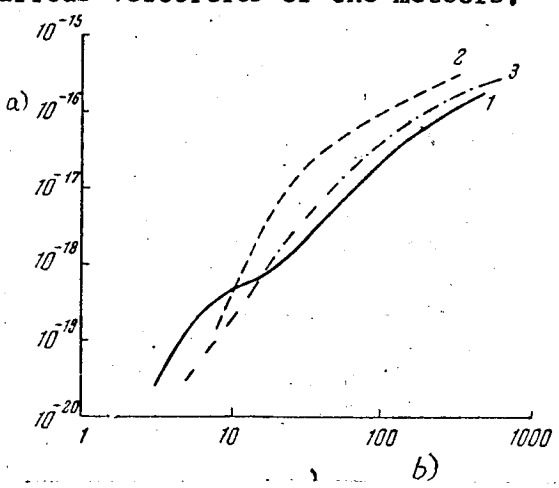

Fig. 1.15. Effective Sections of Ionization for the Collisions of Molecules: 1- N_2 with N_2; 2- O_2 with O_2; 3- N_2 with O_2 [65,66]. Key to figure: a) Q_i, cm^2; and b) $(E_r - E_i)$, ev.

Table 1.10

He — He			Ar — Ar		
E, ev	$Q_i \cdot 10^{16}$, см²		E, ev	$Q_i \cdot 10^{16}$, см²	
	[Rozen]	[Rostagni]		[Rozen]	[Rostagni]
40	0.0110	0.0057	100	0.207	0.396
50	0.209	0.0095	150	0.696	0.588
60	0.0285	0.0151	250	2.23	0.93
70	0.0342	0.0227			
80	0.0385	0.0312			
90	0.0417	0.0378			
100	0.0437	0.0400			

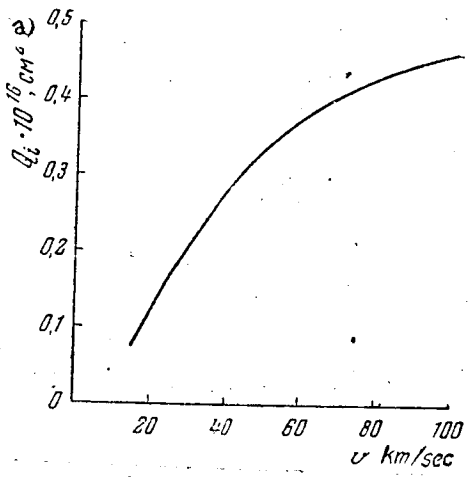

Fig. 1.16. Theoretical Dependence Upon Velocity of Effective Section of Ionization for Collisions of the Atoms of Na and O [69]. Key to figure: a) $Q_i \cdot 10^{16}$, cm^4 (?).

For the collisions of the atoms of Ca with the molecules N_2 and O_2, the dependence of Q_i upon v in the velocity range of 60 - 100 km/sec can roughly be represented in the form

$$Q_i = Q_i^0(v - v_0). \tag{1.189}$$

For Ca and N_2, $Q_i^0 = 0.76 \cdot 10^{-23}$ cm sec, and $v_0 = 3 \cdot 10^6$ cm/sec. For Ca and O_2, $Q^0_i = 1.4 \cdot 10^{-23}$ cm/sec and $v_0 = 4 \cdot 10^6$ cm/sec. From (1.179), (1.188) and (1.189), we derive

$$\beta = \frac{4Q_i^0}{C}\int_{v_0}^{v}(v - v_0)\,dv = \frac{2Q_i^0}{C}(v - v_0)^2. \tag{1.190}$$

For the collisions of the molecules of O_2 with the molecules of N_2 in the range of velocities from 20 - 90 km/sec, the dependence of Q_i upon v can roughly be represented in the form

$$Q_i = Q_i^0 v^{1.3}, \tag{1.191}$$

where $Q^0_i = 3.2 \cdot 10^{-25}$ cm · sec. From (1.179), (1.188) and (1.191), we derive

(see next page)

$$\beta_{O_2, N_2} = \frac{4Q_i^0}{C}\int_{v_0}^{v} v^{1.3}dv = \frac{4Q_i^0}{2.3C}(v^{2.3} - v_0^{2.3}). \qquad (1.192)$$

At v = 83.6 km/sec, Öpik [10] for the stony meteor bodies, found β = = 0.80. In this connection, around 90% of all the ions in the trail, according to Öpik, comprise the ions of the molecules of the atmosphere. From (1.190) for Ca and N_2 at v = 83.6 km/sec, we get β = 0.26; for Ca and O_2 - β = 0.32. For an atmosphere consisting of 80% N_2 and 20% of O_2, we get β = = 0.27. Converting the β-value to the average atomic weight of stony meteor bodies adopted by us, μ = 23, we get for a meteor body consisting of Ca at v = 83.6 km/sec, β_{Ca} = 0.16. The effective ionization sections for the collisions of the atoms of Fe, Si and Mg with molecules of N_2 and O_2 are of the same order of magnitude as for Ca; hence, also the value of β for Fe, Si and Mg will be of the same order as for Ca. For the collisions of O_2 and N_2, from (1.192) at v = 83.6 km/sec, in the conversion to the atomic weight μ = 23, we get $\beta_{O_2N_2}$ = 2.0. In the stony meteor bodies, there is around 40% of oxygen. Thus, for the stony meteor bodies at v = 83.6 km/sec, we get β ≈0.9, which agrees well with the results obtained by Öpik. For the stony meteor bodies at v = 83.6 km/sec, Öpik found β = 2.12. As is evident from the estimations presented above, this value is exaggerated.

In the case of meteors with average velocities, the ionization occurs basically at the first impact of an evaporated meteor atom with the atmospheric molecules. Since the section of ionization diminishes, while the section of diffusion increases with a decrease in the velocity of a particle, the chance of ionization during the second and following collisions is considerably less than during the first. After 2 - 3 collisions, the energy of the meteor atoms proves to be lower than the ionization threshold. Thus, for meteors with average velocities (and even more with the slow velocities), the integration in (1.179) loses sense. In this case, the lower estimation of the value for β can be obtained if we take into account the ionization occurring only at the first collision:

$$\beta \approx \frac{Q_i}{Q_d + Q_i}. \qquad (1.193)$$

At v = 40 km/sec, there are measurements of Q_i for the collisions of Na, K, Rb, Cs, N_2 and O_2 with the molecules of N_2 and O_2, and also for the collisions of atoms of inert gases. We have presented below the β-values found on the basis of (1.193), for various pairs of colliding particles which were converted to the average atomic weight μ = 23. N_2+O_2 signifies that the ionization coefficient pertains to the collisions of a given particle with the molecules of the atmosphere consisting of 80% N_2 and 20% O_2.

Colliding particles	K, $N_2 + O_2$	Na, $N_2 + O_2$	Ne, Ne	Ar, Ar	N_2, N_2	O_2, N_2+O_2
Values for β	0.05	0.03	0.04	0.09	0.04	0.09

Evidently, at v = 40 km/sec, we can assume β = 0.05. Then the β-values for the various pairs of colliding particles presented above will differ from the assumed value by not more than two times. Öpik [10] at v = 40 km/sec for the stony meteor bodies obtained β = 0.09 and for the iron bodies, he obtained

$\beta = 0.3$. As is evident from the estimations presented above, the last of the values for β is clearly exaggerated.

At $v = 20$ km/sec, there are measurements of Q_i for the collisions of the molecules of N_2 and O_2 with the molecules of N_2 and O_2, and also the theoretical calculations by Lazarus and Hawkins [69] for the collisions of Na with O. For the collisions of O_2 with N_2 and O_2 we get $\beta_{O_2, N_2} = 0.0008$ and $\beta_{O_2, O_2} = 0.005$. For the collisions of O_2 with the molecules of the atmosphere $\beta_{O_2, N_2 + O_2} = 0.002$. For Na and O at $v = 20$ km/sec, $Q_i = 1.2 \cdot 10^{-17} cm^2$ and $\beta_{Na, O} = 0.014$. We assume at $v = 20$ km/sec $\beta = 0.005$. Opik [10] at $v = 20$ km/sec obtained for the stony meteor bodies $\beta = 0.005$ and for the iron ones $\beta = 0.02$.

Lazarus and Hawkins [69] from the theoretical calculations obtained for the stony meteor bodies at $v = 40$ km/sec $\beta = 5 \cdot 10^{-4}$. Since this value is less by two orders than according to our estimations, let us consider the study by Lazarus and Hawkins in more detail. As we already mentioned above, the effective ionization section obtained by them for the collisions of Na with O agrees well with the measurement results obtained by Bydin and Bukhteyev for the collisions of Na with O_2 and evidently are valid. In the calculation of the effective section of diffusion, Lazarus and Hawkins utilized the first Born approximation, although in this same study it was indicated that the Born approximation is not applicable in the range of meteor velocities. As a result of this assumption, they obtained at $v = 40$ km/sec, $Q_d = 10^{-14} cm^2$, which is even higher than the section of the diffusion of the atmospheric molecules under the gas-kinetic conditions from a comparison with Eq. (1.188), it is evident that the value for Q_d in the study by Lazarus and Hawkins is exaggerated by more than two times, and hence the β-value for the collisions of Na with O is depressed by just as many times.

In an assessment of the β-value for the other meteor atoms, Lazarus and Hawkins utilized the formula

$$\beta \sim \frac{n\mu}{E_i^6}, \qquad (1.194)$$

where n = the number of valence electrons in the atom. Eq. (1.194) was not substantiated by them in any way, and evidently is invalid. For instance, from (1.194), for the atoms of Na and Ne, the masses of which are about the same, we obtain (even if we consider as valence all of the ten electrons in Ne and only one in Na) $\beta_{Na} / \beta_{Ne} \approx 600$. From Fig. 1.13, it is evident that at $v = 60$ km/sec, for the collisions of Na with N_2, $Q_i \approx 3.5 \cdot 10^{-18} cm^2$, while for the collisions of Ne with Ne, $Q_i \approx 6 \cdot 10^{-18} cm^2$. Since the diffusion section for these two pairs of particles differ but little, the ionization factor for Na proves to be about 17 times less than for Ne. We obtain a discrepancy with Eq. (1.194) of four orders of magnitude. The same discrepancy occurs if we compare the ionization sections for the collisions of Na and O_2 with the same molecule of N_2. Using Eq. (1.194), Lazarus and Hawkins found that the value of β for Mg, Si and Fe is less than about three times than four Na, while for oxygen, in effect $\beta = 0$. From the data presented on

pages 55 - 57, it is evident that at the average meteor velocities, the β-value for Na as a rule is less than for the other atoms and molecules. In this manner, the value of the ionization coefficient in the report by Lazarus and Hawkins is depressed by about two orders of magnitude as a result of these two assumptions.

The data introduced on page 59 indicate that at the average velocity of meteors $v = 40$ km/sec, for the six pairs of atoms and molecules and various electron shells (from the alkali metals to the inert gases), we find a spread in the values for β by less than two times in one direction or other relative to the value $\beta = 0.05$. We can expect that the information available at the present time concerning the effective sections of the ionization of atoms and molecules, at average velocities of the meteors, permit us to establish the value of the ionization factor with an error of not more than two times. In the case of the fastest and the slowest meteors, somewhat higher errors are possible.

Assuming $\beta = 0.9$ at $v = 83.6$ km/sec, $\beta = 0.05$ at $v = 40$ km/sec and $\beta = 0.005$ at $v = 20$ km/sec, we find that in the broad range of velocities, we can assume the following dependence of the ionization factor on the meteor's velocity:

$$\beta = 4 \cdot 10^{-25} v^{3.5}, \tag{1.195}$$

where v is expressed in cm/sec.

From (1.127) and (1.195), we obtain the following scale of the masses of the radio meteors: flying vertically at the velocity $v_0 = 40$ km/sec, a meteor body with the mass $M_0 = 8 \cdot 10^{-4}$ g in the point of maximal evaporation forms an ionized trail with a linear electron density $\alpha_m = 10^{12}$ electrons/cm.

As the parallel visual and radar observations of meteors [70] indicate, the linear electron density of the trail $\alpha = 10^{12}$ electrons/cm corresponds to the meteor of approximately $+5^m$ visual stellar magnitude. By analogy with the scales of visual and photographic stellar magnitudes of meteors, it is convenient to introduce a scale of the values of the radio meteors m_r in the following manner

$$m_r = 35.0 - 2.5 \log \alpha, \tag{1.196}$$

here α is expressed in cm^{-1}. Since the coefficients of luminosity and ionization can depend differently upon the velocity of the meteors, the scales of the stellar magnitudes of the radio meteors and of the visual meteors may not coincide at all values of the velocity. The constant in (1.196) is chosen in such a way that these scales would coincide at $v = 40$ km/sec.

INITIAL RADIUS OF AN IONIZED METEOR TRAIL

In the first studies on the physical theory of radio meteors [70, 71], it was assumed that the initial radius of the ionized meteor trails is very small and about equal to the length of the mean free path of the atmospheric molecules at the corresponding height. In this connection,

it was not taken into account that the particles, evaporating from the surface of a meteor body have velocities close to the velocity of the meteor, v_0. Prior to the establishment of heat equilibrium with the ambient atmosphere, there occurs a rapid initial expansion of the meteor trail.

The initial expansion of the meteor trails were first considered by Manning [72] in 1958. By analogy with the collisions of the elastic spheres, Manning assumed that the velocity of a meteor atom or ion after one collision with a molecule of the atmosphere decreases on an average by 1.5 times. The velocity of an atom or ion after k collisions

$$v = v_0 e^{-\alpha k}, \tag{1.197}$$

where α varies from 0 to 0,4 in dependence on the relationship of the masses of the colliding particles. In the case of equality of masses, $\alpha = 0{,}4$.

In the case of the usual concentration diffusion, the radius of the trail after the time t after the passing through of the meteor body

$$r = \sqrt{4Dt}, \tag{1.198}$$

where D equals the diffusion factor. If the effective section of the diffusion is constant or can be replaced by a certain average value, the diffusion factor equals [25]

$$D = \frac{\bar{v}_r}{3nQ_d}, \tag{1.199}$$

where $\bar{v}_r$ equals the mean relative velocity of the colliding particles, n equals the concentration of the molecules of the atmosphere.

If the velocity of the diffusing particles is much higher than the heat velocity v_a of the molecules of the atmosphere, the mean relative velocity $\bar{v}_r \approx \bar{v}$, where $\bar{v}$ equals the mean value of v for the given time interval. The length of the free path

$$\lambda = \frac{1}{nQ_d}. \tag{1.200}$$

If Q_d does not depend on velocity, from (1.198) - (1.200), we obtain

$$r = \sqrt{\frac{4}{3}\lambda \bar{v} t} = \sqrt{\frac{4}{3}N\lambda^2}, \tag{1.201}$$

where n equals the number of free runs, traversed by a particle during the time t.

Under the gas-kinetic conditions, in the case of equality of masses of colliding particles, the mean relative velocity and the length of the free path

$$\bar{v}_r = \sqrt{2}\, v_a, \quad \lambda^0 = \frac{1}{\sqrt{2}\, nQ_d^0}, \tag{1.202}$$

where Q^0_d equals the effective section of diffusion under gas-kinetic conditions. From (1.200) and (1.202), we obtain $\lambda = \sqrt{2}\,\lambda^0$. Then, (1.201) can be rewritten as

$$r = \sqrt{\frac{8}{3}N\lambda^{0^2}}. \tag{1.203}$$

Equation (1.203) is derived under the assumption that the successive lengths of the free path are haphazardly oriented in relation to each other. If a fast particle encounters a practically stationary molecule of the atmosphere, after collision, the initial direction of motion is partly retained. Manning indicated that in the case of the collisions of solid elastic spheres with varying masses, owing to the partial retainability of the original direction of velocity (persistence of velocity), the resulting path being covered by the fast particle after a large number of runs (increases by $\sqrt{p}$ times, where p = 5. Then, instead of (1.203) we obtain

$$r = \sqrt{\frac{8}{3} pN \lambda^{02}}. \tag{1.204}$$

From (1.197), we find the average time, during which a particle traverses the path between k and (k + 1) with the collisions:

$$\Delta t_k = \frac{\sqrt{2}\lambda^0}{v} = \frac{\sqrt{2}\lambda^0}{v_0} e^{\alpha k}.$$

For N free runs, a particle expends the time

$$t = \sum_{k=0}^{N-1} \Delta t_k \approx \frac{\sqrt{2}\lambda^0 (e^{\alpha N} - 1)}{\alpha v_0}.$$

From this

$$N = \frac{1}{\alpha} \ln \left(\frac{\alpha v_0 t}{\sqrt{2}\lambda^0} + 1 \right). \tag{1.205}$$

From (1.204) and (1.205), we get

$$r = \lambda^0 \sqrt{\frac{8p}{3\alpha}} \ln^{1/2} \left(\frac{\alpha v_0 t}{\sqrt{2}\lambda^0} + 1 \right). \tag{1.206}$$

Manning assumes that the initial expansion of the trail is completed when the rate of the increase in the radius of the trail based on (1.206) becomes less than the rate of expansion as a result of the ambipolar diffusion. From (1.198) and (1.206), we obtain

$$r_0 = \sqrt{\frac{8p}{3\alpha}} \lambda^0 \ln^{1/2} \frac{8pv_0}{3\sqrt{2}(4D/\lambda^0)}. \tag{1.207}$$

Under the gas-kinetic conditions, the length of the free path of the ions λ^{i0} is about five times less than of the neutral particles λ_a [73]; hence, the initial radius of an ionized meteor trail according to (1.207) is about five times less than that of an atom trail. During a variation in the velocity of the meteors from 11 to 72 km/sec, the initial radius of the ionized trail changes from 12.3 λ^{i0} to 14.5 λ^{i0}. On an average, Manning assumes

$$r_0 = 14\lambda^{i0} = 2.8\lambda_a. \tag{1.208}$$

According to the results obtained from the rocket measurements [8], at a height of 95 km, λ_a = 5 cm; hence, according to Manning, at this height the initial radius of an ionized meteor trail should be around 14 cm.

In Manning's study, he did not take into account the dependence of the effective section of diffusion Q_d upon the velocity of the colliding particles, and in case of the meteor velocities, he assumed the Q_d-value

as the same as during the gas-kinetic conditions. From (1.188), we can see that in case of the meteor velocities, the effective section of diffusion is less by about an order than during the gas-kinetic conditions. In this manner, the value, obtained by Manning, of the initial radius of the trail must be greatly depressed.

Öpik [74] presents the results of the calculation of r_0, conducted by him, however he does not report anything concerning the calculation method. The numerical values for r_0 obtained by him can be represented by the following formula

$$r_0 = \frac{9 \cdot 10^{-12} v_0^{3/2}}{\rho}.$$

At v = 40 km/sec, at a height of 95 km, we get r_0 = 1.6 m, which exceeds by more than an order of magnitude the r_0-value found by Manning.

In 1961, there were published the studies by Yu. A. Loshchilov [75], B. L. Kashcheyev and V. N. Lebedinets [76], in which the initial radius of the meteor trails was calculated with allowance for the dependence of the effective section of diffusion upon the velocity of the colliding particles [52].

For finding the radius of a trail, we will utilize Eq. (1.201). However, with allowance for the difference of the successive lengths of the free path of the diffusing particles, let us replace in (1.201)

$$N\lambda^2 \to \sum_{k=0}^{N-1} \lambda_k^2,$$

where λ_k equals length of free path of a fast particle after k collisions. Then the radius of a trail after N runs of the diffusing particles

$$r^2(N) = \frac{4}{3} \sum_{k=0}^{N-1} \lambda_k^2. \qquad (1.209)$$

As was indicated above, the dependence of the effective section of diffusion upon velocity of the colliding particles can be roughly approximated by an expression of the form

$$Q_d = \frac{C_1}{v + C_2}. \qquad (1.210)$$

At $C_1 = 1.8 \cdot 10^{-9}$ cm^3/sec, $C_2 = 3 \cdot 10^5$ cm/sec, Eq. (1.210) provides approximately true values for Q_d both at the meteor velocities and at the gas-kinetic conditions [77].

The difference in the effective sections of diffusion for the collisions of molecules with the atoms Q_d and with the corresponding ions Q^1_d is connected chiefly with the effect of the inductive forces, which develop as a result of the polarization of the molecules in the field of ions [78]. The inductive forces play a significant part at energies of the colliding particles of not more than several electron-volts. At the meteor velocities, they are much less than the forces of repulsion, originating during the overlapping of the electron clouds of colliding particles. As was shown by Massey and Sida [52, 79], at the meteor velocities, the allowance for the effect of the external

valence electrons of atoms of Ca and K during the collisions with the atoms of Ne and Ar does not exert a significant influence upon the value for Q_d. Thus, in the range of meteor velocities, the sections of the diffusion for the atoms and ions should have similar values, while at the gas-kinetic conditions, for ions they are about five times higher than for atoms.

Let us represent the dependence of Q^i_d upon v also by Eq. (1.210), but with other values of the constants: $C_1 = 1.7 \cdot 10^{-9}$ cm^3/sec, $C_2 = 3 \cdot 10^4$ cm/sec. Then at the meteor velocities, we will have $Q^i_d \approx Q_d$, while under the gas-kinetic conditions, $Q^i_d \gtrsim 5Q_d$.

From (1.200) and (1.210), let us find the length of the free path of the ions at $v >> v_a$:

$$\lambda^i = \frac{v + C_2}{nC_1}; \tag{1.211}$$

According to [23], in the case of a spherically symmetrical dispersion for the particles with equal masses, the velocity of a fast particle after k collisions with stationary particles on an average equals

$$v_k = v_0 e^{-0.406k}. \tag{1.212}$$

Then the average length of the free run of the ion after k collisions with the molecules of the atmosphere

$$\lambda^i_k = \frac{v_0 e^{-0.406k} + C_2}{nC_1}. \tag{1.213}$$

The successive lengths of the free run decrease very quickly, therefore the allowance for the persistence of the velocity increases only slightly the resulting path, being traversed by the ions after a large number of runs.

From (1.209) and (1.213), we obtain

$$r^2(N) = \frac{4}{3n^2C_1^2} \sum_{k=0}^{N-1} (v_0 e^{-0.406k_i} + C_2)^2.$$

Transferring from the sum to the integral, we find

$$r^2(N) = \frac{4}{3n^2C_1^2} \int_0^N (v_0 e^{-0.406k} + C_2)^2 \, dk = \tag{1.214}$$

$$= \frac{4}{3n^2C_1^2} [1.24v_0^2(1 - e^{-0.81N}) - 4.93v_0C_2(1 - e^{-0.406N}) + C_2^2N].$$

From (1.212), we find the average number of collisions which are experienced by the meteor atoms or ions prior to the establishment of heat equilibrium with the atmosphere:

$$N_0 = 2.46 \ln \frac{v_0}{v_a}. \tag{1.215}$$

From (1.214) and (1.215), we find the initial radius of the trail

$$r_0^2 = \frac{4}{3n^2C_1^2} \left[1.24v_0^2 \left(1 - \frac{v_a^2}{v_0^2}\right) - 4.93C_2v_0 \left(1 - \frac{v_a}{v_0}\right) + 2.46C_2^2 \ln \frac{v_0}{v_a} \right].$$

Dropping the terms of the second order of smallness in relation to v_a/v_o and C_2/v_o, we get

$$r = \frac{v_0}{nC_1}\sqrt{1.64\left(1+\frac{4C_2}{v_0}\right)}.$$

For the entire range of meteor velocities $4C_2/v_o \leq 0.1$, hence, we can approximately write

$$r_0 = \frac{1.3v_0}{nC_1}. \qquad (1.216)$$

From (1.212) and (1.213), we find the range of time between k and (k + 1) collisions of an ion:

$$\Delta t_k = \frac{1+\frac{C_2}{v_0}e^{0.406k}}{nC_1}.$$

The time spent in N runs,

$$t(N) = \frac{1}{nC_1}\int_0^N\left(1+\frac{C_2}{v_0}e^{0.406k}\right)dk = \frac{1}{C_1 n}\left[N-\frac{2.46C_2}{v_0}\left(e^{0.406N}-1\right)\right].$$

The time of the initial expansion of the trail

$$t_0 = t(N_0) = \frac{2.46}{nC_1}\left(\ln\frac{v_0}{v_a}-\frac{C_2}{v_a}+\frac{C_2}{v_0}\right). \qquad (1.217)$$

At v_o = 40 km/sec at a height of 95 km, from (1.216), we get the initial radius r_o = 1 m of the ionized meteor trail, which is seven times higher than according to Manning, and 1.6 times less than according to Öpik. The time of the initial expansion according to (1.217) $t_o = 2 \cdot 10^{-4}$ sec.

In the cited calculation of the initial radius of the meteor trail, the process of the initial expansion was regarded as a diffusion process. Such an approach is rigorous, if prior to the establishment of heat equilibrium with the atmosphere, the meteor atoms or ions undergo a large number of collisions. From (1.215), it is easy to observe that for the meteors with varying velocities, the number of collisions N_o comprises 10 - 12 in all. With allowance for the dependence of Q_d upon the velocity of the particles, the successive lengths of the free run of the atoms and ions decrease rapidly; therefore, the basic contribution to the initial radius of the trail is made by the first several runs. In connection with this, for the purpose of verifying the value for r_o obtained by us (1.216), it is feasible to consider the contribution of the first several paths to the initial radius.

Assume that the velocity v_o of a meteor body is directed along the axis z (Fig. 1.17, a). Since the particles, evaporating from the surface of a body fly away from it at velocities considerably less than v_o, they form weakly diverging beams in respect to the axis z, and in a first approximation, we can assume that prior to the first collision, the particles have the velocity v_o, directed along the z-axis. Since $v_o \gg v_a$, the molecules of the atmosphere can be considered stationary. The direction of the motion of a particle after impact (collision) is characterized by the angle of deviation θ from the initial direction, and by the azimuth φ. The average value for θ depends on the relationship of the masses of the colliding particles. All

the φ-values are equiprobable, therefore after collision, a particle will move along one of the generatrices of the cone with the opening span 2θ and with the axis directed along the velocity of the particle prior to the collision. The value of the generatrix equals the mean free path λ, depending on the particle's velocity.

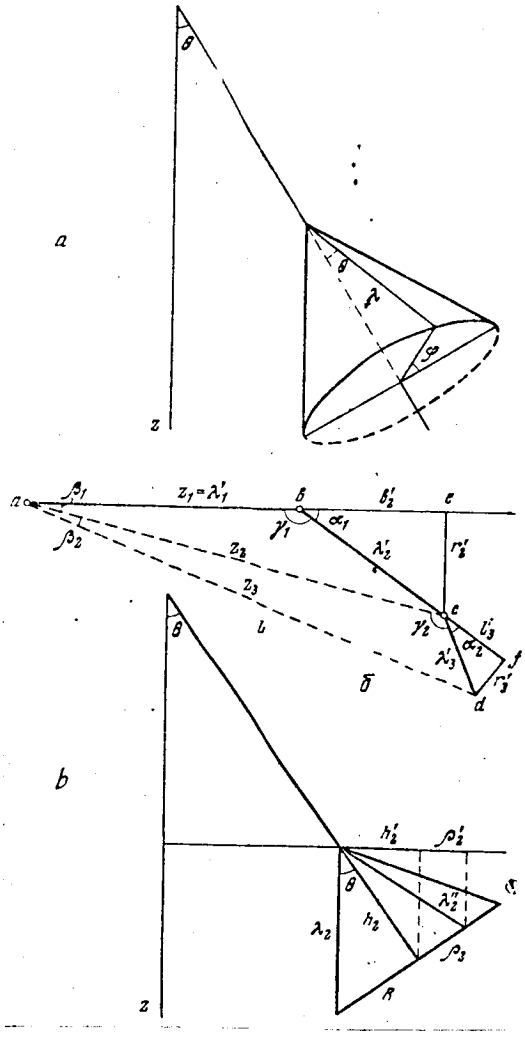

Fig. 1.17. Calculation of Initial Radius of Meteor Trail.

After the first collision, a particle will separate from the axis of the trail for the distance $z_1 = \lambda'_1 = l_1 \sin\theta$, after the second and third--for the distances z_2 and z_3 respectively. For determining z_2 and z_3, let us consider the projections λ'_1, λ'_2, λ'_3 of the generatrices of the cones λ_1, λ_2, λ_3, along which a particle has moved after the first, second and third collisions (Fig. 1.17, b), onto the plane z, perpendicular to the axis of the trail. The angles α_1 and α_2 are determined by the azimuths φ_1 and φ_2.

From the triangles abc and cfd, we find [see next page]

$$z_2^2 = z_1^2 + \lambda_2'^2 - 2z_1\lambda_2' \cos\gamma_1;$$
$$\gamma_1 = \pi - \alpha_1;$$
$$z_3^2 = z_2^2 + \lambda_3'^2 - 2z_2\lambda_3' \cos\gamma_2;$$
$$\gamma_2 = \pi + \beta_1 - \alpha_1 - \alpha_2;$$
$$\cos\beta_1 = \frac{l_2' + \lambda_1'}{z_2}; \quad \sin\beta_1 = \frac{z_2'}{z_2}; \qquad (1.218)$$
$$\cos\alpha_1 = \frac{l_2'}{\lambda_2'}; \quad \sin\alpha_1 = \frac{r_2'}{\lambda_2'};$$
$$\cos\alpha_2 = \frac{l_3'}{\lambda_3'}; \quad \sin\alpha_2 = \frac{r_3'}{\lambda_3'}.$$

In order to express the values entering Eq. (1.218) by λ_1, λ_2, λ_3, and θ, let us examine the sections of a cone with the plane, passing through its axis and perpendicular to the plane L. In Fig. 1.17, c, we have portrayed such a section for the second cone. Here h_2 equals the height of the cone, R equals radius of the base, λ''_2 equals the projection of λ_2 onto the plane of the section, h'_2 equals the projection of h_2 onto the plane L, ρ'_2 equals the projection of ρ_2 onto the plane L. From Fig. 1.17,b, c, it is easy to obtain

$$h_2' = \lambda_2 \cos\theta \sin\theta; \rho_2' = l_2 \sin\theta \cos\varphi_1 \cos\theta; l_2' = h_2' + \rho_2' = \lambda_2 \sin\theta \cos\theta (1 + \cos\varphi_1);$$
$$r_2' = \lambda_2 \sin\theta \sin\varphi_1; \lambda_2'^2 = \lambda_2^2 \sin^2\theta [\sin^2\varphi_1 + \cos^2\theta (1 + \cos\varphi_1)^2]. \qquad (1.219)$$

Similar constructions can be made for the third cone. Having signified the appropriate values for the index 3, we get

$$h_3' = \frac{\lambda_3 \sin\theta \cos^2\theta (1 + \cos\varphi_1)}{\sqrt{\cos^2\theta + \sin^2\theta \cos^2\varphi_1}}; \qquad \rho_3' = \frac{\lambda_3 \sin\theta \cos\varphi_2 (\cos^2\theta - \sin^2\theta \cos\varphi_1)}{\sqrt{\cos^2\theta + \sin^2\theta \cos^2\varphi_1}};$$
$$r_3' = \lambda_3 \sin\theta \sin\varphi_2; \quad l_3' = \lambda_3 \sin\theta \left[\frac{\cos^2\theta (1 + \cos\varphi_1) + \cos\varphi_2 \cos^2\theta - \sin^2\theta \cos\varphi_1}{\sqrt{\cos^2\theta + \sin^2\theta \cos^2\varphi_1}}\right]; \qquad (1.220)$$
$$\lambda_3'^2 = \lambda_3^2 \sin^2\theta \left\{\sin^2\varphi_2 + \frac{[\cos^2\theta (1 + \cos\varphi_1) + \cos\varphi_2 (\cos^2\theta - \sin^2\theta \cos\varphi_1)]^2}{\cos^2\theta + \sin^2\theta \cos^2\varphi_1}\right\}.$$

From (1.218) - (1.220), we find z^2_2:

$$z_2^2 = \lambda_1^2 \sin^2\theta + \lambda_2^2 \sin^2\theta [\sin^2\varphi_1 + \cos^2\theta (1 + \cos\varphi_1)^2] + 2\lambda_1\lambda_2 \sin^2\theta \cos\theta (1 + \cos\varphi_1).$$

Conducting the averaging in respect to φ_1, we get

$$\overline{z_2^2} = \lambda_1^2 \sin^2\theta + \frac{1}{2}\lambda_2^2 \sin\theta (1 + 3\cos^2\theta) + 2\lambda_1\lambda_2 \sin^2\theta \cos\theta. \qquad (1.221)$$

With the aid of Eqs. (1.218) and (1.220), it is easy to demonstrate that

$$-2z_2\lambda_3' \cos\gamma_2 = 2\left\{l_3'\left[\frac{l_2'}{\lambda_2'}(\lambda_1' + \lambda_2') + \frac{r_2'^2}{\lambda_2'}\right] - r_3'\left[\frac{r_2'}{\lambda_2'}(\lambda_1' + l_2') - \frac{l_2}{\lambda_2'} r_2'\right]\right\}. \qquad (1.222)$$

Since $\overline{r'_3} = \lambda_3 \sin\theta \overline{\sin\varphi_2} = 0$, averaging (1.222) in respect to φ, we derive

$$-\overline{2z_2\lambda'_3\cos\gamma_2} = 2\left(\frac{\overline{l'_3 l'_2 \lambda'_1}}{\lambda'_2} - \frac{\overline{l'_3 l'^2_2}}{l'_2} - \frac{\overline{l'_3 r'^2_3}}{\lambda'_2}\right). \tag{1.223}$$

Let us calculate each of the terms in the right hand part of (1.223) separately:

$$\frac{\overline{l'_3 l'_2 \lambda'_1}}{\lambda'_2} = \frac{1}{4\pi^2}\int_{-\pi}^{\pi} d\varphi_1 \int_{-\pi}^{\pi} d\varphi_2 \times$$

$$\times \frac{\lambda_1\lambda_3 \sin^2\theta\cos\theta\,(1+\cos\varphi_1)[\cos^2\theta\,(1+\cos\varphi_1)+\cos\varphi_2(\cos^2\theta-\sin^2\theta\cos\varphi_1)]}{\sqrt{(\cos^2\theta+\sin^2\theta\cos^2\varphi_1)\,[\sin^2\varphi_1+\cos^2\theta\,(1+\cos\varphi_1)^2]}} = \tag{1.224}$$

$$= \frac{\lambda_1\lambda_3\sin^2\theta\cos^3\theta}{2\pi}(I_1 + 2I_2 + I_3),$$

where

$$I_k = \int_{-\pi}^{\pi} \frac{\cos^{k-1}\varphi_1 d\varphi_1}{\sqrt{a_1\cos^4\varphi_1 + a_2\cos^3\varphi_1 + a_3\cos^2\varphi_1 + a_4\cos\varphi_1 + a^5}}. \tag{1.225}$$

Here

$$a_1 = -\sin^4\theta; \quad a_2 = 2\cos^2\theta\sin^2\theta; \quad a_3 = \sin^2\theta;$$
$$a_4 = 2\cos^4\theta; \quad a_5 = \cos^2\theta(1+\cos^2\theta);$$

$$\frac{\overline{l'_3 l'^2_2}}{\lambda'_2} = \frac{1}{4\pi^2}\int_{-\pi}^{\pi} d\varphi_1 \int_{-\pi}^{\pi} d\varphi_2 \times \tag{1.226}$$

$$\times \frac{\lambda_2\lambda_3\sin^2\theta\,[\cos^2\theta\,(1+\cos\varphi_1)+\cos\varphi_2(\cos^2\theta-\sin^2\theta\cos\varphi_1)\cos^2\theta\,(1+\cos\varphi_1)^2]}{\sqrt{(\cos^2\theta+\sin^2\theta\cos^2\varphi_1\,[\sin^2\varphi_1+\cos^2\theta\,(1+\cos\varphi_1)^2]}} =$$

$$= \frac{\lambda_2\lambda_3\sin^2\theta\cos^4\theta}{2\pi}(I_1 + 3I_2 + 3I_3 + I_4);$$

$$\frac{\overline{l'_3 r'^2_3}}{\lambda'_2} = \frac{1}{4\pi^2}\int_{-\pi}^{\pi} d\varphi_1 \int_{-\pi}^{\pi} d\varphi_2 \times$$

$$\times \frac{\lambda_2\lambda_3\sin^2\theta\sin^2\varphi_1\,[\cos^2\theta\,(1+\cos\varphi_1)+\cos\varphi_2(\cos^2\theta-\sin^2\theta\cos\varphi_1)}{\sqrt{(\cos^2\theta+\sin^2\theta\cos^2\varphi_1)\,[\sin^2\varphi_1+\cos^2\theta\,(1+\cos\varphi_1)^2]}} = \tag{1.227}$$

$$= \frac{1}{2\pi}\lambda_2\lambda_3\sin^2\theta\cos^2\theta(I_1 + I_2 - I_3 - I_4).$$

Substituting (1.224), (1.226) and (1.227) into (1.223), we get

$$-\overline{2z_2\lambda'_3\cos\gamma_2} = \frac{1}{\pi}\lambda_3\sin^2\theta\cos^2\theta\,[(\lambda_1\cos\theta+\lambda_2\cos^2\theta+\lambda_2)I_1 +$$
$$+(2\lambda_1\cos\theta+3\lambda_2\cos^2\theta+\lambda_2)I_2+(\lambda_1\cos\theta+3\lambda_2\cos^2\theta-\lambda_2)I_3+(\lambda_2\cos^2\theta-\lambda_2)I_4]. \tag{1.228}$$

From (1.220), we find the average value for λ'^2_3:

$$\overline{\lambda'^2_3} = \frac{1}{4\pi^2}\int_{-\pi}^{\pi} d\varphi_1 \int_{-\pi}^{\pi} d\varphi_2 \lambda_3^2\sin^2\theta \times$$

$$\times\left\{\sin^2\varphi_2 + \frac{[\cos^2\theta\,(1+\cos\varphi_1)+\cos\varphi_2(\cos^2\theta-\sin^2\theta\cos\varphi_1)]^2}{\cos^2\theta+\sin^2\theta\cos^2\varphi_1}\right\} = \tag{1.229}$$

$$\lambda_3^2\sin^2\theta\left[\frac{1}{2}+\frac{3}{2}\cos^2\theta+\left(\operatorname{ctg}^2\theta-\cos^2\theta+\frac{1}{2}\sin^2\theta\right)(1-\cos\theta)\right].$$

From (1.218), (1.221), (1.228), and (1.229), we derive

$$\overline{z_3^2} = \sin^2\theta\left\{\lambda_1^2 + \frac{1}{2}\lambda_2^2(1+3\cos^2\theta) + 2\lambda_1\lambda_2\cos\theta + \right.$$
$$+ \frac{1}{\pi}\lambda_3\cos^2\theta\left[(\lambda_1\cos\theta + \lambda_2\cos^2\theta + \lambda_2)I_1 + (2\lambda_1\cos\theta + 3\lambda_2\cos^2\theta + \lambda^2)I_2 + \right. \quad (1.230)$$
$$+ (\lambda_1\cos\theta + 3\lambda_2\cos^2\theta - \lambda_2)I_3 + (\lambda_2\cos^2\theta - \lambda_2)I_4] +$$
$$\left. + \lambda_3^2\left[\frac{1}{2} + \frac{3}{2}\cos^2\theta + \left(\operatorname{ctg}^2\theta - \cos^2\theta + \frac{1}{2}\sin^2\theta\right)(1-\cos\theta)\right]\right\}.$$

The integrals I_k entering (1.230) were found by numerical integration. In the case of the equality of the masses of the colliding particles during spherically-symmetrical dispersion, the average value $\overline{\cos}\ \theta = 2/3$ [23]. At $v >> v_a$, from (1.213), we get

$$\lambda_k = \frac{v_0}{C_1 n} e^{-0.406k}. \quad (1.231)$$

From (1.225), (1.230) and (1.231), we obtain

$$\overline{z_3} = 0.93\frac{v_0}{C_1 n}. \quad (1.232)$$

Since the initial expansion of the trail also continues after four free runs of the ions, it is obvious that the initial radius of a trail will be larger than z_3. The value z_3 can be assumed as a minimal estimation of the initial radius, r_{min} of the trail. For obtaining the maximal estimation r_{max}, we add to z_3 sum of the lengths of all the remaining paths of the ions prior to the establishment of heat equilibrium with the atmosphere. With the aid of Eqs. (1.213), (1.215) and (1.232), we get $r_{max} = 1.5\ v_0/C_n$. In this manner, the true value of the initial radius of a meteor trail is included in the limits

$$0.93\frac{v_0}{C_1 n} < r_0 < 1.5\frac{v_0}{C_1 n}. \quad (1.233)$$

The value of the initial radius which we have obtained (1.216) $r_0 = 1.3\ v_0/C_{1n}$ satisfies condition (1.233) and is close to the average of the minimal and maximal estimations of r_0.

DISRUPTION OF AN IONIZED METEOR TRAIL

After the establishment of the heat equilibrium with the ambient atmosphere, the further decrease in the electron concentration in the ionized meteor trail occurs as a result of the diffusion-type expansion of the trail, and also of the processes of recombination and adhesion of the electrons. In case of a duration of existence of a trail comprising more than 10 seconds, a significant role is acquired by the expansion of the trail as a result of turbulent diffusion [80]. We will be interested basically in the trails having a reflection duration of less than one second, therefore we will not take into account the expansion of a trail as a result of turbulent diffusion.

The theory of diffusion-type expansion of ionized meteor trails was studied by Kaiser [71]. Since the longitudinal dimensions of the trail are much larger than the transverse ones, we can restrict ourselves to a study of the diffusion in a plane perpendicular to the trail's axis. Let us assume that the trail is situated in heat equilibrium with the atmosphere and we

will not consider the effect of the magnetic field. The equations of diffusion in cylindrical coordinates for ions and electrons have the following forms:

$$\frac{\partial n_e}{\partial t} = \frac{D_e}{r}\frac{\partial}{\partial r}\left(r\frac{\partial n_e}{\partial r}\right) + \nabla'\left(\frac{eEn_e}{m\nu_e}\right),$$

$$\frac{\partial n_i}{\partial t} = \frac{D_i}{r}\frac{\partial}{\partial r}\left(r\frac{\partial n_i}{\partial r}\right) - \nabla\left(\frac{eEn_i}{m_i\nu_i}\right), \tag{1.234}$$

where n_e, n_i equals the density of electrons and ions: D_e, D_i equals the coefficients of diffusion for the electrons and ions, e, m equal the charge and mass of an electron; m_i equals the mass of the ion; ν_e, ν_i equal the frequencies of collisions for the electron and ions; **E** equals the field strength developing as a result of the high mobility of the electrons as compared with the ions.

Since in the central part of the trail, $n_e \approx n_i$, from (1.234), we can exclude **E**:

$$\frac{\partial n_e}{\partial t} = \frac{D}{r}\frac{\partial}{\partial r}\left(r\frac{\partial n_e}{\partial r}\right), \tag{1.235}$$

where D equals the coefficient of ambipolar diffusion:

$$D = \frac{D_i + \frac{m\nu_e}{m_i\nu_i}D_e}{1 + \frac{m\nu_e}{m_i\nu_i}}. \tag{1.236}$$

From the kinetic theory of gases

$$\frac{m\nu_e}{m_i\nu_i} = \frac{\lambda_i}{\lambda_e}\left(\frac{T_e m}{T_i m_i}\right)^{1/2} \ll 1,$$

$$\frac{D_e}{D_i} = \frac{\lambda_e}{\lambda_i}\left(\frac{T_e m_i}{T_i m}\right)^{1/2}, \tag{1.237}$$

where λ_i, λ_e equal the length of the free path of the ions and electrons; T_i, T_e equals the temperature of the ion and electron gases. Assuming $T_i = T_e$, from (1.236) and (1.237), we derive

$$D \approx D_i\left(1 + \frac{T_e}{T_i}\right) = 2D_i. \tag{1.238}$$

Integrating (1.235), we find the distribution of the electron density along the section of the trail

$$n_e = \frac{\alpha}{4\pi D(t - t_0) + \pi r_0^2} e^{-\frac{r^2}{4D(t-t_0)+r_0^2}}. \tag{1.239}$$

where α equals the linear electron density of the trail. According to (1.217), at the heights of 80 - 110 km, the period of the initial expansion of the ionized meteor trail t_0 is of the order of 10^{-3} - 10^{-5} sec. Disregarding in (1.239) the value t_0, we get

$$n_e = \frac{\alpha}{4\pi Dt + \pi r_0^2} e^{-\frac{r^2}{4Dt + r_0^2}}. \tag{1.240}$$

Let us examine the processes of recombination and adhesion (sticking) of electrons in the meteor trails. With allowance for recombination, we will write the equation of the electrons' diffusion in the form

$$\frac{\partial n_e}{\partial t} = \frac{D}{r}\frac{\partial}{\partial r}\left(r\frac{\partial n_e}{\partial r}\right) - \alpha_e n_e^2, \qquad (1.241)$$

where α_e equals the recombination factor. Assuming that in this case also, there occurs a Gaussian-type distribution of the electron density along the section of the trail, and integrating (1.241) along the trail's section, we get

$$\frac{d\alpha}{dt} = -\frac{\alpha_e \alpha^2}{8\pi D(t + t'_0)} \qquad (1.242)$$

and

$$\frac{1}{\alpha} - \frac{1}{\alpha_0} = \frac{\alpha_e}{8\pi D}\ln\left(\frac{t}{t'_0} + 1\right), \qquad (1.243)$$

where t'_0 is found from the equation

$$r_0^2 = 4Dt'_0. \qquad (1.244)$$

The time during which α decreases by two times,

$$t_e = \frac{r_0^2}{4D} e^{\frac{8\pi D}{\alpha_e \alpha_0}}. \qquad (1.245)$$

Assumming for the average height of a meteor zone h equals 95 km, D equals $6 m^2/sec$ and $r_0 = 1m$, we get

$$t_e = 4 \cdot 10^{-2} e^{\frac{1.5 \cdot 10^4}{\alpha_e \alpha_0}}. \qquad (1.246)$$

In the case of atomic ions, the recombination coefficient with radiation is of the order of $10^{-12} cm^3/sec$ [25]. From (1.246), it is easy to observe that the effect of recombination can be disregarded at $\alpha_0 \lesssim 10^{17}$ electron/cm, i.e. at practically any values for α_0.

In the case of the molecular ions, the coefficient of dissociative recombination is of the order of 10^{-8} cm^3/sec [25]. From (1.246), we find that the dissociative recombination decreases by two times during the period of less than one sec at $\alpha_0 \gtrsim 5 \cdot 10^{13}$ electron/cm. As we have seen, in the trails of fast meteors, a large number of molecular ions is forming. In this manner, in the calculation of the duration of the reflection of the radio waves from the trails, being formed by the brilliant fast meteors, it is necessary to take into account the reduction in the electron density in the trail as a result of the dissociative recombination.

With allowance for the adhesion of electrons, the equation of the electron's diffusion can be written as follows:

$$\frac{\partial n_e}{\partial t} = \frac{D}{r}\frac{\partial}{\partial r}\left(r\frac{\partial n_e}{\partial r}\right) - \beta_e n_e n_m, \qquad (1.247)$$

where β_e equals the adhesion factor, n_m equals the density of the particles, free to form negative ions. Integrating (1.247) along the section of the trail, and then in respect to time, we obtain [see next page]

$$\alpha = \alpha_0 e^{-\beta_e n_m t}. \qquad (1.248)$$

In the upper part of the meteor zone (h > 90 km), the adhesion of the electrons occurs mainly toward the molecules and atoms of oxygen during the dual collisions [81, 82]. The value $\beta_2 \approx 10^{-15}$ cm^3/sec. At the height h = 90 km, $n_m = 2 \cdot 10^{13}$ cm^{-3}; hence, at h > 90 km, the effect of the electrons' adhesion must be taken into account for the meteor trails with a duration of the radio waves' reflection of more than 10 seconds. The effect of the adhesion of electrons during the dual and triple collisions upon the duration of the radio waves' reflection from the meteor trails is examined in detail in Refs. [82, 83].

CHAPTER 2

RADIOWAVE SCATTERING ON METEOR TRAILS AND NOTICEABILITY OF RADIO-METEORS

In the first studies on the scattering of radiowaves in the ionized meteor trails, it was assumed that the trail has the form of an infinite cylinder, the radius of which is much shorter than the wave length. Considering the scattering in each electron as independent and coherent, Lovell and Clegg [84] obtained the following expression for the strength of a signal scattered by a meteor trail, at the input of a receiver:

$$P_2 = \frac{P_t G_r G_t \lambda^3 \alpha^2}{32\pi^2 R^3} \left(\frac{e^2}{mc^2}\right)^2, \qquad (2.1)$$

where p_t equals the power of the transmitter, G_r, G_t equals the coefficients of the directivity of the receiving and transmitting antennas (in relation to an isotropic emitter), λ equals the wave length of the radar set (station) (RS), α equals the linear electron density of the trail, R equals the slant range from the RS to the point of the mirror reflection on the trail, e, m equals the charge and mass of the electron, and c equals the speed of light.

In a general form, the problem of the scattering of radio waves in the ionized meteor trails was studied by Herlofson [85] and Kaiser and Gloss [86].

As Kaiser and Gloss [86] demonstrated, if the initial radius of the trail $r_o < \lambda/2\pi$, one should differentiate the ionized meteor trails of three types:

1) Nonsaturated trails. At $\alpha << 2{,}4 \cdot 10^{12}$ electron/cm, the incident wave without significant distortions penetrates into any point of the trail, and the scattering in each electron can be regarded as independent and coherent.

2) Saturated trails. At $\alpha > 2{,}4 \cdot 10^{12}$ electron/cm, the reflection of the radio waves from the trail takes place as if from a metal cylinder with the radius r_c, which is found as the larger of the roots of the equation:

$$\varkappa(r_c)(kr_c)^2 = -1, \qquad (2.2)$$

where $k = 2\pi/\lambda$, $\kappa(r)$ equals the dielectric permeability for the distance r from the axis of the trail

$$\varkappa = 1 - \frac{4\pi n_e e^2}{k^2 mc^2}, \qquad (2.3)$$

n_e equals the electron density.

3) Trails of intermediate type. At α of the order of 10^{12} electron/cm and $r_0 < \lambda/2\pi$, the electron density on the axis of the trail can be higher than the critical one. In this case, the amplitude of the reflected wave depends on the orientation of the electrical vector of the incident wave relative to the trail's axis. For a wave with longitudinal polarization, the amplitude of the reflected wave will be the same as in the case of the non-saturated trails. For a wave with a transverse polarization, in the case of trails of the intermediate type, it is possible to have the phenomenon of resonance, which leads to an increase in the amplitude of the reflected signal. In the case of a Gaussian distribution of the electron density along the radius of the trail, the maximum of resonance occurs at the moment when the dielectric permeability on the axis of the trail $\kappa(0) \simeq -1.4$. The maximal increase in the amplitude of the reflected signal is twofold.

If $r_0 > \lambda/2\pi$, according to Kaiser and Gloss, the phenomenon of resonance is impossible. In this case, the critical value for α between the saturated trails and the trails of the intermediate type is found from the condition $\kappa(0) = 0$. From (1.240) and (2.3), we find

$$\alpha_c = \frac{mc^2}{e^2} \frac{\pi^2 r_0^2}{\lambda^2}. \qquad (2.4)$$

The trails will be nonsaturated if the electron density in any point of the trail is appreciably below the critical value.

SCATTERING OF RADIO WAVES IN UNDERDENSE METEOR TRAILS

If the electron concentration in any point of the trail is considerably less than the critical, the scattering in each electron can be regarded as independent and coherent. The effective section of back scattering for an electron

$$\sigma_e = (\mathbf{e}_r \mathbf{e}_t) \left(\frac{e^2}{mc^2}\right)^2 d\Omega, \qquad (2.5)$$

where $\mathbf{e}_t$, $\mathbf{e}_r$ equals the vectors of the polarization of the incident and reflected waves, d equals the solid angle in which the reflected wave is registered. If the plane of the polarization of the incident and receiving antennas coincide, $(\mathbf{e}_i, \mathbf{e}_r) = 1$.

At the distance R from the radar station, the density of the flow of the radiated energy

$$\frac{P_t G_t}{4\pi R^2}. \qquad (2.6)$$

The effective collecting surface of the receiving antenna

$$\frac{G_r \lambda^2}{4\pi}. \qquad (2.7)$$

From (2.5) - (2.7), we find the strength of the signal scattered by one electron, at the input of the receiver:

$$\Delta P_r = \frac{P_t G_t G_r \lambda^2}{16\pi^3 R^4} \left(\frac{e^2}{mc^2}\right)^2. \qquad (2.8)$$

Dropping the time factor, the voltage in the input of the receiver in case of scattering in one electron can be written as follows:

$$\Delta E_r = (2R_{\text{вх}}\Delta P_r)^{1/2} e^{2\pi i \frac{2R}{\lambda}}, \tag{2.9}$$

where $R_{вх}$ equals the input resistance of the receiver.

An element ds of the trail's length contains αds electrons. In the case of a linear trail, these electrons scatter in a cophased manner, and the total signal scattered by the element ds of the trail's length,

$$dE_r = (2R_{\text{вх}}\Delta P_r)^{1/2} \alpha e^{2\pi i \frac{2R}{\lambda}} ds. \tag{2.10}$$

Integrating (2.10) along the trail, let us find the voltage at the input of the receiver, being created by the signal, scattered in a linear trail:

$$E_r = (2R_{\text{вх}}\Delta P_r)^{1/2} \int_{-\infty}^{s_0} \alpha e^{2\pi i \frac{2R}{\lambda}} ds. \tag{2.11}$$

Here, s is reckoned from the point of the specular reflection in the trail in the direction of the meteor's motion; s_0 typifies the position of the trail's head.

The main contribution to E_r is provided by the sections of the trail close to the point of the specular reflection, for which $s \ll R$ and the value R vary but little, therefore in (2.11), ΔP_r is taken from under the sign of the integral. R can be represented in the form

$$R = \sqrt{R_0^2 + s^2} \approx R_0 + \frac{1}{2}\frac{s^2}{R_0^2}. \tag{2.12}$$

Let us conduct the substitution of the variables

$$x = \frac{2s}{\sqrt{R\lambda}}, \quad x_0 = \frac{2s_0}{\sqrt{R\lambda}}. \tag{2.13}$$

In the substitution of (2.12) and (2.13) into (2.11), in the phase factor, we drop the constant term $4\pi i R_0/\lambda$, and we write R in place of R_0:

$$E_r = \frac{\sqrt{R\lambda}}{2}(2R_{\text{вх}}\Delta P_r)^{1/2} \int_{-\infty}^{x_0} \alpha e^{i\frac{\pi}{2}x^2} dx. \tag{2.14}$$

At $x_0 = \infty$ and constant α, from (2.8) and (2.14), we obtain the Lovell-Clegg equation.

According to (2.14), at constant α-value, the variation in the amplitude of a signal scattered in the forming meteor trail is described by the Frenel integral. The positions [found according to (2.14)], of the maximums and minimums of the diffraction pattern can be utilized for determining the velocity of meteors [87].

If we compare the radius r_c of a trail with the wave length, in (2.10), it is necessary to take into account the difference in the phases of the waves, scattered by various electrons of an element ds of the trail's length. In this case, instead of (2.10), we derive

$$dE_r(r_c) = 2e^{2\pi i \frac{2R}{\lambda}} (2R_{\text{вх}}\Delta P_r)^{1/2}\, ds \int_0^\infty n_e(r)\, dr \int_0^\pi e^{4\pi i \frac{r\cos\theta}{\lambda}}\, d\theta, \tag{2.15}$$

$$\int_0^\pi e^{4\pi i \frac{r\cos\theta}{\lambda}}\, d\theta = \pi J_0\left(\frac{4\pi r}{\lambda}\right), \tag{2.16}$$

where J_0 equals the Bessel function. In the case of a Gaussian distribution of the electrons along the section of the trail, from (1.243), (2.15) and (2.16), we get

$$dE_r(r_c) = \frac{2\alpha}{r_c^2} e^{2\pi i \frac{2R}{\lambda}} (2R_{\text{вх}}\Delta P_r)^{1/2} \int_0^\infty J_0\left(\frac{4\pi r}{\lambda}\right) e^{-\frac{r^2}{r_c^2}}\, dr. \tag{2.17}$$

According to [88]

$$f(r_c) = \frac{2}{r_c^2} \int_0^\infty J_0\left(\frac{4\pi r}{\lambda}\right) e^{-\frac{r^2}{r_c^2}}\, dr = e^{-\frac{4\pi^2 r_c^2}{\lambda^2}}. \tag{2.18}$$

From (2.10), (2.17) and (2.18), we get

$$dE_r(r_c) = dE_r e^{-\left(\frac{2\pi r_c}{\lambda}\right)^2}. \tag{2.19}$$

According to (1.240),

$$r_c^2 = r_0^2 + 4Dt, \tag{2.20}$$

where t equals the time having elapsed from the moment of the passage of a meteor body through a given transverse section of the trail. It is obvious that

$$s_0 - s = vt, \tag{2.21}$$

where v equals the velocity of the meteor. From (2.20), (2.21), we find

$$r_c^2 = r_0^2 + \frac{4D}{v}(s_0 - s). \tag{2.22}$$

From (2.13), (2.18) and (2.22), we obtain

$$f(r_c) = e^{-\left(\frac{2\pi r_0}{\lambda}\right)^2} e^{-\Delta(x_0 - x)} = f(r_0)\, e^{-\Delta(x_0 - x)},$$

where

$$\Delta = \frac{8\pi^2 D \sqrt{R}}{v\lambda^{3/2}}. \tag{2.23}$$

From (2.10), (2.12), (2.19) and (2.23), we find

$$dE_r(r_c) = (2R_{\text{вх}}\Delta P_r)^{1/2} f(r_0)\, e^{-\Delta(x_0 - x)} e^{i\frac{\pi}{2}x^2}\, ds. \tag{2.24}$$

Integrating along the trail, we find

$$E_r = \frac{\sqrt{R\lambda}}{2} (2R_{\text{вх}}\Delta P_r)^{1/2} \int_{-\infty}^{x_0} \alpha f(r_0)\, e^{-\Delta(x_0 - x)} e^{i\frac{\pi}{2}x^2}\, dx. \tag{2.25}$$

The strength of the signal at the input of the receiver

$$P_r = \frac{E_r^2}{2R_{\text{вх}}}. \tag{2.26}$$

From (2.8), (2.25) and (2.26), let us find a general expression for the strength of a signal scattered by an underdense meteor trail:

$$P_r = \frac{P_t G_t G_r \lambda^3}{32\pi^2 R^3}\left(\frac{e^2}{mc^2}\right)^2 \left| \frac{1}{\sqrt{2}} \int_{-\infty}^{x_0} \alpha e^{-\left(\frac{2\pi r_0}{\lambda}\right)^2} e^{-\Delta (x_0 - x)} e^{i\frac{\pi}{2}x^2} dx \right|^2. \tag{2.27}$$

Eq. (2.27) converts to the Lovell-Clegg formula at $x_0 = \infty$, $\alpha = \text{const}$, $r_0 = 0$ and $D = 0$.

The main contribution to (2.27) at $\Delta \lesssim 1$, provides a section of the trail near the point of the specular reflection with a length of the order of $\sqrt{R\lambda}$. At $R = 200$ km, and $\lambda = 8$ m, $\sqrt{R\lambda} \approx 1{,}3$ km. In such a small section of the trail, in a first approximation we can disregard the variation in α and r_0; then, (2.27) will be written:

$$P_r = \frac{P_t G_t G_r \lambda^3 \alpha^2}{32\pi^2 R^3}\left(\frac{e^2}{mc^2}\right)^2 f^2(r_0)\, I^2, \tag{2.28}$$

where

$$I = \left| \frac{1}{\sqrt{2}} \int_{-\infty}^{x_0} e^{i\frac{\pi}{2}x^2} e^{-\Delta (x_0 - x)} dx \right|. \tag{2.29}$$

The maximal value I

$$\varphi(\Delta) = I_{\max} = \frac{1 - e^{-\sqrt{2}\Delta}}{\sqrt{2}\Delta}. \tag{2.30}$$

The maximal value of the strength of the scattered signal

$$(P_r)_{\max} = \frac{P_t G_t G_r \lambda^3 \alpha^2}{32\pi^2 R^3}\left(\frac{e^2}{mc^2}\right)^2 f^2(r_0)\, \varphi^2(\Delta). \tag{2.31}$$

In a measurement of the velocity of the meteors and of the coefficient of the ambipolar diffusion, we usually do not consider the expansion of the trail during the time of the formation in it of the basic Frenel zones. Taking $e^{-\Delta(x_0 - x)}$ from under the integral sign, in (2.29), and considering that $\Delta (x_0 - x) = 16\ \pi^2\ Dt/\lambda^2$, in this case we get

$$I = \frac{1}{\sqrt{2}} e^{-\frac{16\pi^2 Dt}{\lambda^2}} \left| \int_{-\infty}^{x_0} e^{i\frac{\pi}{2}x^2} dx \right|. \tag{2.32}$$

Kaiser [71] reached the erroneous conclusion that the use of the approximate Eq. (2.32) in place of (2.29) does not alter the position of the successive maximums (A, C, E, G ...) and of the maximums (B, D, F ...) of the diffraction pattern of a signal, scattered in a forming trail, and, hence, does not introduce errors into the measurements of the velocity of meteors. In Fig. 2.1, we have presented the amplitude-temporal characteristics of the signals, scattered in the underdense trails, at various values for Δ. The calculation was conducted based on Eq. (2.29) by numerical integration. It is easy to observe that with an increase in Δ, we have a significant displacement of the first maximum of the diffraction pattern. The position of the remaining extremums varies much less.

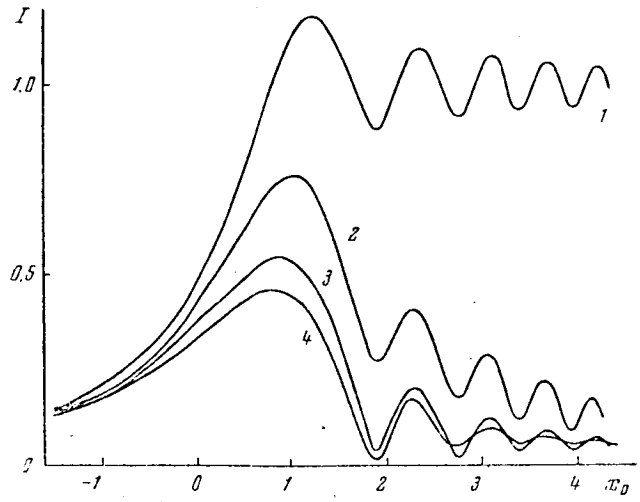

Fig. 2.1. Amplitude-Time-Dependent Characteristics of the Signals, Scattered in the Underdense Meteor Trails, at Values of the Parameter $\Delta = 8\pi^2 D \sqrt{R}/v\lambda^{3/2}$. 1- $\Delta = 0$; 2- $\Delta = 0.5$; 3- $\Delta = 1$; 4- $\Delta = 1.2$.

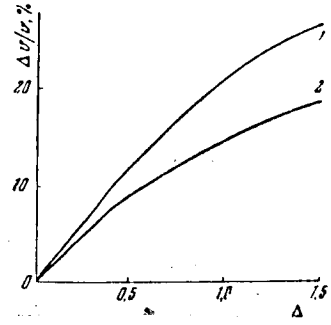

Fig. 2.2. Errors in the Determination of the Velocity of Meteors with the Aid of the Approximation Formula (2.32). 1- According to the AC zone; and 2- According to the AE zone.

In Fig. 2.2, we have presented the errors in the velocity found according to the zones AC and AE, which are introduced from the use of the approximation formula (2.32), at various Δ-values. At $\Delta = 0.5$, the error in velocity found in respect to the AC zone comprises 12%, and in respect to the AE zone it is 9%. At $v = 40$ km/sec, $R = 200$ km and $\lambda = 8$ m, the value $\Delta = 0.5$ corresponds to the height $h \approx 100$ km. According to the data contained in Tables 1.1 and 1.4, the average heights of the beginning of the intensive evaporation of the meteor bodies with $v = 40$ km/sec lie between 100 and 108 km. Thus, at utilization of Eq. (2.32), the radar measurements will yield, at the point of appearance of the faint meteors, the velocity values depressed by several km/sec. This effect was actually found during the radar observations conducted on meteors [89]. Usually, it is ascribed to the considerable braking of the small meteor bodies.

B. L. Kashcheyev and V. N. Lebedinets [76] measured, in respect to a large number of Frenel zones, the velocities for 10 meteors, forming underdense trails with varying Δ-values. They obtained a good agreement with Eq. (2.29). The errors ascribable to the use of Eq. (2.32) can be considerably

reduced if in the determination of the velocity, we do not utilize the position of the first maximum.

Equation (2.32) is also normally employed in finding the coefficient of ambipolar diffusion. According to (2.32), the amplitude of a reflected signal decreases exponentially with time. The duration of the reflection (time of reduction of amplitude by e times)

$$\tau = \frac{\lambda^2}{16\pi^2 D}. \tag{2.33}$$

According to the more precise formula (2.29), approximately the exponential decrease in the amplitude of a reflected signal with time occurs only at $\Delta < 0.5$, when the reflection of the radio waves from the meteor trails has a specular (mirror) nature.

At $\Delta > 2$, the expansion of the trail as a result of diffusion occurs so rapidly that in effect, the reflecting sector of the trail is displaced after the meteor body. In this case, we find the so-called front (head) echo. From (2.29) at $\Delta > 2$, we derive

$$I \approx \frac{1}{2} \frac{1}{\sqrt{(\pi x_0)^2 + \Delta^2}}. \tag{2.34}$$

In this manner, at $\Delta > 2$, the variation in amplitude with time occurs according to a parabola. In this case, a diffraction pattern does not occur.

At the values $0.5 < \Delta < 1.5$, the reflection initially has a specular nature, and then (the more quickly, the higher the Δ), converts to reflection from the head part of the trail. This is readily visible from Fig. 2.1. At $\Delta = 1$, the value of the coefficient of ambipolar diffusion, found according to the decrease with time of the amplitude of the reflected signal with the aid of Eq. (2.32), proves to be depressed by about 30%.

A study of the integral (2.29) indicates that the minimal duration of reflection (i.e. the time of reduction in the signal's amplitude by e times) for the underdense (unsaturated) trails is obtained at $\Delta = 1.2$. In this connection, the duration equals

$$\tau_{min} = 1.4 \frac{\sqrt{R\lambda}}{v}. \tag{2.35}$$

At $\lambda = 8$ m, $v = 40$ km/sec and $R = 200$ km, we derive $\tau_{min} = 0.04$. In this manner, at a frequency of pulse repetition of more than 100 - 200 cps, the noticeability of the faint meteors hardly depends on the repetition frequency.

In the derivation of Eqs. (2.28), (2.29), the following assumptions were made: 1) the linear electron density of the trail does not change perceptibly in the limits of several basic Frenel zones and 2) the electron concentration in the trail is sufficiently low so that we can overlook the weakening of the incident wave during passage through the trail. If even one of these assumptions is not fulfilled, Eqs. (2.28) - (2.31) become inaccurate.

Based on the external appearance of the actual amplitude-time characteristics of the reflected signals, it is often difficult to separate the underdense trails with an approximately constant α-value from the trails of the intermediate type or the trails with quickly changing linear electron

density. At the same time, it is very important to know how to distinguish the trails for which Eqs. (2128) - (2,31) are accurate, since only based on the measurements of such trails can we determine the parameters r_0 and D required for the physical theory of radio meteors. In [91], quantitative criteria were offered for such a selection.

According to (2,29), the ratios of the amplitudes at the moments of successive maximums of the diffraction pattern, and also the ratios of the distances between the various extremums depend only on Δ . The ratio of the amplitudes at the moments of the first and second maximums (Fig. 2,3) and the ratio AB/BC of the zones' lengths (Fig. 2,4) depend particularly greatly upon Δ. Thus, for each trail, we can find the Δ-value by three methods: Δ_1 - according to Eq. (2,24), measuring the drop in amplitude, velocity and range; Δ_2 -based on the ratio of the amplitudes at the moments of the first and second maximums; Δ_3 based on the ratio AB/BC of the zones' lengths. A condition of the applicability of Eqs. (2-28) - (2,31) is the equality $\Delta_1 = \Delta_2 \Delta_3$.

REFLECTION OF RADIO WAVES FROM DENSE (SATURATED) METEOR TRAILS

In the case of dense meteor trails, the electron concentration on the axis of the trail is higher than the critical $n_{e_{kr}}$ for the given frequency.

According to (2,3)

$$n_{e_{kr}} = \frac{\pi mc^2}{\lambda^2 e^2}. \tag{2,36}$$

From (1,243) and (2,36), let us find the distance r_e from the axis of the trail, at which $n_e = n_{e_{kr}}$:

$$r_c^2 = (4Dt + r_0^2) \ln \frac{\alpha \lambda^2 e^2}{\pi^2 mc^2 (4Dt + r_0^2)}. \tag{2,37}$$

If $r_c > \lambda/2\pi$, the incident wave does not penetrate into the trail and the reflection of the radio waves occurs from the boundary of the critical density in the trail. In a first approximation, the trail can be replaced by a metal cylinder with radius r_c. For an infinite metal cylinder with radius $r_c >>$, the effective reflecting surface

$$\sigma_c = \pi R r_c. \tag{2,38}$$

Then the strength of the signal, reflected from the dense meteor trail can be written

$$P_r = \frac{P_t G_t G_r \lambda^2 r_c}{64\pi^2 R^3}. \tag{2,39}$$

From (2,37), let us find the duration of the reflection as the time of reduction in the electron concentration on the trail's axis to the critical value:

$$\tau = \frac{\alpha \lambda^2}{4\pi^2 D} \frac{e^2}{mc^2} - \frac{r_0^2}{4D}. \tag{2,40}$$

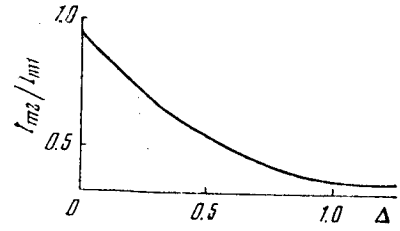

Fig. 2.3. Dependence on Δ of the Ratio of Amplitudes of a Signal Scattered by an Underdense Meteor Trail, at the Moments of the First and Second Maximums of the Diffraction Pattern.

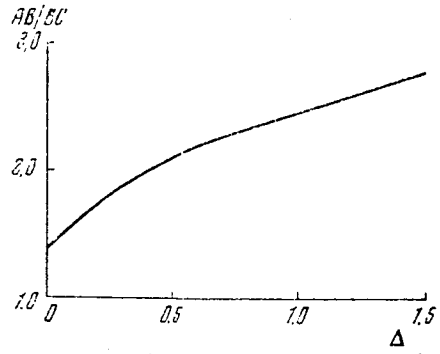

Fig. 2.4. Dependence on Δ of the Ratio AB/BC of the Lengths of the Frenel Zones.

Equating to zero the derivative from (2.37), let us find the time t_m, at which r_c reaches its maximal value:

$$t_m = \frac{\tau}{2,72} = \frac{\alpha\lambda^2}{10,9\pi^2 D}\frac{e^2}{mc^2} - \frac{r_0^2}{10,9D}. \qquad (2.41)$$

The maximal value of r_c

$$(r_c^2)_{\text{макс}} = \frac{\alpha\lambda^2}{2,72\pi^2}\frac{e^2}{mc^2}. \qquad (2.42)$$

From (2.39) and (2.42), we find the maximal value of the strength of the signal reflected from the dense meteor trail:

$$(P_r)_{\text{макс}} = \frac{P_t G_t G_r \lambda^3}{10^2\pi^3 R^3}\left(\frac{\alpha e^2}{mc^2}\right)^{1/2}. \qquad (2.43)$$

In the derivation of (2.43), we did not take into account the refraction of the radio waves. In the external part of the trail where the electron concentration is less than the critical. The allowance for the refraction of the radio waves can reduce the strength of the reflected signal by several times [92], however it does not affect the duration of the reflection. We also assumed that the decrease in the electron concentration in the trail occurs only as a result of the ambipolar diffusion. As was shown in the preceding chapter, in the case of the atomic ions, essentially this condition is fulfilled at $\tau < 10$ sec. At $\tau > 10$ sec, there begins to be reflected the influence of the overlooked factors: the adhesion (sticking) of the electrons, the expansion of the trail as a result of turbulent diffusion, and also the distortion of the trail by the turbulent motions in the atmosphere. All these factors have relatively little influence on the value of the maximum

amplitude of the reflected signal, however they can reduce by many times the duration of the reflection from the trails with $\alpha > 10^{14}$ electron/cm. Therefore, although according to Eq. (2.40) for the meteors -5^m--6^m, we could expect a duration of several hours, in reality, a duration of more than 200 - 300 sec never takes place.

INITIAL RADIUS OF IONIZED METEOR TRAILS

The initial radius of the ionized meteor trails can be measured directly from the radar observations. The value r_0 is found most simply from the simultaneous observations of the same underdense trails with two radar stations (sets) operating on different wave lengths: λ_1 and λ_2. Signifying by the indexes 1 and 2 all the data pertaining respectively to the first and the second radar station, from (2.31), we find the ratio of the maximal amplitudes of the signals registered by the two radar stations:

$$\frac{E_{r1}}{E_{r2}} = \left(\frac{P_{t1}G_{t1}G_{r1}\lambda_1^3}{P_{t2}G_{t2}G_{r2}\lambda_2^3}\right)^{1/2} \frac{\varphi_1(\Delta)}{\varphi_2(\Delta)} e^{4\pi^2 r_0^2\left(\frac{1}{\lambda_2^2}-\frac{1}{\lambda_1^2}\right)}. \qquad (2.44)$$

In the utilization of identical antennas, Eq. (2.44) is simplified somewhat. In this case

$$r_0 = \frac{\left[\frac{1}{2}\ln\frac{P_{t2}}{P_{t1}} + \ln\frac{E_{r1}}{E_{r2}} + \frac{3}{2}\ln\frac{\lambda_2}{\lambda_1} + \ln\varphi_2(\Delta) - \ln\varphi_1(\Delta)\right]^{1/2}}{2\pi\left(\frac{1}{\lambda_2^2}-\frac{1}{\lambda_1^2}\right)^{1/2}}. \qquad (2.45)$$

The relative error involved in the determination of r_0

$$\delta r_0 = \frac{\left\{(\delta E_{r1})^2 + (\delta E_{r2})^2 + \frac{1}{4}(\delta P_{t1})^2 + \frac{1}{4}(\delta P_{t2})^2 + \left[\delta\frac{\varphi_1(\Delta)}{\varphi_2(\Delta)}\right]^2 + \left[\delta\frac{G_1}{G_2}\right]^2\right\}^{1/2}}{8\pi^2\left(\frac{1}{\lambda_2^2}-\frac{1}{\lambda_1^2}\right)r_0^2}. \qquad (2.46)$$

In 1960, measurements were made of r_0 during parallel observations on the waves $\lambda_1 = 8$ m and $\lambda_2 = 4$ m [90]. For the reception and transmission in both radar sets, use was made of identical five-element wave channels. The identical condition of the directional diagrams of the antenna systems was established with an error of not more than $\pm$ 10% from special measurements of the diagrams and also were checked according to the ratios of the amplitudes for the meteors with a duration of reflection for λ_1 1 - 5 sec. In the process of measurements, we recorded continuously the strength of the transmitters. During each day of measurements, a set of standard calibrated signals was transmitted several times, based on which the amplitude characteristics of the receivers were constructed. These characteristics were used for monitoring their linearity (which is necessary in the measurement of the diffusion factor), and also for the conversion of the measured amplitudes of the signals to absolute units.

For each meteor, we measured R, D, P_{t_1}, P_{t_2}, E_{r_1}, E_{r_2}, and also the relative positions of all the extremums of the diffraction patterns and the ratios of the amplitudes at the moments of the successive maximums respectively to E_{r1} and E_{r2}. From several hundred meteors that were observed, we selected 39, for which there was fulfilled the condition of the applicability of Eqs. (2.28) - (2.31): $\Delta_1 = \Delta_2 = \Delta_3$.

As a result of the studies of the equipment, we obtained the following estimations of the accuracy of the measurements of the various parameters

$$|\delta P_{r1}| \leqslant 0.1, \quad |\delta P_{r2}| \leqslant 0.1, \quad |\delta E_{r1}| \leqslant 0.1,$$
$$\left|\delta \frac{G_1}{G_2}\right| \leqslant 0.1, \quad \left|\delta \frac{\varphi_1(\Delta)}{\varphi_2(\Delta)}\right| \leqslant 0.1. \qquad (2.47)$$

The accuracy of measuring the amplitude of the signal E_{r2} for $\lambda_2 = 4$ m depends on the value of the amplitude. At higher values for E_{r2} $|\delta E_{r2}| \leqslant 0.1$, and also at the least values for E_{r2}, which are still used for the measurements, $|\delta E_{r2}| \lesssim 0.3$.

From (2.46) and (2.47), we get:

at high values for E_{r2} $\quad \delta r_0 \pm \frac{0.06}{r_0^2}$,

at low values for E_{r2} $\quad \delta r_0 \pm \frac{0.11}{r_0^2}$, $\qquad (2.48)$

where R_o is expressed in meters.

According to (2.48), at $r_o = 0.5$ m, $\delta r_o = \pm 25\%$, while at $r_o = 1$ m, $\delta r_o = \pm 11\%$. At $r_o < 0.5$ m, the errors involved in measuring r_o increase quickly. At $r_o > 1$ m, the observations of the underdense trails for $\lambda_2 = 4$ m, become impossible as a result of the intensive decrease in the amplitude of the reflected signal. In this manner, the measurements of r_o were possible in the narrow range of values 0.5 - 1.0 m. The maximum reliance can be placed on the values of $r_o \approx 75$ cm, for which the measurement errors are not more than $\pm 0\%$.

For 39 selected meteors, we obtained the average value $r_o = 0.8$ m and the average values of the velocity and coefficient of ambipolar diffusion $v_o = 32$ km/sec and $D = 6.4$ m^2/sec.

Let us compare the results derived with the theory of the initial expansion of ionized meteor trails. According to (1.216), at $v_o = 32$ km/sec

$$r_0 = \frac{2.4 \cdot 10^{15}}{n}. \qquad (2.49)$$

According to the measurements carefully made by B. L. Kashcheyev [93], $D = 6.4$ m^2/sec corresponds to the height 93.5 km, while according to the measurements made by Greenhow and Hall [94, 95], it corresponds to a height of 95.5 km. According to [8], the concentration of molecules of the atmosphere at these heights equals respectively $n_1 = 3.9 \cdot 10^{13}$ cm^{-3} and $n_2 = 2.6 \cdot 10^{13}$ cm^{-3}. Assumming $D \sim n^{-1}$ and taking the average from the values for n_1 and n_2, we can represent the empirical dependence of n upon D by the following formula:

$$n = \frac{2 \cdot 10^{14}}{D}, \qquad (2.50)$$

where n is expressed in cm^{-3} and D in m^2/sec.

From (2.49) and (2.50) at $D = 6.4$ m^2/sec, we get the theoretical value $r_o = 0.77$ m, which agrees well with the measurement results. In Fig. 2.5, we have presented the values for r_o/D as a function of velocity for 39 observed meteors. The solid line indicates the measured dependence of r_o on v_o, while

the broken line indicates the theoretical relationship. We find a satisfactory agreement of the theoretical and measured dependences of r_o on v_o.

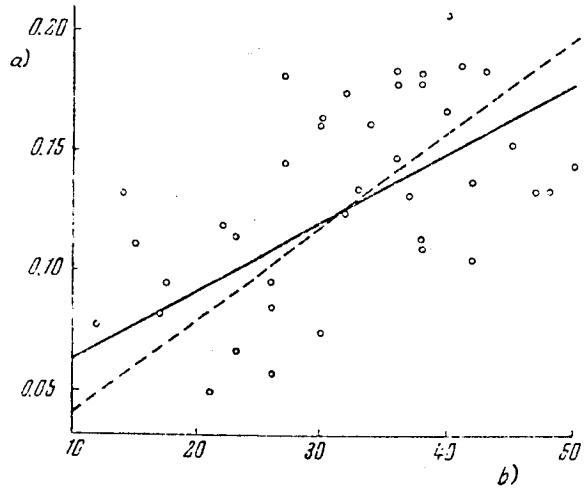

Fig. 2.5. Dependence of Initial Radius of Ionized Meteor Trails on Velocity of Meteors: solid line equals measured, broken line equals theoretical. Key to figure: a) r_o/D, sec/m; and b) v, km/sec.

Similar measurements of the initial radius of the ionized meteor trails were conducted by Greenhow and Hall [96] for the waves $\lambda_1 = 17$ m and $\lambda_2 = 8.3$ m. As was shown above, at such values of λ_1 and λ_2, the measurements of r_o are possible in the range from 1 to 2 m. The maximum rel ance can be placed on the values of r_o, close to 1.5 m. At $D = 14$ m^2/sec, Greenhow and Hall obtained the mean value $r_o = 155$ cm, which agrees satisfactorily with the measurements made by Kashcheyev and Lebedinets, and with the theory of the initial expansion of meteor trails [97].

Extending their measurements to a wide range of heights, and not applying the quantitative criteria for the selection of the underdense trails, Greenhow and Hall obtained a very slight dependence of r_o on D and the absence of a dependence of r_o on v_o. This result evidently should be explained by the use for the measurements of a large number of the trails of the intermediate type, to which Eq. (2.45) is inapplicable. As a result of the limited state of the sensitivity of the equipment at $r_o > 2$ m, the observations of the underdense trails for $\lambda_2 = 8.3$ m, were practically impossible; hence, in the case of the high and fast meteors, only the trails of the intermediate type could be registered. Since the faster meteors are simultaneously the higher ones, at this time, the dependence of r_o on v_o should be distorted with particular intensity.

I. V. Bayrachenko [90], using a technique suggested by Kashcheyev and Lebedinets, measured the initial radius of the ionized meteor trails for the waves $\lambda_1 = 9.6$ m and $\lambda_2 = 6.5$ m. For 50 underdense meteor trails, he obtained the following values: $v_o = 41$ km/sec, $D = 8.2$ m^2/sec and $r_o = 1.0$ m. According to (1.216), at $v_o = 41$ km/sec [see next page]

$$r_0 = \frac{3.1 \cdot 10^{15}}{n}. \qquad (2.51)$$

From (2.50) and (2.51), we obtain the theoretical value $r_o = 1.27$ m, which is only slightly more than the measured value. The relationship of r_o to the velocity of the meteors ($r_o \sim v_o^{0.79}$) proved to be somewhat weaker than the theoretical.

NOTICEABILITY OF RADIO METEORS

In the statistical processing of the results obtained from the radar measurements of meteors, the most complex is the consideration of the selectivity of the observations in relation to various parameters of the meteor bodies. The noticeability of the radio meteors can be represented in the form of the product of two co-factors: of the geometric factor $1/P_1$, characterizing the relative noticeability of meteors with varying coordinates of the radiants, and of the physical factor $1/p_2$ which expresses the relative noticeability of the meteors with varying velocities.

The strength of a radio signal reflected by an ionized meteor trail is a complex function of the parameters of the meteor body, forming the trail, the parameters of the radar set and of time. Since most of the observers, for the calculation of the maximal value of the strength of the signal, reflected from an underdense trail, in place of the precise Eq. (2.31) use the approximate Lovell-Clegg formula, let us introduce the concept of the effective linear electron density of the trail, $\alpha_{э\phi\phi}$. Let us define $\alpha_{э\phi\phi}$ in such a way that upon the substitution of $\alpha_{э\phi\phi}$ in place of in the Lovell-Clegg formula for the underdense trails, we would obtain Eq. (2.31), while for the dense trails, we would derive Eq. (2.43). From (2.1) and (2.31), we derive for the underdense trails:

$$\alpha_{э\phi\phi} = \alpha\varphi(\Delta)\, e^{-\left(\frac{2\pi r_0}{\lambda}\right)^2}. \qquad (2.52)$$

For the dense trails, from (2.1) and (2.43), we get

$$\alpha^2_{э\phi\phi} = 0{,}1 \left(\frac{mc^2}{e^2}\right)^{3/2} \alpha^{1/2}. \qquad (2.53)$$

The critical effective sensitivity of the radar set will be characterized by the minimal value of the effective linear electron density of the trails, which can be detected with a given radar set in the direction of maximal radiation, $\alpha^{мин}_{э\phi\phi}(\varphi_m, A_m)$ (where φ_m, A_m equals the angle of elevation and the azimuth of the direction of maximal radiation). From (2.1), we get

$$\alpha^{мин}_{э\phi\phi}(\varphi_m, A_m) = \left[\frac{32\pi^2 P_{r\,мин} R_m^3}{P_t G_{rm} G_{tm} \lambda^3}\right]^{1/2} \left(\frac{mc^2}{e^2}\right), \qquad (2.54)$$

where $P_{r\ min}$ equals the minimal strength of the signal being registered by the receiver; R_m equals the average range of the meteors, being registered in the direction of maximal radiation; G_{rm}, G_{tm} equals the coefficients of the directivity of the receiving and transmitting antennas for the direction of maximal radiation.

For the other directions being typified by the angle of elevation φ and the azimuth A, the value $\alpha^{мин}_{эфф}(\varphi, A)$, generally speaking will differ from $\alpha^{мин}_{эфф}(\varphi_m, A_m)$:

$$\alpha^{мин}_{эфф}(\varphi, A) = \frac{1}{K(\varphi, A)}\alpha^{мин}_{эфф}(\varphi_m, A_m). \qquad (2.55)$$

According to (2.1) and (2.54)

$$K(\varphi, A) = \frac{R_m^{1/2}G_r^{1/2}G_t^{1/2}}{R^{1/2}G_{rm}^{1/2}G_{tm}^{1/2}}, \qquad (2.56)$$

where G_r, G_t equal the coefficients of directivity of the antennas for the given direction (φ, A), R equals the average range of the meteors, being recorded at the angle of elevation φ.

With allowance for the random position of the point of the specular reflection in the meteor trail, the probability of the detection in the given direction of a trail formed by a meteor body with the mass M_0, velocity v_0 and zenith distance of the radiant z, is proportional to the length l of the trail's sector (M_0, v_0, z, $\alpha^{мин}_{эфф}$), at which $\alpha_{эфф} > \alpha^{мин}_{эфф}$. In the static investigation, the relative noticeability of the meteors with varying values for v_0 and z, being recorded in the given direction can be represented as follows:

$$\frac{1}{P_2} = \frac{1}{l_0}\int_0^\infty l(M_0, v_0, z, \alpha^{мин}_{эфф})\, n(M_0)\, dM_0, \qquad (2.57)$$

where l_0 equals a certain average length of meteor trails, n (M_0) equals the differential distribution of the meteor bodies by masses. The distribution of n (M_0) is usually represented in the form

$$n(M_0) = \frac{n_0}{M^s}, \qquad (2.58)$$

where n_0 and s are constants. Generally speaking, the values n_0 and s can vary somewhat for the various intervals of the masses of meteor bodies. The selection of l_0 is arbitrary and affects only the standardization of P_2. We will be interested mainly in the noticeability of the radio meteors weaker than $+3^m$, in which the difference in the heights of the beginning and end of the trail is around 15 km, therefore, let us assume $l_0 \cos z = 15$ km. P_2 is a function of $\alpha^{мин}_{эфф}$, v_0, z, λ and s. For the given radar set in the direction of the maximal radiation, P_2 depends only on v_0, z and s. For the other directions, P_2 also depends on K (φ, A).

For a calculation of the physical factor, it is necessary to know the dependence of the ionization factor on velocity $\beta(v)$, the dependence of the initial radius of the trail on velocity and height r_0 (v, h), and also the average heights and distribution of the ionization along the trails of the meteors, generated by the meteor bodies with various M_0, v_0 and z. The dependences of $\beta(v)$ and r_0 (v, h) were examined in detail above. As was indicated in Chapter 1, the heights of the beginning of the intensive evaporation of meteor bodies and the heights of the maximal evaporation, calculated with allowance for the heating of the meteor bodies prior to the inception of intensive evaporation and energy losses to heat radiation, on the average agree satisfactorily with the observations.

The distribution of the ionization along the trails of faint meteors was measured by Greenhow and Newfield [43]. A radar set was used on the wave $\lambda = 8$ m with one transmitter and two receiving points, separated by the distance $d = 20$ km. With such a base, the difference in the heights of the points of reflection in the trail Δh could vary within the limits from 0 to $d/4 = 5$ km. The average value $\Delta h = 4$ km. For each meteor, they measured the ratio of the maximal amplitudes of the signals registered in two receiving points, and then according to the Lovell-Clegg formula, they found the ratio of the linear electron densities in two points in the trail. They also measured the difference in the heights of the points of reflection in the trail, Δh.

For the trails, which were underdense in both reflecting points, by a statistical method, they obtained the average curve of the distribution of ionization along the trail. Greenhow and Newfield found a significant difference in the ionization curve, obtained by them, from the theoretical curve (1.32), being provided by the simplest physical theory of meteors: 1) the measured curve is considerably shorter than (1.32). The average difference in the heights of the beginning and end of the trail prove to be $h - h_k = 2.4$ H; 2) They found a very rapid change in α with height above h_m. According to (1.32), above h_m at $\Delta h = 4$ km α can not vary by more than two times. From the observations, considerably higher variations in α were obtained. In certain cases, at $\Delta h = 4$ km, α varies by 10 times.

The results obtained by Greenhow and Newfield agree well with the more precise physical theory of meteors, taking into account the heating of meteor bodies prior to the beginning of their intensive evaporation. There were basically measured the meteors $+5^m$ - $+7^m$, which are produced by the meteor bodies heating all the way through. According to (1.128), for such meteors, the difference of the heights of the beginning and end of the trail $h - h_k = 2.3$ H, which coincides practically with the measurement results. For the calculation of the linear electron density, Greenhow and Newfield used the Lovell-Clegg formula; hence, they measured the distribution, along the trail, not of α, but of $\alpha_{э\phi\phi}$. In Fig. 2.6, the distribution is shown of $\alpha_{\phi\phi}$ along the trail of the radio meteor $+5^m$ with $v_o = 40$ km/sec and $\cos z = 2/3$. The broken line shows the ionization curve (1.32), provided by the simplest physical theory of meteors. In the range of heights 99 - 95 km, $\alpha_{э\phi\phi}$ increases by 12 times (from $3 \cdot 10^{10}$ to $3.5 \cdot 10^{11}$ electron/cm). Above h_m, at $\Delta h = 4$ km, $\alpha_{э\phi\phi}$ varies by not less than 2.5 times. In the meteors with various M_o, v_o and z, the rate of the variation in $\alpha_{э\phi\phi}$ with height above h_m changes within wide limits. Below h_m, Greenhow and Newfield notice a satisfactory agreement of the ionization curve, which they obtained, with the theoretical curve (1.32). It is easy to observe that the theoretical curves (1.32) and (1.126) below h_m practically coincide.

In a number of cases, in the upper reflecting point, the trails were underdense, and in all they were lower by 2 - 3 km, and in the lower reflecting point they were dense (saturated). Measuring the duration of the reflection, we were able to estimate that the linear electron density of the trail in this connection increased by tens of times. As was indicated in Chapter 1, near the point of the inception of intensive evaporation, the rate of evaporation of a meteor body in the range of heights 2 - 3 km increases by about 2 orders of magnitude. The results obtained by Greenhow and Newfield for such "anomalous"

trails confirm that the transition from conditions of the heating of a meteor body to the conditions of its intensive evaporation occur very rapidly.

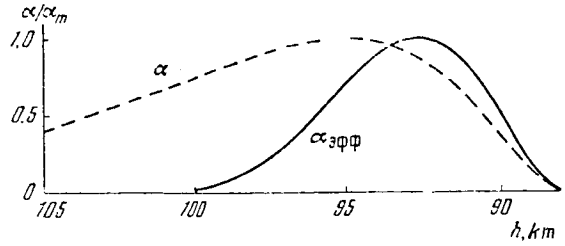

Fig. 2.6. Distribution of Linear Electron Density α and of Effective Linear Electron Density $\alpha_{э\phi\phi}$ Along the Trail of a Radio Meteor $+5^m$ with the Velocity $v_0 = 40$ km/sec.

A good agreement of the observed curves of the luminous intensity of the meteors brighter than 0^m with the theoretical, and also the agreement with the theory of the average distribution (obtained by Greenhow and Newfield) of the linear electron density along the trails of meteors fainter than $+5^m$, indicate that during the statistical studies, for the calculation of the distribution α along the trails of meteors, we can utilize the physical theory expounded in Chapter 1. The anomalies of the curves of the luminous intensity and the braking of the faint photographic meteors is evidently explained by the features of the evaporation of the meteor bodies producing them (the formation of an unstable drop of molten meteor substance, which under the effect of aerodynamic resistance is deformed or broken into parts) and pertain to a narrow range of stellar magnitudes of the meteors 0^m - $+4^m$. As was indicated in Chapter 1, these features do not affect the average heights of the appearance of meteors; for several kilometers, the height of the maximal luminous intensity increases, and leads to a considerable truncation of the meteor's trail.

We calculated the physical factor $1/P_2$ (v_0, z, $\alpha_{э\phi\phi}^{мин}$, λ, s) for a radar set, operating on the wave $\lambda = 8$ m, at various values of v_0, z and s for five values $\alpha_{э\phi\phi}^{мин}$: 10^{10}, $2 \cdot 10^{10}$, $5 \cdot 10^{10}$, 10^{11} and $2 \cdot 10^{11}$ electron/cm. In Fig. 2.7, we have shown the curves of P_2 (v_0), calculated at s = 2 and cos z = 2/3. For all the curves, we have assumed $P_2 = 1$ at $v_0 = 40$ km/sec. As is evident from the drawing, during the observations on the wave $\lambda = 8$ m with a high sensitivity radar set ($\alpha_{э\phi\phi}^{мин} = 10^{10}$ electron/cm), it is best of all to notice the meteors with the velocities 25 - 45 km/sec. At a lower sensitivity of the radar set ($\alpha_{э\phi\phi}^{мин} = 2 \cdot 10^{11}$ electron/cm), the maximum of the noticeability of the radio meteors displaces in the direction of the higher velocities: 40 - 50 km/sec. The poor noticeability of the slow meteors is connected with the low values of the ionization factor at low velocities. In the case of the fast meteors, we have an increase in the initial radii of the ionized meteor trails; according to (2.31), this leads to a decrease in the amplitudes of the signals scattered by the underdense trails. With an increase in the effective sensitivity of the radar set, we record the meteor bodies that are smaller and smaller, which evaporate at high altidue, and their trails have large initial radii. Therefore, with an increase in the effective sensitivity of the radar set, we have a deterioration in the relative noticeability of the fast meteors.

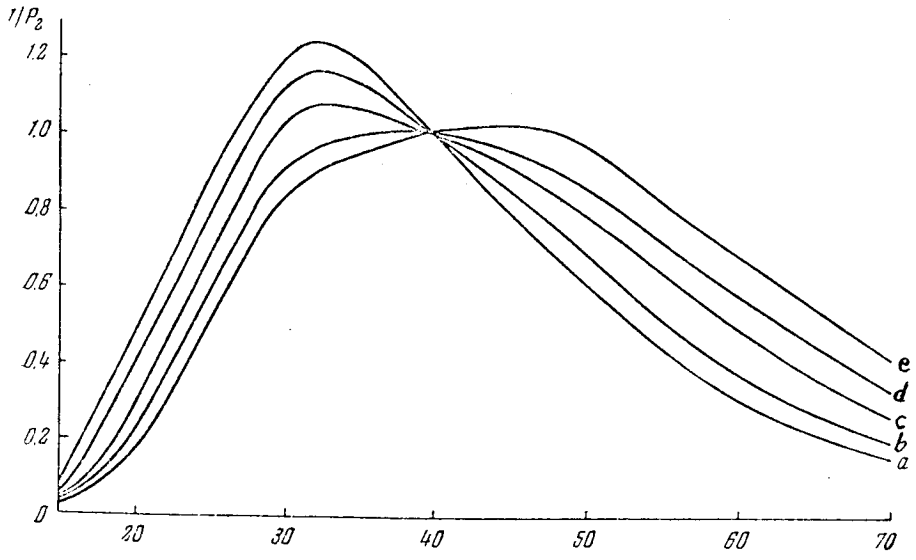

Fig. 2.7. Physical Factor for a Radar Set Operating on the Wave Length λ = 8 m at Various Values of $\alpha_{\text{эфф}}^{\text{мин}}$: a- 10^{10} ; b- $2 \cdot 10^{10}$; c- $5 \cdot 10^{10}$; d- 10^{11} ; e- $2 \cdot 10^{11}$ electron/cm. Key to figure: 1) v', km/sec.

Greenhow [98] in his estimation of the noticeability of radio meteors of various stellar magnitudes assumed that Eq. (1.26) of the simplest physical theory for the height h_m of the maximal evaporation is applicable in case of any masses of the meteor bodies. For the radio meteors $+15^m$ with v_o = 40 km/sec, he derived h_m = 128 km. At a height of 128 km, the initial radius of the trail is so large that even during operation with very powerful radar sets, the observations of such trails, according to Greenhow, are possible for only the waves $\lambda > 30$ m. Since the use of such low frequencies for the radar investigations of meteors is practically impossible (as a result of the high level of interference propagating through the ionosphere and also as a result of the reflection of radio waves from the ionosphere), Greenhow concluded that the radar studies of very faint meteors are practically impossible. This finding is the result of the utilization of the simplest physical theory of meteors which is not applicable to the weak meteors. According to (1.137), at v_o = 40 km/sec, the height of the maximal ionization for the radio meteors $+15^m$ and $+20^m$ is practically the same and equals h_m = 102 km. During the observations on the waves $\lambda > 12$ m, the noticeability of the weak radio meteors with v_o = 40 km/sec is limited only by the effective sensitivity of the radar set. Similarly, for the radio meteor $+15^m$ with a velocity v_o = 60 km/sec, from (1.137), we find the height h_m of maximal evaporation = 110 km, and not 138 km, as Greenhow suggested.

In the majority of the radio meteors being recorded on the waves 8 - 10 m, the points of the reflection lie in a narrow range of heights, 85 - 105 km. Let us assume that the central points of the sectors of the trails (accessible to observations) of all radio meteors lie at the height h_o = 95 km. For the antenna system of the given radar set on a horizontal surface, drawn at the height h_o, let us draw the line of equal values for K (φ , A) from 1.0 to a certain minimal value, K_{min}. In the calculation of the distance to the meteor

according to the given altitude and the angle of elevation, it is necessary to consider the curvature of the Earth's surface. At the same time, in the calculation of the areas of the sectors of the horizontal surface with a dimension of hundreds of kilometers, we can consider it to be flat.

According to the condition of the specular state of the reflection at the given position of the radiant of a meteor stream in the celestial sphere (A, z), the trails of the meteors in the stream can be reflected back to the radar set only as radio waves, being radiated in a plane perpendicular to the direction to the radiant, i.e. in an echo-plane. The intersection of the echo-plane with the line $K(\varphi, A) = K_{min}$ yields two points, the position of which will be assigned by the coordinates A, φ and by the horizontal range d - (A_1, φ_1, d_1) and (A_2, φ_2, d_2). In the observation of the given meteor stream, there can be recorded only those meteorsd the trajectories of which intersect the sector of the horizontal surface drawn at the height h_o, which has the form of a trapezoid with a central line connecting the points (A_1, φ_1, d_1) and (A_2, φ_2, d_2) and with the height l_o cosec z (where l_o equals the average length of the physical sectors of the trails of the meteor stream). The area of the trapezoid (the collecting surface of the radar set for the given position of the stream's radiant in the celestial sphere)

$$z(A, z) = l_0 \operatorname{cosec} z \sqrt{d_1^2 + d_2^2 - d_1 d_2 \cos(A_2 - A_1)}, \qquad (2.59)$$

where z equals the zenith distance of the stream's radiant in relation to the vertical line in the point of the appearance of the meteor (and not in the point of location of the radar set; the consideration of this circumstance becomes significant for the radiants close to the zenith).

In various parts of the viewing field of the radar set, the critical values of the effective linear electron density of the meteor trails $\alpha^{мин}_{э\,\phi\phi}$ being registered are dissimilar. Let us introduce the concept of the effective collecting surface of the radar set, $S_{э\,\phi\phi}$, for the given position of the stream's radiant in the following manner:

$$S_{э\phi\phi}(A, z, v_0) = l_0 \operatorname{cosec} z P_2(v, z, \varphi_m, A_m) \int_{(A_1, \varphi_1, d_1)}^{(A_2, \varphi_2, d_2)} \frac{ds}{P_2[v_0, z, K(\varphi, A)]}, \qquad (2.60)$$

where P_2 (v_o, z, φ_m, A_m) equals the physical factor for meteors with given v_o and z, occurring in a direction of maximal radiation. The integral is taken along the line connecting the points (A_1, φ_1, d_1) and (A_2, φ_2, d_2). For the given radar set, $S_{э\phi\phi}$ is a function of the coordinates of the stream's radiant, and also depends on the velocity of the meteors and on the parameter s of the distribution of meteor bodies in respect to mass.

If at the given position of the stream's radiant in the celestial sphere (A, z), in one second, on an average we register N meteors, the density of the stream of the meteor bodies, forming the ionized trails with the effective linear electron density $\alpha_{э\,\phi\phi} > \alpha_{э\,\phi\phi}(\varphi_m, A_m)$, equals

$$\frac{N}{S_{э\phi\phi}(A, z, v_0)\cos z}. \qquad (2.61)$$

In this connection, it is assumed that the sectors (available to observations) of the trails of all the meteors in the stream have the same length, l_0. As a result of the diurnal motion of the radiant in the celestial sphere, the effective collecting surface of the radar set for the meteors of a given stream varies continually. During the continuous round-the-clock observations, the value of the integral

$$F(\delta, v_0) = \int_0^{24^h} S_{эфф}(A, z, v_0) \cos z \, dt \qquad (2.62)$$

for the given meteor stream is a function of the decliniation of the stream's radiant δ and of the velocity of the meteors. Here t equals the hour angle of the stream's radiant. The function F (δ , v_0) characterizes the relative noticeability during the round-the-clock observations of the meteor streams with varying declinations of the radiants, but with the same velocities. F (δ , v_0) aas a fairly slight dependence on v_0. Let us consider the statistical meaning of the physical factor. Let us find the effective critical mass of the meteor bodies, the trails of which are being registered with the given radar set in the direction of maximal radiation, M_0*, in the following manner:

$$\int_{M_0^*}^{\infty} n(M_0)\, dM_0 = \frac{1}{l_0} \int_0^{\infty} l\,[M_0, v_0, z, \alpha_{эфф}^{мин}(\varphi_m, A_m)]\, n(M_0)\, dM_0. \qquad (2.63)$$

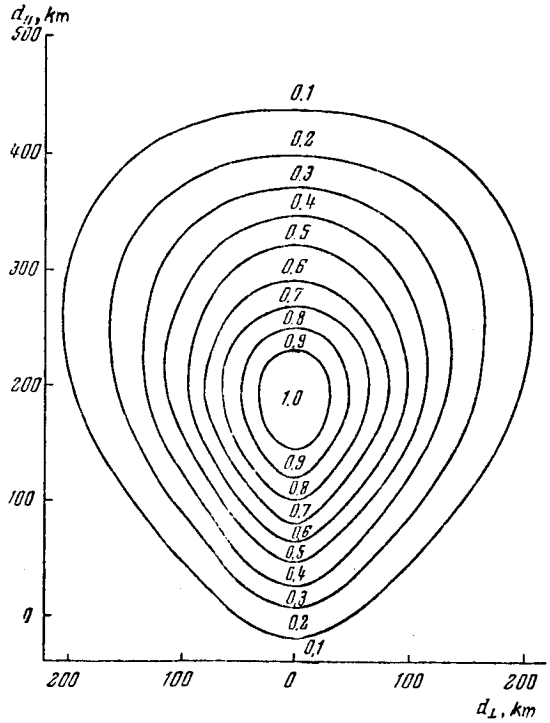

Fig. 2.8. Lines of Equal Sensitivity for the Radar Set at the Kharkov Polytechnical Institute, Drawn for a Horizontal Surface at the Height of 95 km.

For the given radar set, M_0* constitutes a function of v_0 and z, and also depends on the parameter s of the distribution of the meteor bodies in respect

to mass. From (2.57) and (2.63), we derive

$$\frac{1}{P_2(v_0, z)} = \int_{M_0^*}^{\infty} n(M_0)\, dM_0. \tag{2.64}$$

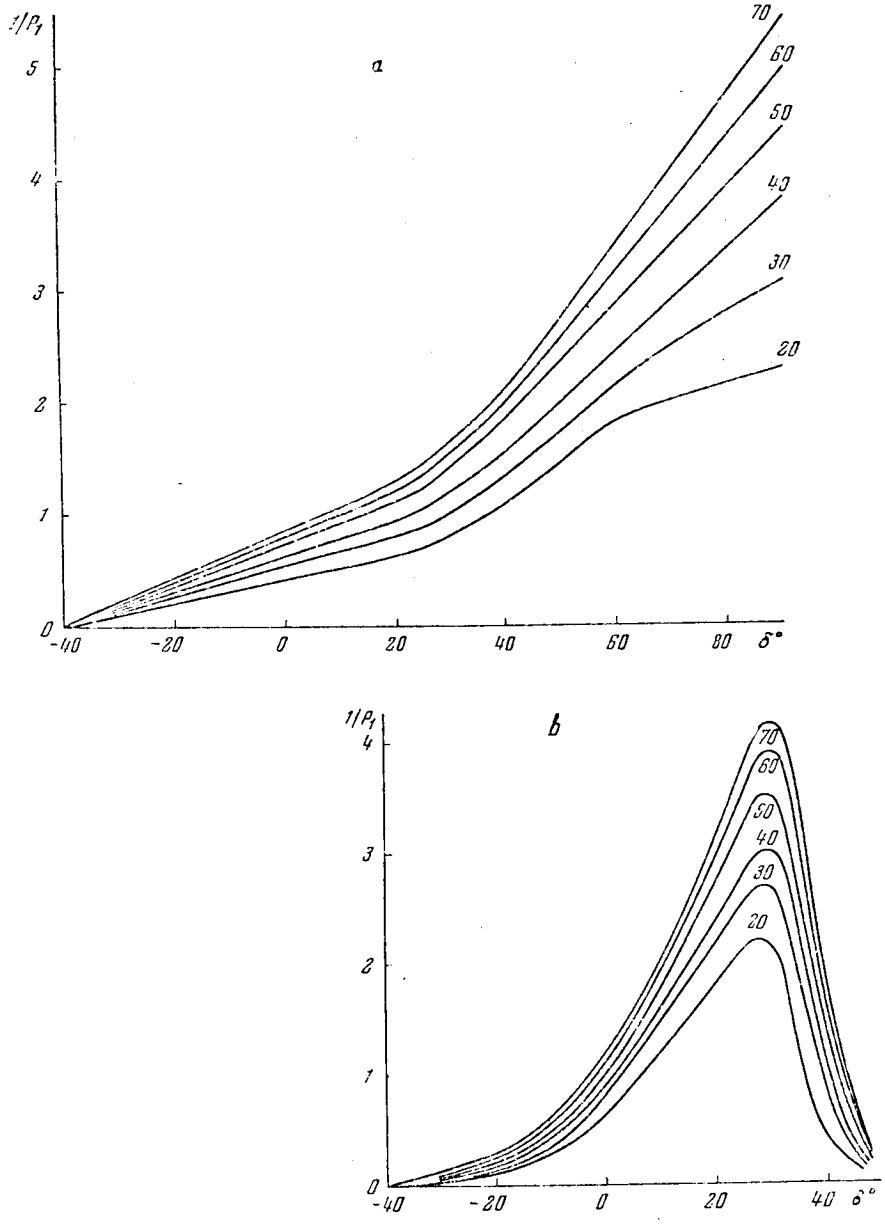

Fig. 2.9. Geometric Factor for Meteors with Varying Velocities (in km/sec). a- At orientation of the antenna toward the east; and b- toward the north.

From (2.58) and (2.64), we find

$$\frac{1}{P_2(v_0, z)} = \frac{n_0}{(s-1)} \times \frac{1}{M_0^{*s-1}} = N(M_0^*), \tag{2.65}$$

where N (M_o) equals the integral distribution of the meteor bodies in respect to mass.

At the given v_o, z and s, the value of the effective critical mass of the meteor bodies M_o* for the given radar set is determined unequivocally from (2.63). Let us signify the value M_o* at v_o = 40 km/sec and cos z = 2/3 $M_{пр}$. Let us select the constant n_o in (2.58) and (2.65) in such a way that for the given radar set at v_o = 40 km/sec and cos z = 2/3 P_2 (v_o, z) = 1. If N equals the number of radio meteors of the stream, registered in the course of the days during continuous observations, at any coordinates of the stream's radiant and at any velocity of the meteors, the density of the flow of meteor bodies with the masses $M_o > M_{пр}$ equals

$$\Phi(M_{пр}) = \frac{NP_2(v_0, z)}{F(\delta, v_0)} = NP_1(\delta, v_0) P_2(v_0, z), \qquad (2.66)$$

where

$$P_1(\delta, v_0) = \frac{1}{F(\delta, v_0)}. \qquad (2.67)$$

In the statistical studies of the distribution of the meteor bodies in respect to various parameters, assigning to the meteors the weights P_1 (δ, v_o) P_2 (v_o, z), we correct the results of the observations for the selectivity of the radar method and transfer from the visible distribution of the radio meteors to the distribution of meteor bodies with the masses $M_o > M_{пр}$. It is natural that in this connection, we can consider only those meteors, the radiants of which are usually visible above the horizon at the point of observation.

We calculated the effective collecting surfaces $S_{эфф}$ (A, z, v_o) and the weights P_1 (δ, v_o) for an antenna system, having been applied at the Kharkov Polytechnical Institute during the measurements of the population of meteors and during the measurements of the coordinates of the radiants and velocities of the meteors (refer to Chapter 4 for a description of the equipment). In Fig. 2.8, we have presented the lines of equal values for K (φ, A) from 1.0 to 0.1 on a horizontal surface, passing at the height h_o = = 95 km. On the y-axis, we have plotted the component of the horizontal range, parallel to the symmetry plane of the directivity diagram of the antenna of the system $d_{\parallel}$, and on the x-axis, we have shown the transverse component of the horizontal range $d_{\perp}$. The calculation of P_1 (δ, v_o) was conducted at various values for δ, v_o and s for two directions of the orientation of the antenna system, i.e. to the east and to the north. In Fig. 2.9, we have shown the relationship P_1 (δ) for two directions of orientation of the antenna system, calculated at s = 2 and at six different values of the velocity of the meteors.

CHAPTER 3

THE STUDY OF WINDS AND CERTAIN PARAMETERS OF THE EARTH'S ATMOSPHERE ACCORDING TO THE RADAR METEOR OBSERVATIONS

The meteor observations as a means for the study of the atmosphere have been used for a long time. As early as the nineteenth century, it was established that the drift of meteor trails occurs about horizontally with a velocity of several tens of meters per second. The meteors permitted us to establish the presence of a minimum of temperature at the height of 80 - 100 km.

Roughly since 1946, for a study of the parameters of the atmosphere, in the Soviet Union and in the USA, use began to be made of instruments established on the geophysical rockets [41], which in a number of cases permitted us to increase the accuracy of the measurements and to expand abruptly the boundaries in respect to altitude.

The investigation of winds in the upper atmosphere comprises one of the most important sections of modern geophysics. Experience has indicated that any method of observing the meteor trails (radar, photographic, visual) permits us to determine their drift. The area of the atmosphere in which meteor trails are observed will be called the meteor zone. The basic method of studying the winds based on the displacement of the meteor trails is the radio method. Experiments have demonstrated that in fact, no kind of anomalous processes in the upper atmosphere, including the ionospheric storms and the high-altitude atomic explosions exert any significant effect upon the radio observations of meteors [99].

We can expect that the displacement of an ionized meteor trail differs from the motion of the neutral air masses. The difference can originate owing to the effect of the Earth's magnetic field. Let us dwell in more detail on this question, having considerable significance for an analysis of the observational results.

A solution of the equation of motion of the neutral component of the weakly ionized gas leads to the following velocity values [85]:

$$U = -\frac{\lambda_1 \frac{\partial p}{\partial x} + \Omega \frac{\partial p}{\partial y}}{p(\lambda_1^2 + \Omega^2)}, \qquad (3.1)$$

$$V = -\frac{\lambda_1 \frac{\partial p}{\partial y} - \Omega \frac{\partial p}{\partial x}}{\rho(\lambda_1^2 + \Omega^2)}, \tag{3.2}$$

where $\lambda_1 = \frac{\sigma_1 H_z^2}{\rho c^2}$; $\Omega = 2\omega_z + \frac{\sigma_2 H_0 H_z}{\rho c^2}$; U and V equal the values ov the velocity components in the direction of north and east; σ_1 equals the conductivity of plasma in a direction across the magnetic field; σ_2 equals the Hall conductivity; ρ equals the density of the medium; c equals speed of light; $\omega_z = \omega_0 \sin\varphi$ equals the vertical component of the Earth's angular velocity at the latitude φ*; p equals the atmospheric pressure; x, y equals the axes of the coordinates, directed to the east and north; H_0 equals the Earth's magnetic field; $H_0 = 0.5 H_p \sqrt{1 + 3\sin^2\varphi}$; $H_z = -H_p \sin\varphi$; H_p equals the magnetic field strength at the pole. If we substitute the values σ_1, σ_2, ρ into Eqs. (3.1) and (3.2), then as was shown in [100, 101], up to the height 110 - 115 km, i.e. to the lower sector of the area E of the ionosphere, we can use the equations of the geostrophic wind:

$$U = -\frac{1}{2\rho\omega_z} \cdot \frac{\partial p}{\partial y}, \tag{3.3}$$

$$V = \frac{1}{2\rho\omega_z} \frac{\partial p}{\partial x}. \tag{3.4}$$

A geostrophic wind is the term used for the horizontal rectilinear motion of the atmosphere under the condition that the frictional forces can be disregarded. As is evident from (3.3) and (3.4), in the absence of the frictional forces, the movement of the air occurs under the effect of the baric gradient and of Coriolis force. For the northern hemisphere, the low pressure area during the circulation of the atmosphere will always remain on the left. The variations in the geostrophic wind with height are determined by the corresponding variation in the baric gradient; the latter is determined by the horizontal temperature distribution.

At the height h $\simeq$120 km, the deviation of the wind direction from the isobaric surfaces, i.e. the separation from the geostrophic wind is approximately 10 degrees. From the theory, it follows that the motions of the meteor trails being registered by a radio meteor have a geostrophic nature and can roughly be analyzed with the use of Eqs. (3.3) and (3.4).

The expounded theoretical concept to the effect that the velocities of drift practically coincide with the wind velocity has been confirmed experimentally. Since the magnetic field of the Earth is inclined at a wide angle to the horizon (for the latitude $\varphi = 50^\circ$, H = 0.46 Gaussian units, $H_y = 0.19$ Gauss, $H_x = 0$), it will cause both a horizontal and a vertical velocity component. At the same time, it is known that the average velocity in a vertical direction comprises ~1.5 m/sec, while in a horizontal direction it comprises tens of meters per second [102].

The primary reason causing the circulation of the atmosphere (in addition to the gravitational effect of the Sun), is the absorption and radiation of energy, being received by oxygen (and possibly nitrogen also) from the Sun. The experimental results indicate that the winds are subjected to regular short- and long-periodic perturbations, which more often have a local nature, and less often, a global nature.

The velocity of the winds in the meteor zone consists of the constant component (velocity of transport motion) and of periodic components, i.e. of diurnal, semidiurnal, 8- and 6-hourly ones. In addition, we find a quite definite annual pattern in the variation in the direction of the winds.

As yet, we do not have a sufficiently complete analysis of the circulation of the upper atmosphere at different heights. This problem is of considerable theoretical difficulty, and requires the accummulation of systematic experimental materials for the various altitudes at a large number of geographic points. So far, there are a number of theories, explaining only individually occurring phenomena (see below). Under such conditions, the role of the results, obtained experimentally for a given region of the upper atmosphere is increasing, and is of unquestioned interest.

Up to the present time, the systematic measurements of the drift of meteor trails have been conducted only at Manchester (53°N, 2°W), Adelaide (35°S, 139°E) and Kharkov (49,4°N, 37°E). In addition, the cycle of radar observations of the trails was conducted in the Antarctic at Mawson. The program of the International Year of the Quiet Sun (1964 - 1965) envisaged a considerable expansion of this type of measurements. The study of the atmosphere is conducted by various methods, including with the aid of rockets and artificial Earth satellites [103, 104]. The meteor studies permit us to determine the height of a homogeneous atmosphere, the diffusion factor, and permit us to calculate the atmospheric density. Comprising a relatively simple and inexpensive method, the meteor observations evidently will find a certain application for finding the qualities of the atmosphere. Let us note that in spite of the apparent extensive data obtained with the aid of rockets, the data concerning the atmosphere at the height of 90 - 100 km, i.e., in the meteor zone to a known degree nevertheless will remain speculative [see, for example, 104].

In recent years in Manchester and Kharkov, a study has been made of the eddy nature of the motion of the atmosphere in the meteor zone [105]. The turbulent state is typical for a meteor zone at least up to the height of about 100 km. Initially, this was established experimentally based on the observations of the diffusion of meteor trails of long duration; the diffusion occurs with a rate which is several times greater than follows from the values of the molecular diffusion.

WINDS IN THE UPPER ATMOSPHERE. METHODS OF INVESTIGATION.

The displacements occurring in the upper layers of the atmosphere can be studied both by direct and by indirect methods. Most of the methods being applied for this purpose in the meteor zone pertain to the indirect methods. Indeed, the first information in general concerning the winds at the height of several tens of kilometers was obtained based on the observations of the Noctilucent clouds ($h \approx 82$ km) and of the bright meteors.

In the upper atmosphere, a circulation of two types exists; the first, when the energy source is situated directly in the upper layers; the second, when the motion occurs owing to the transfer of energy from the lower atmosphere. The temperature gradients (horizontal and vertical) are the direct cause of the

development of winds. In this connection, there takes place a transport of heat from the areas with high to the areas with the decreased temperature.

The Noctilucent clouds can be observed within several hours after sunset and before sunrise, when the clouds are illuminated by the sun's rays because of the horizon. In this connection, in most cases, it is difficult to conduct basic measurements for the finding of the velocity vector of the clouds' motion, and therefore only an estimation of the value is conducted.

The visual and photographic observations of meteors provide broader possibilities than do the observations of the noctilucent clouds, since they occur much more often, and the meteor trail has fairly clearly defined boundaries, permitting one to conduct wind measurements. We are aware of the excellent observations by Whipple [106], I. S. Astapovich [39] and others, permitting us to determine the wind speed at a height of 80 - 110 km. Usually, the velocity field is studied on the basis of the photographs of the bright meteor trails, occurring in minutes. Many measurements (for example, [106]) possessed a relatively high accuracy. The wind speed in a direction to the normal to the trail during the observations for a period of 0.5 sec, was determined with an accuracy not over 10 m/sec. With the possibility of obtaining a group of photographs of the trail at a two second interval, the error involved in determining the velocity dropped to about 4 - 2 m/sec. The complete determination of the velocity vector of the wind requires the photographing of the trail from two - three observation stations simultaneously.

The photographic observations of the brilliant meteor trails yield very valuable information concerning the velocity field of the winds, at the same time encompassing a layer of the atmosphere up to 30 - 35 km. Let us note that the observations can be conducted successfully, utilizing fairly simple cameras [107]. Obtaining, based on the bright meteors, data concerning the motion of the atmosphere, one should take into account that for the meteor zone, as will be demonstrated below, it is typical to have developed turbulent motions. The Reynolds number lies in the range 10^3 - 10^5 [106]. Naturally, it is impossible to obtain patterns of the atmospheric circulation based on individual successful measurements.

In the upper part of the meteor zone (~ 100 - 120 km), the motions of the atmosphere can be studied based on the measurements of the displacement of sporadic formations, $E_{c\,n\,op}$ or according to the motion of the heterogeneities of the ionization in the E-region of the ionosphere. In this region, the motion can be analyzed with the aid of Eq. (3.1) and (3.2).

The appearance of the sporadic layer $E_{c\,n\,op}$, as follows from the name itself, is random. One of the causes for the formation of this layer consists of the fine meteor bodies, evaporating at a height of 100 - 110 km [108, 109]. The ionization potential of the part of the meteor atoms below the ionization potential N_2, O_2 and O, and therefore the photoionization, can lead to an increase in the number of charged particles at the corresponding height. The presence of a high concentration of ions of Ca^+, Mg^+, Fe^+, Ni^+, was confirmed during the rocket measurements [33].

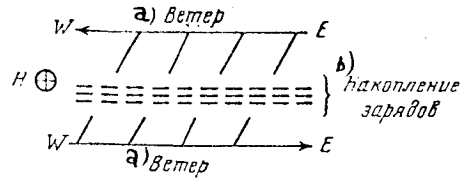

Fig. 3.1. Schematic Diagram of the Formation of the Regions of Increased Ionization During the Variously-Directed Horizontal Motions of the Atmosphere. H- direction of magnetic field. Key to figure: a) wind; and b) accumulation of charges.

The formation of $E_{спор}$ is also sometimes associated with the atmospheric motion. The variation in the wind direction with height, the presence of fixed, fairly clearly outlined layers in respect to altitude, at the boundaries of which the wind has opposite directions, can lead to the development of $E_{спор}$ [110, 111]. Such a process of the origination of a region of increased ionization can be explained as follows. Let us assume that we are considering the upper atmosphere at the magnetic equator (Fig. 3.1, view from the south toward the equator). The motion of the wind eastward brings the positive ions into motion in an easterly direction, wherein the interaction is achieved by means of collisions. The Lorentz forces tend to change the direction of motion. The head wind at a great height brings the ions into motion in an opposite direction. As a result, as this is indicated in Fig. 3.1, between the two layers under consideration, charges accumulate. The electrons tend to follow the ions under the effect of the resultant of the electric field. It is natural that the survey presented is quite approximate. However, the complex nature of the motion of the atmosphere at a different height, the horizontal state of this motion can lead to the accumulation of charges, similar to what has been described.

Most of the meteor trails at the radar stations are observed at a height of 93 - 95 km. This is the zone of eddy motions. In this zone, the formation of $E_{спор}$ similar to the pattern just described is evidently of slight probability. According to the recent reports [111], the height of 100 km can be considered as the upper boundary of developed turbulence. Hines indicates that this occurs as a result of displacing small-scale internal gravitational waves and their unstabilizing effect.

For a study of the motion of heterogeneous ionization in the E-region, use is made of the method of spaced reception of radio signals, reflected from the ionosphere. The reflection of the radio waves occurs most often at the altitude of about 110 - 120 km. An analysis of the system of the electrodynamic equations for an incompletely ionized gas indicates that the motion of the heterogeneities of the ionization can differ significantly from the motion of the neutral air masses.

A study of the motion of the heterogeneities of the ionization is a very common technique, which has been applied during the International Quiet Sun Year (IQSY) (the D_1-method). The method is simple and does not require any special equipment. However, in addition to the indicated appreciable disadvantage (the motion of the heterogeneities will not always typify the wind), there are others as well. Let us consider them.

The nature of the fluctuation of the signals received at scattered points can be greatly distorted owing to the polarization feeding of the usual and unusual components. For the exclusion of this effect, usually at the middle latitudes, it is recommended that measurements be conducted at a frequency of 2,2 $\pm$ 0,2 mc, i.e. at a frequency close to the gyromagnetic, when the unusual component is lacking. If we follow this recommendation, we are required to use a station (set) with a power of tens of kilowatts in a pulse for obtaining data concerning the drift during the daytime (near noon, an intensive absorption takes place).

The measurements of the drift of the ionization heterogeneities in the E-region with the application of a polarimeter, constructed in Kharkov, permitted us to obtain recommendations on increasing the results' reliability [112, 113]. These measurements indicated that at the latitude of Kharkov, the unusual component is absent during the day up to the frequency of 3 mc, with the same probability as at a frequency of 2,4 mc.

Basically, the E-region is typical for the daytime. During the night, the density of the electrons in this region decreases sharply, and in effect prevents us from conducting observations: the diurnal pattern of the drift can not be obtained. It is also difficult to obtain extensive data for the daytime, since frequently the reflections from the E-region has a mirror nature; the method of spaced reception in these cases does not permit us to analyze the drift.

The method of spaced reception characterizes the motion of all of the heterogeneities located at the level of radio waves which is lower than that at which reflection takes place. Strictly speaking, we can in no way determine precisely to which height we should relate the measurements. The observations of the bright meteor trails and of sodium clouds demonstrated that at h 100 - 120 km, the velocity gradient in respect to height can reach several tens of m/sec km.

In a processing of the results of the measurements by the D_1 method, a difficulty develops in the reliable determination of the shifts in respect to time. In reality, the individual time-dependent displacements undergo changes within broad limits for a short period, and the points T_x - T_y in the diagram are not located along a straight line (T_x - T_y are time displacements occurring respectively at E - W and N - S directions, in the recordings of the amplitude-time or phase-time registrations). The wide spread in the points in the diagram basically occurs owing to the variation in orientation of the line for the amplitudes' maximum; in addition, the effect of the chaotic variation in the diffraction curve is quite perceptible.

The winds up to a height of about 95 km can be studied according to the explosions of grenades, ejected from rockets [114, 115]. The presence of a horizontal wind will be reflected in the propagation of a sound wave caused by the explosion: there appears an additional horizontal displacement of the wave during its propagation to the Earth. The modern sound-measuring techniques do not permit us to detect simply and reliably the sounds of the explosions at a great height.

The wind-related measurements can be conducted based on the observations of the motion of artificial clouds made of vapors of sodium and cesium, being created with the aid of rockets at a varying altitude [116 - 118]. The artificial cloud is simultaneously photographed from the stations, spread over a distance of several tens or hundreds of kilometers. Studying a cloud from three scattered points, encompassing a large range of heights, we determine the direction of the wind, and the value of its velocity. With such observations, at the appropriate height we can determine the diffusion factor.

At a height of 60 - 110 km, the wind speed was determined according to the displacement of the trail forming in the sector of the launching of the rocket during the operation of the engines [119].

Up to a height of 90 km, we conducted an observation of the strips of aluminum foil ejected from rockets [120]. The radar sets permit us to determine the angle of drift and the time required for the descent of the strips to a certain height. However, in the upper atmosphere where the pressure is low, while the motion of the atmosphere is basically horizontal, such a method causes a considerable error. The rate of fall of the strips decreases in inverse proportion to the pressure of the atmosphere; we find a considerable horizontal and vertical dispersion of the strips.

The rockets permit us to measure the speed and direction of the wind according to the angle of attack [121]. Such measurements were conducted to a height of 60 km, however the opinion has been expressed that an improvement in equipment will permit us to obtain actual profiles up to a greater height.

The application of rockets expands the possibilities of studying the winds at various times of the day, including fairly large sectors in respect to altitude.

The brief survey given of the techniques used in a study of the atmospheric circulation confirms that the radio observations of meteors are a basic source of information concerning the motion of the atmosphere in the meteor zone. Tens and hundreds of values of the velocity, being obtained hourly at any time of day and year with the aid of one radar complex of equipment, permit us to reproduce reliably the pattern of the motion of the atmosphere at a height of 90 - 100 km.

MEASUREMENTS OF THE DRIFT OF METEOR TRAILS WITH RADIO METHOD

The measurement of the drift of meteor trails by the radio method in effect can be conducted only by way of finding the Doppler shift of frequency, F_D:

$$F_D = \frac{2V_R}{\lambda}, \tag{3.5}$$

where V_R equals the radial component of the drift speed. The determination of the drift rate based on the variation in the distance is difficult, since the reflections of the radio waves from the trails usually occur only for tenths of a second and at an average drift rate of 30 - 40 m/sec, the change in the distance will occur for several meters; the distance to the trail $R \approx$ $\approx$ 200 - 300 km. In the case of the registration of a prolonged reflection

from a dense trail, owing to the distortion of the trail by the eddy motions, new reflecting centers can develop, corresponding to the conditions of the mirror state, or the old reflecting centers will be displaced. The error in calculating the velocity value in this case is also high.

The separation of the Doppler frequency can be conducted either under conditions of the generation of continuous oscillations, or under pulse conditions. The first method has been used for many years in Adelaide [122], while the second has been used in Manchester and Kharkov [123 - 125]. Without going into an analysis of a comparison of the two common types of radar, let us only remark that the pulse method does not require the spreading of the transmitter and receiver; the effect of the moving objects (aircraft, etc.) does not represent any serious operational interference for them. In the pulse, more accurately the pulse-coherent, method, considerable difficulties are represented by the development of the transmitting device (with a master quartz heterodyne) with an output power of around 100 kw in the pulse. The development of a transmitter up to tenuous radiation with the same average power as the pulse type is simple. A simultaneous narrowing of the passband of the receiver permits us to maintain the number (population) of the meteors being recorded. For a determination of the distance to a meteor, use is made of auxiliary equipment (refer to Chapter 4).

A second variant of the pulse system is possible, namely the utilization of self-excited generator, in which the Doppler oscillations are developed owing to the capture of the frequency of the low-power reference oscillator in the receiving-recording device. Under careful engineering development, such a system is promising; it should be more simple in manufacture than the models of the pulse-coherent systems which have been used until recently in meteor research.

The finding of the Doppler frequency can be conducted, as is shown in the present chapter, based on the signal at the output of the phase detector. The signal reflected from the meteor trail, being displaced by the wind, rotates relative to a certain initial reference signal at the angular velocity $\Omega_D = 2\pi F_D$. If the period of the Doppler oscillations is less than the time of recording the reflection from the trail, the finding of the radial velocity component of the wind does not represent any difficulties. In the case of slight changes of frequency, we can proceed as follows. We determine the position of the vector (of the signal) at the time moments t_1 and t_2. During the time $(t_2 - t_1)$, the vector will turn by the angle $\psi = \psi_2 - \psi_1 = \Omega_D (t_2 - t_1)$. The error involved in determining the radial velocity component will actually be determined by the error in determining the angles ψ_1 and ψ_2. The angle ψ can be considerably less than 2π.

Up to the present time, we can by no means consider as solved the question of the measurement, with sufficient accuracy, of the height of occurrence of the meteor trail which is being registered. The amplitude method, having been used during the period of the IGY, of finding the angle of elevation with the aid of two dipoles yields an error not less than $\pm$ (3 - 5) km in the working sector. This error does not permit us to conduct a high-altitude analysis of the distribution of the winds. The amplitude-phase method suggested at the Kharkov Polytechnical Institute decreases considerably the measurement error [126], but it requires a further improvement of the accuracy and simplification of processing the results. The phase technique [176, 209] is promising.

Pulse-Coherent Method of Radio Observations of the Movement of Meteor Trails

The operating principle of a radar set, selecting moving targets, is well known. Comparing the frequency of highly-stable oscillations (being emitted) with the frequency of a signal reflected from a meteor trail, based on Eq. (3.5), we find the radial drift rate. It is known that the momentary instability of quartz is a very low value. In the equipment used for a study of the drift of the trails, most of the trails occur for not longer than 100 - 150 millisecs (on the wave of about 8 meters). The variation in the reference frequency, as experience has shown, during this time does not exceed several hundredths of cps, and usually is not taken into account in calculating the error in the drift measurement.

The observations of the meteors are most often conducted in the 6 - 10 meter waves [127]. In case of a truncation of the wave, the number of the meteors being observed decreases, as does the duration of their observation (Chapter 2); at $\lambda > (10 - 12)$, m, powerful interferences develop owing to the reflection from various heterogeneities of the ionization in the ionosphere. In addition, in the waves of the meter band, a major part is played by the cosmic noises, greatly exceeding the internal noise of the receiver. In the range $\lambda = 3 - 12$ m, the effective temperature of the antenna, corresponding to the upper level of the cosmic and atmospheric jamming, $T_a \sim \lambda^2/3$.

The selection of the working length of a wave and of other parameters of the equipment is discussed in detail in the literature (for example, [33, 111]). For practical purposes, for measuring the drift of the meteor trails at pulse power of the transmitter $P_{\text{ип}} \sim 100$ kw, the pulse repetition rate $F > 200$ cps, the gain factor of the antenna is about 15 - 20, the sensitivity of the receiving device $P_{\text{пр}} \simeq 10^{-13}$ watts, it is feasible to utilize $\lambda = 8 - 13$ m.

In a measurement of the drift of meteor trails, it is necessary to conduct a recording of the range to the trail, of the phase-time and amplitude-time (for finding the height) characteristics of the received signals. Use is made of the driven sweep with a duration of 0.15 - 0.3 sec. As soon as the signal exceeds the level of the noise and is recognized by the system for shielding against interference, it should trigger the generator of the saw-tooth pulses of the indicated duration.

The images from the screens of the cathode-ray tubes are photographed on film. Ordinarily, use is made of a frame-by-frame system of registration, with automatic control of the film feed. Sometimes use is made of the recording of the amplitude and phase characteristics of the signals on continually moving film. In this case, the consumption of film is decreased by way of the line-by-line scanning of the signal across a relatively slowly moving film. In the equipment intended for the study of wind, use is usually made of measures for recording only the "mirror" arranged trails (see below), therefore, the second method is unsuitable.

The presence of a large amount of interference of different kinds requires the mandatory application of effective measures for shielding the recorder. In the frame-by-frame system of recording, these requirements are especially rigid, since each signal received will lead to a spurious activation of the

camera. The work experience gained during the IGY indicated the feasibility of the simultaneous application of several types of shielding (in respect to code, repetition rate and duration of pulse. Success was achieved in using a system of shielding, utilizing the difference in the spectral composition of the pulse of a radar set and of the interference [128]. In addition, the stations for observing the meteors were located far from the sources of industrial interference, under field conditions. The driven condition of the operation of the equipment, the fairly wide diversity of the forms, occurring in practice, of the amplitude and phase characteristics of the received signals, the attempt to obtain the maximally accessible data led to the situation that the shielding from interference had to be reliable and flexible. Considerable difficulties are developed during the summer by the atmospheric interference during thunderstorms and the passage of carrier frequencies and the harmonics of radio broadcasting stations owing to the reflection from the sporadic layer, $E_{c\,\pi\,op}$. At the high latitudes, the intensive reflections from the polar aurorae are added.

The coherent equipment for measuring the movement of meteor trails by the radio method consists of: a) a transmitter, b) an antenna-feeder device, and c) systems of shielding from interference, of a receiving-recording device, and of an altimeter. Let us consider the functional systems of the devices, their technical specifications, having taken as a basis the operating equipment at the Kharkov Polytechnical Institute, intended for measuring the drift of meteor trails.

Transmitting Device

The highly-stable oscillations, necessary under the coherent method, are developed by the quartz heterodyne (Fig. 3.2). The heterodyne operates under continuous conditions at the frequency of 6.15 mc (frequency of quartz). On the one hand, it constitutes a master oscillator of a powerful transmitting device, and on the other hand it comprises a source of a reference signal fed to the phase channel of the receiver.

The pulse exciter of the transmitting device, for increasing the stability of operation, is separated in an individual unit. It is carefully shielded and comprises a fully autonomous system. The exciter develops the radio pulses with a duration of 10 microsecs with a carrier frequency of 36.9 mc. The exciter consists of three main types of circuits: a) circuits, operating under continuous conditions, b) forming pulse circuits, and c) terminal pulse amplifier of the exciter. In the continuous conditions, as already noted, there operate a master heterodyne, a tripler and a doubler of the frequency. For increasing the stability of the frequency of oscillations, all these circuits are placed under eased (favored) conditions; their oscillatory power is low. To the receiver, a signal with a frequency of 6.15 mc is fed through an attenuator.

The necessity for the thermostatic control of the quartz in effect is eliminated owing to the short period of the entire cycle: transmission-reflection from trails-reception.

In the forming pulse circuit, the transformation of the narrow pulses, entering from the synchro generator, to pulses with a duration of 10 microsecs takes place. This is achieved with the aid of a kipp-relay, feeding in the output the square pulses of positive polarity. From the kipp-relay, the pulses

arrive at the pulse amplifier, and from it, as modulating pulses, they arrive at the output stage of the power amplifier of the exciter, mounted on the tube GU- 29. The oscillations are tapped from the pulse amplifier by a symmetric cable of type RD - 16 and are fed to the first stage of the powerful amplifiers (GI - 30).

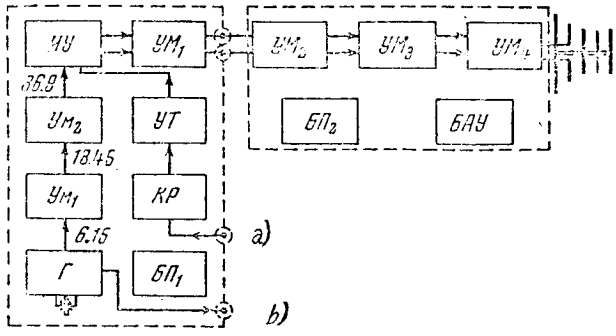

Fig. 3.2. Functional Diagram of the Transmitting Device. Г = quartz heterodyne, $У_{М1, 2}$ = the multipliers; ИУ = the pulse amplifier; KP = the Kipp relay; УТ = the current amplifier; $У_{М_1, 2, 3, 4}$ = the power amplifiers; $БП_{1, 2}$ = the power supply units; БАУ = the unit for the control automation devices. Key to figure: a) 500 cps + 100 cps from the synchro-generators; and b) 6.15 mc, reference signal.

The circuits of the powerful amplifiers consist of three two cycle stages connected in-parallel. The loads in the stages consist of meshes with concentrated constants, with frequency trim owing to the variation in the inductance (the frequency trim is necessary during the changing of the tubes and in other cases). The normal working position of the tubes is blocked, for reducing the average power of the supply units (the stages $У_{М_1, 2, 3, 4}$ are blocked in respect to the control grid).

The necessity of avoiding the stray frequency modulation of a radio pulse, which is quite important in the coherent method, requires the intelligent selection of the parameters L and C of the meshes. The circuits (meshes) provide a wide passband of the frequencies, by the same token, the time is decreased for the transient processes at the beginning and end of each radio pulse. The equivalent resistance of such circuits is low. In this case, the phase of a large part of a pulse is connected rigidly with the phase of the oscillations of the master heterodyne. For the indicated conditions of operation, a selection is made of the type of tubes, providing the largest possible gain factor in respect to power. For example, in the first stage, GI - 30, with about a tenfold power gain, in the second GM I - 83, with the same gain, in the third, the G - 481 with a controlled gain factor up to 4 - 5 (in respect to power). The excitation in the last stage is fed to the cathode oscillatory system. The power at the output of the final stage can be controlled by altering the anode voltage and attains about (100 - 120) kw in the pulse.

Considerable attention should be diverted to the design of the circuits of the powerful amplifiers, in order to avoid self-excitation and to maintain the stability of oscillations.

The basic specifications of the described transmitting device [129] are as follows.

1) Power in the pulse up to 100 kw.
2) Pulse duration equals 10 microsecs.
3) Repetition rate of the basic sequence of pulses equals 500 cps.
4) Repetition rate of the coding sequence of the pulses 100 cps.
5) Displacement in time between the basic and coding sequence equals 167 microsecs.
6) The shape of the pulse si square, the duration of the leading and trailing edges is less than one microsec.
7) Stability of the amplitude of the radiated pulses during a period of the feeding emf (0,02 sec) not worse than 2.5%.
8) Momentary instability of the carrier frequency of oscillations about 10^{-8} .

Antenna-Feeder Devices

The measurement of the drift is conducted in sequence in two directions: N- S- and E-W. This requires either rotating antennas or two antenna systems oriented in different directions.

The attempt to simplify the equipment for measuring the winds usually reduces to the situation that the azimuthal position of the meteor trail being recorded is not determined. In the utilization of sufficiently directed antennas, it is considered that the azimuth of the target roughly coincides with the azimuth of the main lobe of the directivity pattern.

In the meter band, the maximum use is found by the antennas of the "wave channel" type. If use is made of the single wave channel, the number of elements is taken at 3 - 5. Usually, we do not take more than five elements owing to the large sizes of the antenna and the relatively slight improvement in the parameters of the antenna with an increase in the directors above three. The coefficient of directed effect of the single channels that are being used equals roughly 10 - 15. The major error in determining the value of the zonal or meridional component of the wind velocity owing to the width of the directivity diagram (the five-element wave channel in a horizontal plane at the level of three db has a lobe width of 50 degrees) requires the application of more highly directed antennas. Usually, this is a system of cophased horizontal wave channels, mounted on a swivelling base.

Let us consider both types of antenna. The single wave channel, from the design concepts and from the convenience of matching with standard cables, can advantageously be prepared as follows. The basic active vibrator is a loop-vibrator designed by A. A. Pistol'kors. The passive directors are separated by a distance of 0,1 λ, and the reflector by a distance of 1,172 λ . The height of elevating the antenna is selected, proceeding from the principal distribution of the inclination of the orbit of the meteors to the plane of the horizon (see Chapter 4). The most suitable is the arrangement of the maximum of radiation at an angle of 35 - 40 degrees. Therefore, it is advantageous to raise the antenna above the surface of the Earth by $h = 0{,}435$ (the horizontal vibrator raised for such a height has a radiation maximum at the angle of 35 degrees). In addition, we can slant at about the same angle the axis of the wave channel.

The input resistance of the antenna is about 33 ohms. As a basic feeder, we can utilize the RK-3 cable with the wave resistance W = 75 ohms. For matching the antenna with the main RK-3 cable and for the balancing, use is made of the U-elbow from the RK-6 cable with W - 50 ohms; its length equals λ. The feeder is connected to 1/4 of the length of the balancing elbow. In practice, to this same section of the elbow, we connect a short-circuited reactive loop, the length of which is established experimentally during the final matching of the antenna.

Proceeding from the conditions of operation, a relatively powerful transmitter can feasibly be separated somewhat from the recording equipment. Therefore, we proceed from the presence of two separate antennas, i.e. the transmitting and receiving ones; in addition, this is the simplest method of protecting the receiver from "face". The relatively wide directional diagram of each of the antennas permits us to apply two separate antennas. Naturally, the use of one antenna is possible, connected to the output of the transmitter and the input of the receiver through a switching device (segments of the cable and the gas dischargers).

At the end of the feeder connected to the transmitter's input, we place a four-wave transformer and a balancing U-elbow. The input resistance equals about 300 ohms.

In the measurements of the drift, a significant part is played by the directivity of the antenna in a horizontal plane, the absence of large lateral lobes, and of a large trailing lobe. Therefore, we strongly recommend the conduct of a test verification of the directional diagram. The checking can be conducted with the aid of a sounding-balloon, fastened on long lines above the surface of the Earth. To the sounding-balloon, there is attached a pulse quartz-crystal transmitter, having the same frequency and spectral data as the main transmitter. Moving the balloon in different points in space and establishing its position by optical instruments, we photograph the directional diagram of the antennas. We can utilize a slow-moving aircraft or helicopter [126]. Both methods yield good results under a careful preparation and conduct of the experiments.

The coaxiality of the directional diagrams of the transmitting and receiving antennas in various directions can be verified on the basis of the maximum of the recorded number of meteor trails of the underdense type.

Broadside Array of Eight Wave Channels

To increase the accuracy of measuring the wind velocity components, it is feasible to employ antennas having a narrow antenna diagram in the horizontal plane. It is known that if we have n cophased exciting vibrators, separated from each other by the distance d, the width of the diagram $\Delta\varepsilon$ in a horizontal plane can be found from the equation [130, 131]

$$\Delta\varepsilon = 0.88\frac{\lambda}{L}, \qquad (3.6)$$

If [see next page]

$$\frac{d}{\lambda} n \gg 1, \qquad (3.7)$$

where L equals the antenna length, and n equals the number of wave channels; $\Delta\varepsilon$ is given in radians. In the application of the waves $\lambda = 8 - 9$ m, we can develop a broadside array from 4 - 8 wave channels (one rotating or two systems of broadside arrays in the direction N- S and E-W). At $d/\lambda \simeq 1$, according to (3.6), the width of the main lobe of the directional diagram in the horizontal plane equals respectively 16 and 7 degrees.

If we supply the same power to all the channels of the antenna, such an antenna will have a series of lateral lobes with a slight attenuation relative to the main one. In this case, the main purpose is to have the possibility of determining the azimuth of the wind velocity component based on the azimuthal direction of the antenna radiation; this is not accomplished. We can lower the lateral lobes, having accomplished the supply of the antenna according to the method of Dol'f-Chebyshev [130].

The method is used during the application of the individual antennas, powered in a cophased manner, and arranged along one straight line. For the chosen number of channels and the distance between them, the method permits us to compute the law of the distribution of the amplitudes of the current of each of the channels, at which the relative level of the lateral lobes does not surpass a prescribed value, while the main lobe has the least possible width at the given level of the lateral lobes. We should remark that at the connection of the channels according to the Dol'f-Chebyshev method, the diagram expands somewhat, i.e. by 10 - 12%.

An experimental checking indicates the completely satisfactory coincidence of the design parameters of the antenna (according to the Dol'f-Chebyshev method) with the data obtained in actual practice.

/100

Antenna of Altimeter Device

The height of the occurrence of the reflecting area of the meteor trail is found from the equation

$$h = R \sin\theta, \qquad (3.8)$$

where θ equals the angle of elevation. The determination of the angle of elevation was conducted during the measurement of the drift of meteor trails in Manchester and Kharkov with the aid of two half-wave vibrators. The two horizontal vibrators are mounted above a horizontal metal screen at a varying height; $h_1 \simeq 0.5\lambda$, $h_2 \simeq 0.25\lambda$. The directional diagrams of such vibrators in a vertical plane are close to those designed. At the selected height of elevation, the radiation resistances of the dipoles are about the same. We can demonstrate that if we consider the reception of one harmonic signal $E \sin \omega t$ by two antennas, the ratio of the amplitudes of the signals U_1 and U_2 at the output of the antennas equals [see next page]

$$\frac{U_1}{U_2} = \frac{\sin\left(\frac{2\pi}{\lambda} h_1 \sin\theta\right)}{\sin\left(\frac{2\pi}{\lambda} h_2 \sin\theta\right)}. \qquad (3.9)$$

Equation (3.9) usually is represented for the selected antenna system in the form of the curve $\sin\theta = F(U_1/U_2)$, based on which we also find the angle of elevation for each registered meteor. Usually, we record a series of the ratios of the signal's amplitudes; also for increasing the accuracy, we take the average value.

The better the reflecting qualities of the surface above which the altimeter antennas are situated, the closer the calculated angle θ will be to the true value. We recommend making a metal grid. The horizontal dimensions of the grid should be such that it would accommodated in not less than one Frenel zone in the entire working range of the reception angles. The dimension of the Frenel zone can be estimated based on the following equations:

$$b = \sqrt{\frac{h\lambda}{\sin\theta}}; \quad a = \frac{b}{\sin\theta},$$

where b equals the minor half-axis of the ellipse, a equals the major half-axis of the ellipse, and h equals the height of the antenna's elevation. It is important that the surface of the Earth would be smooth and strictly horizontal (at least, within the limits of the zone).

The meshes of the screen (network) are established according to the selected transit factor δ, connoting by this:

$$\delta = \left|\frac{\overline{P_2}}{\overline{P_1}}\right|, \qquad (3.10)$$

where P_2 equals the Umov-Poyting wave vector, penetrating through the network; P_1 equals the Umov-Poyting vector of the wave having arrived from the meteor. The calculation can be conducted, utilizing the nomograms from [131].

In radar technology, the angle of elevation is measured by two methods, namely by the inclination angle of the antenna, and by the method of the equi-signal zones. In the meteor measurements, the first method is not popular owing to the relatively low directivity of the antennas. The second is also unpopular because the appearance of a meteor is a random occurrence, and the reflection exists only for a few tenths of a second. Use is also made of the phase-type altimeters [209].

For the unequivocal determination of the distance to the trail, a code is introduced; each fifth pulse is doubled (we can also use a different sequence of pulses). In this case, in the measurement of the height, one of the antennas of the altimeter receives the signal of the basic sequence of 500 cps, while the second receives the signal of the auxiliary sequence of 100 cps. /101

For increasing the quantity of the meteor trails in which we manage to determine the height of occurrence, it is feasible to employ in the altimeter

an antenna of the "wave channel" type. The increase in the labor expenditure for the production, adjustment and matching of such antennas as compared with the single vibrators is fully justified by the long operation of the equipment installation for measuring the drift of meteor trails (we shortened the necessary number of hours of measurements for a collection of sufficient data).

The amplitude method of determining the angle of elevation is quite simple; however, it has a considerable disadvantage.

Even under the application of the photograph experimental diagram of each vibrator, of a qualitative recording of the signals' amplitudes of the linearity of the amplitude characteristics of the receiver, of the determination of R with an error of not worse than ± 2 km, the error in determining the height is large. Thus, at $R \lesssim 200$ km, the error falls within the limits $\pm$ (2 - 5) km, while at $R \simeq 250$ km, it reaches as much as ± 15 km.

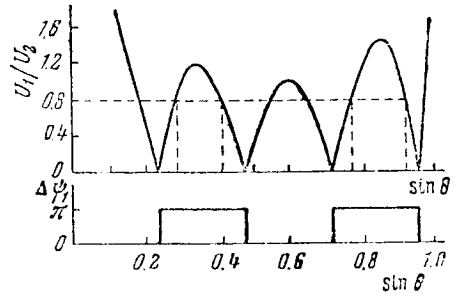

Fig. 3.3. Amplitude and Phase Relationships of Signals for Two Horizontal Dipoles Located at a Height of 2.07 and 0.44 λ.

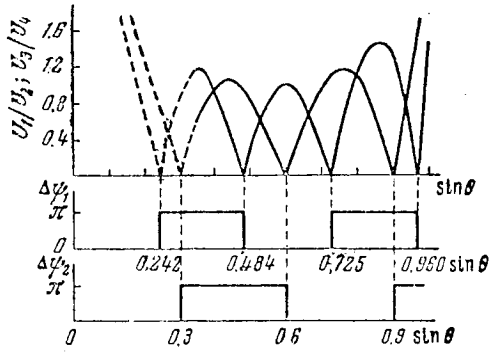

Fig. 3.4. Amplitude and Phase Relationships of Signals in the Antennas of an Altimeter, Consisting of Four Antennas.

The amplitude-phase method of measuring the angle of elevation, developed in the Kharkov Polytechnical Institute, yields a better accuracy than does the amplitude method [126]. Let us examine this method.

An increase in the resolving capability in respect to the angle of elevation θ can be attained owing to the application of a pair of antennas, of which one is raised high ($h \gtrsim 1{,}5\ \lambda$). In this connection, if we utilize the ratio of the amplitudes, we derive an abiguity of the solution: with several angles of elevation, there will be an identical ratio (the single-valued condition disappears at $h > 0{,}5\lambda$).

In Fig. 3.3, we have represented the relationship of the ratio u_1/u_2 to $\sin\theta$ for two half-wave horizontal dipoles, where $h_1 = 2.07\lambda$, $h_2 = 0.44\lambda$ [refer to Eq. (3.9)]. In this same figure, we have shown the difference in the phases between the emf, developing at the output of the first and second antennas, i.e. $\Delta\psi_1$. Within the limits of each of the lobes of the diagram, the phase difference does not alter, while upon a transition to the adjacent lobe, it varies jump-like. The lowermost lobes (the wave arrives at a small angle of elevation) are always cophased.

If we conduct the reception not on two antennas, but on four simultaneously, the ambiguity of the location of the angle is eliminated. Let us select $h_3 = 1.67\lambda$, $h_4 = 0.44\lambda$, then $U_3/U_4 = F(\sin\theta)$ has the form shown in Fig. 3.4. In this same figure, we have plotted the appropriate values of the phase shifts between the signals of the first and second antennas ($\Delta\psi_1$) and the signals of the third and fourth antennas ($\Delta\psi_2$).

The height of the antenna's elevation is so selected that in the working sector of the angles of elevation, we create the maximal resolving capability of the antenna; in this connection, from the convenience of calculation, the height-related factor is taken from a whole number of degrees.

/102

A detailed study of the errors in measuring the heights was made by B. S. Dudnik for the amplitude (AM) and the amplitude-phase methods (APM) [126]. In Table 3.1, we have listed the pertinent values of the errors for the various distances Δh for a meteor trail (in km).

Table 3.1

	R, km							
	100	120	140	160	180	200	220	240
APM	0.4	0.7	1.3	1.5	1.6	1.6	2.0	3.0
AM	3.2	4.2	5.0	6.3	7.8	9.5	11.4	13.0
$\sin\theta$	0.95	0.79	0.68	0.59	0.53	0.47	0.43	0.4

In this connection, for both cases, we assume the same conditions, and we disregard the error of the slant range. For the amplitude method based on a comparison of the signals in two antennas mounted at the heights $h_2 = 0.25\lambda$ and $h_1 = 0.5\lambda$, the dependence of the relationship of the amplitudes of signals upon the angle of elevation, as is known, is expressed by the formula

$$\frac{U_1}{U_2} = 2\cos\left(\frac{\pi}{2}\sin\theta\right). \qquad (3.11)$$

A shortcoming of the amplitude-phase method is the relative complexity: the application of four receiving antennas, the necessity for recording two signals, phases and two ratios of amplitudes, and also the need for the experimental checking of the graduation (calibration) of the altimeter for the various angles of elevation.

From a design standpoint, the dipoles (or the wave channels) are installed in pairs on the vertical masts (the first, with the second, and the third with the fourth). The masts are extended by nonmetallic stays for the absence of distortion of the structure of the incoming field. The dimension of the metallic horizontal network is 60 X 60m^2. In the measurement of the drift of the trails in the W-E direction, the antennas are arranged at a distance of 45 m from the western edge of the radar site. The distance between the antennas is 20 m. During the measurement of the drift in the N-S direction, the antennas of the altimeter can be rearranged.

The antenna of the interference-shielding system can be adopted as single-type with a receiving antenna. In practice, in the application of a shielding system according to the spectral composition, it is sufficient to have a half-wave dipole at the height $h = 0{,}435\lambda$, of which the directional diagram is oriented in the same direction as in the working antennas.

Receiving-Recording Device

The transmitting and antenna-feeder devices described in this section permit us to conduct diverse studies of the meteor phenomena by the radio method. To a considerable extent, the scope of the research questions being included will be determined by the system of the construction of the receiving-recording device.

For the measurement of regular movements in the meteor zone of the atmosphere, the following types of recordings are required: 1) the phase-temporal characteristic of the received signal for finding the Doppler frequencies; 2) the phase-temporal characteristic of the signal displaced relative to the preceding pattern by 90 degrees for determining the sign of the radial velocity component; 3) the recording of the range for finding the height; and 4) one or four recordings for finding the angle of elevation. The actual number of the recordings can be reduced by one (the first), since the velocity of the radial component of the wind can be determined based on one of the altimeter recordings. Thus, from 4 to 7 recordings are needed for measuring the wind at varying height during the investigation of the wind in one point.

/103

The measurement of the parameters of the turbulent motion in the meteor zone requires the development of the extended receiving-rebroadcasting devices [129]. The circuit of the receiving-recording installation in the basic point becomes complicated. Such a circuit (system) is discussed in Chapter 4.

In Fig. 3.5, we have shown the functional diagram of a receiving-recording device in the application of the amplitude altimeter and of a system of protection from the pulse-type interference. In this connection, we assume that the radiation of energy proceeds to the "wave channel" while the reception occurs in the two dipoles. Naturally, such a model of the system is not the only one; however, with its aid, we can analyze the operation of the entire device. For example, the absence of an altimeter permits us to increase the statistics of

the measurements, and to collect data concerning the movements pertaining to a certain central area of altitudes (refer to pages 90 - 93).

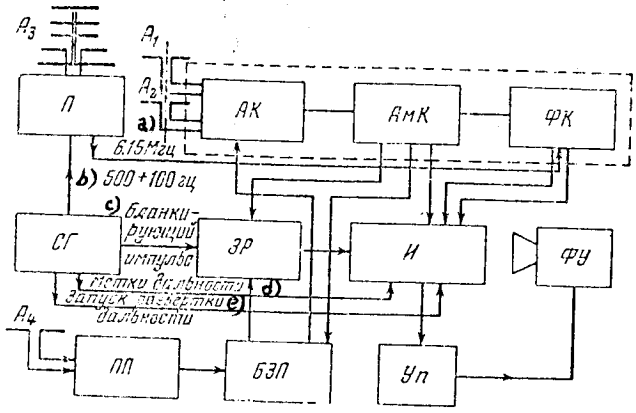

Fig. 3.5. Functional System of a Receiving-Recording Device for Measuring the Drift of Meteor Trails by the Pulse-Coherent Method. П - transmitting device: СГ - synchro generator; ПП - interference receiver; АК - antenna switching device; АмК- amplitude channel of signals' receiver; ФК - phase channel of signals' receiver; ЗР - triggering unit of time scanning and signals' pulse intensification; И - indicating device; ФУ - photographic device; БЗП - unit for shielding against interference; Уп - control unit; A_1 and A_2 - antennas of the amplitude altimeter; A_3 - transmitter antennas; and A_4 - antenna of interference receiver. Key to figure: a) 6.15 mc; b) 500 + 100 cps; c) blanking pulse; d) range markers; e) triggering of range sweep.

The signals from the receiving antennas enter the antenna switch, installed in the receiving-recording stand. The operating principle of the switch is as follows. From the output of one of the antennas, the signal passes freely through the UHF to the input of the mixer and further through all units of the superheterodyne receiver. If the level of the received signal exceeds the level of discrimination, from the unit for shielding from interference, a switching pulse arrives, acting upon the pulse circuits of the antenna switch. After its passage, within 60 microseconds, the second HFA (high frequency amplifier) opens, to which is connected the second antenna; the period of the open condition is 200 microseconds. During this time, there closes automatically the first HFA, etc. The load in both HFA is common, so that the following transformation, amplification and rectification occur for the signals of both sequences (500 and 100 cps). As a result, on the indicator screen, we obtain so to speak the superposition of one amplitude-time-dependent characteristic upon the other (with a shift). The ratio U_1/U_2 can be found repeatedly.

We can switch the antennas A_1 and A_2 in a different way [122]. In this case, the synchrogenerator controls the antenna through which the signals of the main sequence pass, and the antenna through which the coding sequence passes.

/104

The superheterodyne receiver should meet many requirements. The passband is adopted as relatively wide (400 kc) for increasing the accuracy of the range

reading. The sensitivity of the receiver is limited by the level of external noises and equals about $6 \cdot 10^{-14}$ watts at a signal/noise ratio of 2:1. The linearity of the amplitude characteristics of the receiver must be provided.

The complete circuitry of the receiver for the case of switching the antennas with a synchrogenerator is shown in Fig. 3.6. After amplification in the HFA, the signals enter the mixer C_1. To this same mixer, we supply through a buffer stage the oscillations of the quartz-crystal heterodyne of the receiver, preamplified six times up to 48 mc. From the output of the mixer, the signal at the IF (intermediate frequency) of 11.1 mc is fed to the amplitude rectifier, and through the video-amplifier to the range indicator and to the altimeter indicator. The selection of the circuit for the receiver and the frequency of the heterodyne is discussed in Chapter 4.

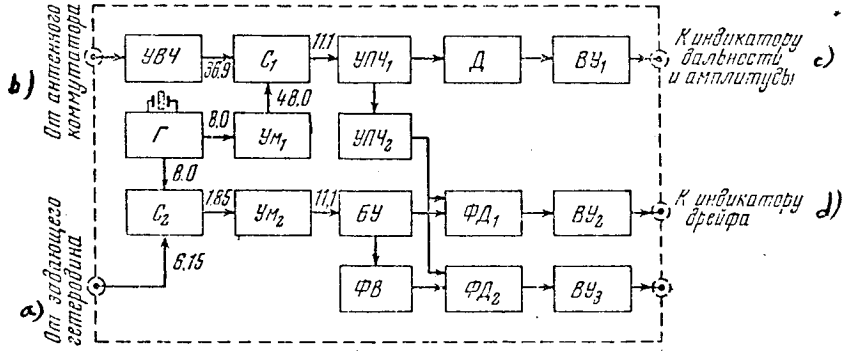

Fig. 3.6. Functional Diagram of the Receiver of the Signals of the Receiving-Recording Apparatus for Studying the Drift of Meteor Trails. УВЧ - amplifier of the high frequency signals; Г - heterodyne; Ум1, 2 - multipliers; $C_{1,2}$ - mixers; $УПЧ_{1,2}$ - amplifiers of the IF oscillations; Д - amplitude rectifier; $ВУ_{1,2,3}$ - video-amplifiers - ФВ - phase-converter; $ФД_{1,2}$ - phase rectifiers; БУ - buffer amplification stage. The frequency of oscillations is indicated in megacycles. Key to figure: a) from the master heterodyne; b) from the antenna switch; c) to the indicator of range and amplitude; and d) to the drift indicator.

The range scanning is linear, type A, and is triggered from the synchrogenerator by a paired pulse. The range sweep is marked with range indications developed by the synchrogenerator. It is convenient to calibrate the indications in two scales, e.g. every 100 and 25 km. For increasing the accuracy of the reading of the distance from the radar set to the trail, it is convenient to have two range scales, namely a coarse and a fine (vernier) scale.

We have noted that to determine the angle of elevation, in fact the amplitude-time-dependent characteristic is recorded. This occurs in the following manner. One of the first signals surpassing the discrimination level, (which is necessary to make regular also in the course of the operation in dependence on the level of the interferences), triggers the time sweep.

All of the subsequent signals will be recorded in the form of a series of patterned pulses.

In the operation at $\lambda \approx 8$ m, allowing for the average values of the observed radial components of the drift velocity and also for the convenience of finding the period of the Doppler frequency and the relationship of the altimeter's amplitudes, we should select a length of the driven sweep 0.15 - 0.25 second.

The sign of the radial velocity of displacement of the trail is found with the aid of the additional rectifier, to which we feed the voltage of the received signal with a shift (see Fig. 3.6). To the first rectifier, we feed the voltage of the reference signal

$$u = U_{m0} \cos \omega_0 t \tag{3.12}$$

and the voltage of the signal arriving from the receiver /105

$$u_n = U_{mn} \cos \omega_n \left[t - \frac{2(R + V_R t)}{c} \right], \tag{3.12}*$$

where R equals range, V_R equals radial velocity of the trail's displacement. At the output of the first rectifier, we obtain the voltage

$$u_{в1} = U_{mв} \cos (\Omega_D t + \varphi_R). \tag{3.13}$$

At the output of the second rectifier, to which the signal u_n is fed with the displacement $\pi/2$, the voltage is developed

$$u_{в2} = U_{mв} \cos \left(\Omega_D t + \varphi_k + \frac{\pi}{2} \right). \tag{3.14}$$

If the direction of the displacement changes to the opposite, the signals at the output of the rectifiers are described by the equations

$$\begin{aligned} u_{в1} &= U_{mв} \cos (\Omega_D t - \varphi_R), \\ u_{в2} &= U_{mв} \cos \left(\Omega_D t - \varphi_R - \frac{\pi}{2} \right). \end{aligned} \tag{3.15}$$

The variation in the phase by π of the signal $u_{в2}$ permits us to determine unequivocally the sign of the radial velocity component of the trail's displacement.

All the signals received by the equipment are automatically photographed. In the absence of signals, the beams of the indicators are attenuated. As soon as a signal is received, in the triggering channel of the sweep, a brightening pulse is formed. The pulses are utilized for brightening the sweep line only during the existence of the received signals in order to eliminate the brilliant exposure of the film after the completion of the reception.

In dependence on the problem presented, we can either record continuously the reflections from the prolonged existing overdense trails, accomplishing the filming in a series of successive frames, or photograph the reflections from the meteors only in the first 0,15 - 0,25 second. The latter approach is used more often, since a distorted trail frequently yields a phase pattern, caused not only by the spatial displacement of the trail. In the changing of the frames, the beam is attenuated for removing the illumination of the film, i.e. to the control electrode, we feed a negative pulse which activates the kipp-relay, triggering the trailing front of the sawtooth voltage of the time sweep.

For photographing, the standard movie cameras are suitable. The system for controlling the feeding of the film depends on the type of apparatus. For economy in using the film, it is advantageous to provide for the control by hand of the triggering channel, i.e. in the case of spurious activations from suddenly developing series of interferences, the operator is able to stop the photorecording.

Let us return to the description of the operation of the receiver (refer to Fig. 3.6). For finding the drift speeds, as we have already previously indicated, one should separate the Doppler frequency. For this purpose, in the receiver there is a unit of the phase rectifier $\Phi Д_1$. The reference signal of the master oscillator (6, 15 mc) enters along the cable to the mixer $С_2$. For this same mixer, there are fed the oscillations from the receiver heterodyne $Г_1$ (8 mc). The signal of difference frequency (1,85 mc) is fed to the multiplier stages, at the output of which the oscillations have the frequency of 11,1 mc. Let us also call these oscillations reference ones. Thus, to the rectifier $\Phi Д_1$, we feed two oscillations with the frequency 11,1 mc differing only in the Doppler frequency in the case of displacement of the meteor trail by the winds. From the output of the phase rectifier, the signals are fed to the video-amplifier, then to the plates of the indicator. In the phase-time-dependent characteristics, there occurs a variation in the amplitudes of the pulses, permitting us to determine the Doppler frequency.

Let us proceed to a consideration of the system of an antenna switching device and of a receiving device for the case of the amplitude-phase method of determining the angle of elevation. In Fig. 3.7, we have shown the functional diagram of such a device. The receiver contains two identical channels, in each of which there function two receiving antennas: respectively $А_1$, $А_2$ and $А_3$, $А_4$. The necessity for the four antennas has been explained above. Let us describe the operation of one of the channels.

/106

The antennas $А_1$ and $А_2$ are connected to the independent units of the HFA. The operation of the HFA is controlled by the switching square pulses, being generated by the pulse circuits - $КР_1$, $КР_2$, $У$, $\Phi И$. The kipp-relay KP of these pulse circuits is triggered by the received signal, having reached the level of discrimination. We have already remarked that the HFA is blocked in respect to the screen grid for 200 microseconds every 60 microseconds after the arrival of each signal pulse. Simultaneously, from the phase-inverter $\Phi И$, there are taken the same positive pulses, opening 100 times per second HFA_2. The signals from the outputs of the HFA_1 and HFA_2 enter the common input circuit of the mixer, $С_1$. In rhythm with the operation of the circuits considered by us, connected with the antennas $А_1$ and $А_2$, there occurs the switching of antennas

A_3 and A_4. The further principle of the operation of the system is quite identical with the functioning of the receiver previously described. To the phase detector, we feed two oscillations at the frequencies 6.9 mc, differing from each other by the Doppler frequency and the initial phase angle.

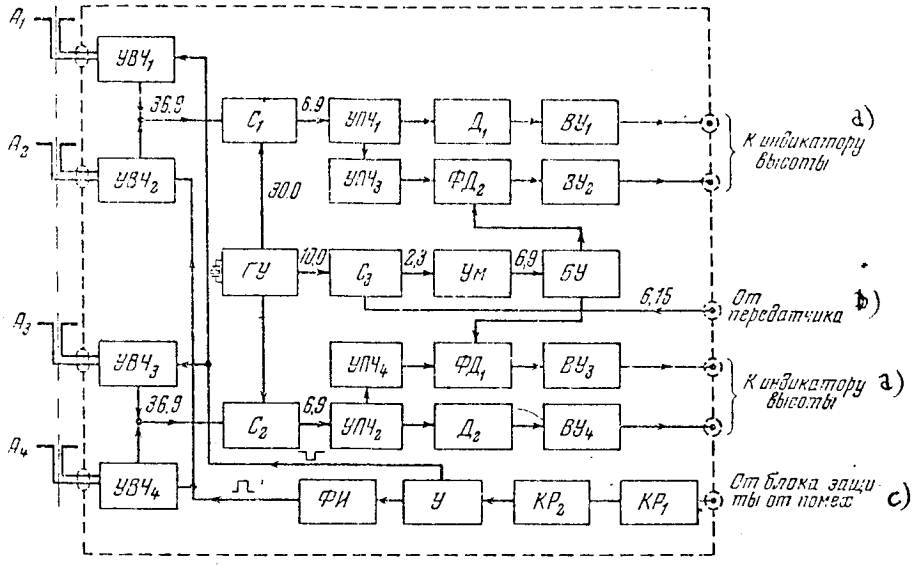

Fig. 3.7. Functional Diagram of a Receiver with an Amplitude-Phase Altimeter. УВЧ$_{1, 2, 3, 4}$-amplifiers of the high frequency signals; С$_{1, 2, 3}$-mixers; УПЧ$_{1, 2, 3, 4}$-amplifiers of the intermediate frequency signals; ВУ$_{1, 2, 3, 4}$-video-amplifiers; ФД$_{1, 2}$-phase rectifiers; ГУ-heterodyne-multiplier; Ум-multiplier; БУ-buffer stage of amplification; КР$_{1, 2}$ - kipp-relay; У-amplifier; ФИ - phase inverter; $A_{1, 2, 3, 4}$ - altimeter antennas; and Д$_{1, 2}$ - rectifiers. The frequency of oscillations is shown in megacycles. Key to figure: a) to the height indicator; b) from the transmitter; and c) from the unit of shielding against interferences.

The altimeter should be periodically calibrated. This can be achieved in the following manner. At a certain distance from both systems of antennas, we set up the horizontal vibrator, to which is connected the standard oscillator on a frequency of 36.9 mc. To the input of the first channel and then to the input of the second one, we connect A_1 and A_3, located at the same height 0.44 ; the operator balances the amplification. Thereby, a triggering is developed in order that we can monitor with an oscillograph the signals in the load of the rectifier Д$_1$ or Д$_2$. The adjustment and checking of the altimeter have been examined in detail in [126]. In the stand of the receiving-recording device, it is also feasible to accommodate a unit of the synchrogenerator, i.e. of the basic control unit of the entire radar set.

The synchrogenerator develops the control pulses for the master oscillator of the transmitting device (500 cps + 100 cps); the blanking pulses (τ = 200 microseconds), being fed to the activation unit of the time sweeps and the brightening of the pulses; the pulses for triggering the range sweep; the pulses for the distance markers of 1500 cps (100 km markers) and 600 cps (25 km markers). The blanking pulses lead all the remaining ones by 45 microseconds. All of the enumerated pulses are formed in the system under study from the oscillations of the master heterodyne for the frequency of 6 kc. The synchrogenerators can also be built according to other systems.

The phase of the oscillations of the master heterodyne of the synchrogenerator is rigidly coupled with the phase of the supply emf of the power system. This permits us to conduct synchronously the operation in other sets operating with the frequency of the network, or a multiple of it (for example, in the case of the study of the initial radius of a meteor trail, there operates simultaneously at least two series of stations at different frequencies).

System of Protection from Pulse Interferences

Let us discuss the operating principle of a system of protection from the pulse interferences, using the difference in the spectral composition of the working and interfering pulses [128]. From a design standpoint, the production of such a system can be various, and does not have to correspond entirely to the system which will be considered by us.

The system contains two channels: a channel ПС for the reception of the useful signals and the channel ПП, tentatively said to be the channel for the reception of interference. It is possible to use the same receivers in both channels.

The receiver ПС is a basic operating receiver, tuned to the frequency f_c of the radar set for measuring the drift of the meteor trails. The receiver of the channel of interferences is tuned to the frequency $f_п$:

$$f_п = f_c \pm k\Delta f_{пр},$$

where $\Delta f_{пр}$ - the pass band of the receiver, and k equals the frequency difference factor. The frequency difference of the receiver is selected experimentally, choosing the best suppression of a given interference. Usually, k equals 4 - 8.

For practical purposes, the difference in the tuning of the receivers is reflected only in the reception of the basic oscillations on the frequency f_c, in which the signal will be at the output only of the receiver ПС. In the presence of the pulse interference, the signals will be at the output of both receivers. This is explained by the fact that the spectral composition of the pulse interference is broad owing to the very diverse form and duration of the interference.

After amplification, clipping and expansion, the signals from the output of the rectifier of the interference receiver, ПП, are converted to negative square pulses. The amplitude of the negative pulses does not depend on the level of interferences; it is sufficient that the interference would exceed the noise level by 1.5 - 2.5 times (the level is regulated by the operator).

The leading edge of a negative pulse practically coincides timewise with the leading edge of the interference.

The negative pulses are fed to the channel of the useful signal and lock it for a time span somewhat surpassing the lifetime of the interference (the pulse is extended). To avoid the dissimilar delay of the received signals in the channel of the useful signals and the channel of interference, the useful signal is delayed for a period of around 5 microseconds. A possible delay system has been examined in [128].

The protection from the pulse interference (the channel ПП and the unit БЗП) is shown in the functional diagram of a grouping of the equipment for measuring the drift of meteor trails (refer to Fig. 3.5).

The shielding system permits us to weaken considerably the effect of the pulse interference, specially those being developed by the ignition of an automatic machine, by the corona discharge of high-voltage electric transmission lines, the sparking of the generator brushes of electric motors, etc. During thunderstorms, the system does not provide complete protection from the effect of atmospheric interference.

/108

Measurement of Drift of Meteor Trails by the Method of Automatic Capture of the Reference Oscillator (Generator)

The development of a multistage transmitting device in the meter band with a master quartz-crystal generator is quite complicated. Let us note that for a long period, in radar practice, it was considered that the observation of moving targets in general is practically realizable only under the continuous conditions of the operation of the transmitter. Subsequently, the pulse-coherent method became popular, and now application is being found for the technique of the capture of the frequency of the reference generator (strictly speaking, the latter method can also be said to be pulse-coherent). In the trapping of the frequency of the reference oscillator, use can also be made of a powerful single-stage self-excited oscillator.

The pulse-coherent technique imposes certain definite requirements on the self-excited oscillator, the heterodyne of the receiver and the reference generator (coherent heterodyne). These requirements can be formulated as follows. The momentary stability of the frequency of the self-excited oscillator should be such that within each successive pulse, the flowing-in of the phase of oscillations owing to the departure of the transmitter frequency relative to a certain reference frequency, would not exceed small fractions π (e.g., let us assume the frequency drift $\Delta\varphi \lesssim 0{,}2\pi$), which corresponds to the deviation in frequency $\Delta f \lesssim 0{,}1/\tau_и$, where $\tau_и$ - the duration in seconds of the self-excited oscillator's pulse. For the pulse durations normally being applied, the stability of the oscillation frequency of the self-excited oscillator is fully achievable. The transmitter should not have a "stray" frequency modulation within the pulse, even with a very low modulation index.

The frequency of the self-excited oscillator should not change from pulse to pulse. The frequency drift should comply with the inequality $\Delta f \lesssim 0{,}1/T_п$, where $T_п$ - the repetition rate of the self-excited oscillator's pulses in seconds. Experience indicates that such a stability is not difficult to attain in the transmitters of average power.

The basic idea of the considered method of measuring the drift of meteor trails consists in the fact that the phase of the reference signal oscillator is trapped by the sonde of the transmitter. At the moment of the arrival of the reflected signal, the phases of the signal and of the coherent oscillator are compared. The phase difference obtained corresponds to the Doppler shift. It is natural that the Doppler shift of the phase will be measured all the more precisely, the more stable the frequency of the reference oscillator. It should correspond to the inequation $\Delta f \leqslant 0.1/T_{ц}$, where $T_{ц}$ - the time of the passage of the signal to the target (if there are several targets, then to the furthermost target) and back, expressed in seconds. Since the frequency of the reference generator is usually chosen at the level of the lowest intermediate frequency, it is easy to make the reference generator with the required stability. It is necessary to divert particular attention to the production of the first heterodyne of the receiver, in which the requirements for absolute stability are the same as in the reference generator; however, the frequency of oscillations is higher by one order of magnitude. Therefore, the receiver is usually made with a double transformation of frequency, in which the first heterodyne is not retuned and is based on quartz-crystal, while the second is not based on quartz-crystal and serves for the final adjustment of the receiver. Under such a model of the construction of the system, the first heterodyne completely complies with the imposed requirements for stability, while from the second there is obtained the necessary stability in a much simpler way.

The pulse of the second intermediate frequency of the receiver, having been received as a result of the effect of the transmitter sonde, is fed through the strobing amplifier to the generator of the reference signal (ГОС). If the radiated pulse of the receiver has a relatively long trailing edge ("tail"), it is necessary to block the strobing amplifier during the completion of the plane part of the probe. This is necessary for the stable capture of the phase of the ГОС. In addition, for the reliable capture of the phase of the ГОС for the shortest time possible, it is desirable to remove its oscillations prior to each probe.

/109

The voltages from the output of the channel of the second intermediate frequency (IF) of the receiver and of the generator of the reference signal are fed to the phase rectifier for the separation of the drift. For obtaining the values of the range to the trail and the angle of elevation, the circuit should be supplemented in a way similar to that which was done in Figs. 3.5 and 3.6; as compared with the previously examined systems, there is nothing basically new in the recordings of these values. In addition, the circuit is supplemented by a system of shielding from the pulse-type interferences.

In the use of the narrow-band receivers, in conjunction with the transmitter-self-excited oscillator, it is necessary to apply the automatic final adjustment of the frequency. If in this connection, in the set, use is made of the pulse-coherent method for the measurement of the drift of meteor trails, it is feasible to operate with a system of automatic frequency control (AFC) to the transmitter. The adjustment of the entire system of the transmitter-AFC-receiver can be conducted on the basis of the sounding pulse (this is equivalent to observing a stationary target).

Both of the pulse-coherent methods of measuring drift of meteor trails considered by us combine the simplicity of the pulse-type radar systems with the property of the continuous radiation radar sets of determining slight changes in the frequency of signals which are being received.

Starting from 1950, initially in the U. S., and then in Australia for measuring the drift of meteor trails, use has been made of the radar equipment of continuous radiation. The radial velocity components of the drift are found based on the Doppler frequency. The receiving point is usually separated from the transmitter, which complicates the operation considerably.

The equipment, the technique of measurements and the processing of the results obtained from studying the drift of meteor trails during continuous radiation are described in sufficient detail [122, 132], and therefore are not considered in the present report.

The work experience at Manchester, Adelaide and Kharkov demonstrated that the further improvement of the radio equipment for investigating the meteor phenomena should be conducted according to an approach, assuring a) the high accuracy of individual measurements; b) the sufficiently reliable data of measurements and c) the complexity of the questions under study.

One of the possible variants of the complication of the equipment in order to expand the obtainment of the possible scientific information, is examined in the next chapter. Let us comment that the latest developments in the equipment (for example, [132, 133]), when use is made of transmitters with a radiating force of millions of watts, antennas with high amplificttion, improved receiving-recording devices with the processing of the information immediately during its obtainment in the electronic computers, expands considerably the information, and permits us to eliminate the effect of the various factors upon the results of measurements.

METHODS OF STUDY OF DRIFT OF METEOR TRAILS

Let us consider the procedure for studying the drift of meteor trails according to the radio observations of meteors.

The parameters of the equipment indicated in the previous section permit us to obtain during the greater part of the year from 50 - 100 recordings of meteors in the hours of the minimum up to several thousands in the hours of the maximum. For various reasons, a considerable part of the recorded reflections does not permit us to obtain data concerning the drift, and only for 20 - 50% of the recordings is a calculation conducted.

The experience in conducting the measurements of the drift of meteor trails has shown that the individual values of the velocity and direction of the displacement of the trail are subjected to large fluctuations. This pertains particularly to those hours of the day when the wind direction is changing. By way of an example, in Table 3.2, we have presented the mean hourly values of velocity (in m/sec) of the zonal component for June 1964 (Kharkov).

The corresponding diurnal pattern of the zonal component, obtained by averaging the 3-day measurements (the measurements alternately taken every day were conducted first in the direction east-west, then in the direction

north-south) are indicated in Fig. 3.8. As already noted [Eq. (3.1) and (3.2)], in the present report, we have assumed the signs of the components of wind velocity common in ionospheric investigations--the positive value corresponds to the eastward direction (for the zonal components) and northward (for the meridional component).

Table 3.2

Date	Local time, hrs					
	18—19	19—20	20—21	21—22	22—23	23—24
9 June. . .	+35	+ 5	—12	—28	—40	—45
11 June. . .	+35	—14	—13	—30	—29	—44
13 June. . .	+10	+24	+13	—27	—33	—43

From Fig. 3.8, it follows that the wind direction varies between 1900 and 2000 hours; for this time, we derive the sign-variable average hourly values of velocity.

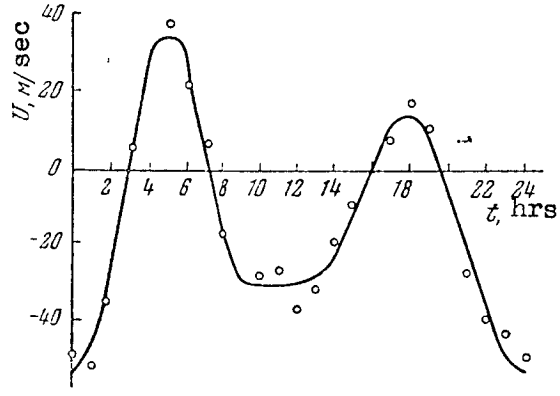

Fig. 3.8. Mean Hourly Values of Meridional Velocity Component of Wind in the Meteor Zone. Local time. Kharkov, June 1964. Positive direction northward.

The many years' measurements of the quantity of meteors, conducted in Kharkov [134], permit us to plan fairly clearly the required number of days of measurements for a collection of sufficient data in the afternoon hours (from 1300 to 2100 hours).

For other equipment, the anticipated quantity can be converted, proceeding from the formulas for the scattering of radio waves in the ionized meteor trails (Chapter 2).

In Fig. 3.9, we have shown an example of the recording of reflections from a meteor trail in the application of the amplitude-phase altimeter. The six beams are used as follows: one beam measures the range, two beams permit us to find the ratios of amplitudes U_1/U_2 and U_3/U_4 [Eq. (3.9)], and three beams are occupied by the phase-time-related characteristics. The phase-type-time-dependent curves permit us to determine the cophased state and the antiphased state of the signals of the basic and auxiliary sequences, and also the sign

of the radial velocity component. Let us note that in Fig. 3.9, each fourth pulse is doubled. We can determine the radial velocity component of the wind, computing the number of pulses in the period of Doppler oscillations. Thus, if f = 36.9 mc, the repetition rate of the sounding pulses is 500 cps, N equals the number of the pulses in the period of the Doppler oscillations, the radial velocity component then equals

$$U_R = 2032/N \text{ m/sec.} \tag{3.16}$$

The drift velocity in the horizontal direction U can be found based on the equation

$$U = \frac{U_R}{\cos\theta} = \frac{2032}{N\cos\theta} \text{ m/sec.} \tag{3.17}$$

/111

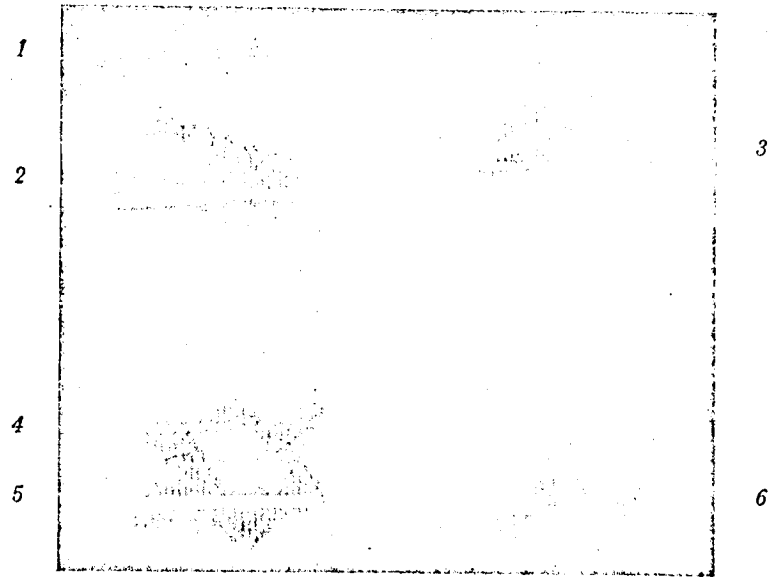

Fig. 3.9. Recording of Reflection from a Meteor Trail. 1- range; 2, 3- amplitudes from four antennas of the altimeter; 4, 5, 6- phase-time-dependent characteristics for determining the Doppler frequency, the sign of the radial component and the elimination of the ambiguity in determining the angle of elevation.

For the selected equipment in the finding of the horizontal component of the wind velocity, Eq. (3.17) reduces to finding the functional dependence U = F(h/R, N); for speeding up the calculations, this functional relationship can feasibly be represented either in the form of tables or in the form of nomograms. Usually, from the experimental data, we find R and N or L/R and N.

Let us consider the first case: we find based on the photographs the range R to the trail, and the number of pulses. Taking into account the various factors, we can find the average value of the height h_{cp} at the working length of wave λ. Thus for λ = 8 m, the height $h_{cp} \approx$ 93 km. Eq. (3.17) for

the equipment of the KPI in this instance is converted to $U = \frac{2032}{N\sqrt{1-(93/R)^2}}$

For an illustration, let us present the part of the auxiliary calculation table, constructed according to this equation.

In Table 3.3, we have selected those distances for the trail R, so that at the given fixed value h_{cp} = 93 km, the variation in the angle θ amounted to 1 degree.

The second case, i.e. the height of the meteor trail, is found by any method (amplitude, amplitude-phase). In this case, the argument is comprised by h/R = sin θ and n (Table 3.4).

Table 3.3

R, km	N-values										
	45	46	47	48	49	50	51	52	53	54	55
190	52.0	50.5	49.5	48.5	47.5	46.5	45.5	45.0	44.0	43.0	42.5
184	52.5	51.0	50.0	49.0	48.0	47.0	46.5	45.5	44.5	43.5	43.0
179	53.0	52.0	51.0	50.0	49.0	48.0	47.0	46.0	45.0	44.0	43.5
176	53.5	51.5	51.5	50.5	49.5	48.5	47.5	46.5	45.5	44.5	44.0

/ 112

Table 3.4

sin θ	N- values										
	45	46	47	48	49	50	51	52	53	54	55
0.500	52.0	50.5	49.5	48.5	47.5	46.5	45.5	45.0	44.0	43.0	42.5
0.515	52.5	51.0	50.0	49.0	48.0	47.0	46.5	45.5	44.5	43.5	43.0
0.530	53.0	52.0	51.0	50.0	49.0	48.0	47.0	46.0	45.0	44.0	43.5
0.510	53.5	52.5	51.5	50.5	49.5	48.5	47.5	46.5	45.5	44.5	44.0

Other methods of facilitating the conduct of the calculations of the velocity based on experimental data are also possible.

The position of the experimental points in Fig. 3.8 indicates that the wind velocity during the day can be described by a Fourier series. As will be indicated during the discussion, this follows from the physics of the processes occurring in the upper atmosphere. During the day, the wind velocity at a sufficient number of measurements for the component N- S or E- W can be described by the following Fourier series:

$$V = V_0 + V_1 \sin\frac{\pi}{12}(t' + \theta_1') + V_2 \sin\frac{\pi}{6}(t' - \theta_2') + V_3 \sin\frac{\pi}{4}(t' + \theta_3'), \qquad (3.18)$$

where V_0 equals the constant determining the average direction for the day and the value of the wind velocity; $V_1 V_2$, V_3 equal the amplitudes of the diurnal, semidiurnal and 8-hour harmonics; t' equals the time of day computed from 0000.

The time is usually assumed to be local, proceeding from an analysis of the causes evoking the appearance of the diurnal and semidiurnal wind components. Let us comment that in certain reports, the time reading is taken differently, i.e. for the component N-S from the moment of the direction of the harmonic wind component to the north, while for the E-W component, it is taken from the moment of the eastward direction.

The wind velocity in the upper atmosphere is normally measured in m/sec. The constant component of the zonal and meridional components are found as the arithmetic mean for the appropriate velocity values. According to the known values for U_o and V_o, we can find the velocity of the transport motion.

If the drift of the meteor trail under the effect of wind is slight, the full period of the Doppler oscillations can not be separated. In this case, we compute the variation in the phase angle for a fixed period based on the phase-time characteristics of the signals being received. The direction of radio component is found according to a comparison of the two phase patterns. An example of such a processing of the recording is shown in [123]. Similarly, there occurs the processing in case of the very brief meteor reflections.

For determining the frequency of the Doppler oscillations, use can be made of the vector phasometer. Knowing by what angle the received signal will turn relative to a reference signal and the corresponding time required for this, based on the photographed sector, we find the angular frequency of the Doppler oscillations. Evidently, the use of the phasometer can increase the number of "useful" reflections during the search for the drift velocity of the trail (in this connection, it is assumed that the conventional phase-time-dependent recordings are underway parallely).

In the determination of the Doppler frequencies, we should discard the variations in phase owing to the diffraction pattern. If the experimental data are found by the calculator by way of the visual processing of each recording, there are selected only the "mirror" reflections and the initial sector of the phase-time recording (approximately to the first maximum of the amplitude-time characteristic) is discarded. Let us recall that in the receiving-recording equipment, provision is made in effect for a single recording of the reflections from the trail during 0,15 - 0,25 sec (although the trail can exist for several seconds and more). During this time, the additional reflecting centers in /113
the trail practically do not develop.

During its existence, a saturated trail can alter its form considerably; the axis of the trail can deflect from the rectilinear by many meters (i.e., by many wave lengths during the radio observations). This a result of the fact that the velocity of the wind in the various sections of the trail is dissimilar. At the reflections of the radio waves from such a trail, the received signal consists of several components having various frequency deviations. The deep feeding of the signal's amplitude takes place.

The main sources of errors in finding the individual values of the drift velocity of the meteor trails are as follows:

1) The relatively broad directional diagram in a horizontal plane. This itself does not allow for the presence of various azimuths, at which the meteor trails are recorded; all the results are considered as pertaining to one of the four directions, namely N, S, E, W;

2) The error owing to the inexact determination of the angle of elevation; and

3) The inaccuracy of determining the Doppler frequencies owing to the limited number of sounding pulses per second, of the "fuzziness" of the passage of the phase-time characteristics of the signals through 0.

As was noted by V. V. Sidorov, the diffusion of the meteor trail can have an effect on the errors in finding the drift velocity. Considering the trails of the saturated and transient type ($\alpha > 2.4 \cdot 10^{12}$ electrons/cm), it is considered that the distribution of electrons in respect to radius is of the Gaussian type. Then, for the saturated trails, the rate of change of the critical dimensions, in dependence on the electron density and the height, can change from 4 to 50 m/sec, i.e. can have values close to the drift velocities. It should be noted that the relative number of such trails during the measurements in Kharkov and Manchester was low. The possibility of introducing corrections into the study of the circulation of the atmosphere in respect to the saturated trails requires a more detailed study of the distribution of the electron concentration.

In theory, on the drift variations, there should be exerted the influence of the occurrence of resonance, developing during the scattering of radio waves by the meteor ionized trail. For practical purposes, as the measurements made in Kharkov have shown (refer to Chapter 4), the role of resonance has been exaggerated by many researchers, and evidently this phenomenon does not exert much influence on the experimentally derived values for the velocity of the trail's drift.

The overall average error of one measurement of the drift velocity during the application of the described equipment and antennas in the form of single wave channels comprises about 30%. Let us note that the indicated errors can be reduced to a considerable extent by complicating the radio equipment. The application of an angle-measuring base device, based on the measurement of the phases of the arrived signals, and the staggered antennas permit us to find the true wind direction [209].

The measurement of turbulences at the height 80 - 100 km can be conducted during the simultaneous measurement of wind velocity in several sectors of the meteor trail. The appropriate equipment has been described in Chapter 4. In the measurements conducted at the KPI, the conditions of coherence included up to 3 extended points [105].

For an analysis of the irregular movements in the meteor zone, use is made of the theory of homogeneous isotropic turbulence [135]. The parameters typifying the turbulent motion are as follows: the pulsation velocity of the large-scale eddies, their typical dimension L, the time τ of disintegration of the large-scale eddies, the rate ε of advance of energy from the side of the external sources, the pulsation velocity U_e of the eddies of the range of energy dissipation, the typical dimension l of these eddies, and their lifetime, t_l. The technique applied for the study of the turbulences in Manchester and Kharkov is practically the same [105, 136, 139].

DISCUSSION OF RESULTS OF THE STUDY OF ATMOSPHERIC CIRCULATION IN THE METEOR ZONE

The most complete and systematic measurements of the atmospheric circulation in the meteor zone have been conducted in Manchester (continuous measurements over a period of five years) and in Kharkov. In the analysis of the motion of the atmosphere, we will utilize these results [124, 140 - 142]. In the measurements (for 27 mc), having been conducted in Southern Australia starting from 1952, equipment was used with low effective sensitivity [122]. As a result, during a day for the analysis of the drift, in all up to 50 - 70 recordings were made that were suitable for processing [132]. Such data do not permit us to make sufficiently reliable inferences concerning the movement of the atmosphere. From 1960, in Adelaide, use was made of quite modern equipment, permitting one to obtain on the frequency of 22.9 mc hundreds of values of the drift velocity every hour [132].

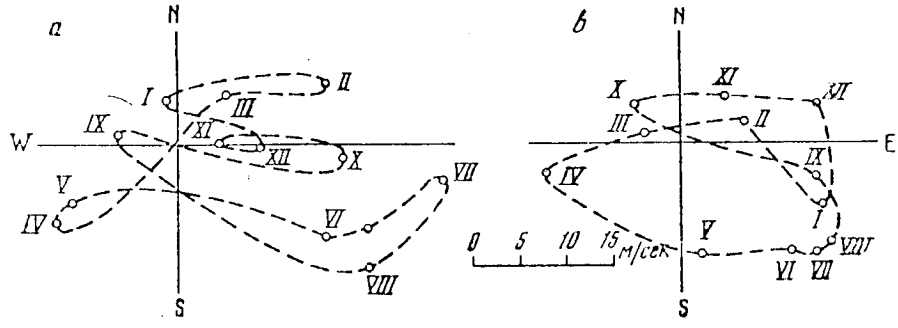

Fig. 3.10. Variation in the Speed and Direction of the Predominant Wind. a- based on measurements in Kharkov from 1962 - 1963; b- averaged data, obtained in Manchester from 1953 - 1958. I - XII - numbers of the months in order.

From March 1962 to March 1963, in the KPI, we conducted monthly measurements of the drift of meteor trails [141]. During the observations, we determined 133,721 individual values of the velocity of the zonal wind component and 79,536 values of the meridional component. In Table 3.5, we have shown the corresponding results obtained from processing the experimental data for each month. The velocity of the prevalent wind $\sqrt{U_0^2 + V_0^2}$ varies from about 2 to about 30 m/sec. The maximum velocity occurs during the summer months. As investigations have shown, the results basically pertain to the height of 92 $\pm$ 3 km.

In Fig. 3.10, we have represented the variations in the velocity vector of the prevalent wind in the meteor zone based on measurements made from March 1962 to March 1963 in Kharkov. For comparison, in this same drawing we have shown the analogous values obtained from 1953 - 1958 in Manchester. In both points, the equipment was operating on the same frequency and had about the same sensitivity. Unfortunately, measurements are lacking conducted in Kharkov and Manchester during the same year.

In order to represent the variations in the velocity of the prevalent wind during several years, in Fig. 3.11, we have presented the values or the velocity

obtained in Manchester during five years (from 1954 to 1958). Let us remark that the results obtained in England permit us to confirm that the solar activity has practically no effect on the value for the constant component of the wind velocity. The solar activity is characterized by various indexes of which the most useful are the relative numbers of the sunspots (the Wolf number). Thus, in 1954, the number of sunspots comprised 4,4, while in 1958 they comprised 180,8 [143]. The states of the ionosphere, including the lower one, change quite appreciably.

The numerous studies of the upper atmosphere conducted in recent years with the aid of rockets and artificial earth satellites so far have not yielded a reliable answer to the question of whether at the height of 80 - 100 km, there are perceptible diurnal and seasonal variations in the temperature.

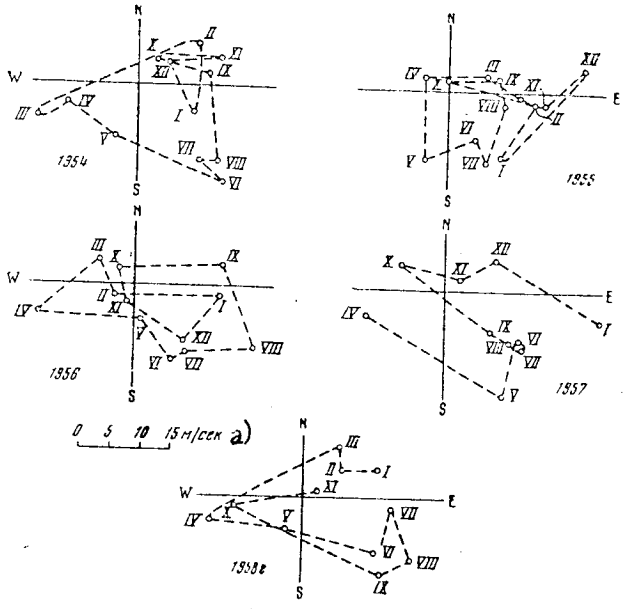

Fig. 3.11. Variation of the Value and Direction of Velocity of Prevalent Wind Obtained in Manchester. The data pertained basically to the height of 90 - 100 km. Key to figure: a) m/sec.

Such variations are clearly expressed, starting from the altitude of 150 - 200 km and close to the Earth. At the same time, if we compare the results of a study of the winds conducted in the same point over a prolonged period (such comparisons permit us to make measurements conducted during the IQSY), we can note a series of previously unknown phenomena. In Fig. 3.12, we have shown the diurnal variations of the zonal component of wind velocity, derived in Kharkov in the same days from December 1963 to April 1964, and from December 1964 to April 1965. It turns out that the diurnal variations (increase or decrease of velocity) occur practically in the same season in different years; in this connection, the values of the constant component and of the amplitudes of the harmonics for the different years may also be different. Thus, in February 1964, $V_0 = 22.0$, $V_1 = 21.9$, $V_2 = 11.2$ m/sec, while in February 1965, $V_0 = 13.7$, $V_1 = 12.5$, $V_2 = 7.3$ m/sec. The initial phase angle both of the diurnal component θ_1 as well as of the semidiurnal θ_2 during the year changes little (refer to Table 3.5); the significant deviations occur usually in not more than 2 - 3 months in the year (most often, this is one of the spring or

one of the autumn months). For December - March 1964 and 1965, θ_1 = 300 - 333 degrees, θ_2 = 179 - 198 degrees (in January 1964, the angles were 251 and 134 degrees respectively). The ratio of the amplitudes of the basic harmonic components, i.e. the semidiurnal V_2 to the diurnal V_1 constitutes:

	December	January	February	March	April
1963-1964	2.3	1.3	0.5	2.1	2.5
1964-1965	1.9	1.0	0.6	2.8	2.6

These data provide evidence that the value of V_2/V_1 from month to month during any year usually varies more considerably than for the same month of the two adjacent years. Let us note that in February 1964 and in February 1965, there occurred approximately a two-fold increase in the amplitude of the diurnal component above the semidiurnal; in February - March 1963, V_2/V_1 equalled 1.0 and 1.3. The results in 1966 differ significantly from the data in Fig. 3.12.

/117

The results presented in Fig. 3.12 for the same month but separated in time by one month evidently typify the winds at the same height.

The diurnal variations of the meridional component of wind velocity obtained for the same month in successive years differ from one another somewhat more than the zonal components. However, even in these cases, we can speak of the analogy in the variation of the velocity (Fig. 3.13).

In Fig. 3.14, we have shown the values of the amplitudes of the semidiurnal harmonics of the zonal and meridional components. We have taken the results of the Kharkov measurements for 1962 - 1963 and the English findings, averaged for five years of measurements [140]. For each of the points, for most of the months, the amplitudes of the 12-hour harmonics of both components have similar values. At the same time, in Manchester, from month to month, the amplitudes of the semidiurnal components changed by about 6 times; in March-July, the amplitudes of the semidiurnal component equalled about 5 - 10 m/sec and were less than the values of the velocity of the prevalent wind during these months. In Kharkov, in 1962 there were registered considerably less variations, than in Manchester, of the semidiurnal component during the year. In all, there occurred a three-fold variation in the amplitudes. The amplitudes of both components have similar values.

The semidiurnal component of wind velocity can be represented in the form of a vector. The vector for all of the months (except September) accomplishes a rotation in a clockwise direction. The shift between the northern and eastern direction of the semidiurnal component in certain months differs appreciably from three hours (90°). The measurements made in Kharkov do not permit us to establish any seasonal regularity in the variation of this displacement.

/118

In Table 3.6, we have shown the values of the angle expressed in hours, by which the northern component of the 12-hour component is ahead of the eastern one. In this same table, we have included the values obtained in Manchester.

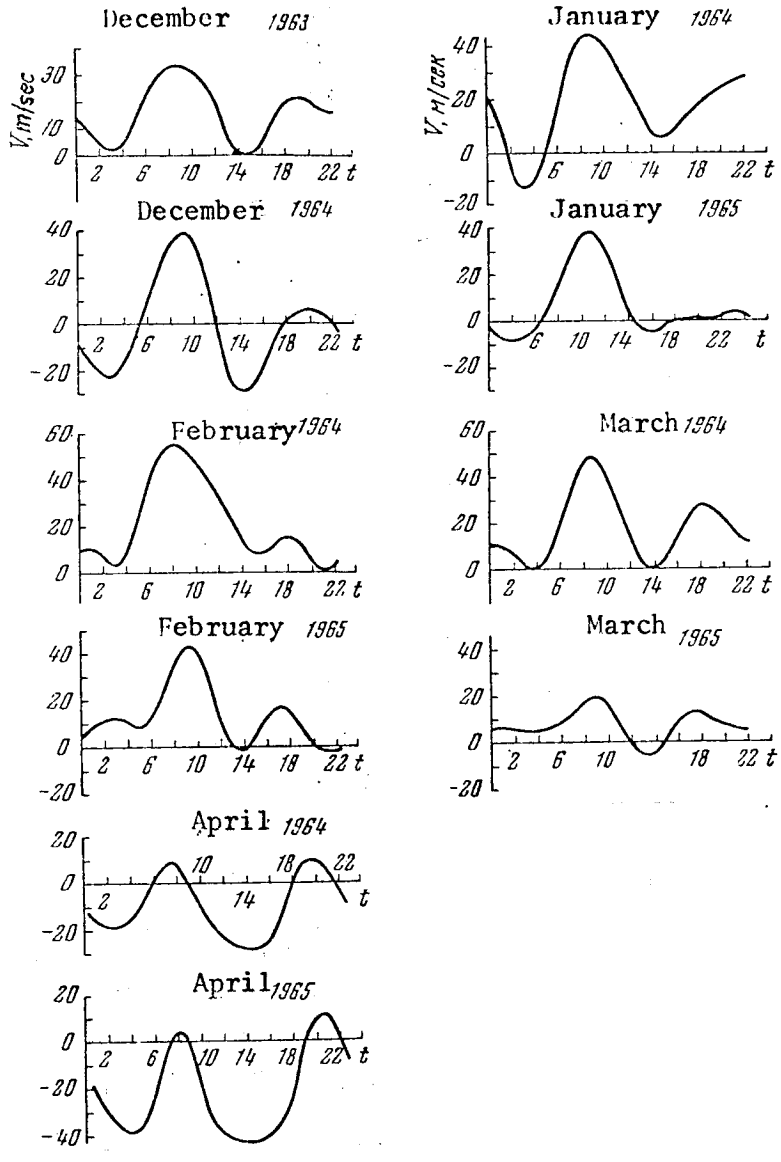

Fig. 3.12. Diurnal Variations in the Wind Velocity Based on the Measurements in Kharkov from 1964 - 1965 (Zonal Component). We have shown the sum of the constant component and four harmonics. The time is local. Positive direction eastward.

It is difficult to compare the diurnal and the 8-hour components, since there are appreciable deviations in the amplitudes and phases from the mean values obtained in both points. Common for these points is the fact that usually the amplitude of the 24 and 8- hourly components is less than the amplitude of the more stable semidiurnal component. The displacement between the northern and eastern components quite often differs significantly from 90°.

Table 3.5

Дата Date	East						
	V_0	V_1	V_2	V_3	V_4	θ_1	θ_2
1962							
Март . . . . . March							
Апрель . . . . . April	—13.4	13.4	18.4	4.8	5.4	15.7	8.0
Май . . . . . May	—11.9	6.7	15.4	6.9	2.0	14.0	7.1
Июнь . . . . . June	16.0	5.0	20.0	4.7	1.7	6.3	8.8
Июль . . . . . July	29.2	7.6	13.0	9.5	5.1	16.9	8.4
Август . . . . August	21.3	3.6	17.8	2.7	0.7	15.4	6.5
Сентябрь . . . September	— 6.6	3.5	14.5	4.9	3.9	20.3	5.8
Октябрь . . . . October	15.3	16.3	15.4	6.8	5.9	13.4	9.2
Ноябрь . . . . November	4.6	6.9	22.2	5.4	2.9	16.1	10.2
Декабрь . . . . December	9.1	7.0	30.0	1.7	1.2	16.7	9.0
1963							
Январь . . . . January	— 1.1	6.8	15.0	4.0	1.6	13.6	11.5
Февраль . . . . February	16.3	11.1	14.9	8.1	6.6	16.6	10.3
Март . . . . . March	5.3	10.1	10.5	5.7	2.3	13.4	9.2

west		North-south								
θ_3	θ_4	U_0	U_1	U_2	U_3	U_4	θ_1	θ_2	θ_3	θ_4
		5.4	3.3	17.4	5.1	2.8	7.4	7.3	7.1	3.2
6.2	2.6	— 8.5	1.5	18.7	1.7	1.4	11.9	5.3	7.7	7.3
6.9	2.8	— 6.4	7.7	18.9	9.5	2.0	11.6	4.9	4.5	2.6
2.2	5.1	—10.0	5.9	24.0	7.2	5.6	11.9	4.9	5.6	4.5
2.5	6.1	— 4.0	6.0	24.1	7.1	4.6	8.9	6.1	7.4	3.4
8.9	3.7	—13.3	3.1	18.5	6.7	4.9	3.7	5.1	4.1	5.5
11.9	7.1	1.2	2.7	18.0	1.5	5.7	11.7	6.4	4.6	6.2
8.5	5.0	— 1.6	8.0	10.2	2.0	2.2	8.7	5.6	8.7	2.8
8.5	5.7	0.6	5.0	12.7	7.8	4.8	4.1	6.1	6.0	6.4
7.0	1.6	— 0.1	11.9	18.6	2.9	4.1	7.2	5.6	7.3	5.5
9.6	1.2	2.5	9.0	18.4	13.8	3.0	6.8	5.7	5.6	2.3
9.2	3.6	6.0	8.4	20.3	10.0	3.6	7.4	6.0	6.6	2.9
9.8	7.5									

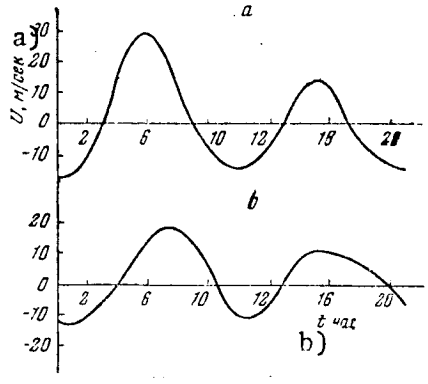

Fig. 3.13 Diurnal Variations of Wind Velocity Based on Measurements Taken in Kharkov in March 1964 (a) and 1965 (b) (Meridional Component). We have shown the sum of the constant component and of four harmonics. The time is local. Positive direction northward. a) U, m/sec; and b) time, hours.

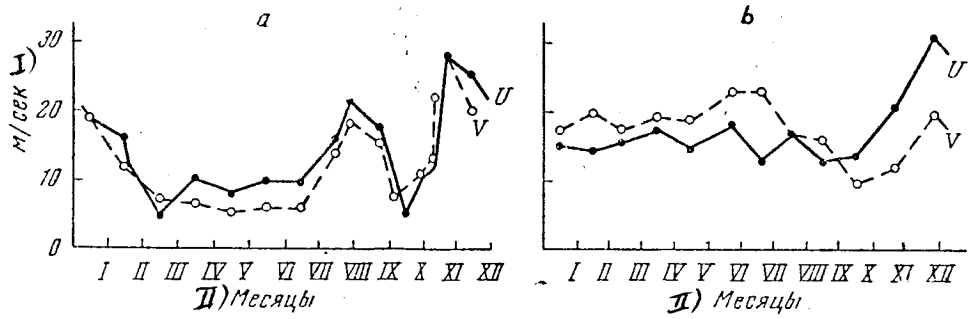

Fig. 3.14. Variation in the Amplitude of Semidiurnal Harmonic Components of Wind Velocity During the Year. a- Kharkov, 1962 - 1963; b- Manchester, averaged data for 1953 - 1958. I) m/sec; and II) months.

Table 3.6

Month	Kharkov	Manchester	Month	Kharkov	Manchester
Jan.	5.8	3.0	July	2.3	0.6
Feb.	3.7	3.0	August	1.4	2.7
March	1.9	3.0	Sept.	—0.6	2.9—3.1
April	2.7	2.8	Oct.	3.6	2.5—3.6
May	2.2	4.4	Nov.	4.1	2.9—3.0
June	3.9	2.3	Dec.	4.4	2.6

Let us proceed to a discussion of the experimental results. As we have already noted, up to the present time a number of hypotheses have been expressed yielding essentially a qualitative but not a quantitative analysis of the pattern of the winds in the upper atmosphere.

Predominant Winds

Proceeding from the measurements of the temperature at a varying height in a few separated points around the globe, starting from 1951, proposals were made of several models of the global pattern of the winds [144 - 147]. It is natural that the development of rocket sounding and the observation of the movements of clouds generated artificially at a great height completely refuted certain of the proposed models, since at the basis of their construction, there lies the unconfirmed variation in the temperature with height (e.g., [147]). From 1963 - 1964, new suggestions have appeared concerning the winds at a varying height (for example, [148]).

In Fig. 3.15, we have presented the seasonal variation of the zonal component of the wind, suggested by Batten [144] for the middle latitudes. This distribution was utilized in a mathematical analysis of the movements in the atmosphere [148] (see below). It is suggested that the 70 - 100 km /119
layer in winter above the pole is warmer than above the equator, and colder than in summer. Kellogg [149] considers that this can be explained, proceeding from the distribution of the atomic oxygen at a various height. As we have

already commented, in the middle latitudes, we also lack reliable experimental data concerning the atmosphere at the height under consideration. It is suggested that a steady (monotonous) variation of the temperature between the pole and the equator takes place. Kellogg considers that in the middle latitudes in winter, the temperature is higher than in summer. The meteor data pertain to a unique type of a transition zone of the atmosphere (90 - 110 km), where we find the beginning of the molecular dissociation of oxygen, and ionization quickly increases (with h = 80 - 85 km). The zone is characterized by a developed turbulence. Kohanskiy [150], having analyzed various data concerning the measurement of wind velocity considers that the turbulent nature of the movement ceases at the altitude of about 100 - 105 km. This process is accompanied by the rapid variation in wind velocity with the increase in the height in the sector 95 - 130 km. In Fig. 3.16, we have shown the mean values of the zonal wind component. In the winter, the velocity in the meteor zone is slight as compared with the velocity at another height; in the summer, it reaches 30 - 60 m/sec. If we supplement the distribution represented in Fig. 3.16 to the height of 110 - 120 km, as the observations of the sodium clouds indicate, the wind velocity quickly increases to 120 - 150 m/sec. Starting from a height of about 100 km, the meridional component equals or surpasses the zonal one.

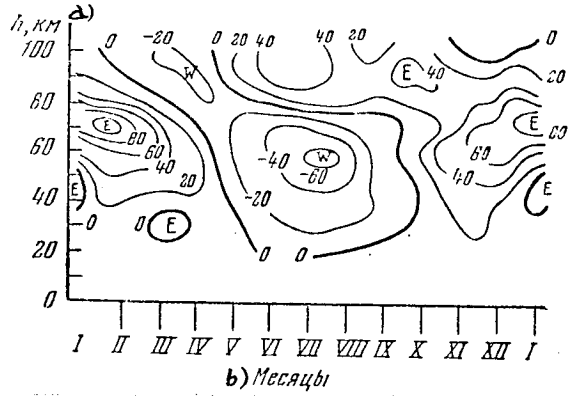

Fig. 3.15. Zonal Component of Velocity of Prevalent Wind for Latitude of Location 30 - 40°. a) h, km; and b) months.

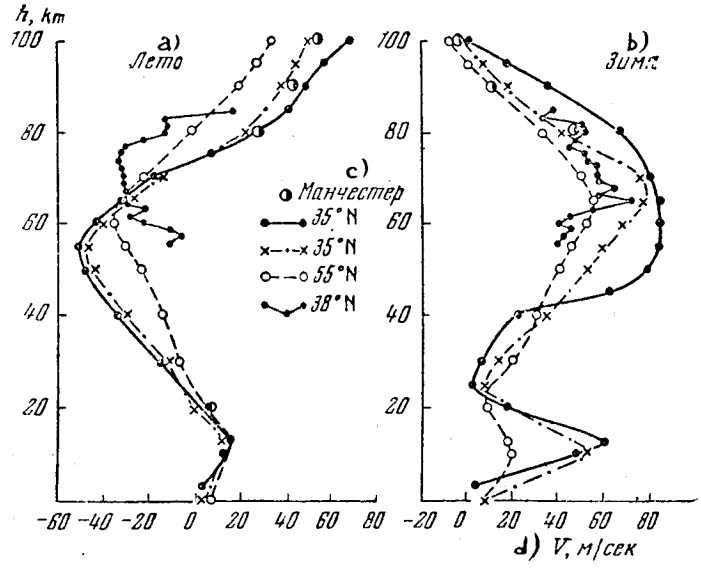

Fig. 3.16. Summer and Winter Values of the Zonal Velocity Component of the Wind Based on Data of Rocket Observations. In addition, values

are shown obtained based on radio observations of the drift of meteor trails in Manchester. Key: a) summer; b) winter; c) Manchester; and d) V, m/sec.

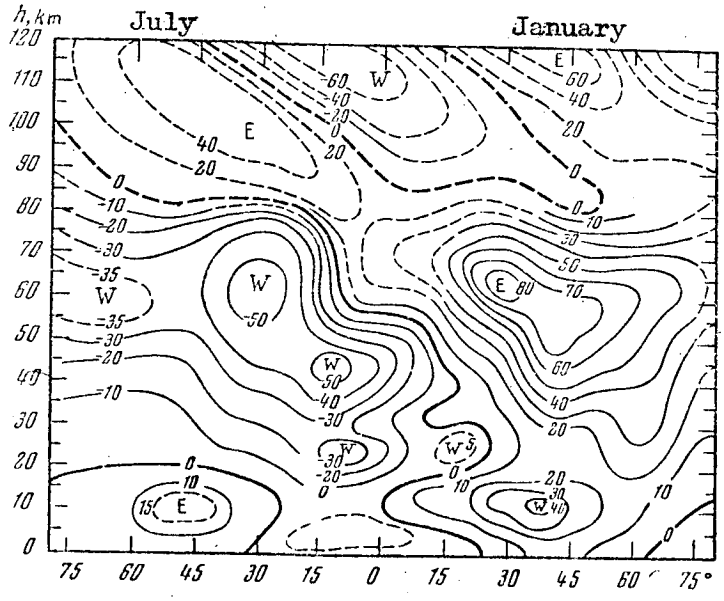

Fig. 3.17. Average Values of the Velocity (Zonal Component) for July and January (in m/sec) [152]. Positive direction eastward. On the x-axis, the geographic latitude is plotted.

Below this height, usually the meridional component is 3 - 4 times less than the zonal component (therefore, in Fig. 3.16, we have shown only the zonal component).

In the reports [150 - 152] for an analysis of the winds in the upper atmosphere, the results of the atmospheric studies published up to 1964 have been involved. The corresponding distribution for the zonal velocity component of the wind is shown in Fig. 3.17; the authors considered the data pertaining to the height of about 80 km and more as insufficiently established (shown by a broken line in the drawing). Let us note that the value of the wind velocity in July (Fig. 3.17) for the latitude of the location 50° and the height 95 km equals 30 m/sec; the same result was obtained in Kharkov (28 - 33 m/sec). In January, the constant velocity component changes by several times from year to year. The maximum difference in the distributions shown in Figs. 3.15 and 3.17 pertains to the height of 55 - 65 km.

The distribution of the winds (refer to Fig. 3.17) permits us to make certain conclusions. In the winter and summer, at a height of about 80 km, in the middle latitudes there forms a fairly stable transition zone; below this height, the winds are westerly, and above it they are easterly. Let us note that this is confirmed not only by the meteor observations but also by the observations of the artificial clouds. During the winter, in the low latitudes, the zonal component is directed westward [152].

The suggested pattern of the seasonal variations of the winds up to a height of 120 km (at the latitude of 30°) is represented in Fig. 3.18 [152];

up to a height of about 80 km, the distribution is based on many experimental results. The stable wind directions are observed at the height between 30 and 80 km; in the winter, these are easterly winds, while in summer they are westerly.

For the meteor zone (900 - 1000 km), the movement in the easterly direction is the basic one from May to November (Fig. 3.17), and in a westerly direction from December to April. For the latitude 50°, such a circulation of the atmosphere was not confirmed. In reality, the results (Fig. 3.19), obtained in Kharkov in 1962 and in the period of the IQSY, testified to the principal motion in southeasterly (summer period) and easterly (autumn-winter period) directions.

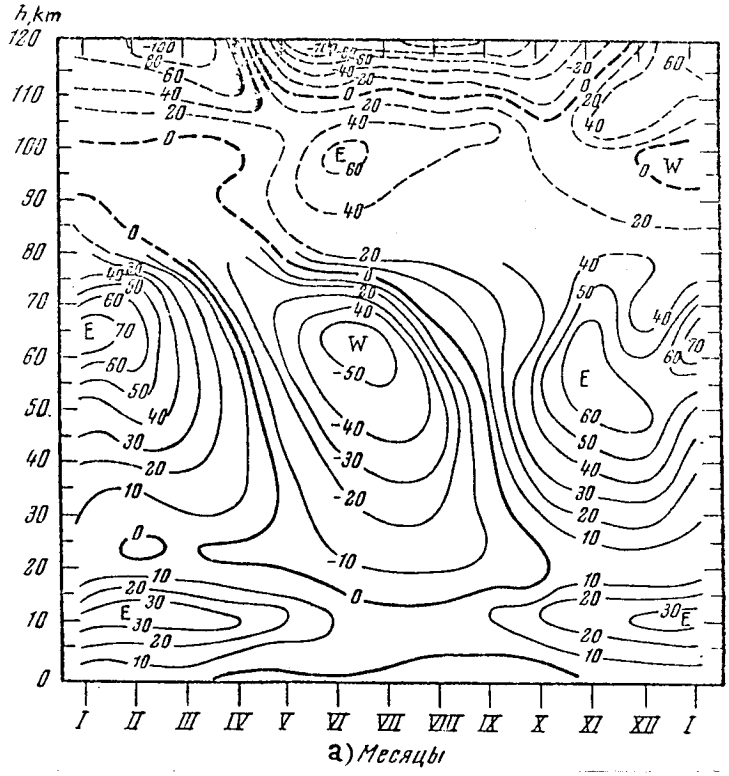

Fig. 3.18. Average Monthly Values of Wind Speed. Geographic Latitude 30° [152]. Positive direction is eastward. a) months

The diurnal wind speed values presented earlier (refer to Figs. 3.12 and 3.13) for various months indicate that the diurnal variations exceed considerably the seasonal ones (see Fig. 3.19), and evidently the latitude ones (refer to Fig. 3.17). This is also indicated by the results of observing the artificial luminescent clouds (Fig. 3.20); four experiments were conducted on 3 December 1962 from 1720 hours to 2245 hours in Eglin (30°N, U. S.) [152].

/122

From year to year, as follows from Fig. 3.19, we find a fairly high frequency of repetition of the results. Unfortunately, as we have already commented, few reliable values of the temperature were obtained for the meteor zone. Particularly scarce are the data for the height starting about from 70 - 80 km (height of elevation of the meteorological rockets) and up to about 200 km (the lower height of movement of artificial earth satellites).

The rate of the constant transport motion has a quite definite nature of variation during the year. Therefore, Kokhanskiy, considering the geostrophic nature of the wind in the meteor zone considers that the temperature above the pole varies periodically, colder in summer and winter and warmer in the remaining time [150].

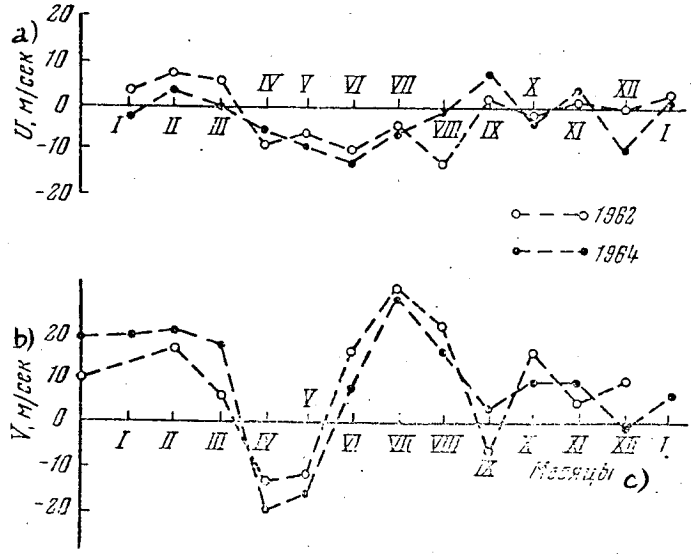

Fig. 3.19. Meridional (Top) and Zonal (Bottom) Components of Predominant Wind Speed, Kharkov, 1962 and 1964. a) U, m/sec; b) V, m/sec; and c) months.

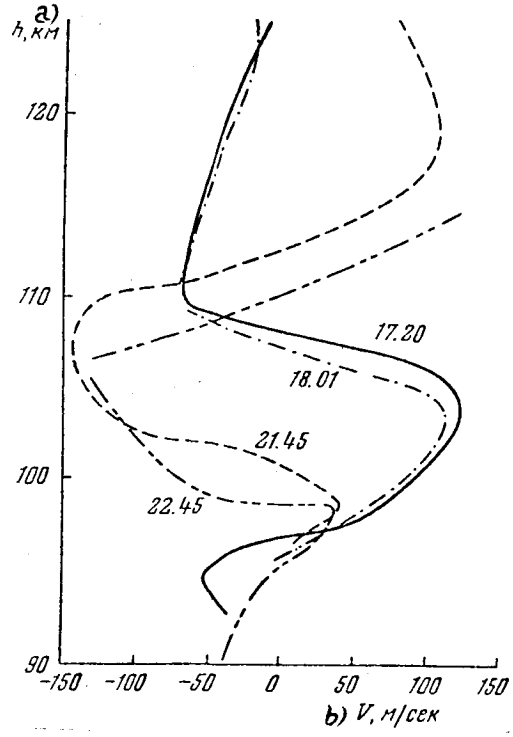

Fig. 3.20. The Zonal Wind Velocity Component Determined Based on Observations of Artificial Luminescent Trails on 3 December 1962. a) h, km; and b) V, m/sec.

Evidently we can consider that the observed displacement of the upper atmosphere is the result of the constant transport motion of the semidiurnal and diurnal harmonic components (tidal components); it also occurs owing to the internal gravitational waves assumed by Hines [153]. A hydrodynamic consideration assumes a broad spectrum of such waves at any height above 50 km. The main types of waves reach their maximal manifestation in the E-area of the ionosphere.

Kokhanskiy attempted to determine the individual velocity components. Based on observations of sodium clouds, for the height of around 95 km, he found that the wind speed, owing to the wave motions, equals about 40 m/sec, while the speed caused by other reasons is around 50 m/sec [152].

The observations of the sodium clouds were conducted in the twilight or predawn hours. This decreases considerably the value of such measurements for revealing the diurnal and semidiurnal components.

Let us return to the data shown in Fig. 3.20. The wind speed at a height of around 105 km reaches 200 - 300 m/sec; the role of the semidiurnal component at this height is appreciable. The variations in wind speed with height are different in different months. In the report [152], the authors consider that one of the possible reasons for the diurnal variations in wind speed is constituted by the pressure waves (induced by the Sun), moving around the surface of the Earth. Assuming the extremums induced by the Sun from 1400 to 1600 and from 0200 to 0400 hours, Kantor and Cole conclude that in December, we can find maximums of a westerly wind at a height of around 112 and 103 km respectively, while the easterly maximums are found at 104 and 95 km; the variations in the height of the maximum are around 8 km. Similarly, in May the eastern wind maximum will occur at a height of 116 and 104 km (the diurnal variation of the height of the maximum is around 12 km). The night (nocturnal) compression of the atmosphere and the daily expansion can explain these significant variations in the position of the wind speed maximum in the eastern and western directions. At a different latitude, the variation in the position of the pressure sur- /123
faces can occur at a varying rate. In the opinion of the authors, the internal gravitational waves and the tidal movements, superimposed on these diurnal pressure waves can explain the variations in the phase and amplitude of the vertical waves and the digression from the geostrophic nature of the winds. For an explanation of the diurnal variations of pressure, as an analysis indicates [152], it is necessary to assume that in the meteor zone, there occur systematic changes in the temperature during the day. In Fig. 3.21, we have shown that the corresponding law of the variation in temperature with height for January and a point at the latitude of 45°. The pressure distribution was found according to the barometric formula. Then, considering the wind to be geostrophic, we determined the values of wind speed. For the conditions indicated in Fig. 3.21, the zonal velocity component at a height of around 95 km equals 25 - 40 m/sec, and is directed westward. This was not confirmed by the Kharkov measurements conducted in January 1964 and 1965 (refer to Fig. 3.12).

The anomalously high value of the semidiurnal wind speed component in the meteor zone in a number of reports is explained by the atmospheric resonance (for example, [148, 154]). After a refinement of the values of the atmospheric temperature at a varying height, the period of oscillations was not derived as equalling 12 hours [148].

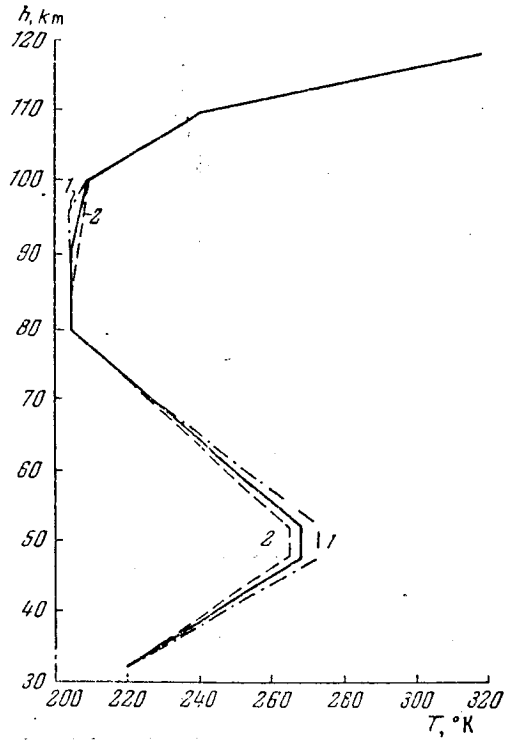

Fig. 3.21. Temperature Profile According to [152] for the Point 45°N, January. 1- day; and 2- night.

A further experimental and theoretical study of the winds in the upper atmosphere is required. It is especially important to obtain reliable statistical data for the meteor zone for each hour of each day.

DETERMINATION OF THE COEFFICIENT OF AMBIPOLAR DIFFUSION AND OF HEIGHT OF THE HOMOGENEOUS ATMOSPHERE

According to the radio waves reflected from the meteors, we can find the coefficient D_a of ambipolar diffusion associated with the pressure and density of the atmosphere; we can compute the height H of homogeneous atmosphere, the atmospheric density ρ and pressure p. Such studies have been conducted fairly extensively in Adelaide and especially in Manchester. Reports are available in which it is indicated that in the processing of the experimental results of the observation of meteors by the radio method, we get contradictory data concerning the atmosphere, disagreeing with the rocket-based data (for example, [95, 155]). The physical factors operating during the scattering of the radio waves in the meteor trails complicate so much the interpretation of the experimental results that the apparent simplicity of obtaining information by such a method concerning the processes in the upper atmosphere is to a considerable extent lost.

/124

Of all the recorded reflections from the meteor trails, we first select the amplitude-time-dependent characteristics, having an exponential law of the attenuation of amplitudes. This is done with the aid of a set of graphs, precalculated at a working value of wave length λ for various τ-values (curves are drawn for log D_a = 4.2, 4.3, 4.4, etc). In Fig. 3.22, we have shown the

results of such a processing of the observations of the sporadic meteors during five days (night hours, September). The measurements were conducted in Kharkov at $\lambda = 8.13$ m; the height was found by the amplitude-phase method. The mean square error of a single measurement of height Δh comprises $\pm$ 2.7 km. In all, around 1000 values were recorded. The spread of the points near any value of log D_a, having the height h_1, h_2..., is tentative; it indicates how many meteors were recorded for a selected height with the same time constant of amplitude attenuation.

Based on experimental points, the linear dependence log $D_a = F(h)$ can be found: a) by way of seeking each value of log D_a of the average value of the height [95], and the subsequent drawing of a straight line through such averaged points; b) by way of finding the averaged points with a preliminary consideration of the error in the measurements of height Δh and $\Delta \log D_a$ [155]; and c) by way of finding the average value of the height based on n of the experimental results, obtained in the limits of variation in height from $(h_1 - \Delta h)$ to $(h_1 + \Delta h)$; in this connection, the mean value of log D_a is found by averaging all of the log D_a-values occurring within the indicated limits of variation in height. Let us note that the first approach of processing (a) is incorrect, since therein, we assume the absence of error in the experimental determination of D_a. Paradoxically, the specific value of H, obtained by such a method coincides with the value found theoretically in the application of rocket data concerning the temperature of the atmosphere.

The wide scattering of the experimental points (refer to Fig. 3.22) once again testifies that we can never determine the height of the occurrence of a recorded meteor based on the time constant of the drop in amplitude (such determinations were conducted in Manchester, in which it was confirmed that the measurement error for the height comprises $\pm$ 3 km [95]). A comparison of the log D_a-values obtained by us for various h-values with the similar 1125
ones obtained in Manchester [95] and Adelaide [156], indicates that the spread in the values is large in all of the measurements. We comment only that the parameters of the equipment, the technique of recording the reflections in Kharkov and Manchester are quite similar.

In Fig. 3.23, we have shown the same values as in Fig. 3.22, only we have allowed for the distortion which is introduced by the terminal velocity of the meteor's motion; we have left only the results with $\Delta \leqslant 0.5$, where $\Delta = \frac{8\pi^2 D_a \sqrt{R}}{V\lambda^{3/2}}$. Hence, it is natural that in this connection, we found a rapid decrease in the quantity of data with a high diffusion factor at a considerable height. The total number of data decreased by about half. With an increase in Δ, the position of the first maximum of the diffraction curve varies appreciably, while the position of the remaining maximums remains almost without changes. Now, if we conduct the calculation $H = dh/d\ln D_a$, it is natural that its value will be exaggerated as compared with the pertinent value found in Fig. 3.22. In Fig. 3.23, most of the meteors are characterized by $\Delta = 0.1 - 0.4$.

After the screening of the curves having $\Delta < 0.5$, there remain many experimental points with a high value of log D_a at a low altitude. One of the reasons for such a distribution may be the resonance effect. It is known that

when the vector of the electric field of an incident wave is perpendicular to the axis of the meteor trail, the resonance of the plasma can develop. As a result, the amplitude-time-related characteristic yields an exaggerated value of the diffusion factor. The resonance dispersion is manifested during the reflection of radio waves by the trails of the underdense and transient types.

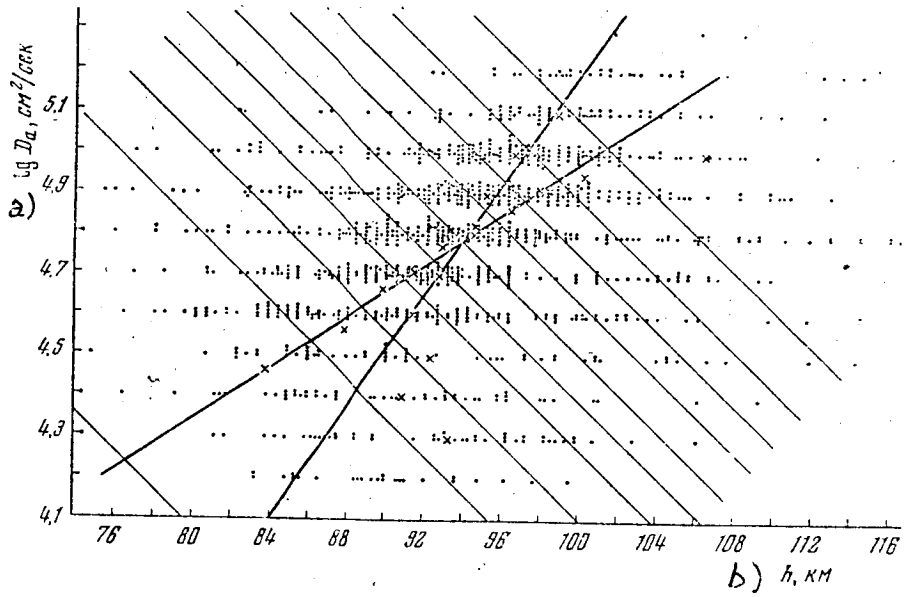

Fig. 3.22. Experimental Values of Log D_a, Obtained for the Exponentially Attenuating Amplitude-Time-Related Characteristics (Kharkov). D_a was determined based on the time constant of reduction in the amplitude. The height of occurrence of the reflecting area was measured by the amplitude-phase method $\lambda = 8.13$ meters. a) log D_a, cm^2/sec; and b) h, km.

For an estimation of the frequency of appearance of the resonance effect during the random orientation of meteor trails relative to the polarization plane, we conducted the following experiment [157]. We used two autonomous /126 transmitters, having about the same parameters (similar to those described in this chapter). The repetition rate of the pulses being generated by each of them is 500 cps. Both systems operated from a common synchrogenerator, wherein the pulses were radiated with a displacement of about 100 microseconds. One transmitter operated on a vertically-polarized antenna, while the other operated on a horizontally-polarized antenna, with the aid of which the investigations of the meteors were conducted daily.

The reception was conducted on one receiver having separate switching HFA to which we connected the vertical and horizontal antennas. The photographic recording was conducted on one beam, which at the high repetition rate (500 + + 500 cps) permitted us to determine easily the mutual position of the maximums of the diffraction curve, and also the polarization ratio of the signals' amplitudes. The receiver had a linear amplitude characteristic in a wide range of amplitudes.

The experiment conducted by us indicated that the presence in the values of a time constant of the damping of the amplitudes of the signals received in

the antennas with a varying polarization in individual cases attained up to 2 - 2,5-fold. This occurred at a height h less than 92 km. The time shift between both curves either was lacking or in most cases did not exceed one pulse.

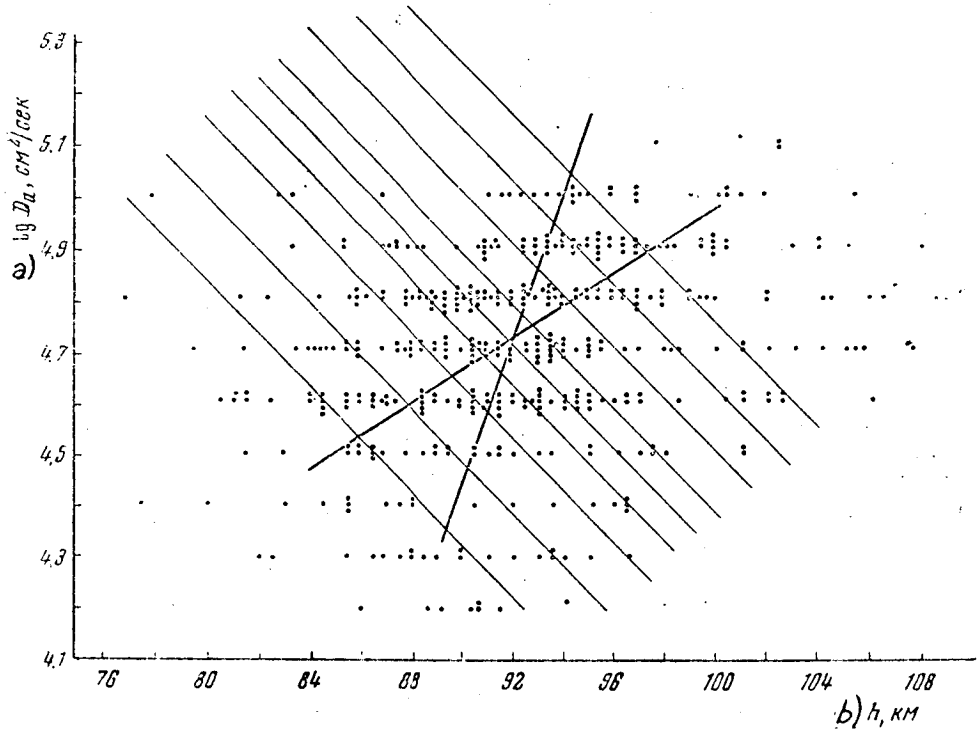

Fig. 3.23. Experimental Values of Log D_a at Varying Height, Obtained for Exponentially-Attenuating Amplitude-Time-Related Characteristics with $\Delta < 0,5$ (Kharkov). The selection was conducted based on the values presented in Fig. 3.22. a) log D_a, cm^2/sec; and b) h, km.

The observation of the sporadic meteors demonstrated that for the underdense trails, approximately in 10% of the total number of recorded trails, the polarization effect was revealed. It is possible that it is specifically such a type of distortion of the amplitude-time characteristics that led to the situation that at the height of 80 - 90 km, there are trails with log D_a = 4.9 - 5.0 (refer to Fig. 3.23).

The wide spread in the values for log D_a and h is sometimes explained by the effect of the winds. Let us discuss this question. One should distinguish the effect of the regular and the irregular motions of the atmosphere. If the wind velocity $V_в$ does not depend on time, the form and the value of the amplitude-time dependence does not change; the diffraction pattern displaces in time as an entirety. In [70], it is shown that the displacement of the amplitude-time characteristic equals $t_o = R_o V_в / V^2$. This occurs practically during the registration of almost all of the meteor trails, and on this is based the measurements of the drift based on the Doppler frequencies.

It is much more complex to estimate the effect of the turbulent wind. It is known that the variation in the speed of a turbulent wind reaches about 100 m/sec • km. At such high velocity gradients, there can develop the displacements of the point of specular reflection; the amplitude-time characteristics

of the signals change; and the maximums and minimums of the diffraction curve are displaced. The specific case when the wind velocity changes linearly along the trail is considered in [158]. The manifestation of the recording of signals in which the exponential law of the variation of amplitude is still retained, but the time constant varied under the effect of eddy motions, is practically impossible. Let us comment only that in the observation of the meteors for $\lambda = 8.13$ m, we recorded the signals with a time constant most often of 0.04 - 0.1 sec, while the mean value of the gradient of the turbulent wind comprises in all 10 m/sec · km (according to the experimental data, the wind gradient above 36 m/sec km occurs in about 7% of the cases, while above 72 m/sec · km, in about 0.6% of the cases). In addition, with a large number of measurements, we can basically expect the effect of the turbulent wind upon the spread in the values, and not on the final averaged values for log D_a and h.

The significant errors in the nature of the experimentally obtained values for log D_a at a varying height h are introduced by the inclusion of the results (refer to Fig. 3.22 and 3.23) of the transient type of meteors. The percentual content of the number of such trails depends on the effective sensitivity, the equipment being used, and the wave length. In Fig. 3.24, we have represented the experimental values for $\Delta \leq 0.5$ for the trails only of the underdense type. A comparison of Figs. 3.22 - 3.24 graphically shows how, from the exponential characteristics of the signals, there remained in all around 200 values.

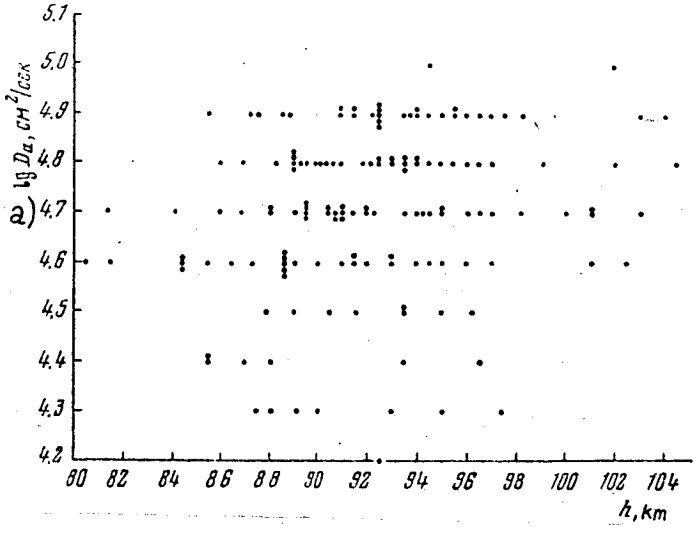

Fig. 3.24. Experimental Values for Log D_a, Found According to the Meteor Trails Only of the Underdense Type. For all of the amplitude-time characteristics Δ was determined by three methods, based on the time constant and the diffraction patterns. a) log D_a, cm^2/sec

Let us discuss further certain causes leading to the situation that the observed distribution by height of the exponential amplitude-time-related characteristics differs from the actual one. The studies conducted by us of the initial radius r_o of the meteor trail indicated that owing to the high value of r_o at a considerable height, it is impossible to obtain reflections from the trails of the underdense type. Only a slight part of the meteors, flying into the upper layers of the Earth's atmosphere with a velocity of

about 50 km/sec and above is recorded during the radar meteor observations. The upper limit of the possibility of observation for $\lambda = 8$ m of the underdense trails equals about 100 km.

In the upper part of the meteor zone, a certain distorting effect on the law of the variation of the amplitudes of the signals reflected from the meteors, is exerted by the magnetic field of the Earth. It is possible that in the scattering of the values for D_a and h, an effect is also exerted by certain diurnal variations in density, variations from day to day (usually the experimental data are combined for several successive days, sometimes weeks or months).

Let us proceed to a discussion of the experimental results.

Reports are available in which according to the D_a-values obtained at a varying height, there are derived the average values of the diffusion factor, and of the fluctuation in the atmospheric density; inferences are made concerning the laws of the diurnal variation D_a, $d\zeta/\zeta$, H. The analysis is extended to a wide range of the variation of height, i.e. from 85 to 105 km. The review conducted above by us of the effect of the various factors indicates that evidently one can by no means be limited simply by a consideration of the error involved in determining h and D_a and change based on a comparison with the previously adopted procedure of processing, the same experimental data as this was done in [95, 155]. Firstly, in these reports a rigorous screening was not conducted of the underdense trails and the distortions were not considered which develop owing to the terminal velocity of the meteor and the high speed of expansion of the trail. Secondly, the data similar to those represented /128
in Fig. 3.22 and 3.23, will always yield an exaggerated value for the height of the homogeneous atmosphere. At $\lambda = 8$ m at a height less than 90 - 92 km, in the results increased as a result of the resonance phneomenon, there enter the D_a-values (the time constant of the amplitude's attenuation decreases). At a height above 95 km, the noticeability of the meteors disappears; by the same token, there are automatically excluded the high values for the diffusion at a great height; based on the spread in the experimental data at this same height, the slowly attenuating amplitudes lead to a depression of the pertinent averaged values for D_a. High values for D_a lead to an increase in Δ. At the values $0,5 < \Delta < 1,5$, the reflection from the trail first has a specular nature, and then converts to the so-called head echo.

The procedure used in processing the data has a considerable significance. We should never select for analysis of the diffusion the data based only on the time constant or should we use the slow scanning. As a rule, in this connection, a large number of the reflections from the trails of the transient type will be assumed as reflections from the underdense trails. A trail can be in the first maximum (or the first and several of the succeeding ones) of the transient type, and then can approach an underdense one. Δ constitutes a quite important value, characterizing the law of the variation of the amplitude-time-dependent characteristic, and without its utilization, the sampling of the data will always be ineffective. With the inclusion in the results of an analysis of the data concerning the trails of the transient type, we have also dealt in the report [159]. In an analysis of the values of the initial radius r_o, in report [96], it was found that r_o does not depend at all on the velocity of the meteor and depends only slightly on diffusion; the values of the initial radius were obtained for h > 95 km as depressed

values. It is understandable that if we attempt to find experimentally r_o for the underdense trails, we will obtain $r_o = 0$; the trails with the linear density $\alpha \approx 10^{12}$ electrons/cm, as is clear from the definition itself, occupy a certain intermediate position between the unsaturated (underdense) and saturated trails.

The experimental results presented in Fig. 3.24 also do not permit one to find sufficiently reliable values for the height of a homogeneous atmosphere. In addition to the resonance effect, upon the dependence $\log D_a = F(h)$, being found experimentally, an effect is exerted by the slight noticeability of the slow meteors; this is reflected in the spread of the D_a-values in case of low h-values.

Thus, we arrive at the conclusion that based on a series of experimental values of the diffusion at a varying height, we find the height of the homogeneous atmosphere only with considerable difficulty. For determining the parameters of the atmosphere, the properties of the meteors must be sufficiently understood. Evidently, so far we must be content with calculated values. The height of the homogeneous atmosphere is calculated from the condition

$$\frac{\zeta_1}{\zeta_2} = \frac{H_2}{H_1} e^{-\frac{2h_1 - h_2}{H_1 + H_2}},$$

where H_1, h_2 equals the height of the homogeneous atmosphere for h_1 and h_2 respectively; ζ_1 and ζ_2 equal the densities of the atmosphere for h_1 and h_2. In the calculation, it is assumed that there occurs a steady variation in the H-value with the variation in the height of the atmosphere. For the height h = 95 km, H varies from 5.4 to 6.8 km. Can we obtain a value of the diffusion factor based on the meteor data? Evidently, we can at $\lambda = 8$ m in the narrow height range h = 91 - 93 km, where the distorting factors have the least effect upon the experimental values of the diffusion factor.

In Table 3.7 based on the data in Fig. 3.23, we have presented the values for $\log D_a$, found based on the linear empirical dependences, constructed: a) without allowance for the error in the determination of diffusion, b) assuming $\Delta h = \pm 2.7$ km, $\Delta D_a \approx 0.3 D_a$ (in analogy with [95]). In addition, / 129 for the sector of the height 92 ± 2.7 km, we found the average values for height h and $\log D_a$ (signified by "в" in the table).

Table 3.7

Type of calculation	h	$\log D_a$	Type of calculation	h	$\log D_a$
а	92.0	4.73	в	92.1	4.72
б	92.0	4.64	а	—	—
в	92.9	4.76	б	92.0	4.73
а	92.0	4.73	в	92.0	4.73
б	92.0	4.71			

As follows from the data presented, all the methods for finding the diffusion factor yield similar values for h = 92 km. In the utilization of the temperature and density of a standard atmosphere, the calculated value of $\log D_a$ for h = 92 km, we obtain 4.5.

Let us comment that based on the experimental data presented in report [155], for the night hours in January-February 1959, at the height h = 92 km, $\log D_a \approx 4.66$; the value of $\log D_a$ was found with allowance for the errors in Δh and D_a. In an earlier report by Greenhow and Neufeld [160], for h = 93 km, $\log D_a = 4.7$.

CHAPTER 4

ORBITS OF METEOR BODIES AND DISTRIBUTION OF METEOR MATTER IN THE SOLAR SYSTEM

MEASUREMENT OF THE VELOCITY OF METEORS

The radar observations permit us to determine both the velocity as well as the position of the meteor radiants, a knowledge of which is required for computing the orbits of the meteor bodies. Currently, in the radio observations on the waves $\lambda \gtrsim 4$ m, the velocity of meteors is usually found by the diffraction method which was described in Chapter 2. In this connection, we find one value of the velocity referring to the moment of passage by the meteor of a point of the specular reflection in the trail.

In the case of extremely brilliant meteors, in addition to the basic specular reflection of radio waves, from the ionized meteor trail, we can observe a weaker reflection from the head part of the trail, the so-called "head echo". If the meteor velocity v remains practically constant, the range R of the head echo varies with the time t according to the hyperbola

$$R^2 = R_0^2 + v^2 t^2, \qquad (4.1)$$

where R_0 is the shortest distance to the trail. According to the curve "range-time", we can determine the meteor velocity. This method was first applied by Hey, Parsons and Stewart [161] during the observations of meteor range of the Draconids in October, 1946. They were able to measure the velocity of 22 meteors. Subsequently, the "range-time" method was developed by McKinley and Millman [162] and was applied for measuring the velocities and braking of meteors.

During the observations with the standard meteor radar sets, the percentage of meteors for which success was attained in measuring the velocity by the "range-time" method is about 1000 times less than that attained by the diffraction method. Therefore, the "range-time" method can not compete with the diffraction method in the statistical measurements of the meteor velocity. However, the diffraction method with the utilization of one receiving station (set) yields a velocity value only in one point in the trail, and does not permit us to measure the braking of the meteors. By the "range-time" method, there can be obtained the variation of meteor velocity during the entire period of visibility of the head echo. In recent years, in a number of meteor observatories [133], radar sets have been developed, including several dispersed receiving points; this permits us to measure by the diffraction method the velocity in several points in the trail and to compute the braking of the meteors.

In the case of observations conducted with very powerful radar sets on the waves $\lambda \lesssim 2$ m, the reflected images from the ionized meteor trails are recorded relatively rarely, and the main type of meteor reflections has become represented by the head echos. At a sufficiently power of the radio set, even on the waves $\lambda < 1$ m, by the "range-time" method during an hour of observations, we can measure the velocities of dozens of meteors. In 1961, Pettengill [163], on the frequency of 440 mc measured the velocity of several hundreds of meteors in the Perseids meteor shower. The average value of the velocity proved to be 62.5 ± 2.5 km/sec, which is close to the velocity of the Perseids, obtained from the photographic observations. /131

STATISTICAL METHODS OF DETERMINATION OF METEOR RADIANTS

The methods of finding the meteor radiants according to the radio observations can be divided into statistical, which permit us to measure the coordinates of the radiants of the meteor showers or the average radiants of groups of meteors, and the methods of finding the radiants of individual meteors. All of the statistical methods utilized the property of the specular state of the reflection of radio waves from the ionized meteor trails.

The "Quantity-Time" Method

In 1945, Hey and Stewart [164] determined for the first time the coordinates of the radiant of the meteor shower δAquarids according to radio observations. Use was made of three radar sets on the frequency of 73 mc, dispersed for a distance of more than 100 km. The axes of the directional diagrams of the antennas intersected at one point at a height of around 100 km. Comparing the diurnal pattern of the quantity of meteors in three radar sets and considering the specular state of the reflection, we were able to compute the coordinates of the radiants of the meteor showers, which yield a perceptible increase in the quantity of the meteors being recorded as compared with the frequency of the background of the sporadic meteors. Since during the measurements, use was made of antennas with a wide directional diagram, the accuracy of finding the radiant of the shower proved to be low (± 10°). This method has not received further development (mainly because it requires the use of three simultaneously functioning radar sets) and currently it is only of historical interest.

The McKinley and Millman Method ("Quantity-Range")

In the observation of the Draconids meteor shower in 1946 [165, 166], we observed the variation in the range of the main mass of the recorded reflections during the diurnal motion of the stream's radiant. The range increases with a decrease in the zenith distance of the radiant. Comparing the distribution of reflections according to range, derived for each hour of observations in the period of action of the shower, with the corresponding distribution in successive days, when the shower was lacking, for each hour, we can obtain the minimal value of the range of the meteors in the shower (R_{min}). Assuming that for the meteors in the shower, all of the points of the reflection lie at a certain average height h_o, based on the value of R_{min}, let us find the zenith distance of the radiant:

$$\sin z = h_o/R_{min}. \qquad (4.2)$$

Having constructed the dependence of z on time, we can find the moment of the culmination of the radiant, to which there corresponds the minimal z-value. Knowing the zenith of the radiant in the upper culmination and the moment of culmination, we can readily find the equatorial coordinates of the radiant.

McKinley and Millman [162] estimate the accuracy of determining the position of the radiants $\pm$ (2 - 4°). The method was applied to the measurements of the coordinates of the radiants of large showers: the Geminids, the Quadrantids and others [162, 167]. In this context, use was made of additional criteria for the establishment of the belonging of the meteors to a shower, i.e. the similarity of the velocities, the appearance of reflections typical in duration in the period of the optimal visibility of the shower.

/132

The "quantity-range" method can be utilized successfully in the observations of the large isolated meteor showers and is not suitable in the case of the simultaneous effect of several faint showers. The problem of detecting the showers becomes even more complex, if additional selection criteria are lacking.

The Clegg Method ("Time-Range")

For measuring the radiants of the meteor showers, most extensive use is made of the technique suggested by Clegg [168] in 1948. The method is based on a study of the variations in the range of reflections during the passage of the shower radiant in the field of view of a pencil-beam antenna, which is oriented at a small angle to the direction toward the east or the west.

According to (2.1), the relative sensitivity of a radar set for the direction characterized by the angle of elevation φ and the azimuth A, is proportional to the value K (φ, A):

$$K(\varphi, A) = \frac{G(\varphi, A)}{R^{2/3}}, \qquad (4.3)$$

where G (φ, A) equals the directional coefficient of the antenna. If we assume that all of the points of reflection for the meteors in a given shower fall in a very narrow range of altitudes near a certain average height h_o, the slant range R is unequivocally connected with φ(in the transition from φ to R, it is necessary to allow for the curvature of the Earth's surface). Let us draw on the horizontal surface at the height h_o the lines of equal values K (φ, A), starting from a certain minimal value K_{min} (the left-hand part of Fig. 4.1, a, b; point o is located above the radar set).

From the condition of the mirror state of the reflection, it follows that at the given position of the radiant of a shower in the celestial sphere of the trail of the shower meteors, there will be reflected back to the radar set only the radio waves being radiated in a plane perpendicular to the direction of the radiant, i.e. in the echo-plane. In Fig. 4.1, a, S_1, S_2, S_3 are the trails of the echo-plane on a horizontal surface at the height h_o, corresponding to the directions for the radiant R_1, R_2, and R_3. In the diurnal motion of the radiant through the celestial sphere, the trail of the echo-plane will occupy the successive positions S_1, S_2 and S_3. The initial reflections

from the meteors in a given shower will be registered at that moment when the trail of the echo plane touches the line $K(\varphi, A) = K_{min}$ (the position

S_1 in Fig. 4.1, a). In the case of a fairly narrow directional diagram, for any position of the shower radiant in the celestial sphere, it is easy to /133 construct the anticipated distribution of reflections based on range. For example, for the position of the radiant R_2 and the trail of the echo-plane S_2, the maximal value of range will be O_0B_1, while the minimal value will be O_0A_1

(where O_0 signifies the position of the radar set). The most probable value of range corresponds to the point of maximum value $K(\varphi, A)$ in the trail of the echo-plane. In Fig. 4.1, a, b, on the right we have shown the contours of the variation in distribution, by range, of the meteors of two showers with varying declinations of radiants in the diurnal motion of the radiants. The line PQ signifies the variation of the most probable range. Along the x-axis we have shown the time, computed from the moment of the radiant's culmination.

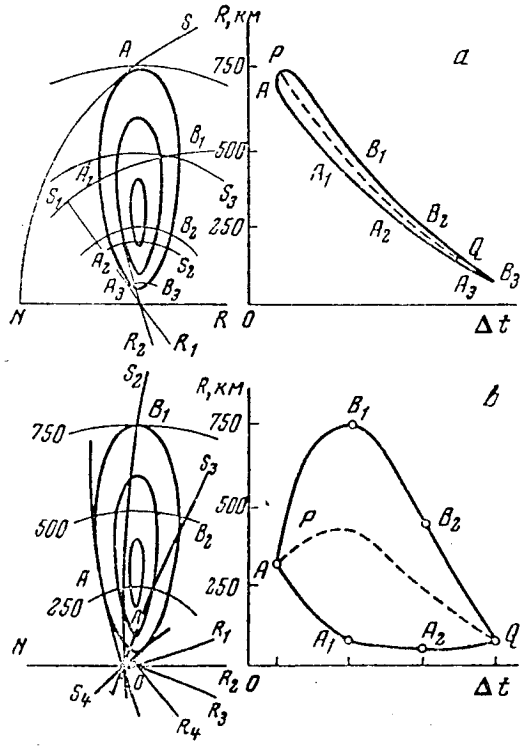

Fig. 4.1. Variation in the Maximal, Minimal and Most Probable Range of Meteor Reflections for an Antenna Oriented Eastward in Case of Two Declinations of the Shower's Radiant.

Comparing the measured distribution of the reflections according to range with the theoretical ones, we can determine the declination of the stream's radiant and the moment of culmination. The problem of determining the stream radiant is simplified in the case of the pencil-beam antenna with a directional diagram pressed to the level line and oriented westward or eastward. If the antenna is directed eastward, the first reflections from the meteor stream will be recorded for the maximal range near the moment of culmination of the radiant, then the range will decrease gradually. In case of the orientation of the antenna westward, the variation in range occurs in the opposite sequence.

For a more precise determination of the stream radiant, the antenna is turned in azimuth by a single angle, and at the second passage of the radiant through the meridian, the declination is found from the difference in the moments of the appearance of the most remote reflections at two positions of the antenna. The accuracy of measuring the coordinates of the radiant depends on its declination and on the quantity of meteors in the shower. The probable errors involved in the measurement of the right ascension α and declination δ of the radiant at a width of the directional diagram of the antenna $\pm$ 10° and the hourly number of meteors in the shower 30 are presented in Table 4.1 [168].

Table 4.1

	δ, degr												
	−30	−20	−10	0	+10	+20	+30	+40	+50	+60	+70	+80	+90
$\Delta\alpha$°	±2	2	1.5	1.5	1.0	1,0	1.0	1,5	3	3	4	5	—
$\Delta\delta$°	±6	6	5	4.5	4	3	2	1,0	0.5	2	3	5	7

For measuring the coordinates of the radiant during one transit of it in Jodrell Bank (England) [169], use was made of a device with two pencil-beam antennas (the width of the directional diagram $\pm$ 5° and the angle of elevation of the diagram's axis was 8.5°), which during the observations remained stationary. The accuracy of measuring the coordinates of the radiants with this device was $\Delta\alpha = \pm 1°$ and $\Delta\delta = \pm 1°.5$. It was possible to separate the streams, for which the time of culmination of the radiants differed by 30 minutes. From 1949 - 1958, the Clegg method was used to conduct a large number of measurements of the coordinates of the radiants of meteor showers; many daily showers were detected, operating from May - July.

The Clegg method was also used in New Zealand [170, 171] and in Australia [172], where the device similar to that described above functioned simultaneously with the equipment of continuous radiation.

For the streams with an hourly number of recorded meteors more than 100, Keay [173] offered a somewhat different procedure for processing the observations. It is assumed that the moment t_m, corresponding to the intersection of the curve of the most probable ranges PQ (refer to Fig. 4.1, a, b) with the mode of distribution of reflections according to the range, coincides with the moment of the appearance of the peak on the curve of the variation of the partial frequency of the meteors with time. The partial quantity is found /134 for the reflections lying in the interval of ranges 50 - 100 km in the vicinity of the mode of distribution of the reflections based on range for each time interval. In this case, the hourly angle of the radiant t in the moment t_m is found from the equation

$$\tan\frac{t}{2} = \frac{\tan\frac{1}{2}(\chi+\psi)\sin\frac{1}{2}(\delta-\xi)}{\cos\frac{1}{2}(\delta+\xi)}, \qquad (4.4)$$

where cos χ = cos φ_m cos A_m; φ_m, A_m equal the angle of elevation and the azimuth of the direction of the maximal value of K (φ, A); ψ equals the parallactic angle; ξ equals the angle depending on the latitude of the point of observation and on the antenna orientation.

In the use of two antennas, we get two moments of the maximums of the partial quantity of reflections t_{m1} and t_{m2}, from (4.4), it is evident that the difference $t_{m1} - t_{m2}$ is specifically connected with the declination δ of the radiant. Knowing δ, from (4.4), we can find the hourly angles of the radiant at the moments t_{m1} and t_{m2}, and hence the right ascension of the stream's radiant. The accuracy of this method decreases considerably if several streams are simultaneously operating.

The Method of Lobing the Diagrams

The method of lobing the diagrams suggested by Ye. I. Fialko [127], combines the methods of Keay and Clegg, supplementing them with the registration of the reflections by several lobes of the directional diagram of an antenna in the vertical plane. In this method, use is made of an antenna having a slight directivity in the horizontal plane. A multi-lobed directional diagram in the vertical plane is formed owing to the reflection of radio waves from the Earth's surface under the condition that the height of elevation of the antenna comprises several wave lengths. In the successive passage of the stream radiant through the plane of maximal sensitivity of each of the lobes, there occurs an increase in the quantity of meteors at the moments t_1, t_2, etc. Knowing the orientation of the lobes in the vertical plane and measuring the moments of the maximums of the meteor frequency, we can find the coordinates of the shower radiant.

Sh. O. Isamutdinov and L. G. Brudnyy [174] measured with this method the radiants of a number of meteor showers, utilizing the two-lobed directional diagram. In the observations of the individual streams with an hourly number of recorded meteors amounting to several tens, the maximums of the meteor frequency, associated with the passage of the radiant through various lobes of the directional diagram, could be determined with an accuracy of $\pm$ 5 minutes. However, in the simultaneous effect of several streams, the pattern of the variation in the meteor quantity becomes very complex. Considerable technical difficulties developed in the determination of the precise position of the maximums of the lobes of the directional diagram and the maintenance of the stability of their orientation. In addition, the limits of the declinations of the optimally recorded radiants are predetermined by the selection of the angles of inclination of the lobes to the level line. For the improvement of the method, we can recommend the use of a selection of reflections, being applied by various lobes of the directional diagram, using a phase displacement by 180° between the signals, received by two adjacent lobes.

The "Quantity-Azimuth" Method

A method was suggested by Weiss [175] as a result of analyzing the possibilities of a radio meteor station of constant radiation in Adelaide

(Australia), which was applied for measuring the coordinates of the reflected centers based on the phase shift of the Doppler patterns of the reflected signals, received by dispersed antennas. The directional diagram of the /135 antennas was oriented vertically upward and permitted the reception of signals in a cone with the angle $\pm$ 50°.

During the diurnal motion of the radiant, at a certain moment there are developed conditions for the registration of the shower meteors. At this time, the reflections are grouped mainly around the direction (φ_o, A_o). The horizontal coordinates of the stream at this moment

$$z = \varphi_0,$$
$$A = A_0 + 180°. \qquad (4.5)$$

Using this method, we found only the radiant of the Geminids meteor shower. Among the disadvantages accruing to the statistical methods, in the given case there is also added the geometric selection. We can establish only the radiants with the zenith distances $40° < z < 90°$. The number of recordings of the coordinates of the reflection points decreases appreciably for the streams with considerable zenith distances of the radiants, since the phase fluctuations of such reflections are slight as a result of the low rate of the vertical displacements of the atmosphere in the meteor zone. The potentialities of the method can be considerably expanded in the case of the application of a phasometer in which are registered the differences in the phases of the high-frequency oscillations of the reflected signals [209]. For the selection of the meteors in the showers, it is feasible to utilize additional characteristics (velocity, etc.).

The above-considered methods of determining the coordinates of the radiants are applied chiefly for studying the individual meteor showers with a large number of reflections. In the application of the statistical methods for processing the results of the observations of the sporadic meteors, we can obtain only several of the most general regularities in the motion of the meteor bodies near the orbit of the Earth [175, 177, 178]. The further progress in the study of the nature of the motion of meteor bodies developing radio meteors, is linked with the application of the methods of measuring the coordinates of the radiants of the individual meteors.

RADAR METHODS OF DETERMINATION OF RADIANTS OF INDIVIDUAL METEORS

Method of Observing a Head Echo

McKinley and Millman [179] in 1949 suggested a method for determining the radiants of individual meteors based on the observations of the head echoes from bright meteors simultaneously for three radar sets dispersed over a wide area. Measuring with a high accuracy the range to the head of the trail from 3 points, for each time moment, we can compute the position of the meteor in space, and hence find both the coordinates of the radiant as well as the velocity and braking. McKinley and Millman using this method measured the coordinates of a radiant of one meteor in the Perseids shower with an error of not over one degree. The velocity of the radio meteor varied during its visibility from 60 to 50 km/sec.

A significant disadvantage of the method is its applicability only to the observations of the very bright meteors, providing head echoes simultaneously for the three scattered radar stations. With the equipment having been used in Ottawa, Canada [179], for 50 hours of observations, there was recorded an average of one meteor, for which by this method the velocity could be determined with an accuracy of ± 1%, and the position of the radiant could be found with an accuracy of 2° [179]. The number of the meteors being processed by this method can be increased by increasing the power of the transmitter and the accuracy of measuring the range.

/136

Pulse-Diffraction Method

If the observations of a forming meteor trail are conducted by two radar sets installed at distance of several kilometers (point A and B in Fig. 4.2), and the trail is so located that the nearer images of the radio waves from it (in the points A' and B') can be observed in both radar sets, the moment of the appearance of the image in point B will be delayed in time by the value

$$\Delta t = \frac{AB\cos\theta}{v}, \qquad (4.6)$$

where AB equals the value of the base, v equals the velocity of the meteors, θ equals the angle formed by the trail with the base AB. The time displacement and the velocity of the meteor can be measured, if in both radar sets we record the pulse-diffraction pattern of the reflected signals. In this manner, the observations with three radar sets provide directed cosines, and hence permit us to find the position of the meteor radiant. The method can be modified somewhat with the application of one transmitter and three receiving points.

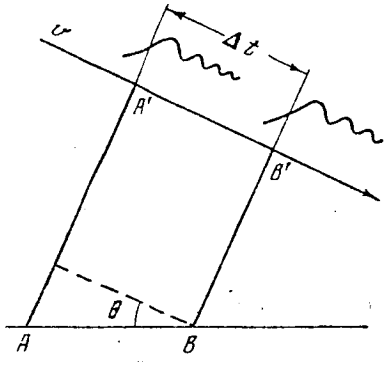

Fig. 4.2. Observation of the Diffraction Pattern of Signals Dispersed in a Forming Trail, with Two Dispersed Radar Sets in the Points A and B. The ratio of the distance between the points of the mirror image in the trail A' and B' to the base length determines the angle between the base and the trail.

This method was initially applied by Gill and Davies [180]. According to their estimation, the accuracy of measuring the radiants' coordinates comprises ± 2° and is limited chiefly by the effect of the turbulent winds in the atmosphere. A similar method was used in the Kharkov Polytechnical Institute [181].

The pulse-diffraction method is most effective in the study of the sporadic meteors brighter than $+12^m$ - $+15^m$. The observations by this method permitted us to reveal a new, previously unknown type of the orbits of the small meteor bodies [182, 76]. Providing a large number of orbits of the individual meteor bodies, this method opens vast possibilities for studying the structures of large meteor showers (streams).

Range Finding-Diffraction Method

In a more complete analysis of the signals reflected by the forming meteor trail for a determination of the orientation of the trail, it suffices to have two radar sets or one transmitter and two scattered receiving points. One of them is located next to the transmitter, while the other is installed at a distance of 5 - 10 km from it. In the base point, in addition to the conventional indicator for recording the amplitude-time-dependent characteristics of the reflected signal, there should be a direction finder for measuring the coordinates of the reflected point. In the outlying point, there is recorded the diffraction pattern and the range to the second point of the reflection in the trail.

Knowing the position of the first reflecting point in the trail, the distance between the reflecting points and the range from the outlying point to the second reflecting point, we are able to compute the orientation of the trail in space. The system of such a calculation was described by Sh. O. Isamutdinov [183].

Until the present time, this method has not yet found experimental realization, which is associated chiefly with the difficulty in producing a sufficiently accurate pulse-type direction finder. The development in the KPI [209] and the Kazan State University [176] phasometer facilitates the problem of introducing this method of measurement of the radiants' coordinates. It /137
should be noted that in the performance of such measurements, the receiving channels of the main and outlying points should be sufficiently wide-band in order to provide the required accuracy of measuring the range. This requirement limits the possibilities of realizing the optimal band of the receiving devices, which in turn decreases the sensitivity of the equipment during the observations of faint meteors.

Range-Finding Method

In the radio observations of meteors fainter than about $+10^m$, one seldom succeeds in obtaining good diffraction patterns of the reflected signals, necessary for the precise determination of the velocity of the meteors by the diffraction method [184]. Therefore, for the faint meteors, it is desirable to have a method which would not require a determination of the velocity according to the diffraction pattern. Such a method was proposed by R. P. Chebotarev [185]. The equipment includes one pulse transmitter and three dispersed receiving points. The ranges are measured from the receiving points to the corresponding points of the mirror image in the trail R_o, R_a, R_b and

the time-related displacements between the moments of the appearance of the mirror image in the outlying receiver points and the main point, Δt_a and Δt_b.

With mutually perpendicular bases, the horizontal coordinates of the meteor radiant are found from formulas [185]

$$\operatorname{tg} A = \frac{\Delta t_a}{\Delta t_b}, \tag{4.7}$$

$$\cos z = \frac{K d_a + d_b}{\sqrt{b^2 (K^2 + 1) - (K d_b - d_a)^2}}, \tag{4.8}$$

where A is calculated from the direction of base Oa; $d_a = R_a - R_o$; $d_b = R_b - R_o$; $K = \Delta t_a / \Delta t_b$; b equals the base length Ob. The meteor velocity can be found from the formula

$$v = \frac{b \sqrt{b^2 - d_a^2 - d_b^2}}{2 \Delta t_b \sqrt{b^2 [K^2 + 1 - (K d_b - d_a)^2]}}. \tag{4.9}$$

From the observations, we also obtained the heights of all three points of the mirror image in the trail.

Up to the present time, this method has not yet been checked experimentally. In order that the method can compete in accuracy with the pulse-diffraction method, it is necessary that all the ranges be measured with errors of not over $\pm$ 50 m. This requires the use of the wide-band channels in the receiving systems (bands $\Delta f \gtrsim 3$ mc), which decreases greatly the effective sensitivity of the equipment. The accuracy of the measurements can be increased owing to an increase in the length of the bases. However, as will be shown below, an increase in the difference of the heights of the reflection points in the trail leads to instability in the position of the first maximum of the diffraction patterns, based on which we find the time-related displacements Δt_a and Δt_b, which in turn leads to an increase in the errors in the measurements. Thus, the sole means of increasing the effective sensitivity of the equipment for the range-finding method is the increase in the pulse power of the transmitter and the directivity of the antenna systems. As is known, this procedure for increasing the sensitivity of the equipment is extremely complex both for engineering and methodological reasons. A compromise solution can be found by means of utilizing the wide-band channels for measuring the range and the narrow-band ones, for a recording of the amplitude-time-dependent characteristics.

In the implementation of the method, additional difficulties develop which are procedural in nature. A high accuracy of typing-in the points is necessary. In case of a deviation of the bases from a mutual perpendicularity, the calculation of the coordinates of the radiant based on the results of the measurements becomes considerably complicated. The presence of delays of the signals in /133 the receiving and antenna-feeder channels requires a careful calibration of the system to avoid systematic errors, etc. In connection with this, for a study of the potentialities of the range-finding method, it is feasible to use parallel measurements with this method and with the pulse-coherent method.

Method of Nonattenuating Radio Waves

The method is employed for measuring the velocities and radiants of meteors in Adelaide, Australia [132, 186]. The main transmitter on a frequency

of 27 mc operates under conditions of continuous radiation. The main receiving point is separated from the transmitter by 20 km, while the two outlying ones are located 5 km to the north and to the east from the main one. While in the pulse-diffraction method, for measuring the velocity in the time-related displacements, use is made of the diffraction of radio waves on a forming meteor trail, in the method of the nonattenuating radio waves, there occurs an interference of the wave, scattered by the forming trail, and a weakened terrestrial wave from the transmitter. For measuring the range, use is made of an additional pulse transmitter. Nilsson [187] estimates the accuracy of measuring the right ascension of radiants as $\pm$ 1,°9, declination $\pm$ 1°,5 and velocity of meteors $\pm$ 1.4 km.

The method of the continuous oscillations has a number of advantages as compared with the pulse-diffraction method. The velocity of a meteor and the time-related displacements in this method can be measured as a result of analyzing the reflected signals both after passage by a meteor of the points of the mirror image in the trail, as well as "during the approach". "During the approach" in the scattering of radio waves, there participates effectively the much smaller section of the trail, and the effect of the heterogeneities in the trail and of the atmospheric turbulence on the accuracy of measurements is reflected less. However, the method of undamped radio waves requires the use of considerably more complex radio engineering equipment. For realizing the possibilities of increasing the accuracy of measurements imposed in this method, the measurement is required of the phase characteristics of the reflected signals at a fairly complex processing of the observations with the purpose of explaining the initial difference in the phases of the reflected wave and the terrestrial wave.

RADAR STATION OF THE KHARKOV POLYTECHNICAL INSTITUTE

Selection of the Basic Parameters of the Radar Set

According to (2.31), the minimal linear electron density of meteor trails which can be registered by a radar set in the case of underdense trails

$$\alpha_{min} = \frac{4\sqrt{2\pi}R^{3/2}\varepsilon^{1/2}}{(P_t G_t G_r)^{1/2}\lambda^{3/2}} \frac{mc^2}{e^2} \frac{1}{\varphi(\Delta)} e^{\left(\frac{2\pi r_0}{\lambda}\right)^2}, \qquad (4.10)$$

where ε equals the minimal signal which can be recorded by the receiver (the ε-value is several times higher than the noise level). The noise level

$$E_{ш} \sim T\Delta f, \qquad (4.11)$$

where T equals the effective temperature of the receiver, with allowance for the external and internal noises, and Δf equals the frequency band of the receiving circuit.

In the meter wave band, the sensitivity of the receivers is limited by the external noises. In this context, the equivalent temperature of the receiving antenna depends in the following manner on the wave length [188]:

$$T \sim \lambda^{(2\div 3)}. \qquad (4.12)$$

From (4.10) - (4.12), it is evident that in the meter wave band, the dependence /139
α_{min} upon λ is basically determined by the exponential factor in (4.10). Most of the radio meteors are recorded at the heights of 90 - 100 km, where the initial radius r_0 of the ionized trails is of the order of 1 m. The faint radio meteors should have higher altitudes and hence r_0-values. Thus, for the observations of the faint meteors, it is necessary to select as much as possible the longer waves (in any case, longer than 4 - 6 m).

With an increase in the wave length of the radar set, we have an increase in the quantity of interference from the remote short wave stations, the extra-long-range propagation of which becomes possible as a result of the scattering of the radio waves in the heterogeneities of the ionization in the ionosphere. In addition, the reflections from the meteors can camouflage the reflections from the aurora polaris, the sporadic layer of the ionosphere E_{spor} and other interferences. In connection with this, the use of the waves longer than 12 - 15 m is disadvantageous. In working with waves longer than 12 - 15 m, there also develops a number of technical difficulties associated with the need to produce very large-scale antenna systems. Proceeding from the concepts outlined above, we selected a wave length for the radar set λ = = 8.13 m (refer to Chapter 3).

At the prescribed wave length, the effective sensitivity of the radar set can be increased owing to the narrowing of the pass band of the receiver, an increase in the pulse power of the transmitter, and an increase in the directivity of the antennas. The pulse power P_t of the transmitter is limited by the power possibilities of the modern oscillator tubes.

The optimal pass band of the receiver is selected from the condition

$$\Delta f = \frac{1}{\tau_и}, \tag{4.13}$$

where $\tau_и$ equals the duration of the transmitter pulse. The pulse duration is determined by the required accuracy of measuring the range, ΔR

$$\tau_и = \frac{2\Delta R}{c}, \tag{4.14}$$

where c equals the speed of light. Under actual conditions, $\tau_и$ is selected to be somewhat less than according to (4.14), which is associated with the procedural features of the equipment designed for measuring the radiants.

In the case of the reception of signals scattered by a meteor trail, in several of the outlying receiving points, the application of pencil-beam antenna systems encounters a number of technical difficulties (for example, we find a complication in the problem of the matching of the electrical axes of their directional diagrams in space). In connection with this, it is necessary to be limited to relatively simple types of the antenna systems.

For increasing the accuracy of measuring the velocity of meteors, the repetition rate of the pulses should be as high as possible. It is desirable to have a repetition rate F of the order of several kilocycles. However, in measuring the radiants, the repetition frequency should not be more than about 1000 cps. This is associated with the requirement for blocking the receiving-indicator channels for the time of radiation of the sounding pulse and the

time of arrival of the "sondes", rebroadcast from the outlying points. In case of a long distance between the outlying points and a high repetition rate of the pulses, and also with allowacce for the reflections from the local objects, the working sector of the ranges, for which the meteors can be recorded, is reduced; this creates an additional factor in the selectivity of the equipment.

For measuring the velocities and the radiants of meteors at the KPI, we produced a meteor radar set with the following specifications [129]:

Wave length $\lambda = 8{,}13$ m
Power in the pulse $P_t = 75 - 100$ kw /140
Frequency of messages $F = 500$ cps
Duration of pulse $\tau_и = 10$ microseconds
Directional coefficient of the receiving and transmitting antennas $G = 16$
Passband of the receiver $\Delta f = 150$ kc
Threshold sensitivity of the receiver $\varepsilon = 2 \cdot 10^{-14}$ watts

For the specific determination of the range, the sequence of pulses is coded (each fifth pulse is doubled). This same equipment was used for measuring the drift velocity of the ionized meteor trails by the pulse-coherent method, and also for studying the turbulent movements in the meteor zone of the atmosphere.

From the listed parameters of the radar sets, we can estimate the critical effective linear electron density of the meteor trails, which can be recorded with the equipment used by us. According to the Lovell-Clegg formula (2.1), we find $\alpha_{эфф}^{мин} \approx 10^{10}$ electrons/cm.

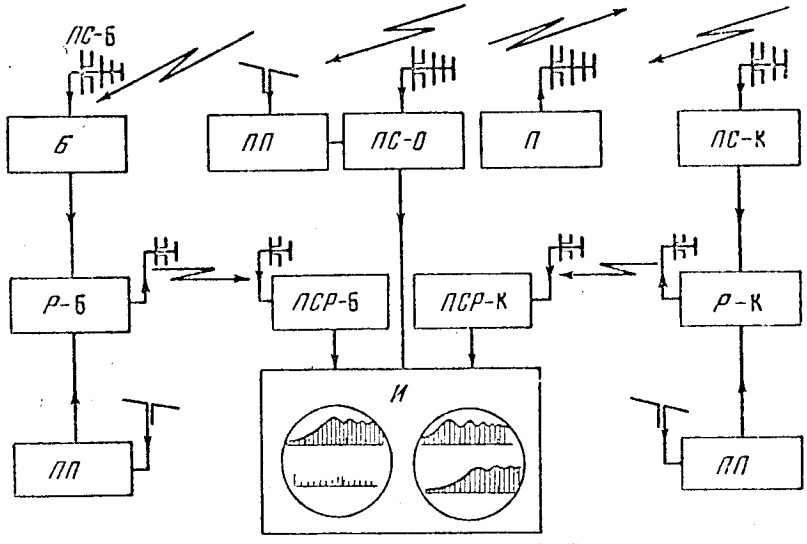

Fig. 4.3. Functional Diagram of the System of Radar Equipment Designed for Determining the Coordinates of Radiants and Velocities of Individual Meteors by the Pulse-Diffraction Method. ПС-Б, ПС-О, ПС-К equal the receivers of the signals; ПП equals the receivers of the interference; П equals transmitter; Р-Б, Р-К equal the relay sets; ПСР-Б, ПСР-К equal the receivers of the relay signals; И equals the indicator.

Operating Principle of the Equipment Facility

The installation of the radar equipment intended for measuring the velocities and radiants of meteors consists of three separate stations, located at different points. In Fig. 4.3, we have shown a functional diagram of the equipment facility. In the base point O, there are located the transmitter and the receiving-recording equipment. The latter includes three receivers, a cathode-ray indicator and a photographic device. One of the receivers located at point O operates on the frequency f = 36.9 mc and is intended for the recording of the signals reflected from a meteor trail and received in the base point. The two other receivers receive the radio echoes, being relayed from the two outlying stations, located several kilometers from the point of the collection of the information (point O).

The equipment in each outlying point has in its makeup a receiver operating on λ = 8.13 m and a relay device. In the latter, the signals are converted to higher frequencies, and after amplification to the required power level, are reradiated in the direction of the base station. The output signals of all three receivers enter the multibeam indicator, operating under driven conditions. The first of the signals which has arrived triggers the scanning of the amplitude-time-dependent characteristic of the radio echoes. In this connection, the range sweep simultaneously becomes brightened. The oscillograms of the signals are recorded by the camera with a normally open lens. After completion of the sweep, there occurs a replacement of the exposed frame, and the system is prepared for recording the next meteor radio echo.

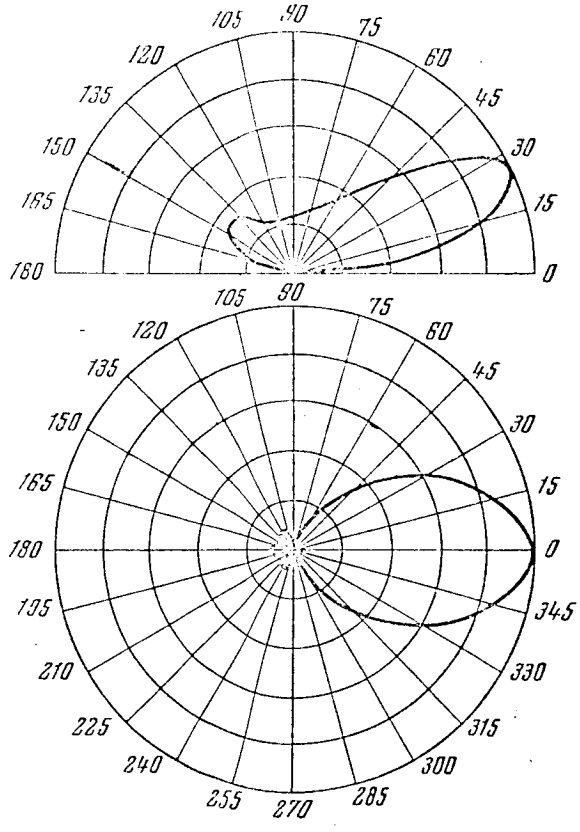

Fig. 4.4. Directional Diagram of the Receiving and Transmitting Antennas for λ = 8.13 m in the Vertical and Horizontal Planes.

The operating effectiveness of the system of recording under review depends on the extent of the noiseproof state of all of the receiving channels. To provide a protection from the pulse interferences in all three points, use is made of additional receivers forming the pulses for the suppression of interference in the signal channels. The disruption of the operation of the breakdown of any of the enumerated elements of the installation makes the determination of the radiant impossible.

During the measurements of the orbits of meteors, use is made of the same transmitter as during the study of the drift of meteor trails (see Chapter 3). Let us examine in more detail the characteristics and the operation of the individual units of the experimental device.

Characteristics of the Antennas for λ = 8.13 Meters

For the radiation of the radio pulses of the transmitter and the reception of reflected signals, use was made of the single-type 5-element antennas of the type "wave channel" (see Fig. 3.3). The height of the antennas above the Earth's surface is $0{,}35\lambda$, the angle of inclination of the indicator to the plane of the horizon is 30°. In Fig. 4.4, we have shown a directional diagram of the antennas in vertical and horizontal planes. The maximum of the radiation is directed at an angle to the horizon $\varphi_m = 27°$. The width of the directional diagram at the level of three decibels (db) in the horizontal plane comprises $\pm$ 25°. This diagram was obtained experimentally (see Chapter 3) and was verified repeatedly during the period of the measurements. The characteristics of the antennas were maintained practically unchanged at a varying degree of the moistness of the soil. The application of the antennas of low directivity permitted us to match easily the electrical axes of the system of four antennas located in various observation points.

/142

Receiver of a Meteor Station

The general requirements imposed on the receivers of coherent radar sets (refer to Chapter 3), also pertain to the receivers of the meteor radar sets designed for measuring the radiants of individual meteors. However, they have a number of specific features. The receiver of the signals in the base point is made according to a superheterodyne circuit. The utilization of a receiver of direct amplification becomes difficult owing to the high requirements imposed on the shielding of the circuits of the phase detector, since the reference voltage in this case coincides in frequency with the carrier frequency (f = 36,9 mc).

The "leakage" of a signal of continuous oscillations of 36,9 mc at the input of a receiver leads to a reduction in the sensitivity of the latter. The frequency of the heterodyne is chosen in the receiver as higher than the signal frequency $f_c < f_r$. Otherwise, the mirror channel proves to be (at $f_{нч}$ = = 11,1 mc) in the shortwave range, where considerable interferences are present from the side of the radio broadcasting stations. In addition, the level of the galactic noises in the shortwave range is higher than for λ = 8,13 m. For increasing the selectivity in respect to the mirror channel, it is necessary to apply high frequency amplifiers (HFA). The application of a receiver with the optimal band ($\Delta f_{опт}$ = 150 kc) provides a measurement of the range with an accuracy equalling ΔR = 1,5 km, which exceeds considerably the required value for ΔR in the calculation of the velocities of the meteors by the pulse-diffraction method.

The $\Delta f_{\text{опт}}$ -band in the case under review can be fully realized, since the instability of the frequency of the transmitter and of the heterodyne f the receiver can be disregarded, since their frequencies are quartz-stabilized. The application in all stages ofsingle circuits, tuned to one frequency provides the maximum stability of the frequency characteristic of the receiver during the replacement of tubes and under temperature variations of the circuits' parameters.

The maximal sensitivity of the receiver at the frequency f_c = 36.9 mc is limited by the level of the external noises. Therefore, the use at the output of the receiver of the tubes of type 6ZH1P and 6ZH4, even in a circuit with grounded cathodes, permitted us to attain the noise-factor $N \approx 2.6$. At such a value of N for 36.9 mc, there always is fulfilled the co dition $T_A \gg T_R$ where T_A equals the effective temperature of the antenna, conditioned by the effect of the galactic noises. The equivalent temperature of the receiver will be $T_R = NT_E$, where $T_E = 290^\circ K$ = room temperature. The question of the

study of external noises has been the topic of many special investigations [188, 189, 190], in which it is shown that the sources of noises are distributed unevenly in the celestial sphere. For the low frequencies, the value $T_A \sim \sim f^{(2-3)}$[188]. In the application of antennas with slight directivity for the frequency f = 20 mc, it was discovered that the maximal and minimal levels of the cosmic noises differ by 1.5 - 2 times. The application of weakly-directed antennas (for example, used in the equipment at the KPI), permits one to assume with sufficient accuracy that for practical purposes, T_A does not change during a 24 hour period.

The temperature of the antenna for λ = 8.13 m ($T_A \approx 14{,}000^\circ K$) was calculated at the base of the graphic averaging of the temperature according to a chart of the isotherms, derived for λ = 7.9 m [190]. The averaging was conducted through an area of the celestial sphere illuminated by the antenna. The experimental measurement of the strength of the external noises confirmed the calculated value for T_A. The stability of the level of the galactic noises was utilized for a coarse monitoring of the sensitivity and the amplification of the receiver (with the exception of the days with elevated solar activity). The switching of the input of the receiver from the antenna to the equivalent with a simultaneous measurement of the excess of the level of external noises above the internal ones permits one to monitor quickly the operation of the receiving circuit, without resorting to the aid of the measuring instruments. The calibration of the sensitivity of the receiver was checked in detail with the aid of the G4-7 device at the beginning and the end of each cycle of measurements. The main diagram of /143
the high frequency circuit of the receiver is similar to the corresponding circuit of the relay device receiver. The video-channels of all the receivers are standard and made according to a system similar to the video-amplifier of the receiver of the relayed signals.

Equipment of the Outlying Points

The basic specifications inherent to the receiving-recording device of the main point during the measurements of the velocities of meteors by the pulse-diffraction method should be provided in the receiving-relay equipment of the outlying points. In order that the sensitivity of all the receiving

channels would be identical, it is necessary that the noise factor of the relay lines would be the same as in the receiver at the base station. This means that the amplifier of the power in the relay set should provide such a level of the relay noises at the output that in the receiving end of the line, they would exceed by approximately 1 order of magnitude the internal noises of the receiver of the relay signals. The operation of the transmitter of the radio relay device during the amplification of the radio noises corresponds to the conditions close to the continuous operating conditions of the amplifier with independent excitation.

Another feature of the radio relay equipment is the fact that, in the entire channel of the transmission and reception of the reflections recorded in the outlying points, it is necessary to preserve the dynamic range being provided in the equipment of the base point. The radio echo from the meteors under the pulse regime of the operation of the installation has the form of a "packet" of radio pulses, the width of which and the amplitudes of the pulses contained in it vary within wide limits. From this it follows that the amplifiers of the transmitter, having a wide range, operate under intermittent-pulse conditions.

The accomplishment of such contradictory and specific requirements led to the need for utilizing several unusual regimes and conditions for the operation of the tubes. Under this fulfillment of the requirements of a wide dynamic range, the power possibilities of the terminal tubes were not fully utilized.

In the planning and manufacture of the radio relay equipment, we pursued the goal of assurring the transmission of the meteor echoes by a simple and most reliable procedure. This problem can be solved, applying various methods of the conversion of the amplitude variations of the signal (into phase, frequency signals, etc.). We can apply various types of the modulation of the carrier frequency of the radio relay procedure. However, all this would have led to a considerable complication of the circuit and hence would have reduced the operating reliability of the installation.

As a result of checking a number of methods for the radio relay procedure, we selected the following method. The signals from the meteors, having entered from the antennas, were preamplified and transformed to a higher carrier frequency, in which we reached the required power level. The frequencies of the relay set were taken in the range of USW, free of interference from the radio broadcasting stations.

Both relaying devices were assembled according to one block-diagram (Fig. 4.5). The required gain factor of the entire channel was divided between the amplifiers, operating on a frequency of 36.9 mc and a relay frequency, in order to obtain the maximum permissible amplification for a lower frequency, in this connection providing the necessary linearity of the amplitude characteristic of the transformer. Prior to the place of the blanking of the interference, all of the stages of the amplifiers were assembled according to the circuit with parallel supply in single circuits, tuned to one frequency.

The total band of the 6-stage amplifier comprises Δf = 200 kc (at a band Δf= 600 kc per stage). For obtaining such a band in the working frequencies, we applied the circuits with low characteristic resistance. /144

In order to provide a stable amplification of the stages, the resistance of the circuits was transformed by a capacity divider, consisting of an output capacitance of the tube and of the transient capacitor.

The noise factor of the receiving channel of the relay device comprised $N \approx 2,6$, when the level of the cosmic noises exceeded the internal noises by approximately 4.5 times. The single-grid transformer was mounted on a pentode. For its functioning, use was made either of the voltage from a local heterodyne, stabilized with quartz, or the voltage of a reference signal received from point O (see Fig. 4.5).

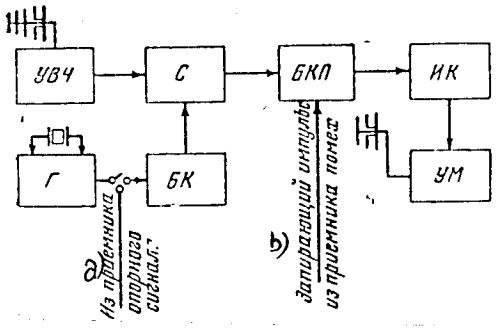

Fig. 4.5. Block-Diagram of a Radio Relay Device of an Outlying Receiving Point. УВЧ equals the amplifier of high frequency signals; С equals mixer; БКП equals the blanking stage of the intermediate frequency; ИК equals the inverse stage of the intermediate frequency amplification; Г equals heterodyne; БК equals buffer stage; УМ equals the power amplifier. Key to figure: a) from the receiver of reference signal b) triggering blanking pulse from the interference receiver.

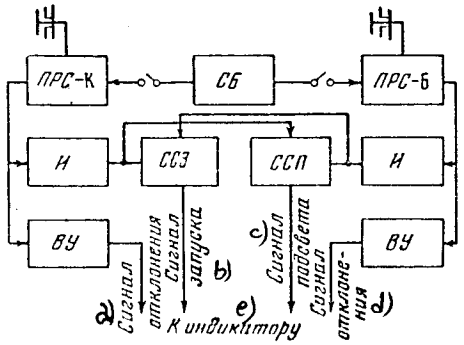

Fig. 4.6. Block-Diagram of the Receivers of the Signals Relayed from the Outlying Receiving Points. ПРС-К, ПРС-Б equals the receivers of the relayed signals; И - inverters; СБ equals the blanking circuits; ССЗ equals the mixer of the triggering signals; ССП equals mixer of intensifier signals; and ВУ equals video-amplifiers. Key to figure: a) deviation signal; b) triggering signal; c) intensifier signal; and d) deviation signal; e) To indicator.

The transition to a two-cycle system of amplification and a special selection of the tube regimes according to the screen grids permitted us to expand considerably the span of the characteristics in respect to the control grids, which in turn provided the possibility of attaining a satisfactory linearity in the amplifiers of the stages.

In the last stage of the relay station, we used the tube GU-29, which provided, under the condition of noise amplification, the power $P \simeq 20$ mw. In the linear regime of the amplification of the noise of pulse signals with the dynamic range (10 - 15), the maximal power reaches $P = 5 - 10$ watts. The circuit of the terminal stage is loaded with a 75-ohm cable, the resistance of which is transformed by a U-elbow with a length $l = \lambda/2$ and a capacity divider made of transient (intermediate) capacitors. From a design standpoint, the relay device is made in one unit. The design of the relay device provides a stable amplification of the entire installation with a gain factor of $10^8 - 10^9$.

For the emission and reception of the relay signals, we apply the standard 3-element director antennas, mounted on masts with a height $h = 10 - 15$ m. The antennas of such a type are simple to produce and are easily matched with the 75-ohm cable with the aid of the U-elbow with length $l = \lambda$. The application of more complex antenna systems is not feasible because of the concepts discussed at the beginning of the present chapter.

The reception of the relayed signals is achieved with the aid of the conventional receivers of the superheterodyne type, the output signals of which arrive directly at the indicator and in the triggering channel.

As will be demonstrated below, proceeding from the requirements of shielding from interference of the receiver band, there should be provided the passage of the remains of the pulses of the interference not blanked in the relay set. Their duration lies in the limits $\tau_0 \geqslant (0.1 - 0.2)\,\tau_u$. As was shown in Chapter 3, the system of shielding from the pulse interference permits one to suppress the interference, the duration of which is less than that of the useful signals. /145

For reducing the influence of the eigen-noises of the receiver on the sensitivity of the relay channel, the level of the latter should be lower by about 1 order of magnitude than the noises being relayed. However, we should recall that the sensitivity of the receiver has an effect on the selection of the parameters of a number of the elements in the relay line. At a low sensitivity of the receiver, in particular, the need arises either to raise the antennas high in order to increase the level of signals, or to increase the power of the transmitter, which greatly complicates the equipment as a whole.

A block-diagram of the receivers is shown in Fig. 4.6. In the receivers, we have used the two-stage USW, based on the 6ZH1P tubes. The noise figure in the receiver is such that the level of the internal noises is commensurable with the cosmic noises in the relay frequency. In this case, the sensitivity of the receiver comprises 85% of the sensitivity of a "completely non-noise-emitting" receiver, attached to the antenna.

IF amplifiers are made on connected circuits. The next to the last stage is blocked for the time of the arrival of the local and relayed sondes. The blanking pulse can be controlled in duration either by disconnection during the control of the tuning of the receivers and in the checking of the operation of the indicator in respect to the relay "sondes". In this same receiver, there are mounted the mixers of the signals of intensification and triggering. The

correction of the identity of the signals in the triggering channels is achieved by changing the amount of the load resistance in the stage of the video-signals' inverter. The necessity for separating the channels of triggering and brightening is caused by the fact that under certain conditions of operation, the channel subjected to the effect of the intensive interference can be disconnected without loss of useful information. In effect, this can be done for a channel of that station in the direction of which the transmitters' radio pulses are being radiated.

System of Shielding from Interference

In connection with the fact that in the experimental apparatus, use is made of the frame-by-frame photographic recording of the reflections, the triggering system should be shielded reliably from the effect of the interfering signals. The photo device is activated from the first signal having exceeded the established level of the clipping and having arrived from any outlying point. Under such a system of triggering, a spurious activation of the recorder under the effect of interference leads to a useless expenditure of photographic materials. At a considerable level of interference, there occurs a premature wear of the electromechanical parts of the camera, and the recorder goes out of operation.

The suppression of interference during the recording of the radiants is conducted in all of the receiving stations based on the method described in Chapter 3 and in which use is made of the difference in the spectra of the periodic signal and of the random pulse interference. The method of the formation and the delay of the pulse signals which is accomplished in the video-channels, cannot be basically realized in the case of the base measurements. This circumstance is caused by the fact that in the relay equipment, there takes place only the conversion of the carrier radio-pulses reflected from the meteors, without the separation of the signals' envelopes. Hence, the necessary delay in the high frequency signals should be realized in the carrier frequency (f_c = 36.9 mc), which represents considerable technical difficulties. Therefore, the suppression of the pulse interferences developing at the site of the station was divided into two stages. In the first stage, we conducted a blanking of interference in the relay set. In this connection, there occurred a "leakage" of the leading edge of the interference. For reducing the duration of the remaining part of the interference, we undertook all measures aimed at reducing the delay in the signals in the receiver as compared with their delay in the relay device up to that point, where the latter are suppressed (see Fig. 4.5). Prior to the stage, in which there /146
occurs the blanking, the band of the relay device channel exceeded the optimal and comprised (1.2 - 1.5) $\Delta f_{опт}$. After this stage, the band was considerably wider, which is necessary for the undistorted amplification of the narrow "remnants" of the unblanked pulse interferences.

The final separation of the interference occurred in the unit for shielding from interference in the base point, in which provision was made for the selection of the signals of interference with a duration $\tau_п$, satisfying the condition

$$\tau_п < \tau_и.$$

The interference is received by a special noise receiver (refer to Fig. 4.5).

Noise Receiver

In order to reduce the delay in the radio pulses of the noise in the receiver of the critical sensitivity, the latter was made based on a circuit with a minimal number of stages. Its band was taken to be considerably wider than in the relay set. This condition must be provided in order that in the stages of the separation and formation of the blanking pulse, an undesirable delay would not develop.

The amplification of the receiver equalling 10^6, with the band $\Delta f \approx 1$ mc was obtained by the application of three mismatched IF circuits, providing the maximum amplification at the given band. In the receiver, we used the tubes with high transconductance of the type 6ZH9P ($s \approx 20$ ma/v).

The calculation of the lag time was conducted based on the pulse characteristics according to the equation

$$t_0 = \frac{\gamma}{\Delta f_{\text{пч}}}, \qquad (4.15)$$

where γ is taken for n single circuits (in our case, $n = 5$, while $\gamma = 0.6$). The lag of the signal in the high-frequency circuit comprised $t_0 = 0.25$ microseconds. The pulses of the interferences were expanded in the video-amplifier.

For the reliable operation of the suppression system, it is important that the level of noise in the channel of the useful signals would be lower than in the noise receiver, since in the clipper separating the interference from the noises, there occurs a loss in the leading part of the pulse. The pulse interferences of industrial origin from the ignition systems of truck transport, remote lightning flashes and other sources have a broad spectrum, the effect of which on the high-frequency circuit with the band Δ leads to the formation of interference pulses with the duration $\tau \approx t/\Delta f$.

Since these interferences arrive at small angles to the horizon, for their reception, we used highly elevated antennas with slight directivity in a horizontal plane. As is apparent from Fig. 4.4, the antennas of the useful signals at small angles have slight amplification. Thus, we obtain the necessary excess of the level of interferences in the receiver of interferences over the level of the latter in the channel of the useful signals.

The disrupting influence of the interferences of a continuous nature can be eliminated by the appropriate selection of the triggering level in the equipment of the base point in respect to any of the three receiving channels.

Equipment Providing the Coherence of Signals Relayed from an Outlying Point

The experimental installation at the KPI permitted us to measure simultaneously with the measurement of the radiants, the velocity of the radial displacements of the meteor trails relative to two observation points. To the relay equipment, we extended the condition of coherence, which provided the obtainment of data required for assessing the influence of the irregular movements upon the accuracy of determining the radiants.

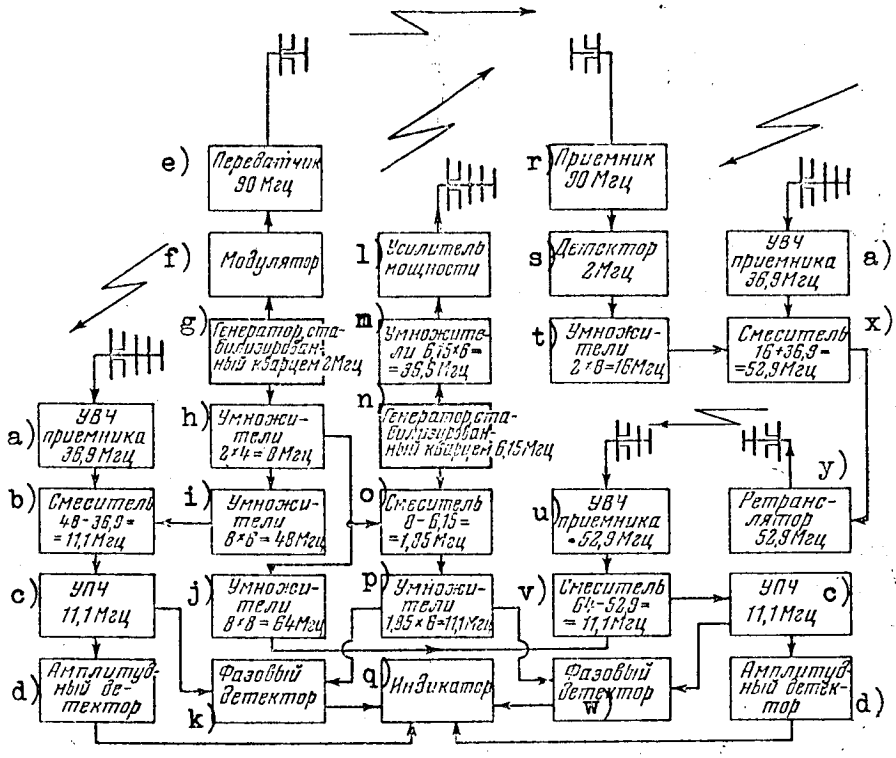

Fig. 4.7. Block-Diagram of Equipment Providing the Coherence of Signals Relayed from the Outlying Receiving Points. Key to figure: a) USW receiver, 36.9 mc; b) mixer, 48 - 36.9 = 11.1 mc; c) IFA, 11.1 mc; d) amplitude detector; e) 90 mc transmitter; f) modulator; g) quartz-stabilized oscillator, 2mc; h) multipliers, 2 x 4 = 8 mc; i) multipliers, 8 x 6 = 48 mc; j) multipliers, 8 x h = 64 mc; k) phase rectifier; l) power amplifier; m) multipliers 6.15 x 6 = 36.9 mc; n) quartz-stabilized oscillator, 6.15 mc; o) mixer, 8 - 615 = 1.85 mc; p) multipliers, 1.85 x 6 = 11.1 mc; q) indicator; r) 90 mc receiver; s) rectifier, 2 mc; t) multipliers, 2 x 8 = 16 mc; u) UHF receiver, 52.9 mc; v) mixer, 64 - 52.9 = 11.1 mc; w) phase rectifier; x) mixer, 16 + 36.9 = 52.9 mc; y) relay unit, 52.9 mc.

The operating principle of the relay unit together with the installation having been applied for measuring the drifts of meteor trails in the base point can be followed with the aid of the block diagram in Fig. 4.7.

It is known that in a fully coherent radar set, the transmitter pulses are formed from the voltage of the highly-stable oscillator, operating under continuous conditions. The phase of this voltage comprises a reference one in the separation of the Doppler variations of the frequency in the reflected signal.

Usually, a comparison of the phases is conducted based on the intermediate frequency. In this connection, the instability introduced by the receiver heterodyne is compensated in the phase rectifier under the condition that the

reference voltage is formed from the voltage of the heterodyne and the signal of the master oscillator of the transmitter. The principle of compensation should always be assured when we conduct the transformation of the signal frequency in the coherent locator. Otherwise, the smallest variations in the frequency of the auxiliary voltage, being utilized during the transformation will distort the true pattern of the phase pulsations, ascribable to the displacement of the object.

The voltage required for the operation of the transformer of the relay unit with the frequency f_4 = 16 mc, is formed from the frequency signal f = 2 mc, being transmitted from the main point with the aid of a special transmitter operating on the frequency $f_{0п} \approx 90$ mc. The oscillations of this same frequency (2 mc) are used in the main point for obtaining the voltage of the heterodyne of the main receiver (f_4' = 48 mc), and also the voltage of the heterodyne of the one of the receivers of the relay signals (the frequency of this heterodyne f_4'' = 64 mc). /148

The main advantages of the suggested system of tying the phase consists in the fact that the channels of the relay and transmission of the auxiliary voltage $f \approx 2$ mc operate in the ultrashortwave range ($f_p \approx 50$ mc, $f_{0п} \approx 90$ mc). This range is free of the interferences inherent to the shortwave sector being used for similar purposes in [191].

The method considered of providing the coherence is convenient, since it permits one to extend the condition of coherence to a larger number of outlying stations, which is important in the study both of the properties of a meteor trail as well as of the turbulent movements in the meteor zone. Let us consider certain elements of this equipment [158].

Transmitter of the reference signal. For the transmission of voltage in the frequency of 2 mc, stabilized by quartz, there serves an additional radio line operating, as already mentioned, on the frequency $f_{0п} \approx 90$ mc. The transmitter with the amplitude modulation is located in the main point, while the receiver is located in an outlying point at a distance of 4.3 km. The master oscillator of the transmitter has been developed on the 6P1P tube based on the Shembel' system with a doubling of the frequency. The power amplifier is made according to a single-cycle system based on the GU-50 tube. The amplitude modulation of the carrier frequency is accomplished according to the pentode grid in the power amplifier.

The transmitter is separated geographically from the receiving-indicating equipment. The voltage f = 8 mc required for the operation of the receivers is formed in the channel of the transmitter multipliers from the voltage f = = 2 mc and is transmitted along the cable with the aid of the cathode follower.

The receiver of the reference signal is assembled according to a circuit with one transformer. For reducing the effect of damping of the signal $f_{0п} \approx 90$ mc in the feeder of the receiving point, the input stages made on the basis of a cascade system, are mounted in the form of attachments to the antenna itself. The frequency voltage f_4 = 16 mc, required for the operation of the relay mixer, is formed after the rectifier in the channel of the multipliers assembled on the 6ZH4 tubes. Through the cathode follower, this voltage is fed along the cable to the buffer stage located in the relay unit. Under

the conditions of noncoherent operation, the input of the latter is connected with the aid of a switch to the autonomous heterodyne, the frequency of which (16 mc) is quartz-stabilized [see Fig. 4.5]. For the emission and reception of the signal of reference frequency, use is made of the standard 3-element antennas.

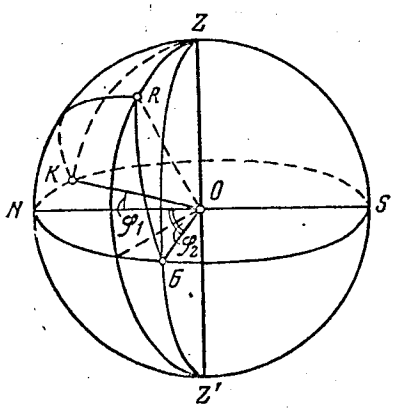

Fig. 4.8. Determination of the Horizontal Coordinates of the Radiant R of a Meteor. K and Б equals projections onto a celestial sphere of the directions of the bases OK and O Б; φ_1 and φ_2 equals angles between the bases and the northward direction.

Receiver of the relay signals and the coherent heterodyne unit. For the coherent functioning with the equipment of the outlying station, use is made of another receiver of the relay signals (see Fig. 4.7). The frequency voltage of the heterodyne f = 64 mc necessary for the operation of the transformer is obtained in the channel of the multipliers of the coherent heterodyne. The oscillations of the frequency 64 mc are formed by way of an 8-fold multiplication of the frequency of 8 mc.

In this same unit, a phase rectifier is located, in which for the intermediate frequency $f_{пр}$ = 11.1 mc, the Doppler pulsations are separated. After amplification, the voltage is fed from the video-amplifier output to the indicator.

By way of the appropriate switching of the phase of the reference voltage at the moment of arrival of the second of the doubled pulses of the code, we can easily determine the sign of the radial component of the drift velocity. The switch is based on two tubes.

/149

METHODS OF MEASUREMENTS AND CALCULATION OF THE ORBITS

Calculating the Coordinates of a Radiant

For measuring the velocities and the coordinates of the meteor radiants, we applied the above-described pulse-diffraction method. The transmitter was located at point O, while the main receiving point was installed along with the transmitter; the two outlying receiving points were located at points K and Б. From the observations, we found the velocity of the meteor and the time-dependent displacements between the diffraction patterns of the reflections, received mainly in the outlying points, Δt_1 and Δt_2.

If the length of the bases OK and OБ is much less than the distance to the meteor trail, the cosines of the angles between the axis of the trail and the bases can be found from the relationships

$$\cos\theta_1 = \frac{2v\Delta t_1}{OK}, \quad \cos\theta_2 = \frac{2v\Delta t_2}{OБ}. \tag{4.16}$$

In (4.16) it is assumed that the velocities of the meteor in three points of the mirror image in the trail differ but little from each other.

In Fig. 4.18, we have presented the projections onto the celestial sphere of the bases and the radiant R of the meteor. The main receiving point is located in the center of the sphere. From the spherical triangles RFБ and RFK

$$\begin{aligned} \cos\theta_1 &= -\sin z \cos(A - \varphi_1), \\ \cos\theta_2 &= -\sin z \cos(A + \varphi_2). \end{aligned} \tag{4.17}$$

From (4.16) and (4.17), we find the horizontal coordinates of the radiant:

$$\sin z = -\frac{2v\Delta t_1}{OK}\sec(A - \varphi_1) = -\frac{2v\Delta t_2}{OБ}\sec(A + \varphi_2), \tag{4.18}$$

$$\tan A = \frac{\cos\varphi_2 - \dfrac{OK\Delta t_2}{OБ\Delta t_1}\cos\varphi_1}{\sin\varphi_2 + \dfrac{OK\Delta t_2}{OБ\Delta t_1}\sin\varphi_1}. \tag{4.19}$$

The quadrant A is selected from the conditions

$$\text{at } \left.\begin{matrix}\Delta t_1 \leqslant 0 \\ \Delta t_2 \geqslant 0\end{matrix}\right\} \quad 90^\circ - \varphi_2 \leqslant A \leqslant 90^\circ + \varphi_1,$$

$$\text{at } \left.\begin{matrix}\Delta t_1 \geqslant 0 \\ \Delta t_2 \geqslant 0\end{matrix}\right\} \quad 90^\circ + \varphi_1 \leqslant A \leqslant 270^\circ - \varphi_2,$$

$$\text{at } \left.\begin{matrix}\Delta t_1 \geqslant 0 \\ \Delta t_2 \leqslant 0\end{matrix}\right\} \quad 270^\circ - \varphi_2 \leqslant A \leqslant 270^\circ + \varphi_1,$$

$$\text{at } \left.\begin{matrix}\Delta t_1 \leqslant 0 \\ \Delta t_2 \leqslant 0\end{matrix}\right\} \quad 270^\circ + \varphi_1 \leqslant A \leqslant 360^\circ \text{ or } 0^\circ \leqslant A \leqslant 90^\circ - \varphi_2.$$

The distances of the outlying points from the basic one and the angles φ_1 and φ_2 were obtained as a result of the geodetic linking of the points to the triangulation system of the closest reference points: OK = 4.3 km, OБ = 7.7 km, $\varphi_1 = 33^\circ 14'$ and $\varphi_2 = 51^\circ 20'$. The difference in the heights of points K and O comprised +26 m, and in points Б and O, it was 7 m. The accuracy of the measurements of the bases and of the angles φ_1 and φ_2 was much higher than the accuracy of determining the time-dependent displacements and the velocity. The maximum accuracy in finding the position of the radiant (other conditions being equal) can be attained if the angle between the bases is close to 90°. In our case, it amounted to about 85°.

/150

Screening and Primary Processing of the Data

The data taken from the film and the primary processing of the results is conducted according to a specially developed procedure. The frame with the photographic recordings of the radio echoes was projected with a 10-fold magnification onto the screen of the "Mikrofot" device. The quality of the recording of the envelopes of the signals recorded in three points, namely the absence of interferences of various origin, of distorting fluctuations of signals of a diffraction nature served as a criterion for the suitability of the meteor for further processing. We processed only those recordings in which in all three diffraction patterns there are at least three distinct Frenel zones. We introduced a special evaluation of the recordings in a 5-point system, considering both the quality of the envelopes, as well as the number of Frenel zones which could be utilized for calculating the velocities and the time-dependent shifts.

For most of the underdense trails (Fig. 4.9, a), the evaluations proved to be lower than for the saturated trails, since in this case, we find a rapid decrease in the signal amplitude to the level of the receiver noises as early as the time of formation of the basic Frenel zones in the trail. In the case of rapid meteors (Fig. 4.9, b), the time of the formation of the second and third (and all subsequent) Frenel zones in the trail can become comparable with the repetition period of the radiated succession of the sounding pulses (T = 2000 microseconds), which leads to a reduction in the accuracy of measuring the velocity. These factors are automatically taken into account by the estimations of the recordings' quality. We did not process the recordings of the radio echoes for which during the period of scanning the signals, we noted intensive fluctuations in the amplitude, evoked by a distortion of the trail by turbulent winds in the upper atmosphere (Fig. 4.9, c).

The reading of the number of pulses for all of the clearly distinguishable maximums (A, C, E, G, ...) and of the minimums (B, D, F, I, ...) of the diffraction patterns for each meteor echo was conducted, assumming for the beginning of the reading the first of the time markers, located near each of the recordings (Fig. 4.9, d). For convenience calculation, we used the scale markers, occurring every ten pulses synchronously with the succession of pulses being radiated. The dimensions of the Frenel zones and the time-related shifts of the similar points of the amplitude-time-related characteristics of the signals, received in the outlying points relative to a signal received in the base point, are computed according to the data and are posted to a special table. In addition, for each meteor, we record: the time of appearance, distance to the point of reflection, estimation of quality of recordings and the type of reflection (A, AB, $\overline{B}$, B), where A equals reflection from an underdense trail (Fig. 4.9, a); AB - from the trail of the intermediate type (Fig. 4.9, b, c); $\overline{B}$ - from a saturated trail (Fig. 4.9, e); B - reflection from a trail with a very high linear electron density, the amplitude of such a reflection increases during the entire scanning period (Fig. 4.9, d). For the reflection of type A, there is recorded the ratio of the amplitudes of the first and second maximums and the coefficient D of the amplitude diffusion.

The time-related shifts Δt_1 and Δt_2 are averaged for all calculated values (according to all extremums of the diffraction patterns). The dimensions of each Frenel zone are determined as weighted averages in respect to

all three diffraction patterns with weights depending on the estimations of the patterns' quality.

According to the adopted technique of screening the recordings, for each meteor we get not less than 12 independent velocity measurements. The calculation of velocity begins from an averaging of the dimensions of the similar zones in three patterns with weights depending on the quality of echo recording. The applicability of such a method of averaging is justified in that the errors in finding the velocity by the diffraction method are much higher than the sys ema ic differences in the meteor velocity in three points of reflection in the trail with a difference in heights between the extreme points of less than two kilometers. The systematic differences in the vel- /151
ocity are mainly caused by the braking of the meteor in the section between the reflection points.

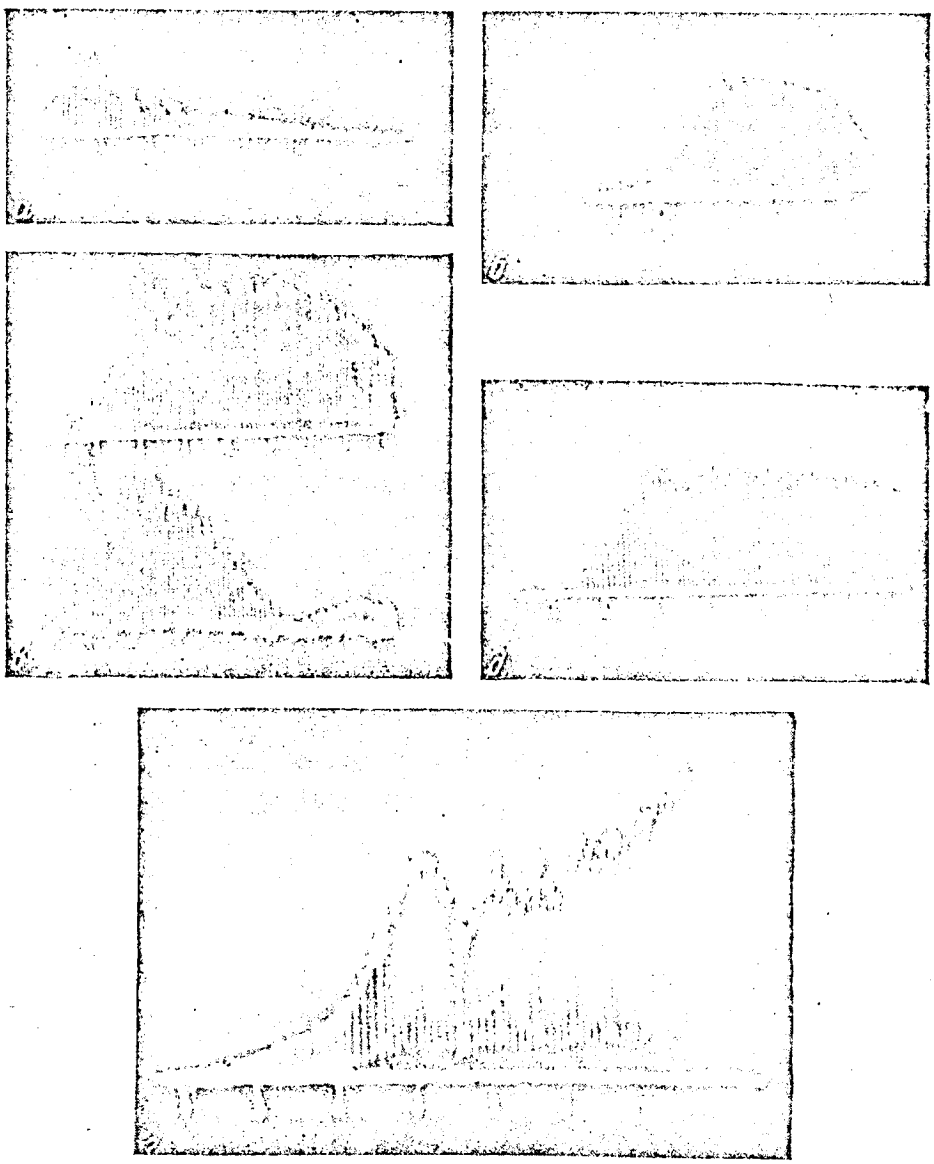

Fig. 4.9. Samples of the Recordings of the Diffraction Patterns of Signals, Scattered in Ionized Meteor Trails of Various Types. a- underdense; b and c- of an intermediate type; e and f- saturated; e- trail with a very high linear electron density.

The velocity of a meteor for each of the Frenel zones is calculated with the aid of the equation

$$v = KY/n \qquad (4.20)$$

where n equals the number of pulses in the corresponding zone for the diffraction pattern; K equals a constant factor for the given equipment, depending on the length of the wave λ of the radar set and the repetition rate of the pulses F, $K = F\sqrt{\lambda}$:

$$Y = \nabla/2\sqrt{R}, \qquad (4.21)$$

where R equals range, ∇ equals length of the corresponding zone expressed in units $\sqrt{R\lambda}/2$. The ∇-value can be calculated with the aid of Eq. (2.32) (as the distance between the points of the extremes of the Frenel integral). The tables of the Y-values as a function of R are presented in [192]. The velocities found for all zones, averaged with the weights which are proportional to the ∇-values for each zone and which are presented in Table 4.2.

Table 4.2

Zone	Weight	Zone	Weight	Zone	Weight
AC	1,10	*CG*	1,34	*BD*	0,86
CE	0,74	*EI*	1,11	*DF*	0,66
EG	0,60	*AG*	2,44	*FH*	0,54
GI	0,51	*CI*	1,85	*BF*	1,52
AE	1,84	*AI*	2,95	*DH*	1,20

The radar equipment of the KPI described in this chapter permitted us to record an average of 500 - 1000 meteors in the course of 24 hours of continuous observations. In Fig. 4.10, we have presented the diurnal pattern of the quantity of recorded meteors for one of the days of observations--13 July 1960. From the total number of meteors, on an average, 15 - 25% meet all of the requirements which are imposed on the recordings selected for finding the coordinates of the radiants and the velocities. Thus, for 24 hours of observations, there can be identified the orbits of 100 - 200 individual meteor bodies. The average number of orbits which can be identified during a day varies from month to month in conformity with the annual varition of the population of meteors [76].

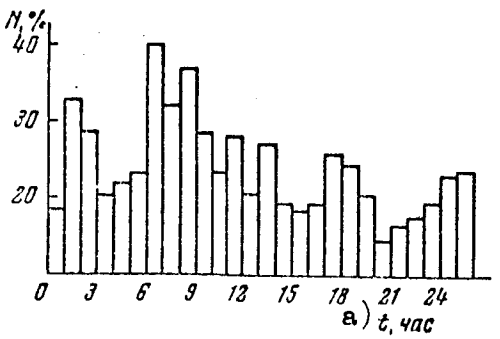

Fig. 4.10. Diurnal Pattern of the Quantity of Meteors for which We Recorded the Amplitude-Time-Dependent Characteristics (based on observations 13 July 1960). Key to figure: a) time, hours.

Calculation of Orbital Elements

The calculation of the coordinates of the corrected radiant of a meteor and of the elements of the orbit of a meteor body was conducted based on the somewhat modified system of I. A. Kleyber [193], which was adapted for the "Ural" computer. As input data, we adopted four values; the time T of the appearance of the meteor, the time-related shifts Δt_1, Δt_2 and the average velocity v of the meteor. All of the values which usually are taken from the Astronomical Yearbook were presented in the form of analytical time functions: distance from Earth to Sun, orbital velocity of the Earth, longitude of the Sun, and sidereal time.

The complete calculation of the radiant and the orbit of one meteor took about 5 minutes machine time. The use of the Ural electronic computer with a fixed scale leads to a considerable complication of the program, since not less than 1/3 of the entire program is taken up by logical conditions related to the indeterminacy of the scale of an entire series of intermediate values entering the calculation. More convenient was the application of calculating /153 machines with the "floating decimal point" (of the Strela type, and others).

The calculation of the coordinate of the radiants and of the orbital elements was conducted in the following order:

1) A, z equal horizontal coordinates of visible radiant;
2) α, δ equal equatorial coordinates of corrected radiant;
3) v_∞, v_g equal the extra-atmospheric and geocentric velocity of the meteor;
4) λ, β equal the ecliptic coordinates of the corrected radiant;
5) λ', β' equal the ecliptic coordinates of the true radiant;
6) v_h equals the heliocentric velocity;
7) E, E' equal the elongation of the corrected and true radiants from the apex; and
8) a, e, q, i, Ω, ω, equal the orbital elements of the meteor body.

MEASUREMENT ERRORS OF VELOCITY AND RADIANT COORDINATES

Effect of the Inaccuracy of Counting the Pulses

In the measurement of the lengths of the Frenel zones for calculating the velocity and the time-dependent shifts for finding the coordinates of the radiant, the relative positions of the extremes of the diffraction patterns of the reflected signals can not be found with absolute accuracy. As a result of the finite state of the repetition rate of the pulses, there is always an uncertainty in the exact position of the extreme of not less than 0,5 distance between two successive pulses. We can expect that at a very good quality of the recordings, the error involved in finding the position of the extremes will be about the same for all of the meteors.

In Table 4.3, we have presented the errors Δv in the velocity of the meteors found based on the zone AC of the diffraction pattern, for various velocities of meteors in the range from 20 to 70 km/sec. We have assumed an average error in the determination of the zone length $\Delta p = \pm 1$ pulse, and an average meteor range R = 200 km. We have given the errors of the average

weighted value of velocity of meteors v_{weigh}, for which there are N separate measurements of the velocity for various zones, at two Δp-values: 1.0 and 0.5.

Table 4.3

v, km/sec	P, pulse	Δv, km/sec	$\Delta v_{weighted}$				Δt
			$N=10$	$N=15$	$N=20$	$N=25$	
20	15,5	±1,3	0,20	0,17	0,15	0,13	0,5
			0,41	0,34	0,30	0,26	1,0
30	10,3	±2,9	0,46	0,37	0,32	0,29	0,5
			0,92	0,75	0,65	0,58	1,0
40	7,8	±5,2	0,8	0,7	0,6	0,5	0,5
			1,6	1,3	1,2	1,0	1,0
50	6,2	±8,2	1,3	1,1	0,9	0,8	0,5
			2,6	2,1	1,8	1,6	1,0
60	5,2	±12,0	1,9	1,6	1,3	1,2	0,5
			3,8	3,1	2,6	2,4	1,0
70	4,4	±16,8	2,6	2,2	1,9	1,7	0,5
			5,3	4,3	3,8	3,4	1,0

/154

Table 4.4

R, km	$v_{взв_1}$, km/sec	N_1	$v_{взв_2}$, km/sec	N_2	Δv, km/sec	$\overline{\Delta v}$, km/sec
127	25,34	27	24,34	28	1,0	
150	25,02	15	25,11	22	0,1	
152	23,59	24	23,82	36	0,2	
130	23,47	14	23,03	29	0,4	±0,6
225	17,20	10	17,30	7	0,1	
137	23,98	14	25,93	22	2,0	
166	23,43	11	23,87	10	0,4	
126	25,19	11	26,12	15	0,9	
123	26,22	22	26,12	15	0,1	
123	29,48	20	28,87	26	0,6	
137	34,02	12	31,38	21	2,6	
145	25,57	24	26,61	28	0,0	
198	30,22	8	30,58	8	0,4	±0,8
178	28,07	29	26,04	30	2,0	
125	29,26	13	29,70	20	0,4	

R, км	$v_{взв_1}$, km/sec	N_1	$v_{взв_2}$, km/sec	N_2	Δv, km/sec	$\overline{\Delta v}$, km/sec
200	32,64	30	32,55	23	0,1	
248	26,53	13	26,39	22	0,1	±0,8
120	33,24	20	34,15	19	0,9	
167	42,00	29	41,30	33	0,7	
140	44,04	12	43,36	18	0,7	
150	39,51	20	38,81	20	0,7	
187	40,18	22	39,68	19	0,5	
170	39,22	12	33,21	20	1,0	
250	41,55	12	39,90	16	1,6	
185	43,32	19	43,61	24	0,4	±0,9
235	43,60	10	44,85	16	1,2	
125	36,95	22	38,25	20	1,3	
148	40,58	36	40,68	30	0,1	
137	36,43	19	35,95	20	0,5	
167	36,62	29	36,46	29	0,2	

[lower index "взв" = "weighted"]

According to the data in Table 4.3, if the errors in counting the pulses in the Frenel zones do not depend on the length of the zones, the corresponding errors in the velocity of the meteors depend greatly on the velocity value ($\Delta v \sim v^2$). For checking the actual accuracy of counting the pulses in the Frenel zones, for 24 radio meteors with an average quality of recording, we conducted two independent s ries of processing by two observers. In Table 4.4, we have presented the derived average for weighted velocity values and the number of individual velocity measurements for various zones for each of the observers. The meteors are divided into three groups by velocity 17 - 25, 25 - 33 and 36 - 44 km/sec. In the last columns, we have presented the difference in the velocity values Δv, obtained by two observers for each meteor, and the average $\overline{\Delta v}$-values for each of the groups of the velocities.

From Table 4.4, it is apparent that the value of the error in the velocity of the meteors associated with the inaccuracy of counting the pulses in the Frenel zones depends slightly on the velocity of meteors ($\Delta v \sim \sqrt{v}$). This is explained by the increase in the accuracy of determining the position of the extremes of the diffraction pattern with a decrease in the number of pulses in the zones. In [194], the weak dependence of Δv upon v is explained by the increase in the number of zones accessible to the measurements, with an increase in the velocity of meteors. In Table 4.5, we have presented the average number of various zones N, based on which there can be measured the velocity for the meteors with different velocities. We have also presented the number n of the meteors in each group of velocities based on which the N-value has been found.

Table 4.5

	v, km/sec					
	20	30	40	50	60	70
n	31	170	444	186	190	20
N	19	26	28	22	18	16

/155

From Table 4.5, it is evident that the number of zones accessible to the measurements is lower for the rapid meteors than for the meteors having average velocities.

For the purpose of evaluating the similarity of the results of finding the velocity based on various zones, and also of the time-related shifts and the coordinates of the radiant according to various extremes of the diffraction patterns for 25 meteors, we found the values of v Δt_1, Δt_2, θ_1 and θ_2 separately for each zone and for each of the extremes. The mean square deviations from the average weighted values of velocity and from the average values Δt_1, Δt_2, θ_1 and θ_2 are presented in Table 4.6. We also present the number N of the individual velocity measurements for each meteor, and an estimation of the quality of the recording of the diffraction patterns of the signals, received in three points.

The values of the mean square deviations presented in this table indicate the excellent face validity of the results. If, at a sufficiently large number

of measurements of the velocity and displacements, the spread of the individual values proves to be higher, this can be explained by the poor quality of the recordings of the diffraction patterns, by the dissimilarities in the distribution of the ionization along the trail (presence of meteor outbursts),

Table 4.6

v, km/sec	N	Estimations	Δv	$\Delta(\Delta t_1)$	$\Delta(\Delta t_2)$	$\Delta\theta_1$	$\Delta\theta_2$	$\sqrt{\Delta\theta_1^2+\Delta\theta_2^2}$	R, km
23,9	24	334	0,25	0,43	0,37	0°62	0°32	0°67	212
36,5	24	434	0,90	0,42	0,24	1,05	0,87	1,34	150
38,5	28	344	0,93	0,24	0,56	1,07	1,27	1,65	215
38,8	29	434	0,78	0,24	0,49	0,52	1,10	1,22	190
40,3	21	433	1,27	0,45	0,54	1,00	1,10	1,46	168
40,7	36	544	0,52	0,06	0,23	0,31	0,23	0,39	210
42,0	13	433	2,50	0,19	0,63	0,65	1,95	1,98	150
42,0	31	444	1,05	0,14	0,29	0,50	0,30	0,55	166
42,8	44	545	0,42	0,20	0,15	0,62	0,21	0,66	250
46,1	24	333	1,05	0,16	0,53	0,57	1,07	1,20	203
49,1	28	534	1,06	0,10	0,59	0,72	0,90	1,24	192
50,7	22	433	1,35	0,16	0,51	0,86	0,90	1,25	185
51,8	20	444	0,83	0,25	0,53	2,06	1,00	2,30	185
53,0	27	433	0,67	0,22	0,11	1,95	0,20	1,96	237
53,3	18	434	1,06	0,20	0,03	1,90	0,30	1,91	268
53,6	18	433	0,96	0,20	0,05	1,00	0,10	1,02	183
55,8	24	434	1,31	0,26	0,40	1,04	0,75	1,40	265
56,1	12	434	1,27	0,13	0,30	0,74	0,56	1,00	248
56,5	22	443	0,33	0,00	0,10	0,28	0,33	0,42	180
57,3	21	444	1,00	0,18	0,19	0,82	0,30	0,87	205
57,5	14	443	1,90	0,39	0,34	1,80	0,74	1,98	145
58,5	18	434	0,76	0,24	0,14	1,10	0,30	1,15	225
59,7	27	444	0,36	0,00	0,00	0,26	0,06	0,27	187
66,0	17	433	1,85	0,10	0,42	1,13	0,90	1,50	176
67,7	12	433	1,26	0,13	0,12	0,60	0,27	0,70	138

The extent of the fluctuations of the amplitude of a signal scattered in a forming meteor trail, and hence the number of zones accessible to measurements, and the accuracy of the measurements, depend on the position of the reflection point on the distribution curve of the ionization along the trail. The fluctuations are extensive in the ascending leg of the curve of ionization, and less extensive in the descending branch. If the point of reflection is close to the end of the trail, the number of extremes in the diffraction pattern can be very low.

Effect of Atmospheric Turbulence

The visual and photographic observations of the persistent meteor trails reveal the irregular nature of the displacement of the air masses in the meteor zone of the atmosphere [106, 195]. According to the results of the photographic [106] and the radar [191] measurements, the velocity gradient of the turbulent wind can reach 100 m/sec km. The presence of such high /156
velocity gradients of the wind can lead to the turning and distortion of the trail even during the formation of the basic Frenel zones [70, 158].

According to (2,12), without allowance for the wind effect, the range to the various points of the trail can be represented as follows: [see next page]

$$R = R_0 + \frac{1}{2}\frac{s^2}{R_0}, \tag{4.22}$$

where R_o equals the distance to the point of the mirror image, s equals the distance along the trail, figured from the point of mirror image in the direction of the meteor's movement.

With allowance for the radial velocity component of the wind u, we will write the distance in the form

$$R = R_0 + \frac{1}{2}\frac{s^2}{R_0} + \frac{(s_0 - s)}{v}u, \tag{4.23}$$

where s_o equals the distance from the point of mirror reflection to the head of the trail. With such a R-value, instead of (2.32), we get:

$$I' = \frac{1}{\sqrt{2}} e^{-\frac{16\pi^2 Dt}{\lambda}} \left| \int_{-\infty}^{x_0} e^{i\frac{\pi}{2}\left[x^2 + \frac{2(s-s_0)}{v\lambda}u\right]} dx \right|. \tag{4.24}$$

Let us expand the radial wind velocity component into a series by the powers of s, and limit ourselves in the expansion to two first terms

$$u \simeq u_o + u's. \tag{4.25}$$

In a linear approximation (4.25), the integral in Eq. (4.24) is reduced to the same form as in (2.32), by the substitution

$$x' = \frac{2\sqrt{1-\delta}(s+k)}{\sqrt{R\lambda}}, \tag{4.26}$$

where

$$\delta = \frac{2Ru'}{v}, \quad k = \frac{\delta v^2 t - 2Ru_0}{\sqrt{R\lambda}}. \tag{4.27}$$

For the head of the trail, from (4.26) and (4.27), we derive

$$x_0' = \frac{(2-\delta)v}{\sqrt{R\lambda}\sqrt{1-\delta}}\left[t - \frac{2Ru_0}{v^2(2-\delta)}\right] = \frac{2v'(t-t_0)}{\sqrt{R\lambda}}. \tag{4.28}$$

In the case of the absence of wind, according to (2.13)

$$x_0 = \frac{2vt}{\sqrt{R\lambda}}. \tag{4.29}$$

From (4.28) and (4.29), it is obvious that in the case of the presence of a gradient of the radial wind velocity component, utilizing Eq. (2.32) we will obtain in place of the meteor velocity v, the value

$$v' = \frac{(2-\delta)v}{2\sqrt{1-\delta}}. \tag{4.30}$$

All the moments of the extremes of the diffraction pattern prove to be displaced by the amount

$$t_0 = \frac{2Ru_0}{v^2(2-\delta)}. \tag{4.31}$$

From (4.27) and (4.31), we find the variation in the time-dependent displacements between the diffraction patterns of the signals, received in two separated points

$$\Delta t' = \frac{2}{2-\delta}\Delta t. \qquad (4.32)$$

/157

From (4.16), we find the total error involved in finding the angle θ between the direction to the radiant and the base, with allowance for the errors in measuring the velocity and the time-dependent shift:

$$\Delta\theta = \cot\theta\left[\left(\frac{\Delta t'}{\Delta t} - 1\right)^2 + \left(\frac{v'}{v} - 1\right)^2\right]^{1/2}. \qquad (4.33)$$

In August 1959, in the KPI, simultaneously with the measurements of the velocity and the meteor radiants, we measured the radial component of wind velocity in two points in a trail [158]. We utilized two coherent devices in the points O and K, separated by a distance of 4.3 km. In Table 4.7, we have shown the distribution of values u = du/ds, obtained on the basis of 302 pairs of measurements. The mean quadratic value u' = 14 m/sec km. For three velocity values 20, 40 and 70 km/sec, we have given the errors in the velocity and position of the radiant, corresponding to each of the u'-values. Dashes are inserted in those cases when the velocity measurements become impossible. We have assummed the average value cot θ= 0.5. We have shown the average quadratic values Δv and $\Delta\theta$. As is evident from the data in Table 4.7, the velocity errors are slight, whereas the errors involved in finding the radiant position prove to be quite appreciable.

Table 4.7

$\frac{du}{ds}$	N	N, %	v, km/sec					
			20		40		70	
			Δv, km/sec	$\Delta\theta$	Δv, km/sec	$\Delta\theta$	Δv, km/sec	$\Delta\theta$
0	119	39,3	0,0	0°0	0,0	0°,0	0,0	0°,0
5	77	25,5	0,0	1,5	0,0	0,7	0,0	0,4
10	55	18,2	0,1	3,2	0,1	1,5	0,1	0,8
15	18	6,0	0,3	5,7	0,2	2,3	0,1	1,1
20	15	5,0	0,7	7,2	0,4	3,2	0,2	1,7
30	4	1,3	2,1	12,3	0,8	5,0	0,4	2,6
40	7	2,3	6,8	19,1	1,2	7,2	0,6	3,7
50	1	0,3	—	—	2,4	10,3	1,0	4,8
60	3	0,1	—	—	4,4	12,2	1,5	6,0
70	2	0,7	—	—	7,6	15,4	2,3	7,2
80	1	0,3	—	—	13,6	19,2	3,1	8,6
Mean quadratic value			±1,2	±4°0	±1,1	±2°7	±0,3	±1°3

In the measurements of the velocities and the radiants of the active meteor streams (showers), the role of errors owing to the turbulent wind decreased somewhat, since the radiants with the values $\Delta\theta \gtrsim 10^o$ will not be related to the screen. Thus, for the Geminids shower (v = 36.4 km/sec), the mean square error owing to the effect of turbulent wind comprised in the velocity $\Delta v = \pm 0.3$ km/sec, and in the position of the radiant $\Delta\theta = \pm 2^o$.

According to (4.33), at various positions of the radiants in the celestial sphere, the errors in the angle θ between the directions to the radiants and the base will be maximum for those radiants for which θ has the minimal values, i.e. for which the time-related shifts are maximal. The role of errors owing to turbulent wind was verified by us for the Geminids shower. In Fig. 4.1, a, b, we have shown the spread in the radiants of the meteors in the Geminids shower for two time spans: when the azimuth of the radiant was close to the azimuth of the base ОБ and of the base ОК.

From Fig. 4.11, it is evident that the spread of the radiants actually occurs chiefly along the anticipated directions. This indicates that the errors owing to the atmospheric turbulent wind are the basic source of the errors involved in finding the position of the radiants of the individual meteors.

/158

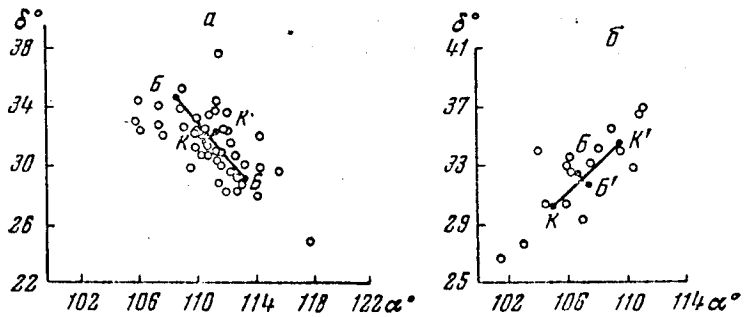

Fig. 4.11. Dispersion of Individual Meteor Radiants in the Geminids Shower for Two Time Spans, When the Radiant Azimuth of the Stream is Close to the Base Azimuth ОБ (a) and of the Base ОК (b). КК' and ББ'--the theoretical displacements of the radiant found under the assumption that the errors in the time-dependent shifts Δt_1 and Δt_2 comprise ± 10%.

Effect of Heterogeneity in the Distribution of Ionization Along the Trail

In the processing of the results of the measurements of velocities and meteor radiants, it is usually assumed that the linear electron density in the trail is constant. Let us examine the variation in the positions of the extremes of the diffraction pattern of a signal, scattered in the forming meteor trail, with allowance for the variation α along the trail. In this case, in place of the Frenel integral (2.32), the fluctuations in the amplitude with time are described by the following equation:

$$I \sim \left| \int_{-\infty}^{x_0} \alpha(x) e^{i\frac{\pi}{2}x^2} e^{-\Delta(x_0-x)}\, dx \right|, \qquad (4.34)$$

where α(x)--the distribution of the effective linear electron density along the trail.

For an estimation of the maximum possible effect of the variation in the effective linear density along the trails of meteors with a smooth curve of ionization, we adopted the ionization curve developed by Greenhow and Neufeld (Fig. 4.12, b), and we computed the diffraction patterns of the reflected signals at two positions of the point of mirror image in the trail: on the

ascending branch of the ionization curve (point O_1 in Fig. 4.12, b) and on the descending branch (point O_2). As was indicated in Chapter 2, the difference in the curves in Fig. 4.12, a and b is caused chiefly by the effect of the initial radius of the ionized meteor trails on the amplitude of the reflected signal. The calculation was conducted based on (4.34) by the numerical integration for two values Δ: Δ = and Δ= 0.5. In Fig. 4.13, a, b, the curves 1 correspond to the point O_1 and the curves 2 correspond to the point O_2 (refer to Fig. 4.12). /159

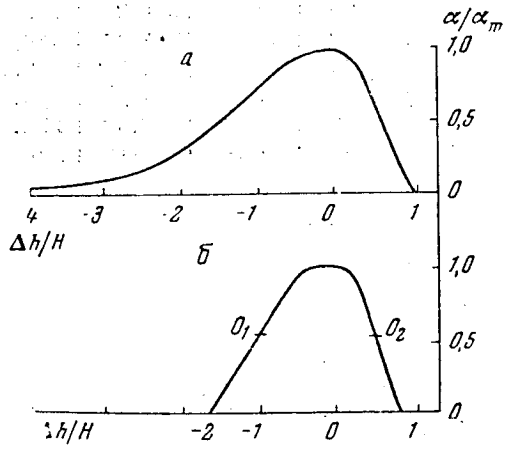

Fig. 4.12. Distribution of Linear Electron Density Along a Meteor Trail. a- theoretical curve for bright meteors; b- average curve of the distribution of effective linear electron density for the meteors $+5^m$ - $+7^m$, obtained by Greenhow and Neufeld [43].

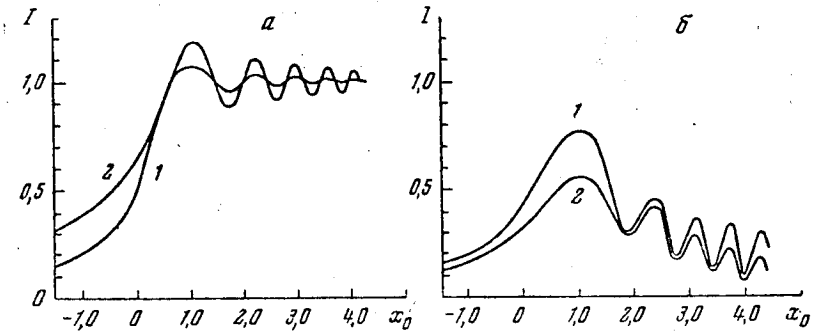

Fig. 4.13. Diffraction Patterns of the Signals Scattered in the Underdense Meteor Trails at Two Positions of the Point of Mirror Image. 1- for the ascending branch of the ionization curve; 2- for the descending branch at 2 values of the parameter $\Delta = 8\pi^2 D \sqrt{R/\lambda^3}/2 v$. a- Δ= 0; b- Δ= 0.5.

For both positions of the point of the specular reflection (mirror image) in the trail, the positions of the diffraction pattern extremes will remain practically the same as in the case α= const. Thus, assuming α = = const for the trails with regular (smooth) ionization curves, we do not introduce appreciable errors into the measurements of the velocities and the meteor radiants.

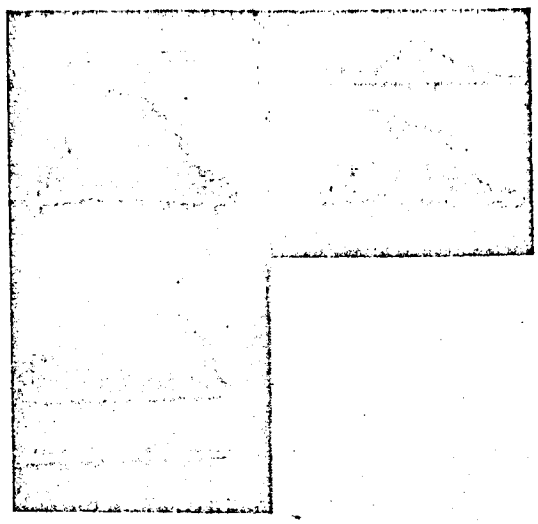

Fig. 4.14. Sample of a Recording of the Diffraction Pattern of a Signal Scattered in the Ionization Trail of a Meteor with an Outburst.

Similar calculations were made for the hypothetical case of a meteor fragmenting greatly, in which the ionization maximum α_m is attained at the distance $\Delta x = \sqrt{2}$ from the point of inception of the intensive evaporation, while the point of the mirror image coincides with the latter. At R = 200 km and λ = 8 m, $\Delta x = \sqrt{2}$ corresponds to the distance along the trail Δs = = 0.9 km. In this case, the extremes of the diffraction patterns prove to be displaced relative to the position which they occupy at α = const. If the point of the mirror image for the second point lies below α_m, this can lead to an error in θ up to 3 - 5°. The velocity measured in the first point proves to be exaggerated by several percents. According to [82], the rapid increase in $\alpha_{э\Phi\Phi}$ is encountered approximately in 0.5% of the total number of meteors. Such meteors are easily recognized by the nature of the envelopes of the diffraction patterns and should be excluded from the processing.

Let us consider the effect of the meteor outbursts upon the diffraction patterns of radio echoes. The presence of an outburst prior to the moment of the passage of a meteor through the point O of the reflected image in the trail is manifested in the form of the fluctuations of the echo amplitude "during the approach" (Fig. 4.14). The effect of the outburst upon the diffraction pattern depends on the force of the outburst and upon the phase difference $\Delta\varphi$ of the signals scattered in the point B, where the outburst occurred, and in point O. If $\Delta\varphi \simeq 0$, the effect of the outburst will be the least.

Let us consider a case, when during a very short outburst, there evaporated practically instantaneously 1% of the original mass of the meteor body, and the outburst occurred near the point of maximal evaporation. For the obtainment of the maximal estimation of the error in the time-related displacements, let us assume that the phase difference $\Delta\varphi$ comprises for one of the points $\Delta\varphi_1 = 0°$, and for the other it is $\Delta\varphi_2 = 180°$. In this case,

for a base with a length of 5 km, the error in θ comprises around $\pm$ 2%. As a result of the possibility of a fairly high error in finding the radiant for the flashing meteors, the radio echoes, which detect the fluctuations in amplitude "during the approach", should be excluded from the processing.

Effect of Diffusion

The effect of the diffusion expansion of an ionized meteor trail during the formation of the basic Frenel zones on the accuracy of finding the velocity by the diffraction method was examined in detail in Chapter 2 (see Fig. 2.2). The velocity errors owing to the diffusion can be reduced practically to zero, if for the determination of the velocity, we did not utilize the position of the first maximum of the diffraction pattern. For finding the velocity based on zone AC, under actual conditions, it is possible to have errors of 10 - 20%. In this connection, the measured velocity proved to be lower than the actual one.

In the measurement of the time-related displacements, the errors can develop owing to the difference in the diffusion factors in two reflection points. In the case of small bases, these differences are also small. In the case of large bases, the absolute error increases in the displacements, but their value also increases at the same time. In connection with this, a relative error in the time-related shifts in all cases proves to be trivial. Sometimes, in one of the reflection points, the trail will be underdense, and in the other it will be saturated. Then, the effect of diffusion leads to a displacement of the first maximum in the first point and does not change its position in the second. In this case, in the calculation of the time-related shifts, it is not necessary to utilize the position of the first maximum of a diffraction pattern.

Effect of the Braking of Meteors

In the radar observations, the most complex is the transition from the measured velocity of a meteor to the extra-atmospheric velocity. Our observations do not permit us to determine in which part of the trail the reflection point lies, therefore in the calculation of the correction to the velocity for the braking in the atmosphere, we assume that all the reflection points lie near the point of the maximal evaporation. As was indicated in Chapter 1, the decrease in the meteor velocity to the point of maximal evaporation Δv_m does not depend on the mass of the meteor body, and depends solely on its velocity. The Δv_m-values are listed on page 11. The adoption of the same correction for the braking for all the meteors with a given velocity leads to the appearance of a random error in the velocity of the order of the actual value for the correction.

For a more precise estimation of the error in the velocity ascribable to braking in the atmosphere, let us adopt the distribution, derived by Greenhow and Neufeld, of the effective linear electron density $\alpha_{э\phi\phi}$ along the trail (Fig. 4.12, b). We will consider that the point of the maximum $\alpha_{э\phi\phi}$ coincides with the point of the maximum evaporation and that the probability of obtaining a reflection from a given point of the trail is proportional to the value $\alpha_{э\phi\phi}$. In this case, the average error in the correction for braking can be found based on the equation [see next page]

$$\overline{\Delta(\Delta v)} = \frac{\int_{h_1}^{h_2} |\Delta v(h) - \Delta v_m| \alpha_{эфф}(h)\, dh}{\int_{h_1}^{h_2} \alpha_{эфф}(h)\, dh}, \qquad (4.35)$$

where h_1 and h_2 equal the heights of the beginning and end of the trail, $\Delta v(h)$ equals the correction for braking at the height h.

Under the assumptions made above, from (4.35), we get $\overline{\Delta(\Delta v)} \simeq 0{,}5\ \Delta v_m$. Thus, for the individual meteors, in which the reflection points lie at the very end of the trail, it is possible to have velocity errors somewhat higher than Δv_m, however, a number of such meteors is low.

For the difference in the heights of the points of reflection in the trail of 1 - 2 km, the meteor velocity is practically the same and hence the braking does not introduce significant errors into the measurement of the time-related displacements and radiant coordinates. The velocity of the individual meteors can be corrected much more precisely for braking, if the measurements of the velocity are conducted simultaneously in several receiving points, distributed at a distance of 40 - 60 km.

Effect of Resonance in the Trail

If the linear electron density of an ionized meteor trail α is of the order of 10^{12} electrons/cm, and the initial radius is short, in the early stages of the existence of a trail, the dielectric permeability κ in its axis is negative. As a result of the diffusion expansion, the electron concentration decreases in the trail with time. In case of a scattering in such trails of radio waves with transverse polarization, it is possible to have the resonance phenomenon, which was reviewed in the reports by Herlofson [85] and Kaiser and Gloss [86].

In the case of resonance, we have a rapid change in the amplitude and phase of the reflected wave with the transverse polarization. A measure of the resonance is: the polarization ratio

$$\rho = \frac{g_\perp}{g_\parallel}$$

(where $g_\perp$, $g_\parallel$ = the coefficients of reflection of radio waves with transverse and longitudinal polarization) and the phase difference of the reflected waves $\Delta\varphi = \varphi_\perp - \varphi_\parallel$. The radius r_m of the trail, at which the polarization ratio ρ reaches the maximum, and the value of the maximum ρ_m depend on the linear electron density of the trail α, and on the distribution of electrons along the section of the trail.

For a homogeneous cylinder of ionization, the resonance sets in at the moment when $\kappa = -1$, if in this connection $kr_m < 1$ (where $k = 2\pi/\lambda$ equals the wave number). Hence, a condition of the possibility of resonance for a homogeneous cylinder is

$$2\alpha \frac{e^2}{mc^2} < 1, \qquad (4.36)$$

where e, m equals the charge and mass of the electron, c equals the speed of light.

The ρ_m-value depends on the kr_m-value:

$$\rho_m = \frac{4}{\pi (kr_m)^2}. \qquad (4.37)$$

At $kr_m \to 0$, $\rho_m \to \infty$. However, under actual conditions, ρ_m can not be infinitely large, since the trail radius always was a finite value (in addition, in this case it is necessary to take into account the energy dissipation owing to the collisions of the electrons and of other processes). At $kr_m > 1$, Eq. (4.37) is no longer applicable and $\rho_m \approx 1$. /162

In the case of a Gaussian distribution of the electrons along the trail section (1.243), the resonance sets in at the dielectric permeability in the axis of the trail $\kappa = -1.4$. The maximal value of the polarization ratio depends on the α-value. At $\alpha < 10^{10}$ electrons/cm, $\rho_m = 2$. With an increase in α, the ρ_m-value decreases, gradually approaching unity. At $\alpha = 5 \cdot 10^{11}$ electrons/cm, Kaiser and Gloss found $\rho_m \approx 1.5$.

The polarization ratio differs noticeably from unity not only at the moment of resonance, but also for a certain time span, the duration of which is about three times longer than the period during which the trail radius, as a result of diffusion, increases from zero to r_m. If the initial trail radius is very short, at the moment of the meteor's passage, the phase difference of the waves with the longitudinal polarization $\Delta\varphi \approx 180^\circ$. Then, $\Delta\varphi$ decreases gradually to zero.

From the condition $\kappa(0) = -1.5$, let us find the trail radius, at which resonance sets in

$$(kr_m)^2 = \frac{\alpha}{0{,}6} \frac{e^2}{mc^2}. \qquad (4.38)$$

At $\alpha > 2.4 \cdot 10^{12}$ electrons/cm, $kr_m > 1$, and the resonance phenomenon according to [86] becomes impossible. In this manner, the upper limit of the α-values at which resonance can occur, $\alpha < 2.4 \cdot 10^{12}$ electrons/cm.

The lower limit of α can be estimated if we consider the finite state of the initial trail radius. From the condition $r_0 < r_m$, we find

$$\alpha > 0{,}6 (kr_0)^2 \frac{mc^2}{e^2}. \qquad (4.39)$$

As was indicated in Chapter 2, at the average velocity of meteors $v = 40$ km/sec, at the average height of radio meteors $h = 95$ km, $r_0 \approx 1$ m. From (4.39), for $\lambda = 8$ m, we get $\alpha > 1.5 \cdot 10^{12}$ electrons/cm. Thus, with allowance for the initial radius of the ionized meteor trails, the resonance phenomenon can occur in a narrow range of α-values, i.e. for a small part of the meteors that are being observed. This span expands for the slow meteors and contracts for the rapid ones.

The effect of resonance upon the measurements of the velocities and the time-dependent displacements was surveyed in a number of reports [196, 197].

As a result of the finite state of the velocity of a meteor and the variation in α along the trail, in various parts of the trail, the resonance will set in at a different time. If we consider α and D as constant, while $r_o = 0$, the length of the resonating sector of the trail $l_{рез}$ is found from (4.38)

$$l_{рез} \approx \frac{v\alpha\lambda^2}{10^{13}\pi^2 D}. \qquad (4.40)$$

It is easy to perceive that at the heights lower than 95 km, at $\lambda = 8 - 12$ m, the length of the resonating sector of the trail can be comparable with the length of the first Frenel zone. In this case, the resonance phenomenon in the trail can lead to considerable displacements in the positions of the extremes of the diffraction patterns, and hence to errors in the velocity. As a result of the difference in the physical parameters in two reflecting points in the trail, the resonance can set in not simultaneously, which leads to errors in the time-related shifts. The errors in the velocity can reach 15 - 20%. In the case of a base of the order of 5 km, the errors in the time-related shifts can reach 10%, which leads to errors in the radiant position of $\Delta\theta \approx 6^o$.

In the theoretical estimations of the effective resonance upon the accuracy of measurement of the radiants and velocity of meteors, we disregarded a number of factors (the initial radius of the trail, the consideration of which leads to a truncation of $l_{рез}$; the variation in α and D along the trail, etc.), therefore at present, it is difficult to state how significant this influence is in the statistical studies of the meteors.

/163

E. K. Nemirova [198] found the criteria of resonance of roughly 50% of the meteors, for which the diffraction patterns were obtained. In this connection, the displacements in the extremes fell in the limits of 20 - 40% of the dimension of the first Frenel zone, A. C. However, these results were obtained based on the observations of a total of 34 meteors. In addition, the study has a number of disadvantages of an equipment-procedural nature.

A significant disadvantage of the previous experimental studies on resonance [197, 198] is the application of the method of the simultaneous radiation of the radio pulses by two antennas with mutually perpendicular polarization planes. Under these conditions, as a result of the turning of the polarization plane of the radio waves in the D-layer of the ionosphere, and also as a result of the application of complex antennas, the effect of the reradiation and other factors, it is impossible to distinguish the signals of varying polarization, having arrived at any of the antennas. The application for the reception and emission, of separate antennas with several different polarization planes leads to the interference of the signals of varying polarization.

For the study of the effect of the polarization phenomena upon the accuracy of measuring the coordinates of the radiants and velocities of meteors, in the KPI, we used the following equipment [157]. Two identical transmitters having operated on the same frequency, generated radio pulses with a repetition rate of 500 cps and with a time displacement of 140 microseconds. For the radiation, use was made of two identical antennas with mutually perpendicular polarization planes. The identical state of the directional diagrams of the antennas was verified from observations.

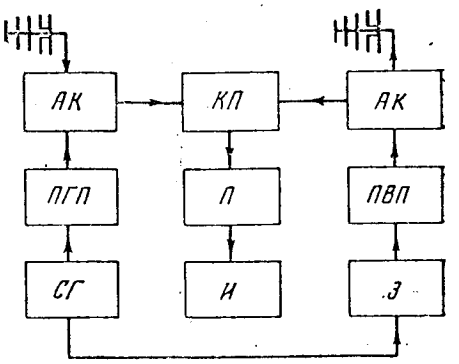

Fig. 4.15. Block-Diagram of a Radar Set Designed for Studying the Resonance Phenomenon During the Scattering of Radio Waves in the Ionized Meteor Trails. А К -antenna switching device; К П - receiver switch; ПГП - transmitter of horizontal polarization; П В П - transmitter of vertical polarization; П - receiver; С Г - synchrogenerator; И - indicator; З - lag by τ = 140 microseconds.

After the antenna switching devices, the signals reflected from a meteor entered the input of one receiver. A special electronic switch, located at the receiver input, connects the antenna with the vertical polarization to the receiver after the signal has been recorded, received by the antenna with the horizontal polarization. With such a method of switching, in one beam of the indicator, there are recorded simultaneously the envelopes of the signals of varying polarization, each of which is formed by the sequence of pulses with a repetition frequency of 500 cps. The amplitude characteristic of the receiving-amplifying channel was linear in the range of amplitudes exceeding the noise level by 20 times. The block-diagram of the equipment is shown in Fig. 4.15.

The measurements were conducted in a westward direction in the first half of the night, and in a northward direction in the morning, in order that the majority of the recorded trails would be close to the vertical planes, drawn through the radar set. The observations were conducted every 6 hours over a period of four days. Approximately for 50% of the meteors, the pulses emitted by the antenna with vertical polarization, after reflection from the trail, were received in the antenna with the horizontal polarization, and vice versa. This phenomenon is usually ascribed to the turning of the polarization plane during the reflection of the radio waves from the trail under resonance conditions, when the reflection factors $g_{\perp}$ and $g_{\parallel}$ do not equal each other. In reality however, such a reception of signals can be explained by the rotation of the polarization plane in the D-layer of the ionosphere and by the reradiation by the local objects.

/164

The polarization ratio of ρ for the trails of the underdense type was both more than and less than unity. In this connection, we did not observe appreciable displacements in the envelopes. A sample of a recording is given in Fig. 4.16, a. In the meteors of the transient type, the ρ-value sometimes increases toward the end of the existence of the echo (Fig. 4.16, b). For the meteors of the saturated type, the increase in ρ occurred both at the end and at the beginning of the reflection (4.16, c).

Of the 540 meteors, for which we obtained diffraction patterns, only in 5% of the cases did we detect relative displacements in the extremes [157]. For half of them, the displacements comprised not more than one pulse, i.e. they corresponded to the critical resolving capability of the equipment. The displacements of a quarter of a period of he first Frenel zone were detected for 1.5% of the meteors. Only one of the recorded diffraction patterns (refer to Fig. 4.16, b) indicated a large displacement. It is typical that basically, we noted displacements of the first maximum, and chiefly for the trails of the transient type.

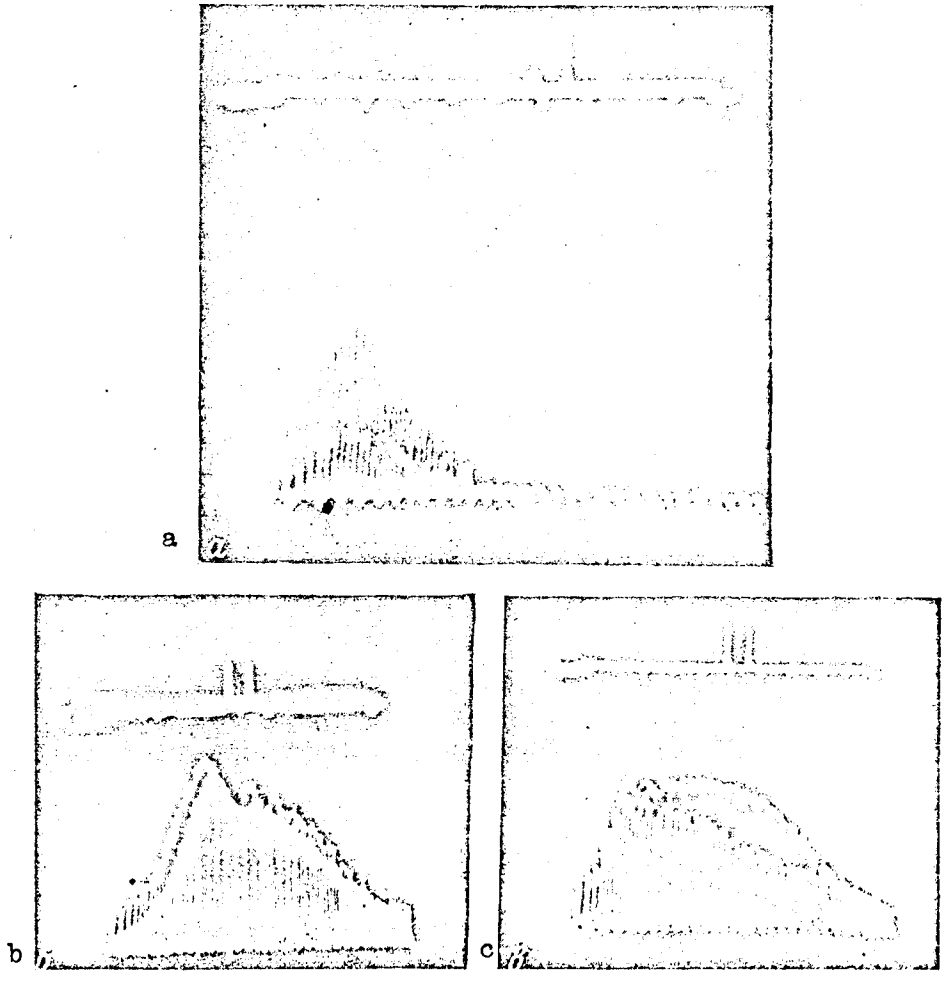

Fig. 4.16. Samples of the Recordings of the Diffraction Patterns of Signals With Horizontal and Vertical Polarization of the Radio Waves Scattered in the Meteor Trails of Different Types. a- underdense; b- transient types; c- saturated type.

/165

In individual cases, we noticed slight displacements in a direction opposite to that predicted by the resonance theory. The decrease in the extent of the fluctuations in the diffraction patterns of the echoes was recorded for the reflections of varying polarization.

The experimental results obtained by us indicate that the errors (predicted by the resonance theory) in the determination of the velocities and the coordinates of the meteor radiants actually occur for individual meteors. However, their statistical weight is quite low. Therefore, the dangers expressed previously that the application of the antennas with horizontal polarization could lead to considerable errors in the measurements of the velocities and meteor radiants are apparently unsubstantiated.

Experimental Verification of the Measurement Accuracy

For the purpose of checking the actual accuracy of the radar measurements of the velocities and coordinates of the radiants of individual meteors, in December, 1959 we conducted systematic observations of the well-known Geminids meteor shower [181]. From 9 - 14 December, we recorded around 700 meteor reflections, suitable for determining the velocities and radiants. For all of the meteors, the orbits were computed. Knowing the velocities, radiants and elements of the orbits of all the meteors, we were able to select reliably among them the meteors in the Geminids shower. The high population of the Geminids leads to the situation that several sporadic meteors, which could erroneously be related to this shower, cannot significantly distort the results for the Geminids. We selected 298 meteors in the shower.

Based on the spread in the individual values of v, α, δ, 1/a, e, q, i and ω, we found the mean square errors of one measurement:

$$\Delta v = \pm 2{,}0 \text{ км/сек}, \qquad \Delta e = \pm 0{,}028,$$
$$\Delta\alpha = \pm 2°{,}7, \qquad \Delta q = \pm 0{,}028,$$
$$\Delta\delta = \pm 2°{,}4, \qquad \Delta i = \pm 5°{,}6,$$
$$\Delta\left(\frac{1}{a}\right) = \pm 0{,}15, \qquad \Delta\omega = \pm 4°{,}3.$$

The basic sources of the errors in the measurement of the velocity are: the inaccuracy of considering the deceleration in the atmosphere, the effect of diffusion and of the atmospheric turbulent wind and the inaccuracy of counting the pulses in the Frenel zones. For the meteors with the velocities 20 - 50 km/sec, Δv should be about the same as for the Geminids. In the case of very slow meteors, Δv increases owing to the inaccuracy of allowing for the deceleration and the effect of the atmospheric wind turbulence. At v > 50 km/sec, the errors increase as a result of the effect of the diffusion and inaccuracy of taking deceleration into consideration. At v <20 and v > 50 km/sec, the average errors involved in measuring the velocity can reach $\Delta v \approx \pm 3$ km/sec.

According to (4,33), the errors in the angles between the bases and the axis of the trail are formed from the errors involved in measuring the velocities and time-dependent displacements

$$\Delta\theta = \operatorname{ctg}\theta \sqrt{\left(\frac{\Delta v}{v}\right)^2 + \left[\frac{\Delta(\Delta t)}{\Delta t}\right]^2}. \qquad (4{,}41)$$

For the Geminids, about half of the resultant errors in θ yield errors in the velocity, and about half yield errors in the displacements. The main source of errors in the measurements of the time-dependent shifts is the effect of the atmospheric turbulent wind. The role of the remaining factors is appreciably less. For the meteors with the velocities $v \gtrsim 30$ km/sec, the values

of the errors in the position of the radiant will be about the same as for the Geminids ($\Delta\delta \approx \pm 2^{\circ}.5$ and $\Delta\alpha \cos\delta \approx \pm 2^{\circ}.5$). At $v \leq 30$ km, the errors increase with a decrease in the velocity, and for the slower meteors, the average errors in a position of the radiants can reach up to $\pm 5^{\circ}$.

/166

ORBITS OF THE METEOR STREAMS AND ASSOCIATIONS

Methods of Sampling the Orbits of Meteor Streams

From November 1959 to December 1960, in the KPI, we conducted an annual cycle of radar measurements of the velocities and radiants of individual meteors. In the course of each month of observations, the measurements were conducted for 7 - 10 days. For several tens of thousands of meteors, the radio echoes were recorded simultaneously in all three receiving points. Among them, for more than 12,500 meteors, the quality of the recordings of the amplitude-time-dependent characteristics was sufficiently good for the possibility of a valid determination of the velocities and of the time-related displacements. For all of the radio meteors sampled in such a manner, we computed the orbits of the meteor bodies producing them.

The presence of a large number of the orbits of the individual meteor bodies permitted us to study the streams and the associations of the radio meteors. In recent years, several reports have been published on the study of the meteor streams and associations based on the photographic and radar measurements of the velocities and the radiants of individual meteors [187, 199, 200]. The term "meteor association" was introduced by Whipple and Jacchia [199] for denoting the aggregations of the orbits, the reality of which was established with less reliability than for the streams. However, the authors themselves [199] indicate that between these two types of groupings of meteor orbits, there is no clear distinction.

Southworth and Hawkins [200] developed a procedure for sampling the meteor streams based on the data of photographic measurements. Since the photographic method provides a high accuracy of results, they assumed that the errors of the measurements are less than the spread of the orbits of the individual meteor bodies in a stream connected with the effect of the perturbations of the planets or other forces, which lead to a gradual disruption of the streams. Therefore, the spread obtained by them in the orbital elements in the streams were considered to be real. In the capacity of a criterion for establishing the generality of the origin of two meteor bodies, A and B, the difference in the elements of their orbits was taken. However, for the different types of orbits, the same differences in any of the elements lead to dissimilar variations in the orbits. For example, at a very slight eccentricity, the variation in the distance of the perihelion from the node does not lead to a significant separation of the orbits in space. Similarly, at a very slight inclination i, the variations in ω and Ω are of little significance if the value $\pi = \Omega + \omega$ will remain constant.

As a measure of the difference in the orbits of two meteor bodies, Southworth and Hawkins took the following quadratic expression, formed from individual orbital elements: [see next page]

$$D^2(A,B) = (e_B - e_A)^2 + (q_B - q_A)^2 + \left(2\sin\frac{1}{2}I_{AB}\right)^2 + \\ + \left\{\frac{1}{2}(e_A + e_B)\,2\sin\frac{1}{2}\left[\omega_B - \omega_A + \right.\right. \\ \left.\left. + 2\arcsin\left\{\cos\frac{1}{2}(i_A + i_B)\sin\frac{1}{2}(\Omega_B - \Omega_A)\sec\frac{1}{2I_{AB}}\right\}\right]\right\}^2, \qquad (4.42)$$

where

$$\left(2\sin\frac{1}{2}I_{AB}\right)^2 = \left(2\sin\frac{i_B - i_A}{2}\right)^2 + \sin i_A \sin i_B \left(2\sin\frac{\Omega_B - \Omega_A}{2}\right)^2.$$

It was established that in the case of the known meteor streams (Quadrantids, Orionids, Perseids, Geminids and others), the value D (A, B) $\leqslant 0{,}20$ for the orbits of any two meteor bodies belonging to the given shower. To the new possible meteor showers, there belong the groups of orbits in which for any pair of orbits, the condition D (A, B) $\leqslant 0{,}20$ was fulfilled.

The accuracy of the radar measurements of the radiants and the velocities of individual meteors is less than for the photographic ones. The divergence of the orbital elements of the meteor bodies of the shower obtained from the radio observations, is explained chiefly by the measurement errors and not by the actual diversity of the orbits of the individual bodies in the shower. In this case, the method of sampling the orbits of showers, developed by Southworth and Hawkins is inapplicable. / 167

Nilsson [187] offered a method for sampling the meteors of streams with application to the radar measurements. Of the 73 meteors observed by him, there were conducted two independent series of the processing of the measurement results from the retrieval of the data from the film to the calculation of the orbital elements. Based on the difference in the orbital elements obtained as a result of the two series of processing, there were estimated the average errors in the orbital elements of the individual meteor bodies: $\Delta e = \pm 0{,}04$; $\Delta i = \pm 3^\circ$; $\Delta\omega = \pm 4^\circ$ and $\Delta(1/a) = \pm 0{,}08$. To the associations, there belonged the groups of meteors in which the differences in the elements of any pair of orbits was less than about the doubled average error of their determination:

$$\left|\frac{1}{a_B} - \frac{1}{a_A}\right| \leqslant 0{,}15, \quad |i_B - i_A| \leqslant 7^\circ, \\ |e_B - e_A| \leqslant 0{,}07, \quad |\nu_B - \nu_A| \leqslant 7^\circ, \qquad (4.43)$$

where ν = the true anomaly.

Relative to the Nilsson report, we should make two comments. 1) The estimations obtained by him for the average errors involved in determining the orbital elements are depressed, since in their calculation, he took into account only the inaccuracy of extracting the data from the film and the errors introduced during the further processing. As was indicated above, one should also take into account a whole series of sources of errors, the most important of which are: the inaccuracy of allowing for the deceleration of a meteor, the effect of the atmospheric turbulent wind upon the measurements of the time-dependent displacements and the velocities, the effect of diffusion upon the velocity measurement. 2) For the various types of orbits, the same errors in finding the radiants and velocities

of the meteors lead to different errors in the orbital elements, therefore the values Δe, i, $\Delta\omega$ and $\Delta(1/a)$ should be assumed different for the different showers.

Even prior to the publication of the Nilsson report, we had developed a method for screening the orbits of the meteor showers, similar to Nilsson's method. This was more convenient in the case when from the observations, there had been obtained a very large number of orbits of the individual meteor bodies.

From the observations for each meteor, there are determined: the time T of its appearance, the velocity v and the radiant coordinates α and δ. We know the accuracy of measurements of v, α and δ, while the permissible spread T can be estimated based on the duration of the effect of the known meteor showers, therefore it would be most simple to separate the meteor associations in a four-dimensional space with the coordinates T, v, α and δ. However, such a sampling method becomes difficult, since the coordinates of the shower radiants vary during the time of their visibility. Therefore, the sampling (selection) of the meteors of the streams and associations was conducted in two stages.

For each period of the observations, having lasted 5 - 10 days, all the meteors were divided into overlapping groups by velocities: 10 - 20, 15 - 25, ..., 65 - 75 km/sec. The meteor radiants of each group were roughly referred to the center of the interval of observations and posted to individual charts. Near each radiant, we posted the meteor velocity. Since each period of observations lasted not over 10 days, the inaccuracy of referring the radiants to the center of the span did not lead to an appreciable spread in the shower radiants, if they existed in the given groups. The associations of the meteors are recorded in such charts.

For each such association, we found approximately the average velocity v, and then for the corresponding section of the chart with a dimension of several tens of degrees in respect to α and δ, we posted the meteors with the velocities v from $-2.5\ \Delta v$ to $+2.5\ \Delta v$. At such a repeated posting in the charts, a part of the previously noted associations was distinguished more clearly against the background of the radiants of the sporadic meteors. On the other hand, several of the associations practically blended in with the background. Such groups of meteors were excluded from the further review.

Table 4.8

Catalog of Orbits of Meteor Showers and Associations

No. of shower	Days of observations (III= March, etc)	N	α	δ	v_∞, km/sec	a	e	q	i	Ω	ω	Shower
1	14—15.III	5	172°	+ 3°	23	1,95	0,67	0,64	0°1	175°	83°	σ Leonids
2	14—16.III	8	177	— 5	29	2,53	0,82	0,47	6	175	100	
3	14—23.III	9	188	+ 1	30	1,94	0,82	0,36	6	356	297	Virginids
4	15—15.III	4	193	— 9	36	1,77	0,90	0,18	6	175	137	
5	15—17.III	4	201	+ 2	32	1,29	0,83	0,22	16	355	316	
6	15—16.III	6	214	+ 9	38	1,27	0,86	0,18	50	355	321	
7	15—15.III	5	258	+33	49	4,59	0,79	0,98	85	354	194	
8	14—20.IV	14	208	+ 6	24	2,19	0,70	0,66	11	28	260	
9	14—26.IV	14	237	—19	40	1,48	0,95	0,07	4	28	336	
10	14—26.IV	14	241	+ 4	30	1,03	0,72	0,29	35	28	315	
11	14—19.IV	11	284	+26	34	0,81	0,27	0,59	69	26	344	
12	14—23.IV	8	256	+20	46	3,03	0,80	0,60	77	28	265	
13	14—19.IV	9	282	+ 6	48	0,84	0,37	0,53	115	26	317	
14	15—22.IV	7	271	+ 6	52	1,44	0,65	0,51	112	28	285	
15	15—19.IV	13	294	+15	45	0,84	0,23	0,65	102	26	26	
16	15.IV—26.V	86	356	+ 8	37	1,27	0,92	0,10	27	32	28	
17	15—20.IV	11	329	+ 9	51	1,60	0,86	0,22	114	27	47	
18	15—20.IV	9	307	+20	39	0,80	0,50	0,40	85	27	35	
19	15—25.IV	34	7	+ 3	31	1,32	0,83	0,22	0,5	30	45	
20	15—19.IV	4	345	+18	33	1,01	0,80	0,20	41	28	37	
21	15—22.IV	16	343	+20	40	1,42	0,85	0,21	61	29	44	
22	15—24.IV	8	346	+28	41	3,32	0,89	0,36	56	28	69	
23	15—19.IV	7	316	+ 4	57	1,40	0,64	0,50	135	28	73	
24	15—19.IV	8	312	+15	51	1,19	0,54	0,55	110	27	72	
25	15—25.IV	16	12	+10	29	1,55	0,78	0,34	6	30	59	
26	15—19.IV	6	342	+24	47	16,1	0,98	0,32	71	26	68	
27	15—19.IV	6	294	+16	52	1,23	0,21	0,98	110	27	148	
28	15—26.IV	18	288	+10	58	1,92	0,50	0,95	120	28	211	
29	15—20.IV	5	293	0	62	1,72	0,42	0,99	142	28	199	
30	15—25.IV	11	13	— 3	31	1,61	0,83	0,28	11	209	233	
31	15—25.IV	16	18	+ 4	27	1,66	0,77	0,39	3	210	246	
32	17—20.IV	2	272	+31	48	5,59	0,84	0,92	82	28	216	Lyrids
33	17—21.IV	5	187	— 5	22	7,14	0,89	0,80	1	209	52	
34	17—20.IV	4	301	+24	52	2,11	0,56	0,93	101	29	143	
35	19—24.IV	14	22	+10	27	2,24	0,79	0,47	0,3	30	78	
36	3—18. V	7	284	+31	31	0,97	0,30	0,68	61	49	293	
37	3—24. V	30	291	+29	34	0,89	0,27	0,65	67	48	309	
38	3—24. V	14	301	+24	33	0,72	0,43	0,41	72	51	343	
39	4— 7. V	11	19	+16	25	1,03	0,69	0,32	8	45	48	
40	4—27. V	16	41	+23	27	1,94	0,77	0,44	6	54	74	
41	4—27. V	43	33	+ 9	31	1,68	0,84	0,27	5	232	233	
42	4—19. V	60	52	+23	30	1,61	0,80	0,31	6	71	57	Perseids
43	4— 7. V	8	306	+36	32	0,85	0,20	0,68	64	45	32	
44	4—27. V	9	330	+16	61	2,59	0,66	0,89	131	57	135	
45	4—19. V	14	8	+21	37	1,31	0,90	0,14	42	48	34	
46	4—27. V	10	307	+24	55	2,44	0,61	0,95	106	57	211	
47	4—27. V	17	17	+19	39	1,64	0,93	0,11	30	53	32	
48	4.V—20.VI	380	43	+23	39	1,66	0,94	0,10	19	77	30	Arietids
49	4—27. V	12	21	+15	40	1,62	0,96	0,07	23	56	26	
50	4—27. V	13	288	+24	33	0,90	0,42	0,52	63	56	308	
51	4—27. V	16	293	+22	33	0,78	0,47	0,41	68	55	327	
52	4—27. V	17	276	+13	33	0,96	0,64	0,35	56	55	312	
53	4—27. V	10	279	+27	34	1,11	0,44	0,62	60	53	284	
54	5—27. V	7	322	5	53	1,00	0,16	0,84	123	56	79	
55	5—20. V	8	359	+18	35	0,91	0,87	0,12	45	45	27	
56	5—27. V	12	323	+23	50	1,05	0,17	0,87	110	60	98	
57	5—17. V	8	7	+26	33	1,07	0,81	0,20	38	50	39	
58	5—27. V	10	289	+11	54	2,16	0,72	0,60	107	52	269	

Table 4.8
(con't.)

No. of showers	Days of observations	N	α	δ	v_∞, km/sec	a	e	q	i	Ω	ω	Shower
	(V = May, etc.)											
59	5 —27.V	12	308°	+11°	61	2,30	0,59	0,94	128°	51°	213°	Arietids
60	5 —27.V	11	313	0	65	2,26	0,57	0,96	149	51	208	
61	5 —27.V	8	23	+23	38	2,54	0,93	0,18	28	53	47	
62	5 —27.V	10	317	+23	52	1,31	0,26	0,97	110	60	201	
63	5 —27.V	11	332	+22	57	1,98	0,60	0,79	119	56	115	
64	5 —27.V	14	335	+16	56	1,25	0,44	0,69	130	58	90	
65	5 —27.V	51	338	0	64	3,34	0,84	0,54	161	47	90	η Aquarids
66	5 —27.V	14	338	— 9	66	4,40	0,85	0,65	179	46	104	
67	5 —26.V	10	282	+ 7	36	0,91	0,74	0,24	62	59	323	
68	5 —27.V	6	334	+20	58	2,36	0,73	0,64	122	51	105	
69	6 —27.V	11	287	+14	31	0,76	0,62	0,28	58	57	330	
70	6 —24.V	7	287	+ 5	55	3,80	0,99	0,42	110	56	284	
71	6 —27.V	18	20	+21	33	1,09	0,86	0,15	23	57	34	
72	16 —27.V	8	288	+19	33	0,87	0,53	0,41	62	60	314	
73	6 —20.VI	8	35	+18	46	1,67	1,00	0,01	78	79	8	
74	6 —20.VI	9	352	+14	52	0,78	0,45	0,43	144	80	31	
75	6 —18.VI	8	7	+28	53	1,47	0,74	0,38	122	79	62	
76	6 —10.VI	7	29	+ 9	52	1,90	0,97	0,05	165	258	202	
77	6 — 9.VI	8	73	+19	24	1,90	0,71	0,56	2	256	265	
78	6 —20.VI	33	44	+12	39	1,34	0,95	0,06	20	258	202	
79	6 —10.VI	15	53	+ 7	37	1,84	0,90	0,18	26	257	223	
80	6 —18.VI	14	64	+15	31	2,20	0,85	0,34	7	258	243	ζ Taurids
81	7 —18.VI	12	18	+15	52	1,12	0,88	0,13	154	79	30	
82	8 —10.VI	11	0	+12	61	1,56	0,60	0,62	156	78	89	
83	8 —20.VI	9	354	+20	60	1,54	0,51	0,76	140	79	105	
84	4 —30.VII	17	6	+27	60	1,59	0,45	0,88	138	116	234	
85	4 —29.VII	23	98	+16	40	5,18	0,97	0,18	16	297	228	
86	4 —28.VII	41	13	+66	42	1,72	0,49	0,87	77	115	126	
87	6 —31.VII	17	330	+ 2	36	0,93	0,90	0,09	41	115	336	Northern
88	6 —29.VII	23	20	+75	42	3,65	0,76	0,87	71	116	133	δ Aquarids
89	6.VII—14.VIII	50	337	— 5	42	2,16	0,97	0,06	18	128	334	Southern
90	4.VII—13.VIII	13	328	—18	33	2,12	0,88	0,26	8	307	126	ι Aquarids
91	4.VII—13.VIII	13	321	— 8	35	1,92	0,89	0,20	12	120	313	Northern ι Aquarids
92	9 —17.VII	5	315	+68	37	3,37	0,70	1,00	60	112	163	
93	15.VII—12.VIII	45	340	— 8	39	1,38	0,96	0,05	1	126	339	
94	14—27.VII	11	327	+11	33	0,85	0,80	0,17	49	113	330	Southern
95	14.VII—14.VIII	151	341	—16	41	2,04	0,96	0,08	28	307	151	ε Aquarids
96	14 —28.VII	10	10	+40	58	2,08	0,53	0,98	121	120	205	
97	14 —28.VII	23	0	+56	41	1,09	0,18	0,90	83	114	107	
98	15 —28.VII	13	44	+21	61	1,42	0,63	0,53	171	119	77	
99	16.VII—13.VIII	32	340	—26	42	4,31	0,96	0,17	45	305	134	
100	26 —28.VII	7	337	—36	42	16,1	0,98	0,30	47	303	114	
101	2 —12.VIII	6	44	+ 3	64	1,75	0,44	0,98	155	314	25	
102	2 —13.VIII	8	38	+33	53	0,79	0,30	0,55	143	134	20	
103	2 —14.VIII	6	42	+25	63	1,36	0,28	0,98	164	135	147	
104	2 —14.VIII	13	25	+41	59	1,92	0,50	0,96	128	134	211	
105	2 —14.VIII	13	29	+28	63	1,78	0,48	0,93	152	133	222	
106	2 —14.VIII	11	44	+33	66	2,60	0,64	0,94	152	134	148	
107	2 —14.VIII	7	23	+61	52	2,38	0,59	0,98	98	135	158	
108	2 —14.VIII	10	57	+49	59	3,01	0,77	0,70	123	134	108	
109	2 — 7.VIII	9	33	+57	54	2,19	0,57	0,95	107	133	144	
110	2 —13.VIII	9	27	+48	55	1,52	0,35	0,98	116	134	206	
111	2 — 5.VIII	4	350	—33	42	6,41	0,95	0,31	54	311	114	
112	3 —14.VIII	18	53	+33	60	1,45	0,54	0,67	152	132	92	
113	3 — 6.VIII	11	62	+29	61	1,84	0,74	0,48	161	132	79	
114	3 —12.VIII	6	30	+ 9	62	1,42	0,48	0,74	173	314	79	
115	3 —14.VIII	10	41	+57	60	11,0	0,91	0,95	113	136	151	Perseids

Table 4.8

No. of shower	Days of observations	N	α	δ	v_∞, km/sec	a	e	q	i	Ω	ω	Shower
	(VII = July, etc.)											
116	3.VII—13.VIII	8	55°	+33°	52	0,81	0,53	0,38	149°	136°	36°	Perseids
117	3—12.VIII	6	46	+36	53	0,83	0,33	0,56	140	135	39	
118	3—13.VIII	9	69	+43	58	2,73	0,84	0,44	129	134	77	
119	3—14.VIII	12	18	+17	60	1,59	0,73	0,43	159	136	291	
120	3—14.VIII	14	41	+44	61	2,73	0,66	0,94	131	135	145	
121	3—14.VIII	8	45	+39	58	1,20	0,27	0,88	138	137	114	
122	2—11.VIII	9	36	+34	67	5,21	0,81	1,00	148	132	164	
123	3—14.VIII	8	36	+30	64	1,78	0,45	0,98	151	136	205	
124	3—11.VIII	5	41	+ 9	67	2,38	0,59	0,98	168	314	22	
125	3—10.VIII	7	54	+16	67	2,62	0,68	0,84	173	313	305	
126	3—10.VIII	9	54	+26	64	1,88	0,61	0,74	168	133	107	
127	3—10.VIII	6	15	+35	62	3,94	0,79	0,83	132	134	232	
128	4—13.VIII	7	29	+16	65	2,02	0,60	0,80	172	135	243	
129	4—14.VIII	15	38	+37	61	1,52	0,35	0,98	141	137	173	
130	4—13.VIII	5	52	— 5	63	2,54	0,61	0,98	138	314	336	
131	4—14.VIII	7	24	+56	52	1,82	0,46	0,99	104	138	203	
132	10—14.VIII	6	39	+12	67	2,72	0,67	0,90	175	319	42	
133	21—27.IX	9	78	+11	68	5,00	0,83	0,85	158	0,2	48	
134	21—28.IX	8	78	+20	70	8,55	0,90	0,84	174	1,2	48	
135	21—27.IX	5	106	+25	64	1,58	0,53	0,75	176	181	106	
136	21—28.IX	10	68	+16	62	1,95	0,75	0,49	167	1,7	101	
137	21—28.IX	6	78	+14	61	1,22	0,46	0,66	163	0,7	95	
138	21—27.IX	6	90	+41	69	13,0	0,92	1,00	150	181	188	
139	21—27.IX	11	82	+26	67	2,30	0,60	0,92	174	180	219	
140	21—28.IX	8	75	+35	66	2,63	0,69	0,81	157	180	238	
141	21—28.IX	4	81	+33	68	3,01	0,70	0,92	162	181	217	
142	21—27.IX	5	77	+27	63	1,51	0,52	0,72	172	182	261	
143	20—28.IX	10	61	+25	61	2,25	0,85	0,34	170	181	296	
144	21—27.IX	5	72	+29	69	11,8	0,94	0,74	168	1,1	242	
145	21—28.IX	9	68	+27	65	3,33	0,81	0,58	168	181	266	
146	21—28.IX	7	99	+ 7	66	2,80	0,67	0,95	151	1,9	332	
147	21—28.IX	83	42	+20	43	2,98	0,98	0,07	16	198	332	
148	20—25.IX	4	99	+18	65	1,65	0,44	0,92	171	1,0	316	
149	20—22. X	73	27	+ 9	31	2,07	0,84	0,33	2,2	15	118	Southern Taurids
150	21—27.IX	16	86	+ 9	63	1,52	0,40	0,91	152	2,1	47	
151	21—25.IX	5	101	+23	69	3,70	0,75	0,92	179	0,9	324	
152	21—27.IX	21	162	+16	45	47,6	1,00	0,11	26	0,4	39	
153	22—25.IX	4	84	+14	57	0,89	0,28	0,64	160	0,5	132	
154	24—28.IX	4	69	+34	67	7,63	0,92	0,65	156	183	254	
155	24—27.IX	9	100	+31	68	2,70	0,64	0,97	165	183	158	
156	10—21. X	21	108	+15	66	1,90	0,51	0,94	166	23	30	
157	10—27. X	13	104	+25	69	3,58	0,75	0,88	175	203	223	Geminids
158	10—22. X	20	81	+29	58	1,69	0,84	0,27	164	201	307	
159	10—22. X	17	88	+12	58	1,48	0,74	0,38	152	23	119	
160	10—21. X	18	40	+15	33	1,74	0,86	0,24	1,2	22	131	Southern Arietids
161	10—21. X	15	34	+20	38	4,05	0,95	0,22	12	201	307	
162	10—22. X	28	44	+14	42	4,46	0,98	0,11	7	22	145	
163	10—21. X	24	52	+15	42	1,74	0,97	0,05	17	21	158	
164	11—21. X	10	110	+24	67	2,07	0,53	0,99	177	201	197	
165	11—27. X	61	93	+16	66	4,76	0,88	0,57	164	25	86	Orionids
166	11—21. X	8	105	+ 6	63	1,62	0,42	0,94	150	21	33	
167	11—20. X	10	96	+30	67	3,10	0,75	0,78	166	199	241	
168	11—21. X	12	106	+31	67	2,29	0,61	0,90	164	202	223	
169	11—18. X	8	122	+16	66	2,13	0,60	0,84	172	20	307	
170	11—21. X	7	119	+17	68	2,90	0,66	0,97	173	22	341	
171	11—22. X	18	142	+23	59	1,36	0,71	0,39	161	203	62	
172	11—17. X	6	99	+12	66	2,21	0,62	0,84	158	20	54	
	(X = Oct. etc.)											

Table 4.8 (Conclusion)

No. of shower	Days of observations	N	α	δ	v_∞, km/sec	a	e	q	i	Ω	ω	Shower
	(X = October, etc.)											
173	11—27. X	12	137°	+25°	68	4,76	0,84	0,74	164°	205°	116°	
174	11—19. X	13	128	+22	65	1,94	0,62	0,75	173	200	110	
175	11—22. X	11	120	+23	68	2,46	0,61	0,97	175	202	159	
176	11—20. X	9	142	+ 8	60	1,90	0,84	0,30	161	22	238	
177	11—16. X	6	119	+ 6	60	1,20	0,37	0,76	151	19	276	
178	11—27. X	13	108	+18	59	0,92	0,24	0,70	170	22	122	
179	11—23. X	13	33	+18	30	2,19	0,84	0,36	5,5	205	295	
180	12—16. X	14	111	+36	65	1,91	0,49	0,97	154	201	200	
181	12—21. X	9	142	+23	67	8,06	0,92	0,61	165	204	100	
182	12—22. X	12	123	+29	68	2,48	0,60	0,98	164	205	164	
183	12—22. X	7	130	+32	66	2,30	0,64	0,83	156	201	124	
184	12—22. X	12	158	+24	57	2,30	0,91	0,20	136	203	48	
185	9—13. XII	10	103	+15	39	2,61	0,94	0,16	20	79	138	
186	9—12. XII	7	85	+19	27	2,07	0,77	0,47	3,6	79	102	
187	9—14. XII	401	111	+33	36	1,31	0,89	0,14	24	260	326	
188	10—16. XII	11	95	+24	31	1,80	0,82	0,32	3,5	260	301	
189	10—14. XII	8	104	+29	40	3,51	0,96	0,14	17	260	320	
190	10—13. XII	9	118	+24	41	1,20	0,97	0,03	16	260	344	
191	10—13. XII	7	103	+43	36	2,46	0,88	0,29	32	260	300	
192	10—16. XII	13	103	+18	32	1,37	0,84	0,22	8,1	80	135	
193	11—16. XII	9	163	+30	64	3,76	0,81	0,71	138	261	249	
194	11—14. XII	12	161	+18	66	2,24	0,68	0,73	162	261	252	
195	22—23. XII	7	190	+75	34	2,60	0,66	0,89	52	270	224	

For each association, we calculated the preliminary average orbital elements e, q, i, ω and the theoretical deviations from the averages Δe, Δq, Δi and $\Delta\omega$, corresponding to the average measurement errors Δv, $\Delta\alpha$, $\Delta\delta$. The further sampling was conducted according to the orbital elements e, q, i and ω. A meteor was assigned to a given association, if for it the conditions were fulfilled.

$$|e-\bar{e}|<2\Delta e,\quad |i-\bar{i}|<2\Delta i,$$
$$|q-\bar{q}|<2\Delta q,\quad |\omega-\bar{\omega}|<2\Delta\omega. \qquad (4.44)$$

After finding the average orbital elements, we conducted a search for the meteors belonging to the given association, which were observed in the successive months.

Orbits of Meteor Showers and Associations

In the processing of the observational material obtained by us, we have not formulated the goal of detecting the meteors in known showers. A comparison with the results of other measurements and the identification of the known meteors was conducted after the average orbital elements were computed of all of the associations detected by us. The only shower which was investigated specially among the measured meteors was the Lyrids shower. In 1958, B. L. Kashcheyev and V. N. Lebedinets [76] detected a very intensive short-period increase in the population of the Lyrids. In 1960, the number of the recorded Lyrids was low, and we managed to find a total of two orbits, similar to the orbit of the shower.

Applying the above-described method of the sampling of the meteor showers to the catalog of orbits developed by us, we discovered that of the total

number of 12,500 meteors, 28% (3500) can be related to the 195 meteor showers and associations. In Table 4.8, for each of the showers and associations, /172 we have presented: the number, day and month of the beginning and end of the observations, the number of the orbits measured, the equatorial coordinates of the corrected average radiant, the extra-atmospheric velocity (corrected for deceleration in the atmosphere and for diurnal rotation of the Earth) and the average elements of the orbit. For the known meteor streams, the orbits of which were obtained previously from the photographic or radar measurements, we have listed their names. In the catalog at the end of the book, we have shown a part of the orbits of the individual meteor bodies, related by us to the showers and associations. Certain of the orbits not included in the catalog were published earlier [76, 201].

The maximum number of orbits was obtained for the two most accurate of the constantly effective meteor showers of the Geminids (401 orbits) and the Arietids (380 orbits). A large number of orbits was also obtained for the known meteor showers: the Southern δ Aquarids (151), the Southern Taurids (73), the Orionids (61), the ζ Perseids (60), the η Aquarids (51) and the Northern δ Aquarids (50). Among these eight showers, we include 1,227 meteors.

For the 104 showers and associations, the number of measured orbits $N >> >> 10$. Most of them apparently constitute actual showers, in which the meteor bodies are connected by the generality of origin. Certain of the associations can prove to be random groups of meteor bodies with similar orbits.

Ninety-three meteors were related by us to the 21 small showers and associations with the number of measured orbits $N \leqslant 5$. A considerable part of such small groups of orbits can be random. However, among them we find the known meteor showers Lyrids and σ Leonids; the orbits of several of them are similar to the orbits of the associations detected by other observers, or with the orbits of the comets. The reality of the individual meteor associations is not linked unequivocally with the number of the measured orbits of the meteor bodies entering them. They are determined chiefly by the compactness of the associations and also by the partial density of the radiants of the sporadic meteors with similar velocities in the given sector of the celestial sphere.

In all 10 orbits were obtained for the Perseids shower, which constitutes one of the most active meteor showers in the photographic and visual observations, and also in the radio observations with the equipment of a low effective sensitivity. During the measurements of the population of the meteors, without equipment, the Perseids were practically not distinguished against the background of the sporadic meteors. The low number of the radio meteors being recorded in the Perseids shower can in no way be explained by the selectivity of the radar method of observations in respect to their velocity, since we find a large number of radio meteors in the showers with even higher velocities, namely the Orionids and the η Aquarids. Evidently, in the Perseids shower, there are relatively few small meteor bodies which produce the main mass of the radio meteors being recorded by us.

Comparison with the Results of Other Observations

Up to the present time, in many Soviet and foreign observatories, according to the basic photographic observations with a shutter, calculations have been made of the individual orbits of about 3500 meteor bodies. In England and Australia, from the base line radar observations of meteors, individual orbits have been obtained of around 4,600 small meteor bodies.

From the available photographic catalogs of the orbits of meteor bodies, for comparison without measurements, the following information was used:

I. In 1954, Whippler [12] published a catalog of the orbits of 144 meteors brighter than about 0^m, in which he assembled the results of the base line photographic observations at the meteor stations of the Harvard Observatory in Massachusetts and New Mexico from 1936 - 1955. Of 144 meteors, 93 belong to 22 previously known and new meteor showers and associations.

/173

II. In 1957, L. A. Katasev [202] published a catalog of 73 orbits. The observations were conducted in Dusha be from 1940 - 1955. In the catalog he included 27 orbits of meteor bodies belonging to three showers: Perseids, δ Aquarids and Taurids.

III. A catalog of orbits 2,529 meteors brighter than about $+3^m$ was developed by McCrosky and Posen [28] as a result of the processing by an approximate graphic method of the observations of the meteors with the photographic cameras "Super-Schmidt", conducted at the Harvard meteor project from 1952 - 1954. They listed 346 orbits of meteors belonging to 25 known meteor showers.

IV. For the 413 meteors, the base line photography of which was obtained with the "Super-Schmidt" cameras under the Harvard meteor project from 1951 - 1954, a precise processing was conducted. Jacchia and Whipple [199] discovered that of these 413 meteors, 268 could be related to 77 previously known and new meteor showers and associations. Catalogs III and IV have 355 common meteors.

V. According to the observations with the cameras "Super-Schmidt", from 1954 - 1957, Hawkins and Southworth [203], obtained the orbits of 359 meteors. The statistical studies of this catalog conducted by Southworth and Hawkins [200] demonstrated that, of the 359 meteors, 129 can be combined into 38 showers and associations.

VI. P. B. Babadzhanov and Ye. N. Kramer [204] based on the photographic observations of meteors brighter than about 0^m, conducted in the IGY period in Dushambe and Odessa, obtained the orbits of 315 meteor bodies. 107 meteors were related by them to 42 meteor showers and associations, of which 15 had not previously been observed.

VII. Z. Ceplecha and others [205] based on the photographic observations of the meteors in the IGY period in Czechoslovakia obtained the orbits of 88 meteor bodies, of which 31 belong to 11 meteor showers.

For a comparison with our measurements, we also make use of the results of determining the orbits of the meteor showers based on the baseline radar measurements of the velocities and coordinates of the radiants of the individual meteors.

VIII. From May, 1954 to April, 1955, Davis and Gill [182] in Jodrell Banka, England, conducted an annual cycle of radar measurements of the velocities and radiants of the meteors, using the pulse-diffraction method. In each month, the measurements were made for a period of 24 hours. They obtained 2,474 orbits for the meteors brighter than about $+7^m$. The catalog of orbits was not published. The special studies of the catalog for the purpose of revealing the meteor showers was not conducted. Davis and Gill present the average radiants and orbital elements for three previously observed and for three new showers, in which they include 74 of the orbits obtained by them.

IX. From December, 1960, to December, 1961, in Adelaide, the base measurements were conducted of the velocities and radiants of the individual meteors by the method of the nonattenuating radio waves. For 1700 hours of observations, 2,200 orbits were obtained for meteors brighter than about $+6^m$. The catalog of orbits was not published. Nilsson [187] conducted special statistical studies of the catalog for the purpose of indicating the orbital groupings. The research method was described above. Nilsson segregated 66 meteor showers and associations, to which 463 meteors belong.

In this manner, based on the results of the baseline photographic and radar observations of the meteors by various authors, there were separated more than 150 meteor showers and associations. The orbits of 24 of them are close to the orbits of the showers and associations obtained from our catalog of 12,500 orbits of individual meteor bodies. We compare below the orbits of a number of showers and associations developed by various authors.

/174

Geminids. The Geminids orbits are listed in 7 of the 10 catalogs enumerated above. In Table 4.9, we have shown the number of the Geminids orbits in each catalog, the average coordinates, the extra-atmospheric velocities and the average orbital elements.

Table 4.9

Radiant and Orbit of Geminids

Author	N	α	δ	v_∞, km/sec	$1/a$	e	q	i	Ω	ω
B.L.Kashcheyev et al	401	111°,4	+32°,6	36,0	0,76	0,89	0,14	23°,7	259°,6	325°,8
Whipple [12]...	13	112,7	+32,4	36,4	0,73	0,90	0,14	23,9	261,2	324,4
McCroskey, Posen [28]	72	111,3	+32,5	36,3	0,71	0,90	0,14	23,1	260,2	324,2
Jacchia, Whipple [199]	20	111,4	+32,5	36,2	0,74	0,90	0,14	23,3	260,2	324,3
Southworth, Hawkins [200]	16	112,6	+32,3	36,3	0,73	0,90	0,14	23,3	261,4	324,1
Babadzhanov, Kramer' [204]	12	111,2	+32,4	36,9	0,76	0,90	0,13	24,8	258,7	326,2
Nilsson [187]	22	109,4	+30,4	34,2	0,79	0,88	0,15	17,4	259,8	325,1

According to our measurements, the average diurnal displacement in the radiant $\Delta\alpha = +0^\circ,83$ $\Delta\delta = -0^\circ,28$. B. L. Kashcheyev and V. N. Lebedinets [76] demonstrated that during the time of the visibility of the stream, there occurs a systematic variation in the velocity of meteors and also of the eccentricity and major semiaxis of the Geminids orbits. From Table 4.9, it is evident that taking into account the differences in the average longitudes

of the Sun for the various authors, our measurements agree well with the results from the photographic observations. The radiant and the velocity of the Geminids, obtained by Nilsson differ somewhat from the results obtained by the other authors, which in the opinion of Nilsson [187], is explained by the relatively large errors in his measurements in connection with the low position of the radiant of Geminids above the horizon for the observers in the Southern Hemisphere.

Arietids. The Arietids radiant is close to the Sun, therefore the orbitt of the shower is determined only from the radar observations in Table 4.10, the measurement results are listed. Nilsson distinguishes two branches of the Arietids shower with quite close radiants, but with different velocities. Since the observations of Davis and Gill and also of Nilsson pertain to the end of the visibility period of the Arietids (15 - 21 June), the results of our measurements from 17 - 20 June are presented separately. In addition to our results, the measurements of the individual Arietids orbits are very scarce, therefore in Table 4.10, for comparison, we have also shown the results of the statistical measurements taken by the Clegg method, conducted at Jodrell Bank from 1950 - 1951 [194]. The average diurnal displacement of the radiant based on our observations, $\Delta\alpha = +0^{\circ},7$ and $\Delta\delta = +0^{\circ},1$.

Table 4.10

Radiant and Orbit of Arietids

Author	N	α	δ	v_∞, km/sec	$1/a$	e	q	i	Ω	ω
B.L.Kashcheyev et al. average..	380	43°,3	+22°,9	38,6	0,60	0,94	0,10	18°,7	76°,6	29°,9
17-20 June	18	52,1	+25,1	39,8	0,60	0,96	0,08	22,8	87,4	25,4
Davis & Gill [182]	6	50,0	+26,0	41,0	0,75	0,97	0,04	46,0	89,0	19,0
Nilsson [187] (1).....	8	46,1	+26,1	39,6	0,67	0,96	0,06	33,4	84,8	23,0
Nilsson [187] (2).....	7	46,6	+25,0	43,6	0,44	0,98	0,04	38,9	84,6	20,3
Lovell [194] 1950..	—	43,8	+21,9	37,7	0,67	0,94	0,10	18,0	77,0	29,0
1951..	—	43,4	+23,9	38,7	0,62	0,94	0,09	21,0	76,8	29,0

The radiant and orbit of the Arietids shower obtained by us agree well /175
with the results from the statistical measurements. From 1950 - 1952, in Jodrell Bank, the determination of the coordinates of the shower radiants was conducted by the Clegg method, using two pencil-beam antennas. In the case of such active showers as the Geminids and the Arietids, the Clegg method provides a high measurement accuracy. The velocity of the meteors was measured by the diffraction method. Use was made of a special procedure of observations for separating the Arietids from the adjacent showers. In 1950, from 31 May to 16 June, the velocity of about 100 Arietids was measured.

The position of the Arietids radiant, found by Davis and Gill, differ from ours by 30°, while the velocity differs by 1 km/sec. Obviously, this difference can be explained in terms of the relatively low accuracy of the radar method used for measuring the radiants of individual meteors. Davis and Gill observed a total of six Arietids.

Already noted above, Nilsson has overestimated the accuracy of his measurements. With such a small number of measurements (8 and 7) by the

radar method, one can scarcely distinguish two simultaneously operating showers, the radiants of which are separated by 1° from each other, while the velocities differ by 4 km/sec. The radiant and the velocity of the first of the showers listed by Nilsson, within the limits of the measurement accuracy, agrees with our results, obtained from 17 - 20 June.

The Southern δ Aquarids. The radiant and the orbit of the shower were determined by many observers. In Table 4.11, we have presented the measurement results. According to our measurements, the average diurnal displacement of the radiant of the Southern δ Aquarids $\Delta\alpha = +0^{\circ}.85$ and $\Delta\delta = +0^{\circ}.35$.

Table 4.11

Radiant and Orbit of the Southern δ Aquarids

Author	N	α	δ	v_∞, km/sec	$1/a$	e	q	i	Ω	ω
B.L. Kashcheyev et al.	151	341°,2	—16°,4	41,2	0,49	0,96	0,08	28°,4	306°,7	151°,1
Katasev [202]	1	339,5	—15,2	44,3	0,18	0,99	0,07	24,0	308,5	150,6
McCroskey, Posen [28]	17	341,6	—14,9	42,4	0,35	0,97	0,08	25,0	309,2	151,1
Jacchia, Whipple [199]	11	341,3	—14,4	42,2	0,36	0,97	0,08	22,7	309,2	151,1
Southworth, Hawkins [200]	3	338,6	—16,7	42,6	0,40	0,97	0,07	28,9	304,6	153,5
Babadzhanov, Kramer [204]	8	341,6	—15,9	40,8	0,37	0,96	0,11	23,7	311,0	145,4
Ceplecha et al. [205]	1	350,7	—13,8	40,1	0,32	0,96	0,14	22,8	322,5	139,4
Davis, Gill [182]	35	339,0	—19,0	43,0	0,44	0,96	0,09	30,0	304,0	150,0
Nilsson [187]	48	339,4	—17,3	41,2	0,43	0,97	0,07	32,5	305,8	152,4

Within the limits of the divergence of the results obtained by individual authors, the radiant and the velocity of the shower obtained by us agree satisfactorily with the data from the photographic observations. The agreement with the data of the radar measurements, especially the Nilsson measurements, is somewhat better.

From the data listed in Table 4.11, we can observe a small systematic difference (approximately by 2° between the positions of the radiant, obtained from the photographic and the radar observations. The Arietids velocity found by the authors and by Nilsson is less by about 1 km/sec than according to the data from the photographic measurements. These differences are less than the divergence of the radiants and the velocities of the individual meteors in the shower, which is obtained during the photographic observations.

Although the systematic differences that have been noted are small, one can scarcely attribute them completely to the measurement errors. They can be explained by the difference in the masses of the meteor bodies, being recorded during the photographic and radio observations. Obviously, the small meteor bodies in a shower on an average will move along less extended orbits. The observed difference of the major semiaxes of the orbits of the meteor /176
bodies producing the photographic meteors and the radio meteors, in the shower of the Southern δ Aquarids can be explained by the effect of the deceleration forces, which change in different ways the orbits of the particles of various sizes.

If the separation of the particles of various dimensions occurs mainly under the effect of the Poynting-Robertson effect, from a comparison of the average orbits obtained from the photographic and radar observations, we can roughly estimate the age of the shower, which proved to be of the order of several milleniums.

Northern δ Aquarids. In Table 4.12, we have shown the radiants and the orbits of a shower, obtained by various authors.

Table 4.12

Radiant and Orbit of the Northern δ Aquarids

Author	N	α	δ	v_∞, km/sec	$1/a$	e	q	i	Ω	ω
B.L. Kashcheyev et al.	50	336°,8	−4°,9	41,8	0,46	0,97	0,06	18°,0	127°,7	333°,8
McCroskey, Posen [28]	2	346,0	0,0	42,2	0,38	0,98	0,08	14,0	142,0	332,5
Southworth, Hawkins [200]	3	346,7	+2,6	39,8	0,41	0,95	0,12	21,2	143,2	324,4
Ceplecha et al. [205]	1	345,4	+0,8	40,9	0,30	0,96	0,12	18,3	142,4	323,4

The average diurnal displacement of the radiant based on our observations $\Delta\alpha = +0^\circ,9$ and $\Delta\delta = +0^\circ,3$.

With allowance for the difference in the average longitude of the Sun during our and the photographic measurements, we find a satisfactory agreement of the radiant and orbit of the shower, obtained by us, with the results of a very low number of photographic measurements.

Southern Taurids. The results of the observations of the shower which were derived by many authors are presented in Table 4.13.

Table 4.13

Radiant and Orbit of the Southern Taurids

Author	N	α	δ	v_∞, km/sec	$1/a$	e	q	i	Ω	ω
B.L. Kashcheyev et al.	73	27°,2	+ 8°,6	30,9	0,48	0,84	0,33	2°,2	14°,6	118°,2
Whipple [12]	8	52,8	+13,9	30,1	0,43	0,84	0,38	5,5	43,3	111,2
McCroskey, Posen [28]	17	42,6	+10,7	28,8	0,53	0,80	0,37	5,3	31,2	114,6
Jacchia, Whipple [199]	13	37,5	+ 9,6	29,8	0,55	0,81	0,34	5,1	24,5	117,8
Southworth, Hawkins [200]	11	28,0	+ 7,5	30,4	0,56	0,82	0,32	5,0	13,7	122,7
Babadzhanov, Kramer [204]	8	24,2	+ 6,2	31,5	0,54	0,83	0,33	3,4	9,5	118,9
Ceplecha et al. [205]	1	28,2	+ 7,0	33,3	0,45	0,88	0,26	6,4	11,9	125,2
Nilsson [187]	17	59,0	+16,6	25,8	0,48	0,76	0,50	4,2	56,1	99,0

We find a good agreement of our results with the data of the photographic measurements. The difference in the orbits obtained by Z. Ceplecha and others [205] and Nilsson [187] from the results of the remaining authors is evidently explained by the fact that their measurements pertain respectively to the very beginning and end of the shower visibility.

Orionids. The radiant and the orbit of the shower based on the observations of various authors are presented in Table 4.14.

With the exception of P. B. Babadzhanov and Ye. N. Kramer, all the remaining observers obtained very close positions of the Orionids radiant. In spite of the large number of measurements, the average velocity of the shower, found by various authors from the photographic observations, varies within fairly wide limits, i.e. from 66.3 to 70.7 km/sec.

/177

Table 4.14

Radiant and Orbit of Orionids

Author	N	α	δ	v_∞, km/sec	$1/a$	e	q	i	Ω	ω
B.L. Kashcheyev et al.....	61	93°,1	+16°,0	65,9	0,21	0,88	0,57	164°,2	25°,4	86°,1
Whipple [12]	2	95,4	+15,5	66,3	0,16	0,92	0,54	162,9	29,3	87,8
McCrosky, Posen [28].	48	94,9	+15,4	68,2	—0,02	1,01	0,58	162,8	30,9	80,3
Jacchia, Whipple [199]	5	95,2	+16,0	67,6	0,06	0,96	0,57	164,4	28,6	82,3
Southworth, Hawkins [200]	12	95,6	+16,2	67,6	0,05	0,97	0,57	164,9	29,2	82,8
Babadzhanov, Kramer [204]	5	95,9	+20,2	70,7	—0,25	1,16	0,63	161,6	28,7	72,5
Ceplecha et al. [205]	4	90,0	+15,4	69,4	—0,05	1,03	0,66	164,0	21,2	70,6
Nilsson [187]	6	96,7	+14,4	65,3	0,16	0,92	0,50	160,3	32,3	90,9

Accordingly, the divergence in the average values of the major semiaxis of the orbit and of the eccentricity is also considerable. The values v_∞, $1/a$ and e for the individual meteors in Orionids in each of the catalogs vary within wide limits. This spread can be explained by the complex structure of the shower (by the simultaneous influence of several showers with similar radiants), which is connected with the extensive perturbations of the producers of the Orionids shower, namely, of Halley's comet. In three of the six photographic catalogs, the average orbit proved to be hyperbolic, which evidently indicates fairly large measurement errors. The major semiaxis of the orbit and the eccentricity based on the data of the radar observations prove to be somewhat less than from the photographic measurements.

ζ Perseids. In Table 4.15, we have presented the radiant and the orbit of this daily shower based on the observations of the authors and Nilsson. The results of both measurements practically coincide.

Table 4.15

Radiant and Orbit of the ζ Perseids

Author	N	α	δ	v_∞, km/sec	$1/a$	e	q	i	Ω	ω
B.L.Kashcheyev et al	60	51°,5	+22°,9	29,8	0,62	0,80	0,31	5°,7	70°,6	57°,0
Nilsson [187]. .	27	50,7	+21,5	29,9	0,59	0,82	0,31	4,8	70,5	56,3

Southern Arietids (Table 4.16). We find a satisfactory agreement of the results, obtained by us, with the data from the photographic measurements by McCrosky and Posen and of the radar measurements made by Nilsson.

Table 4.16

Radiant and Orbit of the Southern Arietids

Author	N	α	δ	v_∞, km/sec	$1/a$	e	q	i	Ω	ω
et al.										
B.L. Kashcheyev/ McCroskey, Posen [28]...	18	39°,6	+14°,7	32,7	0,57	0,86	0,24	1°,2	22°,5	130°,7
Nilsson [187]...	13	38,8	+10,5	30,0	0,57	0,83	0,30	5,8	24,2	122,5
	30	44,8	+12,4	30,2	0,50	0,83	0,34	5,9	33,0	118,3

/178

Table 4.17

Radiant and Orbit of the Southern ι Aquarids

Author	N	α	δ	v_∞, km/sec	$1/a$	e	q	i	Ω	ω
B.L.Kashcheyev, et al	13	327°,8	−17°,6	33,4	0,47	0,88	0,26	7°,5	306°,6	125°,9
McCroskey,Posen [28]	10	330,9	−12,9	35,7	0,36	0,92	0,22	4,2	310,3	129,6
Whipple,Jacchia[199].	6	322,4	−14,8	34,4	0,40	0,90	0,25	3,6	303,3	126,3
Southworth,Hawkins [200]	4	323,8	−14,6	35,5	0,50	0,88	0,23	1,2	301,1	133,5

The Southern ι Aquarids (Table 4.17). In spite of the fact that we have obtained a relatively low number of individual orbits of the meteor bodies of the shower, the average radiant and orbit of the shower found by us agree satisfactorily with the data from the photographic observations.

The Northern ι Aquarids (Table 4.18). From the photographic observations, we have obtained a total of 5 orbits of the meteor bodies of the shower. Three orbits are presented in the Nilsson catalog. In spite of the sparseness of the measurements, the results of the various authors agree satisfactorily with one another.

The Northern Taurids (Table 4.19). From the photographic observations, various authors have obtained around 40 individual orbits of the meteor bodies in the shower.

The results of all the measurements agree well with each other.

/179

Perseids. Of the constantly operating showers, the Perseids yield the largest number of bright meteors, therefore, based on the photographic observations, up to the present time we have obtained several hundreds of individual orbits of Perseids. As already noted above, in the radar observations with equipment of high sensitivity, the number of the shower meteors

being registered is small as compared with the number of the sporadic meteors. In all, we obtained 10 individual Perseids orbits. In Table 4.20, the average radiant and orbit of Perseids obtained by us are compared with the results derived from the photographic observations.

Table 4.18

Radiant and Orbit of the Northern ι Aquarids

Author	N	α	δ	v_∞, km/sec	$1/a$	e	q	i	Ω	ω
et al. B.L. Kashcheyev/	13	320°,7	−8°,2	34,8	0,52	0,89	0,20	12°,0	119° 6	313°,4
McCroskey, Posen [28]	2	332,5	−5,5	33,2	0,49	0,88	0,25	7,5	134,5	308,0
Jacchia, Whipple [199]	2	332,6	−4,2	35,9	0,52	0,91	0,17	15,9	129,4	318,8
Southworth, Hawkins	1	323,8	−6,8	38,5	0,29	0,95	0,18	15,0	124,1	312,8
Nilsson [187].....	3	326,2	−12,3	31,5	0,64	0,85	0,23	6,9	125,3	312,5

Table 4.19

Radiant and Orbit of the Northern Taurids

Author	N	α	δ	v_∞, km/sec	$1/a$	e	q	i	Ω	ω
B.L. Kashcheyev et al.	13	33°,5	+18°,2	30,5	0,46	0,84	0,36	5°,5	205°,4	294°,6
Whipple [12]	7	46,0	+20,9	30,6	0,42	0,85	0,36	3,8	218,1	293,1
Katašev [202]	1	54,2	+20,0	30,7	0,45	0,83	0,39	0,8	226,9	290,3
McCroskey, Posen [28]..	15	53,8	+21,6	30,9	0,43	0,85	0,35	2,9	224,6	294,6
Jacchia, Whipple [199].	6	53,2	+21,1	31,2	0,42	0,86	0,34	2,6	223,6	295,3
Southworth, Hawkins [200]	8	47,9	+20,5	31,9	0,48	0,85	0,31	3,8	216,1	300,9
Babadzhanov, Kramer [204]	1	62,8	+23,2	29,2	0,48	0,81	0,39	2,2	234,8	290,6

Table 4.20

Radiant and Orbit of Perseids

Author	N	α	δ	v_∞, km/sec	$1/a$	e	q	i	Ω	ω
B.L. Kashcheyev, et al	10	41°,0	+56°,6	59,8	0,09	0,91	0,95	113°,1	136°,5	150°,9
Whipple [12]	12	45,2	+56,9	60,7	0,05	0,95	0,95	114,2	138,5	151,9
Katašev [202]	25	46,1	+57,8	60,3	0,12	0,88	0,96	113,0	138,7	150,0
McCroskey, Posen [28]	44	45,6	+58,0	60,2	0,02	0,98	0,94	112,3	138,5	151,1
Jacchia, Whipple [199]	10	46,1	+57,8	60,2	0,05	0,95	0,95	112,8	138,5	150,5
Southworth, Hawkings [200]	9	45,2	+57,1	60,6	0,04	0,96	0,95	113,8	138,0	150,9
Babadzhanov, Kramer [204]	94	45,1	+57,6	61,1	−0,04	1,04	0,95	112,5	137,8	150,5
Ceplecha et al. [205]	15	44,2	+57,8	61,2	0,01	0,99	0,96	112,7	137,5	151,9

Although in certain of the photographic catalogs, a fairly large number of the Perseids enters, we find a relatively large spread in the average positions of the radiant, velocity and orbital elements of the shower, especially a and e), which evidently surpasses the errors in the photographic method of measurements. The spread is very extensive for the individual meteors in each of the catalogs. This indicates the fuzziness of the shower. Our results within the limits of the measurement accuracy, agree with the data from the photographic observations.

Virginids (Table 4.21). In the above-indicated catalogs of the individual orbits of meteor bodies, there is listed a total of 15 Virginids orbits, of which 12 were obtained based on the photographic observations, and three were obtained from the radar observations. Within the limits of the actual accuracy both of the radar and of the photographic measurements, the results obtained by the various authors agree satisfactorily with one another.

Table 4.21

Radiant and Orbit of Virginids

Author	N	α	δ	v_∞, km/sec	$1/a$	e	q	i	Ω	ω
B.L.Kashcheyev et al.	9	188°,2	+1°,2	30,5	0,51	0,82	0,36	5°,7	355°,5	296°,9
Whipple [12]	4	182,3	+4,4	31,6	0,25	0,90	0,42	5,5	353,5	284,0
McCrosky, Posen [28]	5	179,4	+1,0	28,7	0,46	0,80	0,44	0,8	351,4	285,4
Jacchia, Whipple [199]	3	175,6	−0,1	29,4	0,37	0,83	0,45	1,7	170,0	101,9
Nilsson [187]	3	188,5	−3,8	34,3	0,42	0,89	0,26	2,9	354,5	304,3

We do not present the results of the photographic and radar observations of the meteor streams βTaurids, ε Geminids, σ Leonids or Lyrids, for which we obtained a small number of orbits, and also of the shower η Aquarids, for which until now the measurements of the individual radiants have not been conducted.

/180

The orbits of six meteor associations found by us are close to the orbits of the small showers and associations which were found by other authors based on the results of the baseline observations of the meteors:

Association No. 188 - shower VIII from the Whipple catalog [12].

Association No. 186 - shower X from the Whipple catalog [12] and shower 60.12.2 from the Nilsson catalog [187].

Association No. 32 - Association No. 50 from the catalog of Jacchia and Whipple [199].

Associations No. 40, 41 and 185 are respectively similar to the showers 61.5.2, 61.5.6 and 60.12.9 from the Nilsson catalog [187].

Relationship of the Meteor Showers with the Comets

For a comparison with our observations, we will utilize the catalog, published in 1953 by Kramer [206] of 280 cometary radiants, calculated for the comets, the orbits of which approach the orbit of the Earth at a distance of not more than 0.3 A. U.

Of the 195 meteor showers and associations observed by us, 14 have orbits similar to the orbits of 11 comets from the Kramer catalog. In Table 4.22, for each of them we have listed: 1) the average coordinates, obtained by us, of the radiant, velocity and elements of the orbits; 2) the coordinates of the cometary radiant and velocity, the orbital elements of the comet, and also the longitude of the Sun $\lambda_\odot$ at the moment of approaching the Earth with the orbit of the comet, for which the radiant and the velocity are calculated.

Table 4.22

Shower, comet	α	δ	v_∞, km/sec	e	q	i	ω	Ω	$\lambda_\odot$
η Aquarids	338°	0°	64	0,84	0,54	161°	90°	47°	
Orionids	93	+16	66	0,88	0,57	164	86	25	
Halley's comet (1835 III)	337	0	—	0,97	0,59	162	111	55	43°
The same	94	+19	67						207
β Taurids	64	+15	31	0,85	0,34	7	243	258	
Southern Taurids	27	+ 9	31	0,84	0,33	2	118	15	
Northern Taurids	34	+18	30	0,84	0,36	6	295	205	
Enke comet (1937 VI)	85	+13	32	0,85	0,33	12	185	335	98
The same	56	+ 8	32						221
Lyrids	272	+31	48	0,84	0,92	82	216	28	
comet 1861 I	270	+34	48	0,98	0,92	80	213	30	30
Perseids	41	+57	60	0,91	0,95	113	151	136	
comet 1862 III	44	+57	61	0,96	0,95	114	153	137	139
№ 66	338	— 9	66	0,85	0,65	179	104	46	
comet 1698	338	— 8	68	1	0,73	169	151	66	40
№ 108	57	+49	59	0,77	0,70	123	108	134	
comet 1764	51	+45	60	1	0,56	127	105	120	123
№ 124	41	+ 9	67	0,59	0,98	168	22	314	
comet 1946 d	26	+ 4	71	1	1,02	170	22	301	121
№ 161	34	+20	38	0,95	0,22	12	307	201	
comet 1948 g	45	+28	41	1	0,21	23	317	203	213
№ 182	124	+29	68	0,60	0,98	164	164	205	
comet 1366	149	+31	70	0,90	0,98	150	165	227	227
№ 193	163	+30	64	0,81	0,71	138	249	261	
comet 1798 II	158	+34	66	1	0,78	138	215	250	249
№ 195	190	+75	34	0,66	0,89	52	224	270	
Tutlya comet (1926 IV)	210	+76	36	0,82	1,02	55	207	270	270

In Table 4.23, we have listed the orbits of the Jacobini-Zinner, Biel and 1866 I, and the associated meteor showers of Draconids, Andromedids and Leonids, which were not observed by us. The orbits of the showers are taken based on the data of the photographic measurements. / 181

From the data presented in Tables 4.13, 4.14, 4.19, 4.20, 4.22 and 4.23, we can observe that a good agreement of the orbital elements of the comets and the associated meteor showers occurs only in four cases: the comet 1862 III and the Perseids, the comet Jacobini-Zinner and Draconids, the comet 1866 I and Leonids, the comet 1861 I and the Lyrids. In all the remaining cases, the orbits of the comets and of the meteor showers differ significantly from one another.

Table 4.23

Stream, comet	α	δ	v_∞, km/sec	e	q	i	ω	Ω
Draconids [199]	271°	+47°	20	0,70	1,00	25°	177°	196°
Draconids [200]	271	+47	20	0,70	1,00	25	177	196
Giacobinid-Zinner comet (1926 VI)	264	+54		0,72	0,99	31	172	196
Andromedids [199]	26	+32	21	0,71	0,74	9	247	225
" [200]	19	+ 5	22	0,70	0,70	0,4	74	25
Biela's comet (1852 III)	24	+43		0,76	0,86	13	246	223
Leonids [12]	153	+22	72	0,93	0,99	163	174	233
Leonids [199]	152	+23	72	0,92	0,98	162	171	233
Comet 1866 I	150	+23		0,91	0,98	163	171	231

These results are quite natural, if we take into account the value of the approach between the orbits of the comets and the orbit of the Earth. The Earth experiences close approaches with the orbits of four of the above-listed comets. The minimal distances between them equal respectively 0,009, 0,003, 0,007 and 0,002 A. U. For the remaining comets these distances are considerably greater. If the orbit of a comet passes at a great distance from the orbit of the Earth, in order that the meteor shower associated with the comet can be observed on Earth, its orbit should differ appreciably from that of the comet. Since the connection of a number of showers (Andromedids, the Northern and Southern Taurids, and others) with the comets, which do not experience very close approaches with the orbit of the Earth, has been established fairly reliably, the difference in the orbits of the comets and of the meteor showers producing them actually takes place.

This difference can be explained by a number of causes. 1) The contemporary orbit of a comet, as a result of the perturbations from the planets, can differ significantly from that orbit along which the comet moved during the formation of the shower. The partial disintegration of the nucleus of a comet, owing to which the shower is formed, also can lead to a variation in the orbit of the comet. 2) After the formation of a shower, we find the immediate beginning of its gradual breakdown owing to the differential perturbations from the planets, the deceleration of the meteor bodies as a result of the Poynting-Robertson effect, the resistance of the interplanetary environment, etc. From the very beginning, the shower can have a complex structure, if the disintegration of the nucleus occurs at several approaches to the Sun, of a comet with a changing orbit. All these factors lead to a considerable expansion of the shower. The width of the known meteor showers of Perseids, Taurids, and others near the orbit of the Earth are measured by many tens of millions of kilometers. The Earth encounters only a certain part of such a broad shower of meteor bodies. In connection with this, the orbit of the shower, found from the observations of meteors on Earth can differ appreciably from the average orbit for the shower as a whole, and hence from the orbit along which the comet-progenitor of the shower moved during its formation.

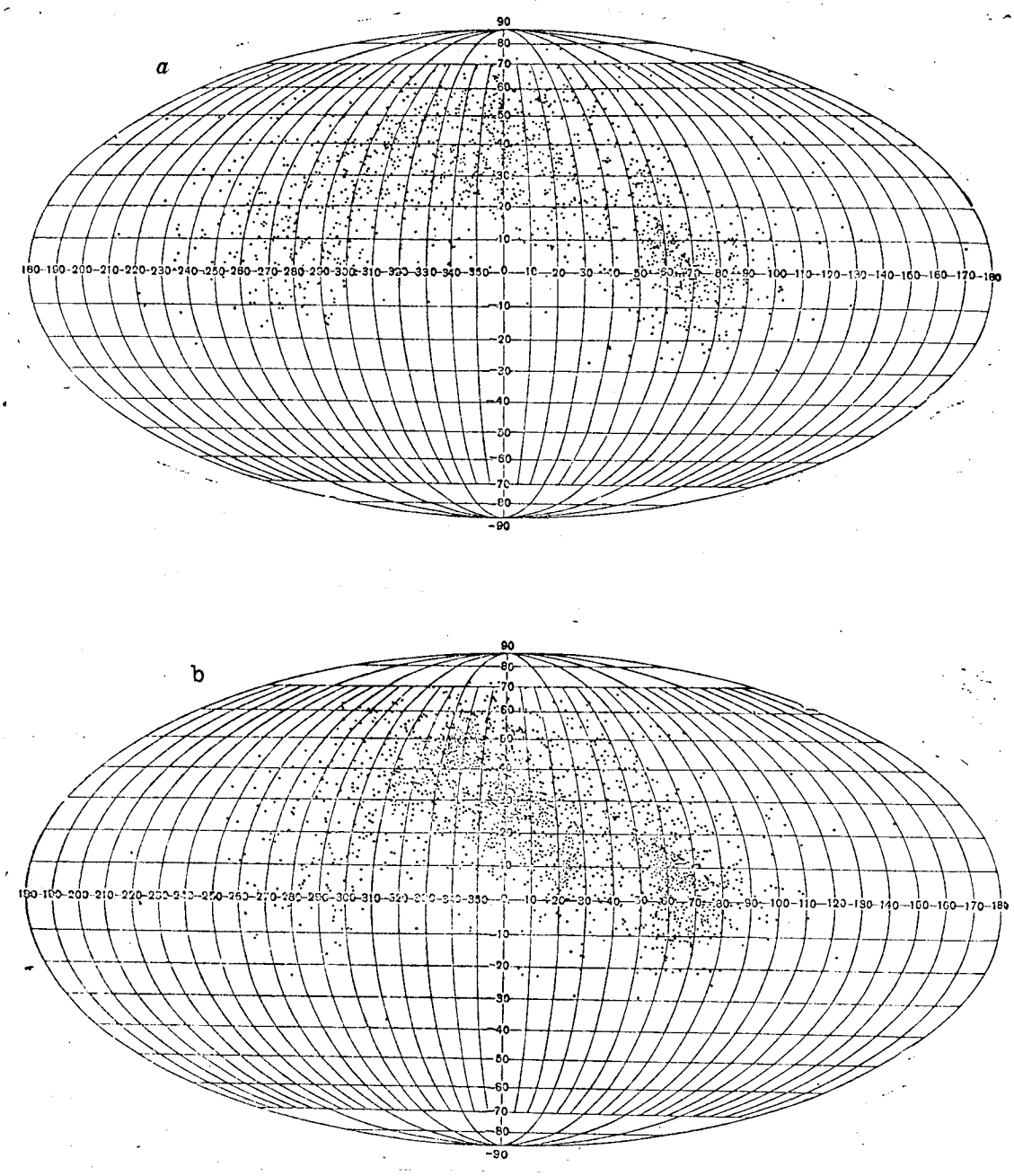

Fig. 4.17. Measured Distribution of Meteor Radiants in 1960.
a- April; b- May

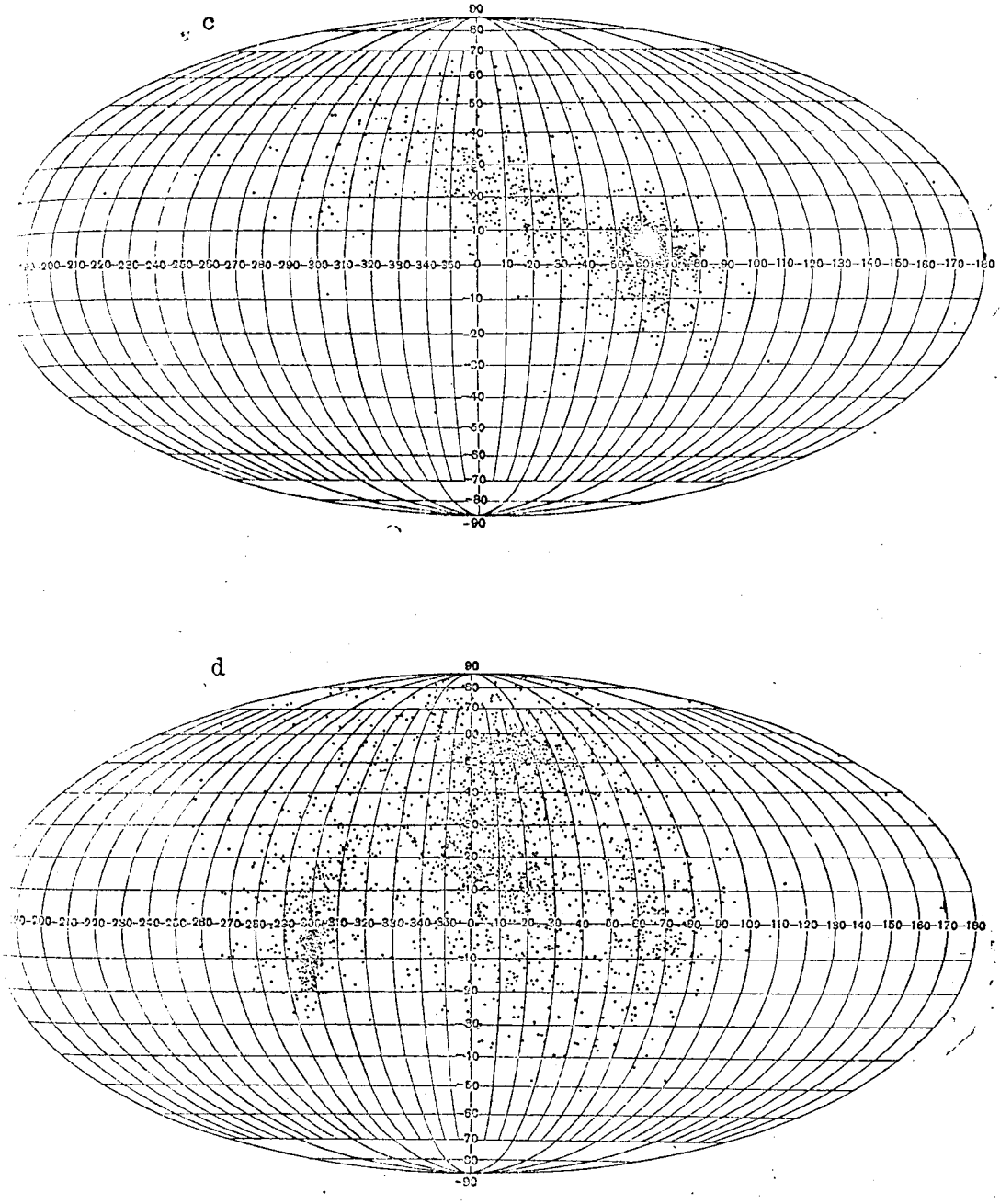

Fig. 4.17. Measured Distribution of Meteor Radiants in 1960. c- June; d- July.

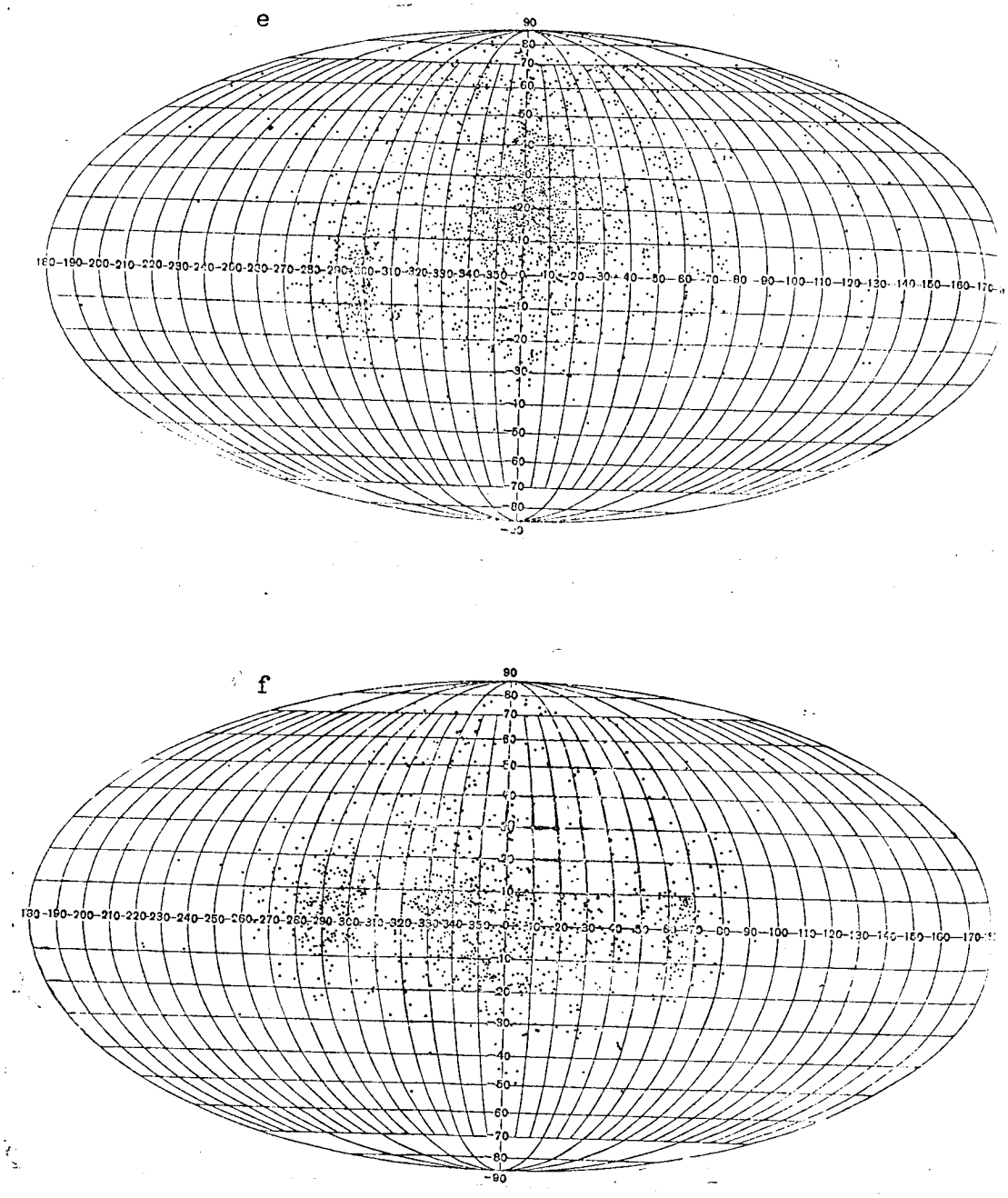

Fig. 4.17. Measured Distribution of Meteor Radiants in 1960.
e- August; f- September.

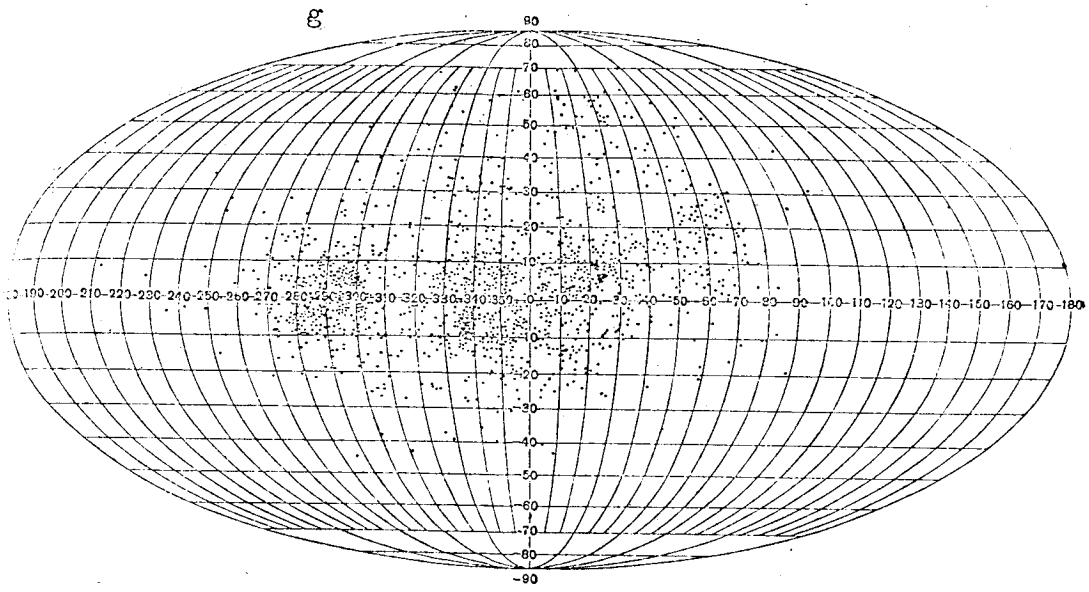

Fig. 4.17. Measured Distribution of Meteor Radiants in 1960.
g - October.

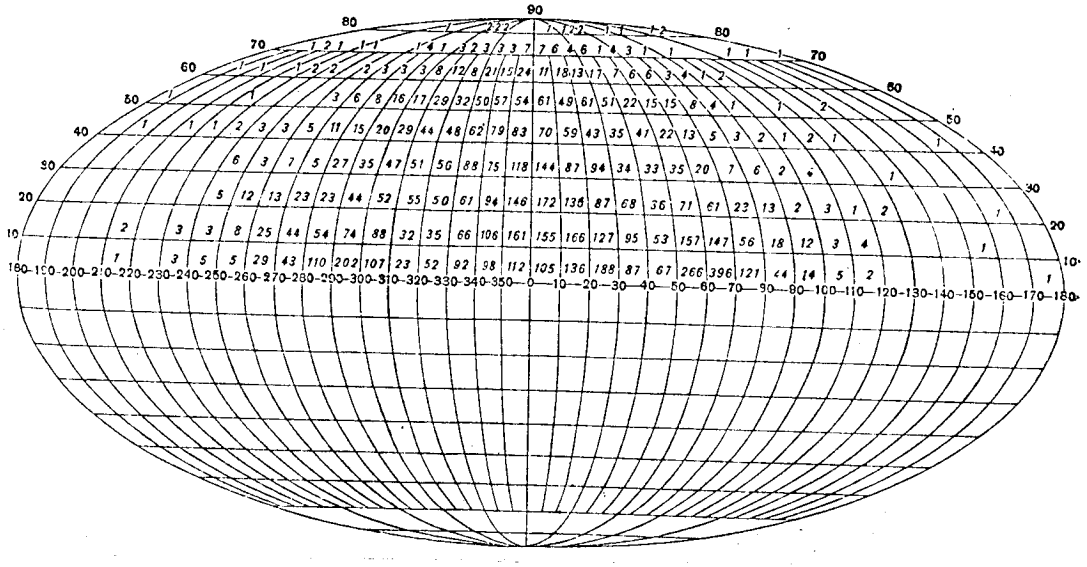

Fig. 4.18. Average Annual Measured Distribution of Meteor Radiants in the Northern Hemisphere.

DISTRIBUTION OF RADIANTS AND VELOCITIES OF METEORS

From the radar measurements of the quantity of meteors /134,177/, we detected three principle groupings of the radiants of faint meteors: apex, solar and antisolar. As was demonstrated by B.L.Kashcheyev, V.N.Lebedinets, and Yu.I.Suvorov /134/, the relative contribution of each of these groups varies in the course of a year. The apex group always contains a large number of radiants. In the Spring-Summer period (May-June), we can distinguish quite perceptably the solar group of radiants, while in the period from August to October we can identify the antisolar group.

For an explanation of these changes in the distribution of the radiants of radiometeors, in /134/. an assumption was expressed concerning the heterogeneity of the structure of the aggregation of meteor bodies, the orbits of which have a perihelion within the Earth's orbit. In the course of a year, the Earth passes through a more or less uniform cloud of meteor bodies, among which we find a prevalence of the particles moving through orbits, similiar to the orbits of the short-period comets, and also through orbits with small eccentricities and relatively high inclinations to the plane of the ecliptic. The combination of the velocity of the meteor bodies and the Earth's velocity leads to a concentration of the visible radiants to the apex, while a high selectivity of the radio observations in respect to the velocity of meteors also permits one to notice a certain concentration of the radiants near the solar and antisolar points from January-March, we observe chiefly this component of the aggregation of the meteor bodies.

From May-October, the Earth, twice in opposite directions, intersects a broad belt of the orbits of the meteor bodies, which is superimposed on the usual background of the meteors of the first component and is manifested in a form of a general increase in the number of meteors and also in the form of broad Summer and Autumn streams (showers).

The identification of a large number of individual radiants of the meteors permits us to refine the radiants' distribution obtained by the statistical procedures. In Fig.4.17, for each of the months in the period from April to October, we have presented the distribution in the celestial sphere, of the corrected radiants of the meteors. For convience in comparing the results, we chose the coordinates $(\lambda - \lambda_a)$ and β (where λ_a equals the ecliptic longitude of the apex). In Fig.4.18, we have presented the mean annual distribution of the meteor radiants for which the orbits were calculated. Since in the course of a year, we have a very intensive variation in the noticeability of meteors with negative ecliptic latitudes of radiants, in Fig.4.18, we have shown the distribution of the radiants only in the Northern Hemisphere.

It is obvious from the drawing most of the observed radiants of the radiometeors belong to the apex group; however, the maximum density of the radiants is obtained not in the direct proximity to the apex, but at a distance of 10-30° from it. This indicates that the concentration of the radiants toward the apex is caused by the combination of the velocity of the meteor bodies and the orbital velocity of Earth. We also clearly notice the fainter, but more concentrated groups of the radiants at distances of

around 60° from the apex or the ecliptic. From April-June, the density of the radiants in the solar group is appreciably greater than in the antisolar group, while from August-October, the opposite relationship takes place. This variation in the relative strength of the sources of the radiants in the solar and antisolar points should by no means be explained only in terms of the variation in the declination of the points during the year. In August, the first of them has a greater declination than the second; however, in the second, the radiants' density at this time is greater than in the first.

/187

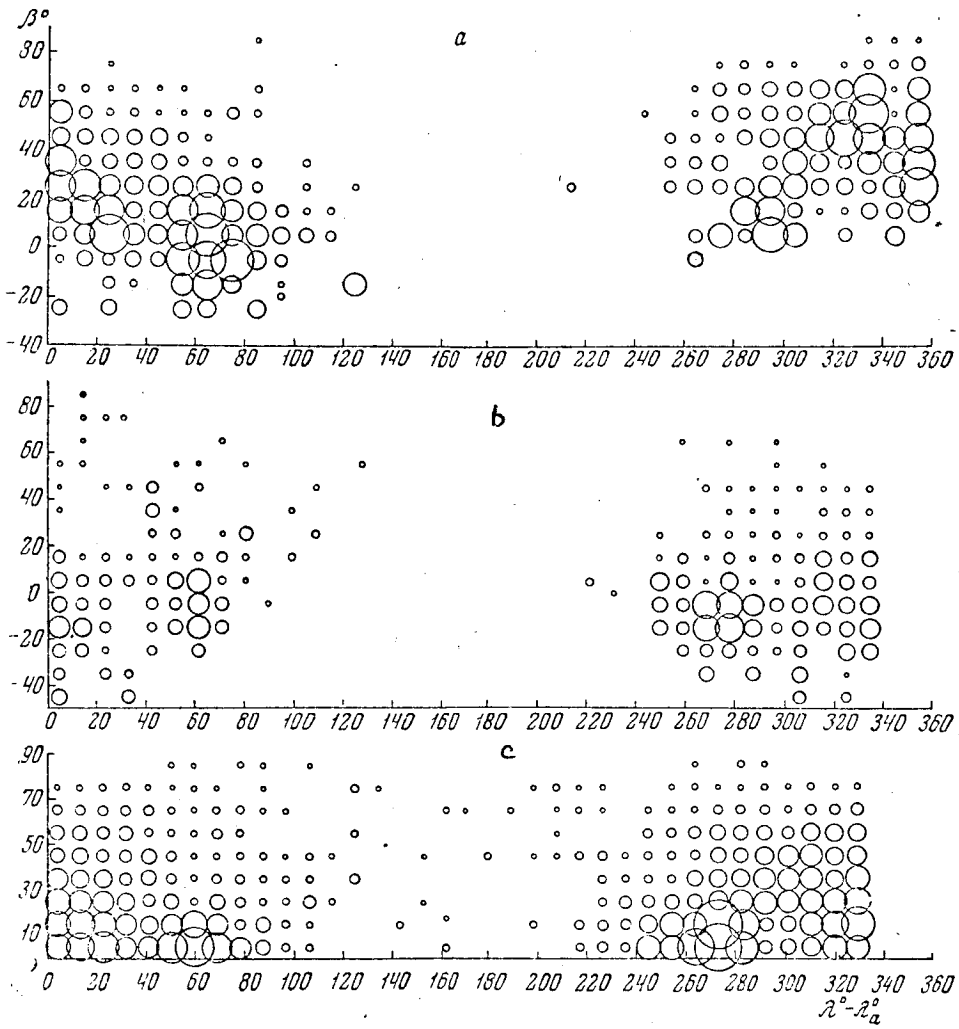

Fig.4.19, Distribution of the Meteor Radiants Corrected for the Geometric Factor. a - May 1960; b - September 1960; c - Mean Annual

It should be explained whether the three cited groupings of radiants comprise the result of the selectivity of the radar method of observing in relation to the velocities and the declinations of the meteor radiants. In. Fig.4.19, we have shown the distribution of the radiants corrected for the selectivity of the apparatus in relation to the declination of the radiants. The areas of the circles in Fig.4.19 are proportional to the sum of the weights P_1 of the meteors, the radiants of which fall in the corresponding area with a dimension of 10 × 10° in respect to λ and β.

In Fig.4.20 for those same periods of observations, we have listed the distributions of the radiants corrected for the similarity in respect to the declination of the radiants and to the velocity of the meteors. To each meteor, we have ascribed the weight P_1P_2. As was indicated in Chapter 2, by the same token we have obtained the distribution of the meteor radiants and gendered by the meteor bodies, falling to Earth, with the masses larger than a certain critical value.

From Fig.4.19, 4.20, it is evident that a allowance for the selectivity of the observations in respect to δ and $\overset{\frown}{v}$ does not alter appreciably the relative distribution of the meteor radiants between the three groups we have mentioned. As in the case of the visible distribution, in May the density of the radiants in the solar group is appreciably greater than in the antisolar one, while in September the reverse is true.

/188

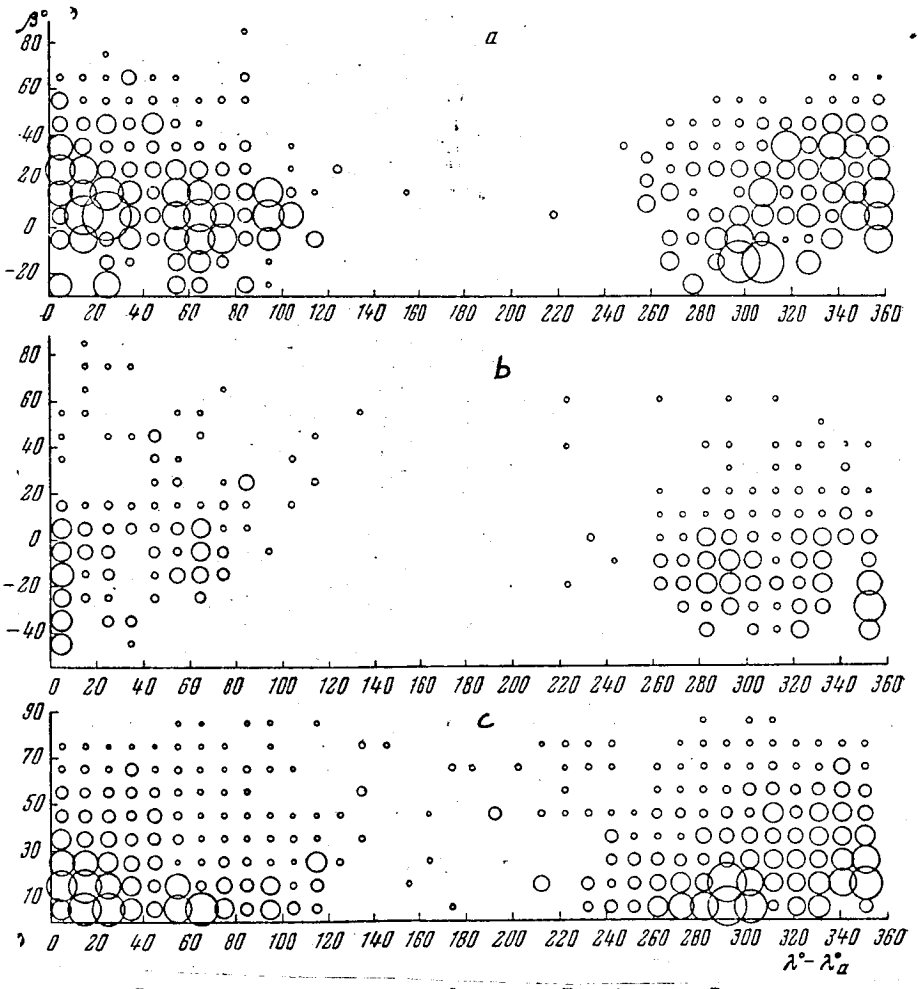

Fig.4.20. Distribution of the Meteor Radiants Corrected for the Geometric and Physical Factors. a - May 1960; b - Spetember 1960; c - Mean Annual

In Fig.4.21, we have shown the distribution by ecliptic latitude of all the observed radiants of the Northern Hemisphere. We find a fairly intensive concentration of radiants towards the ecliptic. 68 percent of the measured

radiants have an ecliptic latitude $\beta<30^{\circ}$. The concentration towards the ecliptic increases with allowance for the discrimination of the observations. After correction for selectivity in respect to δ, 72 percent of the radiants have $\beta<30^{\circ}$, while with consideration of the selectivity in respect to δ and v, they have 81 percent.

In Fig.4.22, we have shown the distribution, obtained at the KPI, of the radiometeors by velocity (corrected form or braking in the atmosphere and for the Earth's rotation). The measured distribution by v has two maximums in the velocity ranges of 30-45 and 50-65 km/sec. The second maximum is less by about 30 percent than the first. After correction for selectivity of the observations in respect to the declinations of the meteor radiants, the relative number of slow meteors increases. With allowance for the physical factor, there appears a sharp maximum in the number of meteor bodies with velocities of 15-25 km/sec. Outside of this range, there occurs almost uniform distribution of the meteor bodies by velocity. The low secondary maximums will remain at velocities of 30-45 and 55-65 km/sec. /189

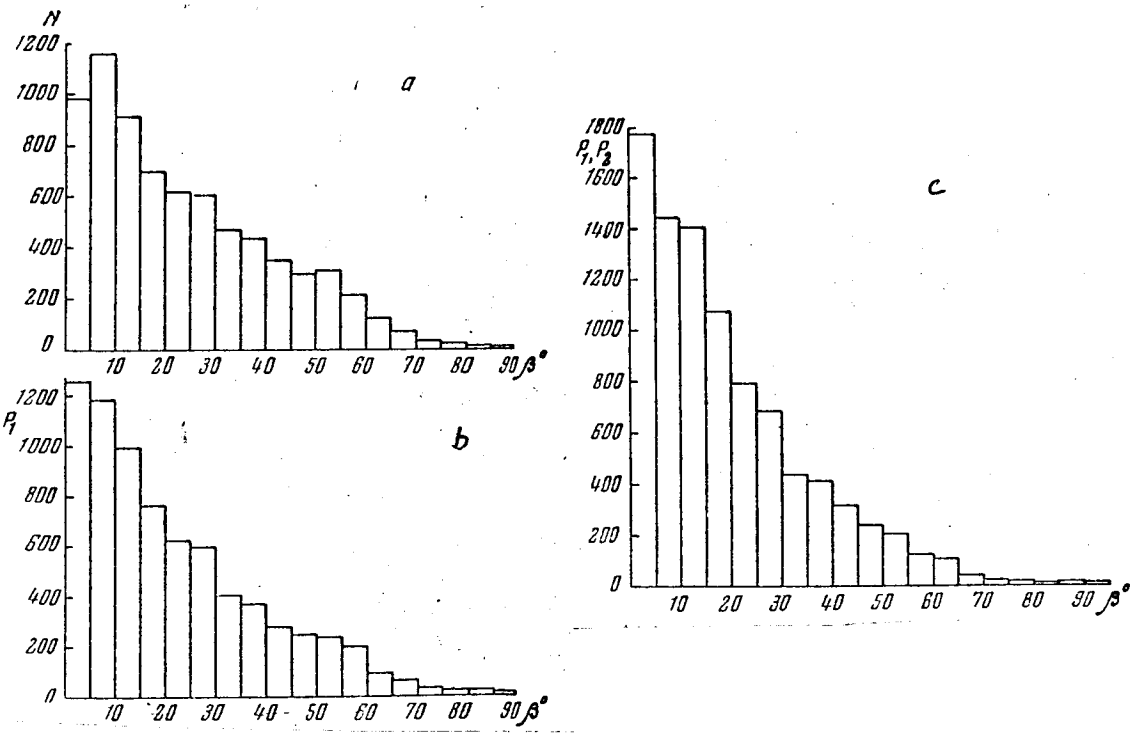

Fig.4.21. Distribution of Ecliptic Latitudes of Meteor Radiants in the Northern Hemisphere. a - Measured; b - Corrected for Geometric Factor; c - Corrected for the Geometric and Physical Factors.

In Fig.4.23, we have presented the distribution by velocity of 2529 meteors, obtained by the photographic observations by McCrosky and Posen /28/.

It can be compared with the results in Fig.4.22b. In the distribution by velocity of the photographic meteors, we also find two maximums. The first of them (20-40 km/sec) is some what broader then for the radiometeors, and is displaced in the direction of lower velocities. The second maximum (60-70 km/sec) is shifted in the direction of higher velocities. These divergences are evidently associated with a varying nature of the motion of the meteor bodies in the solar system, generating photographic meteors, and the finer particles creating the basic mass of the radiometeors.

DISTRIBUTION OF ORBITS OF METEOR BODIES

Assigning to each meteor the weight of the product of the geometric and physical factors for the given radar set, P_1P_2, we can proceed from the

distribution, measured with a given radar set, of radiometeors based on the various parameters, to a distribution based on the same parameters of the meteor bodies, encountered by the Earth, with masses greater than a certain critical value (not depending on the velocity of the meteor bodies). In order to transfer to the distribution of meteor bodies in interplanetary space, it is necessary to take into account the probability of the encounter (with Earth) of the meteor bodies moving through various orbits. The value reciprocal to this probability will be called the astronomical factor (P_3).

It is natural that with the observations of the meteors in the Earth's atmosphere, we can obtain data only concerning those meteor bodies, the orbits of which have a distance from the Sun in the perihelion, $q \leq$ one astronomical units, while in the aphelion, $q' \geq$ one astronomical unit.

/190

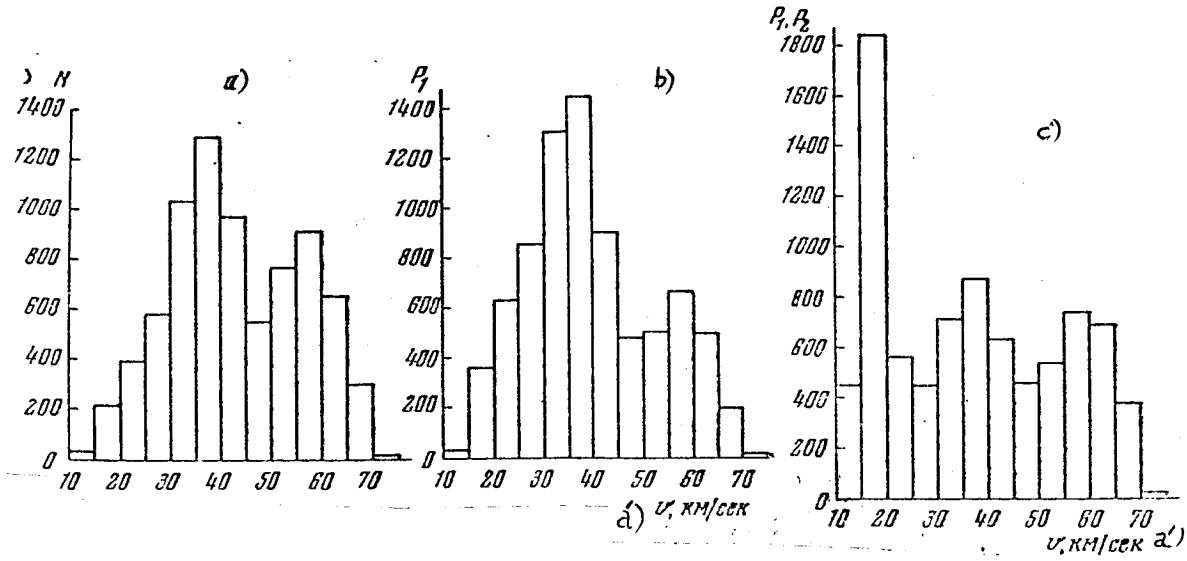

Fig.4.22. Distribution of Extra-Atmospheric Velocities of Radiometeors. Key: a') v, km/sec. a)- Measured; b)- Corrected for Geometric Factor; c)- Corrected for the Geometric and Physical Factors.

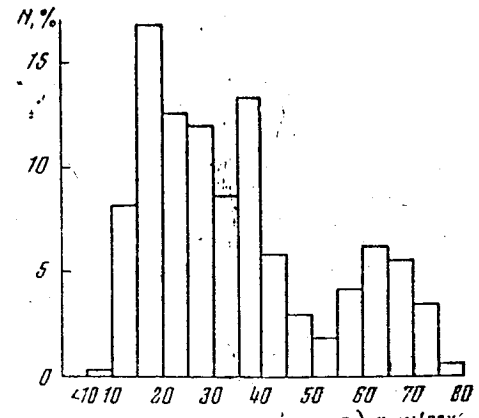

Fig.4.23. Distribution of Extra-Atmospheric Velocities of the Photographic Meteors Brighter than about $+3^m$ /28/.

/191

The probability of the encounter with Earth with meteor bodies moving through various orbits was surveyed by Öpik /207/. Allowing for the variation in latitude of the ascending node and the argument of the perihelion under the effect of perturbations from the part of the plane, Opik obtained the following expression for P_3:

$$\frac{1}{P_3} = \frac{\pi v_g \sin i}{R_3^2 v_\infty^2}\left(2 - \frac{1}{a} - p\right)^{1/2} \qquad (4.45)$$

where R_3 = the radius of the Earth, p = a (1 - e squared). According to (4.45), the probability of encountering Earth is the greatest for the meteor bodies, moving through orbits in which the distance from the Sun in the in the perihelion or the aphelion is close to one astronomical unit.

In Fig.4.24, 4.27,.4.29, and 4.31, we have presented the distribution (obtained by the authors) of the orbital element of the radiometeors: a - measured, b - corrected for the geometric factor (each meteor is taken with the weight P_1, c - corrected for the geometric and physical factors (the meteors are taken with the weight P_1P_2), d - corrected for the astronomical factor (the meteors are taken with the weight P_1,P_2,P_3). Since in the course of a year, we have a very intensive variation in the noticeability of meteors, the radiants of which have negative ecliptic latitudes, the latter are not included in the distributions listed.

In Fig.4.25, 4.28, 4.30, and 4.32, we have presented the distribution of the orbital elements, obtained by McCrosky and Posen /28/ from the photographic observations with the Super-Schmidt cameras, 2529 meteors brighter than about $+3^m$. In Fig.4.26, we have shown the distribution of of the major semiaxes of the orbits obtained by Whipple /12/ from the photographic observations for 144 meteors brighter than about 0^m. Let us consider the distribution of each of the orbital elements separately.

Major semiaxis (Fig.4.24-4.26). The allowance for the selectivity of the radar method of the measurements and also the astronomical factor have practically no effect on the distribution of the orbits by 1/a obtained by the authors. In the large meteor bodies producing meteors brighter than 0^m, we most often find the a-values of the order of 5 A.U. A large number of the meteor bodies have orbits close to the parabolic. Among 144 orbits, there is not one with $a \leqslant 1$ A.U. In the smaller meteor bodies producing the meteors $0^m + 3^m$, we most often find orbits with 3 A.U. The orbits close to the parabolic are found somewhat less often than in the case of the meteors brighter than 0^m. Around 6 percent of the orbits have $a \approx 1$ A.U. and several orbits with $a < 0.56$ A.U.

In the case of even smaller meteor bodies producing the meteors $+5^m - 7^m$, the maximum of the distribution of the orbits by 1/a is shifted into the region of even smaller values: $a \approx 2$ A.U. Around 20 percent of the orbits have $a < 1$ A.U. and several tens of orbits with $a < 0.56$ A.U. The number of orbits close to the parabolic is appreciably less than in the case of the photographic meteors. In this manner, with a decrease in the mass of the meteor bodies, we find a systematic decrease in the average dimensions of the orbits through which they will move.

Around 0.5 percent of the orbits obtained by us prove to be hyperbolic, which in each case can be explained by the measurement errors. Since the observations do not reveal a sufficiently large number of obviously hyperbolic orbits, the insufficient accuracy of the radar measurement methods, used at the present time, of the individual radiants and velocities of the meteors prevent us from solving the question concerning the existence of the hyperbolic orbits of meteor bodies based on the results of the radar observations.

Excentricity of orbits (Fig.4.27-4.28). The radar and photographic observations yield about the same distribution of the orbital eccentricities of the meteor bodies. According to our measurements, we find a steady increase in the distribution function during a variation in the eccentricity from 0 to 1. The allowance for the selectivity for the observations and the astronomical factor leads to a still greater increase in the number of orbits with eccentricities from 0.9. to 1.0. According to the results of the photographic measurements, we most often find orbits with $0.85 < e < 0.90$. The allowance for the selectivity of the measurements and the astronomical factor in the case of the photographic measurements leads to an increase in the number of orbits from $0.85 < e < 0.90$, and to a reduction in the number of orbits from $e > 0.90$. This is associated with the fact that for the small and large meteor bodies, only the distribution of the orbital eccentricities is about the same, while the distribution of the major semiaxes of the orbits differ considerably.

Perihelion distance (in Fig.4.29-4.30). The dissimilarity of the probability of the meteor bodies' encountering the Earth, when they are moving through different orbits, is reflected particularly intensively on the measured orbital distributions by the perihelion distances and inclinations. From the radar observations, we obtain an almost uniform distribution of the orbits by q in the interval $0.2 < q < 0.9$ A.U., and two maximums of the distribution function: at $0.05 < q < 0.2$ A.U. and $0.9 < q < 1.0$ A.U. With allowance for the selectivity of the observations and the astronomical factor, the latter disappears from the maximums. The function of the distribution increases almost steadily at the reduction in q from 1.0 to 0.05 A.U.

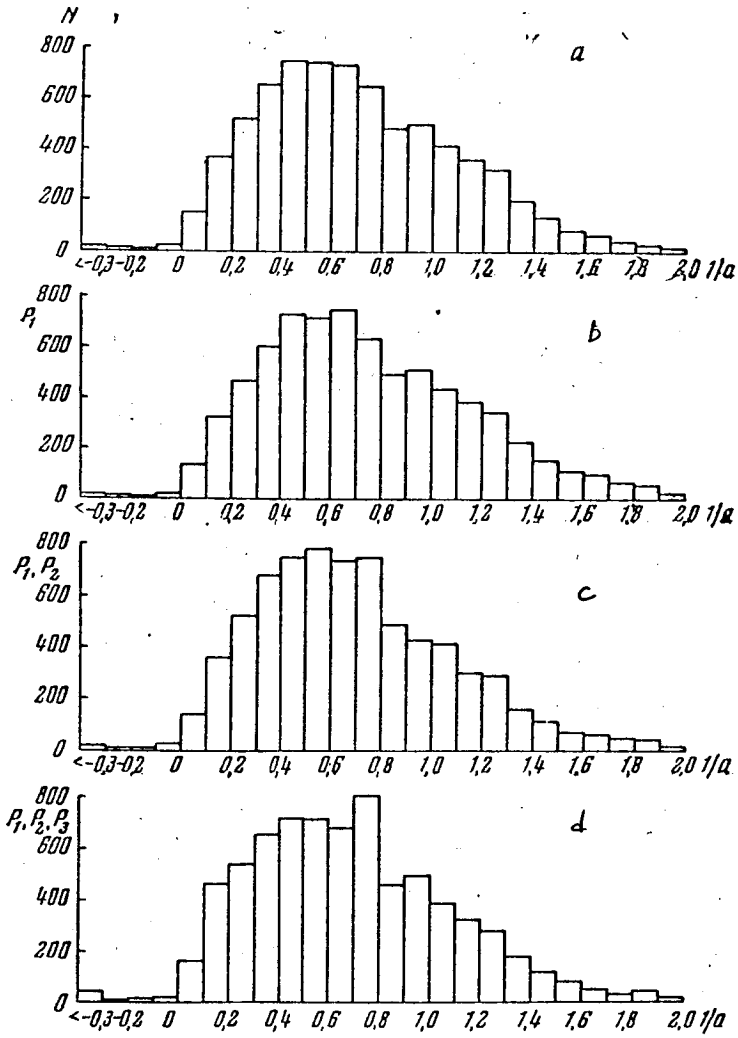

Fig. 4.24. Distribution of Major Semiaxes of the Orbits of Meteor Bodies.
a- measured; b- corrected for geometric factor; c- corrected for geometric and physical factors; and d- corrected for selectivity of observations

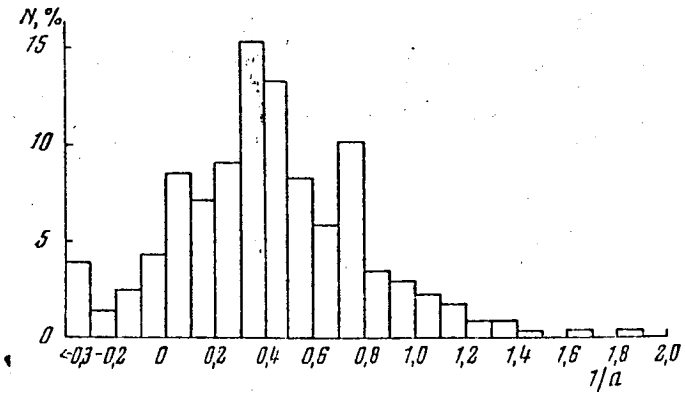

Fig.4.25. Measured Distribution of Major Semiaxes of Orbits of Meteor Bodies Based on Photographic Observations of Meteors Brighter than about $+3^m$ /28/.

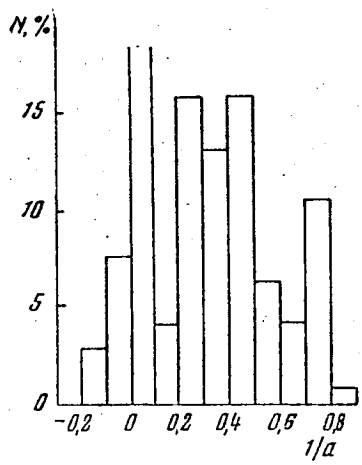

Fig.4.26. Distribution of Major Semiaxes of the Orbits of Meteor Bodies, Based on the Photographic Observations of Meteors Brighter than about 0^m/12/.

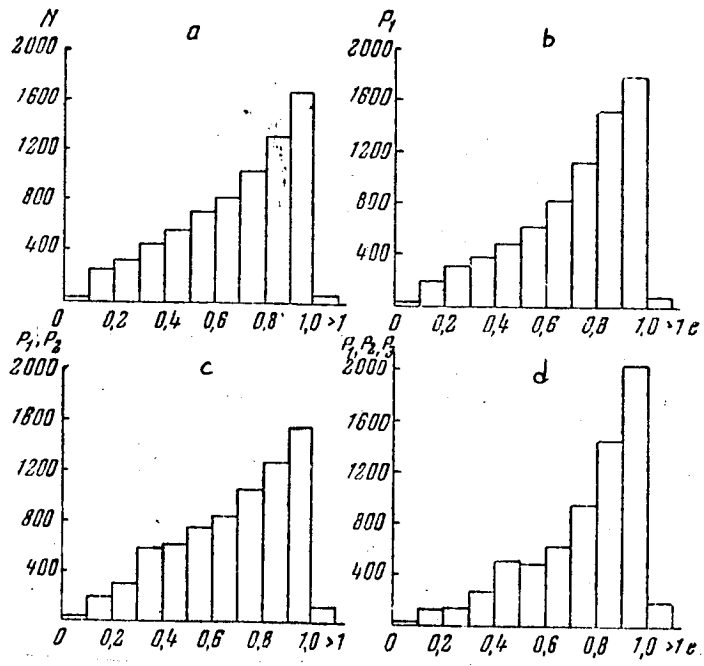

Fig.4.27. Distribution of the Orbital Excentricities According to Radio Observations. The notations are the same as in Fig.4.24.

/194

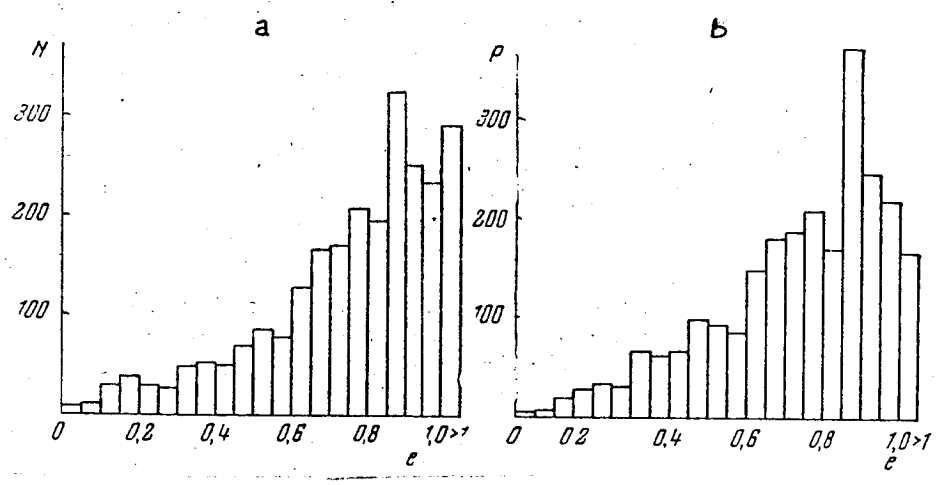

Fig.4.28. Distribution of the Orbital Excentricities Based on Photographic Observations /28/. a - measured; b - corrected for the selectivity of observations.

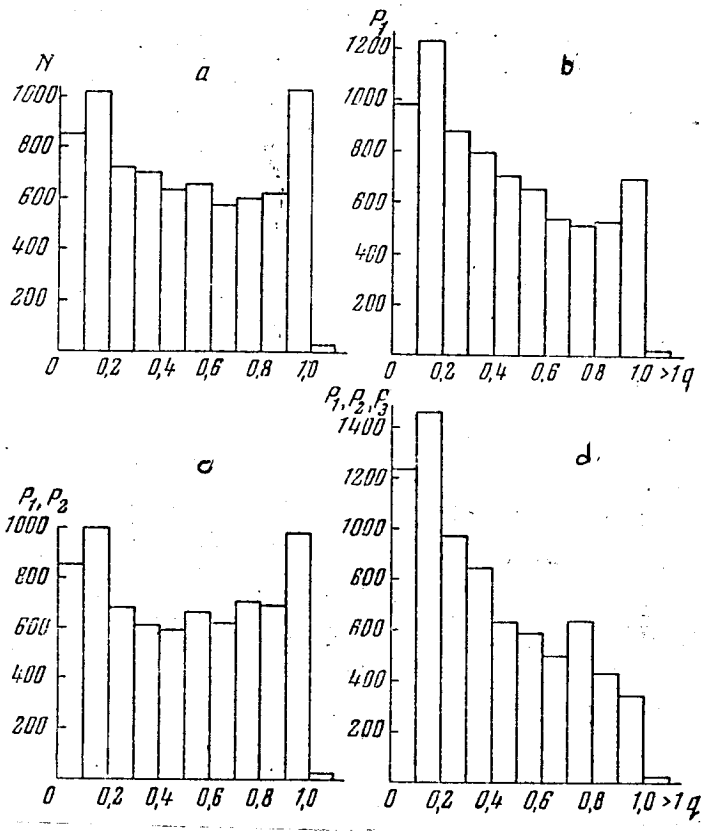

Fig.4.29. Distribution of the Perihelion Distances of Orbits Based on Radio Observations. The notations are the same as in Fig.4.24.

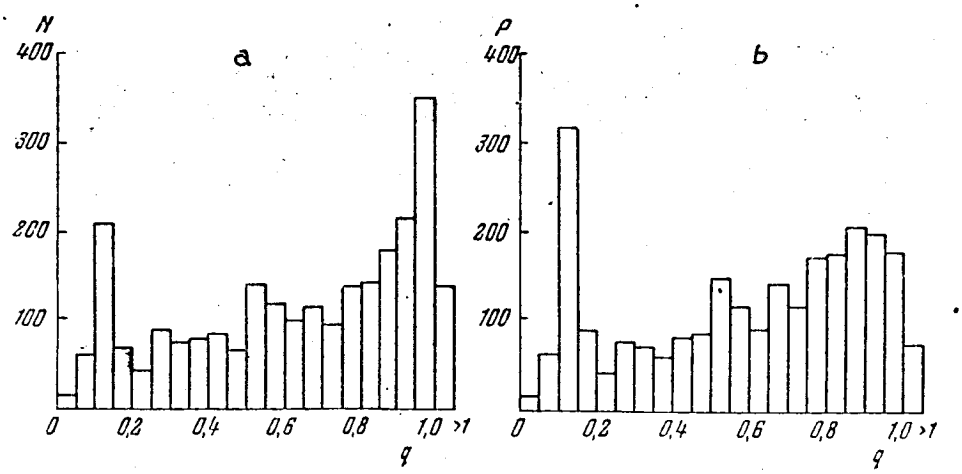

Fig.4.30. Distribution of the Perihelion Distances of Orbits Based on Photographic Observations /28/. The notations are the same as in Fig.4.28.

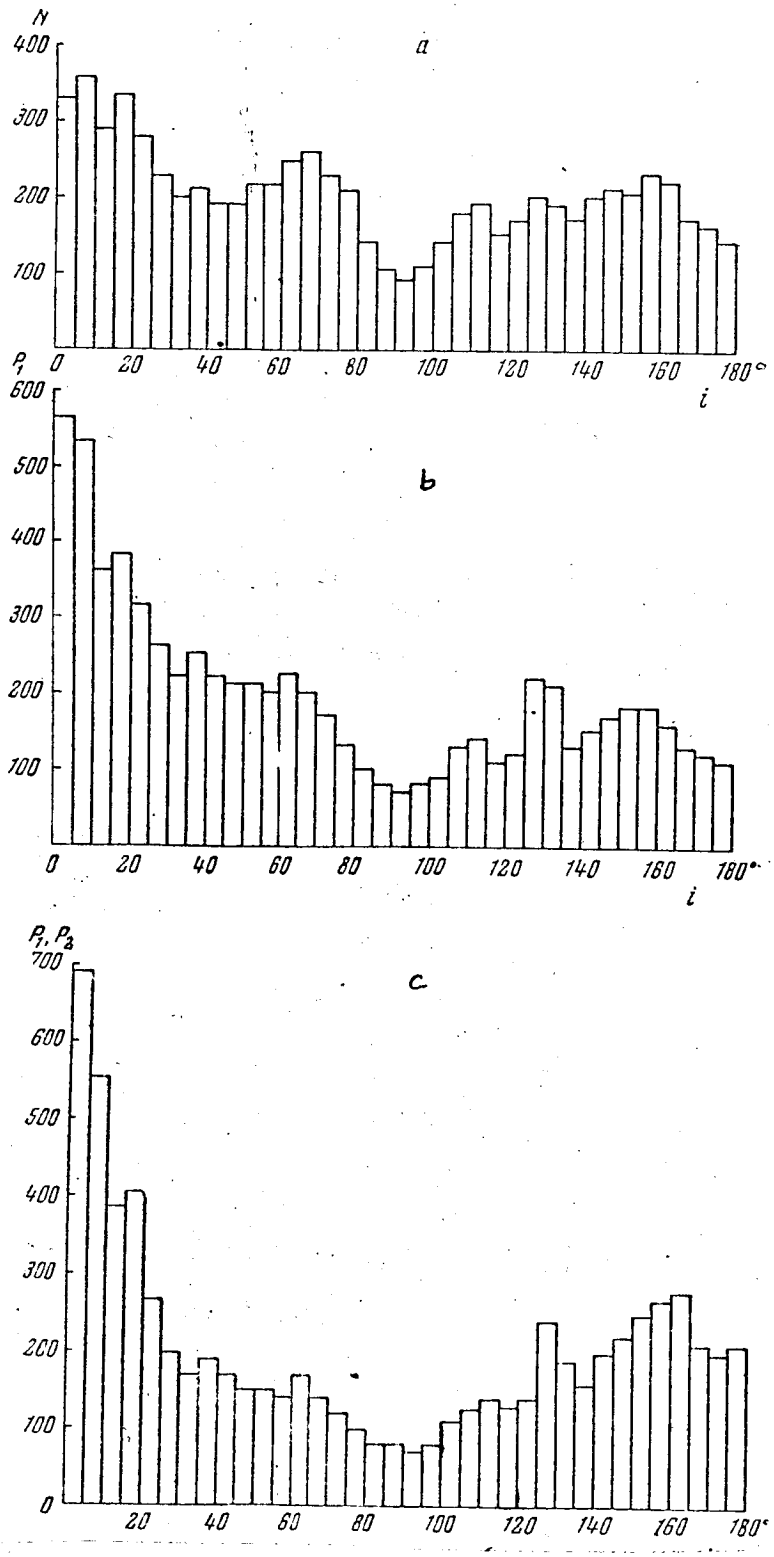
N
400
300
200
100
a
P1
0
20
40
60
80
100
120
140
160
180°
i
600
500
400
300
200
100
b
0
20
40
60
80
100
120
140
160
180°
i
P1, P2
700
600
500
400
300
200
100
0
c
20
40
60
80
100
120
140
160
180°

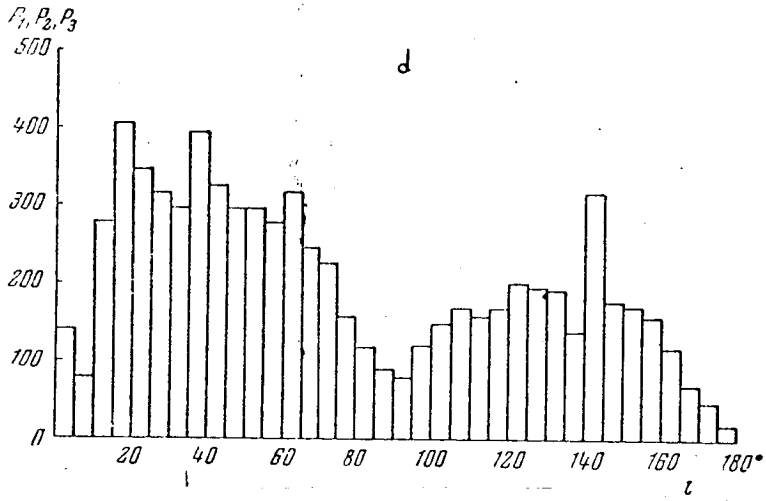

Fig.4.31. Distribution of Orbital Inclinations Based on Radio Observations. The notations are the same as in Fig.4.24.

The distribution of the perihelion distances of the orbits of the larger meteor bodies proves to be quite different. At a decrease from 1 to 0, we find and almost steady (monotonous) decrease in the distribution function. The abrupt maximum at $0.1 < q < 0.15$ appears owing to the meteors in the Geminids shower. The average perihelion distance of the orbits of the small meteor bodies producing the meteors $+5^m - +7^m$ proves to be almost twice as small as for the larger meteor bodies, producing the meteors $0^m - +3^m$.

Inclination of orbits (Fig.4.31-4.32). The radar observations yield an almost uniform distribution of the orbital inclinations of the meteor bodies for the entire range of i-values from 0 to 180°. We find a certain increase in the number of orbits at $i < 30°$ and a decrease in the range $80° < i < 105°$. With allowance for the selectivity for the radar observations, the number of the orbits with small inclinations (obliquities) increases. The large number of orbits with the small orbital inclinations is chiefly explained by the /198 astronomical selection (the probability of a meteor body striking the Earth is proportional to cosec i). After the consideration of the astronomical factor, the number of orbits with $i \lesssim 15°$ decreases abruptly. We have the appearance of two broad maximums of the distribution functions at $15° < i < 65°$ and $120° < i < 160°$. A minimum at $i \approx 90°$ will remain about the same as in distribution obtained directly from the observations.

The distributions in the inclinations of the orbits of the meteor bodies, obtained from a radar and photographic observations differ greatly. In the largest meteor bodies producing meteors $0^m - +3^m$, we find prevalence of the orbits with the small inclinations $i < 30°$. We find that particularly often values $5° < i < 25°$. We find a minimum in the distribution function at i-values close to 90°, and a certain increase in the number of the orbits at $110° < i < 150°$.

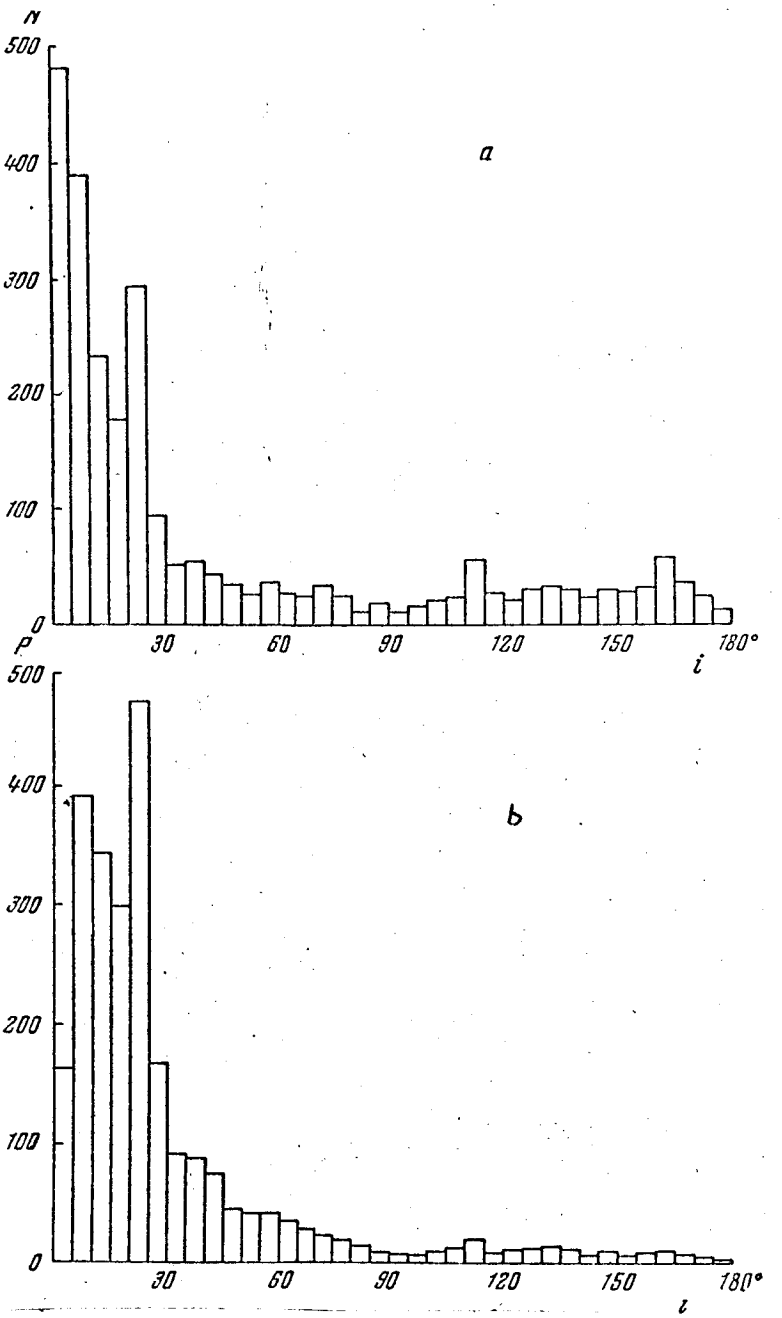

Fig.4.32. Distribution of Orbital Inclinations Based on the Photographic Observations /28/. The notations are the same as in Fig.4.28.

In Figs.4.33, 4.34, 4.36, 4.38, and 4.42, we have listed two-dimensional distributions of various elements of the orbits of the meteor bodies, obtained by the authors from the radar observations and also by McCrosky and Posen /28/. from the photographic observations of the meteors brighter than about $+3^m$ based on the results of the radar observations, we have presented; a - measured distributions; b - the distributions corrected for the geometric factor; c - the distribution corrected for both the geometric and physical factors; d - distributions corrected for the geometric, physical and astronomical factors (i.e., the distributions pertaining to the meteor bodies with the masses larger than a certain value of the orbits of which have perihelions within the Earth's orbit, while the aphelion is outside the Earth's orbit). From the authors' observations, we have taken only those meteors, the radiants of which are located northward from the ecliptic.

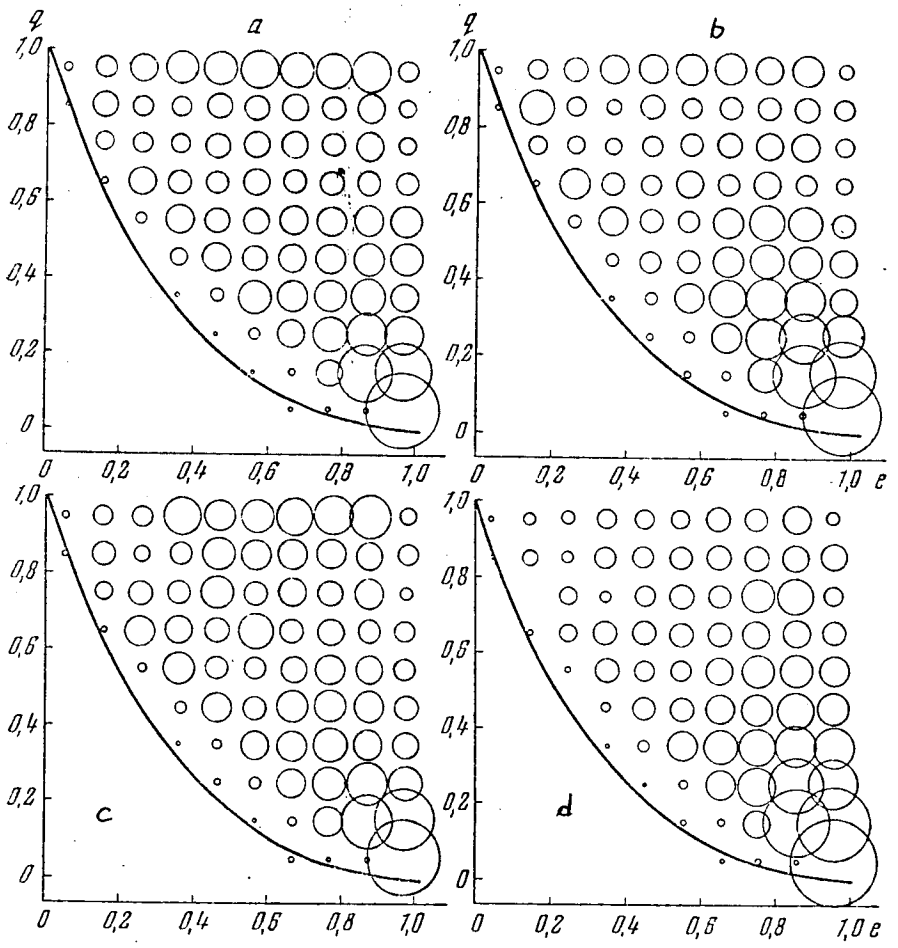

Fig.4.33. Distribution of the Orbits of Meteor Bodies by e and q Derived from the Radio Observations. The notations are the same as in Fig.4.24.

Distribution by e and q in Fig.4.33, we have shown the orbital distribution, obtained by the authors, in respect to the excentricities and the perihelion distances. We have included the critical values for e and q, corresponding to the condition $q' = 1$ (where q' = the aphelion distance). From the observations, we obtain an almost uniform distribution of orbits by e and q. The increase in the number of orbits in the range $0.8 < e < 1$ and $0 < q < 0.2$ A.U. is caused mainly by the meteors in the Geminids, Arietids, and δ Aquarids meteor showers. The allowance for the selectivity for the radar method of observations does not alter significantly the measured distribution. The allowance for the astronomical selection leads to an increase in the number of orbits with small perihelion distances and with eccentricities close to unity.

Distribution by a and e. In Fig.4.34 and 4.35, we have shown the distribution of the major semiaxes and the excentricities of the orbits of meteor bodies based on the data obtained from the radar and photographic observations. The critical values of a and e correspond to the conditions $q = 1$ A.U. and $q' = 1$ A.U. /200

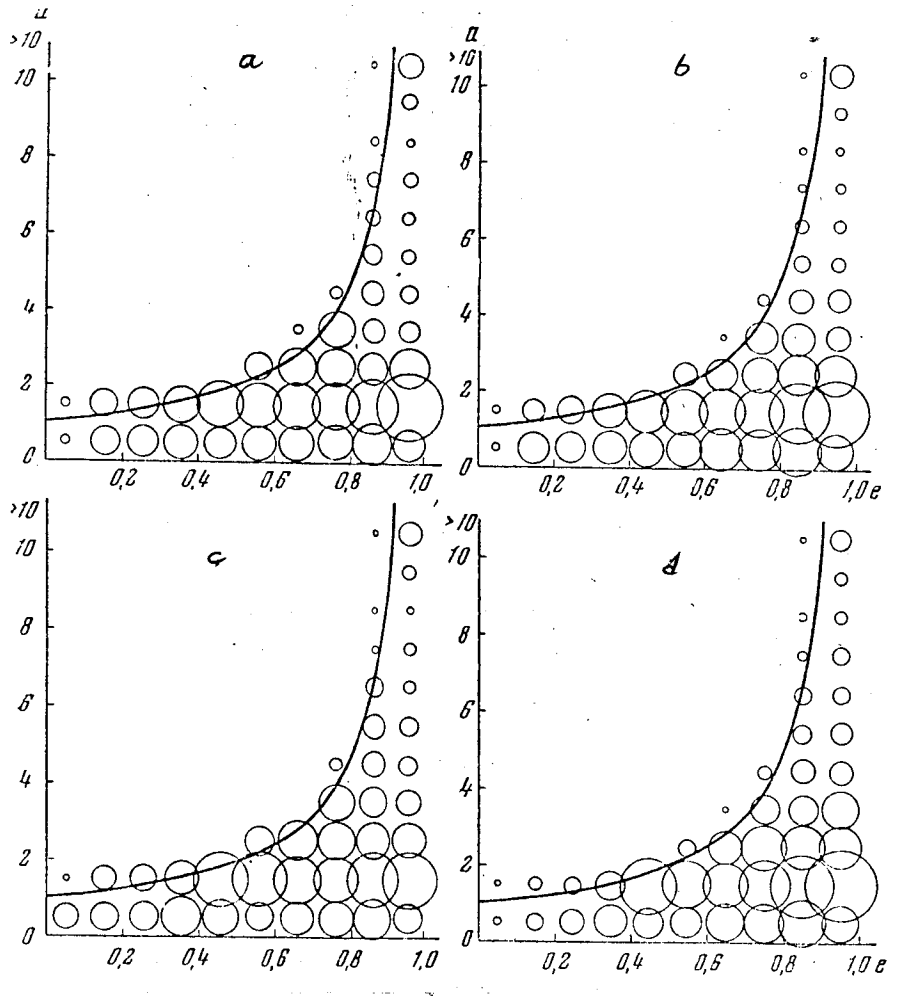

Fig.4.34. Distribution of Orbits by a and e Obtained from the Radio Observations. The notations are the same as in Fig.4.24.

The measured distribution of the orbits in respect to a and e proves appreciably different particles of various sizes. In the case of the larger meteor bodies producing the photographic meteors, we find two main groupings of orbits: namely the orbit with the perihelion distances close to 1 A.U. and the orbits close to the parabolic ($e \approx 1$, $|a| \approx 10$ A.U.). The maximum of the distribution in the range $0.8 < e < 0.9$ and $1 < a < 2$ A.U. yields the meteors in the Geminids shower. The orbits close to the parabolic occur less often in the case of small inclinations to the plane of the ecliptic than in the case of the large inclinations.

According to the data of the radar observations, the orbits of the smaller meteor bodies are concentrated chiefly in range $a \lesssim 3$ A.U. At all of the e-values permitted by the conditions $q \leqslant 1$ A.U. and $q' \geqslant 1$ A.U. The allowance for the selectivity of the radar method of measurements and also of the astronomical selection does not alter significantly the measured distribution of the orbits in respect to a and e. In distinction from the meteor bodies generating the photographic meteors, the orbits of the smaller meteor bodies have greater eccentricities much more often in the case of small inclinations to the plane of the ecliptic than in the case of large inclinations.

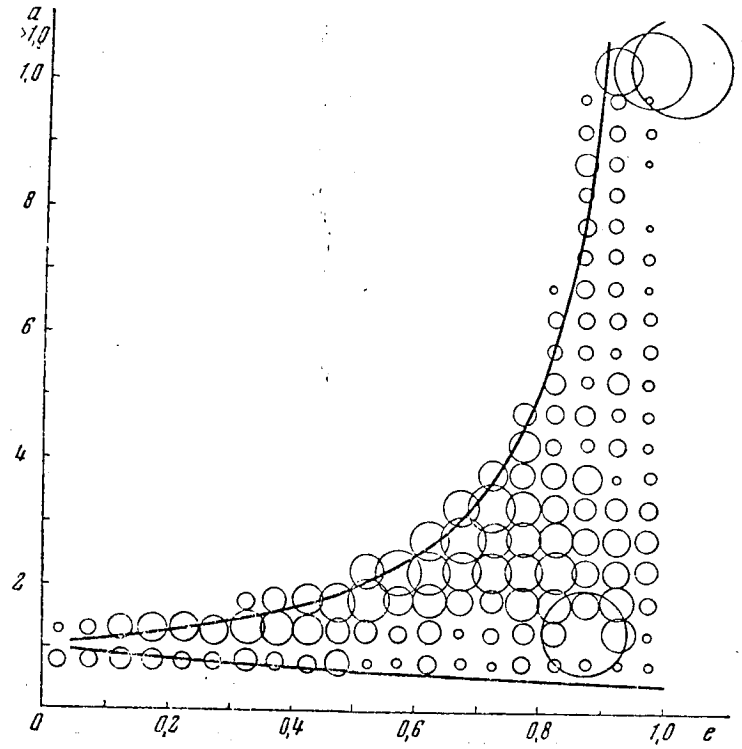

Fig.4.35. Distribution of Orbits by a and e Obtained from the Photographic Observations /28/.

Distribution in respect to i and q (Fig.4.36 and 4.37). The orbits of the small meteor bodies producing the radiometeors are distributed almost uniformly by i and q. We find an increase density in the distribution in the range $5^\circ < i < 50^\circ$ and $0 < q < 0.3$ A.U. With allowance for the selectivity (discrimination of the radar observations and the astronomical selection, we have a de rease in the number of the orbits for which the perihelions are situated close to the Earths' orbit, and an increase in the number of orbits with small inclinations and perihelion distances.

/201

The orbits of the larger meteor bodies producing the photographic meteors are grouped mainly in a range of the small obliquities ($i < 30^\circ$) and the relatively large perihelion distances ($q > 0.7$ A.U.). Thev avoid the ranges $70^\circ < i < 120^\circ$ and $q < 0.7$ A.U. The orbits having perihelions close to the orbit of the Earth, as in the case of the small meteor bodies, are distributed almost uniformly in respect to i in the range $30^\circ < i < 180^\circ$.

Distribution by i and a (Fig.4.38 and 4.39). The distribution of orbits of the large meteor bodies in respect to i prove to be significantly different for the orbits with $a \lesssim 5$ A.U. and $a \gtrsim 5$ A.U. For the first, it is typical to have a clearly expressed prevalence of the direct motions with small obliquities to the plane of the ecliptic. The orbits with $a \gtrsim 5$ A.U. are distributed almost uniformly in respect to i. For the orbits of all of the dimensions, the avoidance of the values $i \approx 90^\circ$ is noticeable.

In the case of the small meteor bodies, the orbits of all dimensions are distributed almost uniformly in respect to i. Most of the orbits have small

dimensions ($a \lesssim 3$ A.U.). The concentration of the orbits of small dimensions to the plane of the ecliptic in expressed much less than for the large meteor bodies.

Distribution by i and e (Fig.4.40 and 4.41). In the case of the large meteor bodies, the distribution by i proves to be different for the orbits with the small and large eccentricities. At $e \gtrsim 0.7$, the orbits are distributed almost evenly by i in the range $30^\circ < i < 180^\circ$. We find a relatively slight increase in the concentration of the orbits in the range of the small inclinations. At e 0.7, almost all the orbits of the large meteor bodies have small obliquities to the plane of the ecliptic ($i \lesssim 30^\circ$).

Such an increase in the concentration to the plane of the ecliptic with a decrease in the eccentricity is especially typical for the orbits of the largest meteor bodies producing the meteors brighter than 0^m. Of 144 orbits listed in the Whipple catalog, only one falls in the range $30^\circ < i < 150^\circ$ and $e < 0.7$. In the meteors brighter than $+3^m$, there are less than 10 percent of such orbits. At the same time, around 30 percent of the radiometeors have orbits of such a type.

In the case of the small meteor bodies producing meteors brighter than about $+7^m$ after allowance for the selectivity of the observations and the astronomical factor, we find a concentration of orbits with $e < 0.7$ in the ranges of the obliquities $30^\circ < i < 80^\circ$ and $110^\circ < i < 160^\circ$.

The comparison of the orbits obtained from the photographic and radar observations permits us to reveal a number of general inherent tendencies in the nature of the motion, in the solar system, of the meteor bodies of various sizes. From the basic photographic observations of several hundred meteors brighter than 0^m, to main types of orbits of large meteor bodies were known: a. The orbits similar to the orbits of the long-periodic comets. For them, it is difficult to find large dimensions, eccentricities very close to unity, and arbitrary obliquities to the plane of the ecliptic. b. The orbits analogous with the orbits of the short-periodic comets. For them, it is difficult to find relatively small sizes ($a \lesssim 5$ A.U.), fairly large eccentricities ($e \gtrsim 0.8$) and small obliquities to the plane of the ecliptic ($i < 30^\circ$). A small number of meteor bodies (around 10 percent) had orbits of an asteroid type (small values for e and i). When we had obtained 2.5 thousandths of orbits of the small meteor bodies producing meteors brighter than about $+3^m$, we revealed a considerably greater diversity of orbits. We found orbits $a < 1$ A.U., almost circular orbits, and also a small number of orbits with slight eccentricities and large obliquities. However, a considerable majority of the orbits nevertheless pertained to the two types of the cometary orbits mentioned.

The basic radar observations of the meteors conducted and Jodrell Bank /128/ and Kharkov /76/ revealed a third basic type of orbits typical for meteors fainter than about $+5^m$. The orbits of this type "β" have small eccentricities ($e < 0.8$) and large obliquities to the plane of the ecliptic ($30^\circ < i < 160^\circ$). The orbits of type "β" have around 30 percent of radiometeors, around 10 percent of faint photographic meteors, and in all a few percents of bright photographic meteors.

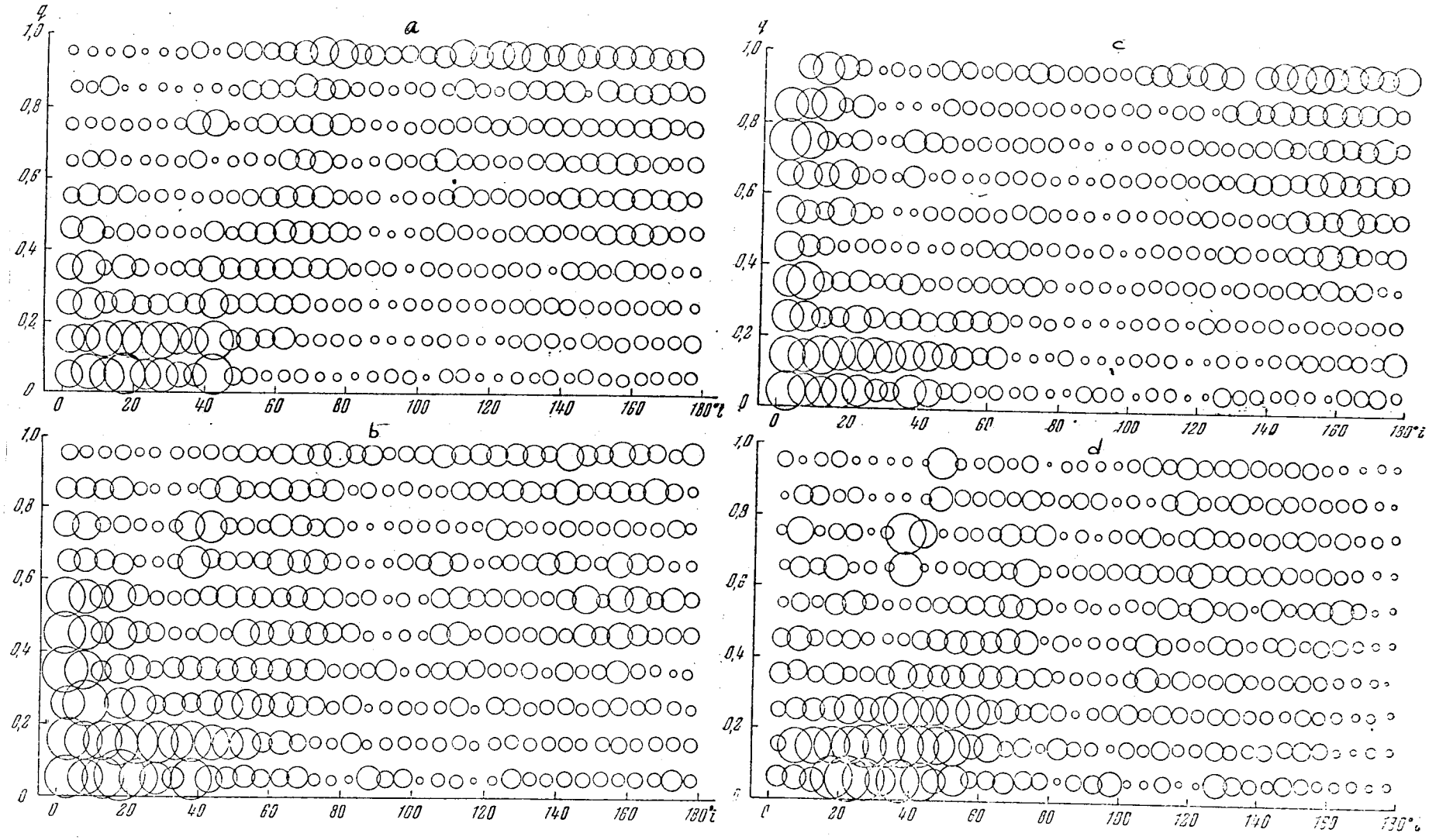

Fig.4.36. Distribution of Orbits in Respect to i and q Obtained from the Radio Observations. The notations are the same as in Fig.4.24.

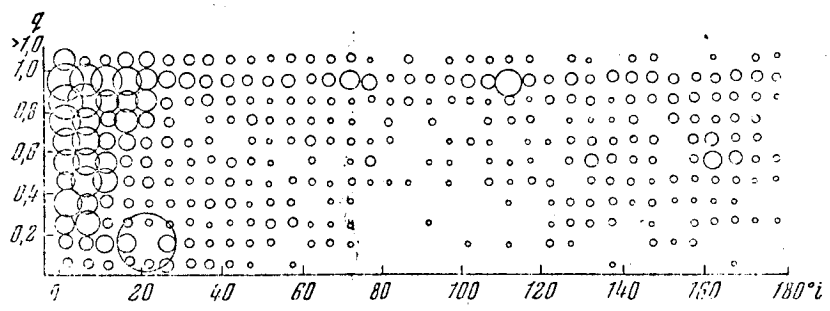

Fig.4.37. Distribution of Orbits in Respect to i and q Obtained from the Photographic Observations /28/.

/204

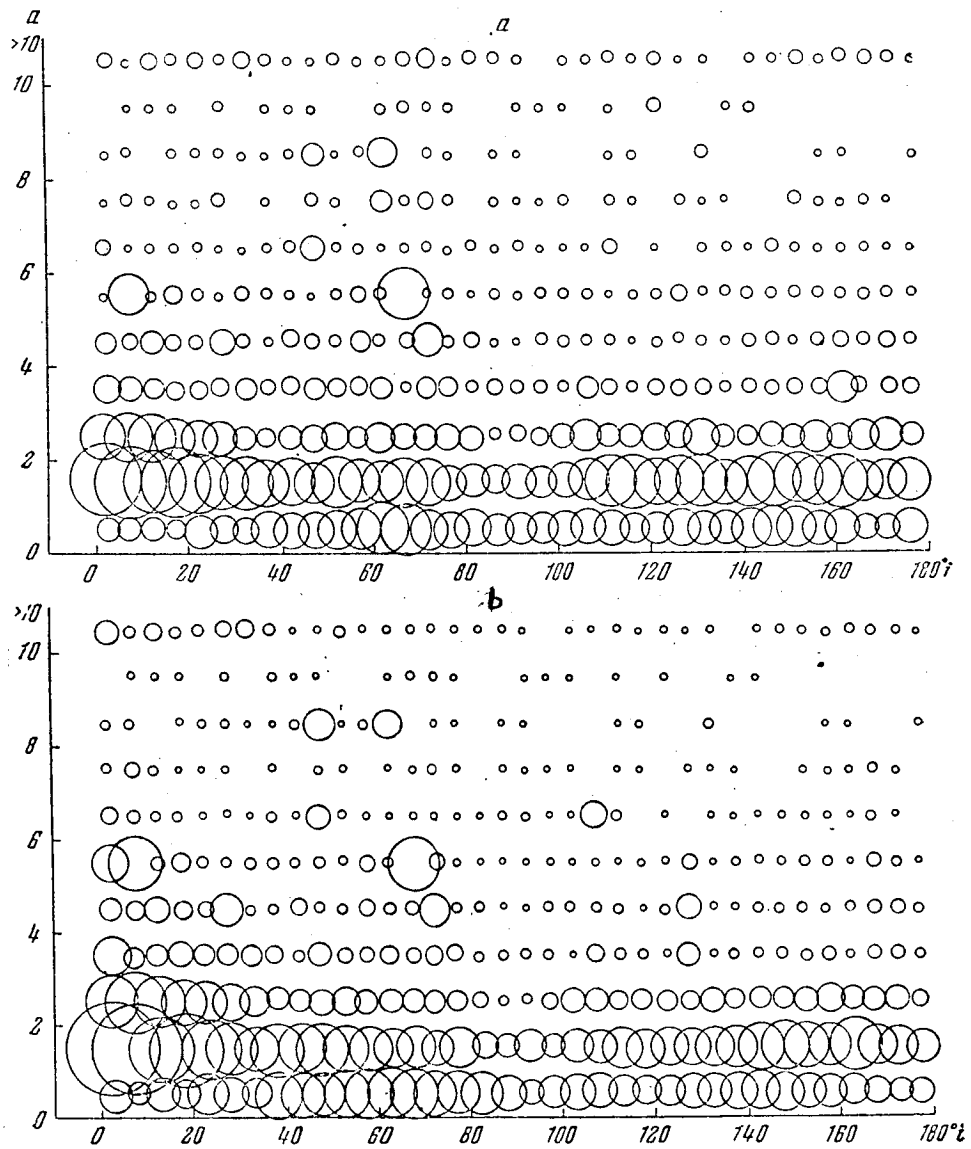

Fig.4.38. Distribution of Orbits in Respect to i and a Obtained from the Radio Observations. The notations are the same as in Fig.4.24.

/205

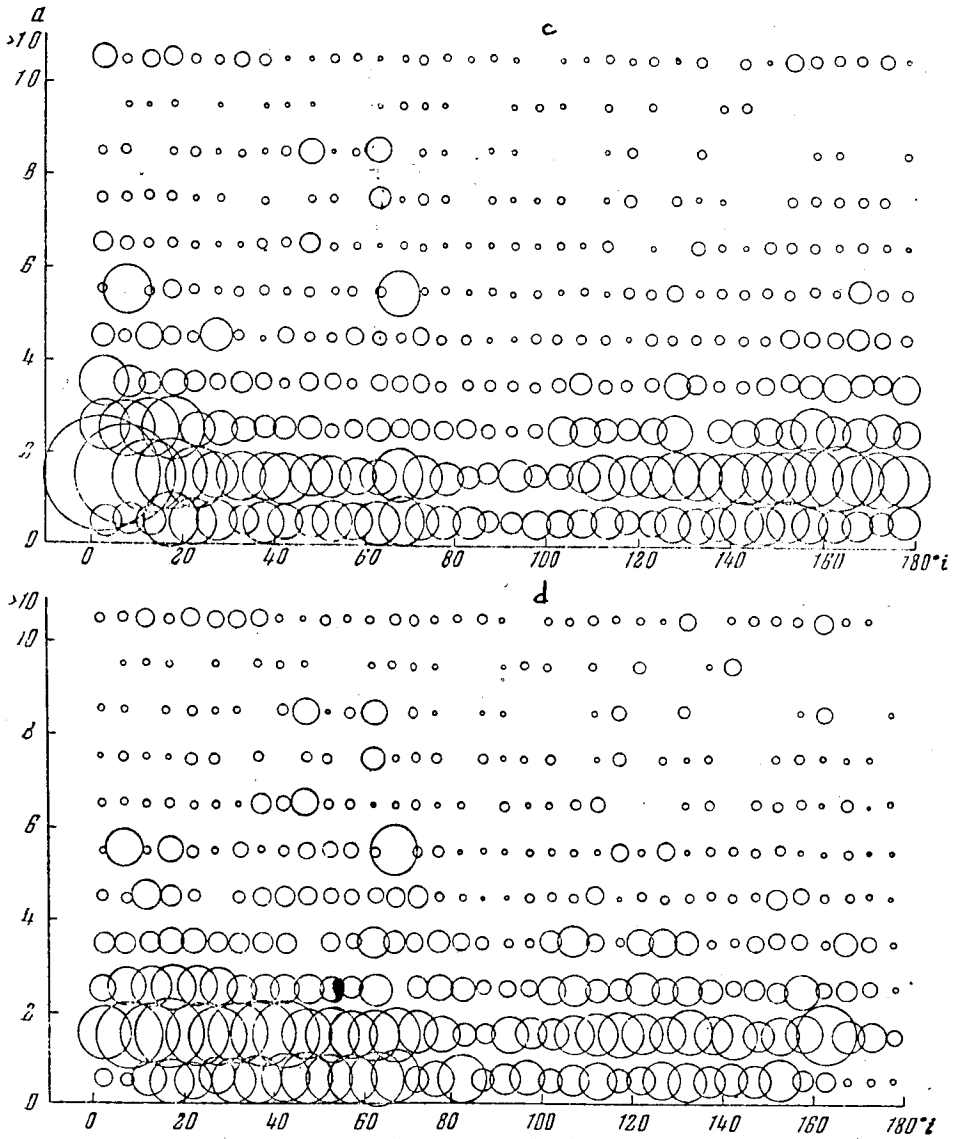

Fig.4.38. Distribution of Orbits in Respect to i and a Obtained from the Radio Observations. The notations are the same as in Fig.4.24.

A statistical analysis of the catalog of 12,500 orbits developed in the KPI (Kharkov Polytechnical Institute) indicates that a large number of the small meteor bodies producing the radiometeors will follow orbits of the fourth type "Γ", which in form and obliquity to the plane of the ecliptic are close to the orbits of the short-periodic comets, but differ from them by small values of the perihelion distance and of the major semiaxes ($q < 0.3$ and $a < 3$ A.U.). The aphelions of the orbits of the type "Γ", lie near the orbit of Jupiter or in a belt of the asteroids. From the photographic observations, the orbits of the type "Γ" were obtained for several meteor showers (Geminids, δ Aquarids and others), for which the comet-precursors were not known. In the case of small meteor bodies, the orbits of this type are especially typical for the meteor bodies in the streams (showers). /206

/206

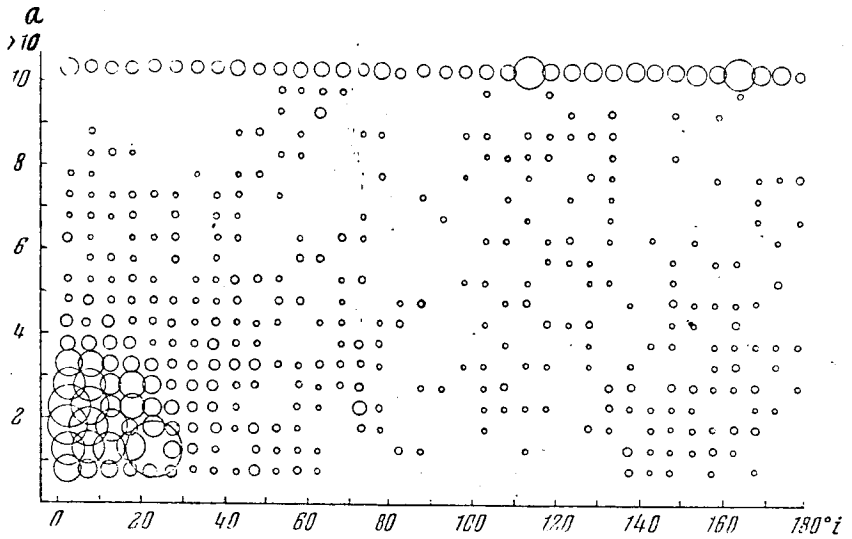

Fig.4.39. Distribution of Orbits by i and a Obtained from the Photographic Observations /28/.

The finding of the two main types of orbits of small meteor bodies has great importance for the study of the origin and evolution of meteoric matter. The two groups of cometary orbits are interconnected, since the perturbations from Jupiter and Saturn can transfer the comets from the orbits of the type "a" to the orbits of type "b". The orbits of type "c" are scarcely found among the larger bodies in the solar system and are not derivatives from the orbit of type "b". The lifetime of the meteoric bodies in the short-periodic orbits is very short as compared to the age of the solar system; hence, the meteor bodies could not have been formed in the orbits of type "c".

Evidently, a considerable part of the small meteor bodies is formed in the orbits of very large dimensions. Under the effect of the force of deceleration (the Poynting-Robertson, the effect of solar corpuscular streams, the resistance of the interplanetary environment, etc), the orbits of the meteor bodies gradually shorten (contract), all the faster, the smaller the mass of the bodies. In this connection, during a short time interval, the orbit proves to be close to the orbit of Jupiter (or of Saturn), and the meteor body can experience close approaches with Jupiter (or with Saturn). For the large meteor bodies, this time span has a long duration, and the probability is high that during this time, the meteor body will be captured by Jupiter, thrown in to an orbit of type "b" or ejected from the solar syste. The orbits of the meteor bodies contract much more quickly, and for them, the probability of passing the "Jupiter barrier" or (Saturn) is considerably higher.

Öpik /207/ demonstrated that in the case of the braking, only as a result of the Poynting-Robertson effect at small i-values, the "Jupiter barrier" can be passed by the small meteor bodies producing meteors fainter than about $+9^m$. At high-value, the probability of close approaches with Jupiter decreases, and the "Jupiter barrier" can be transversed only by the larger meteor bodies. By this mechanism, we can explain the presents of a large number of orbits of the type "c" in the radiometeors and their practically total absence in the bright photographic meteors. In this connection, of considerable interest are the

determinations of the orbits of the even small meteor bodies, producing meteors fainter than $+10^m$. If among them, we find predominating the almost circular orbits with arbitrary obliquities to the plane of the ecliptic, this will comprise a weighty argument in favor of the assumption that most of the very small meteor bodies penetrate the internal areas of the solar system from its remote periphery under the effect of deceleration forces.

/207

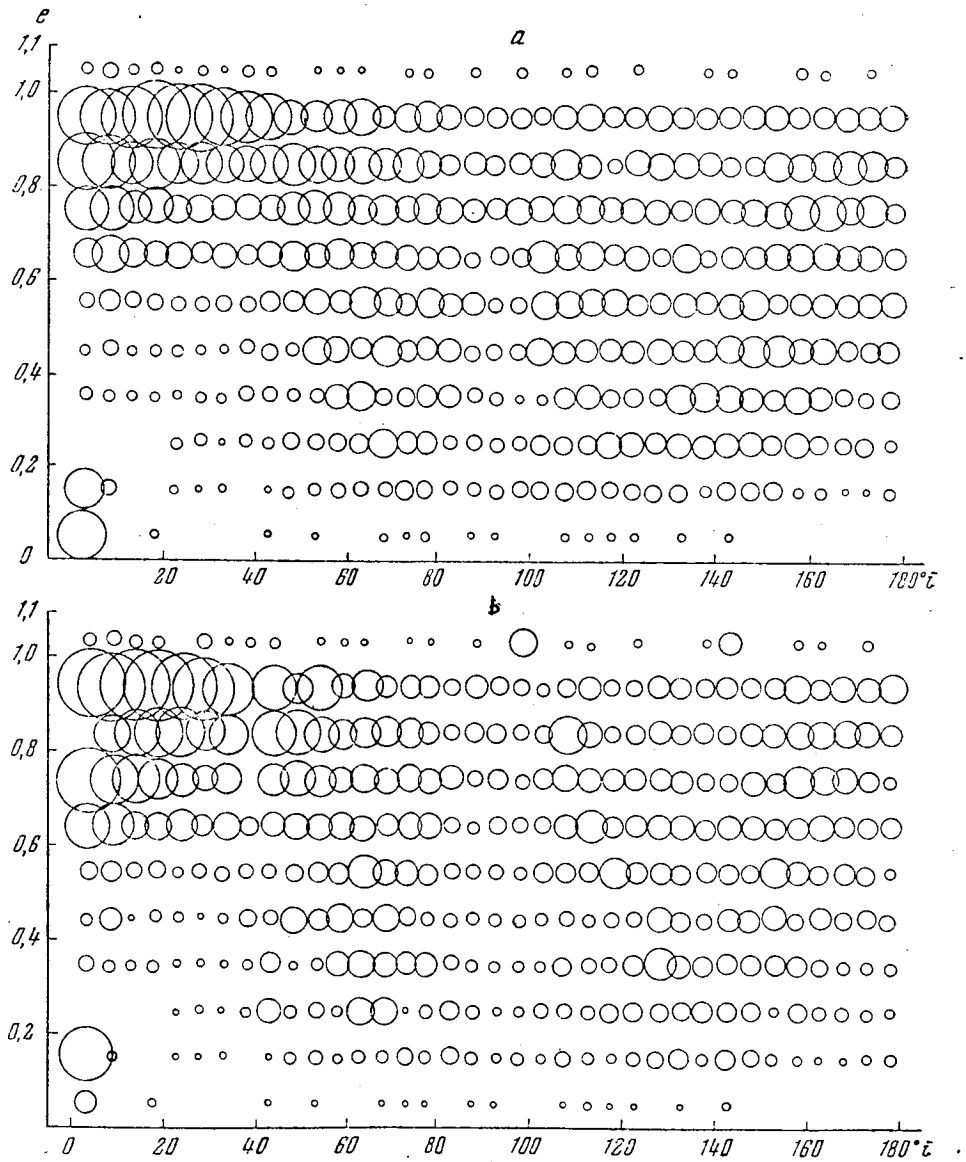

Fig.4.40. The Orbital Distribution in Respect to i and e Obtained from the Radio Observations. The notations are the same as in Fig.4.24.

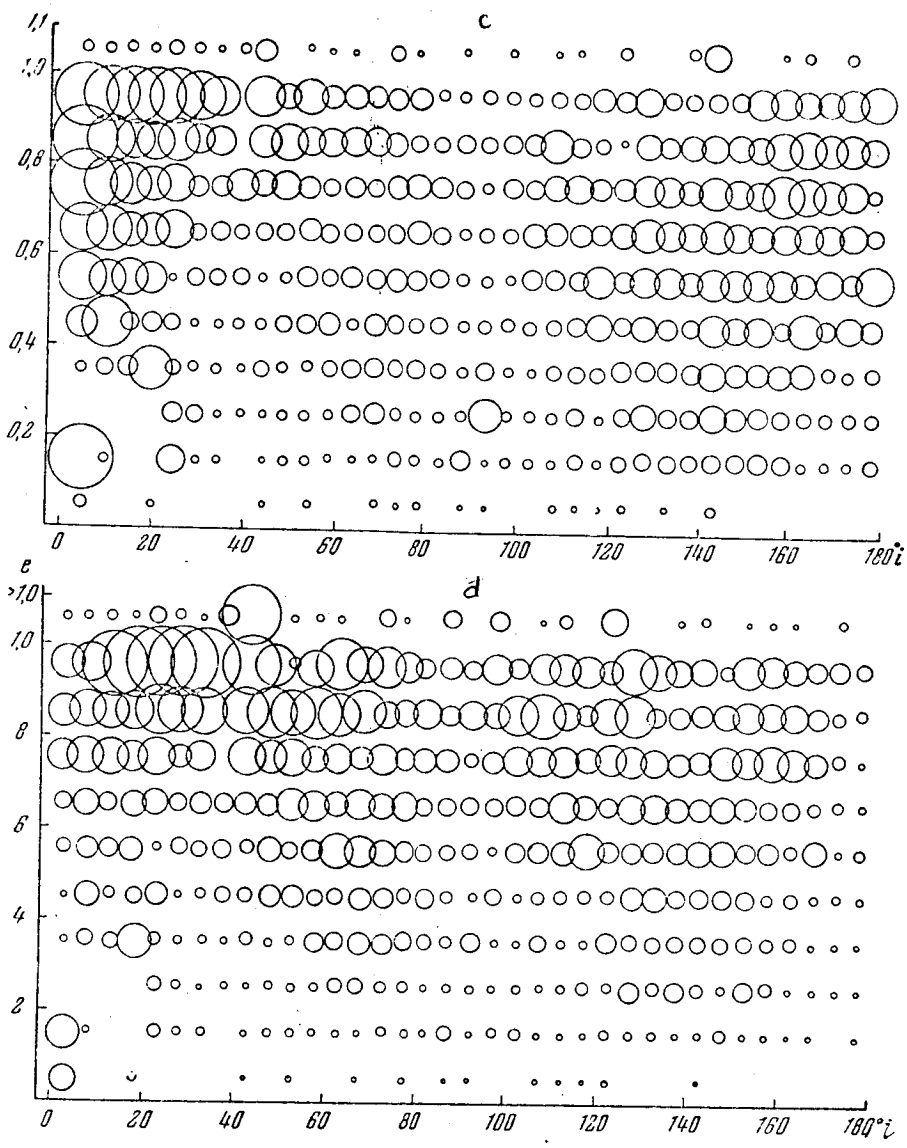

Fig.4.40. The Orbital Distribution in Respect to i and e Derived from the Radio Observations. The notations are the same as in Fig.4.24.

The detection of a very large number of the type "d" orbits for the small meteor bodies demonstrates that in the solar system, there should appear constantly a large number of comets (or of other large bodies, of which the disintegration products are the meteor bodies) in the orbits of such a type. As a result of the frequent approaches to the Sun in the perihelion and the proximity of the entire orbit to the Sun, if we assume the ice model of the comets' nuclei, the lifetime of the comets in the type "d" orbits is quite short (it can be measured in toto by decades), and is many times less than the lifetime of the meteor bodies having orbits of such a type.

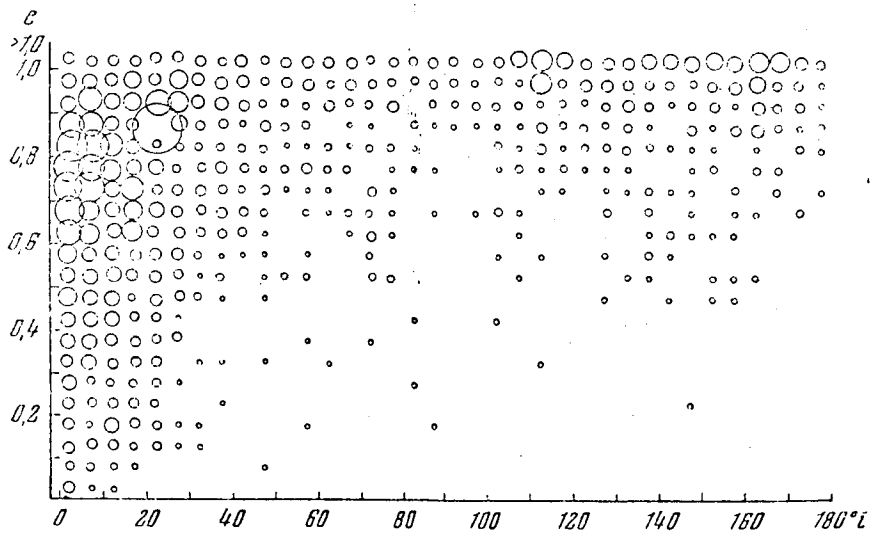

Fig.4.41. Distribution of Orbits by i and e Obtained from the Photographic Observations /28/.

BIBLIOGRAPHY

1. Gaede, W.: The Molecular Air Pump (Die Molecularluftpumpe). Ann. Phys., Vol.41, p.378, 1913.

2. Öpik, E.J.: A Statistical Method of Counting Shooting Stars and its Application to the Perseid Shower of 1920. Publ. Observ. Astron. Tartu., Vol.1, p.25, 1922.

3. Öpik, E.J.: Atomic Collisions and Radiation of Meteors. Acta et Commentat. Univ. Tartuen, Vol.26, Part A, p.2, 1933.

4. Sparrow, G.M.: Physical Theory of Meteors. Astrophys. J., Vol.63, p.90, 1926.

5. Fisher, W.J.: Mass and Velocity of Meteorites and the Air Density along their Luminous Paths. Harv. Cric., Vol.1, p.385, 1934.

6. Öpik, E.J.: Physics of Meteor Flight in the Atmosphere. N. Y., 1958.

7. Jacchia, L.J.: On Two Parameters in the Physical Theory of Meteors. Smithsonian Contribs. Astrophys., Vol.2, p.181, 1958.

8. Table of Standard Atmosphere. Publishing House of Standards, Moscow, 1964.

9. Allen, W.A., Rinehart, J.S., and White, W.C.: Phenomena Associated with the Flight of Ultraspeed Pellets. J. Appl. Phys., Vol.23, pp.132,138,297, 1952.

10. Opik. E.J.: Meteor Radiation, Ionization and Atomic Luminous Efficiency. Proc. Roy. Soc., Series A, pp.230,463, 1955.

11. Hawkins, G.S. and Southworth, R.B.: The Statistics of Meteors in the Earth's Atmosphere. Smithsonian Contribs. Astrophys., Vol.2, p.349, 1958.

12. Whipple, F.L.: Photographic Meteor Orbits and their Distribution in Space. Astron. J., Vol.59, p.201, 1954.

13. McKinley, D.W.: Meteor Science and Engineering. N. Y., 1961.

14. Jacchia, L.G.: Fragmentation as a Cause of the Faint-Meteor Anomaly. Astrophys. J., Vol.121, p.521, 1955.

15. McCrosky, R.E.: Fragmentation of Faint Meteors. Astron. J., Vol.60, p.170, 1955.

16. Levin, B.Yu.: On the Fragmentation of Meteor Bodies (O droblenii meteornykh tel). Astron, Zh., Vol.40, No.2, p.304, 1963.

17. Langmuir, I.: The Vapor Pressure of Metallic Tungsten. Phys. Rev., Vol.2, p.329, 1913.

18. Deshman, S.: Scientific Bases of Vacuum Technology (Nauchnyye osnovy vakuumnoy tekhniki). I.L. (FLP = Foreign Literature Publishing House), 1950.

19. Kubaschewski, O. and Evans, E.L.: Metallurgical Thermochemistry. London, 1951.

20. Stull, D.R.: Vapor Pressure of Pure Substances. Industr. and Engng. Chem., Vol.39, p.517, 1947.

21. Levin, B.Yu.: Elements of a Physical Theory of Meteors (Elementy fizicheskoy teorii meteorov). Astron. Zh., Vol.17, No.3, p.12, 1940.

22. Arifov, U.A.: Interaction of Atomic Particles with the Surface of Metal (Vzaimodeystviye atomnykh chastits s poverkhnost'yu metalla). Tashkent. Izd-vo AN UzbSSR, 1961.

23. Landau, L.D. and Lifshits, Ye.M.: Mechanics (Mekhanika). Izd-vo "Nauka", 1965.

24. Levin, B.Yu.: Physical Theory of Meteors and Meteor Substance in the Solar System (Fizicheskaya teoriya meteorov i meteornoye veshchestvo v solnechnoy sisteme). Izd-vo AN SSSR, 1956.

25. Massey, G. and Barhop, Ye.: Electron and Ion Collisions (Elektronnyye i ionnyye stolknoveniya). FLP, 1958.

26. McKeown, D.: New Method for Measuring Sputtering in the Region Near Threshold. Rev. Scient. Instrum., Vol.32, No.2, p.43, 1961.

27. Levin, B.Yu.: Elements of Physical Theory of Meteors (Elementy fizicheskoy teorii meteorov). Dokl. AN SSSR, Vol.25, No.5, p.372, 1939.

28. McCrosky, R.E. and Posen, A.: Orbital Elements of Photographic Meteors. Smithsonian Contribs. Astrophys., Vol.4, No.1, p.15, 1961.

29. Öpik, E.J.: Research on the Physical Theory of Meteor Phenomena. III. Basis of the Physical Theory of Meteor Phenomena. Publ. Observ. Astron. Tartu., Vol.29, No.5, p.67, 1937.

30. Whipple, F.L.: The Theory of Micrometeorites. I. In an Isothermal Atmosphere. II. In Heterothermal Atmospheres. Proc. Nat. Acad. Sci. U.S.A., Vol.36, No.12, p.687, 1950.

31. Fesenkov, V.G.: On the Question of Micrometeorites (K voprosy o mikrometeoritakh). Meteorikika, Vol.12, p.3, 1955.

32. Levin, B.Yu.: Elements of a Physical Theory of Meteors (Elementy fizicheskoy teorii meteorov). Astron. Zh., Vol.18, No.4-5, p.331, 1941.

33. Istomin, V.G.: Ions of Extraterrestrial Origin in the Earth's Ionosphere (Iony vnezemnogo proiskhozhdeniya v ionosfere Zemli). In the Coll.: "Artificial Earth Satallites" (Iskusstvennyye sputniki Zemli), Vol.2, p.98, 1961.

34. Volynskiy, M.S.: On the Fragmentation of Drops in a Flow of Air (O droblenii kapel' v potoke vozdukha). Dokl. AN SSSR, Vol.62, No.3, p.301, 1948.

35. Volynskiy, M.S.: Study of the Fragmentation of Drops in a Gas Flow (Izucheniye drobleniya kapel' v gazovom potoke). Dokl. AN SSSR, Vol.68, No.2, p.237, 1949.

36. Borodin, V.A., Dityakin, Yu.F., and Yagodkin, V.I.: On the Fragmentation of a Spherical Drop in a Gas Flow (O droblenii sfericheskoy kapli v gazovom potoke). ZhPMTF, No.1, p.85, 1962.

37. Isshiki, N.: Theoretical and Experimental Study on Atomization of Liquid Drop in High Speed Gas Stream. Rept. Transportation Tech. Res. Inst., No.35, 1959.

38. Hinze, I.O.: Critical Speeds and Sizes of Liquid Globuls. Appl. Sci. Res., Vol.1, Series A, p.159, 1949.

39. Astapovich, I.S.: Meteor Phenomena in the Earth's Atmosphere (Meteoriyye yavleniya v zemnoy atmosfere). Fizmatgiz, Moscow, 1958.

40. Jacchia, L.G., Kopal, Z., and Millman, P.M.: A Photographic Study of the Draconid (Giacobinid) Meteor Shower of 1946. Astrophys. J., Vol.111, No.1, p.104, 1950.

41. Poloskov, S.M. and Katasev, L.A.: Meteor Methods of Studying the Upper Atmosphere (Meteornyye metody izucheniya verkhney atmosfery). Byull. Komissii po kometam i meteoram, No.6, p.11, 1961.

42. Whipple, F.L.: On Meteoroids and Penetration. J. Geophys. Res., Vol.68, No.17, p.4929, 1963.

43. Greenhow, J.S. and Neufeld, E.L.: The Variation of Ionization Along a Meteor Trail. Monthly Notices Roy. Astron. Soc., Vol.117, No.4, p.359, 1957.

44. Gerasimenko, V.I. and Oksyuk, Yu.D.: Disassociation of Diatomic Molecules during Rapid Collisions (Dissotsiatsii dvukhatomnykh molekul pri bystrykh stolknoveniyakh). ZhETF, Vol.48, No.2, p.499, 1965.

45. Öpik, E.J.: The Masses of Meteors. Mém. Soc. Roy. Sci., Vol.15, No.1, p.125, Liege, 1955.

46. McCrosky, R.E.: Observations of Simulated Meteors. Smithsonian Contribs. Astrophys., Vol.5, No.4, p.29, 1961.

47. McCrosky, R.E. and Soberman, R.K.: Results from an Artifical Iron Meteoroid at 10 km/sec. Research Note, Air Forces Cambridge Research Laboratory, July, 1962.

48. Jacchia, L.G.: Photographic Meteor Phenomena and Theory, Meteor Photometry, Fundamental Equation and Constants, Duration and Flares. Harvard Observ. Techn. Rept., No.3, 1949.

49. Cook, A.F.: On the Constants of the Physical Theory of Meteors. Astron. J., Vol.60, No.5, p.150, 1955.

50. Verniani, F.: On the Luminous Efficiency of Meteors. Smithsonian Contribs. Astrophys., Vol.8, No.5, p.141, 1965.

51. Mott, N. and Massey, G.: Theory of Atomic Collisions (Teoriya atomnykh stolknoveniy). FLP, 1951.

52. Massey, H.S.W. and Sida, D.W.: Collision Processes in Meteor Trails. Philos. Mag., Vol.46, p.190, 1955.

53. Hartree, D.R. and Hartree, W.: Selfconsistent Field with Exchange for Calcium. Proc. Roy. Soc., Vol.164, Series A, p.167, 1938.

54. Brown, F.R.: Charge Distributions in Fluorine and Neon. Phys. Rev., Vol.44, p.214, 1933.

55. Portnyagin, Yu.I.: Effect of Sections of the Diffusion of Meteor Atoms in the Atmosphere (Effektivnyye secheniya diffuzin meteornykh atomov v atmosfere). Geomagnetizm i aeronomiya, Vol.6, p.707, 1966.

56. Abrahamson, A.A.: Repulsive Interaction Potentials Between Rare-Gas Atoms. Homonuclear Two-Centered Systems. Phys. Rev., Vol.130, p.693, 1963.

57. Abrahamson, A.A.: Repulsive Interaction Potentials Between Rare-Gas Atoms. Hoteronuclear Two-Center Systems. Phys. Rev., Vol.133, p.990, 1964.

58. Rostagni: Ricerche sui raggi positivi e neutrali. V. Ionizazione per urto di ioni e di atomi. Nuovo Cimento, Vol.13, p.389, 1936.

59. Berry, H.W.: The Scattering of Fast Argon Atoms in Argon Gas. Phys. Rev., Vol.75, p.913, 1949.

60. Wolf, F.: Concerning Ion Collisions during Intensive Resonance (Über ionenstösse bei strenger resonanz). Ann. Phys., Vol.29, p.33, 1937.

61. Frische, C.A.: Ionization and Scattering Accompanying Positive Ion Impact in Gases Phys. Rev., Vol.43, p.160, 1933.

62. Moe, D.E.: Ionization of Inert Gases by Positive Potassium Ions. Phys. Rev., Vol.104, p.694, 1956.

63. Bydin, Yu.F. and Bukhteyev, A.M.: Ionization of Fast Atoms of Na, K, Rb, and Cs during Collisions with Molecules of H_2, D_2, N_2, and O_2 (Ionizatsiya bystrykh atomov Na, K, Rb, i Cs pri stolknoveniyakh s molekulami H_2, D_2, N_2, i O_2). ZhTF, Vol.30, No.5, p.546, 1960.

64. Bukhteyev, A.M. and Bydin, Yu.F.: Losses of an Electron by Fast Atoms of Ca, Mg, Si and Fe during Collisions with Molecules of N_2 and O_2 (Poterya elektrona bystrymi atomami Ca, Mg, Si and Fe pri stolknoveniyakh s molekulami N_2 i O_2). Izv. AN SSSR, Series Fiz., Vol.27, No.8, p.1009, 1963.

65. Utterback, N.G. and Miller, G.H.: Ionization of Nitrogen Molecules by Nitrogen Molecules. Phys. Rev., Vol.124, p.1477, 1961.

66. Utterback, N.G.: Ionization of Nitrogen and Oxygen Molecules by Nitrogen and Oxygen Molecules. Phys. Rev., Vol.129, p.219, 1963.

67. Rosen, P.: Low-Energy Inelastic Atomic Collisions. Phys. Rev., Vol.109, p.348, 1958.

68. Rosen, P.: Ionization Cross Section of Argon-Argon Collisions near Threshold. Phys. Rev., Vol.109, p.351, 1958.

69. Lazarus, D.M. and Hawkins, G.S.: Meteor Ionization and the Mass of Meteoroids. Smithsonian Contribs. Astrophys., Vol.7, p.221, 1963.

70. Kayzer, T.R.: Interpertation of a Radio Echo from Meteor Trails.(Interpretatsiya radioekho ot meteornykh sledov). In the Coll.: "Meteors" (Meteory), FLP, 1958.

71. Kaiser, T.R.: Radio Echo Studies of Meteor Ionization. Advances Phys., Vol.2, p.495, 1953.

72. Manning, L.A.: The Initial Radius of Meteoric Ionization Trails. J.Geophys. Res., Vol.63, p.181, 1958.

73. Loeb, L.B.: Kinetic Theory of Gases. London, 1934.

74. Öpik, E.J.: Problems in the Physics of Meteors. Amer. J. Phys., Vol.26, p.70, 1958.

75. Loshchilov, Yu.A.: Concerning the Initial Radius of a Meteor Trail (O nachal'nom radiuse meteornogo sleda). Trudy Gorodskoy Astr. Obs. Kazansk. Un-ta., Vol.33, p.70, 1961.

76. Kashcheyev, B.L. and Lebedinets, V.N.: Radar Studies of Meteor Phenomena (Radiolokatsionnyye issledovaniya meteornykh yavleniy). Series "Results of the IGY" (Rezul'taty MGG). Izd-vo AN SSSR, 1961.

77. Amdur, I., Mason, E.A., and Jordan, J.E.: Scattering of High Velocity Neutral Particles, He - N_2; A - N_2; the N_2 - N_2 Interaction. J. Chem. Phys., Vol.27, p.527, 1957.

78. Girschfelder, J., Curtis, C., and Byrd, R.: Molecular Theory of Gases and Fluids (Molekulyarnaya teoriya gazov i zhidkostey). FLP, 1961.

79. Sida, D.W.: The Scattering of Positive Ions by Neutral Atoms. Philos. Mag., Vol.2, p.761, 1957.

80. Greenhow, J.S.: Eddy Diffusion and its Effect on Meteor Trails. J. Geophys. Res., Vol.64, p.2208, 1959.

81. Davies, J.G., Greenhow, J.S., and Hall, J.E.: Combined Photographic and Radio Echo Observations of Meteors. Proc. Roy. Soc., Vol.253, Series A, p.121, 1959.

82. Davies, J.G., Greenhow, J.S., Hall, J.E.: The Effect of Attachment on Radio Echo Observations of Meteors. Proc. Roy. Soc., Vol.253, Series A, p.130, 1959.

83. Greenhow, J.S. and Hall, J.E.: Attachment Processes in Meteor Trails. J. Atmos. and Terr. Phys., Vol.21, p.261, 1961.

84. Lovell, A.C.B. and Clegg, J.A.: Characteristics of Radio Echoes from Meteor Trails. I. The Intensity of Radio Reflections and Electron Density in the Trails. Proc. Phys. Soc., Vol.60, p.491, 1948.

85. Herlofson, N.: Plasma Resonance in Ionospheric Irregularities. Arkiv fys., Vol.3, p.247, 1951.

86. Kaiser, T.R. and Gloss, R.L.: Theory of Radio Reflections from Meteor Trails. Philos. Mag., Vol.43, p.1, 1952.

87. Davies, J.G. and Ellyett, C.D.: The Diffraction of Radio Waves from Meteor Trails and the Measurement of Meteor Velocities. Philos. Mag., Vol.40, p.614, 1949.

88. Watson, G.N.: Theory of Bessel Functions. N. Y., 1952.

89. Southworth, R.B.: Deceleration of Radio Meteors. Astron. J., Vol.67, p.283.

90. Bayrochenko, I.V.: Physics of Interaction of Radiowaves with Meteor Trails. (Fizika vzaimodeystviya radiovoln s meteornymi sledami). Collection of Reports of the IGY (Sbornik rabot po MGG), No.2, Izd-vo Kiyevskogo Un-ta, p.11, 1963.

91. Dudnik, B.S., Kashcheyev, B.L., and Lebedinets', V.N.:

(Pomilki radiolokatsiynikh vimiryuvan' meteoriv vnaslidok difuziy). Dopovidi AN UkrSSR, Vol.11, No.3, p.299, 1961.

92. Manning, L.A.: The Strength of Meteoric Echoes from Dense Columns. J. Atmos. and Terr. Phys., Vol.4, p.219, 1953.

93. Kashcheyev, B.L.: Concerning the Study of the Proper Atmosphere on Radio Observations of Meteors (Ob issledovanii svoystv verkhney atmosfery po radionablyudeniyam meteorov). In the Coll.: "Meteors" (Meteory), No.2-3, Izd-vo Khar'kovskogo Un-ta, 1963.

94. Greenhow, J.S. and Hall, J.E.: Diurnal Variations of Density and Scale Height in the Upper Atmosphere. J. Atmos. and Terr. Phys., Vol.18, p.203, 1960.

95. Greenhow, J.S. and Hall, J.E.: The Height Variation of the Ambipolar Diffusion Coeficient for Meteor Trails. Planet Space Sci., Vol.5, p.109, 1961.

96. Greenhow, J.S. and Hall, J.E.: The Importance of Initial Radius on the Apparent Height and Number Distributions of Meteor Echoes. Monthly Notices Roy. Astron. Soc., Vol.121, p.183, 1960.

97. Kashcheyev, B.L. and Lebedinets, V.N.: The Initial Radius of Ionized Meteor Trails. Smithsonian Contribs. Astrophys., Vol.7, p.19, 1963.

98. Greenhow, J.S.: Limitations of Radar Techniques for the Study of Meteors. Smithsonian Contribs. Astrophys., Vol.7, p.5, 1963.

99. Dobriner, R.: VHF System Would Use Meteor Trails. Electron Design, Vol.11, p.30, 1963.

100. Dokuchayev, V.P.: Concerning the Effect of the Magnetic Field of the Earth Upon the Winds in the Ionosphere (O vliyanii magnitnogo polya Zemli na ionosfere). Izv. AN SSSR, Series Geofiz., Vol.5, p.783, 1959.

101. Dokuchayev, V.P.: Motion of Ionized Gas in the Upper Atmosphere (Dvizheniye ionizirovannogo gaza v verkhney atmosphere). Izv. Vuzov, Series Radiofiz., Vol.4, p.5, 1961.

102. Manning, L.A.: Conference on the Ionosphere and Fluid Dynamics. J. Geophys. Res., Vol.64, p.2047, 1959.

103. Pushkov, N.V.: Basic Scientific Problems in the Period of IQSY (Osnovnyye nauchnyye zadachi v period mezhdunarodnogo goda spokoynogo solntsa). Geofiz. Byull., No.13, p.3, 1963.

104. Sissenwine, N., Dubin, M., and Wexler, H.: The U.S. Standard Atmosphere. J. Geophys. Res., Vol.67, p.3627, 1962.

105. Delov, I.A., Kashcheyev, B.L., and Borovich, L.I.: Basic Characteristics of Turbulent Flow in the Earth's Atmosphere at Height of 90 - 100km (in Ukraine) (Ocnobni kharakteristiki turbulentnogo rukhu v atmosferi Zemli na visoti 90 - 100km.). Dopovidi AN UkrSSR, No.8, 1051, 1964.

106. Liller, V. and Uippl, F.: Winds in the Upper Atmosphere Based on Photographs of Meteor Trails (Vetry v verkhney atmosfere po fotografiyam meteornykh sledov). In the Coll.: "Rocket Studies of the Atmosphere" (Raketnyye issledovaniya atmosfery). FLP, 1957.

107. Isamutdinov, Sh.O.: In the Collection: "Meteor Propagations of Radiowaves" (Meteornoye rasprostraneniye radiovoln), No.2, Izd-vo Kazanskogo Un-ta, 1964.

108. Lebedinets, V.N.: Density of Meteor Material in the Environs of the Earth's Orbit Based on Radio Observations of Meteors (Plotnost' meteornogo veshchestva v okrestnosti orbity Zemli po radionablyudeniyam meteorov). Astron. Zh., Vol.20, No.4, p.719, 1963.

109. Lebedinets, V.N.: On the Mechanism of Formation of a Region of Higher Atomic Density with Atoms of Meteoric Origin at 100 - 110km. Space Res., Vol.4, p.553, 1964.

110. Whithead, J.D.: The Formation of Sporadic E Layer in the Temperate Zones. J. Atmos. and Terr. Phys., Vol.20, p.49, 1961.

111. Hines, C.O.: The Formations of Midlatitude Sporadic E Layers. J. Geophys. Res., Vol.69, p.1018, 1964.

112. Taran, V.I.: Measurement of the Drift in the Ionosphere with the Simultaneous Study of the State of Polarization (Izmereniye dreyfa v ionosfere s odnovremennym issledovaniyem sostoyaniya polyarizatsii). In the Coll.: "Study of Heteorgeneities in the Ionosphere" (Issledovaniye neodnorodnostey v ionosfere), No.4, Series "Results of the IGY" (Rezul'taty MGG). Izd-vo AN SSSR, 1960.

113. Kashcheyev, B.L. and Taran, V.I.: Measurement of the Drift of Heteorgeneities of Ionization in the E-Region of the Ionosphere at Simultaneous Monitoring of the Polarization of Reflected Radiowaves (Izmereniye dreyfa neodnorodnostey ionizatsii v E-oblasts ionosfery pri odnovremennom kontrole polyarizatsii otrazhennykh radiovoln). In the Coll.: "Meteors" (Meteory), No.2-3, Izd-vo Khar'kovskogo Un-ta, 1963.

114. Stroud, W.G., Bandeen, W.R., Nordberg, W, Bartman, F.L., Otterman, J., and Titus, P.: Temperatures and Winds in the Arctic as Obtained by Grenade Experiment. I.G.Y. Rocket Rept., Ser. I, Nat. Acad. Sci., U.S.A., Vol.58, 1958.

115. Stroud, W.G., Bandeen, W.R., Nordberg, W. Bartman, F.L., Otterman,J., and Titus, P.: Rocket Grenade Measurments of Temperature and Winds in the Mesosphere over Churchill, Canada. J. Geophys. Res., Vol.65, p.2307, 1960.

116. Edward, H.D., Bedinger, J.F., Manring, E.R., and Cooper, C.D.: Emission from a Sodium Cloud Artifically produced by means of Rocket. In: "The Airglow and Aurorae", London, 1956.

117. Manning, B., Bedinger, J., Pettit, H., and Moore, C.: Some Wind Determinations in the Upper Atmosphere using Artifically Generated Sodium Clouds. J. Geophys. Res., Vol.64, p.587, 1959.

118. Edwards, H.D., Cooksey, M.M., Justus, C.G., Fuller, R.N., Albritton, D.L.: Upper-Atmosphere Wind Measurements Determined from Twelve Rocket Experiments. J. Geophys. Res., Vol.68, p.3021, 1963.

119. Kampe, H.J., Smith, M.E., Brown, R.M.: Winds Between 60 and 110 kms. J. Geophys. Res., Vol.67, p.4243, 1962.

120. Smith, L.B.: The Measurement of Wind Between 100,000 and 300,000 ft. by use chaft rockets. J. Meteorol., Vol.17, p.296, 1960.

121. Reising, G.H.: Instantaneous and Continuous Wind Measurements up to the Higher Stratosphere. J. Meteorol., Vol.13, p.448, 1956.

122. Robertson, D.R., Liddy, D.T., and Elford, W.G.: Measurements of Winds in the Upper Atmosphere by means of Drifting Meteor Trails. J. Atmos. and Terr. Phys., Vol.4, p.255, 1953; Vol.4, p.271, 1953.

123. Greenhow, J.S.: Systematic Wind Measurements at Altitudes of 80 - 100 km. Philos. Mag., Vol.45, p.363, 1954.

124. Greenhow, J.S., Neufeld, E.L.: Diurnal and Seasonal Wind Variations in the Upper Atmosphere. Philos. Mag., Vol.46, p.549, 1955.

125. Kashcheyev, B.L., Lysenko, I.A., and Chenura, V.F.: Measurement of the Winds Velocity at a Height of 80 - 120km Based on Reflections from Meteors (Izmereniye skorosti vetra na vysote 80 - 120km po otrazheniyam ot meteorov). Byull. Komissii po Kometam i meteoram, Vol.3, p.9, 1958.

126. Dudnik, B.S.: Amplitude-Phase Method of Measuring the Height of Meteors (Amplitudno-fazovyy metod izmeteniya vysoty meteorov). In the Coll.: "Meteors" (Meteory), No.2-3, Izd-vo Khar'kovskogo Unta, 1963.

127. Fialko, Ye.I.: Certain Problems of a Radar Location of Meteors (Nekotoryye problemy radiolokatsii meteorov). Izd-vo Tomskogo Un-ta, 1961.

128. Dudnik, B.S., Kashcheyev, B.L., Lagutin, M.F., and Lysenko, I.A.: System of Shielding from Pulse Interferences in Equipment Recording in Meteor Activity (Sistema zashchity ot impul'snykh pomekh v apparature, registriruyushchey meteornuyu aktivnost'). Radiotekhnika i elektronika, Vol.3, p.1379, 1958.

129. Kashcheyev, B.L., Dudnik, B.S., Lagutin, M.F., and Lysenko, I.A.: Equipment for the Radar Observations of Meteors (Apparatura dlya radiolokatsionnykh nablyudeniy meteorov). In the Coll.: "Meteors" (Meteory), No.1, Izd-vo Khar'kovskogo Un-ta, 1960.

130. Dolph, C.L.: A Current Distribution for Broadside Areas Which Optimizes the Relationship Between Beam Width and Side-Lobe Level. Proc. IRE, Vol.34, p.335, 1946.

131. Ayzenberg, G.Z.: Antennas of Ultrashort Waves (Antenny ul'trakortkikh voln). Moscow, Svyaz'izdat, 1957.

132. Weiss, A.A. and Elford, W.G.: An Equipment for Combined Geophysical and Astronomical Measurements of Meteors. Proc. IRE Austral., Vol.24, p.197, 1963.

133. Hawkins, G.S.: The Harvard Radio Meteor Project. Smithsonian Contribs. Astrophys., Vol.7, p.53, 1963.

134. Kashcheyev, B.L., Lebedinets, V.N., and Suvorov, Yu.I.: Number of Meteors Based on the Observations Conducted in Harkov in 1957 - 1960 (Chislennost' meteorov po nablyudeniyam, provedennym v Khar'kove v 1957 --1960 gg.). In the Coll.: "Meteors" (Meteory), No.1, Izd-vo Khar'kovskogo Un-ta, 1960.

135. Batchelor, J.: Theory of Homogenous Turbulence (Teoriya odnorodnoy turbulentnosti). FLP, 1955.

136. Greenhow, J.S. and Neufeld, E.L.: Measurements of Turbulence in the 80 to 100 km Region from the Radio Echo Observations of Meteors. J. Geophys. Res., Vol.64, p.2129, 1959.

137. Delov, I.A., Lagutin, M.F., and Lysenko, I.A.: Investigation of Certain Perimeters of the Turbulent Movement by the Method of Radar in Tracing the Meteor Trails (Issledovaniye nekotorykh parametrov turbulentnykh dvizheniy metodom radiolokatsii meteornykh sledov). Izv. Vuzov, Series Radiofiz., Vol.7, p.225, 1964.

138. Delov, I.A.: Turbulent Motions in the Upper Atmosphere at a Height of 80 - 110 km Based on Data from Radio Observations of the Meteor Trails (Turbulentnyye dvizheniya v verkhney atmosfere na bysote 80 - 110 km po dannym radionablyudeniy meteornykh sledov). In the Coll.: "Physics of Comets and Meteors" Fizika komet i meteorov). Science and Thought Publishing House (Izd-vo Naukova Dunka), Kiev, 1965.

139. Delov, I.A.: Investigation of the Turbulent Movements in the Meteor Zone (Issledovaniye turbulentnykh dvizheniy v meteornoy zone). In the Coll.: "Meteors and Comets" (Meteory i kmoety). Izd-vo AN UkrSSR, Kiev, 1966.

140. Greenhow, J.S., Neufeld, E.L.: Winds in the Upper Atmosphere. Quart. J. Roy. Meteorol. Soc., Vol.87, p.472, 1961.

141. Kashcheyev, B.L. and Delov, I.A.: Winds in the Earth's Atmosphere at a Height of 90 - 100 km (in Ukraine) (Rukhi atmosfery Zemli na visoti 90 - 100 km). Dopovidi AN UkrSSR, Vol.7, p.67, 1964.

142. Kashcheyev, B.L., Lysenko, I.A., and Taran, V.I.: The Determination of Wind Velocities at Height of 85 - 130 km by Radio-Echo Methods. Proc. Sympos. URSI, Brussels, September 1959; London, 1960.

143. Dolukhanov, M.P.: Propagation of Radiowaves (Rasprostraneniye radiovoln). Moscow, Svyaz'izdat, 1960.

144. Batten, E.S.: Wind Systems in the Mesosphere. J. Meteorol., Vol.18, p.283, 1961.

145. Kellog, W.W. and Schilling, G.F.: A Proposed Model of the Circulation in the Upper Stratosphere. J. Meteorol., Vol.8, p.222, 1951.

146. Murgatroyd, R.J.: Winds and Temperatures Between 20 km and 100 km. Quart. J. Roy. Meteorol. Soc., Vol.87, p.417, 1957.

147. Pant, P.S.: Circulation in the Upper Atmosphere. J. Geophys. Res., Vol.61, p.459, 1956.

148. Wilkes, M.V.: Oscillations of the Earth's Atmosphere with Allowance for Variation of Temperature with Latitude. Proc. Roy. Soc., Vol.217, Series A, p.44, 1963.

149. Kellog, W.W.: Chemical Heating Above the Polar Mesopause in Winter. J. Meteorol., Vol.18, p.373, 1961.

150. Kochanski, A.: Atmospheric Motions from Sodium Cloud Drifts. J. Geophys. Res., Vol.69, p.3651, 1964.

151. Kochanski, A.: Circulation and Temperature of 70 to 100 Kilometer Height. J. Geophys. Res., Vol.68, p.213, 1963.

152. Kantor, A.J. and Cole, A.E.: Zonal and Meridional Winds to 120 Kilometers. J. Geophys. Res., Vol.69, p.5131, 1964.

153. Hines, C.O.: Internal Gravity Waves at Ionospheric Heights. Canad. J. Phys., Vol.34, p.1441, 1960.

154. Weekes, K. and Wilkes, M.V.: Atmospheric Oscillations and the Resonance Theory. Proc. Roy. Soc., Vol.192, Series A, p.80, 1947.

155. Murray, E.L.: Ambipolar Diffusion of a Meteor Trail and its Relation with Height. Planet Space Sci., Vol.1, p.125, 1959.

156. Weiss, A.A.: Diffusion Coefficients from the Rate of Decay of Meteor Trails. Austral. J. Phys., Vol.8, p.279, 1955.

157. Lagutin, M.F. and Kashcheyev, B.L.: Influence of the Polarization Effect Upon the Radio Signals Dispersed by the Meteor Trails (Vliyaniye polyarizatsionnogo effekta na radiosignaly, rasseivayemyye meteornymi sledami), Radiotekhnika i elektronika, Vol.8, p.158, 1964.

158. Lebedinets, V.N., Lagutin, M.F., and Lysenko, I.A.: Effect of Atmospheric Turbulent Wind on the Measurements of the Velocities and Radiants of Meteors (Vliyaniye atmosfernogo turbulentnogo vetra na izmereniya skorostey i radiantov meteorov). In the Coll.: "Meteors" (Meteory), No.1, Izd-vo Khar'kovskogo Un-ta, 1960.

159. Greenhow, J.S. and Hall, J.E.: The Variation of Meteor Heights with Velocity and Magnitude. Monthly Notices Roy. Astron. Soc., Vol.121, p.174, 1960.

160. Greenhow, J.S. and Neufeld, E.L.: The Diffusion of Ionized Meteor Trails in the Upper Atmosphere. J. Atmos. and Terr. Phys., Vol.6, p.133, 1955.

161. Hey, J.S., Parsons, S.J., and Stewart, G.S.: Radar Observations of the Giacobinid Meteor Shower. Monthly Notices Roy. Astron. Soc., Vol.107, 1947.

162. McKinley, D.W.R. and Millman, P.M.: Phenomenological Theory of Radar Echoes from Meteors. Proc. IRE, Vol.37, p.364, 1949.

163. Pettengill, G.H.: A New Technique for Investigation of Meteor Echoes at UHF. J. Geophys. Res., Vol.67, p.409, 1962.

164. Hey, J.S. and Stewart, G.S.: Derivation of Meteor Stream Radiants by Radio Reflection Methods. Nature, Vol.158, p.481, 1946.

165. Levin, B.Yu.: Observations of the Draconids by the Radar Method. (Nablyudeniya drakonid radiolokatsionnym metodom). Astron. Tsirk., No.57, p.2, 1946.

166. Chechik, P.O.: Observations of Meteors with the Aid of Radar Stations. (Nablyudeniya meteorov s pomoshch'yu radiolokatsionnykh stantsiy). Byuro. Novoy Tekhniki, 1947.

167. Simonenko, A.N. and Suvorov, Yu.I.: The Radiant of 3 September (Radiant 3-go Sentyabrya). Byull. Komissii po Kometam i Meteoram, No.6, p.54, 1961.

168. Clegg, J.A.: Determination of Meteor Radiants by Observations of Radar Echoes from Meteor Trails. Philos. Mag., Vol.39, p.577, 1948.

169. Aspinal, A., Clegg, J.A., and Hawkins, G.S.: A Radio Echo Apparatus for the Delineation of Meteor Radiants. Philos. Mag., Vol.42, p.504, 1951.

170. Ellyett, C.D. and Keay, C.S.L.: Radio Echo Observations of Meteor Activity in Southern Hemisphere. Austral. J. Phys., Vol.9, p.471, 1956.

171. Ellyett, C.D. and Roth, K.W.: The Radar Determination of Meteor Showers in the Southern Hemisphere. Austral. J. Phys., Vol.8, p.390, 1955.

172. Weiss, A.A.: Radio Echo Observations of Geminid Meteor Stream. Austral. J. Phys., Vol.12, p.315, 1959.

173. Keay, C.S.L.: Meteor Radiant Determination from High Echo-Rate Observations. Austral. J. Phys., Vol.10, p.471, 1957.

174. Isamutdinov, Sh.O. and Brudnyy, L.G.: On the Question of Determining the Radiants of Meteor Flows Based on Radar Observations (K voprosy ob opredelenii radnantov meteornykh potokov po radiolokatsionnym nadlyudeniyam). Byull. In-ta Astrofiziki AN TadzhSSR, No.3, 1961.

175. Weiss, A.A.: The Distribution of the Orbits of Sporadic Meteors. Austral. J. Phys., Vol.10, p.77, 1957.

176. Sidorov, V.V.: Angle-Measuring Devise of the KGU-M2 Meteor Station (Uglomernoye ustroystvo meteornoy stantsii KGU-M2). In the Coll.: "Meteor Propagation of Radiowaves" (Meteornoye rasprostraneniye radiovoln), No.2, Izd-vo Kazanskogo Un-ta, 1964.

177. Hawkins, G.S.: A Radio Echo Survey of Sporadic Meteor Radiants. Monthly Notices Roy. Astron. Soc., Vol.116, p.92, 1956.

178. Dudnik, B.S., Kashcheyev, B.L., Lagutin, M.F., Lysenko, I.A., Luk'yashko, D.N., and Lebedinets, V.N.: Radar Observations of Meteors in Kharkov (Radiolokatsionnyye nablyudeniya meteorov v Khar'kove). Series "Results of the IGY" (Rezul'taty MGG), No.8, Izd-vo AN SSSR, 1962.

179. McKinley, D.W.R. and Millman, P.M.: Determination of the Elements of Meteor Path from Radar Observations. Canad. J. Phys., Vol.27, Series A, p.53, 1949.

180. Gill, J.S. and Davies, J.G.: A Radio Echo Method of Meteor Orbit Determination. Monthly Notices Roy. Astron. Soc., Vol.116, p.105, 1956.

181. Kashcheyev, B.L., Lebedinets, V.N., and Lagutin, M.F.: Radar Determinations of the Orbits of Individual Meteors (Radiolokatsionnyye opredeleniya orbit individual'nykh meteorov). Astron. Zh., Vol.38, No.4, p.681, 1961.

182. Davies, J.G. and Gill, J.C.: Radio Echo Measurements of the Orbit of Faint Sporadic Meteors. Monthly Notices Roy. Astron. Soc., Vol.120, p.438, 1960.

183. Isamutdinov, Sh.O.: Concerning One Method of Determing the Coordinates of a Radiant of Separately Studied Meteors (Ob odnom metode opredileniya koordinat radianta otdel'no vzyatykh meteorov). Byull. In-ta Astrofiziki AN TadzhSSR, No.29, p.17, 1962.

184. Eshleman, V.R. and Gallacher, P.B.: Radar Studies of 15-th Magnitude Meteors. Astron. J., Vol.67, 1962.

185. Chebotarev, R.P.: Direction-Finding Time Method of Determining the Radiants and Velocities of Individual Meteors (Pelengatsionno-Vremennoy metod opredeleniya radiantov i skorostey otdel'nykh meteorov). Izv. Vuzov. Radiotekhnika., Vol.6, No.5, p.533, 1963.

186. Avramova, G.V.: Determination of the Meteor Radiants by the Method of Nonattenuating Waves (Opredeleniye meteornykh radiantov metodom nezatukhayushchikh voln). Byull. In-ta Astrofiziki AN TadzhSSR, No.27, p.31, 1959.

187. Nilsson, C.S.: A Southern Hemisphere Radio Survey of Meteor Streams. Austral. J. Phys., Vol.27, p.205, 1964.

188. Shklovskiy, I.S.: Cosmic Radiation (Kosmicheskoye isluchenive). Moscow, Gostekhteorizdat, 1956.

189. Cottony, H.V. and Johler, J.R.: Cosmic Radio Noise Intensities in the VHF Band. Proc. IRE, Vol.40, p.1053, 1952.

190. Costain, J. and Smith, G.A.: The Radio Telescope for λ = 7.9, Mullard Observatory. Monthly Notices Roy. Astron. Soc., Vol.121, p.405, 1960.

191. Greenhow, J.S. and Neufeld, E.L.: Measurement of the Turbulence in the Upper Atmosphere. Proc. Phys. Soc., Vol.14, p.475, 1959.

192. Davies, J.G.: A Table for the Calculation of Meteor Velocity. Jodrell Bank Annals, Vol.1, No.3, 1954.

193. Kleyber, I.L.: Determination of the Orbits of Meteor Streams (Opredeleniye orbit meteornykh potokov). SPb, 1891.

194. Lovell, V.: Meteor Astronomy (Meteornaya astronomiya). Moscow, Fitmatigiz, 1958.

195. Fedynskiy, V.V.: Comparison of the Visual and Radar Determinations of the Drift of Meteor Trails (Sopostavleniye vizual'nykh i radiolokatsionnykh opredeleniy dreyfa meteornykh sledov). Byull. Astron. In-ta Chekhoslovakii, Vol.7, No.3, 1955.

196. Nemirova, E.K.: Concerning the Role of the Resonance Effects during the Measurement of the Velocities of Meteors (O roli rezonansnykh effektov pri izmerenii skorostey meteorov). Astron. Zh., Vol.36, No.3, 1959.

197. Billam, E.R. and Browne, I.C.: Characteristics of Radio Echoes from Meteor Trails. Polarization Effects. Proc. Roy. Soc., Vol.69, Series B, p.98, 1956.

198. Nemirova, E.K.: Resonance Scattering of the Radiowaves by Paraboloid Meteor Trails (Rezonansnoye rasseyaniye radiovoln paraboloidal'nymi meteornymi sledami). Izv. Tomskogo Politekhn. In-ta, Vol.100, p.75, 1962.

199. Jacchia, L.G. and Whipple, F.L.: Precision Orbits of 413 Photographic Meteors. Smithsonian Contribs. Astrophys., Vol.4, p.97, 1961.

200. Southworth, R.B. and Hawkins, G.S.: Statistics of Meteor Streams. Smithsonian Contribs. Astrohpys., Vol.7, p.261, 1963

201. Kashcheyev, B.L., Lebedinets, V.N., and Lagutin, M.F.: The 1959 Orbits of Geminids (Orbita Geminid 1959 goda). In the Coll.: "Meteors" (Meteory), No.1, Izd-vo Khar'kovskogo Un-ta, 1960.

202. Katasev, L.A.: Photographic Methods in Meteor Astronomy (Fotograficheskiye metody meteornoy astronomii). Moscow, Gostekhteorizdat, 1957.

203. Hawkins, G.S. and Southworth, R.B.: Orbital Elements of Meteors. Smithsonian Contribs. Astrophys. Vol.4, p.85, 1961.

204. Babadzhanov, P.B. and Kramer, Ye.N.: Methods and Certain Results of Photographic Investigation of Meteors (Metodika i nekotoryye rezul'taty fotograficheskikh issledovaniy meteorov). Series "Results of the IGY (Rezul'taty MGG). Izd-vo AN SSSR, 1963.

205. Ceplecha, Z., Jezkovy, M., Novak, M., Raichl, J., and Sehnal, L.: Ondrejov Doublestation Meteors during the IGY and IGC. Bull. Astron. Inst. Czechoslovakia, Vol.15, p.144, 1964.

206. Kramer, Ye.N.: Cometary Radiants and the Connection of Meteors with Comets Kometnyye radianty i svyaz' meteorov s kometami). Izv. Astr. Obs. Odesskogo Un-ta, Vol.3, p.613, 1953.

207. Öpik, E.J.: Collision Probabilities with Planets and the Distribution of Interplanetary Matter. Proc. Roy. Irish Acad., Vol.54, Series A, No.12, p.165, 1951.

208. Cook, A.F.: A Criterion for Mode of Ablation of Stone Meteors. Smithsonian Contribs. Astrophys., Vol.4, No.17, p.69, 1963.

209. Dudnik, B.S.: Method of Measuring the Angular Coordinates of a Meteor Radio Echo (Metod izmereniya uglovykh koordinat meteornogo radioekho). Geofiz. Byull., No.17, p.62, 1966.

SUPPLEMENT

/218 (blank)

CATALOG OF ORBITS

/219

No. of meteor	Date	v_∞	α	δ	β	λ	a	e	q	i	Ω	ω	shower
8	03.14.21.49	21	168°	+06°	+01°	166°	1,94	0,63	0,71	000°	354°	254°	1
10	03.14.21.57	30	180	−03	−03	181	2,36	0,82	0,43	003	174	105	2
16	03.15.02.12	34	198	+03	+09	196	1,46	0,85	0,22	016	354	316	5
22	03.14.23.20	23	169	+03	−02	169	2,27	0,71	0,66	001	174	080	1
23	03.14.23.30	29	184	−00	+01	184	1,95	0,79	0,40	001	354	291	3
24	03.14.23.32	28	177	−06	−06	179	2,27	0,44	0,49	006	174	100	2
27	03.14.23.40	32	179	−03	−01	180	4,32	0,28	0,43	004	174	102	2
29	03.14.23.42	32	191	−01	+03	191	1,73	0,84	0,28	005	354	305	3
34	03.14.23.58	29	185	+07	+09	182	2,23	0,80	0,45	009	354	284	3
35	03.15.00.00	28	176	+00	−02	176	2,57	0,80	0,51	001	174	096	2
37	03.15.00.09	34	191	−08	−03	193	1,70	0,88	0,21	006	174	134	4
39	03.15.02.27	31	200	+03	+09	198	1,19	0,81	0,23	016	354	316	5
40	03.15.00.17	37	192	−08	−03	194	2,01	0,91	0,18	005	174	136	4
45	03.15.00.25	31	188	+00	+04	187	1,86	0,83	0,32	004	354	300	3
46	03.15.00.26	30	192	+01	+05	191	1,45	0,80	0,29	007	354	307	3
50	03.15.00.40	27	176	−08	−09	179	2,07	0,77	0,48	008	174	101	2
51	03.15.00.50	24	176	+07	+04	174	2,01	0,70	0,60	003	354	268	1
56	03.15.01.05	33	190	+01	+05	189	2,19	0,86	0,30	006	354	301	3
60	03.15.01.16	36	194	−10	−03	196	1,78	0,90	0,17	007	174	138	4
91	03.15.03.10	39	210	+09	+20	205	1,58	0,88	0,19	047	354	317	6
95	03.15.03.18	40	215	+08	+21	210	1,24	0,87	0,16	056	354	324	6
120	03.15.04.47	48	256	+33	+55	249	4,01	0,76	0,97	084	354	201	7
128	03.15.04.58	51	258	+31	+54	253	6,68	0,85	0,98	088	354	194	7
134	03.15.05.07	49	259	+31	+54	254	3,75	0,74	0,98	087	354	193	7
135	03.15.05.15	49	261	+33	+56	256	5,65	0,82	0,99	085	354	185	7
144	03.15.05.39	47	257	+36	+59	249	4,69	0,79	0,98	080	355	197	7
166	03.15.21.40	31	178	−10	−10	179	2,94	0,85	0,44	010	175	103	2
167	03.15.22.53	30	183	+06	+03	181	2,04	0,80	0,41	008	355	297	3
168	03.15.20.29	23	173	+01	−02	173	2,11	0,71	0,62	001	175	085	1
172	03.15.20.57	22	174	+00	−03	174	1,70	0,63	0,63	002	175	088	1
176	03.15.21.32	37	196	−09	−02	198	1,81	0,92	0,15	005	175	140	4
189	03.16.00.32	36	216	+10	+23	211	1,08	0,82	0,19	048	355	322	6
192	03.16.00.45	36	220	+09	+23	214	0,95	0,82	0,17	053	355	326	6
326	03.15.23.05	27	174	−00	+03	174	2,92	0,81	0,56	002	175	088	2
346	03.15.23.13	40	212	+12	+24	207	1,66	0,86	0,23	052	355	312	6
404	03.16.00.23	30	180	−10	−10	181	2,10	0,80	0,41	010	175	107	2
427	03.16.22.57	30	188	−02	+01	188	1,91	0,82	0,36	002	356	296	3
430	03.16.23.20	32	203	+05	+15	200	1,26	0,81	0,24	021	356	314	5
431	03.23.23.45	39	212	+05	+16	207	1,39	0,89	0,14	046	356	324	6
443	03.23.00.19	30	193	−01	+05	192	2,11	0,82	0,39	009	002	291	3
447	03.17.00.32	32	201	−03	+05	202	1,18	0,84	0,19	009	356	320	5
562	04.14.21.10	24	238	+02	+22	235	0,96	0,63	0,31	022	025	320	10
565	04.14.21.36	33	238	+05	+24	235	1,13	0,77	0,26	039	025	315	10
570	04.14.21.49	40	230	−15	+04	232	1,81	0,95	0,09	011	025	330	9
579	04.14.22.31	26	206	+05	+15	202	3,08	0,80	0,62	011	025	261	8
580	04.14.22.32	22	202	+07	+15	198	2,25	0,69	0,71	009	025	254	8
588	04.14.22.58	36	285	+27	+50	291	0,86	0,17	0,71	074	025	340	11
605	04.14.23.22	45	255	+20	+42	250	2,50	0,77	0,58	078	025	268	12
609	04.14.23.36	47	278	+11	+34	279	0,90	0,39	0,55	104	025	307	13
618	04.14.23.52	30	278	+26	+49	281	0,76	0,36	0,48	061	025	342	11
625	04.15.00.07	40	336	+16	+24	345	1,24	0,86	0,18	066	025	037	21
627	04.15.00.10	55	266	+06	+29	266	2,02	0,73	0,54	113	025	275	14
634	04.15.00.15	51	278	+06	+29	279	0,99	0,40	0,59	117	025	296	13
640	04.15.00.32	45	293	+14	+35	298	0,82	0,25	0,61	104	025	019	15
641	04.15.00.34	51	325	+10	+22	331	1,46	0,83	0,25	111	025	049	17
648	04.15.00.41	31	283	+27	+50	288	0,77	0,32	0,52	062	025	349	11
653	04.15.00.48	36	241	+05	+25	237	1,25	0,81	0,24	049	025	315	10
654	04.15.00.49	61	286	+10	+33	289	3,40	0,71	0,98	123	025	199	28
664	04.15.01.02	46	251	+19	+40	246	3,86	0,86	0,55	076	025	269	12
665	04.15.01.04	54	329	+08	+20	334	2,61	0,91	0,24	116	025	053	17

/220

Continuation

No. of meteor	Date	v_∞	α	δ	β	λ	a	e	q	i	Ω	ω	shower
671	04.15.01.15	37	285°	+26°	+48°	291°	0,85	0,19	0,70	076°	025°	342°	11
678	04.15.01.26	52	292	+16	+38	297	1,34	0,27	0,98	109	025	156	27
681	04.15.01.29	57	282	+14	+36	284	2,31	0,59	0,94	114	025	214	28
682	04.15.01.32	27	240	+05	+25	237	0,90	0,67	0,29	031	025	319	10
685	04.15.01.47	45	095	+14	+35	301	0,82	0,28	0,59	103	250	026	15
686	04.15.01.47	46	283	+05	+28	285	0,75	0,43	0,42	114	025	335	13
694	04.15.02.05	47	281	+07	+30	283	0,80	0,39	0,49	111	025	325	13
705	04.15.02.21	36	308	+23	+40	318	0,78	0,51	0,39	076	025	034	18
706	04.15.02.23	34	285	+27	+49	291	0,82	0,23	0,63	071	025	346	11
708	04.15.02.25	40	346	+30	+33	000	6,13	0,93	0,41	053	025	077	22
711	04.15.02.31	33	282	+28	+51	287	0,81	0,25	0,61	066	025	342	11
722	04.15.03.16	52	330	+07	+18	334	1,78	0,90	0,18	117	025	043	17
724	04.15.03.17	49	282	+08	+31	284	0,90	0,29	0,63	113	025	309	13
731	04.15.03.25	51	282	+04	+27	283	0,88	0,34	0,57	121	025	312	13
736	04.15.03.30	46	290	+17	+38	294	0,94	0,09	0,85	101	025	038	15
742	04.15.03.37	55	311	+01	+19	314	1,11	0,57	0,48	137	025	064	23
743	04.15.03.38	37	343	+20	+25	352	1,42	0,84	0,23	051	025	046	21
746	04.15.03.39	45	291	+14	+36	296	0,83	0,22	0,65	104	025	014	15
753	04.15.03.51	41	351	+07	+10	354	1,92	0,95	0,09	034	025	030	16
754	04.15.03.51	35	350	+07	+10	354	1,15	0,90	0,12	024	025	030	16
755	04.15.03.52	50	310	+19	+36	318	1,38	0,54	0,63	103	025	087	24
761	04.15.04.02	34	284	+28	+50	290	0,84	0,21	0,66	070	025	342	11
767	04.15.04.08	43	254	+22	+44	250	2,32	0,74	0,61	074	025	265	12
771	04.15.04.16	34	282	+27	+49	287	0,82	0,25	0,61	069	025	340	11
774	04.15.04.18	53	293	+14	+36	298	1,30	0,24	0,98	112	025	152	27
778	04.15.04.22	45	299	+14	+34	304	0,80	0,35	0,52	104	025	031	15
785	04.15.04.38	58	283	+17	+39	286	3,77	0,74	0,97	111	025	203	28
787	04.15.04.46	50	285	+02	+25	286	0,79	0,37	0,50	125	025	330	13
790	04.15.04.42	36	350	−00	+04	350	1,05	0,94	0,06	013	025	021	16
792	04.15.04.44	32	341	+18	+24	350	0,98	0,77	0,22	040	025	038	20
793	04.15.04.44	37	352	+01	+04	353	1,20	0,94	0,08	012	025	024	16
802	04.15.04.50	43	291	+19	+40	296	0,85	0,19	0,69	094	025	018	15
803	04.15.04.52	47	291	+13	+34	295	0,85	0,19	0,69	107	025	016	15
807	04.15.04.58	42	314	+21	+36	324	0,98	0,56	0,43	088	025	054	18
808	04.15.04.59	37	349	+10	+13	354	1,34	0,91	0,12	034	025	033	16
809	04.15.05.01	48	334	+24	+33	346	7,71	0,95	0,39	079	025	074	26
812	04.15.05.06	46	252	+19	+41	248	3,64	0,84	0,56	077	025	268	12
816	04.15.05.15	34	348	+11	+15	353	1,09	0,86	0,16	032	025	034	16
817	04.15.05.17	38	352	+07	+09	356	1,50	0,93	0,10	026	025	031	16
819	04.15.05.20	50	332	+13	+23	339	2,19	0,90	0,22	099	025	049	17
821	04.15.05.22	55	326	+08	+20	331	2,34	0,87	0,30	122	025	059	17
822	04.15.05.22	36	306	+23	+40	316	0,77	0,48	0,40	077	025	032	18
826	04.15.05.30	30	016	+03	−04	016	2,69	0,85	0,39	004	205	251	31
827	04.15.05.30	35	009	−05	−08	007	2,38	0,90	0,24	013	205	232	30
829	04.15.05.34	39	348	+11	+15	354	1,59	0,92	0,12	042	025	034	16
830	04.15.05.35	41	343	+29	+33	357	4,31	0,91	0,39	057	025	074	22
831	04.15.05.36	26	006	+11	+07	009	1,30	0,71	0,37	007	025	059	25
832	04.15.05.40	60	291	+07	+29	294	1,87	0,47	1,00	127	025	191	28
834	04.15.05.42	40	354	+04	+06	356	1,83	0,96	0,08	021	025	028	16
836	04.15.05.46	29	013	+06	+01	014	1,99	0,81	0,38	070	025	067	31
841	04.15.05.53	41	340	+30	+35	356	3,49	0,88	0,42	058	025	077	22
842	04.15.05.58	43	345	+25	+29	357	5,58	0,94	0,33	057	025	068	22
843	04.15.06.02	30	001	+05	+04	003	1,28	0,82	0,24	006	025	045	19
847	04.15.06.05	43	353	+03	+06	354	2,33	0,98	0,06	027	025	024	16
848	04.15.06.07	51	309	+16	+33	317	1,24	0,51	0,60	109	025	080	24
849	04.15.06.08	47	340	+23	+29	352	22,52	0,99	0,31	072	025	067	26
851	04.15.06.14	60	288	+07	+29	291	2,00	0,51	0,98	127	025	020	28
855	04.15.06.25	29	359	+03	+04	000	1,08	0,80	0,22	005	025	040	19
857	04.15.06.26	38	352	+01	+04	353	1,36	0,95	0,07	015	025	024	16
859	04.15.06.28	36	359	−01	−00	359	1,50	0,92	0,13	042	205	214	19

Continuation

No. of meteor	Date	v_∞	α	δ	β	λ	a	e	q	i	Ω	ω	shower
862	04.15.06.29	45	339°	+25°	+32°	351°	4,45	0,92	0,35	069°	025°	069°	26
863	04.15.06.31	34	350	+04	+08	352	1,03	0,90	0,11	020	025	027	16
865	04.15.06.34	39	340	+21	+27	350	1,49	0,83	0,25	058	025	049	21
866	04.15.06.34	30	005	—01	—03	004	1,30	0,81	0,24	004	205	226	19
868	04.15.06.35	41	309	+20	+38	318	0,85	0,49	0,43	087	025	044	18
869	04.15.06.35	34	344	+13	+18	351	1,05	0,86	0,15	039	025	033	16
871	04.15.06.40	46	291	+18	+39	296	0,93	0,11	0,82	100	025	037	15
872	04.15.06.43	37	348	+11	+15	353	1,34	0,90	0,13	039	025	039	16
877	04.15.06.48	35	012	—05	—09	009	2,98	0,91	0,27	014	205	237	30
879	04.15.06.52	40	349	—01	+04	349	1,21	0,97	0,03	017	025	016	16
880	04.15.06.52	25	008	+11	+07	011	1,32	0,69	0,40	006	025	063	25
881	04.15.06.54	35	350	+08	+12	354	1,18	0,90	0,12	028	025	031	16
882	04.15.06.55	40	302	+23	+42	311	0,86	0,35	0,56	085	025	044	18
887	04.15.07.17	35	355	+10	+12	359	1,44	0,88	0,17	023	025	010	16
888	04.15.07.21	41	354	+02	+04	355	1,93	0,97	0,06	017	025	025	16
890	04.15.07.31	36	350	—01	+03	350	1,05	0,94	0,06	010	025	020	16
892	04.15.07.43	39	349	+04	+08	351	1,30	0,95	0,06	030	025	022	16
896	04.15.07.57	41	348	+05	+10	351	1,49	0,96	0,06	039	025	024	16
897	04.15.07.57	51	316	+15	+30	324	1,43	0,67	0,47	108	025	071	24
900	04.15.23.42	41	233	—17	+02	235	1,85	0,97	0,06	007	026	336	9
901	04.15.23.58	35	232	—16	+02	233	1,23	0,90	0,13	005	026	328	9
903	04.16.00.19	42	238	—19	+01	240	1,42	0,93	0,03	005	026	345	9
905	04.16.00.32	43	232	—21	—03	235	2,27	0,97	0,06	011	206	155	9
916	04.16.23.47	41	232	—20	—01	235	2,05	0,97	0,07	003	207	153	9
919	04.17.00.46	35	238	—18	+02	240	1,02	0,92	0,08	005	027	337	9
931	04.17.03.27	60	283	+05	+27	285	2,10	0,58	0,88	129	027	228	28
942	04.17.04.14	50	286	+06	+28	289	1,71	0,45	0,93	127	027	219	28
953	04.17.04.53	35	285	+23	+46	290	0,77	0,32	0,53	074	027	345	11
962	04.17.05.29	45	299	+13	+33	305	0,80	0,33	0,54	106	027	090	15
966	04.17.05.37	59	312	+00	+17	315	1,39	0,57	0,59	143	027	083	23
971	04.17.06.03	57	313	+02	+19	316	1,22	0,56	0,54	137	027	073	23
972	04.17.06.26	51	325	+05	+17	329	1,12	0,82	0,20	125	027	040	17
989	04.17.19.53	24	211	+03	+15	208	1,88	0,67	0,61	010	028	268	8
993	04.17.20.17	28	234	+03	+22	231	1,11	0,69	0,34	025	028	308	10
994	04.17.20.21	26	208	—01	+09	206	2,93	0,80	0,59	007	028	266	8
1000	04.17.20.44	23	214	+09	+21	209	1,80	0,65	0,63	014	028	266	8
1003	04.17.21.04	22	207	+09	+19	202	2,18	0,68	0,70	011	028	255	8
1008	04.17.21.20	20	186	—05	+03	188	3,43	0,76	0,81	000	208	056	33
1016	04.17.21.45	25	208	+04	+15	205	2,85	0,78	0,63	011	028	261	8
1017	04.17.21.45	25	208	+05	+15	204	3,03	0,79	0,64	011	028	260	8
1023	04.17.22.06	27	246	+06	+28	243	0,86	0,66	0,29	034	028	322	10
1028	04.17.22.15	23	206	+01	+11	204	2,09	0,68	0,66	007	028	261	8
1042	04.17.22.39	21	185	—05	—02	187	4,72	0,83	0,81	001	208	055	33
1043	04.17.22.40	54	299	+25	+45	309	3,84	0,75	0,96	101	028	152	34
1047	04.17.22.54	29	241	+03	+24	238	1,00	0,72	0,28	038	028	317	10
1050	04.17.23.08	23	208	+10	+20	202	2,24	0,69	0,70	012	028	255	8
1055	04.18.00.22	59	284	+08	+30	287	2,15	0,58	0,91	124	028	222	28
1057	04.18.00.27	41	240	—21	—01	243	1,31	0,98	0,03	005	208	164	9
1059	04.18.00.35	61	291	+08	+30	294	2,62	0,62	0,99	127	028	196	28
1061	04.18.00.40	51	272	+05	+28	273	1,18	0,60	0,48	114	028	294	14
1067	04.18.01.02	21	282	—01	+22	283	0,58	0,74	0,15	027	028	355	9
1075	04.18.01.18	33	287	+27	+49	293	0,79	0,29	0,56	067	028	349	11
1076	04.18.01.32	45	256	+21	+44	252	3,08	0,80	0,62	075	028	262	12
1084	04.18.01.49	55	267	+02	+25	267	1,79	0,76	0,43	117	028	280	14
1085	04.18.01.50	60	321	+04	+18	325	2,88	0,83	0,49	139	028	082	23
1086	04.18.01.50	49	312	+14	+30	319	1,05	0,51	0,51	110	028	064	24
1095	04.18.02.19	48	295	+12	+33	299	0,89	0,15	0,75	111	028	027	15
1107	04.18.03.43	52	296	+16	+37	301	1,28	0,24	0,97	110	028	148	27
1108	04.18.04.00	49	272	+07	+30	273	1,10	0,56	0,48	108	028	296	14
1119	04.18.04.52	39	351	+11	+14	356	1,52	0,93	0,11	040	028	032	16

Continuation

No. of meteor	DATE	v_∞	α	δ	β	λ	a	e	q	i	Ω	ω	shower
1120	04.18.04.53	37	306°	+20°	+38°	314°	0,74	0,49	0,37	083°	028°	025°	18
1123	04.18.04.55	53	336	+05	+14	340	2,57	0,95	0,13	122	028	038	17
1126	04.18.05.02	32	002	+05	+04	003	1,31	0,86	0,18	007	028	039	19
1128	04.18.05.07	50	311	+13	+30	318	1,07	0,49	0,54	113	028	067	24
1140	04.18.05.32	50	312	+17	+33	320	1,04	0,50	0,52	104	028	064	24
1141	04.18.05.33	30	007	+01	−01	007	1,30	0,81	0,24	002	208	226	19
1145	04.18.19.50	26	210	+07	+18	206	3,04	0,79	0,64	013	029	260	8
1149	04.18.20.59	20	210	+04	+15	207	1,56	0,56	0,69	008	029	263	8
1162	04.18.21.58	23	212	+10	+22	206	2,15	0,69	0,67	014	029	259	8
1183	04.18.23.50	30	304	+02	+21	306	0,54	0,87	0,07	066	029	003	9
1226	04.19.01.40	43	298	+20	+40	305	0,87	0,22	0,67	094	029	037	15
1234	04.19.02.15	39	356	+14	+14	002	2,01	0,92	0,16	034	029	041	16
1237	04.19.02.20	43	245	+08	+29	241	2,76	0,89	0,30	063	029	299	26
1242	04.19.02.32	39	309	+15	+32	316	0,70	0,58	0,29	093	029	023	18
1244	04.19.02.36	33	285	+25	+47	290	0,76	0,34	0,50	069	029	345	11
1246	04.19.02.44	52	272	+10	+34	273	1,52	0,60	0,60	106	029	274	14
1251	04.19.03.00	50	295	+16	+37	301	1,09	0,12	0,96	108	029	125	27
1254	04.19.03.08	42	301	+17	+36	307	0,78	0,36	0,50	097	029	026	15
1255	04.19.03.10	59	288	+08	+30	290	1,84	0,49	0,94	124	029	217	28
1258	04.19.03.16	49	312	+15	+31	319	1,00	0,48	0,52	109	029	061	24
1259	04.19.03.19	46	283	+06	+29	284	0,77	0,47	0,41	111	029	328	13
1265	04.19.03.26	35	352	+10	+12	357	1,13	0,89	0,12	028	029	031	16
1280	04.19.04.12	56	293	+15	+36	298	1,69	0,41	1,00	115	029	194	28
1281	04.19.04.14	45	294	+14	+35	299	0,80	0,26	0,60	104	029	012	15
1284	04.19.04.20	40	353	+03	+05	355	1,41	0,07	0,04	025	029	019	16
1287	04.19.04.21	59	294	+17	+38	300	1,46	0,32	0,99	110	029	162	27
1288	04.19.04.22	52	332	+11	+20	338	1,92	0,89	0,92	111	029	048	17
1291	04.19.04.25	34	011	+01	−04	010	2,09	0,89	0,22	006	209	229	19
1292	04.19.04.31	51	334	+09	+19	339	1,66	0,89	0,17	111	029	042	17
1294	04.19.04.32	59	295	+02	+23	297	1,33	0,25	0,99	136	029	202	34
1299	04.19.04.37	37	350	+14	+17	357	1,30	0,88	0,15	040	029	036	16
1304	04.19.04.50	64	293	−02	+19	294	2,17	0,55	0,98	145	029	202	29
1306	04.19.04.54	33	347	+20	+24	357	1,12	0,79	0,23	041	029	042	20
1307	04.19.05.01	40	359	+07	+07	001	2,05	0,95	0,10	021	029	032	16
1308	04.19.05.02	43	341	+22	+28	352	2,07	0,87	0,26	069	029	054	21
1315	04.19.05.19	34	347	+08	+12	351	0,92	0,90	0,10	033	029	024	16
1316	04.19.05.20	27	023	+11	+01	025	2,65	0,81	0,49	084	029	082	35
1321	04.19.05.47	36	359	+01	+01	000	1,40	0,93	0,10	004	029	030	16
1323	04.19.05.49	37	353	−02	+01	353	1,06	0,96	0,04	003	029	018	16
1324	04.19.06.00	40	355	+14	+15	002	2,39	0,94	0,15	039	029	041	16
1325	04.19.06.08	56	316	+12	+27	323	1,76	0,67	0,58	121	029	088	24
1328	04.19.06.25	32	345	+16	+21	352	0,94	0,81	0,17	040	029	033	20
1330	04.19.06.40	51	303	+23	+42	312	1,65	0,46	0,89	101	029	130	34
1331	04.19.06.40	35	358	+05	+06	000	1,30	0,91	0,11	014	029	031	16
1334	04.19.06.44	30	004	+06	+04	006	1,25	0,82	0,22	006	029	043	19
1325	04.19.06.48	28	008	+05	+02	010	1,29	0,78	0,29	192	029	051	19
1336	04.19.06.49	34	346	+16	+20	354	1,04	0,83	0,18	041	029	035	20
1340	04.19.07.00	29	020	+13	+04	023	2,75	0,84	0,45	004	029	078	35
1344	04.19.07.10	35	353	+11	+13	358	1,20	0,89	0,13	031	029	033	16
1345	04.19.07.14	28	009	−05	−08	006	1,12	0,76	0,27	010	209	225	30
1346	04.19.07.20	56	318	+06	+21	323	1,33	0,66	0,46	132	029	068	23
1347	04.19.07.20	43	348	+21	+24	358	3,42	0,23	0,23	059	029	054	21
1349	04.19.07.22	24	018	+04	−03	018	1,39	0,68	0,44	003	209	247	31
1351	04.19.07.28	31	009	+07	+03	011	1,57	0,83	0,27	004	029	052	19
1352	04.19.07.31	28	005	+02	−00	005	1,09	0,78	0,24	000	209	222	19
1357	04.19.07.40	38	350	+07	+10	353	1,16	0,94	0,07	037	029	023	16
1358	04.19.07.42	36	341	+18	+24	349	1,03	0,83	0,18	056	029	035	21
1359	04.19.07.46	34	358	+11	+11	002	1,36	0,88	0,17	023	029	038	16
1363	04.19.07.51	34	006	+03	+01	007	1,63	0,89	0,18	002	029	042	19
1364	04.19.08.05	27	020	−00	−08	018	1,75	0,77	0,41	008	209	248	31

Continuation

No. of meteor	DATE	v_∞	α	δ	β	λ	a	e	q	i	Ω	ω	shower
1367	04.19.08.15	31	013°	−04°	−09°	010°	1,57	0,82	0,28	013°	209°	233°	30
1371	04.19.08.22	34	350	+05	+09	353	0,94	0,91	0,09	023	029	023	16
1372	04.19.08.23	28	018	+08	−00	019	1,98	0,80	0,40	000	209	250	31
1373	04.19.08.23	36	357	+08	+09	000	1,36	0,91	0,12	021	029	032	16
1374	04.19.08.25	30	005	+02	+00	006	1,22	0,83	0,21	000	029	042	19
1375	04.19.08.26	34	007	−01	−04	006	1,56	0,88	0,18	007	209	221	19
1376	04.19.08.27	27	024	+08	−02	025	2,41	0,79	0,50	001	209	262	35
1379	04.19.08.50	33	355	+11	+12	000	1,18	0,86	0,16	025	029	036	16
1383	04.19.09.10	33	352	+05	+08	355	0,97	0,90	0,10	020	029	025	16
1384	04.19.09.14	26	021	+11	+02	023	2,04	0,77	0,48	002	029	078	35
1385	04.19.09.16	25	015	+12	+05	018	1,43	0,69	0,44	001	029	068	25
1389	04.19.09.36	26	013	+04	−02	014	1,29	0,72	0,37	002	209	238	31
1397	04.19.10.06	42	345	+28	+32	358	3,43	0,90	0,36	061	029	069	22
1398	04.19.10.10	38	349	+27	+30	001	2,15	0,84	0,34	050	029	063	22
1400	04.19.10.13	28	012	−04	−08	009	1,26	0,77	0,29	010	209	230	30
1401	04.19.10.14	28	015	−02	−07	013	1,47	0,77	0,33	008	209	238	30
1402	04.19.10.18	34	352	+14	+16	358	1,13	0,86	0,16	032	029	035	16
1404	04.19.10.25	34	006	+05	+02	008	1,73	0,89	0,19	004	029	044	19
1406	04.19.10.26	35	357	+06	+07	360	1,28	0,91	0,11	017	029	031	16
1407	04.19.10.29	35	356	+12	+13	001	1,36	0,89	0,16	027	029	037	16
1409	04.19.10.37	33	003	+04	+02	005	1,32	0,87	0,17	004	029	039	19
1411	04.19.10.38	32	006	−00	−02	005	1,27	0,85	0,19	004	209	220	19
1416	04.19.10.53	24	017	+04	−02	017	1,35	0,68	0,43	002	209	245	31
1425	04.19.11.36	39	340	+18	+24	350	1,23	0,85	0,19	064	029	039	21
1429	04.19.11.46	33	010	+00	−04	010	1,85	0,88	0,22	007	209	229	19
1430	04.19.11.54	25	022	+08	−01	023	1,83	0,73	0,48	001	209	257	35
1431	04.19.11.57	27	023	+07	−03	024	2,47	0,81	0,40	002	209	259	35
1433	04.19.12.34	33	349	+09	+12	354	0,96	0,89	0,11	030	029	026	16
1444	04.19.22.06	38	239	−16	+04	240	1,38	0,94	0,08	014	030	334	9
1457	04.19.22.52	30	242	+07	+27	238	1,11	0,71	0,33	036	030	309	10
1464	04.19.23.05	46	261	+18	+41	259	2,36	0,75	0,59	082	030	268	12
1469	04.19.23.17	50	260	+22	+45	257	4,80	0,86	0,66	080	030	254	12
1482	04.19.23.48	49	287	+09	+32	290	0,88	0,28	0,63	112	029	313	13
1483	04.19.23.48	55	289	+14	+36	292	1,65	0,42	0,96	114	030	212	28
1487	04.20.00.08	35	235	+04	+23	232	1,84	0,83	0,31	036	030	301	10
1506	04.20.01.37	37	342	+22	+27	353	1,18	0,80	0,23	056	030	043	21
1508	04.20.01.45	54	285	+15	+37	288	1,73	0,47	0,91	110	030	225	28
1511	04.20.01.53	56	292	+10	+31	296	1,33	0,27	0,98	121	030	210	28
1512	04.20.01.57	54	289	+12	+34	293	1,30	0,28	0,94	116	030	225	28
1519	04.20.02.22	51	274	+06	+29	275	1,15	0,57	0,49	111	030	294	14
1525	04.20.02.38	34	247	+06	+28	243	1,11	0,75	0,27	047	030	314	10
1532	04.20.02.53	39	350	+18	+20	358	1,59	0,88	0,18	048	030	042	21
1533	04.20.03.00	38	308	+16	+34	316	0,70	0,56	0,31	089	030	022	18
1535	04.20.03.01	47	271	+33	+57	272	7,86	0,88	0,92	079	030	215	32
1544	04.20.03.45	54	302	+23	+42	311	2,44	0,61	0,94	104	030	146	34
1548	04.20.04.15	57	289	+14	+36	293	2,20	0,56	0,97	115	030	205	28
1550	04.20.04.30	35	354	+13	+14	360	1,29	0,89	0,15	032	030	035	16
1551	04.20.04.39	35	004	+08	+07	005	1,66	0,90	0,17	011	030	041	19
1559	04.20.05.16	35	349	+11	+15	354	1,02	0,89	0,12	037	030	028	16
1564	04.20.05.25	27	017	+04	−02	017	1,59	0,77	0,37	003	210	243	31
1565	04.20.05.31	33	016	−02	−08	014	2,30	0,88	0,28	011	210	237	30
1567	04.20.06.17	62	298	−01	+20	300	1,65	0,40	1,00	144	030	194	29
1571	04.20.06.25	35	359	+10	+09	003	1,40	0,89	0,15	020	030	037	16
1572	04.20.06.26	30	008	+12	+08	012	1,52	0,81	0,29	011	030	057	25
1573	04.20.06.43	41	353	+06	+08	356	1,62	0,97	0,05	037	030	022	16
1574	04.20.06.47	39	343	+15	+20	350	1,14	0,88	0,13	061	030	032	21
1579	04.20.06.57	38	356	+02	+03	357	1,28	0,96	0,05	013	030	021	16
1580	04.20.07.00	31	011	+01	−03	011	1,49	0,83	0,25	004	210	229	19
1582	04.20.07.09	43	344	+27	+31	357	3,43	0,90	0,34	064	030	067	22
1588	04.20.07.16	29	018	+08	+01	020	2,19	0,82	0,39	001	030	069	31

Continuation

No. of meteor	DATE	v_∞	α	δ	β	λ	a	e	q	i	Ω	ω	shower
1591	04.20.07.18	29	019°	+08°	+00°	021°	2,31	0,83	0,40	040°	030°	071°	31
1593	04.20.07.20	49	326	+10	+22	332	1,10	0,78	0,24	113	030	043	17
1595	04.20.07.28	40	354	+04	+06	356	1,38	0,97	0,05	028	030	020	16
1596	04.20.07.30	32	006	−02	−04	005	1,23	0,86	0,18	007	210	218	19
1599	04.20.07.34	37	355	+04	+05	356	1,19	0,94	0,07	018	030	023	16
1600	04.20.07.34	39	354	+07	+08	357	1,36	0,95	0,07	028	030	025	16
1601	04.20.07.40	37	336	+18	+26	345	0,93	0,80	0,18	063	030	033	21
1605	04.20.07.40	40	344	+17	+22	352	1,29	0,88	0,16	061	030	037	21
1608	04.20.07.42	37	358	+01	+02	358	1,26	0,94	0,07	007	030	024	16
1610	04.20.07.44	30	345	+12	+13	351	0,83	0,83	0,14	034	030	026	16
1612	04.20.07.52	29	011	+01	−03	011	1,39	0,81	0,27	004	210	230	19
1614	04.20.07.53	40	001	+09	+08	004	2,50	0,95	0,12	022	030	036	16
1615	04.20.07.56	36	347	+08	+13	351	0,97	0,92	0,08	042	030	022	16
1622	04.20.08.37	33	348	+10	+14	353	0,92	0,88	0,11	034	030	025	16
1623	04.20.08.38	30	021	+08	−01	023	3,34	0,88	0,41	001	210	255	35
1625	04.20.08.51	26	020	+09	+01	022	1,74	0,74	0,46	001	030	073	35
1626	04.20.08.52	34	349	+06	+10	352	0,90	0,91	0,08	029	030	021	16
1635	04.20.09.12	30	023	+12	+02	026	4,39	0,90	0,45	002	030	081	35
1636	04.20.09.12	38	007	+01	−02	007	2,26	0,94	0,14	004	210	219	16
1639	04.20.09.18	29	004	+08	+06	007	1,16	0,80	0,24	008	030	043	19
1642	04.20.09.30	27	023	+06	−03	023	2,02	0,77	0,46	003	210	256	35
1643	04.20.09.33	23	014	+09	+02	016	1,17	0,63	0,43	001	030	062	25
1645	04.20.07.17	31	016	+11	+04	018	2,65	0,86	0,36	005	030	067	25
1650	04.20.10.15	29	004	+04	+02	006	1,13	0,81	0,21	003	030	011	19
1651	04.20.10.16	29	011	+07	+02	013	1,48	0,86	0,20	003	030	054	19
1653	04.20.10.18	35	013	+07	+10	354	1,02	0,92	0,08	030	030	024	16
1654	04.20.10.18	39	359	+10	+10	004	2,11	0,94	0,12	026	030	036	16
1658	04.20.10.23	23	023	+10	+01	025	1,63	0,68	0,52	001	030	079	35
1660	04.20.10.26	26	010	+12	+07	014	1,33	0,73	0,36	007	030	058	25
1664	04.20.10.34	39	351	+11	+14	356	1,31	0,92	0,10	043	030	029	16
1665	04.20.10.44	28	014	+11	+05	017	1,65	0,78	0,36	006	030	063	25
1671	04.20.10.52	27	010	−01	−05	009	1,14	0,74	0,29	005	210	228	19
1673	04.20.10.57	27	011	+07	+01	013	1,29	0,75	0,33	002	030	055	25
1676	04.20.11.06	42	345	+18	+23	354	1,65	0,89	0,18	065	030	042	21
1680	04.20.11.13	38	358	+10	+10	002	1,65	0,93	0,12	026	030	034	16
1681	04.20.11.14	26	013	+04	−01	014	1,27	0,73	0,35	001	210	236	19
1683	04.20.11.17	37	008	+04	+01	009	2,32	0,93	0,17	001	030	043	19
1689	04.20.12.16	27	017	+02	−05	016	1,48	0,75	0,36	005	210	241	31
1691	04.20.12.20	25	021	+15	+05	025	1,79	0,71	0,51	004	030	080	35
1694	04.20.12.53	37	358	−00	+01	358	1,20	0,94	0,07	002	030	023	16
1715	04.20.23.42	21	209	+07	+18	204	1,96	0,63	0,72	010	031	254	8
1717	04.20.23.47	25	241	+01	+21	238	0,91	0,65	0,32	022	031	317	10
1736	04.21.21.40	22	188	−04	−00	189	25,68	0,97	0,81	000	212	053	33
1764	04.22.02.42	55	272	+06	+29	273	2,08	0,74	0,54	113	032	275	14
1773	04.22.09.30	40	345	+24	+28	356	1,65	0,84	0,26	062	032	052	21
1774	04.22.09.30	40	345	+23	+27	356	1,58	0,84	0,25	062	032	050	21
1775	04.22.09.37	34	354	+12	+14	359	1,09	0,88	0,13	031	032	031	16
1779	04.22.10.12	29	008	−01	−04	007	1,10	0,80	0,22	005	212	220	19
1780	04.22.10.14	26	019	+05	−02	019	1,47	0,73	0,39	002	212	244	31
1781	04.22.10.18	32	008	−00	−04	008	1,29	0,86	0,19	006	212	220	19
1784	04.22.20.37	26	189	−05	−01	344	−6,28	1,12	0,78	001	212	040	33
1788	04.22.10.37	28	020	+08	−00	022	1,83	0,78	0,40	000	212	249	31
1789	04.22.10.38	28	023	+01	−08	021	1,92	0,79	0,40	008	212	249	31
1790	04.22.10.45	32	005	+07	+05	007	1,27	0,86	0,18	008	032	039	19
1792	04.22.10.52	25	008	+08	+04	010	1,05	0,71	0,30	004	032	047	19
1793	04.22.10.54	33	011	+13	+08	015	2,09	0,87	0,27	012	032	055	25
1796	04.22.12.01	42	344	+23	+28	355	1,79	0,86	0,25	067	032	052	21
1808	04.22.12.43	28	025	+07	−03	026	2,39	0,81	0,45	003	212	256	35
1848	04.23.00.28	36	238	−17	+03	240	1,32	0,91	0,12	006	033	328	9
1850	04.23.00.38	45	255	+21	+43	251	5,12	0,88	0,59	071	033	263	12

Continuation

No. of meteor	DATE	v_∞	α	δ	β	λ	a	e	q	i	Ω	ω	shower
1851	04.23.00.45	40	241°	—17°	+04°	242°	1,71	0,96	0,07	014°	033°	340°	9
1867	04.24.09.55	39	353	+29	+29	006	2,42	0,86	0,33	051	034	063	22
1902	04.25.07.55	41	357	+00	+01	358	1,26	0,99	0,02	009	035	012	16
1908	04.25.08.19	41	358	+14	+13	004	1,90	0,94	0,11	042	035	033	16
1921	04.25.10.16	29	005	+07	+04	008	1,05	0,82	0,19	007	035	037	19
1926	04.25.10.40	37	356	+12	+12	001	1,21	0,92	0,10	036	035	028	16
1928	04.25.10.47	32	019	+00	—07	017	1,92	0,86	0,26	010	215	234	30
1930	04.25.10.48	28	020	+04	—04	020	1,46	0,76	0,34	005	215	239	31
1931	04.25.10.53	33	014	+09	+03	017	1,87	0,87	0,25	004	035	051	25
1932	04.25.12.02	33	015	+04	—02	015	1,73	0,87	0,23	003	215	228	19
1940	04.26.00.59	39	246	—21	+00	248	1,26	0,96	0,06	001	036	339	9
1942	04.26.01.29	33	248	+01	+23	246	1,16	0,79	0,24	039	036	316	10
1973	04.26.04.06	60	294	+11	+32	298	2,60	0,63	0,96	123	036	209	28
1994	05.03.20.53	32	277	+30	+53	280	1,04	0,33	0,70	059	013	284	36
1995	05.03.20.59	31	292	+24	+45	299	0,73	0,42	0,42	065	043	342	38
2000	05.03.21.47	34	286	+26	+49	291	0,88	0,32	0,60	068	043	313	37
2002	05.03.22.01	33	283	+27	+50	288	0,90	0,33	0,60	065	043	309	37
2009	05.04.08.35	37	018	+11	+04	021	2,24	0,93	0,15	008	044	040	48
2010	05.04.08.36	27	021	+15	+06	025	1,27	0,75	0,31	007	044	053	39
2012	05.04.08.40	29	023	+17	+07	027	1,56	0,79	0,32	009	044	057	42
2019	05.04.08.44	28	018	+16	+07	022	1,23	0,78	0,27	010	044	048	39
2021	05.04.08.45	29	023	+14	+04	027	1,48	0,79	0,31	004	044	055	42
2028	05.04.09.12	32	027	+09	—02	028	2,11	0,86	0,29	002	224	237	41
2032	05.04.09.17	41	010	+16	+11	015	2,29	0,96	0,10	034	044	033	47
2039	05.04.09.28	30	023	+13	+03	027	1,58	0,82	0,29	004	044	054	42
2045	05.04.09.34	31	027	+08	—03	028	1,88	0,84	0,29	004	224	237	41
2046	05.04.09.34	25	022	+15	+05	026	1,16	0,70	0,35	005	044	054	39
2047	05.04.09.34	23	014	+19	+12	020	0,96	0,64	0,34	010	044	047	39
2054	05.04.11.50	44	009	+13	+08	014	3,11	0,98	0,06	035	044	027	49
2055	05.04.11.51	38	006	+16	+12	012	1,38	0,92	0,11	035	044	031	16
2056	05.04.19.05	54	294	+22	+43	301	2,95	0,68	0,94	102	044	214	46
2065	05.04.20.33	34	284	+20	+42	288	0,78	0,48	0,41	069	044	327	51
2069	05.04.20.42	33	302	+36	+55	317	0,91	0,15	0,77	065	044	038	43
2116	05.04.22.28	31	277	+28	+51	280	0,94	0,35	0,61	056	044	301	36
2138	05.04.22.56	33	274	128	+51	276	1,09	0,40	0,65	060	044	283	53
2139	05.04.22.57	36	291	+31	+52	300	0,98	0,19	0,79	071	044	291	37
2143	05.04.23.03	37	288	+30	+52	295	1,07	0,25	0,80	073	044	270	37
2146	05.04.23.05	35	290	+29	+51	299	0,91	0,23	0,70	070	044	308	37
2148	05.04.23.08	31	291	+30	+52	300	0,83	0,28	0,59	061	044	331	37
2149	05.04.23.09	30	289	+30	+52	297	0,82	0,30	0,57	059	044	329	37
2156	05.04.23.14	37	292	+28	+49	301	0,93	0,22	0,72	075	044	305	37
2157	05.04.23.16	34	277	+22	+45	279	0,95	0,46	0,51	065	044	304	50
2164	05.04.23.28	34	303	+34	+52	318	0,90	0,16	0,75	069	044	037	43
2169	05.04.23.35	32	283	+30	+53	289	0,95	0,29	0,68	062	044	298	36
2172	05.04.23.29	33	293	+30	+51	303	0,83	0,26	0,62	066	044	332	37
2176	05.04.23.47	32	282	+24	+47	286	0,84	0,41	0,50	063	044	318	51
2177	05.04.23.47	36	286	+27	+49	293	0,96	0,29	0,68	072	044	297	37
2178	05.04.23.47	32	266	+15	+39	266	1,01	0,60	0,40	054	044	307	52
2191	05.05.00.12	34	286	+29	+51	293	0,92	0,28	0,66	066	044	304	37
2198	05.05.00.15	32	299	+24	+43	307	0,71	0,44	0,39	070	044	350	38
2202	05.05.00.17	36	278	+24	+47	281	1,03	0,43	0,59	068	044	293	50
2205	05.05.00.24	32	297	+26	+46	306	0,75	0,37	0,47	069	044	345	38
2206	05.05.00.24	35	297	+25	+45	306	0,77	0,35	0,50	075	044	342	38
2217	05.05.00.45	34	267	+11	+35	267	0,98	0,66	0,33	057	044	313	52
2220	05.05.06.46	61	302	+13	+32	308	3,17	0,69	0,97	123	044	204	59
2224	05.05.00.50	53	283	+11	+34	285	2,21	0,72	0,61	106	044	267	58
2226	05.05.00.50	30	270	+24	+48	270	0,99	0,44	0,55	052	044	299	53
2227	05.05.00.56	37	269	+03	+26	269	0,93	0,80	0,19	065	044	326	67
2229	05.05.00.57	30	265	+10	+33	265	0,88	0,65	0,31	046	044	320	52
2232	05.05.01.03	35	295	+25	+46	304	0,79	0,33	0,52	073	044	338	38

Continuation

No. of meteor	DATE	v_∞	α	δ	β	λ	a	e	q	i	Ω	ω	Shower
2233	05.05.01.03	62	302°	+10°	+29°	307°	3,36	0,71	0,96	127°	044°	207°	59
2235	05.05.01.05	32	304	+36	+54	320	0,86	0,21	0,68	063	044	030	43
2238	05.05.01.08	50	310	+21	+38	319	1,19	0,21	0,94	107	044	127	56
2239	05.05.01.13	31	312	+38	+53	330	0,86	0,27	0,62	061	044	039	43
2242	05.05.01.16	34	287	+22	+44	292	0,82	0,41	0,48	071	044	323	51
2243	05.05.01.16	60	300	+08	+28	304	2,17	0,58	0,91	127	044	222	59
2244	05.05.01.17	58	318	+21	+35	329	3,44	0,74	0,88	115	044	135	63
2252	05.05.01.20	31	304	+36	+53	320	0,85	0,22	0,67	063	044	027	43
2261	05.05.01.28	65	337	−00	+09	338	4,59	0,88	0,57	162	044	004	65
2263	05.05.01.29	56	296	+22	+43	303	5,52	0,83	0,96	105	044	207	46
2269	05.05.01.36	59	303	+12	+31	309	1,93	0,50	0,97	123	044	207	59
2275	05.05.01.39	35	285	+28	+51	291	1,00	0,29	0,70	060	044	289	37
2292	05.05.02.05	58	317	+13	+28	324	1,52	0,42	0,88	127	044	124	44
2293	05.05.02.11	54	323	+23	+35	334	1,94	0,61	0,76	110	044	110	63
2294	05.05.02.15	54	280	+09	+32	281	2,69	0,80	0,53	105	044	023	58
2295	05.05.02.15	56	283	+13	+35	286	5,59	0,88	0,70	108	044	250	58
2297	05.05.02.16	62	334	+02	+11	337	2,53	0,78	0,56	156	044	089	65
2298	05.05.02.17	66	335	+02	+12	337	29,40	0,98	0,63	156	044	104	65
2301	05.05.02.20	53	284	+08	+31	286	1,74	0,69	0,54	110	044	278	58
2306	05.05.02.22	62	308	+01	+19	311	1,61	0,39	0,98	145	044	207	60
2309	05.05.02.26	51	303	+23	+42	313	1,50	0,34	0,99	103	044	202	62
2319	05.05.03.39	59	323	+13	+26	330	1,89	0,58	0,78	129	045	013	64
2323	05.05.03.40	63	335	+01	+11	338	3,01	0,82	0,53	156	045	087	65
2325	05.05.03.44	67	335	−01	−09	337	15,12	0,96	0,62	162	045	102	65
2326	05.05.03.45	39	007	+15	+11	013	1,56	0,94	0,09	036	045	029	47
2329	05.05.03.59	37	005	+20	+16	013	1,42	0,90	0,15	041	045	036	45
2334	05.05.04.09	65	336	−00	+09	338	4,47	0,87	0,56	160	045	093	65
2335	05.05.04.09	33	358	+19	+18	006	0,90	0,85	0,13	042	045	028	55
2342	05.05.04.13	35	358	+18	+18	006	0,95	0,87	0,12	045	045	027	55
2343	05.05.04.15	62	337	+02	+10	339	2,48	0,81	0,47	156	045	079	65
2345	05.05.04.21	56	301	−02	+18	302	0,99	0,37	0,62	142	045	295	55
2347	05.05.04.29	54	322	+12	+25	328	1,12	0,40	0,68	126	045	081	64
2348	05.05.04.32	65	335	+06	+15	339	41,11	0,99	0,58	149	045	099	65
2350	05.05.04.34	65	331	−01	+11	333	2,92	0,77	0,67	159	045	103	65
2354	05.05.04.37	60	334	+02	+12	337	1,67	0,71	0,48	154	045	075	65
2358	05.05.04.50	65	334	−15	−04	330	2,50	0,71	0,72	171	225	288	66
2360	05.05.04.51	60	335	+01	+11	337	1,67	0,72	0,47	155	045	074	65
2363	05.05.04.53	63	337	−00	+09	339	3,42	0,85	0,51	160	045	086	65
2364	05.05.04.53	55	314	+12	+28	321	1,17	0,24	0,89	124	045	113	54
2368	05.05.04.57	56	328	+20	+31	338	2,33	0,71	0,67	116	045	101	68
2370	05.05.04.59	64	336	+04	+13	340	7,80	0,93	0,54	152	045	092	65
2371	05.05.04.59	63	340	+02	+10	342	5,33	0,91	0,45	157	045	081	65
2372	05.05.05.00	34	358	+19	+18	006	0,94	0,86	0,13	043	045	028	55
2374	05.05.05.02	37	009	+18	+13	015	1,49	0,91	0,14	031	045	035	47
2376	05.05.05.05	63	335	−03	+07	336	2,42	0,77	0,55	165	045	087	65
2379	05.05.05.10	63	336	−04	+06	337	2,62	0,79	0,54	168	045	087	65
2381	05.05.05.10	36	004	+19	+16	011	1,19	0,88	0,14	040	045	033	45
2383	05.05.05.10	63	336	−11	−01	333	1,97	0,70	0,59	179	225	269	66
2384	05.05.05.16	63	311	−01	+17	313	1,80	0,45	1,00	150	045	198	60
2385	05.05.05.20	54	322	+10	+23	327	1,04	0,41	0,62	132	045	070	64
2387	05.05.05.20	37	003	+21	+18	012	1,33	0,88	0,15	045	045	036	45
2390	05.05.05.23	61	337	+05	+13	341	2,69	0,84	0,44	149	045	077	65
2392	05.05.05.24	69	332	−12	−02	329	9,33	0,92	0,78	180	225	302	66
2394	05.05.05.24	68	333	−08	+03	333	10,36	0,93	0,72	174	045	114	66
2395	05.05.05.26	58	332	+19	+28	342	4,54	0,87	0,57	121	045	094	68
2397	05.05.05.29	63	336	−01	+08	337	2,59	0,79	0,54	162	045	087	65
2398	05.05.05.29	67	336	−03	+07	336	8,84	0,93	0,61	166	045	101	65
2400	05.05.05.32	66	335	−09	+02	334	3,96	0,84	0,64	177	045	102	66
2402	05.05.05.34	42	005	+15	+12	011	1,75	0,96	0,07	049	045	026	16
2407	05.05.05.36	34	357	+17	+17	005	0,90	0,87	0,11	042	045	025	55

Continuation

No. of meteor	DATE	v_∞	α	λ	β	λ	a	e	q	i	Ω	ω	shower
2409	05.05.05.38	67	310°	−07°	+02°	339°	15,53	0,96	0,55	177°	045°	091°	66
2410	05.05.05.38	66	336	−03	+06	336	5,09	0,88	0,60	166	045	097	65
2414	05.05.05.43	32	033	+10	−03	034	3,61	0,90	0,35	004	225	248	41
2415	05.05.05.44	63	336	+00	+10	337	2,86	0,81	0,54	159	045	087	65
2417	05.05.05.45	38	012	+18	+11	018	1,95	0,93	0,14	027	045	038	47
2418	05.05.05.47	38	001	+16	+14	007	1,15	0,93	0,08	049	045	025	16
2420	05.05.05.48	26	015	+15	+08	020	1,02	0,74	0,27	010	045	043	39
2422	05.05.05.49	41	006	+14	+10	011	1,54	0,96	0,07	040	045	024	16
2423	05.05.05.50	36	356	+16	+16	002	0,89	0,90	0,09	052	045	023	55
2427	05.05.05.53	35	004	+16	+13	011	1,11	0,90	0,11	035	045	029	16
2430	05.05.05.55	37	006	+13	+09	010	1,14	0,93	0,08	029	045	025	16
2433	05.05.05.57	38	020	+20	+11	026	4,65	0,95	0,23	021	045	054	61
2436	05.05.05.57	22	017	+18	+10	023	0,97	0,62	0,37	008	045	041	39
2438	05.05.06.06	38	010	+16	+10	015	1,66	0,93	0,11	030	045	032	47
2439	05.05.06.07	38	004	+15	+12	011	1,29	0,93	0,09	039	045	027	16
2443	05.05.06.11	42	019	+13	+05	023	14,19	0,99	0,12	014	045	041	48
2445	05.05.06.12	32	003	+22	+19	012	1,02	0,81	0,19	034	045	036	57
2447	05.05.06.15	64	335	−03	+07	336	3,00	0,81	0,58	166	045	093	65
2452	05.05.06.20	39	016	+20	+12	022	3,23	0,94	0,18	026	045	046	61
2454	05.05.06.23	37	004	+23	+19	013	1,47	0,88	0,18	014	045	010	45
2455	05.05.06.24	34	022	+08	−01	023	1,85	0,89	0,19	002	225	225	41
2457	05.05.06.25	39	005	+16	+13	011	1,39	0,93	0,09	041	045	028	16
2461	05.05.06.38	35	028	+11	−01	030	3,56	0,92	0,27	001	225	238	41
2462	05.05.06.39	32	005	+28	+23	016	1,25	0,79	0,27	036	045	048	57
2463	05.05.06.39	38	004	+18	+15	011	1,31	0,91	0,11	042	045	031	45
2465	05.05.06.44	38	011	+12	+07	015	1,58	0,94	0,09	022	045	029	49
2466	05.05.06.47	42	017	+12	+04	020	4,63	0,98	0,11	013	045	036	48
2467	05.05.06.48	61	335	−05	+05	335	1,63	0,69	0,50	168	045	077	65
2469	05.05.06.48	64	333	−10	+01	331	2,16	0,69	0,68	177	045	101	66
2470	05.05.06.49	60	337	−03	−06	338	1,66	0,74	0,44	166	045	070	65
2471	05.05.06.51	24	033	+25	+11	040	1,76	0,70	0,53	009	045	082	40
2474	05.05.06.54	31	024	+11	+01	026	1,57	0,83	0,26	082	045	051	41
2475	05.05.06.55	64	307	−03	+15	309	1,95	0,51	0,95	151	045	213	60
2484	05.05.09.57	27	031	+22	+08	036	2,10	0,79	0,45	008	045	075	40
2491	05.05.10.39	33	022	+09	+00	024	1,65	0,87	0,22	000	045	047	41
2500	05.05.12.16	24	037	+21	+06	041	1,82	0,70	0,54	005	045	083	40
2502	05.05.12.20	35	025	+06	−04	025	2,18	0,90	0,21	006	225	228	41
2517	05.05.20.20	36	292	+30	+51	301	0,96	0,20	0,77	072	045	296	37
2568	05.06.06.08	37	014	+18	+12	296	1,84	0,92	0,15	026	046	038	47
2381[a]	05.06.00.03	34	292	+28	+49	301	0,85	0,27	0,61	069	045	324	37
2383[a]	05.06.00.03	33	292	+23	+44	298	0,76	0,41	0,45	070	045	334	38
2385[a]	05.06.00.09	33	288	+20	+42	293	0,75	0,48	0,39	068	045	333	51
2386[a]	05.06.00.11	34	285	+31	+53	292	1,01	0,27	0,74	066	045	286	37
2388[a]	05.06.00.13	34	293	+22	+43	299	0,75	0,43	0,43	072	045	336	38
2398[a]	05.06.00.28	34	285	+23	+45	289	0,86	0,41	0,51	069	045	316	51
2404[a]	05.06.00.34	37	288	+30	+52	295	1,09	0,26	0,80	073	045	269	37
2419[a]	05.06.00.47	65	309	+01	+19	312	2,98	0,67	0,99	146	045	199	60
2424[a]	05.06.00.56	37	013	+12	+06	017	1,52	0,93	0,11	017	045	031	49
2435[a]	05.06.01.19	35	279	+26	+49	283	1,02	0,39	0,62	066	045	291	50
2436[a]	05.06.01.20	30	272	+12	+36	273	0,80	0,62	0,30	051	045	325	52
2437[a]	05.06.01.21	36	292	+31	+52	031	0,96	0,20	0,77	071	045	295	37
2442[a]	05.06.01.23	29	285	+28	+50	291	0,82	0,35	0,53	057	045	324	37
2443[a]	05.06.01.24	65	308	+03	+21	311	2,76	0,64	0,98	142	045	200	60
2445[a]	05.06.01.25	31	277	+27	+50	280	0,95	0,38	0,59	057	045	300	50
2448[a]	05.06.01.25	55	278	+06	+29	279	3,51	0,87	0,46	108	045	280	70
2449[a]	05.06.01.26	31	278	+13	+37	279	0,76	0,61	0,29	057	045	331	69
2453[a]	05.06.01.28	29	274	+14	+37	275	0,79	0,59	0,32	051	045	326	69
2450[a]	05.06.01.33	32	307	+36	+53	324	0,86	0,22	0,67	065	045	033	43
2463[a]	05.06.02.27	61	332	+19	+18	342	13,42	0,95	0,64	124	045	104	68
2468[a]	05.06.02.34	63	838	+01	+09	340	3,09	0,84	0,49	159	045	083	65

Continuation

No. of meteor	DATE	v_∞	α	δ	β	λ	a	e	q	i	Ω	ω	shower
2469[a]	05.06.02.34	64	335°	+01°	+10°	338°	3,07	0,82	0,56	158°	045°	091°	65
2461[a]	05.06.01.31	61	306	+09	+27	309	2,22	0,56	0,98	130	045	203	59
2475[a]	05.06.02.39	67	308	−03	+16	310	3,69	0,74	0,97	152	045	203	60
2480[a]	05.06.02.53	33	004	+25	+21	014	1,13	0,81	0,21	038	045	040	57
2485[a]	05.06.02.57	65	336	−01	+08	337	5,33	0,88	0,61	163	045	099	65
2495[a]	05.06.03.11	65	307	−01	+18	309	2,65	0,64	0,96	148	045	208	60
2501[a]	05.06.03.17	59	325	+18	+30	334	3,07	0,75	0,77	122	045	117	63
2504[a]	05.06.03.20	67	340	−05	+03	340	38,17	0,99	0,55	173	045	095	66
2510[a]	05.06.03.38	64	339	−01	+07	341	4,30	0,89	0,49	163	045	084	65
2515[a]	05.06.03.42	64	338	−02	+07	339	4,41	0,88	0,52	165	045	088	65
2518[a]	05.06.03.50	57	328	+20	+31	338	2,84	0,75	0,70	118	046	106	68
2520[a]	05.06.03.54	50	315	+14	+30	322	0,93	0,22	0,73	118	046	057	54
2524[a]	05.06.04.03	61	336	−01	+08	338	1,88	0,74	0,48	161	046	077	65
2528[a]	05.06.04.09	55	326	+13	+25	333	1,25	0,51	0,61	126	046	081	64
2530[a]	05.06.04.15	54	288	+12	+34	291	1,97	0,65	0,69	109	046	259	58
2544[a]	05.06.05.14	33	011	+17	+11	017	1,18	0,86	0,16	022	046	036	71
2545[a]	05.06.05.14	64	338	−04	+05	338	3,32	0,84	0,54	169	046	089	65
2552[a]	05.06.05.35	34	013	+19	+13	020	1,41	0,87	0,18	024	046	041	71
2553[a]	05.06.05.37	31	029	+17	+05	033	2,53	0,86	0,34	006	046	065	42
2562[a]	05.06.05.49	39	016	+22	+14	023	4,04	0,95	0,20	031	046	049	61
2566[a]	05.06.05.54	63	339	−02	+07	340	2,98	0,84	0,49	165	046	082	65
2568[a]	05.06.05.58	62	337	−04	+05	338	2,15	0,76	0,51	168	046	081	65
2569[a]	05.06.05.58	64	337	−07	+03	336	2,33	0,76	0,57	174	046	089	66
2571[a]	05.06.06.01	37	011	+19	+13	018	1,68	0,91	0,14	030	046	037	47
2572[a]	05.06.06.03	37	012	+12	+07	015	1,42	0,93	0,09	019	046	029	49
2573[a]	05.06.06.05	36	006	+20	+16	014	1,29	0,89	0,15	039	046	035	45
2582[a]	05.06.06.22	36	026	+11	+00	028	3,49	0,94	0,22	050	046	053	41
2584	05.06.06.26	63	336	−01	+08	338	2,42	0,78	0,53	162	046	085	65
2588	05.06.08.00	36	015	+23	+15	023	2,30	0,90	0,22	029	046	050	61
2591	05.06.08.40	30	025	+12	+02	027	1,48	0,81	0,28	002	046	052	41
2596	05.06.08.46	31	028	+06	−06	028	1,74	0,84	0,28	002	226	234	41
2598	05.06.08.47	38	007	+19	+15	014	1,49	0,92	0,12	042	046	034	45
2600	05.06.09.35	26	035	+24	+10	040	2,21	0,77	0,50	009	046	081	40
2605	05.06.09.50	35	016	+13	+06	020	1,59	0,91	0,14	013	046	037	48
2606	05.06.09.54	39	011	+15	+09	016	1,71	0,95	0,09	029	046	029	49
2609	05.06.10.00	33	026	+10	−01	027	1,94	0,87	0,24	001	226	231	41
2615	05.06.10.14	28	033	+24	+10	039	2,37	0,80	0,46	010	046	077	40
2616	05.06.10.17	33	030	+07	−05	030	2,37	0,88	0,29	007	226	298	41
2620	05.06.10.22	23	020	+17	+08	024	1,02	0,66	0,35	007	046	049	39
2629	05.06.11.15	28	034	+06	−07	034	1,88	0,80	0,38	008	226	246	41
2631	05.06.11.18	32	030	+10	−02	031	2,45	0,88	0,29	003	226	239	41
2633	05.06.11.36	34	030	+14	+02	032	3,59	0,92	0,30	003	046	062	42
2641	05.06.21.50	37	273	+26	+49	274	1,38	0,52	0,66	064	046	270	53
2653	05.06.22.26	33	271	+27	+50	271	1,18	0,46	0,64	056	046	280	53
2655	05.06.22.35	33	292	+29	+50	300	0,87	0,26	0,64	067	046	319	37
2656	05.06.22.39	32	276	+11	+34	278	0,78	0,66	0,27	060	046	328	69
2659	05.06.22.46	30	275	+26	+50	277	0,96	0,40	0,58	055	046	299	53
2672	05.07.00.19	37	004	+20	+16	012	1,22	0,90	0,13	044	046	032	45
2673	05.07.00.20	33	270	+12	+35	270	0,93	0,65	0,33	058	046	316	52
2677	05.07.01.03	31	290	+31	+52	299	0,86	0,27	0,62	062	046	322	37
2688	05.07.03.10	66	338	−03	+06	339	6,95	0,92	0,58	167	046	097	65
2698	05.07.06.57	36	007	+12	+08	011	1,03	0,93	0,07	025	047	022	16
2700	05.07.07.01	32	004	+29	+25	016	1,16	0,77	0,26	039	047	046	57
2701	05.07.07.04	32	029	+07	−04	029	1,86	0,86	0,26	006	227	246	41
2706	05.07.07.12	65	336	−06	+04	336	3,15	0,80	0,63	172	047	099	66
2707	05.07.07.14	35	005	+14	+10	010	0,99	0,91	0,08	030	047	023	16
2708	05.07.07.15	26	026	+18	+07	031	1,33	0,73	0,36	007	047	058	42
2710	05.07.07.20	38	018	+13	+05	021	2,15	0,94	0,12	013	047	035	48
2713	05.07.07.25	24	020	+17	+08	025	1,02	0,68	0,32	008	047	048	39
2715	05.07.07.28	28	026	+07	−03	027	1,29	0,78	0,29	004	227	231	41

Continuation

No. of meteor	DATE	v_∞	α	δ	β	λ	a	e	q	i	Ω	ω	shower
2717	05.07.07.33	30	027°	+23°	+11°	033°	2,08	0,83	0,35	013°	047°	064°	42
2718	05.07.07.33	27	019	+17	+08	024	1,09	0,74	0,28	010	047	046	39
2719	05.07.07.37	38	011	+17	+12	017	1,56	0,93	0,11	032	047	032	47
2720	05.07.07.39	37	009	+13	+08	014	1,26	0,94	0,08	026	047	025	16
2723	05.07.07.42	30	029	+03	−08	028	1,53	0,82	0,27	011	227	232	41
2724	05.07.07.44	29	039	+22	+07	043	4,65	0,90	0,48	007	047	084	40
2725	05.07.07.47	62	338	−01	+07	340	2,09	0,77	0,48	163	047	078	65
2735	05.07.08.10	32	306	+37	+54	323	0,87	0,21	0,69	063	047	032	43
2736	05.07.08.10	30	032	+09	−04	033	2,02	0,83	0,34	004	227	242	41
2737	05.07.08.10	31	025	+06	−04	025	1,39	0,83	0,24	005	227	226	41
2738	05.07.08.10	35	358	+22	+21	007	0,98	0,84	0,15	050	047	031	55
2739	05.07.08.14	35	002	+19	+16	010	1,03	0,89	0,12	047	047	028	55
2741	05.07.08.16	36	017	+20	+12	024	2,16	0,91	0,19	024	047	045	61
2742	05.07.08.17	64	341	+02	+09	343	7,88	0,94	0,47	160	047	085	65
2743	05.07.08.17	26	032	+21	+08	037	1,67	0,74	0,44	007	047	071	40
2748	05.07.08.24	33	024	+14	+04	027	1,86	0,88	0,22	006	047	049	42
2751	05.07.08.27	40	009	+16	+11	015	1,69	0,95	0,09	038	047	029	16
2752	05.07.08.35	29	026	+09	−01	027	1,37	0,80	0,27	168	227	230	41
2757	05.07.08.43	24	023	+15	+05	027	1,06	0,67	0,35	005	047	051	39
2758	05.07.08.44	35	010	+15	+10	015	1,20	0,90	0,12	025	047	030	71
2767	05.07.08.54	35	008	+17	+12	014	1,15	0,90	0,11	031	047	030	71
2769	05.07.08.57	31	032	+04	−09	030	1,82	0,83	0,31	011	227	238	41
2772	05.07.09.24	38	016	+15	+07	021	1,90	0,93	0,13	019	047	036	47
2774	05.07.09.29	34	025	+11	+01	027	2,04	0,90	0,21	002	047	048	41
2778	05.07.09.34	32	001	+27	+25	012	1,02	0,77	0,23	041	047	040	57
2780	05.07.09.55	29	030	+06	−05	030	1,53	0,80	0,30	007	227	235	41
2782	05.07.10.00	33	012	+21	+14	019	1,27	0,86	0,18	027	047	039	71
2783	05.07.10.05	25	018	+15	+07	022	1,00	0,72	0,28	007	047	044	39
2794	05.07.10.55	29	032	+06	−07	033	1,72	0,80	0,35	008	227	242	41
2795	05.07.11.02	32	014	+21	+14	021	1,31	0,84	0,21	023	047	043	71
2796	05.07.11.08	34	031	+11	−01	033	3,56	0,92	0,29	002	227	241	41
2798	05.07.11.54	38	005	+15	+12	011	1,17	0,93	0,08	040	047	025	16
2804	05.16.20.30	51	306	+27	+45	318	1,93	0,50	0,97	099	056	209	46
2825	05.16.22.01	36	284	+17	+39	287	0,98	0,58	0,41	069	056	308	72
2835	05.16.22.27	34	278	+14	+37	280	0,98	0,63	0,36	059	056	311	52
2842	05.16.22.44	53	307	+27	+45	318	2,54	0,61	0,98	101	056	204	46
2845	05.16.23.03	39	282	+07	+30	284	0,97	0,75	0,25	073	056	320	67
2848	05.16.23.14	32	300	+31	+50	312	0,82	0,29	0,58	065	060	330	37
2853	05.16.23.24	34	288	+10	+32	291	0,76	0,69	0,23	066	056	332	69
2854	05.16.23.25	33	296	+22	+43	304	0,76	0,47	0,41	068	056	331	51
2856	05.16.23.29	36	282	+10	+32	284	0,90	0,70	0,27	066	056	321	67
2858	05.16.23.31	35	287	+24	+46	293	0,96	0,44	0,54	067	056	302	50
2860	05.16.23.39	34	283	+19	+42	287	0,92	0,53	0,43	062	056	310	72
2861	05.16.23.41	29	286	+13	+36	289	0,75	0,62	0,28	051	056	332	69
2868	05.16.23.49	35	276	+11	+34	277	1,06	0,69	0,32	059	056	311	52
2871	05.16.23.53	35	298	+20	+41	305	0,76	0,49	0,38	074	056	332	51
2877	05.17.00.10	62	332	+17	+27	341	3,93	0,79	0,84	130	056	128	44
2879	05.17.00.20	60	312	+13	+29	319	2,43	0,61	0,96	127	056	211	59
2880	05.17.00.21	36	278	+08	+31	280	0,96	0,72	0,27	062	056	319	67
2882	05.17.00.22	33	302	+22	+41	310	0,71	0,49	0,36	071	056	341	38
2883	05.17.00.23	34	297	+29	+49	307	0,87	0,31	0,60	069	056	316	37
2884	05.17.00.25	31	293	+33	+54	303	0,92	0,26	0,68	059	056	306	36
2888	05.17.00.30	32	288	+23	+45	294	0,87	0,45	0,48	062	056	315	50
2890	05.17.00.35	57	307	+22	+39	316	4,22	0,77	0,96	111	056	208	46
2891	05.17.00.36	51	286	+04	+27	288	2,04	0,83	0,35	105	056	296	70
2893	05.17.00.38	32	289	+11	+33	292	0,73	0,68	0,23	062	056	334	69
2896	05.17.00.45	31	299	+32	+52	311	0,85	0,27	0,61	063	056	326	37
2900	05.17.00.55	29	286	+20	+42	290	0,80	0,52	0,38	054	056	325	72
2906	05.17.01.04	52	295	+10	+32	299	1,63	0,65	0,57	110	056	276	58
2910	05.17.01.09	34	305	+25	+43	315	0,74	0,41	0,44	074	056	341	38

Continuation

No. of meteor	DATE	t$_{00}$	α	δ	β	λ	a	e	q	i	Ω	ω	shower
2912	05.17.01.14	52	290°	+15°	+37°	294°	2,54	0,76	0,61	099°	056°	265°	58
2915	05.17.01.21	55	292	+13	+34	297	3,96	0,83	0,66	107	056	257	58
2919	05.17.01.29	52	313	+23	+39	323	1,50	0,34	0,98	108	056	206	62
2923	05.17.01.39	25	290	+31	+53	299	1,09	0,32	0,74	067	056	276	36
2926	05.17.01.42	56	330	+22	+32	341	1,89	0,57	0,82	118	056	118	63
2928	05.17.01.44	48	314	+24	+39	326	1,09	0,13	0,95	103	056	117	56
2929	05.17.01.56	56	283	+03	+26	285	15,79	0,98	0,36	108	056	287	70
2938	05.17.02.46	66	313	+01	+18	316	4,47	0,79	0,92	147	056	218	60
2939	05.17.02.46	33	308	+23	+40	318	0,68	0,51	0,33	073	056	350	38
2944	05.17.02.57	40	028	+20	+08	033	3,94	0,96	0,15	019	056	042	48
2945	05.17.02.58	32	019	+23	+14	026	1,11	0,84	0,18	026	056	036	71
2950	05.17.03.01	47	321	+22	+35	332	0,92	0,21	0,72	106	056	051	56
2961	05.17.03.16	54	331	+23	+32	342	1,59	0,51	0,77	116	056	107	63
2963	05.17.03.21	61	311	+09	+26	317	2,36	0,61	0,92	132	056	219	59
2966	05.17.03.25	60	332	+15	+25	339	2,13	0,61	0,83	133	056	122	44
2969	05.17.03.34	52	319	+14	+29	326	0,95	0,13	0,83	122	056	052	54
2987	05.17.04.32	38	017	+22	+14	024	1,42	0,92	0,12	038	056	032	45
2989	05.17.04.40	38	011	+22	+16	019	1,18	0,91	0,10	051	056	028	45
2993	05.17.04.40	57	334	+23	+31	346	2,42	0,69	0,75	118	056	112	63
2998	05.17.04.48	63	347	+04	+09	349	2,55	0,80	0,52	161	056	084	65
3000	05.17.04.51	33	012	+25	+18	022	1,01	0,84	0,16	038	056	033	57
3004	05.17.05.06	61	346	+05	+10	349	2,21	0,78	0,49	157	056	080	65
3008	05.17.05.13	31	039	+08	−07	039	1,79	0,84	0,28	092	236	235	41
3010	05.17.05.13	34	014	+25	+18	023	1,00	0,05	0,16	037	056	034	57
3014	05.17.05.17	35	013	+26	+11	023	1,20	0,87	0,16	042	056	036	57
3015	05.17.05.18	43	022	+15	+05	025	2,52	0,98	0,05	024	056	022	49
3018	05.17.05.29	37	016	+24	+16	024	1,41	0,90	0,14	041	056	035	45
3025	05.17.07.47	31	040	+12	−04	041	1,98	0,85	0,30	005	236	238	41
3046	05.18.00.01	36	277	+11	+35	279	1,09	0,69	0,34	062	057	308	52
3049	05.18.00.03	55	289	+07	+29	292	3,45	0,86	0,47	109	057	278	70
3053	05.18.00.26	32	282	+18	+41	286	0,91	0,55	0,40	059	057	313	72
3064	05.18.01.03	64	317	+00	+16	320	2,22	0,57	0,94	151	057	215	60
3067	05.18.01.22	34	231	+06	+29	282	0,86	0,74	0,22	058	057	326	67
3070	05.18.01.27	32	275	+12	+35	276	1,01	0,65	0,35	052	057	310	52
3071	05.18.01.31	34	294	+25	+45	301	0,86	0,41	0,51	069	057	315	51
3072	05.18.01.31	59	314	+09	+25	320	1,48	0,38	0,92	133	057	227	59
3073	05.18.01.37	30	291	+25	+46	298	0,81	0,43	0,46	059	057	323	50
3074	05.18.01.47	31	291	+30	+51	300	0,91	0,35	0,60	061	057	308	36
3082	05.18.02.10	52	325	+13	+26	332	0,90	0,22	0,70	126	057	047	54
3083	05.18.02.10	33	304	+24	+43	314	0,72	0,45	0,40	072	057	342	38
3086	05.18.03.12	54	310	+21	+38	319	1,75	0,46	0,96	110	057	215	46
3091	05.18.04.21	52	313	+24	+40	324	1,52	0,35	0,98	106	057	206	62
3093	05.18.04.31	59	330	+23	+33	342	3,05	0,72	0,86	119	057	131	63
3098	05.18.04.35	48	318	+25	+39	330	1,09	0,15	0,93	104	057	113	56
3099	05.18.04.36	47	323	+22	+34	334	0,89	0,22	0,69	108	057	050	56
3103	05.18.04.52	56	335	+15	+23	343	1,26	0,47	0,67	132	057	088	64
3104	05.18.04.53	62	330	+15	+25	337	2,39	0,62	0,90	134	057	137	44
3107	05.18.05.45	64	314	+13	+29	320	5,86	0,83	0,97	130	057	203	59
3116	05.18.23.21	33	279	+16	+39	281	1,00	0,60	0,40	057	058	306	52
3121	05.18.23.41	33	289	+15	+37	292	0,79	0,59	0,32	065	058	325	69
3122	05.18.23.42	52	315	+24	+39	326	1,44	0,31	0,99	107	058	205	62
3132	05.19.00.42	33	297	+21	+41	304	0,73	0,35	0,78	069	058	331	51
3133	05.19.00.47	33	292	+24	+45	299	0,84	0,44	0,48	066	058	316	50
3139	05.19.01.05	34	306	+23	+41	316	0,70	0,49	0,36	074	058	345	38
3143	05.19.01.18	34	299	+32	+51	310	0,89	0,24	0,68	068	058	309	37
3146	05.19.01.55	34	284	+13	+36	287	0,86	0,63	0,32	062	058	320	52
3148	05.19.02.05	34	281	+09	+32	283	0,89	0,70	0,27	060	058	321	67
3159	05.19.02.39	53	322	+16	+29	330	1,04	0,11	0,93	122	058	107	54
3163	05.19.02.45	53	291	+05	+27	294	1,86	0,78	0,40	111	058	291	70
3170	05.19.03.17	53	317	+20	+35	327	1,27	0,23	0,98	114	058	211	62

Continuation

No. of meteor	DATE	v_∞	α	δ	β	λ	a	e	q	i	Ω	ω	shower
3181	05.19.03.45	60	333°	+18°	+27°	342°	2,39	0,64	0,85	129°	058°	126°	44
3196	05.19.04.58	40	019	+23	+14	027	1,65	0,93	0,11	043	058	033	45
3198	05.19.05.47	37	032	+20	+07	037	2,35	0,92	0,18	014	058	045	48
3199	05.19.05.53	30	045	+12	—04	046	1,98	0,82	0,36	005	238	245	41
3200	05.19.05.59	40	021	+21	+11	028	1,78	0,95	0,09	035	058	031	47
3202	05.19.06.26	38	024	+24	+13	031	1,77	0,92	0,15	032	058	040	47
3203	05.19.06.28	34	027	+20	+08	032	1,33	0,88	0,16	016	058	038	71
3205	05.19.09.16	28	044	+23	+56	048	1,90	0,79	0,40	006	058	070	40
3210	05.19.09.58	27	038	+19	+04	042	1,32	0,75	0,33	004	058	056	42
3215	05.24.00.35	58	335	+21	+29	340	1,83	0,68	0,58	125	063	123	68
3219	05.24.00.53	54	309	+24	+41	320	2,20	0,58	0,92	105	063	220	46
3221	05.24.01.00	56	339	+23	+29	350	1,56	0,53	0,74	121	063	104	63
3224	05.24.01.11	54	313	+18	+34	321	1,44	0,39	0,88	114	063	235	56
3228	05.24.01.20	36	296	+27	+47	305	0,95	0,37	0,60	070	063	298	50
3232	05.24.01.37	42	024	+18	+08	029	1,59	0,97	0,05	038	063	021	16
3233	05.24.01.38	55	339	+15	+22	347	1,10	0,42	0,64	133	063	078	64
3234	05.24.01.39	34	285	+15	+37	289	0,93	0,61	0,36	060	063	313	52
3240	05.24.01.52	31	295	+25	+46	303	0,72	0,43	0,47	061	063	319	50
3249	05.24.02.03	32	299	+23	+42	308	0,76	0,49	0,39	066	063	330	51
3256	05.24.02.19	34	310	+22	+38	319	0,69	0,52	0,33	077	063	344	38
3257	05.24.02.21	53	320	+21	+34	330	1,24	0,22	0,97	115	063	218	62
3261	05.24.02.28	32	301	+21	+40	308	0,73	0,55	0,33	065	063	335	51
3262	05.24.02.23	31	289	+21	+42	294	0,87	0,52	0,42	058	063	315	72
3281	05.24.02.55	31	299	+28	+48	310	0,80	0,38	0,50	062	063	325	37
3289	05.24.03.06	51	322	+25	+37	334	1,17	0,17	0,97	108	063	137	62
3294	05.24.03.10	57	338	+20	+27	348	1,58	0,51	0,77	127	063	109	64
3295	05.24.03.14	35	304	+26	+44	315	0,79	0,37	0,50	075	063	326	37
3297	05.24.03.16	34	293	+21	+42	300	0,85	0,51	0,42	066	063	317	72
3298	05.24.03.16	37	289	+28	+50	297	1,23	0,44	0,69	069	063	270	53
3299	05.24.03.16	35	298	+19	+39	305	0,78	0,53	0,37	073	063	325	51
3304	05.24.03.20	28	292	+25	+46	299	0,81	0,44	0,45	052	063	322	50
3305	05.24.03.22	41	028	+21	+09	033	2,10	0,96	0,09	032	063	030	47
3311	05.24.03.39	52	300	+12	+32	305	1,64	0,65	0,58	108	063	274	58
3315	05.24.03.42	34	045	+07	—10	046	2,26	0,88	0,27	015	243	236	41
3318	05.24.03.49	51	324	+23	+35	335	1,10	0,15	0,94	112	063	121	56
3320	05.24.03.57	31	298	+22	+42	306	0,75	0,49	0,38	063	063	330	51
3321	05.24.04.01	38	285	+07	+30	287	1,02	0,75	0,25	008	063	318	67
3334	05.24.04.32	57	338	+12	+20	344	1,14	0,36	0,73	139	063	090	64
3346	05.24.04.47	42	026	+18	+07	031	1,93	0,97	0,05	031	063	023	49
3348	05.24.04.50	32	041	+21	+05	045	1,67	0,84	0,26	007	063	052	42
3354	05.24.04.55	32	019	+23	+13	026	0,88	0,86	0,12	030	063	026	71
3355	05.24.04.56	29	292	+16	+37	297	1,58	0,68	0,50	115	063	076	69
3357	05.24.05.00	42	032	+26	+13	038	4,75	0,97	0,15	034	063	043	61
3369	05.24.05.12	57	293	+03	+24	295	7,34	0,95	0,10	068	063	012	70
3379	05.24.06.16	31	037	+16	+01	040	2,08	0,96	0,22	002	063	030	41
3380	05.24.06.20	29	042	+16	+00	044	1,37	0,80	0,28	005	063	051	41
3385	05.24.06.27	30	037	+11	—03	039	1,17	0,83	0,20	005	243	221	41
3390	05.24.06.36	37	030	+17	+04	033	1,38	0,93	0,09	012	063	028	49
3397	05.24.06.42	37	034	+20	+06	038	1,88	0,93	0,14	014	063	038	48
3405	05.24.06.55	29	051	+28	+87	056	2,74	0,84	0,43	010	063	077	40
3407	05.24.06.58	66	322	+01	+15	325	2,93	0,68	0,94	154	063	214	60
3409	05.24.07.01	37	025	+20	+09	030	1,24	0,94	0,08	028	063	026	47
3413	05.24.07.24	03	047	+20	+03	051	1,55	0,75	0,39	003	063	065	40
3427	05.24.07.58	40	023	+17	+07	027	1,26	0,97	0,04	034	063	019	16
3430	05.24.08.01	28	042	+22	+06	046	1,37	0,76	0,33	007	063	057	42
3431	05.24.08.01	30	045	+23	+06	049	1,84	0,82	0,33	007	063	062	42
3432	05.24.08.15	39	028	+17	+05	032	1,49	0,95	0,07	017	063	025	49
3433	05.24.08.16	36	030	+20	+08	035	1,41	0,91	0,12	019	063	033	48
3436	05.24.08.49	33	041	+09	—07	042	1,63	0,87	0,21	012	243	226	41
3438	05.24.09.12	33	024	+19	+08	029	1,00	0,90	0,10	021	063	026	71

Continuation

No. of meteor	DATE	m∞	α	δ	β	λ	a	e	q	i	Ω	ω	shower
3439	05.24.09.15	39	031°	+21°	+08°	037°	2,16	0,94	0,12	023°	063°	035°	48
3440	05.24.09.37	31	048	+24	+06	052	2,31	0,84	0,36	007	063	067	40
3460	05.24.09.45	29	048	+23	+05	052	1,73	0,79	0,37	005	064	065	40
3462	05.25.12.10	29	044	+21	+04	047	1,52	0,80	0,31	006	064	056	42
3466	05.25.12.15	26	052	+25	+06	056	1,77	0,74	0,46	005	064	074	40
3474	05.26.00.15	38	272	−37	−14	272	1,64	0,90	0,16	033	245	140	40
3477	05.26.05.48	62	335	+16	+25	343	2,34	0,60	0,93	135	065	142	41
3485	05.26.20.37	55	310	+25	+42	322	1,19	0,51	0,58	052	065	284	46
3488	05.26.21.25	34	293	+24	+45	300	0,93	0,45	0,51	063	065	305	50
3491	05.26.22.38	35	288	+05	+28	290	0,89	0,77	0,21	062	066	326	67
3494	05.26.22.58	31	286	+07	+30	289	0,83	0,71	0,24	049	066	326	67
3496	05.26.23.10	31	296	+15	+36	301	0,74	0,62	0,28	060	066	331	69
3499	05.26.23.15	64	336	+17	+25	345	4,65	0,80	0,94	135	066	147	44
3503	05.27.00.03	61	317	+11	+27	323	2,29	0,62	0,87	130	066	229	59
3504	05.27.00.11	33	293	+20	+41	299	0,87	0,53	0,41	063	066	315	72
3511	05.27.01.00	36	289	+28	+50	296	1,21	0,45	0,67	064	066	273	53
3512	05.27.01.00	64	345	+07	+08	357	3,16	0,82	0,58	162	066	094	65
3514	05.27.01.06	33	288	+26	+48	294	1,05	0,45	0,58	060	066	290	53
3515	05.27.01.14	32	286	+11	+34	288	0,89	0,66	0,30	054	066	319	52
3516	05.27.01.16	34	292	+20	+41	298	0,90	0,53	0,42	065	066	312	72
3528	05.27.01.53	62	335	+18	+27	344	2,65	0,65	0,93	123	066	144	44
3534	05.27.02.06	64	327	+05	+17	331	2,05	0,53	0,97	149	066	207	60
3537	05.27.02.10	36	285	+16	+39	288	1,10	0,64	0,40	062	066	301	52
3541	05.27.02.13	33	285	+17	+40	289	0,98	0,58	0,41	057	066	306	52
3551	05.27.02.20	36	285	+14	+36	286	1,07	0,65	0,37	062	066	307	52
3552	05.27.02.21	59	340	+16	+23	348	1,51	0,47	0,80	135	066	111	64
3554	05.27.02.28	37	289	+26	+48	296	1,22	0,48	0,63	066	066	277	53
3556	05.27.02.30	31	294	+24	+45	302	0,84	0,46	0,45	059	066	317	50
3558	05.27.02.32	31	294	+14	+35	299	0,75	0,64	0,97	057	066	330	69
3560	05.27.02.34	58	316	+21	+36	326	2,79	0,66	0,95	116	066	211	46
3566	05.27.02.44	50	326	+21	+33	336	0,98	0,09	0,89	114	066	080	56
3574	05.27.02.50	50	330	+21	+31	340	0,91	0,18	0,75	115	066	054	56
3583	05.27.03.05	59	341	+22	+28	352	2,11	0,63	0,78	127	066	116	63
3584	05.27.03.05	32	022	+20	+10	028	0,85	0,88	0,10	023	066	023	71
3591	05.27.03.21	50	325	+23	+34	336	1,05	0,11	0,93	112	066	107	56
3597	05.27.03.24	53	328	+16	+26	336	0,94	0,10	0,85	127	066	063	54
3611	05.27.03.43	52	323	+27	+39	337	1,48	0,33	0,99	108	066	154	62
3616	05.27.03.48	31	294	+17	+38	299	0,78	0,58	0,33	058	066	326	69
3618	05.27.03.49	53	320	+19	+33	330	1,20	0,23	0,93	117	066	234	62
3619	05.27.03.50	51	322	+22	+35	333	1,09	0,13	0,95	111	066	238	62
3620	05.27.03.52	55	313	+28	+43	326	3,33	0,71	0,96	104	066	207	46
3622	05.27.03.54	54	299	+10	+30	304	2,15	0,77	0,16	139	066	027	58
3624	05.27.03.55	39	031	+24	+11	038	1,83	0,93	0,12	030	066	035	48
3625	05.27.03.55	35	302	+19	+38	309	0,75	0,55	0,34	073	066	329	51
3639	05.27.04.16	64	357	+03	+04	358	3,08	0,82	0,55	171	066	090	65
3640	05.27.04.19	56	342	+21	+26	352	1,33	0,49	0,68	127	066	092	64
3651	05.27.04.34	40	037	+22	+07	042	2,89	0,96	0,13	018	066	052	48
3654	05.27.04.37	55	014	+05	−00	015	1,98	0,90	0,09	179	246	211	71
3656	05.27.04.39	55	344	+17	+22	352	1,13	0,48	0,59	133	066	075	64
3662	05.27.04.45	54	340	+20	+26	350	1,08	0,39	0,66	126	066	078	64
3663	05.27.04.45	55	342	+24	+29	353	1,43	0,51	0,70	121	066	096	63
3676	05.27.04.58	54	327	+16	+28	336	2,01	0,53	0,94	125	066	112	54
3678	05.27.05.01	49	332	+18	+27	341	0,81	0,27	0,59	121	066	031	48
3681	05.27.05.07	42	036	+18	+03	039	3,08	0,97	0,08	012	066	030	48
3682	05.27.05.08	59	346	+21	+24	355	1,92	0,65	0,68	130	066	100	68
3689	05.27.05.15	52	328	+25	+36	340	1,26	0,25	0,95	112	066	137	56
3690	05.27.05.16	56	340	+18	+24	349	1,22	0,40	0,73	131	066	094	64
3692	05.27.05.20	39	035	+19	+05	039	2,13	0,95	0,10	015	066	033	48
3697	05.27.05.24	32	047	+23	+06	051	2,10	0,86	0,30	008	066	059	42
3704	05.27.05.39	66	351	+03	+06	353	3,58	0,80	0,71	168	066	110	65

Continuation

No. of meteor	DATE	Mag	α	δ	β	λ	a	e	q	i	Ω	ω	shower
3708	05.27.05.53	51	328°	+24°	+34°	340°	1,07	0,16	0,90	113°	066°	107°	56
3709	05.27.04.56	29	029	+22	+08	035	0,94	0,81	0,18	015	066	033	71
3710	05.27.05.58	32	041	+17	+01	044	1,43	0,85	0,21	001	066	014	41
3711	05.27.05.58	38	037	+21	+06	042	2,28	0,94	0,13	014	066	038	48
3718	05.27.06.17	31	040	+22	+07	044	1,34	0,82	0,24	010	066	045	42
3719	05.27.06.17	36	034	+21	+06	039	1,50	0,92	0,12	015	066	034	48
3734	05.27.06.54	32	033	+25	+11	039	1,20	0,85	0,18	019	066	039	71
3736	05.27.06.56	27	053	+23	+04	056	1,68	0,74	0,43	004	066	070	40
3738	05.27.07.03	30	036	+22	+07	041	2,47	0,95	0,12	019	066	037	48
3741	05.27.07.06	40	029	+19	+07	034	1,54	0,96	0,06	026	066	024	47
3745	05.27.07.10	63	351	+03	+06	353	1,91	0,66	0,64	167	066	096	65
3746	05.27.07.13	36	033	+26	+12	039	1,51	0,89	0,16	026	066	039	61
3758	05.27.07.50	37	032	+19	+05	036	1,40	0,94	0,09	016	066	028	49
3766	05.27.08.10	32	025	+20	+09	031	0,93	0,89	0,10	022	066	025	71
3767	05.27.08.10	36	037	+22	+07	042	1,75	0,91	0,16	015	066	040	48
3769	05.27.08.17	28	046	+24	+06	050	1,45	0,77	0,34	007	066	059	42
3770	05.27.08.20	38	021	+18	+09	027	1,02	0,95	0,05	039	066	018	16
3774	05.27.08.32	34	042	+22	+06	045	1,96	0,89	0,21	010	066	047	42
3776	05.27.08.36	66	353	−09	−05	350	2,42	0,68	0,78	170	246	297	66
3783	05.27.08.44	39	026	+19	+08	031	1,28	0,96	0,06	033	066	021	47
3784	05.27.08.45	40	035	+26	+11	041	3,34	0,95	0,15	029	066	042	61
3786	05.27.08.53	29	049	+12	−06	050	1,55	0,78	0,33	007	246	238	41
3790	05.27.09.00	31	016	+17	−01	048	1,65	0,84	0,26	001	246	233	41
3794	05.27.09.06	29	046	+26	+08	051	1,59	0,79	0,34	009	066	061	42
3795	05.27.09.04	35	048	+12	−06	049	2,77	0,91	0,25	009	246	234	41
3796	05.27.09.10	27	040	+11	−05	041	1,01	0,76	0,24	006	246	221	41
3798	05.27.09.10	26	044	+08	−08	044	1,07	0,73	0,29	010	246	227	41
3800	05.27.09.18	32	034	+22	+08	039	1,17	0,86	0,17	015	066	037	71
3808	05.27.09.36	39	037	+22	+07	042	2,52	0,94	0,14	019	066	039	48
3813	05.27.10.24	43	030	+16	+03	033	2,05	0,99	0,03	019	066	018	49
3814	05.27.10.28	33	036	+13	−01	037	1,05	0,87	0,14	003	246	212	41
3820	05.27.12.25	41	028	+21	+09	034	1,65	0,96	0,07	035	066	025	47
3821	05.27.13.15	45	030	+19	+06	035	3,38	0,99	0,04	035	066	022	49
3828	06.06.06.51	40	051	+05	−13	050	2,83	0,94	0,16	032	255	222	79
3854	06.06.07.17	30	058	+21	+01	061	1,96	0,84	0,32	001	008	059	42
3864	06.06.07.20	34	046	+10	−07	047	1,22	0,89	0,13	015	255	212	78
3865	06.06.07.20	54	028	+09	−02	029	2,83	0,98	0,05	165	255	203	76
3877	06.06.07.33	36	048	+10	−08	049	1,61	0,92	0,13	019	255	215	79
3879	06.06.07.34	30	053	+24	+04	057	1,57	0,82	0,27	006	075	052	42
3881	06.06.07.35	35	039	+15	−00	041	1,05	0,93	0,07	001	255	202	78
3896	06.06.07.47	29	057	+20	+00	060	1,65	0,81	0,31	000	075	057	42
3901	06.06.07.53	32	056	+23	+04	059	2,06	0,86	0,29	005	075	056	42
3905	06.06.08.33	20	070	+19	−03	071	1,42	0,59	0,59	002	255	262	77
3908	06.06.07.58	34	060	+17	−03	061	3,34	0,91	0,28	004	255	239	80
3909	06.06.07.59	32	060	+26	+06	063	2,83	0,88	0,34	007	075	065	42
3913	06.06.08.11	26	052	+27	+08	057	1,19	0,72	0,34	009	075	053	42
3914	06.06.08.12	42	039	+12	−03	040	1,62	0,99	0,02	018	255	195	78
3915	06.06.08.12	28	052	+22	+03	055	1,23	0,78	0,27	004	075	048	42
3934	06.06.08.32	52	007	+29	+21	019	1,62	0,79	0,34	114	075	060	75
3936	06.06.08.32	32	061	+24	+03	064	3,30	0,90	0,34	004	075	066	42
3939	06.06.08.34	36	064	+14	−07	065	59,42	0,99	0,32	011	255	248	80
3941	06.06.08.37	23	076	+15	−07	076	2,27	0,73	0,60	005	255	272	77
3942	06.06.08.37	28	064	+16	−05	065	1,95	0,79	0,41	005	255	249	80
3948	06.06.08.47	37	048	+15	−03	050	1,88	0,94	0,12	007	255	214	78
3951	06.06.08.50	32	052	+27	+08	056	1,77	0,86	0,26	012	075	052	42
3952	06.06.08.51	27	061	+23	+03	064	1,70	0,77	0,40	003	075	066	42
3962	06.06.08.59	23	071	+23	+01	072	1,83	0,70	0,56	001	075	085	77
3964	06.06.08.32	32	053	+21	+02	056	1,68	0,85	0,23	003	076	048	42
3967	06.06.09.08	27	068	+20	−02	069	2,29	0,80	0,47	002	256	258	77
3971	06.06.09.16	51	352	+18	+20	360	0,86	0,49	0,44	134	076	043	74

Continuation

No. of meteor	DATE	v_∞	α	δ	β	λ	a	e	q	i	Ω	ω	shower
3977	06.06.10.42	31	053°	+25°	+06°	056°	1,62	0,84	0,26	008°	076°	051°	42
3982	06.06.10.52	47	032	+20	+07	037	2,23	0,99	0,02	078	076	014	73
3991	06.06.11.12	29	061	+16	—04	063	1,88	0,81	0,36	005	256	243	80
3992	06.06.11.13	35	054	+08	—11	054	2,07	0,89	0,21	020	256	228	79
4002	06.06.11.32	29	059	+29	+09	063	1,90	0,80	0,38	010	076	066	42
4013	06.06.12.09	37	043	+07	—09	042	1,28	0,94	0,08	031	256	206	78
4062	06.07.03.59	53	351	+13	+16	357	0,86	0,42	0,50	145	076	044	74
4076	06.07.04.16	43	045	+08	—02	045	2,36	0,97	0,07	038	256	206	78
4087	06.07.04.36	45	032	+16	+03	035	1,46	1,00	0,00	075	076	005	73
4122	06.07.05.58	41	049	+09	—09	049	2,57	0,96	0,11	028	256	214	79
4124	06.07.06.03	26	057	+24	+04	060	1,30	0,72	0,36	004	076	058	42
4129	06.07.06.25	40	046	+10	—07	046	1,80	0,96	0,07	023	256	206	78
4131	06.07.06.53	55	015	+15	+08	020	1,58	0,89	0,18	154	076	041	81
4134	06.07.06.59	52	009	+31	+25	038	1,96	0,82	0,36	112	076	064	75
4139	06.07.07.25	49	010	+13	+08	015	0,86	0,86	0,12	151	076	025	81
4146	06.07.07.49	42	041	+08	—07	041	1,52	0,98	0,04	041	256	198	78
4152	06.07.08.03	38	044	+17	—000	046	1,45	0,95	0,07	028	256	205	78
4153	06.07.08.04	28	060	+28	+08	063	1,67	0,78	0,37	008	076	063	42
4154	06.07.08.05	32	059	+26	+06	062	2,67	0,88	0,31	008	076	061	42
4159	06.07.08.12	27	075	+20	—02	076	3,58	0,85	0,54	003	256	269	77
4168	06.07.08.49	33	063	+13	—08	063	2,94	0,89	0,32	011	256	243	80
4169	06.07.08.51	31	057	+13	—07	058	1,60	0,83	0,27	010	256	232	80
4180	06.08.06.03	44	035	+18	+02	037	1,57	0,99	0,01	050	077	009	73
4188	06.08.02.19	65	003	+10	+08	007	4,28	0,85	0,64	164	077	102	82
4198	06.08.02.40	37	046	+15	—02	048	1,50	0,94	0,09	006	257	208	78
4209	06.08.02.55	39	056	+05	—14	055	4,25	0,95	0,20	030	257	230	79
4217	06.08.03.06	63	353	+18	+20	001	3,09	0,73	0,83	143	077	124	83
4219	06.08.03.08	41	045	+12	—05	046	2,06	0,97	0,06	021	257	203	78
4227	06.08.03.19	58	352	+20	+21	001	1,39	0,47	0,74	137	0770	098	83
4247	06.08.04.01	51	029	+09	—03	030	1,84	0,98	0,04	159	257	199	76
4249	06.08.04.01	53	021	+12	+03	023	1,53	0,93	0,10	166	077	030	81
4250	06.08.04.02	33	061	+11	—09	061	2,59	0,89	0,28	014	257	238	80
4269	06.08.04.36	52	014	+19	+12	020	1,33	0,86	0,18	141	077	039	81
4275	06.08.04.50	53	354	+13	+14	359	0,85	0,46	0,46	147	077	043	74
4279	06.08.04.55	36	056	+05	—14	055	2,23	0,90	0,22	026	257	229	79
4280	06.08.04.56	54	355	+12	+13	360	0,87	0,47	0,46	149	077	045	74
4282	06.08.04.57	53	002	+26	+23	013	—1,34	0,68	0,42	124	077	064	75
4286	06.08.05.02	58	360	+12	+11	005	1,28	0,57	0,53	155	077	072	82
4289	06.08.05.09	63	003	+09	+07	007	1,85	0,70	0,57	164	077	086	82
4292	06.08.05.09	38	043	+15	—01	045	1,34	0,96	0,06	003	257	202	78
4305	06.08.05.26	31	066	+18	—03	067	2,89	0,87	0,38	004	257	249	80
4311	06.08.05.35	57	351	+22	+23	001	1,41	0,47	0,74	133	077	099	83
4318	06.08.05.42	60	359	+12	+11	004	1,52	0,59	0,61	156	077	086	82
4319	06.08.05.42	50	015	+14	+08	019	1,02	0,89	0,11	152	077	028	81
4322	06.08.05.46	51	015	+19	+12	021	1,22	0,88	0,15	139	077	034	81
4323	06.08.05.46	53	005	+26	+22	015	1,36	0,72	0,38	125	077	061	75
4334	06.08.05.56	36	055	+04	—15	054	2,11	0,90	0,21	030	257	227	79
4336	06.08.05.57	42	047	+10	—07	048	2,67	0,97	0,07	030	257	207	78
4353	06.08.06.16	32	063	+24	+03	065	3,31	0,90	0,33	004	077	065	42
4355	06.08.06.21	40	039	+14	—01	041	1,32	0,98	0,03	006	257	194	78
4357	06.08.06.22	28	062	+21	—00	063	1,60	0,78	0,35	000	257	240	42
4362	06.08.06.28	62	356	+15	+15	002	1,93	0,62	0,74	150	077	107	82
4363	06.08.06.39	36	053	+10	—09	053	1,82	0,91	0,16	019	257	220	79
4366	06.08.06.40	26	059	+25	+05	062	1,42	0,74	0,36	005	077	060	42
4367	06.08.06.40	35	045	+13	—04	046	1,18	0,92	0,09	011	257	206	78
4369	06.08.06.44	36	044	+09	—08	043	1,18	0,93	0,08	024	257	204	78
4375	06.08.06.47	29	061	+28	+07	065	1,92	0,80	0,37	008	077	065	42
4376	06.08.06.49	28	063	+14	—07	064	1,66	0,78	0,37	007	257	242	80
4379	06.08.06.52	60	001	+12	+11	005	1,43	0,60	0,56	157	077	079	82
4381	06.08.06.54	35	051	+07	+11	051	1,39	0,88	0,17	023	257	218	79

Continuation

No. of metepr	DATE	v_∞	α	δ	β	λ	a	e	q	i	Ω	ω	shower
4382	06.08.06.55	28	066°	+18°	−04°	067°	2,00	0,80	0,41	004°	257°	249°	80
4389	06.08.07.00	59	000	+12	+11	005	1,43	0,59	0,57	155	077	080	82
4390	06.08.07.02	29	032	+22	+01	036	1,68	0,80	0,34	001	077	060	42
4391	06.08.07.03	34	056	+08	−12	056	1,82	0,88	0,22	020	257	228	79
4392	06.08.07.03	27	025	+29	+08	064	1,55	0,75	0,38	009	077	063	42
4394	06.08.07.04	40	042	+16	−00	046	1,48	0,97	0,05	002	257	200	78
4396	06.08.07.05	40	041	+11	−04	042	1,28	0,97	0,04	023	257	197	78
4405	06.08.07.20	28	063	+23	+02	065	1,78	0,78	0,38	002	077	066	42
4406	06.08.07.22	37	044	+05	−14	057	1,99	0,91	0,18	028	257	224	79
4410	06.08.07.27	62	357	+19	+19	005	2,49	0,71	0,71	143	077	106	83
4411	06.08.07.28	42	043	+10	−06	043	1,78	0,98	0,04	034	257	199	78
4412	06.08.07.28	64	002	+10	+08	005	2,36	0,72	0,66	165	077	100	82
4415	06.08.07.29	61	356	+15	+15	002	1,66	0,57	0,71	150	077	100	82
4420	06.08.07.35	37	051	+03	−15	049	1,61	0,90	0,16	034	257	219	79
4440	06.08.08.10	36	052	+10	−09	052	1,73	0,91	0,16	019	257	219	79
4445	06.08.08.16	32	055	+21	+02	058	1,64	0,85	0,24	003	077	049	42
4446	06.08.08.20	31	056	+25	+05	060	1,71	0,84	0,28	007	077	054	42
4448	06.08.08.37	31	059	+25	+05	062	2,00	0,84	0,31	006	077	059	42
4454	06.08.08.42	40	058	+26	+05	061	2,14	0,87	0,28	007	077	056	42
4462	06.08.08.47	22	074	+18	−05	075	1,61	0,64	0,59	003	257	265	77
4468	06.08.08.51	27	062	+23	+02	064	1,60	0,77	0,37	002	077	023	42
4475	06.08.09.03	25	075	+17	−06	075	2,21	0,75	0,55	004	257	266	77
4481	06.09.04.39	44	035	+15	+01	038	1,46	1,00	0,00	025	078	004	73
4485	06.09.04.52	39	041	+12	−03	043	1,25	0,97	0,04	016	258	197	78
4486	06.09.04.52	58	354	+22	+23	004	1,66	0,57	0,73	133	078	102	83
4495	06.09.05.22	59	000	+13	+12	006	1,38	0,58	0,57	155	078	079	82
4498	06.09.05.28	39	053	+04	−15	051	2,17	0,92	0,16	036	258	221	79
4500	06.09.05.38	51	347	+17	+21	355	0,80	0,36	0,51	144	078	032	74
4503	06.09.05.49	49	349	+12	+16	354	0,69	0,52	0,33	141	078	016	74
4509	06.09.05.59	52	003	+24	+21	013	1,09	0,67	0,36	127	078	052	75
4521	06.09.06.13	53	015	+16	+09	020	1,26	0,87	0,17	149	078	037	81
4522	06.09.06.15	60	352	+19	+20	360	1,66	0,50	0,82	141	078	116	83
4527	06.09.06.27	31	064	+23	+02	066	2,72	0,87	0,34	003	078	065	42
4533	06.09.06.34	39	045	+09	−08	046	1,47	0,95	0,07	029	258	204	78
4536	06.09.06.39	54	030	+10	−03	032	3,28	0,98	0,05	165	258	204	76
4541	06.09.06.42	32	064	+15	−06	065	2,49	0,87	0,32	007	258	242	80
4542	06.09.06.48	30	057	+24	−04	060	1,53	0,81	0,27	005	078	052	42
4546	06.09.06.49	50	023	+15	+05	027	1,34	0,95	0,06	153	078	022	81
4552	06.09.06.58	48	033	+19	+05	037	2,00	0,99	0,01	111	078	011	73
4556	06.09.07.07	35	046	+15	−02	048	1,19	0,91	0,10	006	258	208	78
4564	06.09.07.17	39	042	+09	−06	042	1,22	0,96	0,04	030	258	198	78
4569	06.09.07.26	51	351	+13	+15	356	0,78	0,44	0,43	145	078	027	74
4570	06.09.07.28	31	059	+14	−07	060	1,68	0,84	0,27	009	258	232	80
4575	06.09.07.37	32	056	+24	+04	060	1,86	0,87	0,25	007	078	057	42
4590	06.09.08.55	56	006	+27	+22	017	2,14	0,79	0,45	126	078	075	75
4591	06.09.08.57	25	076	+20	−03	076	2,64	0,79	0,54	002	258	266	77
4596	06.09.09.19	29	059	+25	+05	062	1,58	0,80	0,32	006	078	057	42
4597	06.09.09.20	61	355	+19	+19	003	1,97	0,60	0,77	142	078	111	83
4609	06.09.09.58	30	060	+24	+03	062	1,69	0,82	0,30	004	078	057	42
4627	06.09.10.49	29	063	+23	+01	065	1,77	0,81	0,35	002	078	063	42
4628	06.09.10.52	55	031	+12	−01	033	5,15	0,99	0,04	175	258	203	76
4621	06.09.09.36	39	046	+07	−10	047	1,47	0,94	0,08	036	258	206	78
4632	06.10.04.44	35	060	+07	−13	059	2,22	0,89	0,24	022	259	232	79
4639	06.10.05.20	57	352	+20	+21	001	1,20	0,39	0,73	137	079	091	83
4640	06.10.05.51	49	037	+20	+05	041	3,61	1,00	0,01	095	079	012	73
4645	06.10.06.06	52	009	+29	+23	020	1,46	0,77	0,33	119	079	057	75
4648	06.10.06.08	42	046	+13	−04	047	2,08	0,98	0,04	020	259	200	78
4654	06.10.06.21	28	058	+25	+04	061	1,38	0,77	0,31	005	079	054	42
4655	06.10.06.21	53	018	+12	+04	021	1,22	0,88	0,14	167	079	034	81
4660	06.10.06.24	47	035	+18	+04	039	1,80	1,00	0,01	097	079	007	73

Continuation

No. of meteor	DATE	v_∞	α	δ	β	λ	a	e	q	i	Ω	ω	shower
4666	06.09.10.00	29	064°	+25°	+03°	066°	1,43	0,82	0,36	004°	078°	065°	42
4682	06.10.07.05	59	359	+15	+15	005	1,43	0,54	0,65	150	079	089	82
4684	06.10.05.56	39	040	+15	—01	043	1,15	0,97	0,03	004	259	195	78
4686	06.10.07.07	54	029	+06	—06	029	2,17	0,96	0,10	155	259	212	76
4691	06.10.07.22	41	042	+18	+02	045	1,56	0,98	0,03	012	079	016	48
4692	06.10.07.23	36	040	+21	+05	044	1,12	0,94	0,06	018	079	021	48
4693	06.10.07.23	38	041	+21	+05	045	1,31	0,96	0,05	020	079	021	48
4699	06.10.07.33	39	040	+11	—05	041	1,15	0,97	0,03	028	259	194	78
4704	06.10.07.41	47	016	+14	+07	020	0,84	0,91	0,07	148	079	019	81
4708	06.10.07.43	49	025	+09	—02	027	1,09	0,96	0,04	171	259	197	76
4710	06.10.07.46	41	041	+21	+05	045	1,48	0,97	0,04	021	079	018	48
4711	06.10.07.47	41	046	+09	+08	046	1,65	0,96	0,06	034	259	203	78
4712	06.10.07.47	37	041	+25	+09	046	1,25	0,93	0,08	027	079	026	48
4715	06.10.07.50	39	041	+21	+05	045	1,29	0,96	0,05	023	079	019	48
4716	06.10.07.50	49	029	+10	—00	032	1,28	0,98	0,03	166	259	195	76
4717	06.10.07.55	36	043	+07	—09	042	1,02	0,93	0,07	031	259	201	78
4721	06.10.08.00	39	041	+22	+05	045	1,37	0,96	0,05	022	079	020	48
4728	06.10.08.11	32	060	+25	+04	063	2,00	0,86	0,28	006	079	056	42
4736	06.10.08.17	32	060	+23	+03	062	1,88	0,85	0,27	004	079	054	42
4744	06.10.08.25	43	042	+13	—03	043	1,62	0,99	0,02	026	259	193	78
4749	06.10.08.39	42	040	+20	+04	044	1,64	0,99	0,02	025	079	015	48
4752	06.10.08.44	39	044	+26	+09	049	1,66	0,96	0,09	027	079	029	48
4788	06.18.03.16	53	023	+13	+03	026	1,12	0,85	0,16	171	087	035	81
4796	06.18.03.44	50	351	+12	+14	357	0,71	0,44	0,40	147	087	009	74
4800	06.18.04.05	56	018	+29	+19	028	2,14	0,83	0,36	129	087	065	75
4809	06.18.04.50	38	052	+14	—05	053	1,23	0,95	0,06	017	267	202	78
4813	06.18.05.12	36	052	+11	—07	052	1,26	0,95	0,06	028	267	201	78
4818	06.18.06.16	32	077	+16	—07	077	3,60	0,89	0,38	009	267	251	80
4822	06.18.06.30	34	075	+14	—08	075	4,33	0,92	0,33	011	267	246	80
4829	06.18.07.17	26	062	+28	+07	065	1,10	0,73	0,29	008	087	047	42
4831	06.18.07.50	51	026	+17	+06	030	1,15	0,90	0,11	157	087	029	81
4845	06.20.03.52	59	003	+19	+18	008	1,34	0,44	0,74	147	089	098	83
4848	06.19.10.54	32	071	+23	+02	073	2,36	0,88	0,29	001	088	058	42
4849	06.19.11.00	30	070	+28	+05	072	1,66	0,81	0,32	007	088	057	42
4885	06.20.02.41	50	360	+14	+13	006	0,70	0,52	0,34	149	089	018	74
4891	06.20.07.34	35	049	+11	—07	049	0,88	0,94	0,05	025	269	197	78
4898	06.20.09.10	44	044	+14	—03	045	1,22	1,00	0,00	096	269	185	73
4917	07.04.06.26	58	356	+23	+22	006	1,26	0,63	0,93	137	101	229	84
5027	07.04.08.40	40	082	+16	—08	082	5,65	0,97	0,17	017	282	228	85
5049	07.04.22.50	35	302	—24	—04	299	2,86	0,91	0,25	006	283	125	90
5052	07.04.23.05	44	311	—14	+04	310	4,72	0,99	0,07	018	103	331	89
5057	07.05.23.53	34	305	—08	+12	306	1,61	0,87	0,21	021	103	314	91
5060	07.06.00.55	41	315	—14	+03	312	1,76	0,97	0,05	014	103	337	89
5061	07.06.00.59	42	000	+73	+61	052	7,02	0,87	0,90	069	103	140	88
5062	07.06.01.00	36	321	—00	+14	323	0,92	0,91	0,08	048	103	338	87
5077	07.08.00.16	45	016	+71	+55	055	17,00	0,95	0,85	073	105	133	88
5084	07.08.16.34	43	012	+72	+57	054	5,18	0,83	0,86	072	105	133	88
5104	07.09.19.07	46	010	+62	+61	044	2,36	0,64	0,85	083	106	127	86
5113	07.09.20.42	37	316	+66	+62	020	3,24	0,69	1,00	061	106	163	92
5125	07.10.01.57	41	024	+71	+55	060	2,99	0,73	0,80	069	107	122	88
5132	07.10.02.50	39	019	+76	+59	064	3,95	0,78	0,86	064	107	131	88
5140	07.13.23.44	44	330	+00	+12	332	0,82	0,91	0,07	038	110	342	87
5144	07.14.00.45	30	325	+12	+25	332	0,81	0,77	0,19	043	110	330	94
5146	07.14.00.55	43	324	—07	+07	324	1,88	0,98	0,04	039	110	340	89
5149	07.14.01.26	33	327	+14	+26	334	0,85	0,78	0,19	054	110	329	94
5150	07.14.01.32	42	326	—25	—11	320	2,25	0,96	0,10	038	290	148	95
5151	07.14.01.55	33	325	+05	+18	330	0,88	0,85	0,13	042	110	333	87
5160	07.14.03.15	58	000	+25	+23	011	1,30	0,36	0,83	136	111	249	84
5163	07.14.03.45	64	002	+27	+24	013	3,36	0,72	0,95	138	111	211	84
5166	07.14.04.05	58	004	+33	+29	018	1,69	0,42	0,98	127	111	207	96

Continuation

No. of meteor	DATE	v_∞	α	δ	β	λ	a	e	q	i	Ω	ω	shower
5186	07.14.09.34	42	010°	+66°	+55°	047°	1,87	0,53	0,87	076°	111°	128°	86
5214	07.14.22.21	35	315	—12	+05	314	1,63	0,90	0,17	009	111	318	91
5218	07.14.22.40	34	311	—26	—08	306	2,51	0,88	0,29	012	291	120	90
5223	07.14.23.10	35	316	—10	+07	316	1,59	0,90	0,16	014	111	321	91
5229	07.14.23.26	33	316	—20	—03	312	1,55	0,86	0,21	005	291	134	90
5231	07.14.23.30	40	320	—05	+10	320	1,86	0,95	0,10	033	111	328	89
5232	07.14.23.56	36	312	—13	+05	311	2,32	0,91	0,21	008	111	311	91
5233	07.14.23.57	34	324	+01	+14	327	0,96	0,88	0,12	034	111	333	87
5234	07.15.00.02	33	308	—11	+08	308	2,15	0,87	0,28	011	111	303	91
5236	07.15.00.09	37	326	+10	+22	332	1,01	0,85	0,15	059	111	326	94
5241	07.15.00.51	37	326	+06	+18	330	1,02	0,88	0,12	052	111	331	87
5246	07.15.01.09	43	321	—09	+06	320	2,50	0,98	0,06	024	111	334	89
5248	07.15.01.18	37	329	—09	+04	328	1,01	0,96	0,04	016	111	343	93
5269	07.15.01.56	33	329	+03	+14	332	0,82	0,89	0,09	039	111	338	87
5286	07.15.02.53	59	003	+22	+19	012	1,26	0,35	0,82	142	111	252	84
5290	07.15.03.14	44	355	+56	+51	025	6,38	0,30	0,96	084	111	144	97
5292	07.15.03.32	38	355	+56	+51	027	1,03	0,13	0,90	077	112	096	97
5296	07.15.03.43	61	004	+30	+26	017	2,10	0,54	0,97	133	112	208	84
5317	07.15.04.47	44	004	+54	+46	031	1,20	0,24	0,91	090	112	121	97
5331	07.15.05.08	40	360	+53	+47	028	0,94	0,14	0,81	083	112	063	97
5349	07.15.05.23	45	009	+71	+58	053	5,27	0,83	0,90	075	112	140	88
5353	07.15.05.51	60	039	+21	+05	043	1,40	0,69	0,44	168	112	069	98
5368	07.15.06.08	61	034	+20	+06	039	1,46	0,58	0,61	168	112	087	98
5385	07.15.06.26	45	018	+65	+51	050	2,29	0,63	0,84	081	112	125	86
5391	07.15.06.32	41	355	+59	+54	030	1,25	0,25	0,94	078	112	134	97
5407	07.15.06.50	40	003	+64	+54	041	1,41	0,37	0,89	076	112	127	86
5425	07.15.07.21	60	032	+21	+07	037	1,24	0,52	0,60	164	112	081	98
5460	07.15.08.03	39	017	+69	+54	053	1,54	0,47	0,82	070	112	115	86
5461	07.15.08.06	39	008	+75	+61	058	2,63	0,66	0,89	066	112	135	88
5463	07.15.08.12	43	003	+63	+54	040	1,78	0,48	0,92	080	112	137	86
5482	07.15.09.12	42	018	+63	+50	048	1,46	0,46	0,79	080	112	110	86
5484	07.15.09.12	41	089	+20	—03	089	4,17	0,97	0,12	009	292	219	85
5491	07.15.09.38	41	090	+15	—09	090	4,45	0,97	0,15	022	292	223	85
5511	07.15.10.24	39	001	+68	+58	045	1,56	0,42	0,91	071	112	131	86
5514	07.15.10.32	40	097	+16	—07	097	38,50	0,99	0,23	014	292	238	85
5523	07.15.10.58	46	011	+64	+52	045	2,30	0,61	0,89	083	112	133	86
5535	07.15.11.43	26	000	+57	+51	032	1,20	0,23	0,91	083	112	123	97
5544	07.15.11.59	40	005	+62	+52	040	1,27	0,31	0,88	078	112	118	86
5545	07.15.11.59	41	008	+64	+53	044	1,45	0,40	0,87	078	112	122	86
5549	07.15.12.06	38	096	+19	—05	096	4,94	0,95	0,23	009	292	235	85
5560	07.15.15.02	36	312	+68	+74	023	3,56	0,72	0,99	059	112	163	92
5561	07.15.15.02	36	312	+67	+74	023	3,44	0,71	0,99	059	112	163	92
5573	07.15.18.46	40	021	+72	+56	059	2,05	0,60	0,83	070	112	122	88
5582	07.15.22.43	42	327	—16	—02	324	1,86	0,98	0,03	012	292	161	95
5584	07.15.22.50	36	317	—22	—05	313	2,16	0,91	0,19	010	292	134	90
5585	07.15.22.52	42	319	—06	+09	320	2,97	0,97	0,09	032	112	327	89
5596	07.16.00.04	38	325	+00	+13	328	1,18	0,93	0,08	045	112	334	87
5599	07.16.00.32	37	327	+11	+23	333	1,02	0,84	0,16	060	112	326	94
5617	07.16.01.26	35	325	+09	+21	331	0,96	0,84	0,15	049	112	328	94
5625	07.16.01.58	34	327	+12	+24	333	0,92	0,82	0,17	053	112	328	94
5633	07.16.22.36	40	337	—31	—20	326	1,53	0,90	0,16	053	293	140	99
5639	07.16.23.22	37	315	—12	+05	314	2,22	0,92	0,18	010	113	315	91
5643	07.16.23.45	38	330	—06	+06	330	1,07	0,95	0,05	025	113	342	93
5661	07.17.00.55	34	333	—00	+10	335	0,83	0,93	0,06	036	113	342	87
5662	07.17.00.56	35	333	+06	+16	337	0,82	0,07	0,88	050	113	339	87
5663	07.17.01.02	32	330	+11	+22	336	0,81	0,83	0,14	048	113	334	94
5664	07.17.01.02	41	327	—13	+00	325	1,62	0,98	0,04	094	113	340	93
5665	07.17.01.03	32	330	+05	+16	334	0,80	0,86	0,11	037	113	337	87
5566	07.17.01.09	40	328	—05	+07	328	1,32	0,96	0,05	033	113	340	89
5668	07.17.01.21	41	326	—13	—01	324	1,80	0,98	0,04	003	113	338	93

Continuation

No. of meteor	DATE	t_{Greenw}	α	δ	β	λ	a	e	q	i	Ω	ω	shower
5676	07.17.01.36	36	328°	+01°	+13°	330°	1,02	0,91	0,09	042°	113°	336°	87
5680	07.17.02.12	30	327	+10	+22	333	0,83	0,78	0,18	038	113	330	94
5694	07.17.03.13	39	328	−26	−11	321	1,86	0,94	0,12	031	293	145	95
5709	07.17.03.43	43	019	+80	+61	069	22,79	0,96	0,89	067	113	140	88
5711	07.17.03.46	36	313	+69	+74	027	3,31	0,70	1,00	059	113	163	92
5722	07.17.04.09	40	356	+58	+53	030	1,15	0,18	0,94	078	113	125	97
5723	07.17.04.10	40	360	+54	+48	028	0,99	0,12	0,87	084	113	082	97
5732	07.17.04.21	59	002	+23	+20	011	1,32	0,42	0,76	140	113	258	84
5740	07.17.04.30	41	352	+58	+54	028	1,26	0,23	0,97	079	113	142	97
5743	07.17.04.35	40	354	+55	+50	025	1,03	0,11	0,92	080	113	102	97
5754	07.17.04.40	40	006	+75	+61	058	3,26	0,72	0,91	068	113	139	88
5755	07.17.04.40	60	007	+26	+21	017	1,40	0,34	0,92	140	113	229	84
5762	07.17.04.50	41	357	+55	+50	028	1,09	0,15	0,93	082	113	115	97
5795	07.17.05.30	39	003	+56	+49	033	0,96	0,18	0,79	079	113	069	97
5812	07.17.06.29	60	045	+20	+03	048	1,66	0,75	0,41	173	114	068	98
5843	07.17.09.03	41	010	+67	+55	049	1,60	0,45	0,88	074	114	125	86
5844	07.17.09.03	44	018	+68	+54	053	2,38	0,64	0,86	078	114	128	86
5856	07.17.10.21	38	099	+18	−06	098	6,34	0,96	0,24	010	294	237	85
5858	07.17.18.32	39	320	+70	+72	032	4,77	0,79	1,00	063	114	163	92
5859	07.17.18.39	40	022	+67	+52	054	1,42	0,45	0,78	074	114	107	86
5861	07.17.18.56	37	006	+69	+57	049	1,41	0,38	0,88	069	114	122	86
5863	07.17.19.02	45	021	+64	+50	051	1,91	0,57	0,83	083	114	121	86
5879	07.17.20.00	39	007	+68	+56	047	1,40	0,37	0,88	072	114	123	86
5881	07.17.20.03	38	017	+69	+55	054	1,40	0,41	0,82	070	114	112	86
5884	07.17.20.11	41	007	+64	+54	045	1,45	0,38	0,90	077	114	127	86
5887	07.17.20.16	39	002	+58	+51	034	1,05	0,18	0,86	079	114	097	97
5895	07.17.20.30	41	028	+73	+55	062	2,53	0,68	0,82	071	114	123	88
5898	07.17.20.44	42	019	+64	+50	050	1,50	0,45	0,82	080	114	114	86
5899	07.17.20.45	45	334	−26	−15	326	3,50	0,97	0,11	060	294	144	99
5905	07.17.20.56	41	356	+56	+51	028	1,15	0,17	0,95	081	114	130	97
5906	07.17.20.57	44	037	+75	+55	068	9,08	0,91	0,82	071	114	128	88
5907	07.17.20.57	36	317	−07	+09	317	1,86	0,90	0,18	019	114	317	91
5914	07.17.21.09	38	015	+79	+61	068	1,92	0,55	0,87	068	114	127	88
5916	07.17.21.12	45	029	+70	+53	060	3,78	0,78	0,82	077	114	126	88
5925	07.17.21.38	41	001	+53	+46	028	0,96	0,13	0,84	086	114	070	97
5929	07.17.21.47	31	316	−20	−04	313	1,50	0,83	0,26	005	294	129	90
5935	07.17.21.54	39	003	+67	+57	045	1,50	0,39	0,91	072	114	131	86
5937	07.17.21.56	38	328	−02	+10	330	1,13	0,94	0,07	037	114	337	87
5939	07.17.21.58	44	009	+57	+48	037	1,28	0,30	0,89	088	114	121	97
5941	07.17.22.01	43	017	+66	+52	051	1,69	0,50	0,84	079	114	121	86
5944	07.17.22.07	44	012	+65	+53	047	1,76	0,49	0,89	080	114	130	86
5948	07.17.22.15	42	007	+59	+50	038	1,20	0,27	0,88	083	114	115	97
5953	07.17.22.25	46	320	−07	+08	320	46,84	1,00	0,08	032	114	326	89
5956	07.17.22.30	38	325	+01	+14	328	1,25	0,92	0,10	042	114	331	87
5958	07.17.22.31	43	357	+53	+48	026	1,13	0,16	0,95	086	114	128	97
5976	07.17.23.02	43	008	+54	+45	035	1,04	0,20	0,83	088	114	090	97
5978	07.17.23.10	43	330	−18	−06	326	2,20	0,98	0,04	029	294	158	95
5982	07.17.23.13	39	355	+55	+51	026	1,03	0,11	0,92	080	114	102	97
5985	07.17.23.23	43	005	+64	+54	042	1,60	0,43	0,92	080	114	135	86
5993	07.17.23.38	59	005	+40	+34	023	2,73	0,64	0,99	121	114	199	96
5998	07.17.23.56	58	004	+28	+24	016	1,33	0,40	0,88	133	114	240	84
6039	07.18.02.45	57	038	+22	+06	043	0,65	0,58	0,45	165	114	060	98
6055	07.18.05.04	37	096	+17	−06	096	2,90	0,93	0,21	012	294	231	85
6061	07.18.05.44	39	094	+18	−05	094	3,23	0,95	0,17	012	294	226	85
6067	07.18.06.42	39	101	+17	−06	100	47,05	0,99	0,24	011	294	240	85
6069	07.18.07.17	38	098	+16	−08	098	4,23	0,95	0,23	014	295	235	85
6070	07.18.07.46	38	096	+11	−12	096	4,26	0,94	0,24	023	295	235	85
6074	07.24.22.20	42	010	+64	+53	045	1,33	0,31	0,92	080	121	129	86
6077	07.24.22.24	56	006	+43	+37	025	2,09	0,54	0,97	114	121	208	96
6082	07.24.22.38	42	024	+66	+50	054	1,40	0,41	0,83	080	121	115	86

Continuation

No. of meteor	DATE	v_∞	α	δ	β	λ	a	e	q	i	Ω	ω	shower
6084	07.24.22.42	39	333°	−08°	+03°	332°	1,39	0,96	0,06	010°	121°	336°	93
6091	07.24.22.47	37	338	+04	+12	341	0,94	0,99	0,06	045	121	340	87
6094	07.24.22.53	44	020	+71	+55	058	2,86	0,69	0,90	078	121	137	86
6099	07.24.23.13	34	327	−21	−07	322	1,74	0,89	0,20	014	301	134	90
6100	07.24.23.15	44	022	+71	+55	058	2,45	0,64	0,89	077	121	133	86
6103	07.24.23.19	42	337	−28	−17	328	1,52	0,50	0,17	045	301	135	99
6109	07.24.23.29	41	337	−23	−12	330	1,97	0,94	0,11	039	301	146	95
6110	07.24.23.30	46	337	−25	−14	329	9,81	0,99	0,12	050	301	140	99
6112	07.24.23.38	43	336	−19	−08	331	2,25	0,97	0,06	033	301	154	95
6113	07.24.23.39	55	011	+44	+36	030	1,60	0,38	0,99	114	121	205	96
6115	07.24.23.40	43	337	−19	−09	332	2,38	0,97	0,06	039	301	154	95
6117	07.24.23.42	61	013	+37	+29	027	2,37	0,59	0,98	129	121	204	96
6120	07.24.23.44	61	012	+38	+30	027	2,44	0,60	0,98	127	121	204	96
6128	07.25.01.00	41	337	−20	−10	331	2,10	1,00	0,01	034	301	150	95
6129	07.25.01.03	43	335	−19	−08	330	3,02	0,98	0,07	031	301	151	95
6323	07.25.05.56	41	106	+13	−09	105	40,47	0,99	0,23	018	301	238	85
6326	07.25.06.17	39	102	+17	−06	102	3,80	0,53	0,18	012	301	227	85
6327	07.25.06.27	40	099	+16	−08	099	3,63	0,96	0,15	019	301	223	85
6332	07.25.13.33	45	017	+71	+58	056	3,02	0,70	0,92	079	121	141	86
6347	07.25.22.35	39	341	+21	−12	335	1,48	0,93	0,10	038	303	150	95
6353	07.26.22.48	40	340	−30	−19	330	2,62	0,92	0,20	046	303	132	99
6355	07.26.22.52	42	339	−16	−06	335	1,80	0,97	0,05	029	303	158	95
6361	07.26.23.22	41	337	−18	−08	332	2,01	0,96	0,08	028	303	152	95
6363	07.26.23.38	42	339	−08	+00	338	1,49	1,00	0,02	001	123	346	93
6414	07.27.02.14	40	328	−07	+06	328	2,54	0,95	0,12	016	123	324	89
6415	07.27.02.14	41	342	−11	−03	339	1,28	0,98	0,02	021	303	166	93
6419	07.27.02.28	33	335	+13	+22	342	0,90	0,81	0,17	047	123	328	94
6421	07.27.02.30	42	335	−22	−11	329	3,87	0,97	0,12	033	303	141	95
6433	07.27.03.11	61	012	+28	+21	023	1,63	0,47	0,86	140	123	236	84
6442	07.27.03.32	61	013	+28	+21	023	1,60	0,46	0,86	140	123	237	84
6445	07.27.03.45	64	012	+27	+20	021	2,61	0,67	0,87	143	123	229	84
6455	07.27.04.20	58	015	+43	+33	032	1,92	0,48	0,99	121	123	201	96
6467	07.27.04.50	63	050	+25	+06	054	2,20	0,74	0,57	167	123	089	98
6469	07.27.04.51	42	004	+55	+46	037	0,99	0,10	0,89	089	123	089	97
6477	07.27.04.56	43	011	+66	+54	048	1,67	0,44	0,94	081	123	142	86
6479	07.27.04.58	42	020	+68	+53	055	1,50	0,41	0,88	078	123	125	86
6486	07.27.05.00	44	010	+76	+61	061	4,70	0,80	0,94	073	123	146	88
6490	07.27.05.01	40	028	+66	+50	056	1,21	0,35	0,79	078	123	101	86
6502	07.27.05.22	44	016	+80	+62	070	−40,63	1,02	0,92	071	123	146	88
6507	07.27.05.32	61	015	+32	+23	025	1,71	0,45	0,94	137	126	220	84
6514	07.27.05.47	44	017	+69	+55	053	2,49	0,60	0,92	080	123	140	86
6519	07.27.05.55	45	015	+68	+54	052	2,10	0,71	0,93	081	123	141	86
6522	07.27.05.57	40	021	+74	+58	062	1,04	0,70	0,89	071	123	132	88
6526	07.27.06.00	45	023	+76	+59	066	7,33	0,87	0,91	074	123	141	88
6560	07.27.07.16	43	025	+69	+53	058	1,83	0,52	0,87	079	123	127	86
6589	07.27.21.53	43	338	−15	−06	336	2,34	0,97	0,05	026	304	157	95
6592	07.27.22.07	42	342	−29	−19	332	3,29	0,71	0,18	051	304	133	99
6596	07.27.22.25	44	338	−16	−06	334	2,87	0,98	0,05	031	304	157	95
6598	07.27.22.28	39	340	−15	−06	336	1,45	0,96	0,06	023	304	156	95
6599	07.27.22.28	38	339	−10	−01	336	1,27	0,96	0,05	036	304	159	93
6600	07.27.22.28	40	340	−16	−07	335	1,59	0,40	0,06	027	304	155	95
6601	07.27.22.30	39	336	−06	+03	336	1,37	0,96	0,06	013	124	337	93
6604	07.27.22.35	46	340	−27	−17	331	20,52	0,99	0,15	052	304	134	99
6605	07.27.22.35	39	335	−07	+03	334	1,60	0,96	0,07	011	124	335	93
6608	07.27.22.53	39	343	−10	−02	340	1,13	0,97	0,03	012	304	165	93
6609	07.27.22.57	43	339	−12	−03	336	2,01	0,99	0,03	015	304	162	95
6611	07.27.23.05	36	341	−10	−02	339	1,03	0,94	0,06	007	304	160	93
6612	07.27.23.05	42	341	−22	−13	334	2,19	0,95	0,11	043	304	146	95
6613	07.27.23.05	45	330	−08	+03	330	10,93	0,99	0,07	014	124	329	89
6614	07.27.23.05	41	341	−22	−13	334	1,89	0,94	0,11	042	304	147	95

Continuation

No. of meteor	DATE	v_∞	α	δ	β	λ	a	e	q	i	Ω	ω	shower
6615	07.27.23.07	42	339°	—26°	—11°	331°	8,62	0,96	0,16	044°	304°	136°	99
6618	07.27.23.15	42	338	—10	—01	336	1,80	0,98	0,03	006	304	162	93
6619	07.27.23.16	41	341	—20	—11	335	1,75	0,98	0,09	039	304	150	95
6620	07.27.23.18	45	341	—25	—16	333	4,78	0,97	0,13	052	304	140	99
6621	07.27.23.20	36	337	—11	—01	335	1,17	0,92	0,09	003	304	154	93
6622	07.27.23.21	43	338	—21	—11	332	3,57	0,97	0,10	039	304	146	95
6623	07.27.23.21	39	329	—09	+03	328	2,25	0,95	0,12	008	124	324	89
6624	07.27.23.24	42	339	—21	—11	333	2,38	0,96	0,10	037	304	147	95
6625	07.27.23.25	40	336	—14	—03	333	1,83	0,96	0,07	012	304	153	95
6626	07.27.23.25	43	327	—09	+03	327	9,90	0,99	0,12	012	124	320	89
6627	07.27.23.27	37	339	—13	—03	336	1,25	0,94	0,07	011	304	156	93
6628	07.27.23.30	41	337	—16	—06	333	1,93	0,96	0,08	022	304	152	95
6629	07.27.23.30	41	339	—14	—05	335	1,72	0,97	0,05	020	304	157	95
6631	07.27.23.34	39	339	—03	+05	339	1,21	0,97	0,04	024	124	342	93
6632	07.27.23.34	42	340	—15	—06	336	1,73	0,97	0,05	026	304	158	95
6633	07.27.23.38	43	339	—16	—07	334	2,53	0,98	0,05	032	304	156	95
6635	07.27.23.40	42	341	—14	—05	337	1,62	0,98	0,04	026	304	160	95
6636	07.27.23.41	43	336	—13	—02	333	1,60	0,97	0,05	011	304	156	95
6638	07.27.23.42	40	337	—23	—13	331	2,34	0,94	0,13	035	304	141	95
6640	07.27.23.45	41	345	—24	—16	336	1,76	0,94	0,12	052	304	145	99
6642	07.27.23.47	40	336	—19	—09	331	2,14	0,95	0,11	026	304	146	95
6645	07.27.23.49	41	334	—21	—09	328	3,52	0,96	0,13	026	304	141	95
6646	07.27.23.50	40	341	—19	—10	336	1,61	0,41	0,08	037	304	153	95
6648	07.27.23.57	42	344	—35	—26	331	4,59	0,94	0,29	055	304	118	100
6649	07.27.23.57	42	344	—19	—12	338	1,68	0,96	0,07	048	304	154	95
6651	07.27.23.59	45	334	—10	+00	332	5,03	0,99	0,04	002	124	337	89
6654	07.28.00.00	42	341	—20	—11	335	1,96	0,96	0,08	042	304	152	95
6656	07.28.00.00	41	338	—14	—05	335	1,75	0,97	0,05	020	304	157	95
6657	07.28.00.00	42	334	—15	—04	331	2,87	0,97	0,08	015	304	151	95
6658	07.28.00.03	41	338	—11	—01	336	1,60	0,98	0,04	007	304	161	93
6661	07.28.00.05	37	335	—12	—02	333	1,40	0,94	0,09	006	304	152	93
6664	07.28.00.10	39	338	—14	—04	334	1,47	0,95	0,07	014	304	155	95
6665	07.28.00.12	38	338	—06	+03	337	1,20	0,95	0,06	012	124	339	93
6667	07.28.00.13	40	338	—13	—03	335	1,49	0,97	0,05	012	304	158	95
6668	07.28.00.15	41	338	—25	—15	330	2,80	0,95	0,15	039	304	138	99
6670	07.28.00.15	40	338	—15	—05	335	1,55	0,95	0,07	020	304	155	95
6671	07.28.00.15	39	336	—12	—02	333	1,63	0,20	0,07	018	304	154	95
6677	07.28.00.18	39	336	—17	—06	331	1,86	0,95	0,10	019	304	148	95
6680	07.28.00.20	43	340	—18	—09	334	2,27	0,57	0,07	036	304	153	95
6682	07.28.00.26	45	329	—30	—20	329	145,08	0,99	0,21	050	304	125	99
6685	07.28.00.29	42	336	—18	—08	332	2,81	0,97	0,08	027	304	149	95
6686	07.28.00.30	42	339	—21	—12	333	2,54	0,96	0,10	040	304	147	95
6687	07.28.00.31	42	338	—24	—14	331	2,84	0,95	0,14	040	304	140	99
6689	07.28.00.34	39	342	—04	+03	342	1,05	0,97	0,03	020	124	346	93
6690	07.28.00.36	44	340	—21	—12	334	3,00	0,97	0,09	044	304	148	95
6691	07.28.00.36	39	337	+02	+12	339	1,22	0,94	0,07	042	124	336	87
6692	07.28.00.37	42	339	—13	—04	336	1,81	0,97	0,04	019	304	161	95
6694	07.28.00.40	44	341	—20	—11	335	2,89	0,98	0,07	046	304	151	95
6695	07.28.00.42	44	337	—27	—16	329	9,49	0,98	0,16	044	304	133	99
6701	07.28.00.45	43	336	—25	—14	328	7,14	0,98	0,15	039	304	135	99
6702	07.28.00.45	46	339	—17	—08	334	4,30	0,99	0,05	049	304	155	95
6708	07.28.00.50	42	340	—20	—11	334	2,24	0,96	0,09	038	304	149	95
6713	07.28.00.55	37	342	—11	—03	339	1,10	0,95	0,05	012	304	161	93
6715	07.28.00.57	40	337	—15	—05	333	1,72	0,96	0,07	018	304	153	95
6716	07.28.01.03	40	340	—18	—08	335	1,66	0,95	0,08	030	304	153	95
6720	07.28.04.15	58	010	+44	+36	027	2,84	0,65	0,98	117	124	204	96
6735	07.28.04.22	59	015	+27	+19	024	1,22	0,34	0,81	143	124	255	84
6758	07.28.04.41	59	012	+41	+33	029	1,25	0,22	0,98	122	124	205	96
6759	07.28.04.42	42	022	+65	+50	052	1,25	0,31	0,86	082	124	115	86
6764	07.28.04.44	41	011	+56	+45	038	0,95	0,12	0,84	087	124	069	97

Continuation

No. of meteor	DATE	v_∞	α	δ	β	λ	a	e	q	i	Ω	ω	shower
6808	07.28.06.20	60	048°	+21°	+03°	051°	1,26	0,56	0,56	173°	124°	078°	98
6817	07.28.06.24	40	032	+76	+57	068	2,08	0,59	0,86	069	124	127	88
6828	07.28.06.46	62	054	+20	+00	057	1,75	0,73	0,48	179	124	077	98
6834	07.28.06.53	60	046	+21	+03	049	1,18	0,50	0,59	172	124	078	98
6852	07.28.07.30	41	027	+77	+58	067	2,76	0,68	0,88	071	124	135	88
6881	07.28.09.37	39	101	+16	−07	101	2,66	0,64	0,14	017	304	220	85
6883	07.28.09.38	42	100	+15	−08	100	3,85	0,75	0,11	024	304	217	85
6892	07.28.09.48	38	101	+17	−07	100	1,98	0,93	0,14	016	304	219	85
6974	07.29.10.30	41	101	+15	−08	101	3,28	0,96	0,12	023	305	218	85
7001	07.29.12.52	43	102	+17	−06	102	5,85	0,98	0,11	019	305	218	85
7009	07.29.14.57	39	031	+74	+56	066	1,62	0,48	0,85	070	125	122	88
7012	07.29.15.36	44	041	+75	+55	071	3,29	0,74	0,85	074	125	130	88
7033	07.29.20.10	40	338	−11	−01	336	1,73	0,44	0,06	006	306	157	93
7038	07.29.22.28	38	341	+18	−10	336	1,50	0,37	0,10	029	306	150	95
7041	07.29.23.28	40	335	+20	−08	320	2,85	0,66	0,13	023	306	141	95
7042	07.29.23.34	46	335	−04	+06	335	6,74	0,99	0,04	034	126	336	89
7050	07.29.23.50	37	345	−02	+01	344	0,97	0,97	0,03	005	126	346	93
7051	07.29.23.56	41	339	−07	+02	338	1,58	0,97	0,04	008	126	340	89
7052	07.29.23.59	38	341	−20	−11	335	1,55	0,40	0,11	029	306	147	95
7053	07.30.00.06	40	346	−18	−11	340	1,42	0,33	0,07	042	306	155	95
7055	07.30.00.54	41	339	−21	−11	333	2,57	0,69	0,80	031	305	142	95
7057	07.30.00.58	40	339	−21	−11	332	2,25	0,98	0,05	031	306	142	95
7073	07.30.03.41	62	016	+25	+17	024	1,64	0,50	0,82	147	126	243	84
7105	07.30.22.06	34	340	−12	−03	337	2,23	0,98	0,04	015	306	160	95
7106	07.30.22.07	44	339	−13	−04	336	3,76	0,99	0,05	019	307	156	95
7110	07.30.22.12	40	339	−13	−03	336	1,64	0,96	0,07	012	306	155	95
7112	07.30.22.20	39	343	−13	−06	339	1,32	0,95	0,06	022	307	158	95
7113	07.30.22.20	41	346	−17	−10	340	1,47	0,96	0,06	045	306	157	95
7116	07.30.22.31	43	337	−03	+06	338	1,89	0,97	0,05	031	126	338	89
7120	07.30.22.44	39	341	−12	−03	338	1,44	0,96	0,06	012	307	157	95
7121	07.30.22.45	44	345	−27	−19	335	4,55	0,96	0,17	054	307	133	99
7124	07.30.22.52	42	339	−20	−10	334	3,33	0,97	0,10	033	307	145	95
7125	07.30.22.52	42	340	−22	−13	333	3,64	0,96	0,13	038	307	140	95
7127	07.30.22.54	40	339	−16	−07	335	1,92	0,96	0,08	023	306	151	95
7128	07.30.22.54	42	339	−23	−13	332	3,77	0,96	0,15	036	307	137	95
7130	07.30.22.56	42	343	−17	−09	338	1,86	0,97	0,06	040	306	154	95
7131	07.30.22.58	41	340	−16	−07	335	1,98	0,96	0,07	027	306	153	95
7132	07.30.22.59	41	339	−13	−04	336	1,95	0,97	0,06	015	307	154	95
7135	07.30.23.01	42	342	−17	−09	337	1,95	0,96	0,07	037	306	154	95
7136	07.30.23.01	42	343	−18	−09	337	2,11	0,96	0,08	036	307	152	95
7137	07.30.23.08	41	341	−10	−01	339	1,64	0,98	0,04	008	307	160	93
7138	07.30.23.08	41	341	−15	−06	337	1,76	0,96	0,06	026	306	156	95
7139	07.30.23.10	41	341	−18	−09	336	1,89	0,96	0,08	032	306	151	95
7141	07.30.23.22	42	337	−05	+04	337	2,16	0,98	0,05	019	127	336	89
7142	07.30.23.22	43	337	−03	+06	338	1,92	0,98	0,04	029	126	339	89
7145	07.30.23.24	42	338	−14	−04	334	2,65	0,97	0,08	016	307	151	95
7146	07.30.23.25	40	339	−13	−04	336	1,86	0,96	0,07	015	307	154	95
7150	07.30.23.30	40	340	−12	−03	337	1,62	0,96	0,06	013	307	156	95
7151	07.30.23.34	43	341	−23	−14	334	3,71	0,96	0,13	043	307	140	95
7153	07.30.23.42	44	340	−05	+03	340	2,08	0,99	0,02	021	126	346	89
7154	07.30.23.42	44	342	−31	−21	331	−32,54	1,01	0,24	050	307	121	99
7155	07.30.23.45	42	341	−22	−13	334	3,42	0,96	0,13	040	307	141	95
7157	07.30.23.47	39	345	−20	−13	338	1,53	0,93	0,10	040	307	149	95
7159	07.30.23.48	41	341	−21	−12	335	2,34	0,95	0,12	037	307	144	95
7160	07.30.23.50	41	341	−12	−03	338	1,82	0,97	0,05	015	307	158	95
7162	07.30.23.52	41	340	−15	−06	336	1,95	0,96	0,08	022	307	152	95
7166	07.30.23.56	41	340	−14	−05	337	1,71	0,96	0,06	020	306	156	95
7170	07.31.00.04	34	342	+06	+13	346	0,87	0,91	0,08	038	127	338	87
7171	07.31.00.05	36	337	+05	+14	340	1,11	0,90	0,11	036	127	331	87
7173	07.31.00.07	39	341	−10	−02	338	1,44	0,96	0,06	008	307	157	93

Continuation

No. of meteor	DATE	v_∞	α	δ	β	λ	a	e	q	i	Ω	ω	shower
7178	07.30.23.59	42	340°	−17°	−08°	335°	2,68	0,97	0,08	030	307°	150°	95
7187	08.02.04.05	61	020	+27	+15	034	1,32	0,31	0,91	150	130	232	105
7188	08.02.04.05	61	018	+41	+30	033	2,68	0,64	0,97	126	130	208	104
7189	08.02.04.06	52	032	+17	+40	040	0,77	0,31	0,53	142	130	016	102
7203	08.02.04.46	64	038	+01	−14	036	1,80	0,46	0,97	155	310	029	101
7207	08.02.05.07	66	039	+29	+13	046	2,43	0,61	0,96	156	130	149	106
7215	08.02.05.08	52	037	+29	+14	044	0,76	0,37	0,48	149	130	021	102
7212	08.02.05.30	51	033	+34	+19	043	0,77	0,32	0,52	137	130	018	102
7254	08.02.19.37	35	331	−04	+07	331	1,97	0,90	0,20	013	130	314	91
7261	08.02.20.10	50	018	+56	+44	043	1,63	0,39	0,99	100	130	156	107
7266	08.02.20.21	58	049	+49	+30	060	2,47	0,69	0,76	121	130	114	108
7283	08.02.21.25	41	337	−06	+04	336	2,74	0,97	0,09	011	130	328	89
7286	08.02.21.31	41	342	−25	−16	333	5,42	0,96	0,20	038	310	129	99
7288	08.02.21.37	32	329	−03	+09	331	1,60	0,85	0,24	014	130	310	91
7289	08.02.21.37	36	330	−06	+06	330	2,34	0,92	0,20	011	130	312	91
7294	08.02.21.44	45	353	−34	−27	340	9,42	0,96	0,31	062	310	113	111
7297	08.02.21.58	43	350	−34	−32	337	6,75	0,95	0,31	056	310	114	111
7298	08.02.22.00	37	345	−14	−07	341	1,35	0,93	0,09	020	310	152	95
7311	08.02.22.25	41	340	−08	+01	339	2,29	0,97	0,07	003	130	133	89
7312	08.02.22.28	55	033	+57	+41	053	2,88	0,67	0,94	107	130	145	109
7316	08.02.22.36	41	345	−23	−15	337	2,88	0,95	0,15	041	310	138	99
7321	08.02.22.42	43	345	−18	−11	339	3,32	0,94	0,09	039	310	148	95
7322	08.02.22.44	41	344	−16	−08	339	2,29	0,97	0,08	028	310	150	95
7326	08.02.22.50	39	347	−16	−09	342	1,57	0,95	0,08	031	310	152	95
7328	08.02.22.52	55	021	+50	+37	041	1,77	0,44	0,99	112	130	159	110
7334	08.02.23.01	41	343	+01	+07	345	1,49	0,97	0,05	035	130	339	89
7336	08.02.23.05	42	344	−17	−09	339	2,59	0,97	0,09	033	310	149	95
7342	08.02.23.16	62	027	+25	+13	034	1,38	0,35	0,90	155	130	234	105
7349	08.02.23.23	64	028	+26	+14	035	1,97	0,51	0,97	154	130	210	105
7356	08.02.23.28	40	343	−10	−03	340	1,65	0,96	0,06	009	310	155	95
7357	08.02.23.29	43	341	−23	−14	334	13,16	0,91	0,16	036	310	133	99
7360	08.02.23.31	39	345	−21	−13	338	1,94	0,93	0,14	034	310	142	95
7365	08.02.23.38	66	033	+33	+19	042	3,01	0,67	1,00	146	130	163	122
7374	08.02.23.48	40	342	−00	+07	143	1,50	0,96	0,06	029	130	337	89
7377	08.02.23.52	40	340	−07	+01	339	1,91	0,96	0,07	004	130	334	93
7393	08.03.00.06	60	023	+42	+30	038	2,19	0,55	0,99	126	130	201	104
7407	08.03.00.19	63	027	+31	+18	036	1,72	0,44	0,96	147	130	212	105
7417	08.03.00.30	58	065	+45	+24	071	2,77	0,83	0,48	124	130	082	118
7418	08.03.00.32	61	036	+42	+26	048	1,96	0,52	0,94	133	130	144	120
7422	08.03.00.35	60	010	+18	+12	016	1,74	0,74	0,45	151	130	287	119
7423	08.03.00.36	62	023	+31	+20	034	1,82	0,49	0,93	143	130	220	105
7426	08.03.00.40	62	052	+29	+10	057	1,54	0,58	0,65	160	130	093	112
7427	08.03.00.41	52	042	+36	+19	050	0,82	0,38	0,51	137	130	038	117
7428	08.03.00.44	41	343	−12	−05	340	2,06	0,97	0,06	019	310	155	95
7431	08.03.01.10	64	025	+09	−01	027	1,72	0,58	0,73	178	311	075	114
7432	08.03.01.10	59	047	+36	+17	054	1,27	0,44	0,71	144	131	093	112
7433	08.03.01.10	58	040	+37	+20	049	1,18	0,29	0,84	140	131	106	121
7436	08.03.01.13	66	038	+01	−13	036	2,42	0,60	0,97	156	311	028	101
7437	08.03.01.15	69	034	+31	+16	042	7,27	0,86	1,00	152	131	164	122
7440	08.03.01.18	63	026	+31	+19	036	2,07	0,53	0,97	145	130	209	105
7443	08.03.01.25	61	052	+48	+28	063	5,37	0,86	0,74	124	131	115	108
7445	08.03.01.27	63	026	+08	−03	027	1,67	0,56	0,73	175	311	075	114
7446	08.03.01.27	54	043	+35	+17	051	0,89	0,34	0,59	142	131	054	117
7451	08.03.01.30	63	031	+30	+16	039	1,71	0,42	0,99	151	131	203	123
7458	08.03.01.40	61	036	+55	+38	054	−50,73	1,02	0,94	115	131	149	115
7462	08.03.01.46	61	051	+31	+12	057	2,62	0,73	0,64	155	131	090	112
7486	08.03.02.10	63	027	+28	+15	035	1,67	0,43	0,95	152	131	216	105
7495	08.03.02.20	66	052	+25	+06	055	2,77	0,72	0,77	169	131	117	126
7497	08.03.02.24	58	052	+30	+11	057	1,09	0,51	0,53	155	131	068	112
7498	08.03.02.30	59	069	+42	+20	074	3,78	0,89	0,40	129	131	074	118

Continuation

No. of meteor	DATE	v_{∞}	α	δ	β	λ	a	e	q	i	Ω	ω	shower
7500	08.03.02.31	64	041°	+03°	−12°	039°	1,74	0,43	0,99	159°	311°	023°	101
7513	08.03.02.52	57	068	+44	+22	073	2,68	0,85	0,41	125	131	073	118
7518	08.03.02.56	64	054	+32	+13	059	2,30	0,72	0,68	155	131	103	112
7519	08.03.03.00	68	053	+12	−07	054	4,40	0,81	0,83	167	311	308	125
7522	08.03.03.02	58	057	+30	+10	062	1,17	0,63	0,43	157	131	062	113
7526	08.03.03.15	59	051	+34	+15	057	1,25	0,50	0,62	149	131	083	112
7534	08.03.03.20	67	039	+11	+04	040	2,22	0,55	0,99	172	311	018	124
7537	08.03.03.26	67	037	+10	−05	038	2,37	0,59	0,98	171	311	023	124
7594	08.03.20.22	42	338	−03	+06	338	3,16	0,97	0,08	020	131	329	89
7611	08.03.21.41	54	024	+47	+34	041	1,42	0,30	0,99	116	131	207	110
7616	08.03.21.53	40	341	−01	+07	342	1,61	0,96	0,07	025	131	335	89
7625	08.03.22.08	41	345	−20	−12	339	2,34	0,94	0,13	036	311	143	95
7626	08.03.22.10	40	348	−32	−25	335	3,99	0,94	0,30	047	311	117	111
7627	08.03.22.14	43	347	−20	−14	340	3,24	0,96	0,12	044	311	142	95
7632	08.03.22.22	59	022	+39	+27	036	1,72	0,06	0,96	130	131	214	104
7636	08.03.22.24	55	031	+53	+37	049	1,86	0,14	0,96	112	131	147	109
7638	08.03.22.31	52	028	+57	+42	049	1,77	0,46	0,96	104	131	147	109
7639	08.03.22.32	64	032	+33	+19	041	2,13	0,54	0,99	146	131	199	123
7646	08.03.22.38	39	339	−02	+06	340	1,81	0,95	0,09	019	131	330	89
7648	08.03.22.40	40	345	−21	−13	338	2,42	0,94	0,14	035	311	140	95
7654	08.03.22.47	53	020	+62	+49	049	4,42	0,78	0,98	096	131	159	107
7656	08.03.22.49	41	349	−16	−11	344	1,69	0,46	0,07	040	311	153	95
7663	08.03.23.01	61	015	+16	+09	020	1,70	0,71	0,50	160	131	282	119
7669	08.03.23.07	40	345	−11	−05	342	1,67	0,96	0,07	017	311	155	95
7670	08.03.23.08	39	345	−03	+04	345	1,36	0,26	0,05	016	131	340	93
7678	08.03.23.22	61	013	+12	+06	017	1,87	0,78	0,42	165	131	289	119
7681	08.03.23.25	40	349	−11	−06	345	1,37	0,96	0,05	026	311	160	95
7683	08.03.23.25	40	343	−16	−08	338	2,16	0,95	0,11	024	311	146	95
7684	08.03.23.26	61	015	+32	+24	027	2,37	0,65	0,82	135	131	238	127
7698	08.03.23.37	39	343	−09	−02	341	1,60	0,96	0,07	006	311	154	95
7711	08.03.23.52	67	034	+32	+17	043	3,52	0,72	1,00	150	131	164	122
7718	08.04.00.07	60	037	+46	+30	050	2,46	0,62	0,94	127	131	145	120
7721	08.04.00.08	58	026	+42	+29	040	1,52	0,35	0,99	127	131	206	104
7724	08.04.00.13	41	345	−13	−06	341	1,86	0,96	0,07	023	311	153	95
7731	08.04.00.18	59	021	+39	+28	035	1,74	0,45	0,95	128	131	217	104
7733	08.04.00.22	67	039	+07	−08	039	2,41	0,59	0,99	166	311	021	124
7737	08.04.00.24	36	341	−04	+04	341	1,32	0,92	0,10	010	131	331	93
7739	08.04.00.24	41	343	−16	−08	338	2,65	0,96	0,10	026	311	146	95
7743	08.04.00.28	43	346	−13	−07	342	2,36	0,98	0,05	030	311	156	95
7748	08.04.00.36	58	018	+43	+32	034	2,16	0,56	0,95	121	131	213	104
7751	08.04.00.39	68	034	+36	+21	044	9,34	0,90	0,99	144	131	163	122
7754	08.04.00.44	44	349	−11	−05	346	2,01	0,99	0,03	036	311	164	95
7755	08.04.00.45	60	035	+45	+29	048	2,27	0,58	0,96	128	131	151	120
7759	08.04.00.47	58	052	+50	+30	063	2,63	0,72	0,73	120	131	110	108
7760	08.04.00.48	58	037	+41	+25	048	1,30	0,29	0,92	132	131	128	121
7765	08.04.00.53	59	033	+37	+23	044	1,37	0,28	0,98	138	131	148	129
7770	08.04.00.59	65	049	+25	+07	054	1,92	0,57	0,82	167	131	119	126
7775	08.04.01.03	42	346	−09	−03	343	1,77	0,98	0,04	013	311	160	95
7783	08.04.01.13	64	037	+30	+14	045	1,82	0,46	0,98	154	131	154	106
7788	08.04.01.18	66	033	+38	+24	044	5,54	0,82	1,00	139	131	163	122
7795	08.04.01.31	60	038	+41	+24	049	1,74	0,47	0,93	135	131	139	120
7796	08.04.01.31	63	041	+44	+26	052	3,68	0,75	0,92	133	131	142	120
7809	08.04.01.48	64	037	+42	+26	049	3,70	0,74	0,96	135	131	152	120
7810	08.04.01.49	61	050	+35	+17	057	1,57	0,54	0,72	147	131	102	112
7816	08.04.01.55	64	040	+31	+15	047	1,97	0,51	0,96	153	132	147	106
7817	08.04.01.56	64	031	+08	−05	031	1,57	0,47	0,83	171	312	063	114
7821	08.04.02.03	64	038	+24	+09	043	1,50	0,35	0,98	163	132	152	103
7825	08.04.02.05	65	029	+25	+12	036	1,90	0,50	0,95	157	132	214	105
7826	08.04.02.06	65	051	+17	−02	053	2,03	0,59	0,83	177	312	301	125
7827	08.04.02.07	65	027	+12	+01	030	1,97	0,59	0,81	178	132	242	128

Continuation

No. of meteor	DATE	v_∞	α	δ	β	λ	a	e	q	i	Ω	ω	shower
7829	08.04.02.11	60	016°	+16°	+08°	021°	1,47	0,66	0,50	161°	132°	285°	119
7831	08.04.02.15	63	048	+25	+07	053	1,58	0,49	0,81	167	132	115	126
7832	08.04.02.15	65	024	+13	+03	027	2,10	0,65	0,74	174	132	251	128
7850	08.04.02.38	63	053	+32	+12	053	1,89	0,63	0,70	155	132	103	112
7854	08.04.02.44	60	061	+29	+08	064	1,54	0,70	0,46	160	132	072	113
7860	08.04.02.52	64	063	+30	+09	067	3,51	0,86	0,50	160	132	086	113
7863	08.04.02.55	62	062	+27	+06	065	1,91	0,75	0,47	166	132	077	113
7878	08.04.03.15	64	064	+29	+07	067	3,76	0,86	0,50	163	132	086	113
7879	08.04.03.16	63	060	+29	+08	064	2,54	0,78	0,56	162	132	090	113
7882	08.04.03.17	66	054	+25	+06	058	2,94	0,75	0,74	169	132	112	126
7885	08.04.03.20	65	051	+14	—04	052	1,72	0,51	0,85	172	312	302	125
7892	08.04.03.29	59	058	+31	+11	062	1,37	0,64	0,49	156	132	073	113
7908	08.04.03.47	68	055	+18	—01	057	4,26	0,80	0,79	177	312	302	125
7918	08.04.04.46	63	051	—08	—25	047	2,85	0,66	0,98	135	312	336	130
7943	08.04.16.32	54	019	+53	+41	041	2,17	0,54	0,99	107	132	199	131
7966	08.04.22.10	52	022	+47	+35	039	1,18	0,20	0,95	113	132	227	110
7973	08.04.22.22	55	036	+58	+41	056	2,87	0,68	0,93	107	132	142	109
7981	08.04.22.39	68	033	+38	+23	044	—102	1,01	1,00	141	132	266	122
7984	08.04.22.49	50	024	+60	+46	049	1,89	0,49	0,97	098	132	152	107
7985	08.04.22.53	59	039	+44	+27	051	1,61	0,45	0,92	129	132	137	120
7988	08.04.22.53	56	023	+47	+35	040	1,65	0,40	0,99	116	132	204	110
7991	08.04.22.57	39	344	—04	+03	344	1,42	0,96	0,06	010	132	337	93
7996	08.04.23.28	41	341	—07	+01	340	2,36	0,97	0,08	005	132	331	89
7999	08.04.23.34	67	038	+33	+17	047	4,37	0,79	0,92	149	132	159	106
8005	08.04.23.44	54	033	+59	+43	054	2,64	0,64	0,95	104	132	147	109
8006	08.04.23.44	40	346	—16	—09	341	1,90	0,95	0,10	027	312	148	95
8007	08.04.23.44	60	024	+42	+30	039	2,18	0,55	0,98	127	132	203	104
8009	08.04.23.46	53	036	+57	+40	055	1,97	0,53	0,92	106	132	138	109
8010	08.04.23.47	39	346	—11	—05	343	1,55	0,95	0,07	017	312	155	95
8013	08.04.23.52	59	035	+35	+20	044	1,23	0,01	0,97	141	132	141	129
8016	08.05.00.04	61	030	+08	—04	031	1,27	0,43	0,72	172	312	086	114
8020	08.05.00.07	46	345	—20	—13	338	—20,17	1,01	0,12	044	312	139	99
8025	08.05.00.15	57	025	+47	+34	042	1,88	0,47	0,99	118	132	201	110
8028	08.05.00.25	62	018	+36	+26	031	2,68	0,67	0,89	132	132	224	127
8034	08.05.00.35	62	028	+42	+28	041	2,60	0,62	0,99	130	132	198	104
8035	08.05.00.35	58	038	+54	+37	054	3,54	0,74	0,93	114	132	144	115
8039	08.05.00.41	62	037	+25	+10	043	1,25	0,22	0,98	161	132	145	103
8040	08.05.00.46	53	038	+33	+17	047	0,82	0,27	0,60	143	132	029	102
8050	08.05.01.02	62	034	+38	+23	045	1,77	0,44	0,99	139	132	157	129
8055	08.05.01.11	61	052	+27	+08	056	1,36	0,49	0,70	164	132	095	126
8059	08.05.01.18	54	036	+32	+16	044	0,83	0,23	0,64	145	132	026	102
8063	08.05.01.23	59	049	+31	+12	054	1,15	0,39	0,70	155	132	086	112
8068	08.05.01.27	56	065	+42	+21	070	1,70	0,74	0,44	130	132	072	118
8071	08.05.01.30	55	051	+30	+11	056	0,89	0,47	0,47	154	132	050	116
8075	08.05.01.33	65	041	+32	+15	049	2,19	0,57	0,95	153	132	147	106
8085	08.05.01.52	65	027	+18	+06	031	2,03	0,59	0,83	168	132	237	128
8090	08.05.01.53	65	028	+16	+04	032	2,03	0,58	0,85	172	132	236	128
8092	08.05.01.54	65	052	+40	+21	060	9,67	0,92	1,00	140	312	344	130
8095	08.05.02.02	63	053	+33	+14	058	1,86	0,61	0,72	153	132	105	112
8097	08.05.02.06	61	049	+35	+16	055	1,47	0,45	0,77	148	132	106	112
8099	08.05.02.08	61	034	+38	+22	045	1,59	0,38	0,98	139	132	154	129
8101	08.05.02.08	60	064	+42	+21	070	3,27	0,84	0,53	134	132	089	118
8106	08.05.02.51	63	055	+32	+12	061	2,07	0,67	0,68	155	132	101	112
8115	08.05.03.08	59	055	+46	+26	064	2,39	0,71	0,69	127	133	105	108
8118	08.05.03.14	67	045	+32	+14	052	3,44	0,73	0,92	155	133	142	106
8125	08.05.03.37	60	040	+58	+40	059	9,35	0,90	0,93	111	133	148	115
8129	08.05.03.50	64	061	+28	+07	064	2,82	0,79	0,58	165	133	093	113
8131	08.05.03.59	61	051	—06	—24	047	1,71	0,43	0,97	136	313	330	130
8132	08.05.04.03	63	051	—04	—22	047	2,30	0,57	0,98	140	313	335	130
8211	08.06.00.15	61	042	+47	+29	054	2,98	0,69	0,92	127	133	141	120

Continuation

No. of meteor	DATE	α_{∞}	α	δ	β	λ	a	e	q	i	Ω	ω	shower
8214	08.06.00.22	64	056°	+27°	+07°	060°	1,93	0,65	0,68	166°	133°	101°	126
8215	08.06.00.22	70	036	+31	+15	044	—230	1,00	1,00	153	133	167	127
8216	08.06.00.25	59	027	+42	+29	041	1,86	0,47	0,99	127	133	203	108
8218	08.06.00.34	58	059	+48	+27	067	2,20	0,71	0,64	124	133	098	116
8224	08.06.00.40	67	038	+31	+15	045	3,77	0,74	1,00	153	133	163	108
8226	08.06.00.42	63	036	+35	+20	046	1,80	0,45	0,99	144	133	157	95
8231	08.06.01.02	65	042	+36	+19	051	2,86	0,67	0,95	143	133	148	95
8238	08.06.02.57	63	066	+29	+07	069	2,94	0,84	0,47	163	133	081	105
8278	08.06.19.45	53	020	+61	+47	047	3,13	0,68	0,99	099	134	163	103
8297	08.06.22.23	54	030	+54	+38	049	1,65	0,41	0,98	110	134	152	89
8302	08.06.22.50	51	023	+64	+49	052	2,95	0,67	0,98	094	134	158	89
8303	08.06.22.58	54	036	+61	+43	058	3,30	0,72	0,94	103	134	146	95
8315	08.06.23.38	54	027	+51	+36	046	1,55	0,36	0,99	113	134	456	99
8319	08.07.00.38	59	070	+43	+20	074	2,82	0,84	0,45	131	134	078	89
8321	08.07.00.45	61	060	+50	+29	069	8,44	0,92	0,71	123	134	113	95
8342	08.07.23.28	52	032	+59	+43	075	1,90	0,49	0,96	103	135	148	95
8343	08.07.23.28	62	056	+23	+03	059	1,44	0,50	0,72	174	135	099	126
8346	08.07.23.47	61	013	+37	+29	028	4,06	0,80	0,82	126	135	235	122
8348	08.08.00.04	63	058	+46	+25	066	7,19	0,90	0,75	132	035	118	104
8349	08.08.00.07	51	058	+27	+87	022	0,79	0,63	0,29	146	135	033	108
8364	08.08.01.06	57	062	+52	+30	070	2,75	0,76	0,67	118	135	103	122
8400	08.09.00.17	38	351	—09	—05	348	1,33	0,95	0,07	016	316	156	129
8401	08.09.00.52	38	350	—15	—10	345	1,51	0,93	0,11	027	316	147	106
8410	08.09.04.17	65	029	+31	+17	038	2,43	0,62	0,92	148	136	219	113
8415	08.09.04.52	62	043	+23	+06	047	1,21	0,20	0,97	168	136	141	107
8424	08.09.23.16	41	343	—04	+04	343	2,77	0,96	0,10	011	137	326	109
8425	08.09.23.19	40	345	—03	+03	345	2,00	0,96	0,08	012	137	331	107
8426	08.09.23.20	40	348	—09	+04	345	1,91	0,96	0,08	013	317	151	109
8427	08.09.23.28	40	345	—25	—17	336	9,22	0,97	0,25	033	317	122	110
8428	08.09.23.35	43	346	+01	+06	348	2,54	0,98	0,05	030	138	336	118
8434	08.10.00.18	40	348	—17	—11	342	2,67	0,95	0,14	027	317	140	108
8438	08.10.00.32	44	348	—17	—11	343	7,19	0,98	0,11	034	317	142	109
8440	08.10.00.33	38	349	—12	—06	345	1,65	0,94	0,10	018	317	149	95
8442	08.10.00.39	41	349	—00	+04	350	1,54	0,97	0,04	018	137	340	89
8444	08.10.00.44	42	348	—00	+04	349	1,77	0,98	0,04	021	137	339	89
8445	08.10.00.52	40	347	—03	+02	347	1,62	0,96	0,07	007	137	335	93
8449	08.10.01.40	32	336	—08	+02	335	1,67	0,84	0,26	003	137	307	91
8457	08.10.02.34	58	016	+19	+12	022	1,44	0,74	0,38	151	137	298	112
8459	08.10.02.48	70	038	+13	—02	039	9,12	0,90	0,94	177	317	031	132
8462	08.10.03.02	61	022	+16	+06	026	1,57	0,69	0,48	166	137	285	119
8465	08.10.03.18	69	035	+12	—01	037	5,28	0,83	0,88	177	317	044	132
8470	08.10.03.22	65	038	+11	—04	039	1,81	0,51	0,89	172	317	050	132
8472	08.10.03.28	64	037	+31	+15	045	1,97	0,50	0,98	153	137	203	123
8474	08.10.03.34	57	031	+50	+35	047	1,91	0,48	0,99	118	137	200	110
8486	08.10.03.53	65	018	+35	+25	031	14,07	0,94	0,83	134	137	230	127
8490	08.10.04.03	69	042	+08	—07	042	3,92	0,75	0,97	169	317	025	124
8495	08.10.04.24	50	023	+57	+44	047	1,49	0,34	0,99	099	137	020	131
8500	08.10.04.30	61	043	+38	+20	052	1,59	0,39	0,97	042	137	149	129
8515	08.10.04.50	63	041	+29	+13	047	1,51	0,34	0,99	156	137	205	123
8520	08.10.05.05	59	044	+40	+22	063	1,30	0,29	0,92	138	137	130	121
8524	08.10.05.08	64	040	+29	+13	047	1,62	0,39	0,99	156	137	203	123
8528	08.10.05.13	67	058	+15	—05	059	2,23	0,62	0,85	170	317	306	125
8529	08.10.05.14	67	058	+14	—06	058	2,72	0,68	0,87	169	317	311	125
8531	08.10.05.16	66	048	+33	+15	055	2,73	0,65	0,95	153	137	147	106
8532	08.10.05.18	66	051	+36	+17	058	3,05	0,70	0,90	149	137	138	106
8549	08.10.05.57	49	054	+35	+15	060	0,71	0,58	0,30	141	137	025	116
8552	08.10.06.03	63	062	+27	+06	065	1,89	0,65	0,66	168	137	097	126
8569	08.11.00.48	33	334	—11	—01	332	2,72	0,89	0,29	001	318	120	90
8571	08.11.01.00	41	344	—06	+01	343	1,08	0,97	0,10	003	138	326	89
8572	08.11.01.09	44	349	—01	+04	350	2,55	0,99	0,03	021	138	341	89

Continuation

No. of meteor	DATE	v_∞	a	δ	β	λ	a	e	q	i	Ω	ω	Shower
8576	08.11.03.20	65	031°	+17°	+04°	035°	2,20	0,65	0,77	171°	138°	246°	128
8578	08.11.03.42	61	035	+09	—04	036	1,28	0,45	0,70	171	318	088	114
8590	08.11.04.08	59	019	+19	+10	025	1,56	0,71	0,45	156	138	289	119
8591	08.11.04.08	56	033	+46	+31	048	1,31	0,25	0,98	122	138	211	110
8593	08.11.04.10	51	027	+55	+40	048	1,37	0,28	0,98	106	138	208	131
8595	08.11.04.13	63	049	+06	—12	048	1,52	0,35	0,99	158	318	025	101
8602	08.11.04.20	66	041	+34	+17	050	2,70	0,63	1,00	149	138	163	122
8607	08.11.04.28	64	044	+57	+38	060	—4,01	1,24	0,96	116	138	154	115
8620	08.11.05.04	62	023	+14	+01	026	1,82	0,74	0,48	171	138	283	119
8634	08.11.05.12	64	049	+04	—13	048	1,66	0,40	0,99	155	318	022	101
8637	08.11.05.15	59	048	+38	+19	056	1,27	0,31	0,88	142	138	119	121
8640	08.11.05.16	57	046	+41	+22	055	1,16	0,25	0,87	136	138	110	121
8643	08.11.05.19	59	045	+44	+25	056	1,02	0,17	0,85	124	138	088	120
8645	08.11.05.20	52	046	+37	+19	054	0,81	0,31	0,56	138	138	030	117
8647	08.11.05.22	55	047	+08	—09	046	1,89	0,48	0,99	163	318	023	124
8649	08.11.05.22	58	042	+61	+43	061	12,50	0,92	0,95	106	138	152	115
8650	08.11.05.22	61	058	+35	+14	063	1,61	0,55	0,73	152	138	104	112
8655	08.11.05.27	57	046	+40	+22	055	1,09	0,22	0,85	136	138	101	121
8668	08.11.05.47	53	048	+39	+21	056	0,86	0,29	0,61	135	138	045	117
8669	08.11.05.48	53	056	+31	+11	061	0,80	0,49	0,41	154	138	038	116
8671	08.11.05.49	55	055	+33	+13	060	0,86	0,42	0,50	151	138	046	116
8692	08.11.22.58	38	349	—11	—06	346	1,72	0,94	0,11	016	319	147	95
8693	08.11.23.00	39	350	—17	—11	344	2,59	0,94	0,15	028	319	139	95
8701	08.11.23.45	41	354	—16	—13	348	2,16	0,95	0,11	038	319	145	95
8703	08.11.23.48	43	349	—01	+04	349	2,59	0,98	0,04	018	139	338	89
8704	08.11.23.50	40	344	+01	+07	346	2,15	0,95	0,10	022	139	327	89
8713	08.12.00.24	41	350	+01	+05	351	1,61	0,97	0,05	021	139	338	89
8714	08.12.00.30	40	348	—04	+01	347	2,03	0,97	0,07	005	139	333	89
8716	08.12.00.33	39	354	—07	—04	352	1,34	0,96	0,05	016	319	159	93
8717	08.12.00.40	42	346	—10	—04	343	5,51	0,98	0,10	012	319	145	95
8720	08.12.01.02	36	352	—01	+03	352	1,15	0,94	0,07	011	139	337	93
8744	08.12.02.38	51	036	+10	—04	038	1,22	0,42	0,71	172	319	089	114
8775	08.12.04.07	63	051	+00	—18	049	1,66	0,40	0,99	147	319	022	101
8777	08.12.04.08	60	017	+16	+09	022	2,06	0,83	0,26	158	139	294	119
8782	08.12.05.15	53	042	+34	+17	050	0,80	0,26	0,59	143	139	019	102
8783	08.12.05.17	59	040	+57	+39	058	6,39	0,85	0,97	113	139	157	115
8785	08.12.05.37	61	056	+32	+12	061	1,30	0,42	0,76	156	139	101	112
8789	08.12.05.48	53	048	+34	+15	055	0,79	0,34	0,98	142	139	153	117
8790	08.12.05.50	62	044	+39	+21	053	1,74	0,44	0,98	142	139	153	129
8791	08.12.05.50	52	042	+36	+19	050	0,77	0,31	0,53	140	139	015	102
8811	08.12.23.57	46	356	—10	—08	353	3,11	0,99	0,04	045	320	159	95
8817	08.13.00.07	40	347	—22	—15	339	14,47	0,98	0,25	031	320	122	99
8821	08.13.00.22	39	353	—10	—07	350	1,56	0,94	0,09	022	320	151	95
8823	08.13.00.27	36	341	—12	—03	339	2,70	0,92	0,22	006	320	129	90
8825	08.13.00.50	35	340	—00	+08	341	1,94	0,90	0,20	015	140	314	91
8831	08.13.01.26	46	348	—04	+01	348	10,15	0,99	0,04	006	140	336	89
8833	08.13.01.29	40	354	—06	—03	353	1,50	0,97	0,05	014	320	159	93
8834	08.13.01.31	33	343	—14	—07	339	1,82	0,87	0,24	011	320	129	90
8858	08.13.02.53	38	351	—11	—07	347	1,80	0,94	0,11	018	320	147	95
8864	08.13.03.15	59	028	+44	+30	043	2,12	0,55	0,95	125	140	215	104
8884	08.13.03.49	65	034	+19	+05	038	2,03	0,61	0,80	170	140	243	128
8885	08.13.03.52	64	035	+27	+13	041	1,74	0,49	0,88	156	140	231	105
8888	08.13.03.55	60	020	+19	+10	026	1,76	0,76	0,43	156	140	288	119
8896	08.13.04.09	64	060	—03	—23	057	3,18	0,69	0,97	139	320	333	130
8903	08.13.04.22	53	026	+55	+40	047	1,72	0,43	0,98	107	140	205	131
8908	08.13.04.38	53	028	+59	+44	051	2,23	0,56	0,99	103	140	162	107
8910	08.13.04.39	67	048	+37	+18	056	4,66	0,79	0,98	148	140	157	106
8911	08.13.04.45	60	045	+56	+37	060	5,31	0,82	0,96	116	140	151	115
8925	08.13.05.02	63	041	+37	+21	050	2,12	0,53	0,99	143	140	198	129
8927	08.13.05.04	53	023	+54	+41	045	1,83	0,47	0,97	106	140	207	131

Continuation

No. of meteor	DATE	v_∞	α	δ	β	λ	a	e	q	i	Ω	ω	shower
8929	08.13.05.07	51	025°	+60°	+45°	050°	1,85	0,46	0,99	099°	140°	200°	131
8933	08.13.05.09	59	041	+41	+24	051	1,40	0,30	0,98	135	140	152	129
8934	08.13.05.12	59	051	+39	+20	059	1,28	0,33	0,86	141	140	116	121
8937	08.13.05.18	60	042	+38	+22	050	1,37	0,25	0,98	141	140	149	129
8942	08.13.05.26	53	044	+33	+16	051	0,77	0,30	0,54	146	140	015	102
8946	08.13.05.32	55	033	+48	+33	048	1,37	0,29	0,98	119	140	211	110
8953	08.13.05.40	60	039	+37	+21	049	1,36	0,28	0,98	141	140	211	129
8954	08.13.05.41	51	059	+31	+10	063	0,72	0,58	0,30	155	140	025	116
8955	08.13.05.42	59	042	+54	+36	058	3,14	0,69	0,97	117	140	154	115
8958	08.13.05.45	64	050	+25	+07	054	1,52	0,37	0,97	168	140	148	103
8961	08.13.05.47	61	045	+47	+28	057	2,59	0,63	0,97	130	140	152	120
8966	08.13.07.55	57	079	+42	+19	081	2,10	0,82	0,38	131	140	068	118
8970	08.13.08.19	59	075	+45	+23	079	2,91	0,82	0,51	128	140	085	118
8992	08.13.23.12	32	341	—18	—09	336	2,34	0,87	0,31	013	321	119	90
8999	08.13.23.47	39	350	—09	—04	348	1,00	0,95	0,33	094	321	113	95
9000	08.13.23.48	38	356	—06	—04	354	1,30	0,95	0,06	016	321	158	93
9001	08.13.23.52	39	350	+03	+07	352	1,55	0,95	0,07	023	141	335	89
9002	08.13.23.57	32	339	—12	—03	336	2,19	0,87	0,29	004	321	122	90
9005	08.14.00.13	42	355	—03	—01	355	1,67	0,98	0,03	006	321	164	93
9011	08.14.00.39	42	355	—08	—05	353	1,83	0,97	0,05	024	321	158	95
9014	08.14.01.10	42	354	—15	—11	349	3,09	0,96	0,11	036	321	144	95
9048	08.14.03.24	66	034	+27	+13	041	2,52	0,65	0,88	157	141	227	105
9049	08.14.03.25	43	353	—14	—10	348	3,48	0,97	0,10	034	321	145	95
9053	08.14.03.36	64	035	+29	+14	042	1,93	0,54	0,89	154	141	154	105
9064	08.14.03.50	67	042	+10	—06	043	2,53	0,64	0,91	170	321	041	132
9066	08.14.03.55	57	022	+18	+08	027	1,30	0,72	0,36	160	141	302	119
9073	08.14.04.34	60	032	+40	+25	044	1,71	0,46	0,93	133	141	222	104
9079	08.14.04.40	63	038	+33	+17	046	1,83	0,48	0,96	148	141	212	123
9084	08.14.04.49	65	054	+31	+12	059	1,94	0,18	0,92	158	141	138	106
9090	08.14.04.55	60	033	+40	+25	045	1,63	0,15	0,94	133	141	220	104
9091	08.14.04.55	58	029	+43	+19	044	1,65	0,44	0,93	126	141	222	104
9092	08.14.04.55	63	039	+32	+16	047	1,61	0,40	0,96	151	141	214	123
9096	08.14.05.02	63	046	+28	+10	052	1,49	0,34	0,99	161	141	156	103
9100	08.14.05.08	63	041	+36	+19	050	1,77	0,44	0,99	145	141	203	129
9102	08.14.05.09	60	040	+35	+19	048	1,29	0,26	0,96	144	141	220	129
9107	08.14.05.12	57	028	+57	+42	050	2,93	0,66	1,00	107	141	196	131
9113	08.14.05.16	66	040	+15	—01	042	1,97	0,55	0,88	018	321	050	132
9114	08.14.05.44	67	043	+14	—02	044	2,37	0,61	0,91	143	321	044	132
9116	08.14.05.49	58	050	+39	+20	058	1,11	0,23	0,86	141	141	105	121
9139	08.14.05.56	63	041	+38	+21	051	1,93	0,49	0,99	142	141	199	129
9140	08.14.05.59	50	030	+65	+48	057	2,23	0,56	0,99	094	141	159	107
9120	08.14.06.21	57	044	+37	+59	064	2,59	0,63	0,96	115	141	152	115
9129	08.14.06.55	57	060	+36	+15	065	1,04	0,41	0,61	149	141	072	112
9135	08.14.07.06	62	059	+35	+15	064	1,63	0,52	0,79	151	141	112	112
9146	08.14.07.11	62	047	+47	+28	058	3,03	0,68	0,97	130	141	154	120
9148	08.14.07.17	60	072	+31	+08	075	1,52	0,72	0,43	161	141	070	113
9151	08.14.08.14	62	048	+46	+27	058	2,59	0,63	0,96	131	141	150	120
9157	09.20.23.54	61	057	+25	+05	060	12,33	0,85	0,35	168	178	294	143
9160	09.20.23.58	65	097	+20	—03	096	1,61	0,45	0,89	173	358	310	148
9161	09.21.00.00	32	014	+08	+02	016	1,67	0,85	0,26	310	178	308	149
9164	09.21.00.08	41	022	+14	+05	026	2,50	0,97	0,08	016	178	331	147
9168	09.21.00.14	63	075	+29	+06	077	1,39	0,45	0,76	168	178	256	142
9177	09.21.00.23	62	058	+25	+04	062	2,64	0,84	0,41	169	178	286	143
9178	09.21.00.04	61	075	+12	—10	075	1,29	0,46	0,70	159	358	087	137
9189	09.21.00.36	70	086	+42	+19	087	45,83	0,98	1,00	148	178	189	138
9195	09.21.00.40	64	094	+04	+19	094	2,88	0,66	0,97	145	358	334	146
9196	09.21.00.42	67	072	+36	+13	075	4,32	0,81	0,84	155	178	230	140
9201	09.21.00.47	43	025	+12	+02	025	2,78	1,00	0,05	009	178	337	147
9202	09.21.00.47	64	102	+24	+01	101	1,53	0,50	0,76	177	178	106	135
9206	09.21.00.53	28	015	+12	+05	018	1,23	0,78	0,27	156	178	311	149

Continuation

No. of meteor	DATE	v_∞	α	δ	β	λ	a	e	q	i	Ω	ω	shower
9210	09.21.00.57	66	076°	+11°	−11°	076°	2,86	0,70	0,84	158°	358°	052°	133
9215	09.21.01.05	70	071	+36	+08	074	18,00	0,95	0,82	166	178	230	133
9216	09.21.01.07	67	078	+33	+10	080	2,62	0,65	0,92	162	178	217	141
9219	09.21.01.08	36	010	+10	+05	013	4,27	0,94	0,26	008	178	301	149
9220	09.21.01.14	65	080	+24	+01	081	1,69	0,47	0,90	178	178	276	139
9226	09.21.01.26	67	076	+07	−15	076	4,56	0,86	0,86	152	358	046	133
9229	09.21.01.27	61	065	+19	−02	066	1,58	0,71	0,46	175	357	107	136
9238	09.21.01.57	62	056	+22	+03	059	3,25	0,89	0,34	173	178	292	143
9239	09.21.01.58	66	069	+35	+13	073	3,22	0,75	0,78	156	178	242	140
9245	09.21.02.02	65	083	+26	+03	084	1,54	0,39	0,95	174	178	214	139
9253	09.21.02.11	69	072	+17	−05	073	10,00	0,92	0,80	171	358	054	131
9273	09.21.03.35	68	079	+33	+10	081	3,19	0,71	0,93	162	178	213	141
9282	09.21.03.44	60	073	+13	−10	073	1,24	0,59	0,61	159	358	099	137
9284	09.21.03.47	64	107	+25	+03	104	1,85	0,64	0,67	174	178	008	135
9286	09.21.03.48	63	063	+17	−04	065	2,44	0,79	0,49	171	358	098	136
9287	09.21.03.52	69	082	+28	+05	083	3,65	0,73	0,97	171	178	224	139
9240	09.21.01.04	67	066	+27	+05	069	6,16	0,89	0,68	169	178	251	141
9269	09.21.04.44	67	159	+19	+09	153	−45,42	1,00	0,09	035	178	037	152
9275	09.21.04.50	64	063	+29	+08	066	2,57	0,73	0,55	163	178	271	145
9277	09.21.04.58	69	093	+23	−01	098	4,25	0,78	0,90	180	358	319	151
9279	09.21.04.58	44	159	+19	+10	153	6,06	0,98	0,11	031	178	038	152
9281	09.21.05.01	68	081	+26	+04	082	2,64	0,64	0,95	173	178	209	139
9287	09.21.05.07	66	075	+13	−09	075	3,11	0,73	0,81	162	358	058	133
9289	09.21.05.10	61	083	+08	−15	082	1,28	0,29	0,91	151	358	053	150
9292	09.21.05.22	67	098	+06	−18	098	4,79	0,80	0,92	148	358	325	146
9293	09.21.05.23	70	072	+19	−03	073	3,86	0,79	0,80	172	358	053	134
9296	09.21.05.23	43	161	+16	+07	156	8,99	0,98	0,14	021	178	043	152
9298	09.21.05.27	48	159	+18	+08	154	−7,99	1,01	0,09	031	178	036	152
9299	09.21.05.27	44	160	+18	+09	155	−8,11	0,99	0,12	027	188	040	152
9300	09.21.05.32	48	162	+15	+69	158	−3,16	1,04	0,12	022	178	044	152
9319	09.21.06.39	45	159	+17	+07	154	10,78	0,99	0,10	024	178	037	152
9324	09.21.07.04	62	082	+05	−18	081	1,49	0,40	0,90	145	358	047	150
9325	09.21.07.05	45	161	+17	+08	157	−21,90	0,50	0,13	024	178	043	152
9341	09.21.09.08	44	161	+17	+09	156	39,34	1,00	0,13	026	178	042	152
9348	09.21.10.25	44	158	+17	+07	153	5,43	0,98	0,09	024	178	034	152
9374	09.21.23.53	34	010	+12	+07	014	2,64	0,89	0,28	010	179	301	149
9376	09.22.00.08	33	012	+14	+08	017	1,98	0,88	0,25	012	179	307	149
9401	09.22.02.31	57	083	+12	−11	083	0,88	0,26	0,65	157	359	133	153
9406	09.22.02.47	45	026	+13	+02	029	3,59	0,99	0,03	010	179	340	147
9427	09.22.23.48	45	021	+15	+06	025	43,25	1,00	0,08	024	180	327	147
9428	09.22.23.54	44	021	+12	+03	024	19,83	1,00	0,08	011	180	325	147
9430	09.23.00.32	42	026	+12	+01	029	3,00	0,98	0,06	003	180	335	147
9438	09.23.01.18	33	016	+12	+04	019	1,85	0,88	0,23	007	180	310	149
9460	09.23.02.43	61	077	+15	−08	077	1,28	0,45	0,70	163	360	088	137
9466	09.23.02.53	66	064	+29	+08	067	6,97	0,92	0,58	164	180	263	145
9474	09.23.03.12	62	068	+14	−08	068	2,00	0,74	0,52	162	360	098	136
9489	09.24.00.04	44	026	+13	+03	029	3,87	0,98	0,06	011	181	334	147
9500	09.24.00.49	28	013	+10	+04	016	1,50	0,77	0,34	005	180	300	149
9542	09.24.03.17	45	026	+15	+04	029	0,51	0,99	0,05	019	181	334	147
9561	09.24.04.17	68	076	+37	+14	079	5,90	0,85	0,86	155	181	225	140
9564	09.24.04.18	65	079	+37	+14	081	2,34	0,62	0,88	154	181	227	140
9565	09.24.04.20	57	084	+12	−11	084	0,92	0,26	0,68	156	001	122	153
9570	09.24.04.24	69	086	+46	+23	087	−21,00	1,05	0,99	144	181	194	138
9574	09.24.04.28	67	067	+33	+22	070	7,13	0,91	0,66	157	181	254	154
9575	09.24.04.30	70	078	+11	−11	077	29,00	0,97	0,85	159	001	045	133
9581	09.24.04.42	64	082	+07	−16	082	1,92	0,54	0,89	149	001	046	150
9600	09.24.04.57	70	100	+25	+02	099	5,35	0,82	0,94	176	181	150	151
9603	09.24.05.02	69	077	+10	−13	077	4,50	0,98	0,84	157	001	048	133
9614	09.24.05.22	60	089	+07	−16	089	1,21	0,20	0,97	149	001	036	150
9623	09.24.06.07	68	096	+34	+11	095	3,13	0,69	0,98	116	181	162	155

Continuation

No. of meteor	DATE	v_∞	α	δ	β	λ	a	e	q	i	Ω	ω	shower
9651	09.24.17.07	43	028°	+15°	+04°	031°	2,62	0,98	0,05	017°	181°	337°	147
9669	09.24.20.03	30	015	+09	+02	017	1,67	0,81	0,31	003	182	303	149
9674	09.24.20.14	30	014	+12	+05	017	1,65	0,81	0,31	006	182	303	149
9677	09.24.20.17	44	029	+18	+05	033	2,52	0,98	0,04	008	182	338	147
9684	09.24.20.51	62	065	+16	+06	066	2,25	0,82	0,40	167	002	109	136
9694	09.24.21.34	31	013	+12	+06	017	1,82	0,83	0,31	007	182	301	149
9703	09.24.23.38	29	019	+14	+06	023	1,23	0,78	0,27	007	182	312	149
9704	09.24.23.42	63	061	+21	+01	063	3,47	0,90	0,36	178	181	290	143
9706	09.24.23.47	69	104	+20	—02	103	4,04	0,78	0,88	176	002	317	151
9712	09.24.23.56	68	096	+29	+06	096	2,40	0,59	0,98	169	182	162	155
9715	09.25.00.07	65	097	+05	—18	097	2,27	0,57	0,97	148	002	345	146
9719	09.25.00.15	65	076	+36	+13	078	2,60	0,69	0,81	154	182	238	140
9727	09.25.00.33	65	085	+12	—11	085	1,98	0,53	0,93	159	002	046	150
9734	09.25.00.38	59	078	+14	—09	078	1,12	0,47	0,59	160	002	105	137
9749	09.25.00.58	69	074	+30	+07	076	12,00	0,93	0,78	166	182	238	144
9756	09.25.01.05	68	100	+21	—01	099	2,71	0,65	0,94	177	002	327	151
9757	09.25.01.08	68	086	+29	+15	086	2,61	0,63	0,96	170	182	208	139
9773	09.25.02.29	63	089	+12	—11	084	1,42	0,39	0,87	158	002	057	150
9778	09.25.02.45	67	078	+10	—13	078	4,74	0,82	0,83	155	002	052	133
9787	09.25.02.51	65	099	+22	—01	099	1,67	0,44	0,93	177	002	320	148
9791	09.25.02.55	62	072	+17	—05	073	1,72	0,67	0,56	167	002	096	136
9793	09.25.02.58	64	076	+32	+10	078	1,95	0,61	0,76	161	182	249	140
9801	09.25.03.03	69	083	+27	+04	084	4,09	0,78	0,92	173	182	215	139
9805	09.25.03.07	64	088	+08	—15	088	1,70	0,43	0,97	152	002	098	150
9810	09.25.03.1	64	075	+28	+05	077	1,84	0,63	0,70	170	182	257	142
9812	09.25.03.11	67	098	+09	—14	098	3,25	0,71	0,96	154	002	335	146
9813	09.25.03.12	67	067	+26	+04	070	6,25	0,91	0,58	171	182	203	145
9814	09.25.03.12	57	086	+16	—07	086	0,85	0,29	0,60	165	002	141	153
9832	09.25.03.34	43	027	+11	+12	029	3,48	0,98	0,06	017	182	333	147
9835	09.25.03.37	65	099	+17	—07	098	1,64	0,43	0,94	167	002	322	148
9843	09.25.03.46	67	099	+07	—16	099	5,84	0,85	0,85	151	002	048	133
9849	09.25.03.55	61	087	+08	—16	086	1,30	0,29	0,92	150	002	050	150
9853	09.25.04.03	47	164	+14	+07	160	—5,37	1,02	0,11	024	182	040	152
9861	09.25.04.12	69	101	+23	+01	100	3,30	0,28	0,94	179	182	147	151
9863	09.25.04.15	61	061	+25	+04	064	2,18	0,85	0,33	170	182	297	143
9866	09.25.04.22	63	085	+11	—12	085	1,50	0,40	0,90	157	002	050	150
9868	09.25.04.22	72	081	+20	—03	082	—32,03	1,03	0,91	175	002	234	134
9874	09.25.04.29	63	078	+28	+05	079	1,45	0,50	0,72	169	182	261	142
9878	09.25.04.36	64	084	+10	—13	084	1,76	0,49	0,90	155	002	045	150
9883	09.25.04.39	60	062	+22	+01	064	1,98	0,85	0,32	177	182	299	143
9889	09.25.04.47	61	071	+15	—07	074	1,48	0,68	0,48	164	002	107	136
9898	09.25.05.15	64	107	+24	+01	105	1,57	0,52	0,75	178	182	106	135
9901	09.25.05.21	65	099	+16	—07	099	1,68	0,45	0,93	167	002	320	148
9903	09.25.05.25	44	164	+14	+07	159	10,89	0,99	0,12	021	182	040	152
9913	09.25.05.44	68	101	+32	+09	099	3,29	0,71	0,95	163	182	152	155
9916	09.25.05.48	45	162	+17	+09	157	8,28	0,99	0,10	031	182	036	152
9930	09.25.06.07	46	163	+13	+05	160	—30,94	1,00	0,16	017	182	038	152
9953	09.25.07.12	43	164	+15	+08	159	6,92	0,98	0,12	023	182	040	152
9962	09.25.07.28	47	163	+17	+09	158	—8,60	1,01	0,10	032	182	038	152
9968	09.25.07.52	43	164	+16	+08	159	5,42	0,98	0,13	025	182	041	152
9975	09.25.08.00	44	162	+14	+06	157	6,47	0,99	0,09	021	182	034	152
9986	09.26.07.47	69	095	+38	+15	094	5,34	0,81	1,00	154	183	173	138
10007	09.26.20.02	35	019	+11	+03	022	2,45	0,91	0,22	004	184	309	149
10012	09.26.21.07	31	013	+12	+06	017	2,21	0,85	0,33	007	184	297	149
10013	09.26.21.08	33	018	+09	+01	002	0,88	0,26	0,89	002	184	304	149
10019	09.26.21.41	68	072	+28	+06	075	10,13	0,93	0,69	168	184	249	144
10020	09.26.21.47	68	069	+31	+09	073	61,48	0,99	0,65	161	184	252	154
10023	09.26.22.14	31	014	+09	+03	016	2,35	0,85	0,33	003	184	296	149
10027	09.26.22.26	33	013	+09	+03	016	3,16	0,70	0,33	004	184	295	149
10030	09.26.22.35	35	017	+13	+06	021	2,60	0,91	0,24	009	184	306	149

Continuation

No. of meteor	DATE	v_∞	α	δ	β	λ	a	e	q	i	Ω	ω	shower
10064	09.26.23.22	66	068°	+36°	+14°	072°	7,79	0,92	0,64	179°	004°	047°	154
10068	09.26.23.28	59	065	+26	+04	068	1,55	0,78	0°,34	169	184	301	143
10088	09.27.00.13	60	064	+28	+07	067	1,82	0,80	0,36	162	184	296	143
10090	09.27.00.15	72	093	+38	+15	092	−11,39	1,09	1,00	155	184	188	138
10091	09.27.00.15	62	087	+08	−15	087	1,45	0,37	0,91	152	004	048	150
10092	09.27.00.15	65	084	+29	+05	085	1,79	0,51	0,88	170	184	230	139
10097	09.27.00.42	65	103	+33	+10	101	1,90	0,51	0,94	161	184	144	155
10098	09.27.00.45	66	083	+24	+01	084	2,18	0,61	0,86	179	184	232	139
10100	09.27.00.51	62	073	+15	−07	074	1,82	0,70	0,55	164	004	095	136
10104	09.27.01.00	69	074	+28	+06	076	28,20	0,97	0,73	169	184	243	144
10111	09.27.01.15	66	102	+31	+08	101	2,06	0,54	0,94	165	184	146	155
10113	09.27.01.17	69	101	+32	+09	099	3,40	0,71	0,97	164	184	159	155
10123	09.27.01.30	68	080	+17	−06	081	4,49	0,81	0,83	169	004	052	134
10129	09.27.02.02	61	070	+14	−08	071	1,75	0,74	0,45	161	004	107	136
10136	09.27.02.33	64	087	+11	−12	087	1,75	0,47	0,93	157	004	040	150
10138	09.27.03.57	63	086	+08	−15	085	1,60	0,45	0,88	151	004	052	150
10139	09.27.03.57	64	087	+09	−15	087	1,71	0,48	0,93	153	004	040	150
10145	09.27.04.05	63	079	+25	+02	080	1,57	0,55	0,70	175	184	261	142
10148	09.27.04.07	61	085	+05	−18	085	1,43	0,40	0,86	144	004	059	150
10163	09.27.04.33	60	090	+08	−15	090	1,15	0,19	0,93	151	040	057	150
10164	09.27.04.40	69	104	+31	+08	102	4,23	0,78	0,94	165	184	150	155
10168	09.27.04.48	46	164	+15	+08	160	−122	1,00	0,10	027	184	036	152
10179	09.27.05.28	64	105	+26	+03	103	1,30	0,37	0,82	174	184	110	135
10180	09.27.05.28	46	165	+13	+06	161	−15,07	1,01	0,10	023	184	038	152
10192	09.27.05.37	68	096	+29	+06	095	2,52	0,60	1,00	170	184	172	155
10202	09.27.23.40	31	014	+15	+08	018	2,08	0,84	0,33	010	185	297	149
10224	09.28.03.17	61	065	+27	+07	067	1,92	0,82	0,34	166	185	297	143
10232	09.28.03.42	69	079	+18	−05	080	6,50	0,88	0,78	170	005	057	134
10243	09.28.03.57	59	083	+15	−08	083	1,05	0,39	0,64	164	005	106	137
10251	09.28.03.58	66	072	+34	+12	075	3,10	0,87	0,66	156	185	254	154
10264	09.28.04.27	64	080	+32	+09	081	1,93	0,61	0,76	163	185	248	140
10266	09.28.04.29	65	100	+09	−14	100	1,96	0,51	0,97	154	005	336	146
10346	09.28.22.31	63	071	+19	−03	073	2,12	0,78	0,47	174	006	102	136
10347	09.28.22.35	65	075	+27	+04	076	2,50	0,75	0,62	171	186	264	145
10348	09.28.22.35	43	031	+15	+02	034	3,10	0,98	0,06	010	186	334	147
10349	09.28.22.36	67	084	+32	+09	085	3,18	0,72	0,88	163	186	225	141
10358	09.28.23.01	44	027	+15	+03	030	9,74	0,99	0,80	011	186	327	147
10366	09.28.23.12	44	030	+14	+01	033	4,53	0,98	0,07	009	186	332	147
10371	10.10.20.38	36	035	+10	−04	036	2,55	0,91	0,22	007	017	130	160
10372	10.10.20.38	39	030	+21	+09	035	5,86	0,96	0,96	000	017	197	161
10373	10.10.20.40	43	041	+13	−03	042	5,99	0,98	0,09	009	175	147	162
10378	10.10.21.04	30	030	+07	−05	030	1,89	0,81	0,35	006	017	116	149
10383	10.10.21.27	29	033	+13	+00	035	1,39	0,78	0,30	000	197	306	149
10384	10.10.21.32	43	041	+21	+05	045	3,26	0,98	0,07	019	197	332	147
10386	10.10.21.38	54	084	+11	−12	084	1,01	0,71	0,29	147	017	135	159
10388	10.10.21.43	45	037	+22	+07	042	−50,4	1,00	0,10	025	198	324	147
10389	10.10.21.50	33	034	+07	−06	034	2,08	0,87	0,27	009	018	124	149
10390	10.10.21.53	44	047	+14	−03	048	2,42	0,98	0,04	016	018	160	163
10394	10.10.22.08	29	025	+06	−04	026	2,32	0,82	0,42	004	018	106	149
10395	10.10.22.10	42	042	+17	+01	044	2,89	0,98	0,07	003	198	331	162
10398	10.10.22.15	31	031	+05	−07	033	1,83	0,83	0,32	009	018	120	149
10400	10.10.22.17	37	041	+20	+04	045	1,53	0,93	0,11	010	198	328	147
10405	10.10.22.20	31	031	+03	−09	030	2,38	0,85	0,35	011	018	114	149
10407	10.10.22.22	44	039	+20	+04	043	7,07	0,99	0,09	015	198	328	147
10409	10.10.22.23	40	032	+20	+07	036	6,26	0,97	0,18	014	198	311	161
10414	10.10.22.30	31	034	+06	−08	034	1,72	0,83	0,30	010	018	123	149
10416	10.10.22.37	31	033	+09	−04	033	1,75	0,83	0,30	005	018	123	149
10417	10.10.22.37	33	030	+24	+12	036	1,97	0,87	0,26	018	198	306	161
10418	10.10.22.40	41	046	+21	+01	049	1,67	0,97	0,05	015	198	338	147
10419	10.10.22.40	42	042	+14	−02	044	3,46	0,97	0,08	006	018	150	162

Continuation

No. of meteor	DATE	v_∞	α	δ	β	λ	a	e	q	i	Ω	ω	shower
10428	10.10.22.57	28	031°	+10°	−03°	032°	1,47	0,76	0,35	003°	018°	120°	149
10429	10.10.23.00	39	033	+16	+03	036	5,01	0,96	0,19	005	198	310	161
10431	10.10.23.01	32	032	+03	−10	031	2,32	0,85	0,34	012	018	116	149
10433	10.10.23.03	37	031	+19	+06	036	3,51	0,94	0,21	011	198	309	161
10435	10.10.23.05	39	041	+18	+02	044	1,91	0,95	0,10	007	198	328	147
10436	10.10.23.06	57	084	+13	−11	084	1,18	0,70	0,35	154	018	125	159
10439	10.10.23.10	31	033	+15	+01	036	1,52	0,83	0,26	002	198	309	160
10440	10.10.23.10	35	031	+11	−01	032	3,54	0,93	0,27	002	018	122	149
10441	10.10.23.12	46	040	+20	+04	044	110	1,00	0,06	016	198	332	147
10443	10.10.23.14	29	028	+05	−06	027	2,15	0,81	0,40	006	018	110	149
10445	10.10.23.16	59	079	+30	+07	080	1,60	0,81	0,31	162	198	302	158
10449	10.10.23.17	47	047	+16	−01	049	5,15	0,99	0,02	009	018	164	163
10450	10.10.23.18	47	040	+16	+01	042	9,82	0,15	0,06	004	198	330	162
10452	10.10.23.21	31	028	+09	−02	029	2,37	0,85	0,35	003	018	114	149
10453	10.10.23.22	43	042	+19	+03	046	2,95	0,98	0,06	011	198	333	147
10455	10.10.23.31	44	040	+22	+06	044	4,72	0,98	0,08	023	198	328	147
10456	10.10.23.31	61	081	+32	+09	083	1,85	0,78	0,41	158	198	290	158
10458	10.10.23.37	35	032	+16	+03	036	1,86	0,85	0,22	006	198	309	160
10459	10.10.23.38	32	033	+08	+05	034	0,96	0,89	0,28	007	018	124	149
10463	10.10.23.42	67	100	+27	+04	099	2,12	0,58	0,89	173	198	225	157
10478	10.11.00.03	38	048	+15	−03	050	1,28	0,95	0,06	010	018	157	163
10480	10.11.00.04	40	048	+15	−03	050	1,40	0,97	0,05	012	018	159	163
10483	10.11.00.47	66	108	+21	−02	106	1,70	0,44	1,00	177	018	005	164
10484	10.11.00.47	32	030	+21	+08	035	1,79	0,84	0,28	011	198	305	179
10485	10.11.00.47	41	049	+15	−03	051	1,43	0,97	0,04	015	018	161	163
10491	10.11.00.52	60	103	+15	−08	103	0,98	0,19	0,79	164	018	107	178
10493	10.11.00.53	41	036	+15	+00	038	6,90	0,98	0,15	001	198	317	162
10494	10.11.01.17	40	048	+14	−04	049	1,49	0,96	0,06	014	018	157	163
10495	10.11.01.17	67	123	+22	+02	121	2,44	0,67	0,81	175	198	122	174
10496	10.11.01.24	65	098	+16	−07	098	1,72	0,50	0,86	167	018	055	172
10499	10.11.01.26	67	096	+29	+06	095	3,00	0,73	0,81	170	198	236	167
10504	10.11.01.40	46	043	+13	−03	045	19,95	1,00	0,05	014	018	153	162
10505	10.11.01.42	70	115	+15	−06	114	2,58	0,63	0,97	169	018	339	170
10508	10.11.01.47	66	089	+18	−05	089	3,53	0,81	0,65	169	018	077	165
10510	10.11.01.48	70	115	+25	+03	112	3,61	0,73	0,98	174	198	164	175
10518	10.11.02.01	64	088	+21	−03	088	2,11	0,73	0,57	175	018	091	165
10521	10.11.02.03	69	114	+22	+00	112	2,78	0,65	0,98	165	018	281	175
10522	10.11.02.04	38	029	+15	+03	033	8,07	0,97	0,24	005	198	303	161
10524	10.11.02.06	59	135	+22	+05	131	1,28	0,70	0,38	168	198	060	171
10527	10.11.02.08	64	101	+04	−19	102	1,85	0,49	0,95	145	018	030	166
10528	10.11.02.08	31	027	+06	−05	027	3,04	0,87	0,38	005	018	109	149
10530	10.11.02.08	65	113	+25	+03	111	1,56	0,37	0,98	174	198	162	175
10531	10.11.02.08	57	080	+29	+06	081	1,26	0,79	0,27	163	198	311	158
10534	10.11.02.12	40	048	+10	−03	048	1,63	0,95	0,08	027	018	152	163
10537	10.11.02.14	61	083	+10	−13	083	1,93	0,77	0,45	150	018	105	159
10538	10.11.02.16	33	032	+09	−03	034	2,12	0,87	0,28	005	018	123	149
10542	10.11.02.22	67	108	+24	+02	107	1,98	0,50	0,99	178	198	187	164
10543	10.11.02.22	39	040	+12	−04	042	2,37	0,95	0,13	010	018	142	162
10549	10.11.02.27	58	084	+10	−13	084	1,55	0,75	0,39	148	018	117	159
10553	10.11.02.37	67	115	+25	+03	112	2,07	0,53	0,97	174	198	159	175
10554	10.11.02.38	67	104	+30	+07	102	2,29	0,59	0,95	168	198	208	168
10556	10.11.02.38	66	105	+16	−07	105	1,69	0,42	0,98	167	018	020	156
10561	10.11.02.48	35	039	+09	−06	039	2,01	0,90	0,20	010	018	134	160
10569	10.11.03.01	68	116	+17	−04	114	2,47	0,62	0,95	173	018	331	170
10570	10.11.03.01	69	117	+22	+01	115	3,60	0,74	0,95	179	198	152	175
10574	10.11.03.07	67	125	+23	+04	122	2,55	0,69	0,78	173	198	118	174
10575	10.11.03.11	66	122	+17	−04	121	2,17	0,63	0,80	173	018	300	169
10585	10.11.03.44	61	102	+20	−03	102	1,04	0,22	0,81	173	018	093	178
10587	10.11.03.47	68	100	+25	+02	099	2,45	0,63	0,90	176	198	222	157
10589	10.11.03.47	59	085	+13	−10	085	1,43	0,71	0,42	156	018	113	159

Continuation

No. of meteor	DATE	v_∞	α	δ	β	λ	a	e	q	i	Ω	ω	shower
10590	10.11.03.52	63	103°	+07°	+16°	103°	1,44	0,33	0,96	149°	018°	032°	166
10591	10.11.03.53	45	043	+21	+04	047	4,08	0,99	0,05	020	198	335	147
10597	10.11.04.01	59	135	+20	+03	132	1,23	0,72	0,34	173	198	055	171
10598	10.11.04.04	63	138	+05	−10	139	5,52	0,93	0,37	153	018	252	176
10599	10.11.04.04	59	118	+07	−14	119	1,08	0,34	0,71	152	018	263	177
10600	10.11.04.05	65	105	+14	−09	105	1,52	0,36	0,98	164	018	022	156
10603	10.11.04.14	67	123	+14	−06	121	2,42	0,67	0,81	169	018	302	159
10606	10.11.04.17	70	095	+23	−01	095	11,33	0,93	0,84	178	018	047	157
10607	10.11.04.27	65	120	+14	−06	119	1,60	0,48	0,83	167	018	298	169
10608	10.11.04.30	66	122	+22	+02	120	2,00	0,59	0,83	176	198	122	174
10611	10.11.04.37	68	102	+32	+09	100	3,38	0,72	0,94	163	198	212	168
10615	10.11.04.40	66	123	+26	+06	120	2,24	0,59	0,83	168	197	123	174
10619	10.11.04.52	65	091	+19	−05	091	2,26	0,78	0,68	170	018	076	165
10620	10.11.04.52	59	133	+09	−09	133	1,33	0,74	0,35	158	018	238	176
10622	10.11.04.58	64	128	+20	+01	125	1,68	0,62	0,64	178	198	093	174
10623	10.11.05.01	65	128	+21	+02	125	1,95	0,65	0,68	175	198	101	174
10626	10.11.20.46	38	030	+22	+09	035	5,26	0,95	0,24	016	198	330	161
10628	10.11.20.54	42	044	+20	+03	048	2,46	0,98	0,06	011	198	335	147
10632	10.11.21.08	34	027	+09	−02	028	7,44	0,96	0,34	002	018	111	149
10633	10.11.21.09	43	047	+25	+67	052	1,87	0,98	0,04	034	198	340	147
10634	10.11.21.12	29	031	+04	−08	030	1,86	0,80	0,38	008	018	113	149
10637	10.11.21.28	39	035	+18	+03	038	4,30	0,96	0,17	008	198	314	161
10638	10.11.21.35	22	042	+15	−01	044	0,87	0,63	0,33	098	019	137	149
10639	10.11.21.35	32	039	+19	+03	042	1,28	0,84	0,20	005	198	319	160
10642	10.11.21.57	30	031	+13	+01	033	1,74	0,82	0,32	001	198	301	149
10643	10.11.21.58	29	031	+02	−10	030	2,01	0,81	0,39	001	019	112	149
10646	10.11.22.31	39	047	+26	+08	052	1,32	0,96	0,06	029	199	337	147
10649	10.11.22.36	31	028	+20	+08	033	1,98	0,84	0,32	010	199	299	179
10650	10.11.22.41	42	051	+19	+00	054	1,47	0,99	0,02	001	199	347	163
10652	10.11.22.44	44	043	+20	+03	046	3,58	0,98	0,06	013	199	334	147
10657	10.11.22.47	29	036	+14	−00	038	1,29	0,79	0,27	000	018	131	160
10658	10.11.22.52	61	075	+28	+06	077	3,24	0,91	0,29	165	199	300	158
10659	10.11.22.52	41	038	+19	+04	041	4,16	0,97	0,12	011	199	321	147
10663	10.11.22.58	28	032	+05	−07	031	1,70	0,78	0,37	008	019	115	149
10664	10.11.23.03	68	088	+20	−04	089	8,32	0,92	0,66	173	019	074	165
10667	10.11.23.17	29	028	+04	−07	027	2,38	0,82	0,42	007	019	107	149
10669	10.11.23.18	31	033	+10	−03	034	1,79	0,83	0,30	004	019	122	149
10670	10.11.23.20	59	082	+25	+02	083	1,49	0,78	0,33	176	199	302	158
10672	10.11.23.28	46	044	+14	−03	046	13,31	1,00	0,06	014	019	153	162
10673	10.11.23.34	43	040	+16	+01	043	6,52	0,98	0,10	002	199	325	162
10674	10.11.23.35	46	049	+25	+07	053	2,59	0,99	0,03	049	199	343	147
10675	10.11.23.35	37	050	+13	−05	051	1,18	0,93	0,08	016	019	157	163
10676	10.11.23.36	40	040	+26	+09	046	2,15	0,95	0,11	027	199	132	147
10678	10.11.23.40	40	051	+14	−04	052	1,42	0,96	0,05	018	019	160	163
10679	10.11.23.45	35	032	+24	+11	038	2,25	0,90	0,23	018	199	309	161
10680	10.11.23.45	41	044	+19	+02	048	2,03	0,97	0,07	008	199	334	147
10682	10.11.23.47	31	029	+09	−03	030	2,44	0,85	0,36	003	019	113	149
10683	10.11.23.47	29	030	+07	−05	030	1,04	0,89	0,11	159	199	332	149
10685	10.11.23.52	40	044	+24	+07	048	1,77	0,95	0,08	025	199	332	147
10689	10.11.23.55	47	043	+18	+01	046	−200	1,00	0,04	006	199	336	147
10690	10.11.23.55	44	043	+21	+05	047	3,74	0,98	0,06	022	199	334	147
10691	10.11.23.56	43	045	+20	+03	049	2,26	0,98	0,05	014	199	337	147
10692	10.12.00.11	54	086	+21	−02	086	2,50	0,80	0,51	175	019	096	165
10693	10.12.00.12	34	037	+14	−00	039	1,76	0,89	0,20	001	019	135	160
10696	10.12.00.18	44	040	+16	+01	043	15,34	0,99	0,08	001	199	327	162
10700	10.12.00.23	31	032	+03	−09	031	2,34	0,85	0,35	011	019	115	149
10705	10.12.00.26	64	102	+32	+08	100	1,54	0,44	0,86	164	199	236	168
10707	10.12.00.29	55	078	+28	+05	079	1,18	0,81	0,19	165	199	321	158
10708	10.12.00.30	68	093	+32	+19	092	4,96	0,88	0,75	063	099	143	167
10710	10.12.00.33	58	120	+07	−13	121	0,97	0,37	0,61	152	019	244	177

Continuation

No. of meteor	DATE	v_∞	α	δ	β	λ	a	e	q	i	Ω	ω	shower
10717	10.12.00.38	65	098°	+11°	−12°	099°	1,85	0,54	0,85	157°	019°	054°	172
10718	10.12.00.38	33	032	+07	−05	032	2,56	0,88	0,31	007	019	119	149
10724	10.12.00.48	43	045	+17	+00	047	2,79	0,98	0,06	002	199	335	147
10725	10.12.00.48	59	101	+17	−06	101	0,93	0,30	0,65	168	019	120	178
10727	10.12.00.48	44	042	+18	+02	045	5,22	0,99	0,07	006	199	331	147
10731	10.12.00.53	57	104	+17	−06	104	0,82	0,28	0,59	168	019	150	178
10733	10.12.00.54	68	107	+17	−06	107	2,29	0,57	0,99	169	019	010	156
10737	10.12.01.02	58	088	+14	−09	088	1,18	0,66	0,40	158	019	120	159
10741	10.12.01.10	63	102	+07	−16	103	1,44	0,35	0,93	151	019	043	166
10743	10.12.01.15	66	099	+32	+08	098	2,20	0,62	0,84	164	199	234	167
10744	10.12.01.17	60	077	+30	+07	079	2,22	0,87	0,30	160	199	301	158
10750	10.12.01.25	41	010	+12	−03	011	4,28	0,96	0,13	008	019	140	162
10751	10.12.01.27	31	033	+08	−05	034	1,92	0,84	0,31	007	019	121	149
10752	10.12.01.28	59	087	+12	−11	087	1,40	0,68	0,45	155	019	111	159
10754	10.12.01.29	33	027	+05	−06	027	5,73	0,93	0,38	007	019	106	149
10757	10.12.01.35	56	076	+29	+06	077	1,43	0,87	0,19	161	199	318	158
10758	10.12.01.36	63	100	+08	−16	101	1,67	0,46	0,90	151	019	047	166
10763	10.12.01.38	69	105	+27	+04	104	3,01	0,68	0,97	172	199	202	164
10765	10.12.01.39	63	104	+16	−07	104	1,28	0,28	0,92	167	019	049	156
10766	10.12.01.40	54	088	+08	−15	088	0,97	0,63	0,36	143	019	131	159
10767	10.12.01.43	65	125	+30	+10	120	1,82	0,55	0,83	161	199	122	183
10768	10.12.01.43	68	094	+28	+04	094	4,51	0,83	0,78	172	199	239	167
10769	10.12.01.55	57	101	+15	−08	100	0,88	0,32	0,60	163	019	130	178
10784	10.12.02.19	61	043	+21	+06	138	2,17	0,85	0,32	164	199	062	171
10788	10.12.02.25	57	079	+28	+05	080	1,40	0,82	0,91	168	199	220	158
10789	10.12.02.26	67	102	+30	+07	100	2,56	0,64	0,91	168	199	220	157
10792	10.12.02.30	66	097	+30	+07	096	2,38	0,66	0,80	167	199	240	167
10793	10.12.02.44	69	096	+32	+08	095	8,55	0,90	0,82	164	199	231	167
10795	10.12.02.45	67	106	+17	−06	105	1,94	0,49	0,98	169	017	020	156
10796	10.12.02.45	67	136	+27	+10	131	5,16	0,88	0,61	159	199	100	181
10801	10.12.02.50	39	046	+16	−01	048	1,62	0,96	0,07	003	019	154	163
10803	10.12.02.52	59	081	+30	+06	083	1,46	0,78	0,32	164	199	304	158
10804	10.12.02.52	45	039	+16	+00	041	−31,57	1,00	0,10	001	199	323	162
10807	10.12.02.56	48	046	+22	+04	049	9,36	1,00	0,03	029	199	342	147
10808	10.12.02.57	68	098	+30	+07	097	3,65	0,77	0,85	168	199	229	167
10811	10.12.03.05	65	137	+23	+06	133	3,43	0,85	0,53	166	199	088	181
10814	10.12.03.10	60	139	+25	+09	134	1,53	0,74	0,40	158	199	065	171
10815	10.12.03.11	60	108	+17	−06	107	1,95	0,51	0,95	168	019	094	178
10816	10.12.03.11	68	117	+29	+08	114	2,37	0,59	0,97	166	199	157	182
10821	10.12.03.26	67	115	+28	+07	112	2,12	0,53	0,99	168	199	168	182
10822	10.12.03.30	66	091	+12	−11	091	3,52	0,80	0,69	157	018	072	165
10825	10.12.03.34	62	105	+04	−18	106	1,49	0,34	0,98	146	019	020	166
10829	10.12.03.37	63	127	+25	+06	123	1,39	0,51	0,68	168	199	093	174
10839	10.12.04.06	61	137	+23	+06	132	1,50	0,72	0,42	165	199	068	171
10844	10.12.04.17	60	119	+04	−16	120	1,23	0,36	0,78	147	019	280	177
10846	10.12.04.22	66	129	+36	+17	122	3,11	0,73	0,84	148	199	129	183
10848	10.12.04.25	67	097	+12	−11	097	2,75	0,69	0,85	159	019	051	172
10850	10.12.04.25	65	128	+22	+03	125	1,96	0,65	0,69	174	198	109	174
10854	10.12.04.30	66	129	+35	+16	122	2,74	0,70	0,83	151	199	126	183
10855	10.12.04.30	66	106	+25	+02	104	1,85	0,48	0,96	176	199	208	164
10856	10.12.04.30	68	122	+17	−04	120	3,05	0,72	0,86	173	019	313	169
10858	10.12.04.51	64	108	+15	−08	107	1,43	0,31	0,99	165	019	009	156
10860	10.12.04.52	66	129	+32	+13	123	2,62	0,89	0,80	156	199	192	183
10864	10.12.04.56	58	158	+28	+17	149	5,29	0,96	0,23	126	199	056	184
10865	10.12.04.57	61	138	+23	+07	133	1,69	0,75	0,42	164	199	070	171
10868	10.12.05.04	60	154	+23	+12	147	5,00	0,96	0,21	142	199	053	184
10885	10.12.05.52	61	118	+06	−15	118	1,23	0,33	0,82	151	019	286	177
10886	10.12.05.52	58	138	+23	+06	134	1,24	0,73	0,33	164	199	054	171
10896	10.12.06.15	54	126	+20	+01	124	1,62	0,57	0,70	179	199	100	174
10898	10.12.06.22	63	119	+07	−14	120	1,43	0,43	0,82	154	019	294	177

Continuation

No. of meteor	DATE	v_∞	α	δ	β	λ	a	e	q	i	Ω	ω	shower
10900	10.12.06.27	56	154°	+21°	−09°	148°	2,00	0,94	0,13	143°	199°	037°	184
10903	10.12.06.38	63	137	+23	+07	133	2,07	0,77	0,47	165	199	078	171
10922	10.12.20.02	44	040	+21	+05	044	8,43	0,99	0,09	019	199	326	147
10923	10.12.20.04	32	031	+04	−08	030	2,87	0,87	0,36	010	019	118	149
10926	10.12.20.17	42	041	+20	+04	044	4,27	0,98	0,10	013	199	326	147
10931	10.12.20.56	45	053	+10	−08	053	2,54	0,98	0,04	048	019	159	163
10947	10.12.21.52	47	044	+23	+06	048	19,37	1,00	0,05	031	199	335	147
10951	10.12.21.59	44	046	+16	−01	048	3,68	0,99	0,05	006	019	156	162
10955	10.12.22.22	37	037	+20	+05	041	2,39	0,93	0,17	012	200	317	161
10967	10.12.23.23	68	106	+36	+13	103	3,42	0,72	0,95	157	200	208	180
10984	10.13.00.01	55	081	+26	+02	082	1,10	0,82	0,20	173	200	321	158
10986	10.13.00.14	57	086	+11	−12	086	1,17	0,70	0,35	149	020	125	159
11005	10.13.00.30	56	108	+15	−08	107	0,80	0,26	0,59	164	020	163	178
11012	10.13.00.52	69	121	+31	+10	117	3,52	0,73	0,95	161	200	153	182
11013	10.13.00.58	36	179	+65	+56	139	1,24	0,33	0,83	065	200	109	168
11017	10.13.01.07	68	107	+37	+14	104	3,18	0,69	0,97	155	200	203	180
11028	10.13.04.46	56	156	+26	+15	148	2,28	0,91	0,20	130	200	047	184
11059	10.13.19.09	69	107	+36	+13	104	4,40	0,78	0,96	156	200	204	180
11068	10.13.21.08	31	038	+07	−08	038	1,62	0,83	0,28	010	020	126	149
11084	10.13.23.58	61	079	+31	+08	081	2,66	0,88	0,32	160	201	297	158
11093	10.14.00.57	65	107	+12	−11	107	1,56	0,38	0,97	160	021	026	156
11094	10.14.00.57	64	097	+31	+08	096	1,82	0,61	0,71	164	201	256	167
11097	10.14.01.00	68	096	+31	+07	095	3,80	0,80	0,76	166	201	243	167
11100	10.14.01.03	65	099	+10	−13	099	2,29	0,63	0,84	155	021	054	172
11101	10.14.01.08	64	091	+16	−08	091	2,07	0,73	0,57	164	021	091	165
11106	10.14.01.20	65	110	+23	+00	108	1,43	0,31	0,99	179	201	197	164
11107	10.14.01.21	52	091	+15	+09	091	1,62	0,67	0,54	161	021	098	165
11111	10.14.01.26	61	112	+38	+16	108	1,19	0,19	0,96	149	201	217	180
11119	10.14.01.58	65	113	+37	+15	109	1,79	0,44	1,00	153	201	186	180
11122	10.14.02.16	76	116	+23	+01	114	2,06	0,52	0,99	177	201	168	175
11124	10.14.02.28	64	102	+11	−12	102	1,56	0,45	0,86	157	021	057	172
11135	10.14.03.35	55	152	+22	+10	146	1,50	0,90	0,15	146	201	038	184
11168	10.14.20.55	41	044	+27	+09	049	2,42	0,96	0,10	029	201	327	147
11169	10.14.21.22	34	043	+13	−04	044	1,53	0,88	0,19	006	021	137	160
11171	10.14.21.30	30	036	+01	−13	034	2,11	0,82	0,38	014	021	112	149
11177	10.14.22.33	61	082	+33	+10	083	2,59	0,86	0,37	154	202	292	158
11185	10.14.23.15	60	082	+29	+06	083	1,90	0,83	0,32	165	202	300	158
11189	10.15.00.02	64	088	+15	−09	088	2,96	0,82	0,52	161	022	094	165
11194	10.15.00.16	61	113	+37	+15	109	1,22	0,21	0,97	151	202	213	180
11197	10.15.00.21	68	104	+22	−01	103	2,60	0,65	0,90	079	022	041	157
11208	10.15.01.40	66	118	+19	−01	117	2,82	0,65	0,98	177	202	341	170
11209	10.15.01.42	60	108	+19	−03	107	0,99	0,17	0,82	174	022	102	178
11210	10.15.01.44	65	115	+40	+18	110	2,01	0,50	1,00	147	202	183	180
11211	10.15.01.44	62	112	+38	+16	108	1,37	0,29	0,97	150	202	210	180
11213	10.15.01.55	64	108	+29	+07	106	1,48	0,38	0,93	167	202	222	168
11214	10.15.02.02	65	113	+34	+13	116	1,70	0,42	0,98	156	202	161	180
11222	10.15.02.34	65	131	+33	+15	125	2,04	0,60	0,82	152	202	122	183
11223	10.15.02.38	70	121	+33	+12	116	6,47	0,85	0,98	158	202	167	182
11224	10.15.03.45	58	136	+25	+08	131	1,07	0,59	0,44	161	202	059	171
11226	10.15.03.56	59	141	+11	−04	140	1,48	0,81	0,28	169	022	232	176
11235	10.15.04.37	56	141	+07	−08	141	1,22	0,80	0,24	157	022	225	176
11241	10.15.05.07	58	144	+08	−06	144	1,74	0,87	0,22	161	022	228	176
11252	10.15.19.37	45	049	+19	+01	051	4,30	0,99	0,04	004	202	337	147
11256	10.15.20.22	29	032	+11	−02	034	2,00	0,81	0,38	003	022	113	149
11259	10.15.20.29	45	047	+21	+03	050	5,79	0,99	0,05	015	202	335	147
11261	10.15.20.47	45	049	+22	+03	052	4,07	0,99	0,04	018	202	339	147
11263	10.15.20.48	44	050	+28	+09	055	2,19	0,97	0,06	043	202	336	147
11264	10.15.20.48	28	033	+04	−09	032	1,89	0,76	0,43	008	022	108	149
11270	10.15.21.02	40	049	+24	+06	053	1,69	0,96	0,07	021	202	335	147
11272	10.15.21.04	46	053	+20	+00	056	2,57	0,99	0,02	003	202	346	147

Continuation

No. of meteor	DATE	v_∞	α	δ	β	λ	a	e	q	i	Ω	ω	shower
11276	10.15.21.18	41	052°	+20°	+01°	054°	1,69	0,97	0,04	006°	202°	340°	147
11277	10.15.21.30	39	048	+25	+07	053	1,51	0,43	0,86	021	202	332	147
11278	10.15.21.30	39	042	+20	+04	046	2,51	0,95	0,13	009	202	322	147
11280	10.15.21.36	44	055	+14	−06	056	1,93	0,98	0,04	033	022	161	163
11291	10.15.22.54	59	081	+34	+11	083	1,86	0,85	0,29	151	203	303	158
11302	10.15.23.45	67	111	+37	+14	107	2,16	0,74	0,97	154	203	202	180
11311	10.16.00.07	67	091	+15	−08	091	6,34	0,90	0,62	163	023	079	165
11312	10.16.00.15	64	087	+16	−07	087	3,22	0,85	0,47	163	023	099	165
11319	10.16.00.34	69	106	+33	+10	103	4,72	0,81	0,91	162	203	216	168
11323	10.16.00.48	69	104	+32	+09	102	4,86	0,82	0,89	164	203	221	168
11327	10.16.00.57	63	113	+32	+10	110	1,30	0,25	0,98	161	203	304	180
11337	10.16.01.33	64	110	+35	+13	107	1,50	0,39	0,92	156	203	222	180
11346	10.16.01.39	65	111	+11	−11	111	1,67	0,41	0,99	160	023	011	156
11350	10.16.01.56	69	136	+25	+07	131	7,27	0,90	0,72	166	203	115	173
11351	10.16.01.56	65	123	+16	−07	121	1,52	0,41	0,89	173	023	309	169
11360	10.16.02.31	66	103	+16	−07	103	1,97	0,56	0,86	166	023	052	156
11362	10.16.02.37	62	106	+09	−14	106	1,26	0,29	0,89	154	023	059	166
11369	10.16.03.16	67	140	+21	+05	136	5,02	0,89	0,56	169	203	004	181
11376	10.16.03.48	61	121	+05	−15	122	1,25	0,34	0,82	151	023	287	177
11400	10.16.19.28	30	039	+06	−09	040	1,76	0,82	0,32	012	023	121	149
11401	10.16.19.35	29	036	+04	−10	036	1,94	0,81	0,37	011	023	114	149
11404	10.16.20.07	34	040	+13	−02	041	2,06	0,88	0,24	004	023	129	160
11413	10.16.21.20	45	047	+24	+06	052	5,17	0,99	0,06	027	203	332	147
11415	10.16.21.40	37	047	+16	−06	047	2,05	0,93	0,15	014	023	140	162
11423	10.17.01.52	66	111	+30	+08	108	1,95	0,51	0,95	166	104	212	168
11438	10.17.05.09	62	144	+05	−09	145	2,92	0,89	0,33	157	024	244	176
11452	10.17.23.36	71	112	+26	+04	110	7,39	0,87	0,97	173	205	199	164
11454	10.17.23.39	38	045	+26	+08	050	1,99	0,93	0,13	020	205	322	147
11464	10.17.23.54	31	031	+18	+05	035	2,71	0,87	0,36	006	205	292	179
11465	10.17.23.56	31	033	+07	−06	033	3,42	0,89	0,39	007	025	107	149
11474	10.18.00.13	68	100	+10	−13	100	7,35	0,89	0,81	156	025	053	172
11475	10.18.00.14	39	037	+23	+08	042	6,48	0,97	0,22	015	205	306	161
11476	10.18.00.15	44	055	+16	−03	057	2,17	0,98	0,04	019	025	161	163
11483	10.18.00.24	73	105	+26	+04	104	14,11	0,95	0,89	173	205	219	157
11484	10.18.00.25	48	050	+25	+07	054	28,22	1,00	0,04	038	205	336	147
11486	10.18.00.29	65	091	+16	−07	091	3,47	0,85	0,53	165	025	091	165
11492	10.18.00.38	64	090	+12	−12	090	3,60	0,86	0,50	154	025	094	165
11491	10.18.00.38	64	109	+11	−11	109	1,45	0,35	0,94	153	025	089	156
11496	10.18.00.43	62	094	+17	−06	093	1,63	0,70	0,49	166	025	104	165
11497	10.18.00.43	38	050	+22	+04	053	1,54	0,94	0,09	011	205	331	147
11500	10.18.00.50	56	106	+06	−17	106	0,42	0,55	0,65	144	025	123	168
11501	10.18.00.23	64	107	+16	−06	107	1,48	0,40	0,88	168	025	053	156
11503	10.18.00.54	44	054	+24	+04	058	2,09	0,99	0,03	024	205	342	147
11504	10.18.01.00	65	112	+07	−15	113	1,90	0,48	0,99	153	025	006	166
11508	10.18.01.08	62	091	+15	−09	091	2,12	0,78	0,46	160	025	103	165
11509	10.18.01.11	69	093	+21	−02	093	203	1,00	0,63	176	025	075	165
11510	10.18.01.13	36	035	+19	+05	039	4,58	0,94	0,27	008	205	301	161
11512	10.18.01.15	71	094	+18	−05	093	−6,29	1,11	0,67	170	025	068	165
11517	10.18.01.40	62	094	+19	−04	094	1,70	0,71	0,49	170	025	103	165
11520	10.18.01.42	66	095	+13	−10	095	3,47	0,82	0,63	160	025	079	165
11522	10.18.01.46	32	034	+18	+04	038	2,50	0,31	0,32	005	205	208	179
11524	10.18.01.47	67	107	+13	−10	107	2,56	0,64	0,92	162	025	037	156
11528	10.18.01.54	46	043	+15	−02	045	−4,62	1,03	0,12	005	025	138	162
11530	10.18.02.02	40	046	+20	+02	050	2,57	0,96	0,11	008	205	326	147
11531	10.18.02.04	69	122	+24	+04	119	3,04	0,68	0,98	173	205	165	175
11532	10.18.02.06	65	091	+14	−09	091	4,24	0,88	0,53	159	025	090	165
11538	10.18.02.20	44	051	+26	+08	056	2,43	0,98	0,06	033	205	336	147
11544	10.18.02.45	71	104	+27	+05	102	243	1,00	0,87	172	205	222	157
11545	10.18.02.49	66	092	+13	−11	092	5,19	0,89	0,57	158	025	085	165
11550	10.18.03.11	67	133	+30	+12	128	2,86	0,71	0,84	158	205	128	183

Continuation

No. of meteor	DATE	Mo	α	δ	β	λ	a	e	q	i	Ω	ω	shower
11554	10.18.01.48	58	143°	+10°	−04°	142°	1,30	0,79	0,27	169°	025°	230°	176
11555	10.18.03.53	69	088	+14	−10	088	−5,33	1,10	0,53	159	025	084	165
11559	10.18.04.04	62	144	+06	−08	144	2,48	0,86	0,34	161	025	245	176
11561	10.18.04.07	69	113	+26	+04	111	2,86	0,66	0,98	172	205	197	184
11564	10.18.04.18	67	110	+31	+09	107	2,58	0,64	0,92	164	205	216	168
11566	10.18.04.21	68	104	+28	+05	102	3,16	0,74	0,82	171	205	234	157
11570	10.18.04.32	67	136	+23	+11	130	3,08	0,74	0,79	159	205	120	173
11572	10.18.04.34	66	108	+12	−11	108	1,92	0,52	0,93	160	025	037	156
11577	10.18.04.53	68	142	+22	+07	138	10,71	0,94	0,61	166	205	101	181
11578	10.18.04.55	64	133	+24	+06	128	1,54	0,52	0,74	168	205	103	174
11581	10.18.05.04	58	111	+15	−07	110	0,88	0,22	0,69	166	025	136	178
11582	10.18.05.09	66	130	+23	+05	126	1,99	0,58	0,83	171	205	123	174
11583	10.18.05.17	60	141	+25	+10	136	1,28	0,64	0,46	158	205	067	171
11590	10.18.05.38	66	126	+16	−03	125	1,72	0,50	0,86	173	025	307	169
11600	10.18.06.28	56	152	+25	+13	146	1,43	0,82	0,26	144	205	049	184
11601	10.18.06.29	61	146	+24	+10	140	1,67	0,75	0,42	156	205	070	171
11602	10.18.06.31	57	143	+24	+09	137	1,05	0,67	0,35	157	205	051	171
11613	10.18.07.31	55	157	+25	+14	149	1,43	0,86	0,20	134	205	044	184
11615	10.18.07.37	55	160	+25	+15	152	1,77	0,89	0,19	128	205	044	184
11618	10.18.07.48	56	164	+22	+14	157	3,02	0,95	0,14	126	205	041	184
11639	10.18.19.43	28	032	+14	+01	034	2,07	0,79	0,42	070	205	289	179
11640	10.18.19.45	29	034	+19	+05	038	1,88	0,81	0,36	005	205	296	179
11647	10.18.20.28	42	044	+14	−03	045	14,87	0,99	0,15	007	025	135	162
11649	10.18.20.35	45	057	+15	−05	058	2,41	0,99	0,03	033	025	162	163
11651	10.18.20.43	35	042	+13	−03	044	2,28	0,89	0,23	005	025	129	160
11653	10.18.20.50	44	051	+22	+04	054	3,59	0,99	0,05	016	205	335	147
11657	10.18.21.17	37	049	+15	−04	051	1,80	0,93	0,13	009	025	145	162
11661	10.18.21.42	30	033	+06	−07	033	2,99	0,89	0,42	008	025	105	149
11663	10.18.21.58	29	034	+17	+03	037	1,96	0,82	0,36	003	205	295	179
11664	10.18.22.07	54	086	+26	+03	086	1,08	0,85	0,16	170	205	326	158
11679	10.18.23.41	48	053	+22	+03	056	8,52	0,88	1,02	008	106	042	147
11682	10.19.00.00	67	093	+24	+01	093	6,32	0,91	0,56	179	206	266	165
11686	10.19.01.40	65	093	+17	−07	093	3,79	0,85	0,56	166	026	088	165
11691	10.19.02.16	66	094	+17	−07	093	4,01	0,86	0,57	165	026	086	165
11694	10.19.02.27	66	093	+18	−05	093	3,91	0,86	0,56	169	026	088	165
11695	10.19.02.27	59	093	+14	−09	093	1,36	0,70	0,41	158	026	116	159
11697	10.19.02.25	68	108	+15	−07	108	2,83	0,68	0,91	167	026	037	156
11701	10.19.02.47	70	092	+17	−07	092	−4,27	1,14	0,61	166	026	074	165
11702	10.19.02.48	65	108	+30	+08	006	1,66	0,49	0,85	166	206	237	168
11705	10.19.03.06	69	123	+19	−01	121	2,61	0,63	0,97	178	026	341	170
11707	10.19.03.15	67	139	+25	+10	134	3,21	0,79	0,69	162	206	108	173
11711	10.19.03.33	66	094	+17	−07	094	4,32	0,87	0,58	165	026	085	165
11714	10.19.03.41	69	096	+16	−07	096	38,15	0,98	0,68	166	026	069	165
11726	10.19.04.29	67	122	+27	+06	119	1,94	0,01	0,99	169	206	170	182
11728	10.19.04.34	66	142	+20	+04	138	3,12	0,82	0,57	171	206	093	181
11730	10.19.04.38	69	127	+22	+03	124	3,22	0,71	0,93	175	206	148	175
11732	10.19.04.46	57	145	+28	+13	138	1,10	0,66	0,38	148	206	055	171
11733	10.19.04.46	57	111	+16	+06	110	0,82	0,29	0,58	166	257	148	178
11735	10.19.04.50	63	096	+18	−05	096	1,79	0,70	0,54	168	026	096	165
11743	10.19.05.22	62	120	+19	−02	118	1,45	0,32	0,99	177	026	352	170
11744	10.19.05.23	61	144	+25	+10	138	1,56	0,69	0,49	156	206	075	171
11747	10.19.06.58	58	159	+25	+15	151	2,53	0,89	0,27	136	206	057	184
11754	10.19.19.36	35	040	+14	−01	042	3,10	0,92	0,91	026	026	124	160
11758	10.19.20.35	27	036	+18	+04	039	1,49	0,75	0,38	004	206	297	179
11759	10.19.20.44	42	050	+13	−05	051	4,33	0,98	0,10	015	026	146	162
11760	10.19.20.50	29	030	+21	+08	035	2,23	0,81	0,42	008	206	287	179
11761	10.19.21.00	38	039	+24	+09	044	5,33	0,96	0,22	017	206	306	161
11764	10.19.21.13	65	091	+11	−12	091	5,94	0,91	0,53	153	026	089	165
11766	10.19.22.09	32	044	+12	−05	045	1,62	0,85	0,25	007	026	129	160
11767	10.19.22.09	35	049	+19	+01	055	1,92	0,94	0,12	002	206	325	147

Continuation

No. of meteor	DATE	T_{00}	α	δ	β	λ	a	e	q	i	Ω	ω	shower
11768	10.19.22.09	32	041°	+18°	+02°	044°	1,79°	0,86	0,25	003°	206°	308°	160
11769	10.20.03.51	70	143	+23	+08	138	−55,93	1,01	0,68	164	207	015	181
11771	10.20.04.24	68	096	+18	−05	096	6,76	0,91	0,63	170	027	077	165
11775	10.20.04.35	70	136	+27	+10	131	12,86	0,93	0,86	162	207	135	173
11778	10.20.04.51	58	163	+22	+14	156	3,15	0,94	0,19	134	207	048	184
11782	10.20.05.31	66	125	+23	+04	122	1,60	0,39	0,97	174	207	153	175
11786	10.20.06.49	60	149	+20	+07	144	1,73	0,19	0,35	162	207	062	171
11788	10.20.07.07	65	141	+27	+11	135	2,19	0,70	0,66	158	207	100	173
11791	10.20.07.34	62	147	+07	−06	147	2,51	0,87	0,33	166	027	244	176
11797	10.20.20.03	42	050	+24	+05	034	3,12	0,97	0,09	017	207	327	147
11799	10.20.20.08	46	055	+24	+05	058	3,81	0,99	0,04	027	207	339	147
11800	10.20.20.12	43	051	+11	−07	051	5,83	0,98	0,12	022	027	142	162
11801	10.20.20.19	28	037	+10	−04	038	1,79	0,77	0,41	004	027	111	149
11802	10.20.20.21	32	040	+20	+04	044	1,94	0,86	0,28	006	207	305	160
11805	10.20.20.24	44	048	+25	+07	052	10,18	0,99	0,10	022	207	324	147
11812	10.20.21.03	32	046	+13	−04	047	1,59	0,85	0,24	006	028	131	160
11820	10.20.21.22	39	047	+14	−03	048	3,65	0,95	0,16	008	027	136	162
11823	10.20.21.42	39	047	+19	+01	050	2,97	0,95	0,14	003	207	320	147
11824	10.20.21.52	42	047	+24	+07	051	3,87	0,97	0,12	018	207	321	147
11825	10.20.21.54	29	038	+13	−02	039	1,82	0,80	0,37	002	027	115	149
11826	10.20.21.58	38	052	+25	+06	056	1,59	0,69	0,10	017	207	329	147
11827	10.20.22.04	41	047	+16	−01	049	5,92	0,98	0,13	003	027	140	162
11828	10.20.22.15	44	045	+20	+02	048	−12,75	1,01	0,13	007	207	317	147
11830	10.20.22.25	43	057	+11	−09	057	2,63	0,97	0,08	034	027	051	163
11833	10.20.22.27	30	043	+16	−00	046	1,51	0,82	0,27	000	027	128	160
11834	10.20.22.30	39	040	+17	+01	043	18,13	0,98	0,22	002	207	304	161
11835	10.20.22.31	65	007	+99	+12	084	2,42	0,74	0,64	166	207	261	167
11839	10.20.23.25	30	039	+14	−01	041	1,81	0,82	0,33	002	028	119	149
11842	10.20.23.39	31	039	+13	−02	040	2,23	0,84	0,33	003	028	117	149
11844	10.21.00.08	66	096	+15	−09	096	4,29	0,86	0,59	162	028	084	165
11847	10.21.00.12	54	094	+17	−07	094	2,83	0,83	0,49	165	028	097	165
11850	10.21.00.28	29	039	+10	−05	040	1,80	0,80	0,37	005	028	115	149
11852	10.21.00.40	41	059	+19	−01	061	1,50	0,98	0,03	007	028	162	163
11855	10.21.00.45	67	096	+12	−11	096	6,38	0,90	0,63	157	027	027	165
11856	10.21.00.46	70	146	+23	+09	140	−10,48	0,94	0,65	162	208	109	181
11857	10.21.00.49	49	050	+21	+03	053	− 3,84	0,99	0,05	015	208	333	147
11858	10.21.00.49	58	087	+28	+05	088	1,68	0,85	0,25	166	203	310	158
11859	10.21.00.50	60	092	+17	−06	092	1,74	0,79	0,36	164	028	116	170
11860	10.21.00.52	70	111	+20	−02	110	4,48	0,78	0,93	176	028	032	156
11861	10.21.00.56	38	055	+20	+01	058	1,39	0,94	0,08	002	208	334	147
11862	10.21.00.57	62	096	+16	−07	096	1,72	0,72	0,48	064	008	014	165
11863	10.21.01.03	63	094	+18	−05	094	2,12	0,79	0,45	167	023	104	165
11867	10.21.01.09	67	096	+12	−14	096	9,10	0,93	0,62	157	028	078	165
11868	10.21.01.13	58	082	+26	+03	083	2,31	0,92	0,18	121	208	316	158
11870	10.21.01.17	67	094	+16	−07	094	2,41	0,93	0,55	164	028	086	165
11871	10.21.01.17	67	094	+17	−06	094	13,78	0,96	0,57	166	028	083	159
11873	10.21.01.21	64	114	+18	−03	113	1,33	0,30	0,93	174	028	044	156
11874	10.21.01.22	69	097	+19	−04	096	−75,39	1,01	0,64	171	028	073	165
11876	10.21.01.24	66	094	+18	−06	094	6,89	0,92	0,54	168	028	088	165
11877	10.21.01.25	65	095	+14	−09	094	4,18	0,87	0,55	160	028	088	165
11878	10.21.01.26	63	095	+16	−07	095	1,96	0,56	0,49	165	028	101	165
11879	10.21.01.27	66	093	+14	−10	093	8,87	0,94	0,54	159	028	087	165
11882	10.21.01.31	69	126	+27	+07	122	2,90	0,65	0,98	167	208	165	182
11884	10.21.01.35	68	111	+23	+01	102	2,61	0,66	0,90	178	208	222	157
11885	10.21.01.39	66	110	+16	+06	109	1,99	0,55	0,90	169	028	044	156
11886	10.21.01.40	67	013	+13	−10	096	5,96	0,90	0,61	159	028	079	165
11887	10.21.01.40	69	095	+16	−07	095	−52,66	1,00	0,61	166	028	077	165
11888	10.21.01.44	70	095	+14	−09	095	− 4,88	1,13	0,64	161	028	071	165
11889	10.21.01.45	64	095	+13	−10	095	2,87	0,82	0,53	158	028	093	165
11894	10.21.01.58	69	094	+14	−10	094	− 6,74	1,09	0,61	160	028	075	165

Conclusion

No, of meteor	DATE	φ_{obs}	α	δ	β	λ	a	e	q	i	Ω	ω	shower
11896	10.21.02.12	67	129°	+28°	+09°	124°	2,21	0,57	0,95	164°	208	150°	182
11899	10.21.02.34	55	093	+12	−11	093	1,06	0,75	0,27	150	028	135	150
11900	10.21.02.35	69	126	+28	+08	122	3,11	0,68	0,99	165	208	168	182
11903	10.21.02.40	69	113	+17	−05	112	2,89	0,65	0,96	071	003	024	156
11905	10.21.02.54	70	098	+18	−05	028	−86,54	1,00	0,68	170	028	068	165
11906	10.21.02.55	64	094	+19	−04	094	3,05	0,83	0,49	171	028	097	165
11909	10.21.03.06	69	115	+24	+03	113	3,00	0,68	0,97	175	208	200	161
11910	10.21.03.08	66	093	+15	−09	093	8,41	0,93	0,54	161	028	087	165
11911	10.21.03.16	61	089	+11	−12	089	2,93	0,86	0,38	150	028	109	159
11912	10.21.03.20	65	094	+15	−08	094	4,17	0,88	0,52	162	028	092	165
11917	10.21.03.37	66	127	+28	−09	122	1,87	0,48	0,98	114	208	161	182
11918	10.21.03.40	67	145	+23	+08	140	4,84	0,87	0,61	162	208	100	181
11920	10.21.03.44	65	151	+20	+08	146	5,51	0,92	0,42	162	208	078	182
11933	10.21.04.13	67	095	+17	−07	095	6,20	0,91	0,56	166	028	085	165
11935	10.21.04.16	56	145	+24	+09	140	0,98	0,66	0,33	157	208	018	171
11936	10.21.04.17	65	110	+33	+11	107	1,90	0,56	0,84	159	208	236	168
11938	10.21.04.21	61	111	+21	−01	110	1,01	0,28	0,75	178	028	099	178
11978	10.21.19.52	33	036	+23	+08	041	2,83	0,89	0,32	011	208	296	179
11979	10.21.19.57	43	050	+18	+00	053	4,88	0,98	0,09	004	208	326	147
11983	10.21.20.55	31	039	+08	−07	039	2,50	0,85	0,37	008	028	112	149
11985	10.21.21.39	45	050	+24	+05	054	8,81	0,99	0,08	019	208	329	147
11986	10.21.21.39	36	040	+21	+06	045	4,01	0,94	0,24	009	208	304	161
11988	10.21.22.11	43	052	+15	−03	053	5,75	0,98	0,09	011	028	147	162
11989	10.21.22.13	43	055	+18	−01	057	2,71	0,98	0,06	005	028	155	163
11990	10.21.22.21	29	042	+19	+03	046	1,46	0,79	0,30	004	208	306	160
11991	10.21.22.27	32	037	+16	+01	037	3,18	0,89	0,34	001	208	293	179
11992	10.21.22.28	59	090	+09	−16	020	2,01	0,81	0,38	141	028	112	159
11995	10.21.22.37	38	062	+13	−08	063	1,22	0,94	0,07	029	028	157	163
11996	10.21.22.49	55	089	+13	−10	089	1,22	0,83	0,21	149	028	138	159
11997	10.21.22.53	29	036	+16	+01	039	1,84	0,80	0,39	001	208	292	179
12000	10.21.23.02	47	051	+20	+01	054	−11,05	1,00	0,06	006	208	331	147
12001	10.21.23.04	42	053	+15	−02	054	3,08	0,97	0,09	007	028	149	162
12004	10.21.23.21	32	040	+08	−07	040	3,14	0,89	0,35	009	028	112	149
12005	10.21.23.31	58	089	+12	−12	089	1,70	0,82	0,30	149	029	124	159
12007	10.21.23.37	44	047	+21	+03	051	142,16	1,00	0,11	010	209	321	147
12008	10.21.23.37	44	054	+16	−03	056	4,06	0,98	0,06	012	029	152	163
12009	10.21.23.44	42	053	+25	+05	057	2,31	0,97	0,07	019	209	332	147
12013	10.22.00.06	67	094	+17	−07	094	3,43	0,97	0,54	166	029	085	165
12015	10.22.00.20	38	047	+12	−05	048	3,06	0,94	0,18	011	018	134	162
12016	10.22.01.44	67	096	+15	−08	095	16,58	0,95	0,58	163	029	081	165
12020	10.22.02.28	68	130	+27	+08	115	2,40	0,60	0,96	165	209	154	182
12021	10.22.02.29	59	099	+17	−06	098	1,25	0,66	0,43	166	029	116	159
12025	10.22.03.10	58	147	+20	+07	143	1,22	0,72	0,34	163	209	055	171
12026	10.22.03.16	68	140	+22	+06	135	4,56	0,84	0,75	169	209	117	173
12028	10.22.03.52	59	162	+23	+14	154	3,40	0,92	0,27	138	209	059	184
12033	10.22.05.12	70	129	+24	+05	125	4,05	0,76	0,96	172	209	158	175
12034	10.22.05.19	68	127	+23	+09	124	2,48	0,61	0,97	174	209	161	175
12040	10.22.06.41	60	149	+22	+08	144	1,42	0,73	0,38	159	209	062	171
12046	10.22.22.19	34	037	+19	+04	049	4,99	0,93	0,34	005	210	291	179
12047	10.23.22.43	26	038	+13	−02	039	1,73	0,74	0,44	002	030	108	149
12052	10.24.04.04	64	121	−05	−24	124	2,49	0,60	0,99	136	031	353	165
12057	10.26.04.26	68	116	+25	+04	114	2,45	0,64	0,89	173	213	224	157
12060	10.27.02.46	69	147	+24	+10	141	6,41	0,88	0,75	161	214	118	173
12064	10.27.03.48	66	145	+25	+11	140	2,67	0,71	0,77	159	214	117	173
12065	10.27.03.52	57	121	+19	−01	119	0,82	0,27	0,69	178	034	151	178

-END-